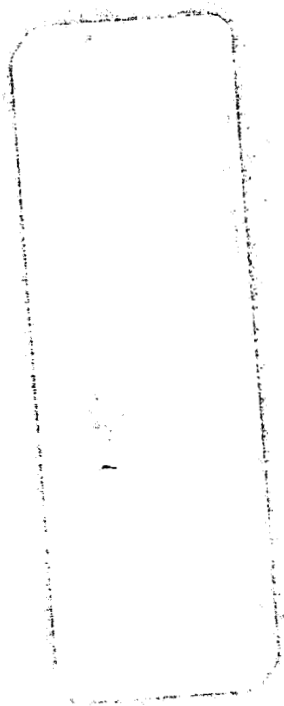


2 (mix)



LESC-5001397
22 FEB 1971

INVESTIGATION OF EXTERNAL REFRIGERATION SYSTEMS FOR LONG TERM CRYOGENIC STORAGE



PREPARED FOR
MANNED SPACECRAFT CENTER
UNDER CONTRACT NAS 9-10412

FACILITY FORM 602	N71-20279	(THRU)
	450	03
	CR-114920	23
	(NASA CR OR TMX OR AD NUMBER)	(CATEGORY)

FINAL REPORT

Reproduced by
**NATIONAL TECHNICAL
INFORMATION SERVICE**
Springfield, Va. 22151

LOCKHEED MISSILES & SPACE COMPANY

A GROUP DIVISION OF LOCKHEED AIRCRAFT CORPORATION
3251 SPACE SYSTEMS DIVISION 4, 40 GUNNERY ROAD, PALMDALE, CALIFORNIA 91364

IMSC-A981632
22 Feb. 1971

CF-114970

INVESTIGATION OF EXTERNAL REFRIGERATION SYSTEMS
FOR LONG TERM CRYOGENIC STORAGE
FINAL REPORT

Prepared for

Thomas L. Davies

Propulsion and Power Division
Manned Spacecraft Center
National Aeronautics and Space Administration

Prepared by

H. L. Jensen, T. C. Nast, A. P. M. Glassford,
R. M. Vernon, W. F. Ekern

Lockheed Missiles & Space Company
Sunnyvale, California

Approved by



S. C. De Brock, Manager
Propulsion Systems

FOREWORD

A 14-month study was conducted by Lockheed Missiles & Space Company for the Propulsion and Power Generation Branch of the Manned Spacecraft Center of the National Aeronautics and Space Administration under Contract NAS9-10412. The study entitled an Investigation of External Refrigerators for Long Term Cryogenic Storage was initiated to present sufficient information and procedures for evaluating the usefulness of a small closed cycle cryogenic refrigeration systems for space applications. The resulting data are presented in four documents, as follows:

An Investigation of External Refrigeration Systems for Long Term Cryogenic Storage - Systems Review Report. LMSC-A903162
May 28, 1970

An Investigation of External Refrigeration Systems for Long Term Cryogenic Storage - Final Report. LMSC-A981632, 22 Feb 1971

Handbook of External Refrigeration Systems for Long Term Cryogenic Storage. LMSC-A984158, 22 Feb 1971

An Investigation of External Refrigeration Systems for Long Term Cryogenic Storage. LMSC-A984159, 22 Feb 1971

This report is the second of these documents and contains the basic data and rationale from which the Handbook (or third of these documents) was produced. It also includes an updating of most of the information presented in the first document.

Sincere appreciation is given to Thomas L. Davies and other NASA personnel for the suggestions and guidance in this study.

CONTENTS

Section		Page
	FOREWORD	ii
	ILLUSTRATIONS	vii
	TABLES	xiv
1	SUMMARY	1-1
2	INTRODUCTION	2-1
	2.1 Introduction	2-1
	2.2 Study Purpose	2-2
	2.3 State of Refrigerator Technology	2-2
	2.4 Study Scope	2-4
	2.5 Study Organization	2-6
	2.6 Report Contents	2-8
	2.7 Remarks	2-11
3	REFRIGERATORS	3-1
	3.1 Introduction	3-1
	3.2 Basic Refrigeration Cycles	3-4
	3.3 Basic Refrigerator Components	3-13
	3.3.1 Compressors	3-13
	3.3.2 Expanders	3-22
	3.3.3 Heat Exchangers	3-25
	3.3.4 Motors	3-28
	3.4 Existing Refrigerator Systems	3-33
	3.4.1 The Stirling Cycle Refrigerator	3-35
	3.4.2 The Vuilleumier Refrigerator	3-54
	3.4.3 The Joule-Thomson Refrigerator	3-60

Section	Page	
3.4.4	Split Component Regenerator Refrigerators (Gifford-McMahon, Solvay and Taconis)	3-74
3.4.5	Brayton/Claude Cycles	3-103
3.5	Additional Operating Data	3-120
3.5.1	Cooldown Time of Refrigerators	3-120
3.5.2	Effect of Heat Rejection Temperature on Refrigerator Performance	3-125
3.6	Summary of Performance Data for Various Cycles	3-126
3.6.1	Coefficient of Performance Versus Cooling Load	3-129
3.6.2	Coefficient of Performance Versus Temperature	3-133
3.6.3	Refrigerator Weight Versus Power Input	3-141
3.6.4	Weight Versus Cooling Capacity	3-145
3.6.5	Weight Versus Temperature	3-151
3.6.6	System Volume	3-154
3.6.7	System Volume Versus Cooling Rate	3-155
3.6.8	System Volume Versus Temperature	3-155
4	FAILURE CHARACTERISTICS OF REFRIGERATORS	4-1
4.1	Introduction	4-1
4.2	Reliability Terminology	4-2
4.3	Failure Rate Patterns	4-4
4.3.1	Use of Redundancy	4-10
4.4	Failure Rate of Refrigerators	4-10
4.4.1	Conventional Technology Refrigerators	4-12
4.4.2	Advanced Technology Refrigerators	4-17
4.5	Discussion	4-19
5	THERMAL ENVIRONMENTS	5-1
5.1	Definition of Thermal Environment Parameters	5-1
5.2	Direct Solar Heat Flux	5-2
5.3	Planetary Heat Flux	5-3
5.4	Temperature of Near-Earth Satellites	5-7

Section		Page
6	TANKAGE AND HEAT LEAKS	6-1
	6.1 Introduction	6-1
	6.2 Tank Volume and Surface Area	6-1
	6.3 Weight Estimate of Cryogen Tanks	6-4
	6.3.1 Tank Support System Weights	6-7
	6.3.2 Baffles	6-7
	6.3.3 Vacuum Jackets	6-7
	6.3.4 Access Covers	6-10
	6.4 Heat Leak to Tanks	6-10
	6.4.1 Heat Leak Through Insulation	6-10
	6.4.2 Heat Leak Through Supports	6-16
	6.4.3 Heat Leak Through Lines and Instrumentation	6-19
7	HEAT REJECTION SYSTEMS	7-1
	7.1 Introduction	7-1
	7.2 Radiator Design	7-2
	7.2.1 Preliminary Design of Radiators for Space Operation	7-2
	7.2.2 Approximate Method for Radiator Design	7-20
	7.2.3 Fluid Selection for Radiator Design	7-24
	7.2.4 Pressure Drop in Coolant Ducts	7-25
	7.2.5 Radiator Weight and Area Requirements	7-28
	7.3 Design of Heat Pipe Radiators	7-31
	7.4 Fluid Circulation	7-33
	7.5 Heat Pipe Design	7-33
	7.5.1 Fluid Selection	7-36
	7.5.2 Wick Design	7-45
	7.5.3 Size and Weight	7-51
	7.5.4 Design Procedure for Optimized Homogeneous Wick Heat Pipes	7-53
8	HEAT ABSORPTION	8-1
	8.1 Introduction	8-1
	8.2 Tank Wall Heat Exchangers	8-1

Section	Page
8.2.1 Design Analyses	8-1
8.2.2 Optimum Tube Spacing	8-6
8.2.3 Design Procedure	8-7
8.2.4 Sample Calculations	8-8
8.3 Fluid Circulation Pumps	8-11
8.4 Cryogenic Heat Pipes	8-11
8.4.1 Fluid Selection	8-11
8.4.2 Evaporator and Condenser Temperature Drops	8-14
8.4.3 Wick Design	8-19
8.4.4 Size and Weight	8-19
8.4.5 Heat Pipe Insulation	8-22
8.5 Solid Conduction Devices	8-26
9 POWER SUPPLIES	9-1
9.1 Summary	9-1
9.2 Electrical Power Systems	9-3
9.2.1 Solar Photovoltaic Power Source	9-3
9.2.2 Battery Power Systems	9-6
9.2.3 Fuel Cell Power System	9-10
9.2.4 Radioisotope Thermoelectric Generators (RTG)	9-17
9.2.5 Radioisotope-Brayton-Cycle Power System	9-21
9.2.6 Nuclear Reactor Power Systems	9-24
9.2.7 Power Conditioning	9-34
9.3 Thermal Energy Sources	9-35
9.3.1 Radioisotope Heat Source	9-35
9.3.2 Solar Collector/Receiver System	9-43
9.3.3 Heat Storage	9-46
10.0 CRYOGEN PROPERTIES	10-1
11.0 CONVERSION UNITS	11-1

ILLUSTRATIONS

Figure		Page
3-1	Mechanically-Powered Refrigerator Operation	3-5
3-2	Heat-Powered Refrigerator Operation	3-5
3-3	The Carnot Refrigeration Cycle	3-9
3-4	The Ericsson Refrigeration Cycle	3-9
3-5	The Stirling Refrigeration Cycle	3-11
3-6	The Brayton Refrigeration Cycle	3-12
3-7	The Heat Powered Brayton Refrigeration Cycle	3-12
3-8	Theoretical Isentropic Work for Single Stage Compressor	3-18
3-9	Compressor Weight as a Function of Power Required	3-20
3-10	Compressor Volume as a Function of Power Required	3-21
3-11	Efficiency of Reciprocating Expansion Engine	3-24
3-12	Efficiency of Radial Impulse Turbines	3-24
3-13	Schematic of a Counterflow Heat Exchanger	3-26
3-14	Schematic of a Regenerative Heat Exchanger	3-26
3-15	Weight of Exchanger-Expanders Versus Temperature	3-29
3-16	Volume of Exchanger-Expanders Versus Temperature	3-30
3-17	Weight of Exchangers-Expanders Versus Cooling Power	3-31
3-18	Specific Weight of Electric Motors	3-32
3-19	Cycles Included for Analysis	3-34
3-20	The Practical Stirling Refrigerator - Two Piston Version	3-37
3-21	The Stirling Refrigerator - Displacer Version	3-38
3-22	Refrigeration Versus Temperature (Stirling Cycle)	3-46
3-23	Refrigeration Versus Temperature (Stirling Cycle)	3-47
3-24	Refrigeration Versus Temperature (Stirling Cycle)	3-47
3-25	Refrigeration Versus Temperature (Stirling Cycle)	3-48
3-26	Refrigeration Versus Temperature (Stirling Cycle)	3-49
3-27	Coefficient of Performance Versus Cooling Capacity (Stirling Cycle)	3-50
3-28	Coefficient of Performance Versus Temperature (Stirling Cycle)	3-51

ILLUSTRATIONS (Cont.)

Figure		Page
3-29	Percent Carnot Efficiency of Stirling Cycle Refrigerators	3-52
3-30	Specific Weight Versus Cooling Capacity (Stirling Cycle)	3-53
3-31	Specific Weight Versus Temperature (Stirling Cycle)	3-55
3-32	Specific Volume Versus Refrigeration Load (Stirling Cycle)	3-56
3-33	Vuilleumier Cycle	3-57
3-34	Coefficient of Performance Versus Cooling Capacity (Vuilleumier Cycle)	3-63
3-35	Coefficient of Performance of Prototype Vuilleumier Refrigerators (Small Units)	3-64
3-36	Percent Carnot Efficiency of Vuilleumier Prototype Refrigerators	3-65
3-37	Specific Weight Versus Temperature (Vuilleumier Cycle)	3-66
3-38	Specific Weight Versus Refrigeration Capacity (Vuilleumier Cycle)	3-67
3-39	Specific Volume Versus Refrigeration Capacity (Vuilleumier Cycle)	3-68
3-40	Joule-Thomson Cycle	3-69
3-41	A Three-Fluid Cascaded Joule-Thomson Refrigerator	3-71
3-42	COP Versus Temperature for Joule-Thomson Closed Cycle Systems	3-77
3-43	COP Versus Capacity for Joule-Thomson Closed Cycle Systems	3-78
3-44	Percent Carnot Efficiency for Joule-Thomson Systems	3-79
3-45	Specific Weight Versus Capacity for Closed-Cycle Joule-Thomson Units	3-80
3-46	Specific Volume of Closed Cycle Joule-Thomson Units Versus Capacity	3-81
3-47	The Solvay Expansion Process	3-84
3-48	The Taconis Expansion Process	3-86
3-49	Refrigeration vs. Temperature (Gifford-McMahon Cycle)	3-93
3-50	Refrigeration vs. Temperature (Gifford-McMahon Units)	3-94
3-51	Refrigeration vs. Temperature (Gifford-McMahon Units)	3-95
3-52	Refrigeration vs. Temperature (Gifford-McMahon Units)	3-96

ILLUSTRATIONS (Cont.)

Figure		Page
3-53	Refrigeration vs. Temperature (Gifford-McMahon Units)	3-97
3-54	COP Versus Refrigeration Capacity for Gifford-McMahon, Solvay and Taconis Systems at 20°K, 77°K, and 110°K	3-98
3-55	COP vs. Refrigeration Capacity for Gifford-McMahon, Solvay, and Taconis Systems at 12°K and 15°K	3-99
3-56	COP of Gifford-McMahon, Taconis, and Solvay Refrigerators	3-100
3-57	Specific Weight vs. Refrigeration for Gifford-McMahon, Solvay and Taconis Refrigerators	3-101
3-58	Specific Weight Versus Temperature of Gifford-McMahon, Solvay, and Taconis Refrigerators	3-102
3-59	Specific Volume Versus Capacity of Gifford-McMahon Systems	3-104
3-60	Percent Carnot Efficiency of Gifford-McMahon Systems	3-105
3-61	The Brayton Cycle	3-106
3-62	The Claude Refrigeration Cycle	3-112
3-63	Thermodynamic Performance of Brayton/Claude Cycle for Prototype Units and Prediction	3-118
3-64	Specific Weight of Brayton/Claude Cycle Refrigerators for Prototype Units and Prediction	3-119
3-65	Estimated Cool-Down Characteristics of Various Refrigerators for 25°K Cooling	3-122
3-66	Estimated Cool-Down Characteristics of Various Refrigerators for 77°K Cooling	3-123
3-67	Cool-Down Times for Various Refrigerators (from 300°K)	3-124
3-68	Summary of Refrigerator Coefficient of Performance for Various Cycles at 20°K and 4.2°K	3-131
3-69	Summary of Refrigerator Coefficient of Performance Versus Refrigeration for Various Cycles at 77°K	3-135
3-70	Coefficient of Performance at 5 Watts Versus Temperature	3-137
3-71	Coefficient of Performance at 100 Watts Versus Temperature	3-139
3-72	Refrigerator System Weight Versus Power Input for Various Machines	3-143
3-73	Summary of Refrigerator Weights Versus Refrigeration for Various Cycles at 20°K and 4.2°K	3-147

ILLUSTRATIONS (Cont.)

Figure		Page
3-74	Summary of Refrigerator Weight Versus Refrigeration for Various Cycles at 77°K	3-149
3-75	Summary of Refrigerator Weights Versus Temperature at 5 Watt Cooling Capacity	3-152
3-76	Summary of Refrigerator Weights Versus Temperature at 100 Watt Cooling Capacity	3-153
3-77	Refrigerator System Density Versus System Weight	3-157
3-78	Summary of Refrigerator Specific Volume Versus Refrigeration at 20°K	3-159
3-79	Summary of Refrigerator Specific Volume Versus Refrigeration at 77°K	3-161
3-80	Summary of Refrigerator Specific Volume Versus Temperature for Various Cycles at 5 Watts	3-163
3-81	Summary of Refrigerator Specific Volume Versus Temperature for Various Cycles at 100 Watts	3-165
4-1	The "Bathtub" Curve	4-6
4-2	Weibull Failure Rate Distributions	4-8
4-3	Life Ratio Vs. Reliability	4-9
5-1	View Factors from Vehicle Surfaces to Planetary Terrain	5-5
5-2	Planetary View Factor for Infrared Exchange	5-6
5-3	Lunar Surface Temperatures	5-9
5-4	Diurnal Temperature Variation of the Surface of Mars	5-10
5-5	Polar Orbit Geometry	5-11
5-6	Planet Reflection Coefficient for Flat Surface Element	5-12
5-7	Time Average Temperature as a Function of the α/ϵ Ratio (Surfaces 1 and 2)	5-14
5-8	Time Average Temperature as a Function of the α/ϵ Ratio (Surface 3)	5-14
5-9	Time Average Temperature as a Function of the α/ϵ Ratio (Surface 4)	5-15
5-10	Time Average Temperature as a Function of the α/ϵ Ratio (Surface 5)	5-15

ILLUSTRATIONS (Cont.)

Figure		Page
6-1	Tank Volume	6-2
6-2	Tank Area	6-3
6-3	Aluminum Tank Shell Weight	6-5
6-4	Tank Support Weight	6-8
6-5	Vacuum Jacket Volume	6-9
6-6	Total Unit Weight as a Function of Actual-to-Design Layer Density Ratio for Four Multilayer Insulations	6-11
6-7	Heat Flux Through Goldized Mylar/Silk Net Insulation	6-13
6-8	Heat Leaks Through Fiberglas Supports	6-17
6-9	Heat Leak Through Lines and Instrumentation	6-20
7-1	Radiator Duct with Trapezoidal Fins - Two Exposed Sides	7-3
7-2	Correction Factor for Interradiation Between Coolant Tube and Fins	7-7
7-3	Nomogram for Solution of Dittus-Boelter Equation	7-8
7-4	Fin Effectiveness for Rectangular Fins	7-13
7-5	Fin Effectiveness for Trapezoidal Fin, $c/H = 0.75$	7-14
7-6	Fin Effectiveness for Trapezoidal Fin, $c/H = 0.50$	7-15
7-7	Fin Effectiveness for Trapezoidal Fin, $c/H = 0.25$	7-16
7-8	Fin Effectiveness for Trapezoidal Fin, $c/H = 0.01$	7-17
7-9	Film Resistance Number for Radiator Heat Rejection	7-18
7-10	Radiation Number for Radiator Heat Rejection	7-19
7-11	Heat Transfer Parameter for Various Liquids	7-27
7-12	Radiator Area for Deep Space and Lunar Surface Operation	7-29

ILLUSTRATIONS (Cont.)

Figure		Page
7-13	Radiator Weight for Deep Space and Lunar Surface Operation	7-30
7-14	Rectangular Fin Radiator with Integral Heat Pipes	7-32
7-15	Weight of Circulation Pump and Motor	7-34
7-16	Power Required for Circulation Pump	7-35
7-17	Heat Pipe Schematic	7-37
7-18	Vapor Pressure Vs. Temperature for Various Liquids	7-38
7-19	Liquid Parameter for Various Liquids	7-41
7-20	Fluid Property Groups at Moderate Temperatures	7-42
7-21	Cross-Sections of Three Wick Structures	7-43
7-22	Heat Pipe Schematic and Pressure Diagram	7-46
7-23	Heat Pipe Performance for Moderate Temperatures	7-52
7-24	Weight of Moderate Temperature Heat Pipes	7-54
7-25	Nucleate Boiling Heat Fluxes for Moderate and High Temperature Fluids	7-56
8-1	Tank Wall Heat Exchanger	8-2
8-2	Wall Temperature Distribution	8-5
8-3	Tube-Wall Attachment Geometry	8-5
8-4	Heat Exchanger Surface Area Requirements	8-9
8-5	Tank Wall Heat Exchanger Weight	8-10
8-6	Helium Circulation Fan and Motor Weight	8-12
8-7	Helium Circulation Power	8-13
8-8	Fluid Property Groups at Low Temperatures	8-15
8-9	Fluid Property Groups at Low Temperatures (Hydrogen)	8-16
8-10	Cryogenic Heat Pipe Fluids	8-17
8-11	Nucleate Boiling Heat Fluxes for Cryogenic Fluids	8-18
8-12	Homogeneous Wick Heat Pipe Performance	8-20
8-13	Channel Wick Heat Pipe Performance	8-21
8-14	Compressibility Factor of Real Gases	8-23
8-15	Relative Operating Pressures for Nitrogen, Oxygen, and Fluorine Heat Pipes	8-24

ILLUSTRATIONS (Cont.)

Figure		Page
8-16	Cryogenic Heat Pipe Weight	8-25
8-17	Heat Leak as a Function of Heat Pipe Radius for a 5-ft Long Pipe with No Exterior Insulation	8-27
8-18	Heat Leak as a Function of Heat Pipe Radius for a 5-ft Long Pipe with a Multilayer Insulation	8-27
8-19	Weight of Solid Conductor for Liquid Oxygen Storage	8-29
9-1	Schematic of Hydrogen-Oxygen Fuel Cell Power System	9-13
9-2	Fuel Cell Power System Weight 0.1 KW Unit	9-14
9-3	Fuel Cell Power System Weight 1.0 KW Unit	9-15
9-4	Fuel Cell Power System Weight 10 KW Unit	9-16
9-5	Schematic of Radioisotope Thermoelectric Generator	9-18
9-6	Radioisotope Brayton-Cycle Power System	9-22
9-7	Direct Radiating Thermoelectric Power System	9-31
9-8	SNAP-8 Type Tankine Cycle Power System	9-32
9-9	Nuclear Reactor Brayton-Cycle Power System	9-33
9-10	Schematic - Direct Coupling of Radioisotope Heat Source with Heat-Powered Refrigeration Unit	9-37
9-11	Schematic - Heat Pipe Coupling of Radioisotope Heat Source with Heat-Powered Refrigeration Unit	9-39
9-12	Schematic - Large Isotope Heat Source for Heat-Powered Refrigeration Unit	9-40
9-13	Solar Collector Diameter - Ft	9-48
10-1	Hydrogen - Density - Heat of Vaporization - Temperature	10-1
10-2	Hydrogen - Pressure - Internal Energy	10-3
10-3	Properties of Liquid Oxygen	10-4
10-4	Oxygen Pressure Versus Internal Energy	10-5
10-5	Properties of Liquid Fluorine	10-6
10-6	Fluorine Pressure Versus Internal Energy	10-7
10-7	Properties of Liquid Nitrogen	10-8
10-8	Nitrogen Pressure Versus Internal Energy	10-9

TABLES

Table		Page
3-1	Existing Stirling Cycle Refrigerators	3-43
3-2	Existing Vuilleumier Prototype Refrigerators (Small Units)	3-61
3-3	Closed Cycle Joule-Thomson Refrigerators (Small Units)	3-75
3-4	Existing Gifford-McMahon Refrigerators	3-91
3-5	Prototype Brayton Cycle Refrigerators	3-117
3-6	Areas of Application of Cryogenic Cooling	3-127
5-1	Representative Values of Solar Absorptance and	5-4
5-2	Physical Characteristics of Earth's Moon and the Planets	5-8
5-3	Equilibrium Tank Surface Temperatures	5-16
6-1	Typical Properties of Aluminized, Low-Emittance Micro-Spheres	6-15
6-2	Heat Leak Through Supports and Lines and Administration	6-18
7-1	Thermophysical Properties of Liquids at One Atmosphere	7-26
7-2	Wick Permeability Values	7-49
9-1	Solar Photovoltaic Power System Characteristics	9-5
9-2	Battery Power System Characteristics	9-9
9-3	Hydrogen-Oxygen Fuel Cells	9-12
9-4	RTG Characteristics	9-20
9-5	Reactor Power System Characteristics (Typical)	9-30

TABLES (Cont.)

Table		Page
9-6	Typical Radioisotope Heat Source Characteristics	9-42
9-7	Characteristics of a Solar Heat Source Designed by Minneapolis-Honeywell	9-46
9-8	Typical Absorber Aperture Diameters (Ft)	9-49
9-9	Typical Characteristics of Solar Collector/ Absorber Heat Sources	9-50
Section 11 - Conversion Units		
1	Defined Values of Basic Units and Equivalentents	11-4
2	Secondary Units in the International System	11-5
3	Values of Physical Constants in SI Units	11-7
4	Length	11-8
5	Area	11-9
6	Volume	11-10
7	Linear Velocity	11-12
8	Angular Velocity	11-13
9	Linear Acceleration	11-14
10	Angular Acceleration	11-15
11	Mass and Weight	11-16
12	Density	11-17
13	Force	11-18
14	Pressure or Force per Unit per Area	11-19
15	Torque	11-20
16	Moment of Inertia	11-21
17	Energy, Work, and Heat	11-22
18	Power, Heat Flux, Radiant Flux	11-23
19	Power Density, Heat Flux Density	11-24
20	Temperature	11-25
21	Thermal Conductivity	11-26
22	Thermal Resistance	11-27

TABLES (Cont.)

Table		Page
23	Thermal Capacitance	11-28
24	Thermal Diffusivity	11-29
25	Specific Heat	11-30
26	Latent Heat	11-31
27	Viscosity	11-32
28	Kinematic Viscosity	11-33

Section 1
SUMMARY

This report is the culmination of a 14 month study initiated by the National Aeronautics Space Administration at the Manned Spacecraft Center to provide data and material on external cryogenic refrigeration systems. The data was prepared so that it could be used to evaluate the usefulness of using an external cryogenic refrigerator to cool cryogenic storage systems over long periods of time in space. One of the main purposes of the study was to produce a handbook* that could be used to aid the engineer/planner in performing the trade-off studies that are necessary to evaluate the various options that arise when one considers the use of cryogens in space.

Several elements which contribute to the refrigeration system were investigated and procedures for estimating performance, weight, and volume of each element were established. The major elements of the refrigeration system are the refrigerator itself, the mechanisms to transfer heat from the cryogenic tankage to the radiator, the cryogenic tankage and its insulation, mechanisms to reject heat from the system, and power supplies.

Information and data were prepared for a wide range of parameters. The initial range parameters that were covered in the initial phases of this study are:

- o Cooling load 5 to 100 watts (17 to 341 BTU/hr)
- o Temperature at which heat
 is to be absorbed 20 to 110°K (36 to 200°R)
- o Mission duration 6 to 24 months
- o Tank size 20 to 200 ft³
- o Heat sink temperatures 78 to 340°K (140 to 610°R)

The heat sink temperatures were evaluated in terms of a set of thermal environments that would cover the above temperature range rather than actually determining the effective sink temperature. For example, heat flux parameters were evaluated considering surfaces in various earth orbits, in deep space, and on the lunar surface for various sun lighting conditions.

* Handbook of External Refrigeration Systems for Long Term Cryogenic Storage.
LMSC-A984153, 22 Feb 1971.

As potential applications and additional information became available during the course of the study, the ranges of the above mentioned parameters were extended. The cooling loads were extended down to fractions of a watt and the temperature was extended down to the 4 to 12°K regime. The tank data was extended to cover ranges up to 280 ft³.

The data and information developed for the various elements and parameters are presented in this report along with qualifying data and explanations.

The pertinent data has been extracted from this report and used in a succinct fashion to provide a handbook for cryogenic refrigeration systems analyses. The handbook presents curves, data, and procedures to obtain system weight, volume and performance for a variety of cryogenic refrigeration systems space applications.

Section 2 INTRODUCTION

2.1 INTRODUCTION

During the process of planning future space missions and determining the role of cryogenic fluids for use in those missions it is necessary to evaluate many different options. One option that the designer/planner may want to evaluate is the use of refrigeration systems to maintain the cryogenic state of the fluids of interest. Cryogenics can be stored in space for a considerable time, with proper care and appropriate design conditions the storage time can be six months or more. Boil off nearly always occurs; however, for cryogenics like hydrogen that have a high heat of vaporization the penalty paid from a weight standpoint is sometimes acceptable. Other constraints such as volume and orbit control may make it more effective to utilize a refrigeration system.

In order to provide the needed data the National Aeronautic and Space Administration at the Manned Spacecraft Center initiated a timely study to investigate external refrigeration systems for cooling cryogenic storage systems in long term space applications. The study was a 14 month effort extending from December 22, 1969 to February 22, 1971.

A cryogenic refrigeration system is simply a device that will transfer heat from a very low temperature source to a high temperature sink. In order to conduct tradeoff studies something has to be known about each element of the heat transfer system so that the proper consideration can be given to it. In this study the complete system that was evaluated is made up of the refrigerator unit itself, the heat transfer mechanisms used to reject the waste heat and to absorb the heat, and the power supply. The power supply is included in the system because the efficiency of cryogenic refrigerators is low enough that the type of power and the way it is put into the system becomes an important design consideration.

2.2 STUDY PURPOSE

The purpose of performing this study is to provide the designer/planner with sufficient basic information to conduct rapid and accurate cryogenic refrigeration systems studies. The data and material presented in this report provides the base from which a refrigeration systems handbook was prepared. All the data that are contained in the handbook are presented in this report, but more detailed and descriptive information is usually provided here. The handbook will be used to conduct step-by-step tradeoff analyses of refrigeration systems. Each element of the system including refrigerator units, failure characteristics, thermal environment, tankage, waste heat rejection, cryogen to refrigerator heat exchanger, and power supply have been evaluated and data for each is given in this report and in the handbook. For completeness and to facilitate the use of the report and handbook a limited amount of cryogenic property data is included. Also included is a comprehensive set of conversion units particularly applicable to thermal work. The conversion units have been included because a great deal of information on refrigeration systems is in terms of mixed International and English units; whereas, in general, the engineer has a better "feel" for the subject if the units are in terms familiar to him. Therefore the data in this report have been presented in units customarily used, resulting in a mixed set of units. With the complete conversion system readily available, little time will be wasted in converting to whatever units the engineer is comfortable in handling.

2.3 STATE OF REFRIGERATOR TECHNOLOGY

During the nineteenth century, the principal interest in attaining very low temperatures was to attempt to liquefy the so-called permanent gases, culminating in the liquefaction of hydrogen in 1898 and helium in 1908. Early very low temperature refrigeration was achieved by a relatively inefficient cycle involving one or more stages of compression, heat exchange and throttling, known as the Linde or Joule-Thomson cycle.

After this first liquefaction of helium considerable research was performed on the behavior of helium and other substances at the newly-attainable low

temperatures in apparatus which included integral liquefiers or in the very small numbers of laboratories in the world which possessed a self-contained but inevitably temperamental and inefficient liquefier. These early low temperature experiments gradually revealed the vast possibilities of basic research at very low temperatures and the demand for liquid helium as a basic laboratory utility rapidly increased. In the late 1940's, Arthur D. Little, Inc., began marketing a commercial version of a significantly more efficient and practical helium liquefier using expansion engines and operating on a modified Claude cycle which was developed by Dr. S. C. Collins. Several hundred units of this refrigerator/liquefier and its derivatives have been built to date and its introduction, in retrospect, marked the beginning of the commercial low temperature refrigerator market. During the 1950's, a small number of other laboratory model refrigerators appeared on the market and several large scale gas liquefiers were built. These all worked on basically similar Claude or Brayton cycles, or the simple Joule-Thomson cycle. A second most significant event in the development of practical very low temperature refrigerators was the introduction in the late 1940's and early 1950's of a Stirling-cycle-based refrigerator by Phillips Electrical Company. This Stirling cycle refrigerator also developed into a highly successful commercial product. The most significant feature of this cycle is the use of regenerative rather than counterflow heat exchangers. Since that time many types of refrigerators using regenerative heat exchangers have been built which are basically related to the Stirling refrigerator, for example, the Taconis, Gifford-McMahon, Solvay and Vuilleumier Systems.

From the late 1950's to the present day several new fields of application for refrigerators and liquefiers developed whose influence is almost entirely responsible for the present shape of technology. With the development of the space program, liquid fueled ballistic missiles, and the large scale use of liquefied natural gas came a demand for very large scale liquefaction plants. At the same time there was a growing interest in the field of very low temperature electronics which led to a demand for convenient laboratory-type refrigerators for basic research, and for small flight weight

units for airborne detection systems. Although many other particular applications could be noted, it is in these three areas that the greatest amount of design effort, cumulative experience and reliable hardware can be found.

In general, these existing refrigerators are not immediately suitable for space flight use although the technology developed for the airborne detection system refrigerators is to a large extent appropriate to the spaceborne application. A substantial number of research and development programs have been pursued by the U. S. Government in order to reduce or eliminate these inadequacies. Some of the programs have been general in nature and have been intended to raise the overall level of technology. Others have aimed at procuring a refrigerator for a particular mission. This research and development activity is sufficiently established and intense to be considered as the major aspect of the current state of refrigerator technology of interest to spacecraft designers.

2.4 STUDY SCOPE

The study was mainly oriented toward developing procedures and information that can be used to determine the performance, weight, and the size of a complete refrigeration system. As mentioned before there are several elements in the refrigeration system, any one of which could easily occupy the time and effort available for this study. Therefore, by necessity, only enough analyses was conducted in each area to provide the designer with the information required for him to determine the overall system performance, weight, and volume and to conduct system operating tradeoffs. The data provided include the range of parameters indicated below.

- o Cooling load 5 to 100 watts (17 to 341 BTU/HR)
- o Cryogenic tankage 20 to 200 cu. ft.
- o Temperatures at which cooling is required 36° to 200°R (20 to 110°K)
- o Mission duration 6 to 24 months

A significant amount of cryogenic refrigeration development has been conducted at cooling loads of less than 5 watts (0.1 to 1 watt) and at temperatures below 20°K (4 to 12°K). Therefore where this information was available the lower limits of 5 watts and 20°K were extended to lower levels. To

help in evaluating larger tanks, especially hydrogen tanks, the volumes and associated data were extended to 280 cu. ft. A variety of thermal environment conditions were studied in order to obtain the heat rejection rates of the radiators and the heat absorption rates to the cryogenic tankage. Initial consideration was given to examining a temperature range of 140 to 610°R (78 to 340°K); however, it seemed more prudent to define the thermal environment that a radiator or tank would experience in space and compute the heat rates directly. Therefore, several mission profiles were defined and the appropriate methods to compute view factors, planet albedo, and solar incidence were developed. The mission profiles were generally categorized into planetary orbit operation, Martian and Lunar surface operations, and deep space operation, such as translunar or transmartian flight.

Information has been included on refrigerator maintenance and failure characteristics; however, this is relatively limited primarily because of the limited operating experience available for space based cryogenic refrigerators.

With the information given in this report and in the handbook the designer can identify the optimum refrigeration system for his particular application and can determine the sensitivity of the operating characteristics to variations in each element of the system. He can obtain an insight to what areas of development would best profit by additional effort. He can obtain bounds on operating conditions in order to establish preliminary specifications. The most important single function of the material given here is to aid the designer in determining whether or not an active external refrigerator should be used for his application.

The data and information given in these reports are not intended to be used for refrigerator design or for detail designs of heat exchanger or heat pipe designs. The procedures outlined for calculating radiator channel and fin dimensions are quite comprehensive and could be used for detail configuration definition if the situation demands it. However, the procedures outlined in the handbook are somewhat simplified and can be used more rapidly.

2.5 STUDY ORGANIZATION

The study was initiated by reviewing reports, data sources and development programs available on small cryogenic refrigerators. A bibliography was obtained from the National Bureau of Standards and the pertinent reports were reviewed. This activity was conducted over the first four months of the contracted effort and a refrigerator systems review report* was published in May 1970. Following this effort additional information was collected on refrigeration systems and the data in the report was continuously updated and extended. Effort was also initiated for other elements of a refrigeration system. Power supplies were reviewed and descriptive information developed on all types of power supplies that might be used in conjunction with refrigerators. In some cases, e.g., a nuclear reactor power source, it is not likely that the power source would be used only for refrigerator operation; however, it was felt that enough descriptive information should be given so that if an application arises the designer will have a handy source of information to provide him understanding and insight to the problem areas. He can also evaluate ways of integrating the power supply requirements with the refrigerator requirements. Environmental conditions were evaluated with the effort being aimed at establishing the thermal environments, mainly because the thermal environment contributes the greatest interaction to system tradeoff analyses. Other environments that are encountered during terrestrial (salt, wind, rain transportation, etc.) and ascent (max. acceleration, vibration, acoustic) operation are generally specified and little tradeoff interaction is available.

Refrigerator analyses were conducted to develop procedures and methods for estimating cool down times, for estimating performance over operating regions where no data presently exists, and for estimating refrigerator characteristics at various heat rejection temperatures. The approach used for most of these analyses was to utilize data on existing cryogenic refrigerators and modifying it by consideration of the ideal performance characteristics. It is very difficult, and sometimes misleading to predict the performance of a cryogenic refrigerator on analytical procedures alone. To develop methods of accurately doing this was beyond the scope of this study. However, by careful evaluation

* Investigation of External Refrigeration Systems for Long Term Cryogenic Storage, LMSC-A903162, 28 May 1970.

of the operating performance and characteristics of existing and in-development refrigerators, a great deal of useful data and curves were generated.

The failure characteristics of the cryogenic refrigerators were examined. Most existing refrigerators require frequent maintenance intervals and no refrigerator presently exists that will operate in an unattended space environment for 6 to 24 months. The effort in evaluating the failure characteristics was primarily directed toward developing means to permit the designer/planner to estimate overall system weight and reliability characteristics. A convenient measure of system advantages and disadvantages from a refrigerator failure point of view is the probability of failure. These probability numbers, as used in this report, are not meant to give hard and exact values because none really exist on these systems. Rather, they are meant to give the user a "feel" for what is required in the way of necessary operating life and/or redundancy.

An extremely large variation in operating life of the various refrigerator systems is obtained as one consults various manufacturers. Consequently, it would be prudent for the user to directly ascertain the expected operating life of a particular machine for a particular application after he has performed the desired trade-off studies and has obtained some insight to his requirements and problems.

Analyses of waste heat rejection and heat absorption methods were performed. The primary emphasis for the waste heat rejection portion was placed on radiator definition and design. Detailed and simplified procedures were developed to determine tube and fin size for radiators suitable for rejecting the amount of heat and in the environments appropriate to this study. A comprehensive discussion of heat pipe designs was also prepared and should provide the user with one of the most up to date sources of heat pipe information available at this time.

In order to provide the engineer with information to estimate complete system performance, methods of transferring heat from the cryogenic tank to the refrigerator were also investigated. A great deal of time could be devoted to defining the exact performance parameters; however, to stay within the scope of this study only sufficient data and material was developed to give the designer approximate weights and performance characteristics. The use of cryogenic heat pipes was also investigated and included in this section.

To facilitate the use of the material in this report a limited amount of cryogen properties data and conversion charts were prepared. In evaluating the processes involved with intermittent operation of a refrigeration system, it is necessary to investigate the pressure profiles in cryogen tanks. To aid the designer in the computational process a set of pressure-internal energy charts were prepared. A considerable amount of effort was required to put the data in this format but having it thus will markedly increase the speed of calculating intermittent refrigerator operations.

The conversion units are quite comprehensive, especially in the thermodynamics area and should also facilitate the use of the material in this report.

2.6 REPORT CONTENTS

This report has been primarily organized in sections according to major elements of a cryogenic refrigerator system. The sections are:

- o Summary
- o Introduction
- o Refrigerators
- o Failure Characteristics
- o Thermal Environments
- o Tankage and Heat Leaks
- o Waste Heat Rejection
- o Heat Absorption
- o Power Supplies
- o Cryogen Properties
- o Conversion Units

A major requirement of this study was to produce a handbook that could be easily used to quickly evaluate cryogenic refrigeration systems for space applications. With this in mind this report was written in terms of sections that would contribute directly to the handbook.

This report has all of the pertinent and detailed information developed and provides rationale, discussion, limitations, qualifications, and procedures in the study. The handbook is an extraction of this report giving only the pertinent data and procedures required for systems trade-off analyses.

The discussion of refrigerators given in Section 3 is an extension and an up-dating of the Systems Review Report prepared earlier in this study. Much of the material presented in the earlier report is given here so that a complete and comprehensive set of refrigerator and systems data will be available as a single source of material. Also, additional material was developed and became available after the Systems Review Report was prepared and it was felt that the material would be disjointed and confusing if presented separately.

Section 3 provides the basic information to obtain external autonomous refrigerator performance, weight and size.

Following this section Section 4 describes the basic failure characteristics of the refrigerators and develops a means by which the engineer can estimate performance-reliability trade offs.

Section 5 presents the thermal environments and methods of computing average surface temperatures for cryogenic tanks and heat rates for radiator designs.

Section 6 provides estimates of cryogen tank weights and vacuum jacket shell weights. Also presented are the heat rates to the cryogenic tanks for various temperature conditions. These data are presented so the engineer can obtain trends and weight increments in conducting trade-off studies and are not meant to represent the ultimate in tank design, weights and insulation.

Section 7 presents the information required to determine radiator design and provides means of estimating weights of the major elements required to transport the heat from the refrigerator to the radiator. Heat pipe design procedures are also given.

Section 8 provides information for estimating the weights of the devices required to transfer heat from the cryogen tank to the refrigerator. Weight estimates of tank heat exchangers, helium circulation compressors, and cryogenic heat pipes are presented.

Section 9 presents data and descriptions of almost all power sources that are or might be applicable to refrigeration systems evaluations. The power sources range from batteries to nuclear reactors. This complete spectrum was covered so that rapid estimates of a broad range of potential future applications can be made without a lengthy search for relevant material.

Section 10 provides a limited amount of property data on cryogens. Data on hydrogen, oxygen, fluorine, and nitrogen in the form of pressure-internal energy charts have been provided to aid the engineer in making rapid heat-pressure balances for intermittent refrigerator operation calculations.

Section 11 provides a comprehensive set of units conversion charts. The engineer can work in whatever units are familiar to him and rapidly convert the data to be compatible with other data normally made available to him.

With the material in each of these sections the designer/planner has the necessary information to estimate the performance, weight, and volume of a complete cryogenic refrigeration system for whatever space application he may be interested in. A large range of the pertinent parameters has been given and this data should be useful for a large variety of space-oriented studies.

2.7 REMARKS

Generally speaking, non-vented cryogenic refrigeration systems show an advantage over the vented systems having no self-contained external refrigeration only for long-term (approximately six months or more) applications. This is basically caused by additional fixed weight that must be added to the system for refrigerator power supply and radiators. If a large power supply is available, and does not have to be added for the refrigerator operation, then a tradeoff might be expected for shorter duration missions.

The refrigerator operating at cryogenic temperatures does so at relatively low efficiencies, requiring anywhere from 250 to 5,000 watts of input power to achieve 10 watts of cooling. Therefore, the power supply and the heat rejection devices become important, and an associated weight penalty must be attached to the system.

At the present time, little failure characteristic data is available on refrigerators that would be applicable to cryogenic and space applications. Before embarking upon a program that utilizes a closed cycle external refrigerator, one must carefully assess the development situation and the potential refrigerator failure rates.

The material developed in this study and presented in the handbook should be used to review the missions and functions for which cryogenic refrigerators may have potential applications. Having thus identified the potential applications and having examined the relative tradeoffs, the refrigeration system requirements and characteristics can be roughly specified. The detail characteristics of the refrigeration system can then be studied and particular design features such as types of refrigerator, its cooling capacity, its performance, size, and weight, its heat rejection temperature, its lifetime, the type of heat rejection system, the type of power supply, and the heat transfer devices can be accurately specified. System cost and development time can thus be established. A complete picture of the refrigeration system will then be available for decisions as to what type research and development program are required to achieve the goals.

Section 3 REFRIGERATORS

3.1 INTRODUCTION

The purpose of this section is to summarize the current available information on small refrigerator systems that are applicable to in-space cryogenic cooling operations. Most of the data are applicable to cooling loads of 1 to 100 watts and cooling temperatures of 20°K to 110°K. To date no closed cycle refrigeration system has been used in space, although a few elementary short life open cycle systems have been flown and a few programs presently underway will place closed cycle refrigerators in space in the near future. Consequently, such systems must be developed and proven for space use, and this report must necessarily be directed towards assembling the data needed to assess potential performance rather than providing hard data. The assessment of the possible performance of a refrigerator in a given cooling task in this context will thus depend upon the current performance, development potential and peculiarities of the task.

The current state of refrigerator technology is governed largely by a combination of technical performance limitations and prevailing economic market. The interaction of these influences may be divided into three categories. In the first would be those purely technical limitations imposed by an incomplete understanding of the basic physical processes, or by fundamental limits of the processes themselves. Refrigerator designs are based on the best available heat transfer, fluid flow and material property data and an upper limit as thermodynamic performance will be set by the adequacy of these data, the methods of handling the data for design purposes, and the techniques for obtaining the performance of actual machines. These limitations are discussed in the sections describing particular configuration systems. In a second category of influences would be the influence of the market on refrigerator technology. One of the reasons that spaceborne refrigerators are not available is

that until recently there has been no demand for them. Although a need for such refrigerators is now emerging it does not promise to be profitable and private development is unlikely. This can only be remedied by support of the refrigerator market by research and development programs such as those funded by various agencies of the Defense Department. These programs effectively permit systems of limited economic appeal to be developed to their full technical capabilities. In the third category are those limitations placed by an interaction between market requirements, mechanical design and refrigerator performance. For example, the thermodynamic performance, reliability and physical dimensions of commercial refrigerators are optimized with respect to terrestrial, physical, and economic conditions. It is very probable when configured for space application many existing types of refrigerators would seem far more attractive than their terrestrial versions. The cost of such relatively minor design must be compared with that of establishing radically different designs.

From a knowledge of the current state of technology one may select a suitable refrigerator system, define a program leading to the design or development of a satisfactory hardware from existing technology, or define a program of research and development on one or more new types of refrigeration systems. The selection process must be based upon a complete specification of the total spacecraft environment in which the refrigerator must operate. Such a specification must include the following parameters:

- o Magnitudes and temperature levels of cooling loads
- o Interface requirements between load and refrigerator such as permissible level of vibration; whether the refrigerator can be integrated with the cooling load or whether the heat must be transferred by heat pipe, convective loop or other thermal link from a remote location; duty cycle, heat flux and temperature level control requirements, etc.
- o Nature of spacecraft power supply, particularly as defined in terms of system penalties for both primary thermal power and generated electrical power, since both electrically and thermally powered refrigerators exist.

- o Interface requirements between power source and refrigerator. For electrically powered systems this requirement would be quite simple. For thermally powered systems it must be decided whether the source can be integrated with the load or should be located remotely and heat transferred by some device.
- o Interface requirements between refrigerator and spacecraft heat rejection systems. Heat must be rejected from the refrigerator at temperatures in the general range of earth ambient temperatures. It must be transported from the refrigerator to the radiator by some thermal link.
- o Maintenance possibilities. Depending upon the particular mission, this will range from zero maintenance to a maximum value considerably less than that permissible for ground and airborne units.
- o Required operational lifetime.

This portion of the report is concerned with the refrigerator unit itself. The subject of interfacing with power supply, cooling load and heat rejection system are covered in Sections 9, 7 and 8.

The main body of data relating to refrigerator performance is contained in Section 3.4 which gives performance and weight characteristics of existing refrigerators. Several types of refrigerator can be separated into components, however, and it is appropriate to provide some data on the performance of the individual components. As an example, the compressors used by most terrestrial Gifford-McMahon/Solvay systems are not weight optimized and if a realistic assessment of the possible performance of these systems in the space application is to be made, possible compressor weight reduction must be estimated. These factors are discussed in Section 3.3.

In Section 3.2 background material is presented relating to some of the basic thermodynamic cycles used by refrigerators.

3.2 BASIC REFRIGERATION CYCLES

3.2.1 General Theory

A refrigerator is a device which absorbs heat at one temperature and rejects it at a higher temperature. In order to perform this operation, an expenditure of mechanical work is required, as shown in Fig. 3-1. According to the Second Law of Thermodynamics, this operation must result in a zero or positive change in entropy. In terms of the quantities shown in Figure 3-1

$$\frac{q_a}{T_a} \geq \frac{q_c}{T_c} \quad (3-1)$$

According to the First Law of Thermodynamics

$$q_a = q_c + W \quad (3-2)$$

Thus,

$$W \geq q_c \left[\frac{T_a - T_c}{T_c} \right] \quad (3-3)$$

Eq. 3-1, 3-2 and 3-3 relate to a system of heat source, heat sink, mechanical, refrigerator and mechanical work source. It is sometimes desirable to include the work source in the definition of the refrigerator, in which case the situation shown in Fig. 3-2 applies. In this case the work input required by the refrigerator is generated by an engine, which takes heat from a high temperature source, rejects heat to a lower temperature sink and produces work. For the whole system the operation must produce a zero or positive production of entropy. If both engine and refrigerator share a common sink then

$$\frac{q_a}{T_a} \geq \frac{q_h}{T_h} + \frac{q_c}{T_c} \quad (3-4)$$

According to the First Law of Thermodynamics

$$q_a = q_h + q_c \quad (3-5)$$

thus,

$$q_h \geq q_c \left[\frac{T_h}{T_c} \cdot \frac{T_a - T_c}{T_h - T_a} \right] \quad (3-6)$$

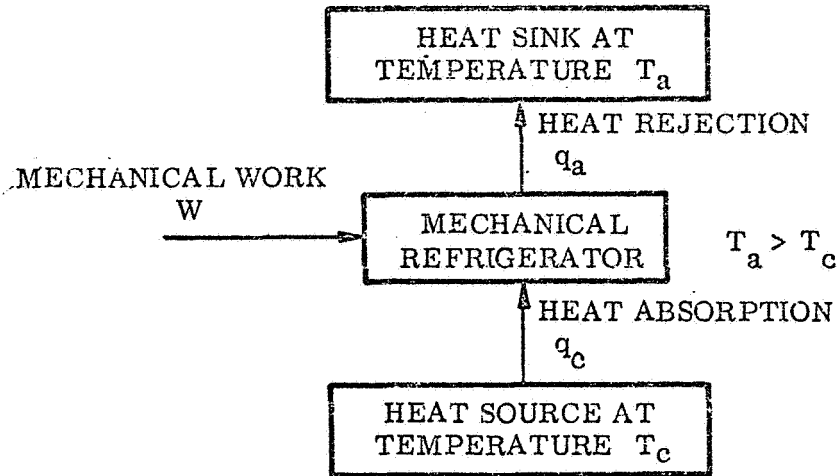


Figure 3-1 Mechanically-Powered Refrigerator Operation

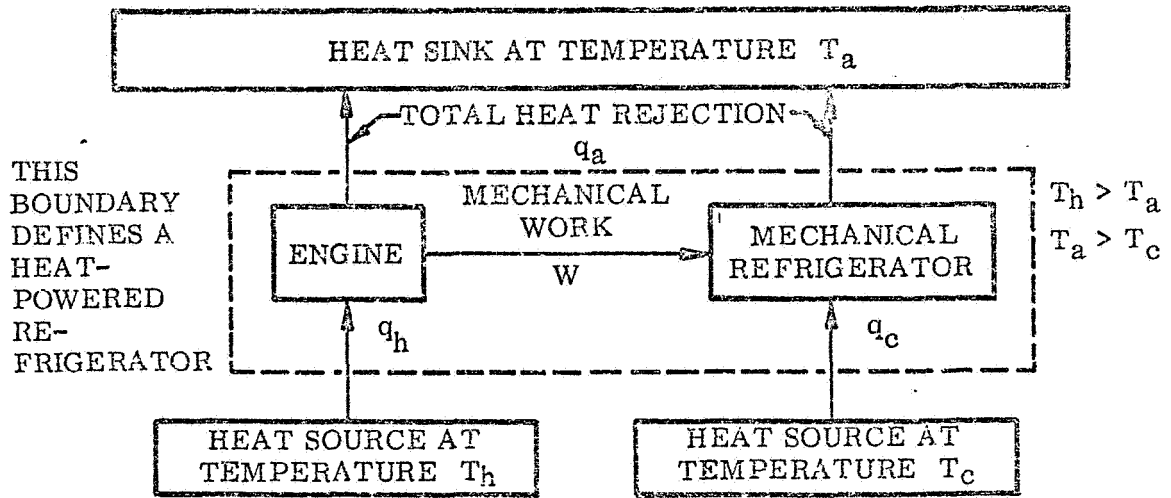


Figure 3-2 Heat-Powered Refrigerator Operation

There is no input of mechanical work to the system. Energy is supplied as heat and the whole system may be called a heat powered refrigerator. The performance of a refrigerator is customarily expressed by its "coefficient of performance" "c.o.p."

$$\text{c.o.p.} = \frac{\text{refrigerative effect}}{\text{powered supplied}}$$

This function is a satisfactory basis for comparison if all systems are of the type of Fig. 3-1. For most mechanical refrigerators the source of power will be electrical energy converted to mechanical power via an electric motor. The electrical energy will originally have been produced by some process whose operation is completely independent of the refrigerator and its influence may be neglected for comparison purposes. In the case of heat powered refrigerators the coefficient of performance is of less value as a standard. Some heat powered refrigerators operate by electrical resistance heating, while others operate on heat input from a primary source, such as radioisotope or solar collector. If the heat input, q_h , in Eq. 3-6 were to be provided by an electrical heater then based upon electrical power consumption, q_h , would clearly be greater than W in Eq. 3-3 and the refrigerator of Fig. 3-1 would be always superior in efficiency. If, however, the means of obtaining heat and electrical/mechanical power are included in the assessment of power required, then a different conclusion may possibly be reached.

The heat and work interactions implied by the devices shown in Fig. 3-1 and 3-2 are produced by circulating a fluid through the system and causing it to undergo appropriate processes at the heat source and sink. The First Law of Thermodynamics can be written for working fluid in a given process as follows:

$$\begin{array}{l} \text{heat addition} \\ \text{to the fluid} \end{array} = \begin{array}{l} \text{increase in internal energy} \\ \text{of the fluid} \end{array} + \begin{array}{l} \text{work performed} \\ \text{by the fluid} \end{array}$$

Heat may be transferred from the load to the fluid by causing the latter to perform expansion work and replacing this energy with heat from the load either during or after expansion. Heat may be transferred from the fluid to the sink by performing work on the fluid by compressing it and rejecting this energy to the heat sink during or after compression. In either case, the

system requires a compressor and sink heat exchanger, and an expander and load heat exchanger. The device of Fig. 3-1 will require a source of mechanical work which may be provided by some type of separate motor. The device of Fig. 3-2 produces the necessary mechanical work by incorporating a heat engine within the system. A heat engine is a reversed refrigerator so this system will require an expander and source heat exchanger and a compressor and heat sink exchanger in addition to the refrigerator components. These components are essential to all refrigerators. Very low temperature refrigerators are distinguished from other refrigerators by the use of a heat exchanger between the load and sink temperatures. Working fluid flowing from the compressor to the expander is pre-cooled by fluid returning to the compressor from the expander. This process permits operation of the refrigerator over a much greater temperature differential than could be obtained by a single expansion.

3.2.2 Thermodynamic Cycles

It is desirable to keep the values of W and q_h in Eq. 3-3 and 3-6, respectively, as small as possible with respect to q_c . Their values will be a minimum when all cycle processes are reversible, i.e., they produce no overall increase in entropy. Cycles based upon reversible processes can be conceived but are impossible to execute in practice. In fact, practical refrigeration cycles are notable for their very high degree of irreversibility, and the design of successful practical cycles is usually based on expeditious juggling of the many sources of performance loss. This characteristic highly irreversible behavior is traceable to the basic expression for entropy change, dq/T . It is apparent that the entropy changes associated with a given quantity of transferred heat is very much greater at low temperatures than at high temperatures. Much more emphasis must, therefore, be placed upon cold end performance than ambient or hot end performance and the resulting practical cycles frequently bear little resemblance to textbook ideal cycles. Nevertheless, it is useful to review the basic ideal cycles in order to obtain a better understanding of their faults and to indicate why the variations shown in the practical cycles of Section 3.4 are necessary.

Carnot Cycle

The Carnot Cycle is the best known reversible cycle, shown on the temperature entropy diagram of Fig. 3-3. The compression/cooling and expansion/heating processes are accomplished isothermally. The heat transfer processes during these phases are effected over negligibly small temperature differences, resulting in no overall increase in entropy. The fluid is cooled and heated between these temperatures by isentropic expansion and compression, respectively. In practice, the isothermal processes require an infinitely long duration if finite quantities of heat are to be transferred across infinitesimal temperature differences. It is necessary to run practical machines at relatively high speeds and compression is generally accomplished so fast that the process is adiabatic and the working fluid temperature rises. The heat of compression would thus be rejected to the sink after compression and across a finite temperature difference. The same comment applies to the expander and the heat from the cooling load. Another serious limitation of the Carnot cycle is that the ratio of the minimum sink temperature to the load temperature is governed by the pressure ratio used in the compression and expansion processes.

$$\frac{T_a}{T_c} = \left(\frac{P_2}{P_1} \right)^{\frac{\gamma-1}{\gamma}} \quad (3-7)$$

This places a severe restriction upon the practical temperature range.

Ericsson Cycle

A second reversible cycle is The Ericsson Cycle, shown in Fig. 3-4 on a temperature-entropy diagram. Compression and expansion are performed isothermally as they are, in the Carnot cycle and the same comments apply. However, heating and cooling is accomplished at constant pressure in a heat exchanger. If the exchanger is 100 percent efficient, which is to say that the temperature difference between the working fluid and exchanger is zero at all points, the cycle is reversible. The Ericsson cycle has the desirable quality of being able to span large temperature differences. It would undoubtedly be the most popular refrigeration cycle were it possible to perform reversible heat transfer in all the components. In practical machines the compression and expansion

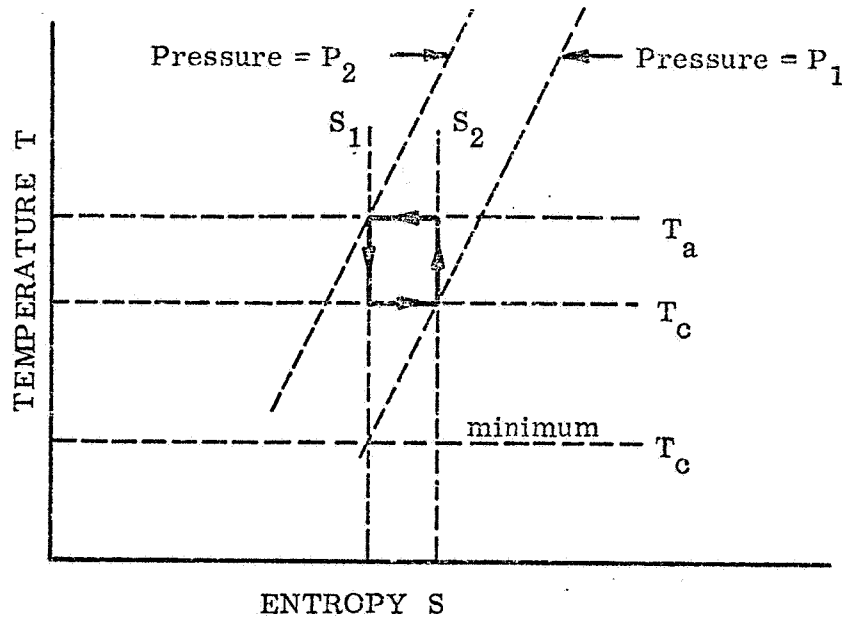


Fig. 3-3 The Carnot Refrigeration Cycle

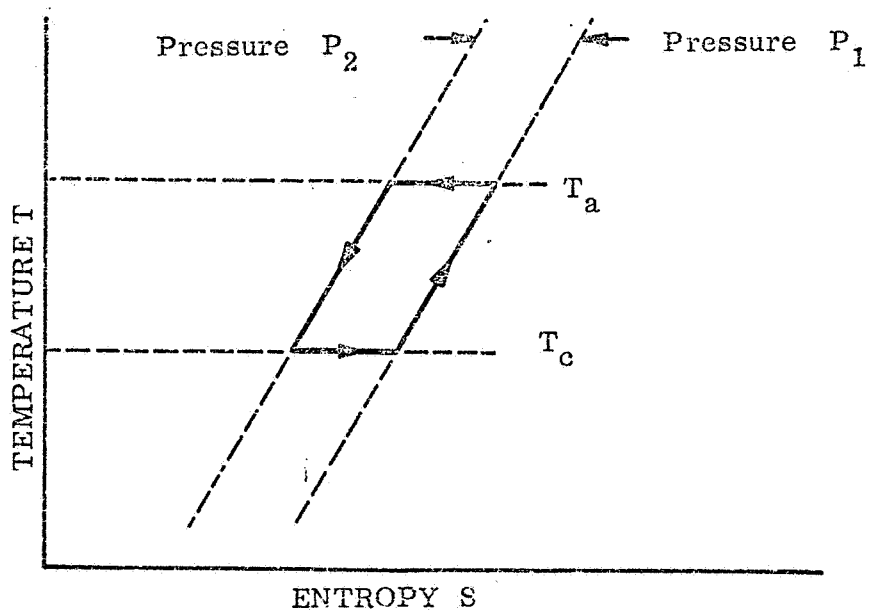


Fig. 3-4 The Ericsson Refrigeration Cycle

processes are performed so rapidly that they are closer to being adiabatic than isothermal. The Ericsson cycle then more closely resembles the non-reversible Brayton cycle, as shown in Fig. 3-6.

Stirling Cycle

The Stirling cycle shown in Fig. 3-5 is similar to the Ericsson cycle, with the major difference being that the fluid is cooled and warmed at constant volume rather than at constant pressure. It is difficult though not impossible, to conceive even ideally a device that would perform this reversible constant volume heat exchange. Using such a device the Stirling cycle has an ideal efficiency.

Brayton Cycle

The Brayton cycle is basically an Ericsson cycle operated rapidly. It deserves its own name because recognition of this speed of operation requires that separate heat exchangers be provided downstream of the compressor and expanders for transferring the heat that in the Ericsson cycle would have been transferred inside these components. It is a reasonable generalization that most practical refrigerators operate on cycles which are modifications or variations of this Brayton cycle because of the need to operate at practical speeds. The principal variations are the use of differing types of compressors, heat exchangers and expanders, and the use of varying numbers of these components to exploit the benefits or avoid the problems of non-ideal behavior of the working fluid and the components themselves. The Brayton cycle is non-ideal if heat can only be exchanged with constant temperature sink and source because of the inevitable presence of finite temperature differences in the sink and source heat exchangers.

Heat Powered System

Fig. 3-7 shows the cycle which would be followed by a heat powered system such as that shown in Fig. 3-2. It is composed of a coupled engine and refrigerator which both operate on the Brayton cycle. The compressor handles working fluid for both the refrigerator and the engine. The power produced by the engine is equal to the power required by the refrigerator. This power may be transmitted directly through the fluid or may be transmitted from component to component by mechanical linkages.

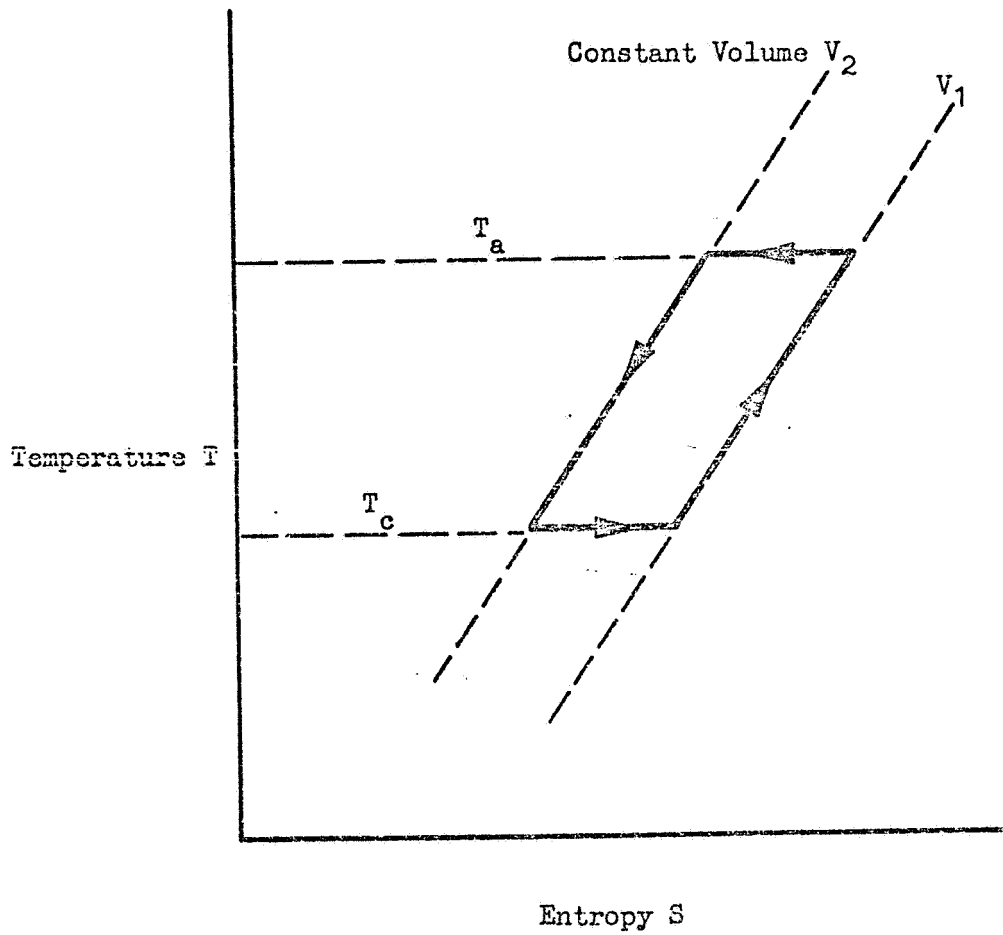


Fig. 3-5 The Stirling Refrigeration Cycle

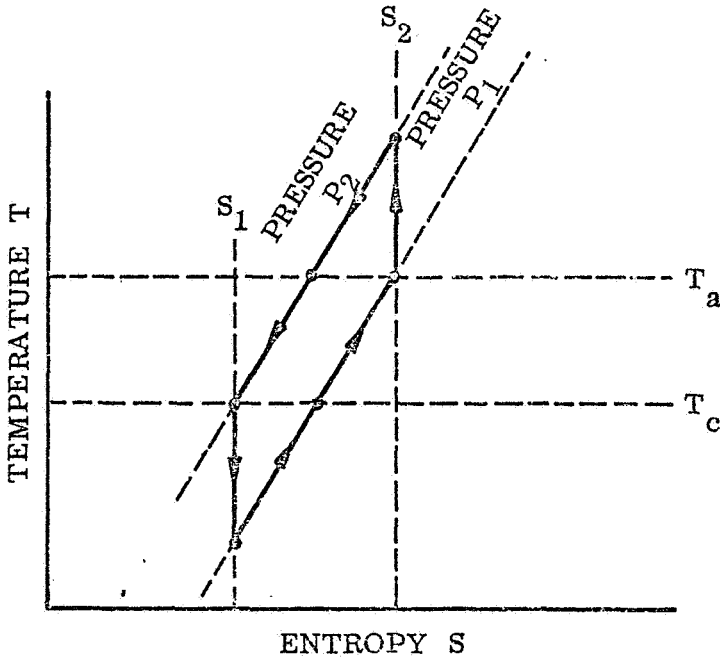


Fig. 3-6 The Brayton Refrigeration Cycle

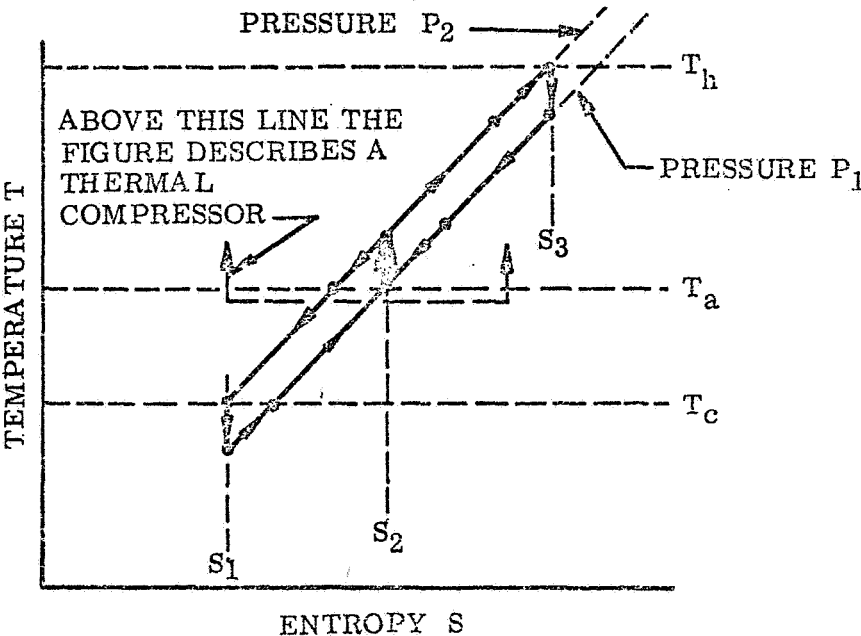


Fig. 3-7 The Heat Powered Brayton Refrigeration Cycle

The thermodynamic cycles described above represent the basic theoretical possibilities for refrigeration cycles. It is impossible in practice to design a refrigerator to operate on any one of the ideal cycles. Practical refrigerators tend to become known by the names of the cycles which they most closely approximate or by the type of components that they use. It is important to observe this distinction. Practical refrigerators are described in Section 3.4.

3.3 BASIC REFRIGERATOR COMPONENTS

The basic components of a refrigerator are compressor, expander or expansion device, and heat exchangers. Some practical refrigerators exist in which some or all of these components are incorporated in the same mechanical device, for example, the Stirling and Vuilleumier refrigerators. Others represent a system comprised of separable components which may be studied and selected independently. In this section, a brief survey is given of the state of development of these three types of components.

3.3.1 Compressors

3.3.1.1 General Consideration: The compressor is the component in which most or all of the power required for refrigeration is supplied to the working fluid. It can be seen from Eq. 3-3 that for very low temperature refrigeration even in the ideal case the compressive work will be many times the cooling capacity and the compressor is therefore usually the largest and is always the most heavily stressed component in the system. For many terrestrial refrigeration applications the compressor can be located remotely from the heat exchanger, and need not be subjected to much weight and volume optimization. The most important requirements of a stationary compressor are that it should be reliable and that it should not contaminate the working fluid.

Compressors designed for terrestrial use are thus generally much heavier than they need to be. Refrigeration cycles usually require relatively high compression ratios and reciprocating machines are most commonly used. Contaminant-free compression is obtained by using carbon or Teflon piston rings, or by using an oil lubricated compressor fitted with a very efficient gas cleanup unit. The

oil-free reciprocating compressors on the market tend to fall into two categories. There are many relatively high capacity compressors designed for process plants which are characterized by high reliability and low operating cost but high weight and volume. There is also an extensive family of simple dry lubricated compressors of under about 2 h.p. capacity which are designed to be portable and which consist of little more than an electric motor with light-weight compression cylinders attached. The weight of these units is largely that of the motor.

An alternative approach to providing oil-free compressed gas is to use a conventionally lubricated compressor and apply the design effort to removing the oil from the high pressure discharge stream. If this approach is acceptable, it is possible to use hermetically sealed freon compressors, whose weight is relatively low. The overall operational weight would have to include the weight of the oil separation equipment, however. All other things being equal, the solid lubricated system should show a lighter weight, at the expense of a shorter lifetime. The oil lubricated system would be difficult to modify for use in a zero-g environment.

The possibility of using welded metal bellows to seal the space between piston and cylinder has always been considered an attractive concept but until recently bellows technology has not been able to provide the lifetime necessary to permit design of a competitive unit. At the present time, however, there are several small capacity bellows compressors on the market which have demonstrated impressive lifetimes and low unit weight. This type of compressor is not yet fully proven nor have all its possibilities been adequately explored, and it is thus deserving of greater attention.

For relatively high flow rates, rotary dynamic machines are generally found to be more suitable than reciprocating machines in that the system size and weight can be reduced considerably for a given throughput. Dynamic compressors raise fluid pressure by increasing the kinetic energy of the flow stream and thus converting the kinetic energy to pressure head. This can be achieved by a variety of machine configurations. Generally speaking, rotary dynamic compressors do not provide as much pressure rise per stage as reciprocating

positive displacement machines and it is thus found that those rotary machines which provide the highest pressure ratio per stage are the first to become attractive as flow rates are increased and reciprocating compressors become less attractive. With increasing flow rates first the regenerative or drag compressor, then centrifugal compressors, then axial compressors would be considered. The compression efficiency of the regenerative compressor is quite low, that of the centrifugal compressor is somewhat better while the axial flow compressor has the highest efficiency of dynamic compressors. Normally, drag and centrifugal compressors are not attractive by comparison with positive displacement and axial compressors from the point of view of efficiency. They are, however, compatible with gas bearings and retain considerable appeal because of this feature.

Between the fields of application of reciprocating positive displacement and rotary dynamic compressors are rotary positive displacement compressors. This type of compressor can attain compression ratios and efficiencies comparable to those obtained in reciprocating compressors, but at higher flow rates. They are, like the reciprocating compressor, quite heavy, and are not likely candidates for spaceborne refrigeration systems, since at the higher flow rates gas bearing dynamic compressors will be more attractive.

In recent years, more attention has been given to lightweight long-life, contaminant-free compressors suitable for aircraft and spacecraft use. A number of experimental compressors exist in the relatively small size range which eliminate solid seals, bearings or crank shaft. Among these are high speed rotary compressors using gas bearings; a reciprocating compressor operated by linear actuator and metallic spring, and using clearance seals; a reciprocating compressor with linear actuation, gas springs, clearance seals and rotary motion for centralization and valve port alignment; and an electro-dynamically operated free piston compressor. These compressors are all in the early development stage.

Work on heat-powered compressors is in a very early stage of development. Such compressors may be defined as a single device which compresses a fluid while accepting heat from a high temperature source and is ejecting it to a

lower temperature sink but which does not consume or produce mechanical work. Such systems may be rotary or reciprocating in action. They would effectively constitute the upper portion of Fig. 3-6, in that the thermal compressor constitutes a Brayton cycle engine whose output is exactly sufficient to compress the working fluid of the refrigerator. Also, the working fluid is common to both the engine and the refrigerator.

3.3.1.2 Performance of Practical Compressors: The minimum amount of power required to compress unit mass of a fluid from a pressure P_1 to a pressure P_2 is that required by the isothermal process and is equal to $RT \ln (P_2/P_1)$. The actual work required is increased by power losses in transmitting energy from the power supply to the working fluid, such as motor losses and friction losses at bearing and seal surfaces. If the compressor has valves then the flow pressure losses through these valves will require that the fluid in the compressor be compressed from a lower to a higher pressure than the corresponding fluid pressures in the outside circuit, hence increasing the power requirement. During the compression process some heat will be transferred from the fluid to the walls of the compressor, but it will invariably be insufficient to prevent the fluid temperature from rising and the process will thus not be reversible and will require more power than isothermal compression. Also during compression there will be turbulence within the compression spaces which will result in further heating of the fluid by internal friction, and hence further deviation from the isothermal process. Finally, not all the fluid compressed will be available in the refrigeration cycle because there will be leakage from high to low pressure sides through clearance spaces, and in the case of gas bearing systems a portion of the flow will be required by the bearings.

In the case of the thermal compressor the losses associated with the valves, leakage, and non-isothermal compression will still be present. The bearing and seal losses will usually be much less since there will be no moving boundary to the device through which mechanical work must be transmitted. Since the thermal compressor is an integrated heat engine and compressor there will be heat losses associated with the heat engine function as well as the compressor function.

The thermodynamic performance of a compressor takes into account all effects internal to the compressor and is usually expressed by the isentropic efficiency, η_{ad} , or the isothermal efficiency, η_{is}

$$\eta_{ad} = \frac{\text{actual work required for compression}}{\text{isentropic work, } W_{ie}} \quad (3-8)$$

$$\eta_{is} = \frac{\text{actual work required for compression}}{\text{isothermal work, } W_{is}} \quad (3-9)$$

$$W_{ad} = RT_1 \frac{\gamma}{\gamma-1} \left[\left(\frac{P_2}{P_1} \right)^{\frac{\gamma}{\gamma-1}} - 1 \right] \quad (3-10)$$

$$W_{is} = RT_1 \ln (P_2/P_1) \quad (3-11)$$

The theoretical isentropic work of a single stage, compressor is shown on Fig. 3-8. The actual work of compression is obtained using Eq. 3-8 and a known value for isentropic efficiency η_{ad} . The value of η_{ad} varies with the type of compressor, fluid and operating conditions, and cannot be presented in a convenient graphical or tabular form but representative values may be quoted for good typical designs. For reciprocating compressors an adiabatic efficiency of 0.85 to 0.90 may be assumed. For centrifugal compressors η_{is} can range from 0.50 and lower for very small units, up to about 0.82 for well designed high capacity machines. Drag or regenerative compressors have η_{is} figures characteristically less than 0.50. In calculating the required motor size allowance must be made for motor efficiency, mechanical efficiency, leakage or loss of compressed fluid, etc.

Having determined the required motor input power Figs. 3-9 and 3-10 may be consulted to obtain compressor weight and volume, respectively. These figures were obtained by plotting data for comparatively low weight electrically driven compressors for terrestrial applications. The data are plotted against input power because a substantial portion of the weight is that of the electric motor. The weight of the compression components will also vary with number of compression stages and operating pressure, but the variations due to these effects are less than those between different design concepts. The data shown for Zefex ⁽³⁻¹⁾ and Gast ⁽³⁻²⁾ compressors are typical of commercially

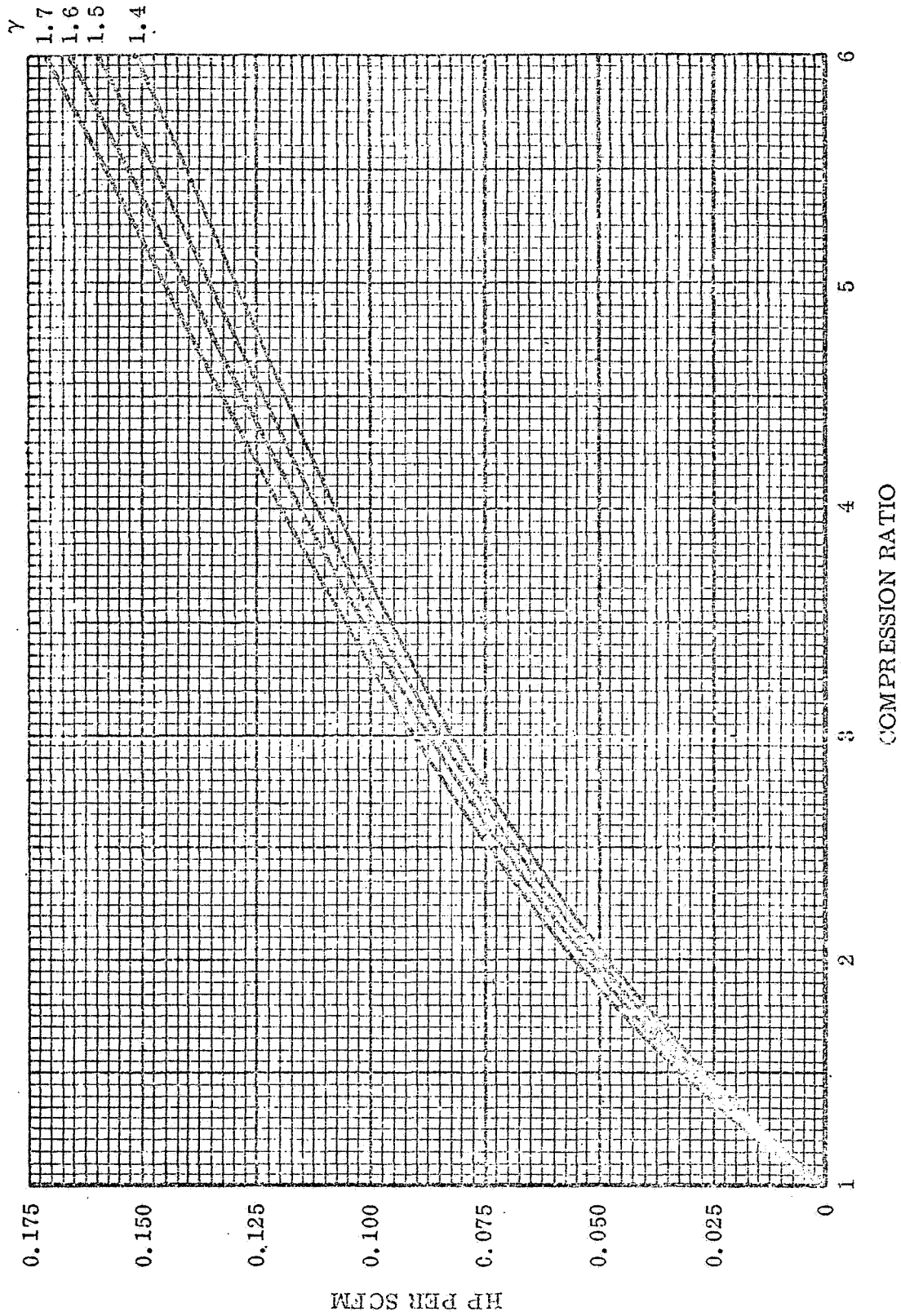


Fig. 3-8 Theoretical Isentropic Work for Single Stage Compressor

available, lightweight, oil-free, solid lubricated compressors. Their range of application, as dictated by the market rather than technology, is up to 1 to 2 HP for compression from 14.7 psia to 35-175 psia. They consist of little more than lightweight compression cylinders attached to conventional low cost electric motors. The extent to which their weight could be reduced would be dependent mainly on possible motor lightening and to a much lesser extent on compression piston and cylinder lightening. Data are also shown for Tecumseh (3-3) and Bendix-Westinghouse (3-4) hermetically sealed oil-lubricated freon compressors. The weights shown are for the bare compressor, excluding the oil separation components that would be needed for a low temperature refrigeration application. The data are significant in that some attention has been given to reducing the weight of this type of compressor. The electric motor is integrated with the compression cylinders in these designs. They are known to be strong enough to operate as helium compressors at pressure levels up to 350 psig and are offered as part of many split component refrigerators. Their power range is generally up to about 3 HP. Also plotted in Figs. 3-9 and 3-10 are data for Copeland hermetically sealed freon compressors (3-5). These compressors are not weight optimized and are built in the more conventional manner of detachable motor and compression cylinders. However, Copeland makes a range of similarly designed compressors from $\frac{1}{4}$ HP to 35 HP and a plot of the weight and volume data for these compressors is helpful in showing trends. The Copeland data show two linear relationships reflecting air cooling for lower powers and water cooling for the higher powers.

Also shown on Figs. 3-9 and 3-10 are data for two prototype dry lubricated, reciprocating, compressors designed for low weight by U. S. Philips Corporation and Air Products and Chemicals, Inc. Both these designs show substantial weight reduction through the use of 400 Hz rather than 600 Hz electric motors. It can be seen that a very substantial reduction in compressor weight can be obtained using current technology.

Meaningful data on the prototype systems mentioned earlier are difficult to obtain but an indication of the performance of gas bearing compressors can be obtained from the following figures. Maddocks (3-6) reports a gas-bearing

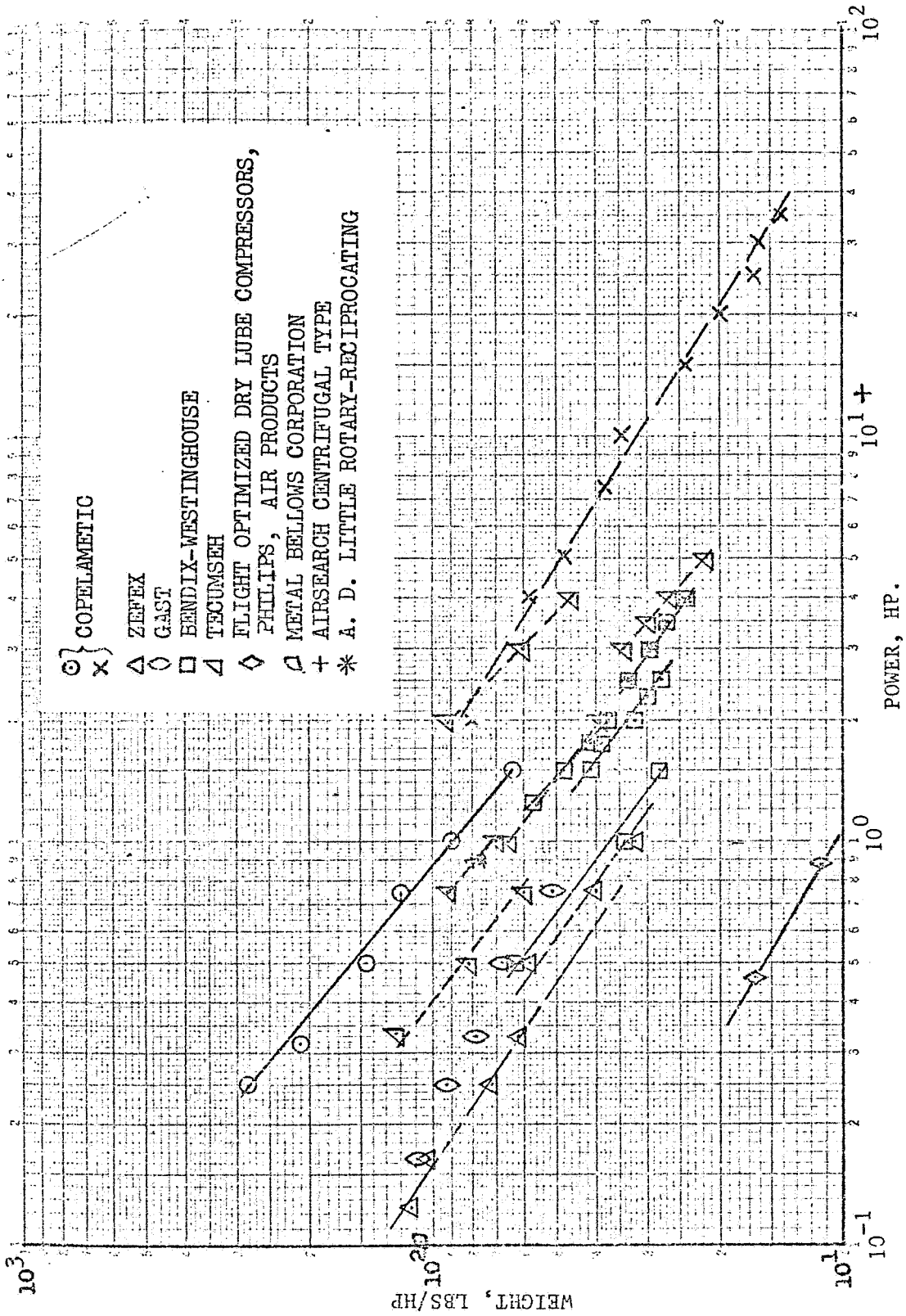


Fig. 3-9 Compressor Weight as a Function of Power Required

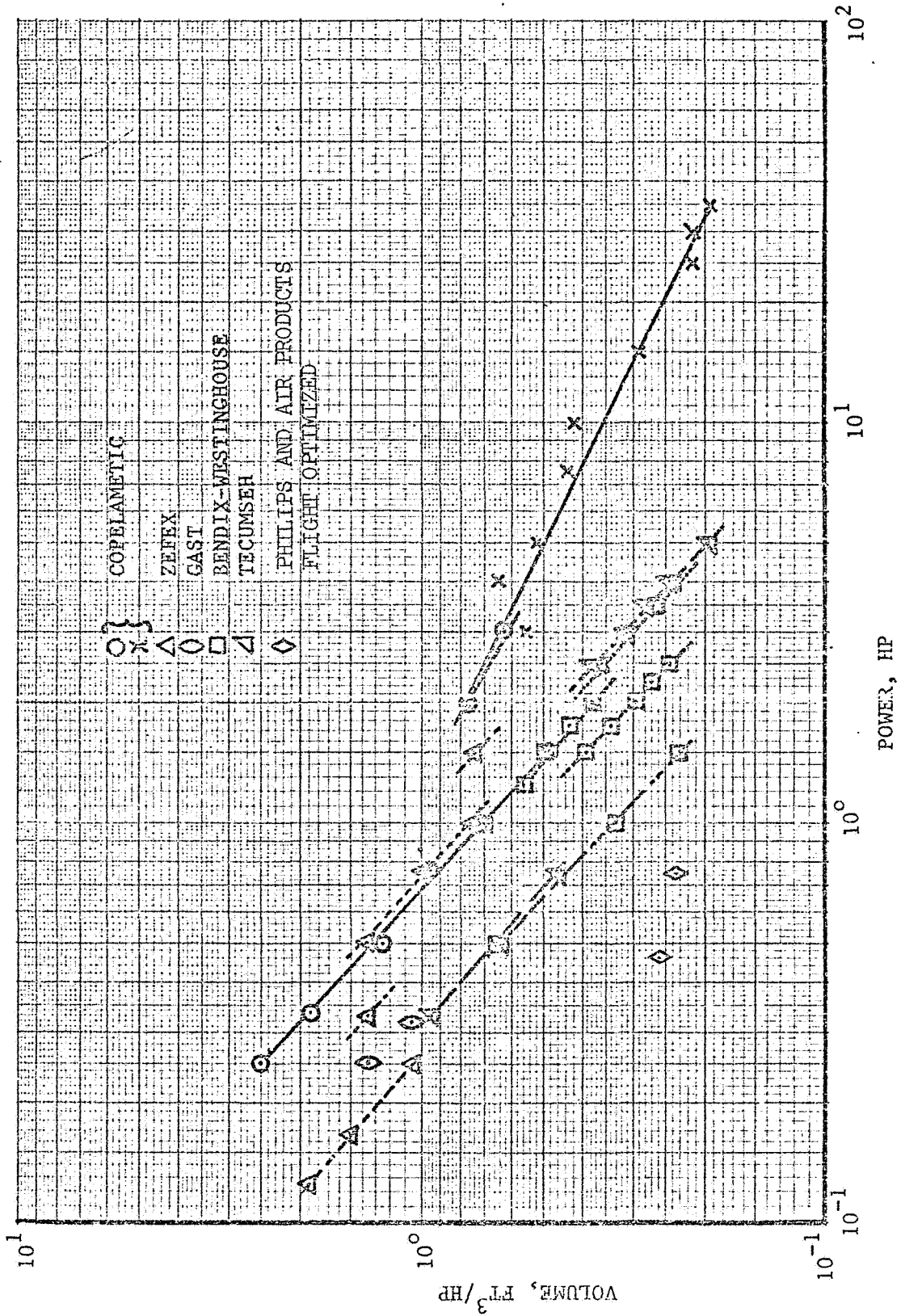


Fig. 3-10 COMPRESSOR VOLUME AS A FUNCTION OF POWER REQUIRED

six-stage centrifugal compressor of 9600 watts input, whose weight in developed form would be about 110 lbs., giving a weight of 8.9 lbs./HP. Breckenridge (3-7) reports a gas-bearing two-stage rotary-reciprocating compressor design of about 72 lbs. and 746 watts input, giving a weight of 77 lbs/HP at 0.93 HP.

These latter figures are, of course, for single examples of relatively early development units. They do suggest that gas bearing machinery will tend to be heavier than the optimized conventional designs.

3.3.2 Expanders

3.3.2.1 Configurations: An expander is a device in which a fluid may perform work against the environment which, in the context of refrigeration system, means the environment outside the refrigerator. Two principal types of expanders are commonly used - reciprocating positive displacement and rotary dynamic. The work produced by these expanders can be transmitted to the environment mechanically or, in the case of the rotary expander, by generating electricity at the low temperature and dissipating it to the external environment.

The reciprocating expander is much like a reversed reciprocating compressor in operation. Fluid is admitted to an expansion cylinder at high pressure, is expanded against a piston and is then discharged from the cylinder at low pressure. Rotary dynamic expanders, or turbines, can be constructed in a variety of ways. For lower flow rates radial impulse turbines are generally used. For higher flow rates axial impulse and radial reaction turbines appear superior. A survey of individual applications (3-8) suggests that the range of flow rates and cooling loads covered by this report is best handled by radial impulse machines. The flow rates usually encountered in relatively small capacity turbines are usually so low that even with radial impulse turbines partial admission must be used. In a pure impulse turbine the pressure head of the working fluid is converted entirely to kinetic energy in the inlet nozzles and the turbine wheel operates essentially like a Pelton wheel to remove the kinetic energy. Reaction turbines require a static pressure differential across the wheel since part of the expansion is performed in the wheel passages. As size is reduced it becomes increasingly difficult to maintain this pressure head. The axial turbines, both impulse and reaction, have a

generally higher flow capacity than radial turbines and are thus to be found in high flow applications.

3.3.2.1 Performance of Practical Expanders: Representative unit data for expander weight and volume are difficult to obtain since few have been built by comparison with compressors. However, practical refrigerator systems show values of coefficient of performance of about $1/20$ at 100°K to $1/200$ at 20°K so that the expander power will be between 5 and 0.5% of the compressor power. Thus its unit weight and volume need not be known to as high a degree of accuracy as those for the compressors. In order to obtain a conservative estimate of the order of magnitude of size of expanders it is suggested that the following approximations be made. Compressors and expanders are both power transmission devices and it is proposed that the assumption be made that the system size per unit power transmitted are the same for both types of devices at a given value of transmitted power. Expander weight and volume should thus be estimated from Figs. 3-9 and 3-10, in which case the abscissa will refer to expander power rather than compressor power. This gross rule of thumb is proposed solely to serve the immediate requirements of this report and should not be used out of this context without extreme caution.

It is important to know the isentropic efficiency of the expander in order to perform a cycle analysis because the efficiency of the expander will have a great bearing on the overall system size and weight. The remarks and equations relating to compressor work and efficiency apply to the expansion process. The loss mechanisms are the same, with one important exception. In the compressor, heat transfer from the hot fluid to the compressor walls during compression will tend to increase compression efficiency. In the expander the walls will be warmer than the fluid and heat transfer from them to the expanding fluid will tend to decrease expansion efficiency. Data for isentropic efficiency of reciprocating expansion engines and overall efficiency (including electric generator) for radial impulse turbines are shown in Figs. 3-11 and 3-12. The data are to be regarded as showing the rough order of magnitude and the trends, rather than exact information, since each expander is designed for a different application. Efficiency is not a function of pressure ratio or output primarily and these parameters have been selected only for graphic convenience.

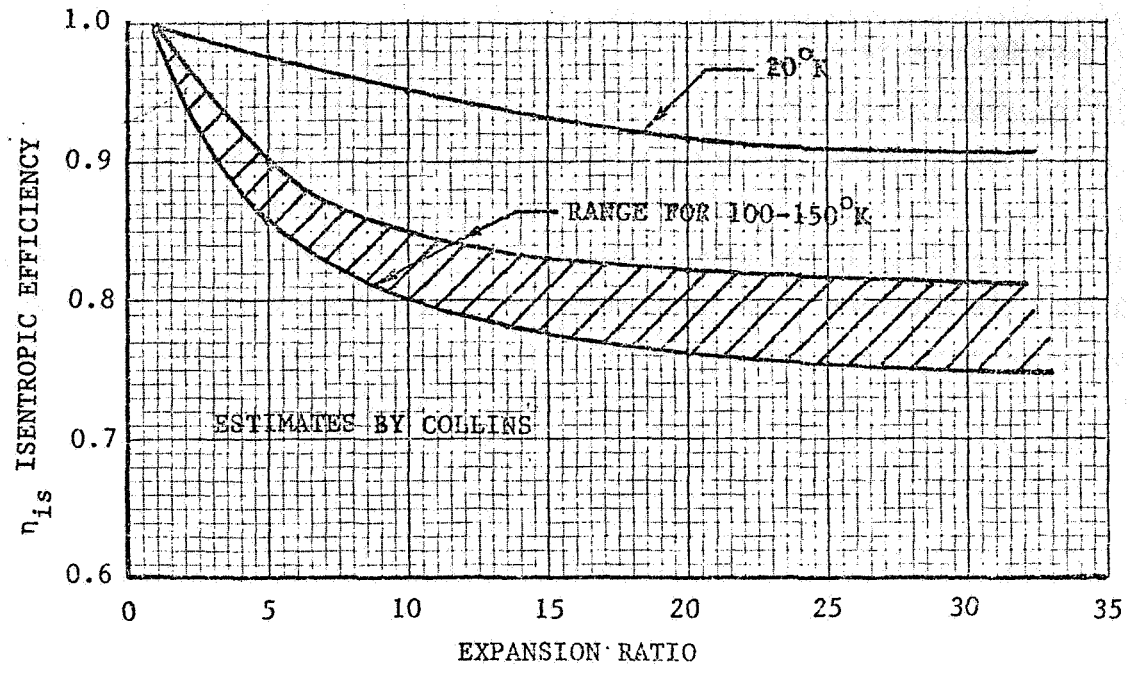


Fig. 3-11 Efficiency of Reciprocating Expansion Engine

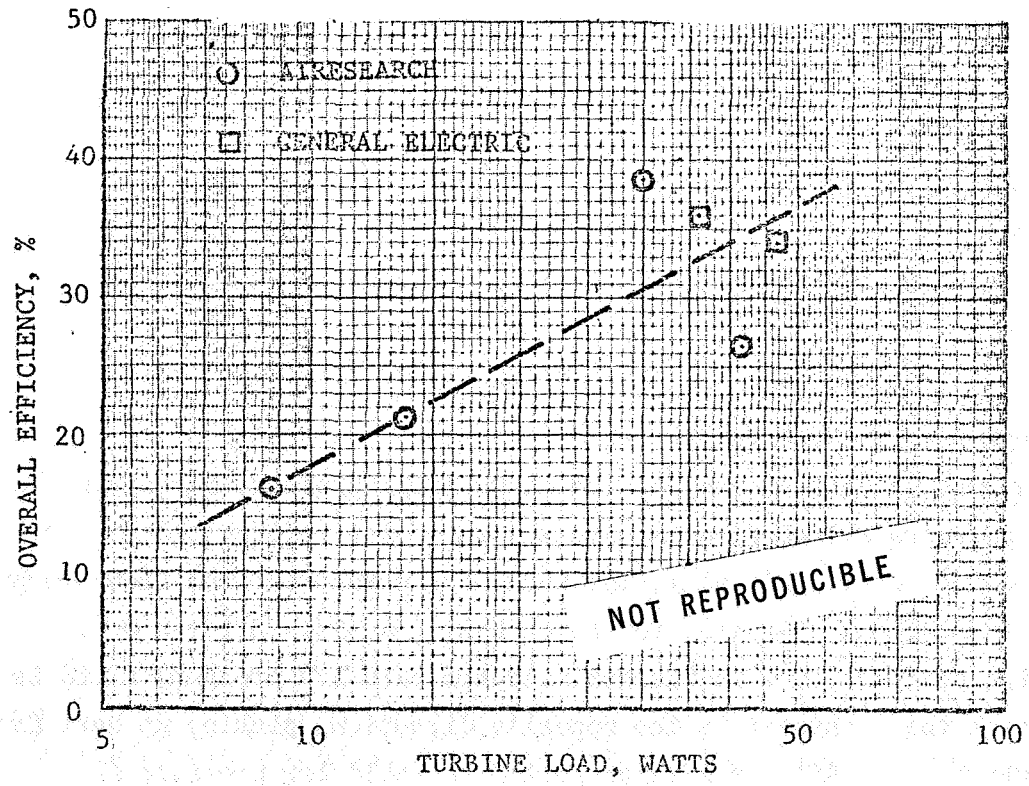


Fig. 3-12 Efficiency of Radial Impulse Turbines

3.3.3 Heat Exchangers

3.3.3.1 General Consideration.

There are three principal types of heat exchangers in a refrigerator system - the compressor after-cooler, the cooling load exchanger and the main heat exchanger in which heat is exchanged between the working fluid streams passing to and from the expander. The performance of these three types of exchangers influences refrigeration systems in differing ways. The most important heat exchanger is the main exchanger because it must operate over the relatively large temperature range of load temperature to sink temperature. The two principal configurations used for this exchanger are the counterflow heat exchanger (Fig. 3-13) and the regenerative heat exchanger (Fig. 3-14).

3.3.3.2 Counterflow Heat Exchangers

In the counterflow heat exchanger the high pressure and low pressure fluid streams pass continuously through separate flow channels which are in thermal contact. Heat is transferred from the warm high pressure fluid through the channel walls to the cooler low pressure fluid. At each point in the exchanger the properties and parameters of the fluid flows are constant with time. The counterflow heat exchanger has the disadvantage that fluid containment and heat transfer are accomplished in the same channels. This leads to less efficient use of materials of construction and increased weight per unit heat transfer area. Miniaturization is difficult for this reason. The counterflow exchanger does not, however, depend upon the specific heat of the walls for its operation and thus can operate at all temperatures. It is also considerably easier to design, since its performance is not time dependent.

3.3.3.3 Regenerative Heat Exchangers

In the regenerative heat exchanger, the warmer high pressure stream and the cooler low pressure stream flow alternately in opposite directions through the same flow channel. Initially, the warm high pressure fluid flows through the exchanger giving up its heat to the exchanger walls. After a period of time the high pressure flow is discontinued and cold low pressure fluid is passed through the exchanger in the opposite direction, picking up heat from the exchanger walls. After a similar period the cold low pressure flow is

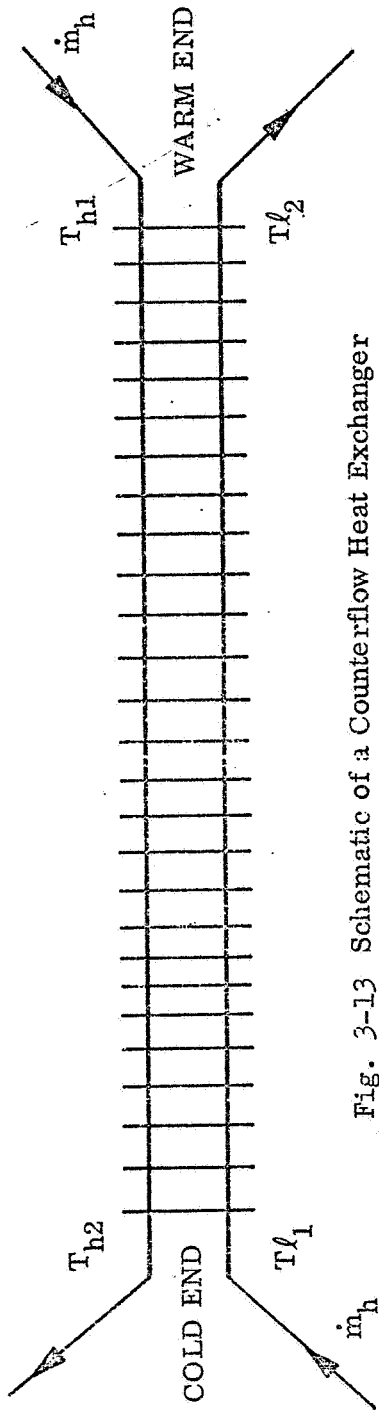
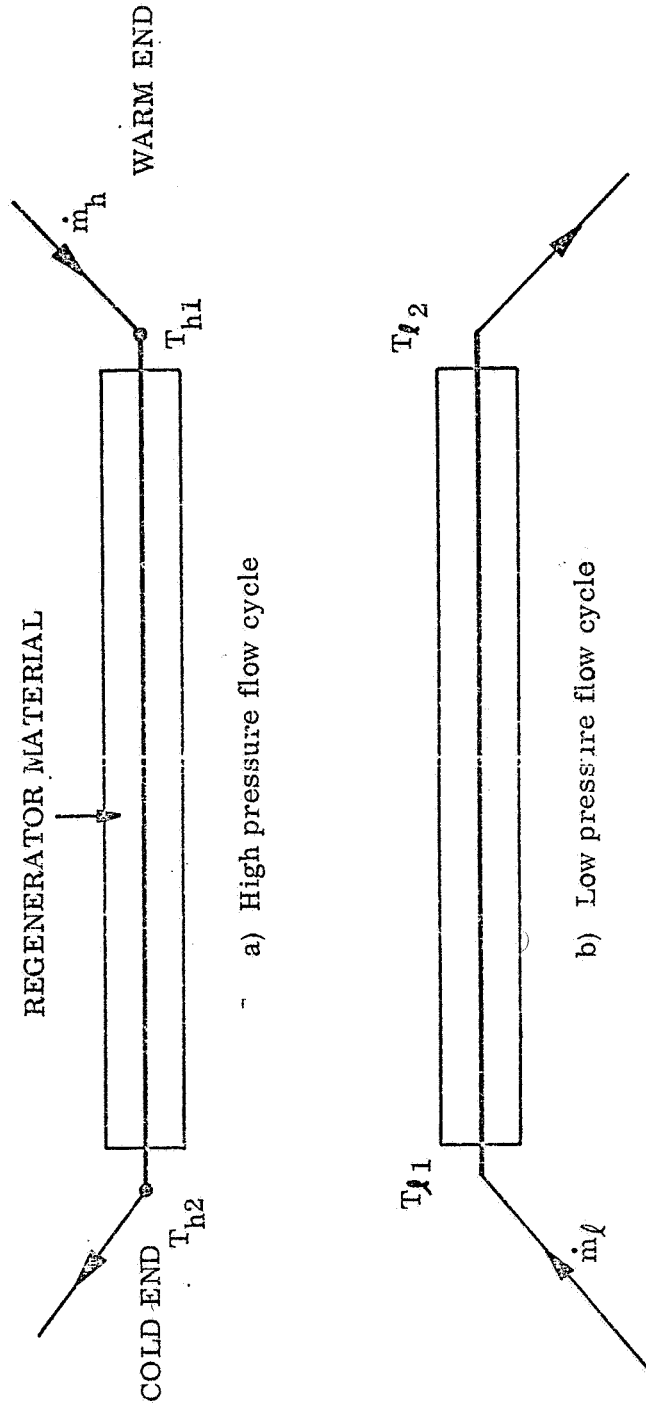


Fig. 3-13 Schematic of a Counterflow Heat Exchanger



a) High pressure flow cycle

b) Low pressure flow cycle

Fig. 3-14 Schematic of a Regenerative Heat Exchanger

stopped and the warm high pressure flow resumes. This type of exchanger achieves its heat transfer by temporary heat storage on the exchanger walls rather than heat transfer through the walls of the flow channels. The heat transfer area per unit volume can be increased considerably since the transfer area has no structural responsibility such as maintaining separation of the flows. Materials such as fine screen or small spheres can be used to pack the regenerator to provide heat storage capacity. At low temperatures the specific heat of solids falls off very markedly, however, and the thermal storage capacity of practical regenerators becomes very small. Refrigerators using regenerative exchangers currently have a lower limit of operation of about 7°K , with poor performance due to this effect appearing below about 20°K . The intermittent nature of the flow in the regenerator tends to reduce the rate of heat exchanger fouling. A disadvantage of the regenerator is that its operating pressure must vary cyclically and losses are introduced because this process cannot be performed reversibly. For this reason, regenerative exchangers are best applied to systems in which the exchanger is in constant communication with a reciprocating expander and, in some cases, a reciprocating compressor, so that the cyclic pressure variation is at least accomplished smoothly. Alternatively, the flow reversal would have to be performed by valve operation, resulting in large losses due to sudden expansion of either the inflowing high pressure stream or the outflowing regenerator contents.

3.3.3.4 Heat Exchanger Design

It is impossible to present generalized heat exchanger performance data in the manner that is possible for compressors and expanders. This is because heat exchanger performance is not limited by natural phenomena so much as by system optimization criteria. Heat exchangers can be built to virtually any desired degree of efficiency as long as the weight, volume and pressure loss penalties can be paid. There is a virtual infinity of possible heat transfer surfaces, each with its own heat transfer and pressure drop characteristics and, many materials of construction may be considered. For actual design data the literature must be consulted, for example Kays and London, "Compact Heat Exchangers" (McGraw Hill, 1954).

It was noted above that regenerative heat exchangers are often used in systems in which the expander and heat exchanger are built as a unit. A system employing such an expander-exchanger combination requires only a compressor to form a complete refrigeration system.

Some weight and volume data for practical exchanger-expanders are presented in Figs. 3-15 and 3-16. They refer to several different types of expansion process but a degree of correlation which is satisfactory for the present purposes is apparent. It may be assumed that the weight and volume figures could be reduced somewhat by careful design, but not by a large factor. Although these expanders are not necessarily flight items, their weight has been quite low so as to minimize heat leakage. Most of the weight lies in the drive mechanism. Figs. 3-15 and 3-16 show clearly the rapid rise in weight and volume with decreasing operating temperature. Fig. 3-17 is a less satisfactory correlation of weight against cooling power for various temperatures.

The weight and volume of split component refrigeration systems can be found from the component data. For a given cooling load and temperature the weight and volume of the expander can be found from Figs. 3-15 to 3-17. The compressor power required is found from the coefficient of performance given in Section 3.4.4. The compressor weight and volume is found from Figs. 3-9 and 3-10.

3.3.4 Motors

A limited survey was made of the weight of electric motors. The results are shown in Fig. 3-18, where the specific weight is shown as a function of the power input. Data are shown for both 60 cycle and 400 cycle AC motors. Fairly extensive data was readily available on 60 cycle motors up to 50 h.p. and 400 cycle motors up to 1 h.p. No attempt was made to differentiate between units whose use required weight optimization and those which did not. As shown in the figure, the 400 cycle units represent a substantial weight improvement over the 60 cycle units and this advantage is utilized on a preponderance of flight designed refrigerators. Comparison of the motor weights with the light-weight compressors shows that a substantial fraction of the compressor weight is a result of the electric motor.

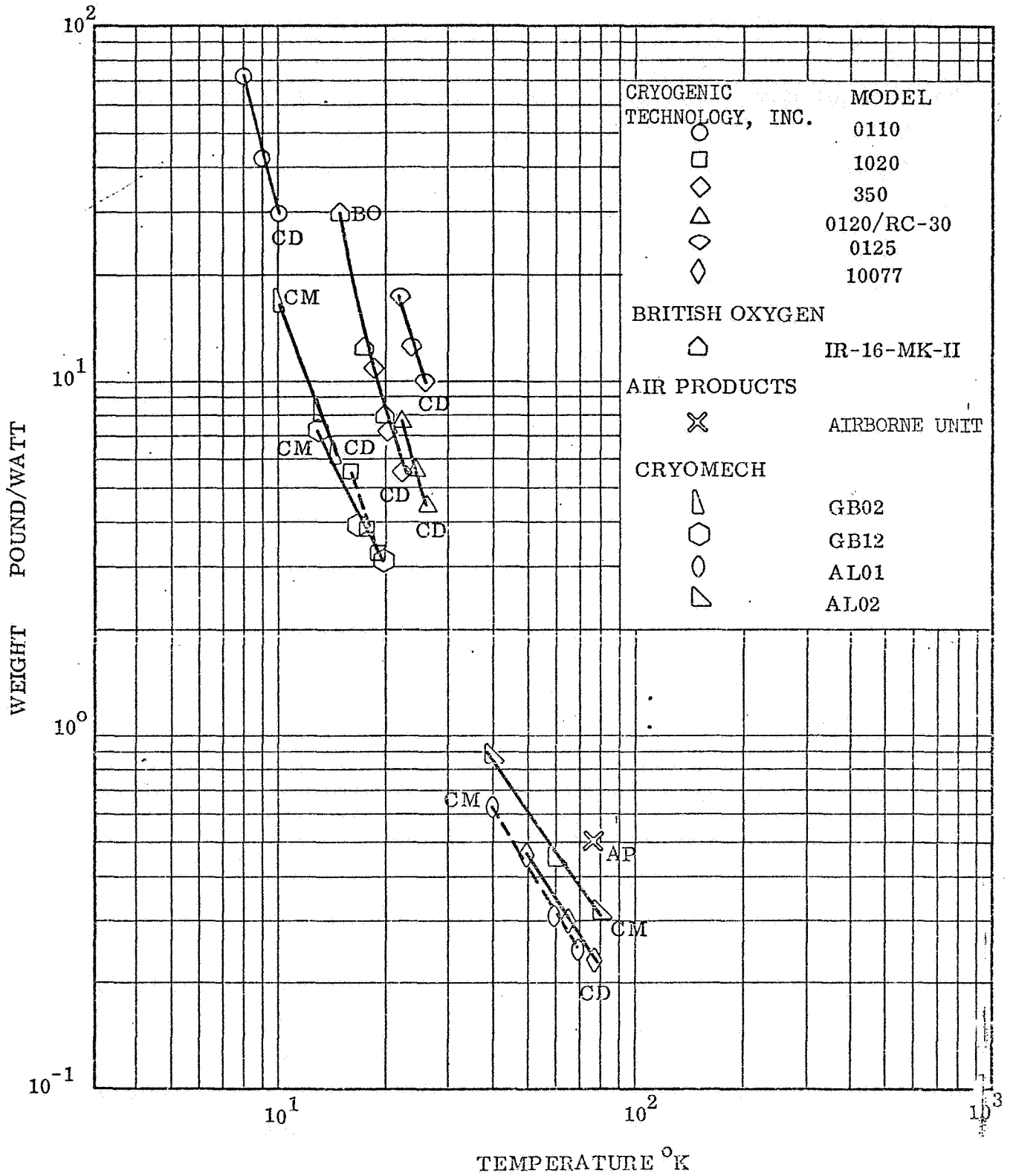


Fig. 3-15 Weight of Exchanger-Expanders Versus Temperature

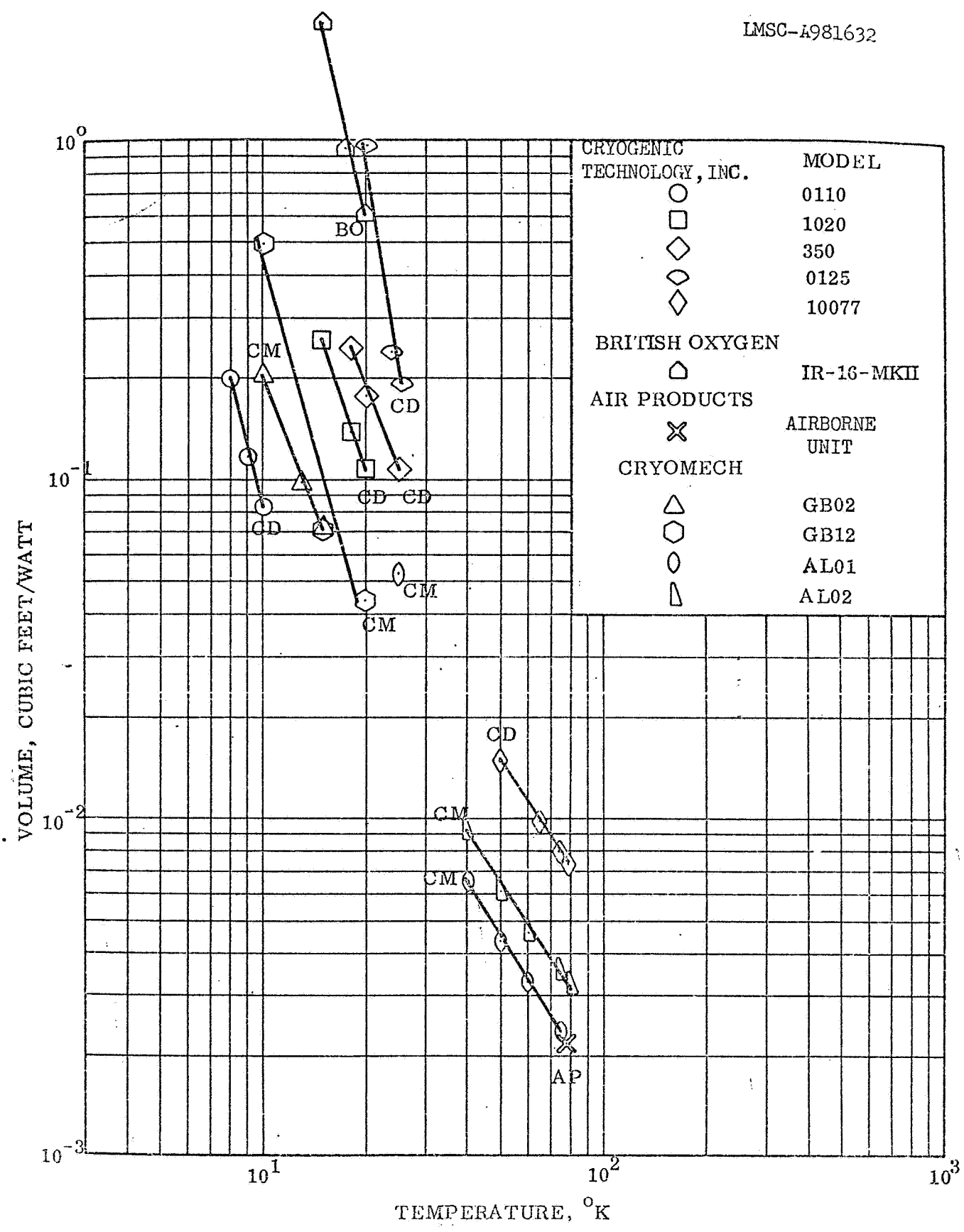


Fig. 3-16 Volume of Exchanger-Expanders Versus Temperature



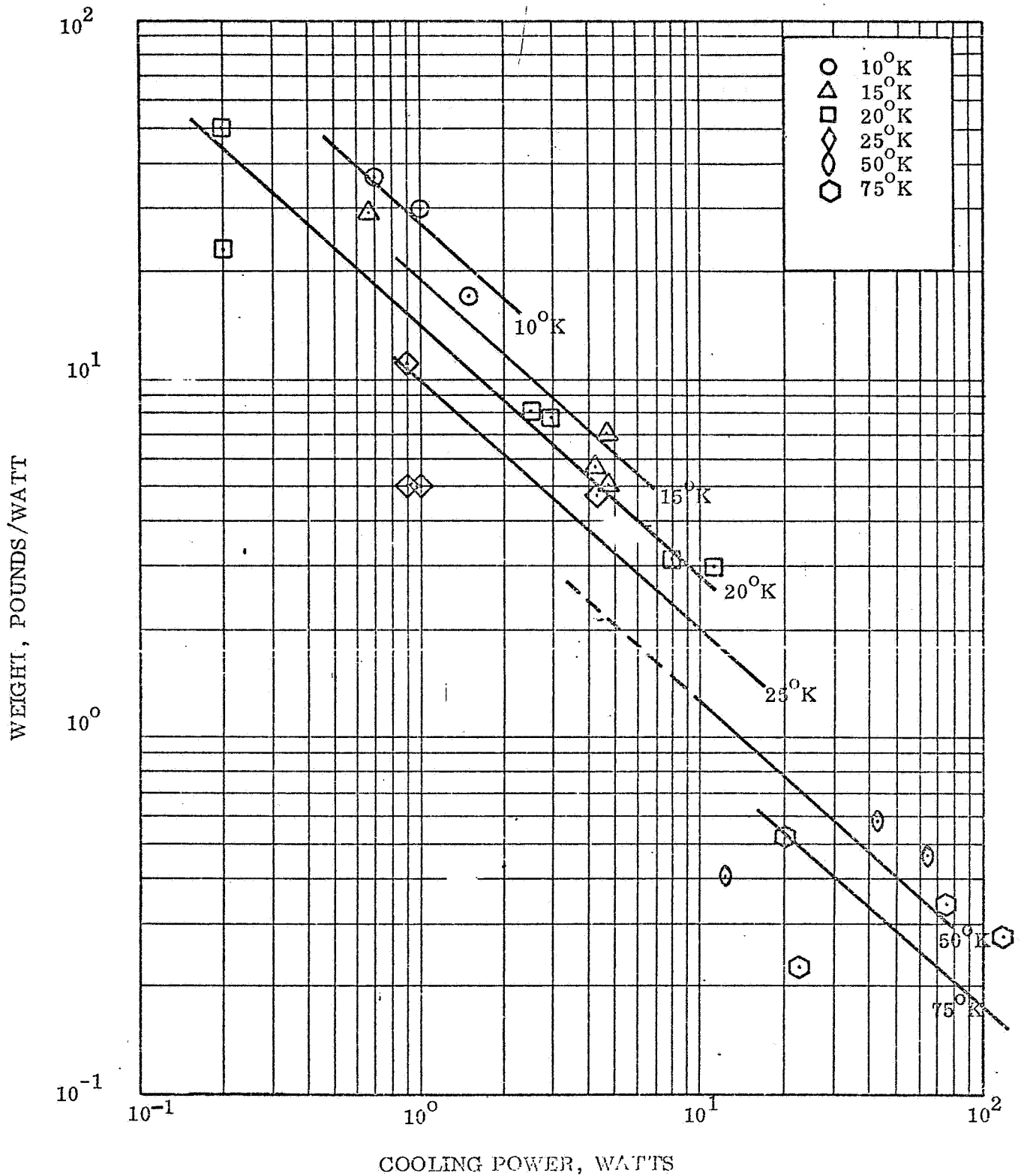


Fig. 3-17 Weight of Exchangers-Expanders Versus Cooling Power

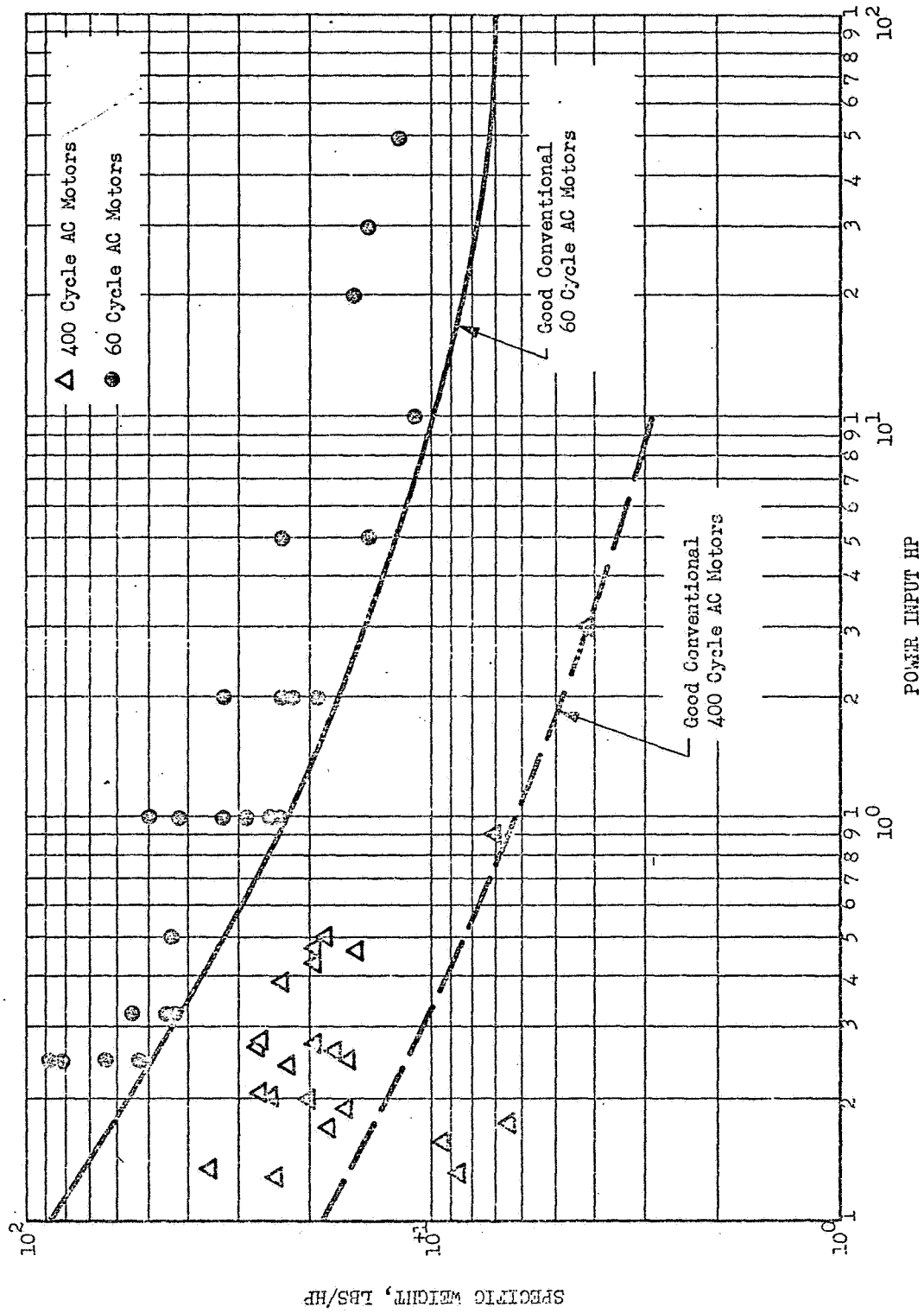


Fig. 3-18 SPECIFIC WEIGHT OF ELECTRIC MOTORS

3.4 EXISTING REFRIGERATOR SYSTEMS

This section describes practical refrigeration cycles which use the thermodynamic principles and the components described in the previous sections. The cycles selected for discussion were limited to those which it was felt had potential for satisfying the requirements of this study, i.e., potential for long term operation, low weight and volume and high thermal efficiency. The data on operating characteristics of the various units has been obtained from an extensive search of the literature and from contacts and discussions with the companies and agencies engaged in the production and development of the units.

Although most cycles are basically related to the Brayton cycle, their practical execution has led to a wide variety of machine configurations. Most refrigeration systems can, however, be placed into one of two subgroups whose members are closely related. These systems are as follows: those employing counterflow heat exchangers and those employing regenerative heat exchangers (see Fig. 3-19). If counterflow exchangers are used then the working fluid flow rate at any point in the refrigeration system is constant with time. The working fluid flows at constant rate and direction through all the system components. These components can hence be designed for continuous steady state operation at prescribable conditions. This category includes Claude, Joule-Thomson, and orthodox Brayton cycle systems. On the other hand those systems which employ regenerative heat exchangers must make some provision for intermittently reversing the direction of flow and alternately compressing and decompressing the working fluid in the regenerator. This can be performed in a refrigerator in which the cycle processes are executed successively in different regions of the same component. The working fluid is compressed while it occupies the warm end and the regenerator spaces, and is expanded while it occupies the cold end and regenerator spaces.

It is noted that the work of compression can always be reduced by multistaging in those systems which use separate compressors. The efficiency of expansion can similarly be improved by multistage expansion. The efficiency of heat exchange may be improved by what might be referred to as multistage heat exchange by splitting the exchanger into sections to reduce the temperature

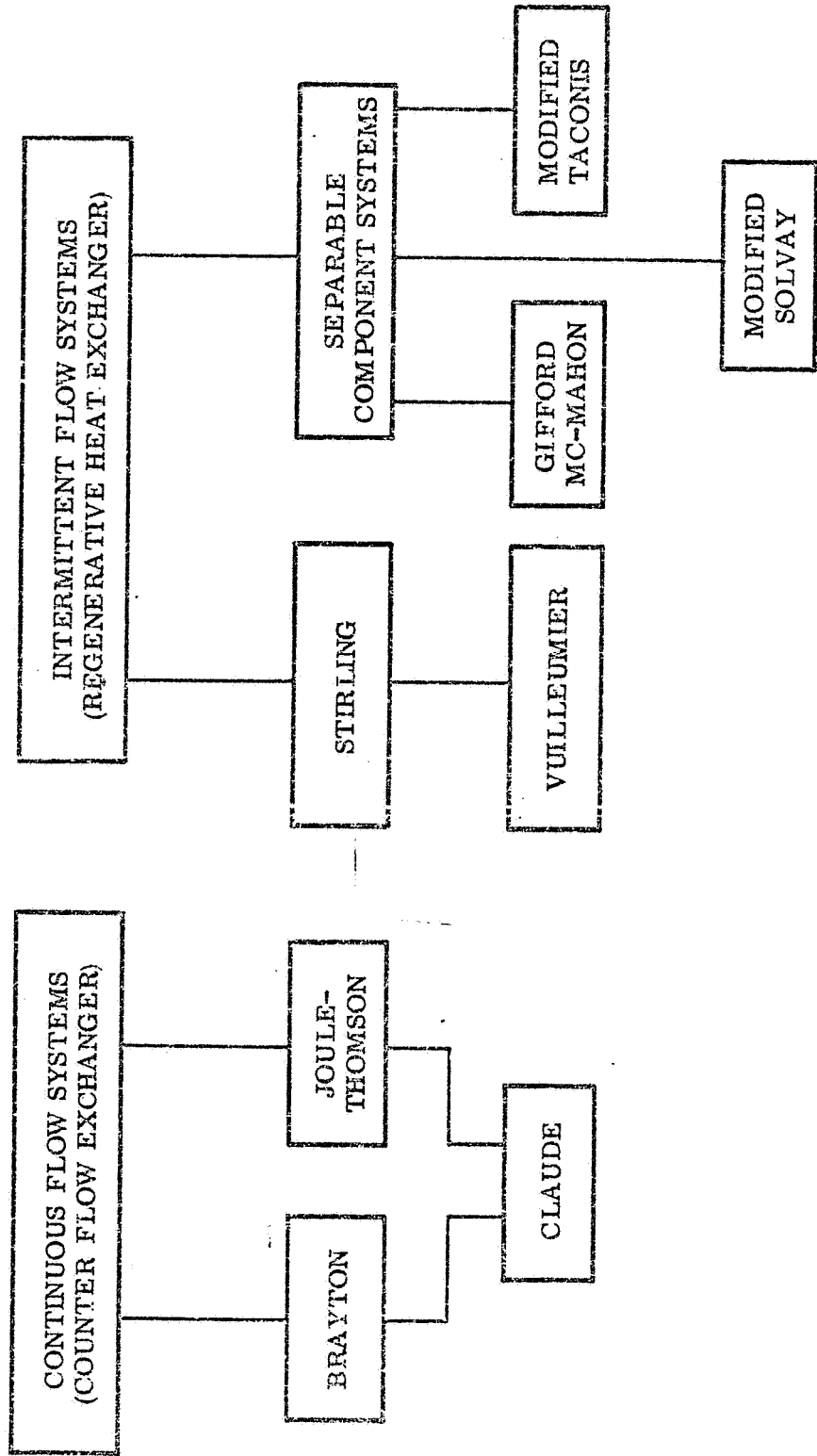


Fig. 3-19 Cycles Included for Analysis

range. Between heat exchange stages the temperatures of the two streams are brought together by supplying refrigeration at this point by means of an intermediate expansion engine. The additional refrigeration required for staging the heat exchanger can be supplied by expanding a portion of the working fluid at the chosen interstage point. Likewise cooling of external loads at intermediate temperatures can be achieved by expanding working fluid at that temperature. The possibility of staged compression or expansion, or expansion at more than one temperature level introduces complexity and arbitrariness to the basic cycle types and so such possibilities will be noted but not discussed further in this report.

3.4.1 The Stirling Cycle Refrigerator

It was noted earlier that these refrigerators which are commonly called Stirling refrigerators do not in practice operate on the ideal Stirling cycle. Due to the speed of operation heat cannot be transferred to and from the working spaces fast enough to permit isothermal compression and expansion. As a result these processes are carried out under conditions closer to adiabatic and the necessary heat transfer is effected in separate heat exchangers. This operation is more characteristic of the Brayton cycle. The truly characteristic feature of the practical so-called Stirling refrigerator and its derivatives is the use of regenerative heat exchangers.

In the refrigeration application heat exchangers are used to exchange heat between high and low pressure gas streams meaning that the single flow passage in the regenerator must be alternately pressurized and depressurized. This could be achieved by using a continuously operating compressor and expander, ballast tanks or dual regenerators, and reversing valves between compressor and regenerator and expander and compressor. Such a system would incur substantial losses due to irreversible sudden compression and expansion when the valves were switched and due to the pressure drop through the valves. The practical Stirling refrigerator avoids these losses because the regenerator is in communication with the expander and compressor at all times, resulting in smooth and therefore less irreversible pressure cycling in the regenerator and elimination of flow losses through the valves.

3.4.1.1 Operation

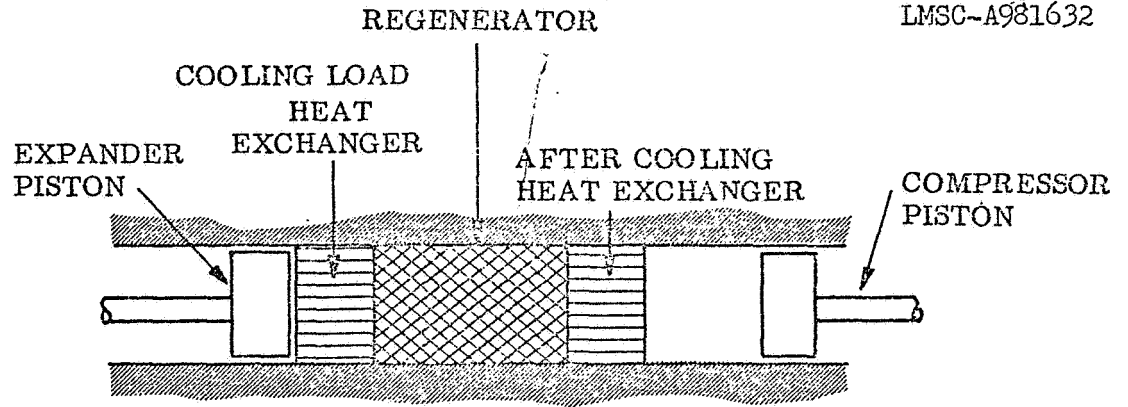
The operation of a Stirling refrigerator is shown in Fig 3-20.

In position 1 the working fluid occupies the ambient space, after-cooler and regenerator. From 1 to 2 the fluid is compressed by inward motion of the compression piston. From 2 to 3 the compressed fluid is transferred from the ambient end to the cold end at constant overall volume by equal increments of both pistons. During this process heat of compression is rejected to the after cooler and the fluid temperature is reduced to the cold end temperature in the regenerator. With the fluid now occupying the cold space, load heat exchangers, and regenerator the fluid is expanded by outward movement of the expander piston, 3 to 4. The fluid is returned from the cold end to the ambient end at constant volume by equal movement of both pistons. During this transfer the energy lost in expansion is replaced in the load exchanger and the temperature is raised to the ambient temperature in the regenerator.

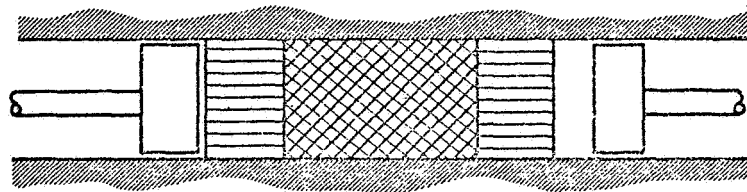
This cycle can equally well be executed using just one piston to perform both expansion and compression processes, and using a passive displacer to move the fluid from one space to another. This configuration of refrigerator is shown in Fig. 3-21.

In practice, it is not practical to move either the two pistons or the piston and displacer in the intermittent manner shown. It is customary to drive both components from the same crank shaft for practical convenience. Both components are thus continually in motion but the cycle can be satisfactorily executed by phasing the piston or displacer motions such that compression occurs with most of the fluid in the warm space and expansion occurs with most of the fluid in the cold space.

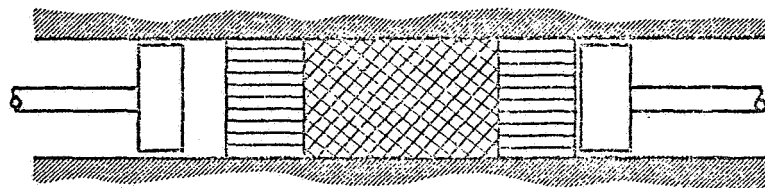
Because of the cyclic operation of the practical Stirling refrigerator and the fact that working fluid will be distributed through several temperature regimes during compression and expansion, it is impossible to show the steady state cycle processes on a temperature entropy diagram in the conventional way. It is also very difficult to perform a reliable thermal analyses of this type of system without resort to quite complex digital and/or analog computational techniques. For approximate engineering analysis purposes simplified repre-



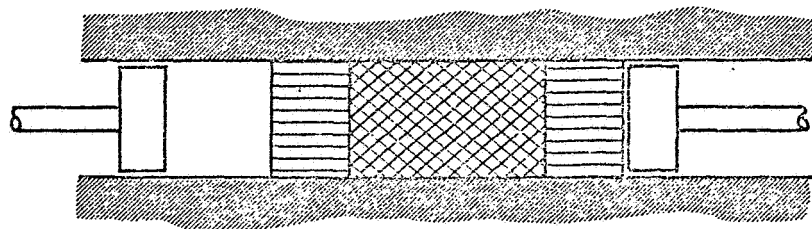
1.



2.



3.



4.

Fig. 3-20 The Practical Stirling Refrigerator
Two Piston Version

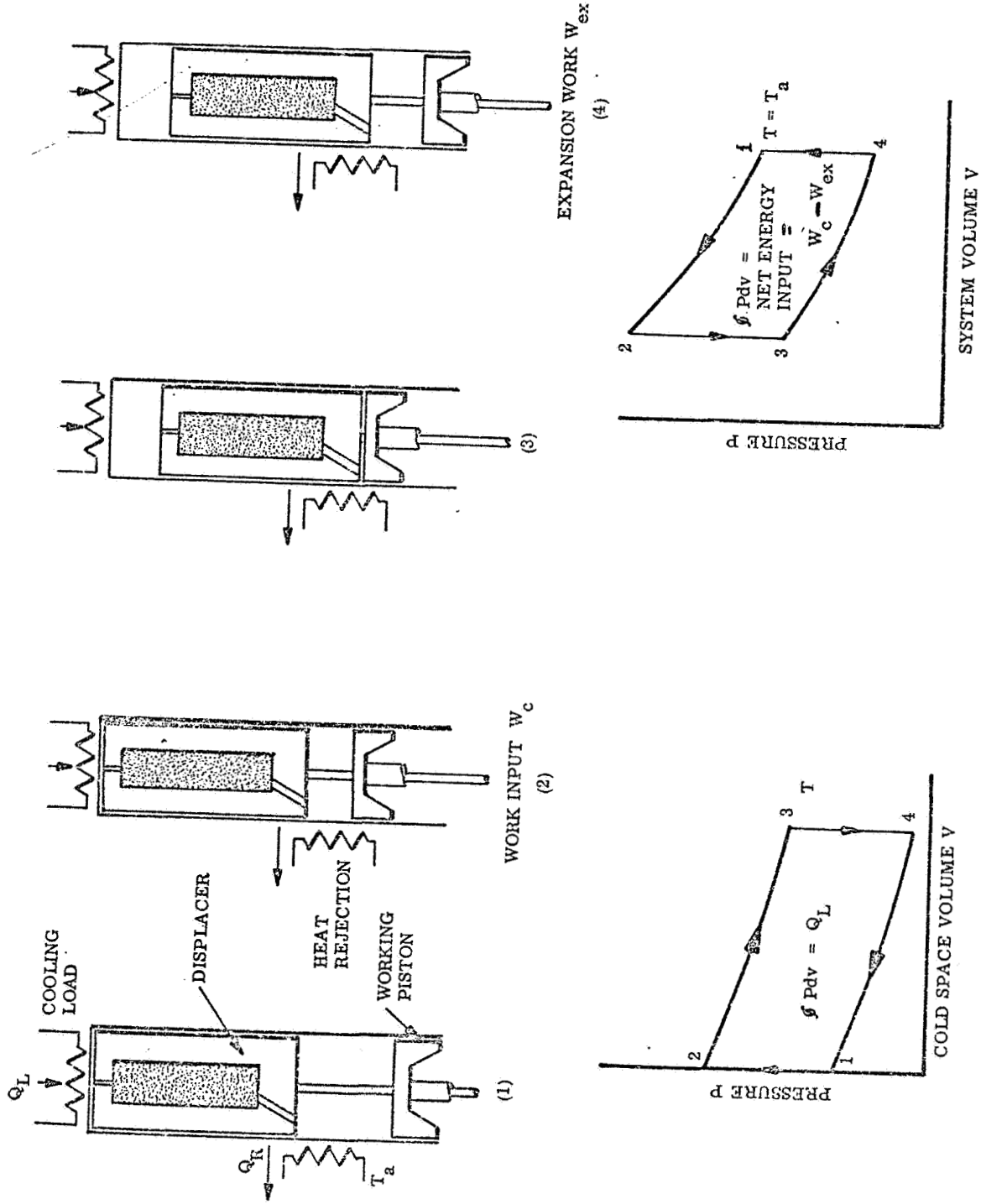


Fig. 3-21 The Stirling Refrigerator - Displacer Version

sentation of the processes can be made which provide a more accessible if less reliable method.

The detailed analysis of a practical Stirling refrigerator requires that the processes occurring in the various locations of the machine be characterized by a set of partial differential equations. There are five major locations; the compression space, after-cooler, regenerator, load exchanger, and expansion space. Within these regions there will be property variations which can be allowed for by averaging or by subdivision of the region. Equations are written to characterize the mass and heat flow rates into these regions and subdivisions in terms of pressure and temperature differentials, fluid properties and system geometry. The equations are then solved for the boundary conditions of total mass conservation, given load and after-cooler temperature and given compressor and expander displacement, speed and phase relationship. Such a system of equations can only be solved by numerical techniques on a digital computer, or by analog methods. This approach has been extensively developed by Finkelstein (3-71). It has been found that solution by these methods is quite difficult because of the length of time required both to write a program and then to solve the problem on the computer. As time progresses it is likely that improved numerical techniques will be found to reduce the amount of machine time, but currently this exact analysis approach is usually rejected in favor of the more convenient approximate approach.

In the approximate analysis the performance of the refrigerator is assessed by writing the cooling capacity of the machine, q_c , as

$$q_c = \oint_c Pdv - \sum \text{losses}$$

Here, $\oint_c Pdv$ is the gross work performed by the cold end of the refrigerator, equal to the gross cooling capacity. The losses due to the various undesirable mechanisms which introduce heat from the environment to the cold end and reduce the effective cooling capacity are considered to be analytically separable effects. The work input to the ambient end, W , is

$$W = \oint_a Pdv$$

The terms $\oint_C Pdv$ and $\oint_A Pdv$ can be evaluated by writing mass and energy conservation equations for the working spaces. In the simplest case these equations can be solved by assuming isothermal conditions in the spaces and modifying the answer by means of an empirical constant to allow for non-isothermal behavior. This so-called Schmidt analysis permits analytic expressions to be written for the integrals. The separable loss mechanisms are generally accepted to be as follows:

- a) Heat conduction from ambient to cold end by conduction through the structural members.
- b) Heat transfer by radiation and convection from the ambient environment.
- c) Heat transfer from the ambient end to the cold end due to the relative motion of the displacer or expander and cylinder walls.
- d) Heat flux into the cold space due to regenerator inefficiency.
- e) Heat loss due to cyclical pressurization and depressurization of the clearance spaces.
- f) Non-ideal heat transfer in the load and after-cooler exchangers.

These losses can be assessed by performing simple individual engineering analyses of the mechanisms, assuming that they are decoupled from each other. Generalized expression for these loss mechanisms cannot be written because the most appropriate analytical model may be different from one case to another. An example of this procedure is given by Gifford (3-51).

The analysis based upon decoupled loss mechanisms is a great deal easier to use than the complex analysis but it cannot allow for the strong interaction that may occur between the loss mechanisms, particularly a), c), e) and heat transfer within the working spaces. This method will continue to be used until the complex analysis can be made more available and less costly in computer time.

3.4.1.2 Companies Engaged in Production and Development of Stirling Refrigerators

The following companies are presently engaged in production and development of Stirling cycle refrigeration systems:

U. S. Philips Corporation
Malaker Corporation
Hughes Aircraft Corporation

U. S. Phillips: Phillips was the pioneer in development of the Stirling refrigerator, having built their first machine in 1954 for the purpose of air liquification. Initial research on the Stirling cycle as a refrigeration device was initiated in 1945 by Phillips, and in 1950 the first drops of liquid air were obtained from a Stirling-cycle refrigerator. Additional history on the development of the Stirling refrigerator at Phillips is given in Refs. 3-9 to 3-12.

Presently, Phillips produces a variety of Stirling cycle machines for laboratory and industrial use as well as miniature units for aircraft use. The miniature flight units, designated "Cryogem", include models 42100 and 42151 which are two stage units which provide cooling in the range of 1 watt at 25°K and 2 watts at 30°K. These units are intended primarily for aircraft usage in cooling infra-red detectors and as such provide lower refrigeration capability than required for this study.

Of particular interest for long-term cryogenic storage requirements is Phillips Model A-20 "Cryogenerator." This unit appears to be the only one which provides 20°K refrigeration at levels near 100 watts. Other available production units generally provide 1-10 watts of refrigeration at that temperature, or else are very large, heavy industrial units. The unit is a two-stage machine based on the Phillips-Stirling cycle and provides refrigeration at two temperature levels, one over the 60-90°K range and the second stage between 15 and 30°K. This unit has the potential of cooling two different cryogens at the two temperature levels. Conceivably all two-stage Stirling cycles have this capability. However, development along these lines has not been pursued in many units. Different arrangements of the A-20 cryogenerator have been selected by Phillips for various usages including gas liquification and experiment cooling. The weight of this unit is approximately 660 lbs. Discussions with Phillips indicate that this weight could be reduced to the neighborhood of 200 - 300 lbs

by redesigning the base plate and converting to a 400 cycle motor. The unit, of course, is not capable of operation in space because of its wet lube system, however, it does provide a data point for weight estimates at the higher cooling levels.

Malaker Corporation: Malaker has been engaged in the development of Stirling cycle refrigerators since the 1950's. The majority of their research and development has been applied to the Stirling cycle and has been concentrated on small units. Malaker has produced units with very high thermal efficiencies, and is actively engaged in additional development and modification of their units. Some of their earlier work under contract to WPAFB is reported in Ref. 3-17. Recent work of interest here has been devoted to the modification of one of their units to make it adaptable to space operation (Designated Model SS-I). The primary modifications consist of providing an all welded case around the units to allow larger temperature excursion during operation without freezing up the existing O-ring seals and leaking the working gas. Malaker has concentrated on miniature units for laboratory use, for aircraft support and various field uses. They have not built large industrial units. Units are available for cooling down to approximately 15°K in two stages and to near 60°K in a single stage.

Hughes Aircraft Corporation: Hughes Aircraft Corporation produces Stirling cycle machines for various uses. The majority of their units manufactured to date are for infrared cooling on aircraft. Refrigeration units are not commercially available from HAC but essentially provide a support function for in-house activities.

One of the prototype models (3-13) provides 15W at 80°K and therefore falls within the study range, while the other units provide only a few watts. HAC is extensively engaged in research and development on the Vuilleumier cycle unit and these activities are discussed in another section (3.4.2.2)

3.4.1.3 Analysis of Stirling Cycle Data

Data has been assembled on the characteristics of the Stirling refrigerators as shown in Table 3-1.

FOLDOUT FRAME I

Manufacturer	Malaker Corp.	Malaker Corp.	Malaker Corp.	Malaker Corp.
Trade Name	Cryomite	Cryomite	Cryomite	Cryomite
Model	Mark VII-C	Mark XIV-A	Mark VII-R	Mark XX
I.D. Number	1	2	3	4
Refrigeration Range	17.5 - 80°K	44 - 100°K	40 - 125°K	40 - 120°K
Cycle	Stirling	Stirling	Stirling	Stirling
Working Fluid	Helium	Helium	Helium	Helium
High Pressure	NI	NI	NI	NI
Low Pressure	17 atm Fill	NI	NI	NI
Minimum Temp	17.5°K	44°K	40°K	40°K
Cool-Down Time	8 min	7 min	3.8 min	7.4 min
Expander RPM	NI	NI	NI	NI
Volts-Phase-Frequency	208 - 3/4 - 400/60	208 - 3 - 400	208 - 3 - 400	208 - 3 - 400
Cooling Means	Air or Water	Air	Air	Air or Liquid
Ambient Temp Reqrts				
Required Attitude	Any	Any	Any	Any
Cryostat Dimensions	4.8"D x 11.5"L	2.9"D x 13"L	6 1/2"D x 23 1/2"L	19" x 18" x 15 1/2"
Compressor Dimensions				
System Volume	209 in. ³	86 in. ³	781 in. ³	1500 in. ³
System Weight	15.5 lb	5.5 lb	40 lb	65 lb
MTBF	40,000 hr	40,000 hr	40,000 hr	40,000 hr
Maintenance Interval	1,000 hr	1,000 hr	1,000 hr	1,000 hr
System Cost	\$5,195	\$9,000	\$17,500	\$24,000
15°K	Refrigeration			
	Power Input			
	COP			
	% Carnot			
	Lb/Watt			
20°K	Refrigeration	1 watt		
	Power Input	480W		
	COP	.00208		
	% Carnot Eff.	2.92%		
	Lb/Watt	15.5		
77°K	Refrigeration	17.7W	2.8W	60W
	Power Input	395W	108W	1220W
	COP	.0448	.0259	.0492
	% Carnot	13%	7.5%	14.3%
	Lb/Watt	0.876	1.97	0.667
110°K	Refrigeration	23.7	5W	90W
	Power Input	395	96W	1220W
	COP	.073	.0522	.0738
	% Carnot	12.6%	8.25%	11.7%
	Lb/Watt	0.654	1.10	0.445
	In. ³ /Watt	8.8	17.2	8.7

FOLDOUT FRAME 2

er Corp.	Phillips Lab.	Phillips Lab.	Hughes Aircraft	Phillips Lab.	Malaker Corp.
ite XX	None A-20 5	Prototype X-20 6	Prototype 7	Cryogem 42100 1- S	Cryomite Mark XV 2- S
120°K ing m	12 - 300°K Stirling Helium	12 - 300°K Stirling Helium	45°K up Stirling Helium	20°K up Stirling Helium	54 - 100°K Stirling Helium
in 3 - 400	427 psia 12°K 40 min 1450 - 1750 400 - 3 - 50/60	NI NI 12°K 15 min 1750 2000 VA - 3 - 50/60	NI NI 45°K 3 min NI 115 - 3 - 400	125 psig NI 20°K 12 min 208 - 3 - 400	NI NI 54°K 8 min 24V DC
r Liquid 18" x 15 1/2"	198 gal/hr H ₂ O 43.5" x 37.4" x 19.7"	Air or Liquid Any (g = 0) 4"D x 7.5"L 18.5" x 13.8" x 13"	Air or Liquid -55 to +71°C Any 8" x 6" x 6"	Air Any 5.87" x 4.81" x 10.9"	Air Any 2.9"D x 12.2"
in. ³ C h4 hr 00	15,000 in. ³ 660 lb 500 hr	112 lb NI 4,000 hr NI	10 lb NI 500 hr NI	119 in. ³ 12 lb 1000 NI	66 in. ³ 5 lb 40,000 hr 1000 hr \$9,000
	20W 8300W .0024 4.5% 33.0	5W 1750W .00286 5.4% 22.4			
	100W 8300W .0121 17% 6.60	10W 1750W .00572 8% 11.2		1W @ 25°K 350 .0029 3.2% 12 119	
		36W 1750W .0206 6% 3.12	14W 500W .0280 8.1% 0.715		1W 29.5W .03 9.9% 5 66
		NI			1.9% 29.5 .064 11% 2.63 24.7

Table 3-1 Existing Stirling Cycle Refrigerators

Lab.	Malaker Corp.	Malaker Corp.	Malaker Corp.	Phillips Lab.	Phillips Lab.
	Cryomite Mark XV 2-S 54 - 100°K Stirling Helium	Cryomite Mark XVII-1 3-S 77°K Stirling Helium	Mark XVI-3 4-S 77 - 110°K Stirling Helium	Prototype 5-S 7 - 300°K Stirling Helium	Micro-Cryogen 6-S 40-300°K Stirling Helium
	NI NI 54°K 8 min	NI NI 54°K 9 min	NI NI 77°K 7 min	6 atm 3.7 atm 7°K 15 min 600 RPM	8.5 ATM 4.5 ATM 40°K 3 min 1800 RPM
3 - 400	24V DC	24V DC	24V DC	320-3-60	24 VDC
	Air Any 2.9"D x 12.2"L	Air Any 3.2"D x 14"L	Air Any 3.5"D x 15.5"L	Water Any 6" x 12" x 24"	Air or Liquid -55°C to 75°C Any 4" x 4" x 8"
	66 in. ³ 5 lb 40,000 hr 1000 hr \$9,000	88 in. ³ 13 lb 40,000 hr 1000 hr	137 in. ³ 10 lb 40,000 hr 1000 hr	35 lb	128 in. ³ 3 lb 250 to 500 Hz \$4,000 to \$6,500
				1.3W (est.) 700W .00186 26.9	
	1W 29.5W .034 9.9% 5 66	4.3W 280W .015 4.35% 3.02 20.4	8.2W 208W .039 11.3% 1.22 16.7		1.5W 90W .0167 4.8% 2.0 85.5
	1.9W 29.5 .064 11% 2.63 34.7		12.5W 195W .064 11.1% 0.8 11.0		

The parameters of the various units are tabulated in Table 3-1 for the seven units. The tabulation also includes the calculations which were made to provide the basis of the curves which are plotted.

Figs. 3-22 through 3-26 present the cooling capacity as a function of the temperature for the individual units. Also included is the power input vs. temperature where available.

Fig. 3-27 presents the coefficient of performance (C.O.P.) of the units as a function of net refrigeration provided. The data is presented at four temperatures of interest: 15°K, 20°K (LH₂), 77°K (LN₂) and 110°K. The 20°K and 110°K temperatures represent the lower and upper limits of the study and the 77°K point is a convenient intermediate temperature at which operating data is commonly reported. 15°K is the minimum temperature at which data was available. The data at the four temperatures was curve fit as shown on Fig. 3-27. In general, the curve fitting was done so that the curve represented maximum performance (highest value of C.O.P.).

Fig. 3-28 presents the C.O.P. as a function of temperature. The Carnot efficiency is also shown for comparison, and represents the maximum theoretical performance of the Stirling cycle. Curve fits are also shown for 100 watt and 5 watt capacity, and were obtained from the previous figure. The figures, as expected, show a pronounced effect of both temperature and capacity. It is interesting to note that the slope of the 5 and 100 watt curves are nearly parallel to the slope of the Carnot C.O.P. vs. temperature.

Fig. 3-29 shows the percent Carnot efficiency which the units have achieved as a function of refrigeration capacity. The units provided from 6% to a maximum of 20% of the theoretical efficiency, and this is the best performance of any of the cycles as will be seen in later sections.

Fig. 3-30 presents the specific weight of the systems as a function of cooling capacity. The data are fitted with lines at 77°K and 110°K as for the C.O.P. data. The data at higher cooling rates at 20°K is for heavy ground based units only, and an estimated weight for flight weight units is shown at 20°K. The

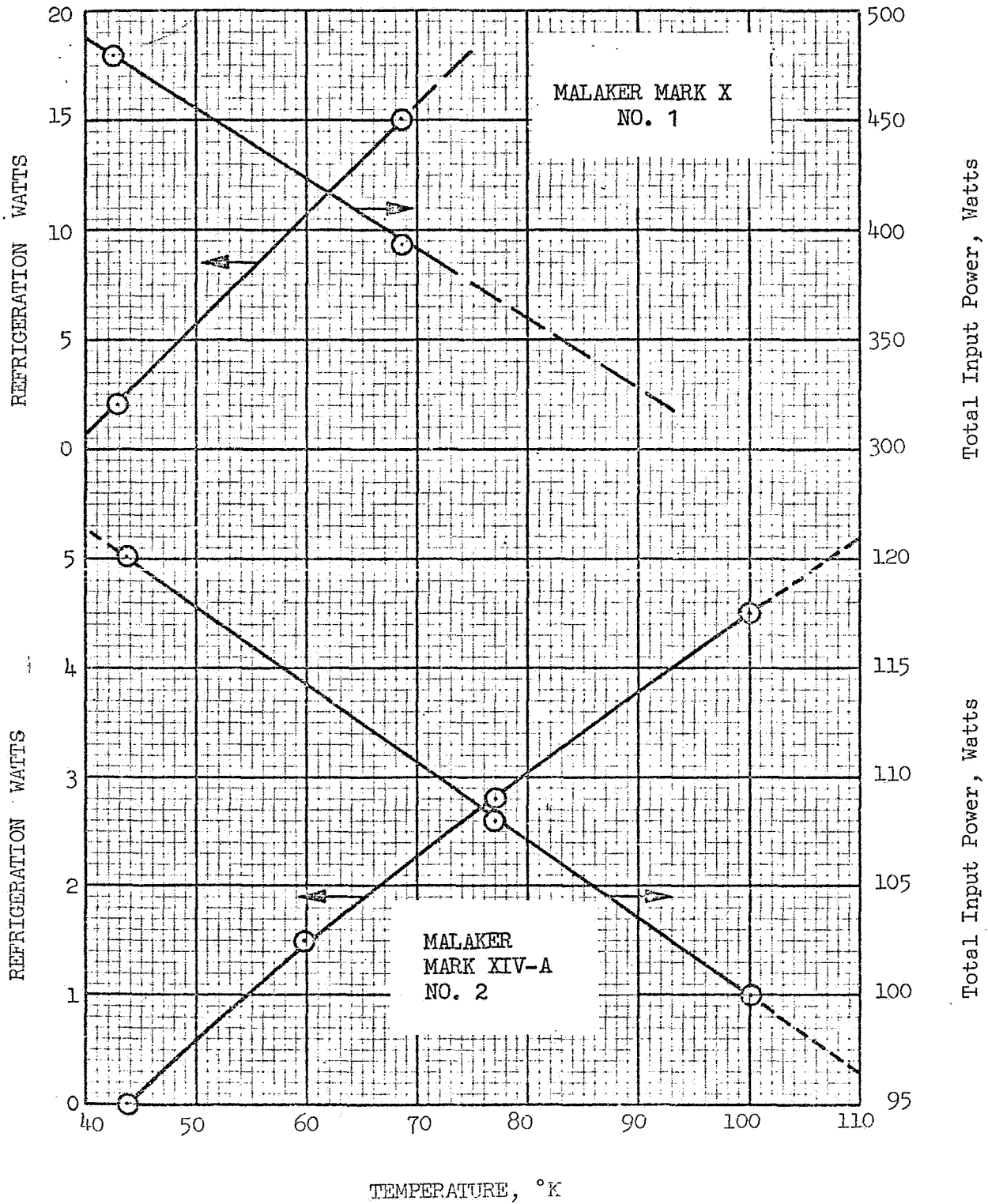


Fig. 3-22 Refrigeration Versus Temperature (Stirling Cycle)

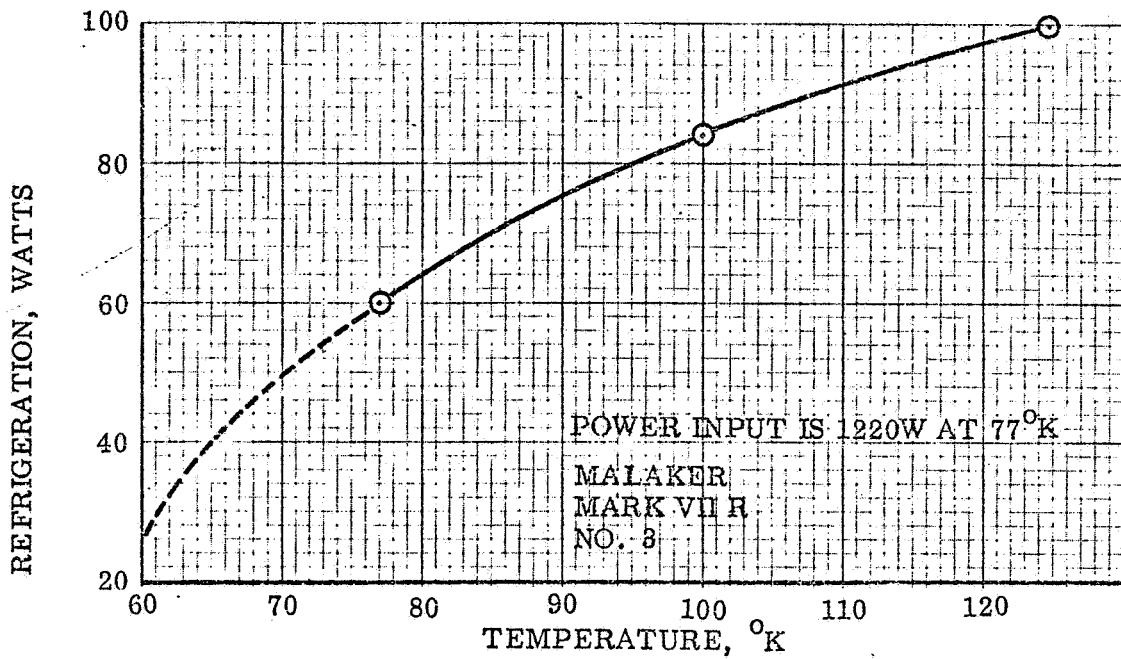


Fig.3-23 Refrigeration Versus Temperature (Stirling Cycle)

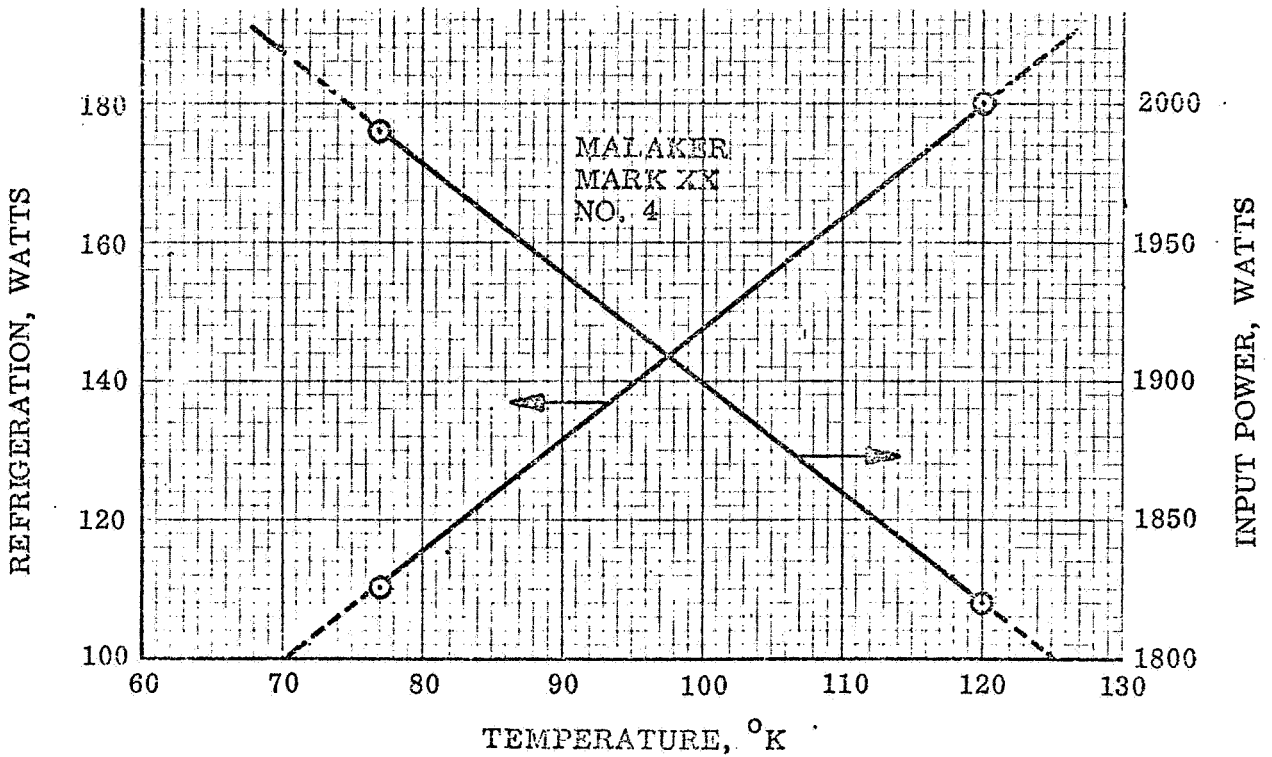


Fig.3-24 Refrigeration Versus Temperature (Stirling Cycle)

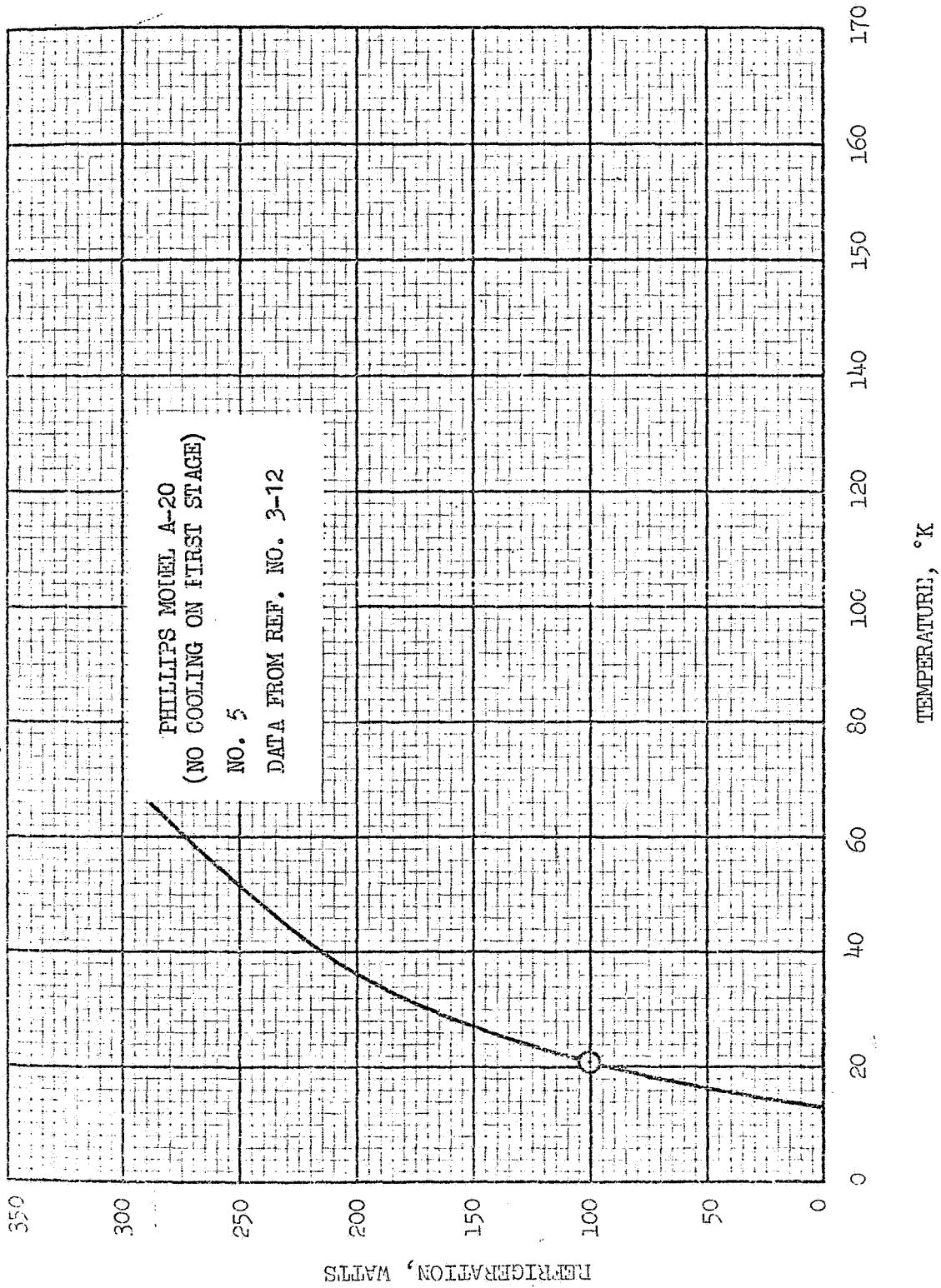


Fig. 3-25 Refrigeration vs. Temperature (Stirling Cycle)

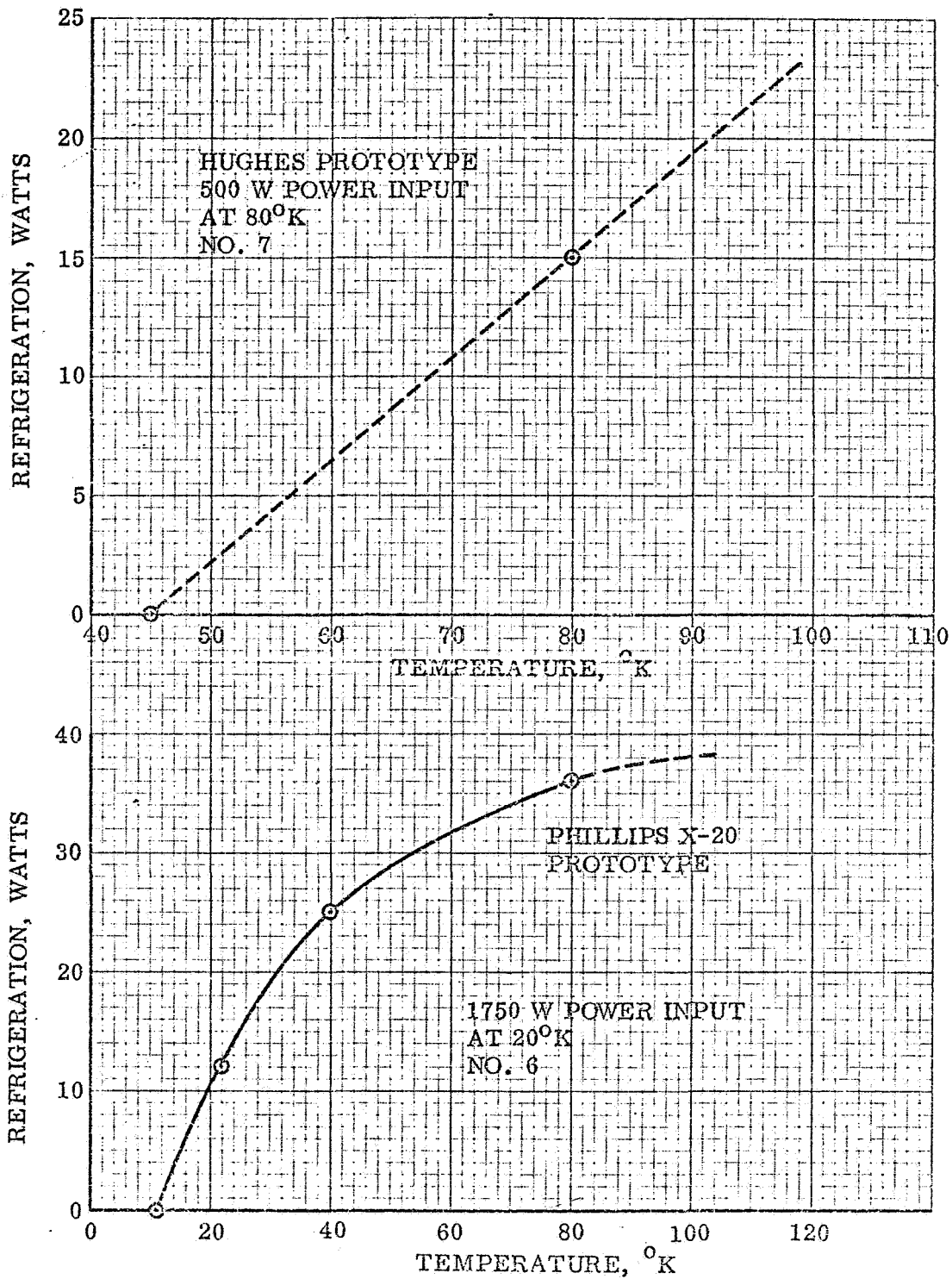


Fig. 3-26 Refrigeration Versus Temperature (Stirling Cycle)

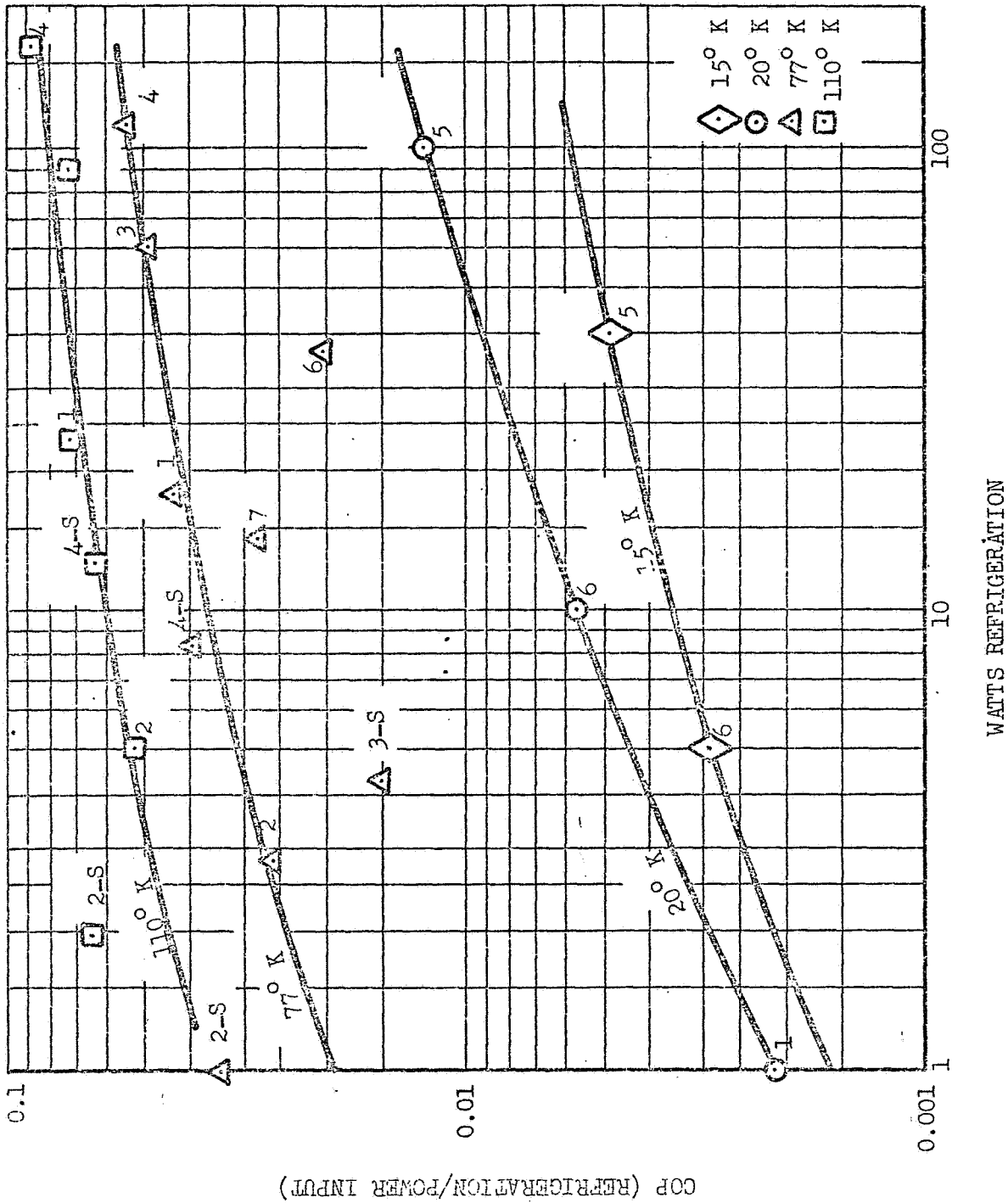


Fig. 3-27 Coefficient of Performance Versus Cooling Capacity (Stirling Cycle)

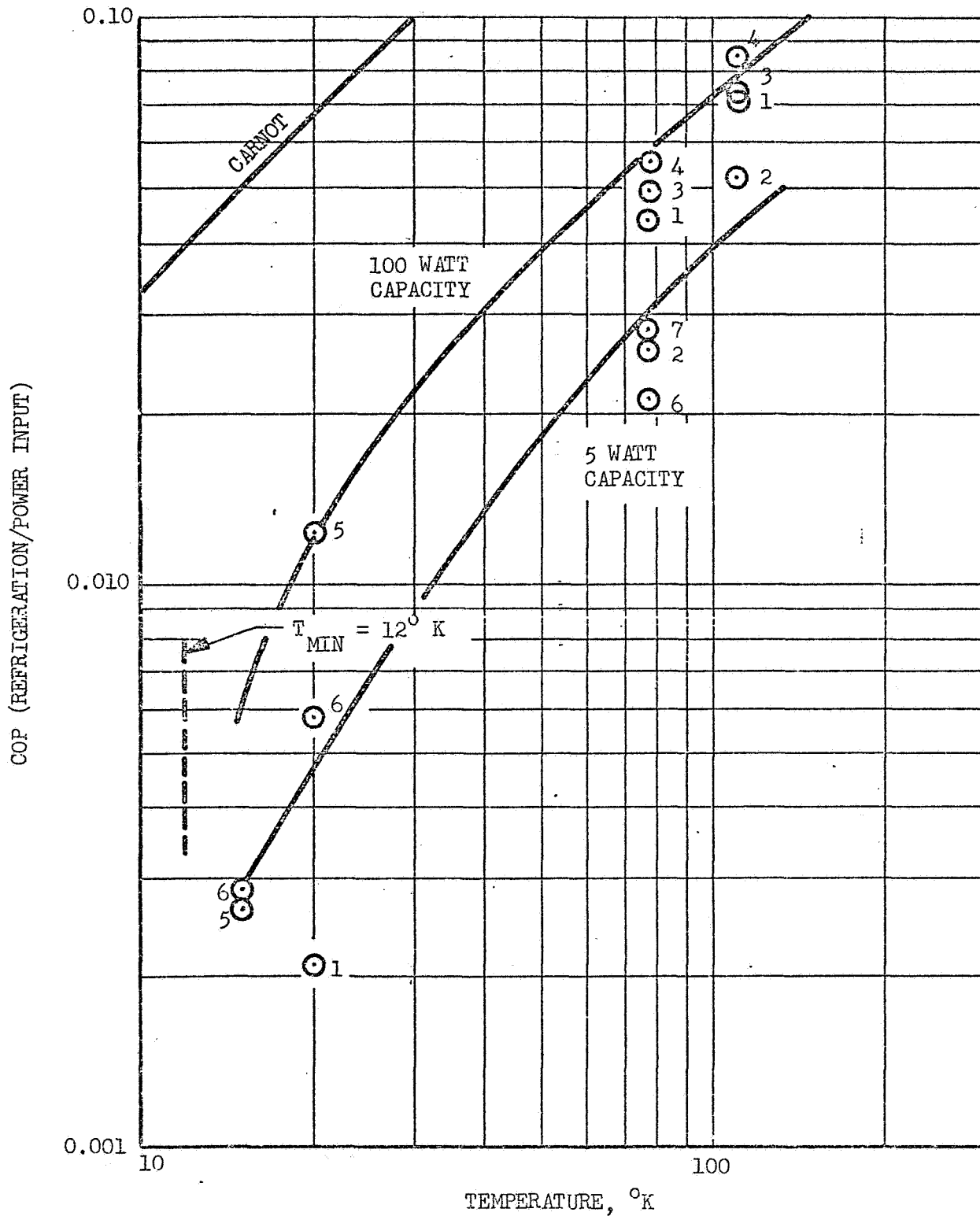


Fig. 3-28 COEFFICIENT OF PERFORMANCE, VERSUS TEMPERATURE (STIRLING CYCLE)

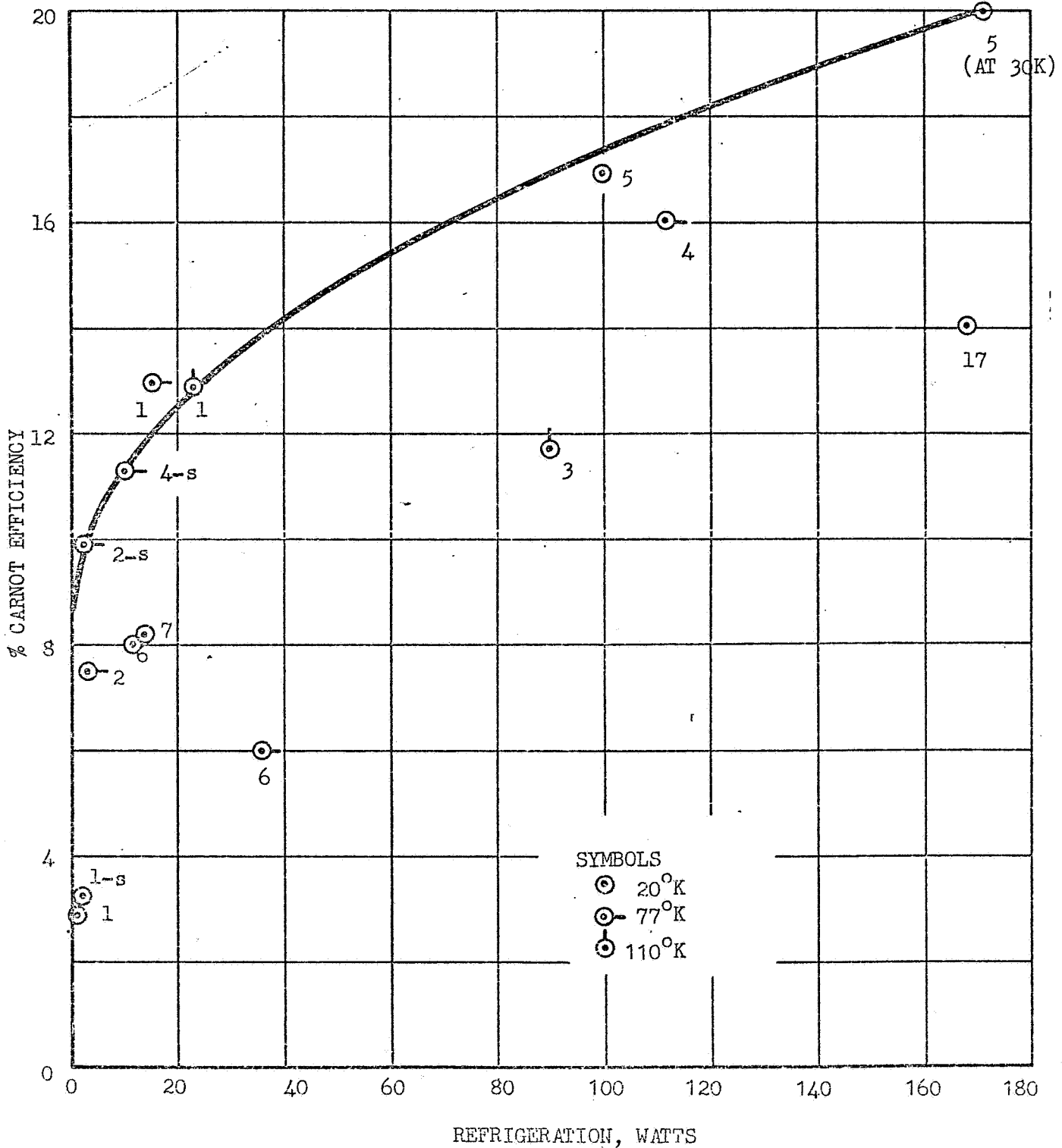


Figure 3-29 Percent Carnot Efficiency of Stirling Cycle Refrigerators

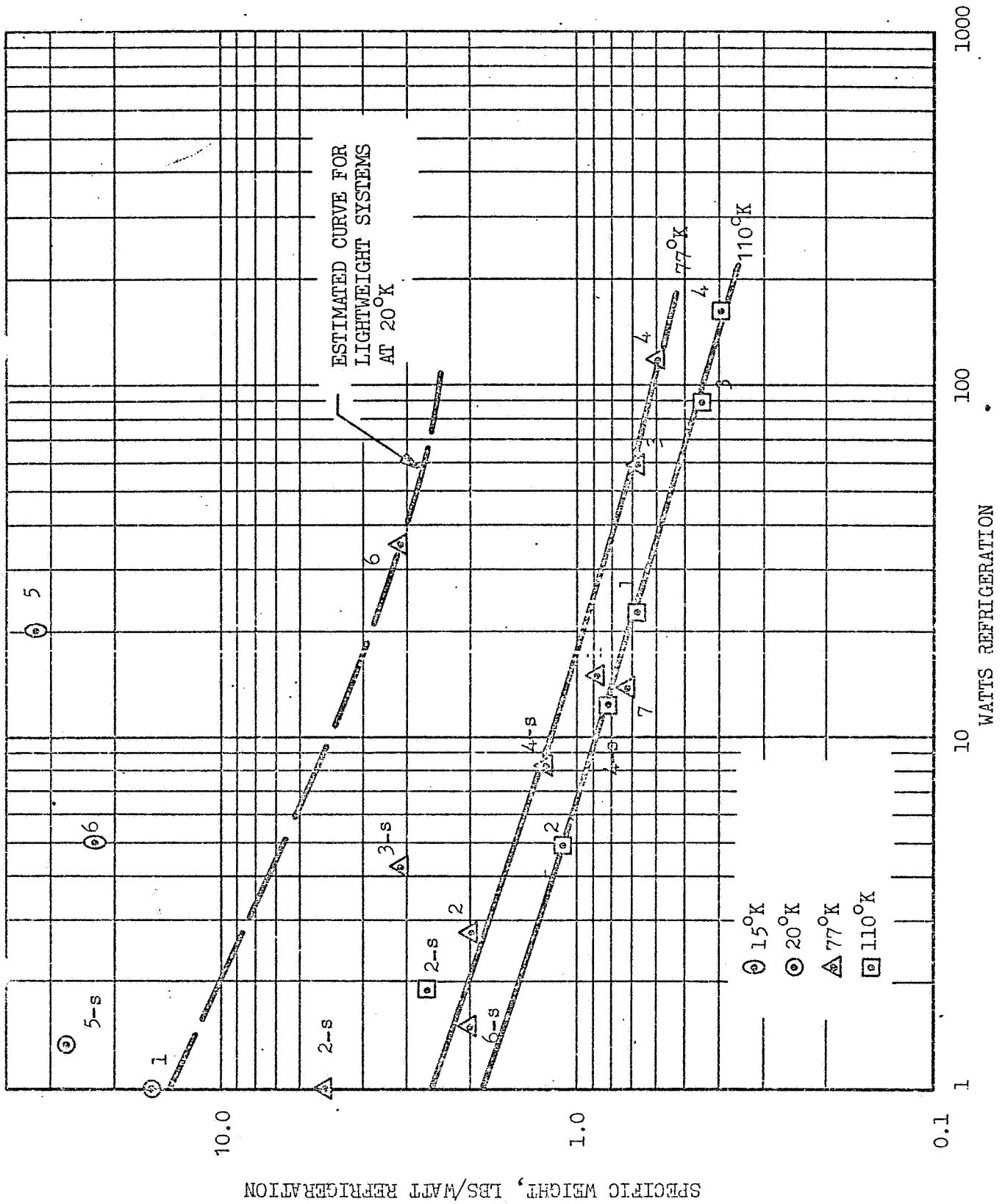


Figure 3-30 Specific Weight Vs. Cooling Capacity (Stirling Cycle)

manner of obtaining this estimated weight curve is described in Section 3.6. It is shown here for comparison with the data points for existing units.

Fig. 3-31 shows the data points plotted as specific weight vs. temperature, with lines at 5 watt and 100 watt capacity. The capacity lines were obtained by cross-plotting the result of the previous plot. The results show the expected strong dependence on both capacity and temperature.

Fig. 3-32 shows the specific volume of the various units vs. cooling capacity at the three temperatures selected.

3.4.2 The Vuilleumier Refrigerator

3.4.2.1 Operation

The Vuilleumier (VM) refrigerator is in essence a practical Stirling refrigerator in which compression and expansion of the working fluid is effected thermally instead of mechanically. This modification is best illustrated in connection with the Stirling refrigerator configuration of Fig. 3-21. The working piston of the Stirling refrigerator can be removed and replaced by a thermal compressor/expander consisting of a hot space, ambient space regenerative heat exchanger and displacer. The cycle of operations shown in Fig. 3-33 closely parallels that of the Stirling refrigerator. In position 1, the fluid is all in the ambient space. From 1 to 2, the compressor displacer moves from hot to ambient end, causing fluid to move from ambient to hot spaces as constant volume, resulting in an increase in system pressure and hence compression of the fluid remaining in the ambient space. From 2 to 3 the expander displacer is moved to displace this remaining fluid to the cold end. From 3 to 4 the pressure is reduced by displacing fluid from the hot space back to the ambient space, thereby expanding the fluid in the cold space. From 1 to 2 the cold gas is returned to the ambient space by movement of the expander displacer. The heat interactions in the exchangers are similar to those in the Stirling refrigerator. In addition to the load and after-cooler heat exchangers, however, there is also a power heat exchanger required at the hot end through which the energy required to compress the fluid is supplied. As noted in Section 3.2 this energy will be higher than the actual work of compression since the device is in essence a combined engine and compressor, and thus the supplied energy

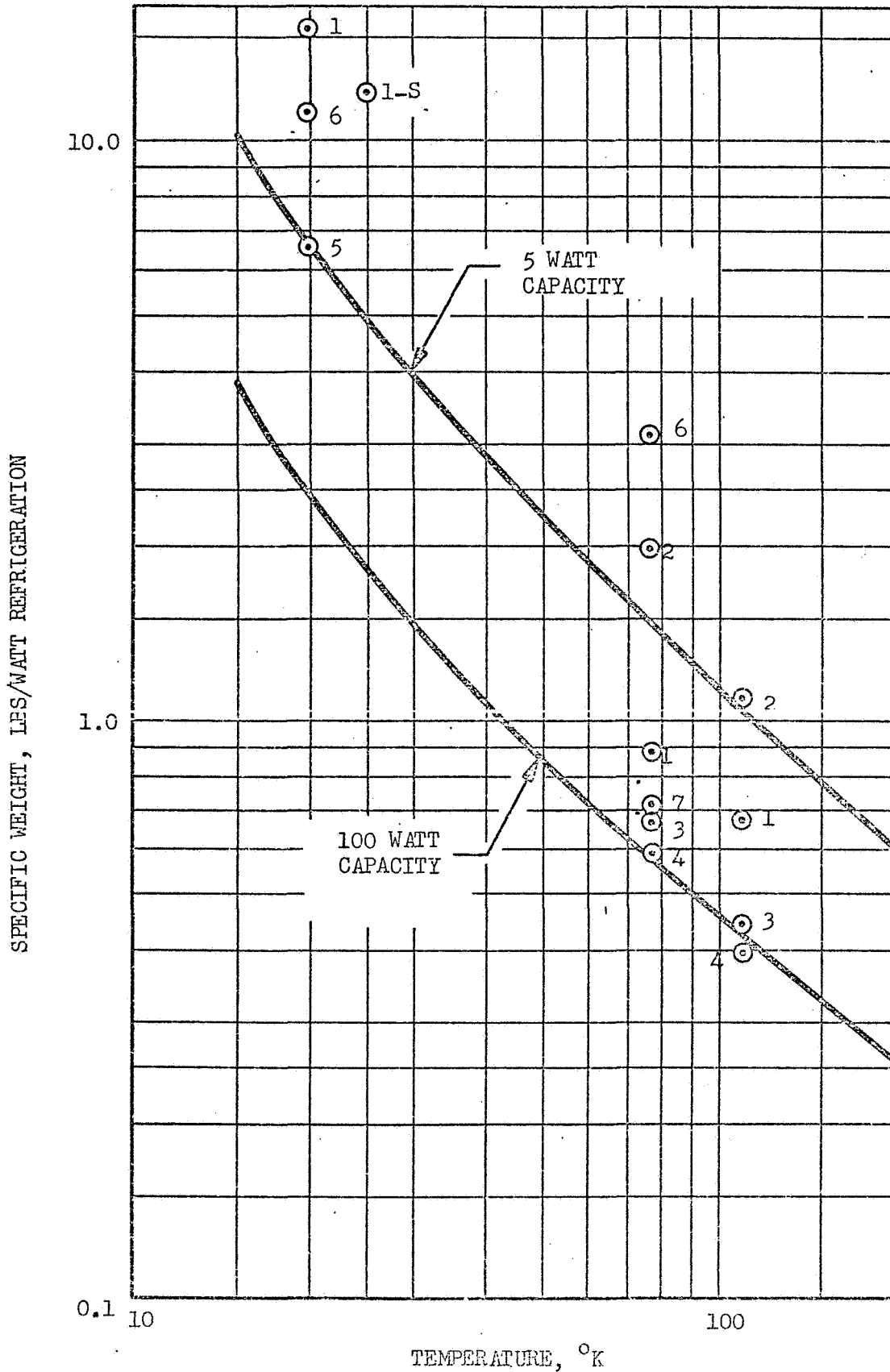
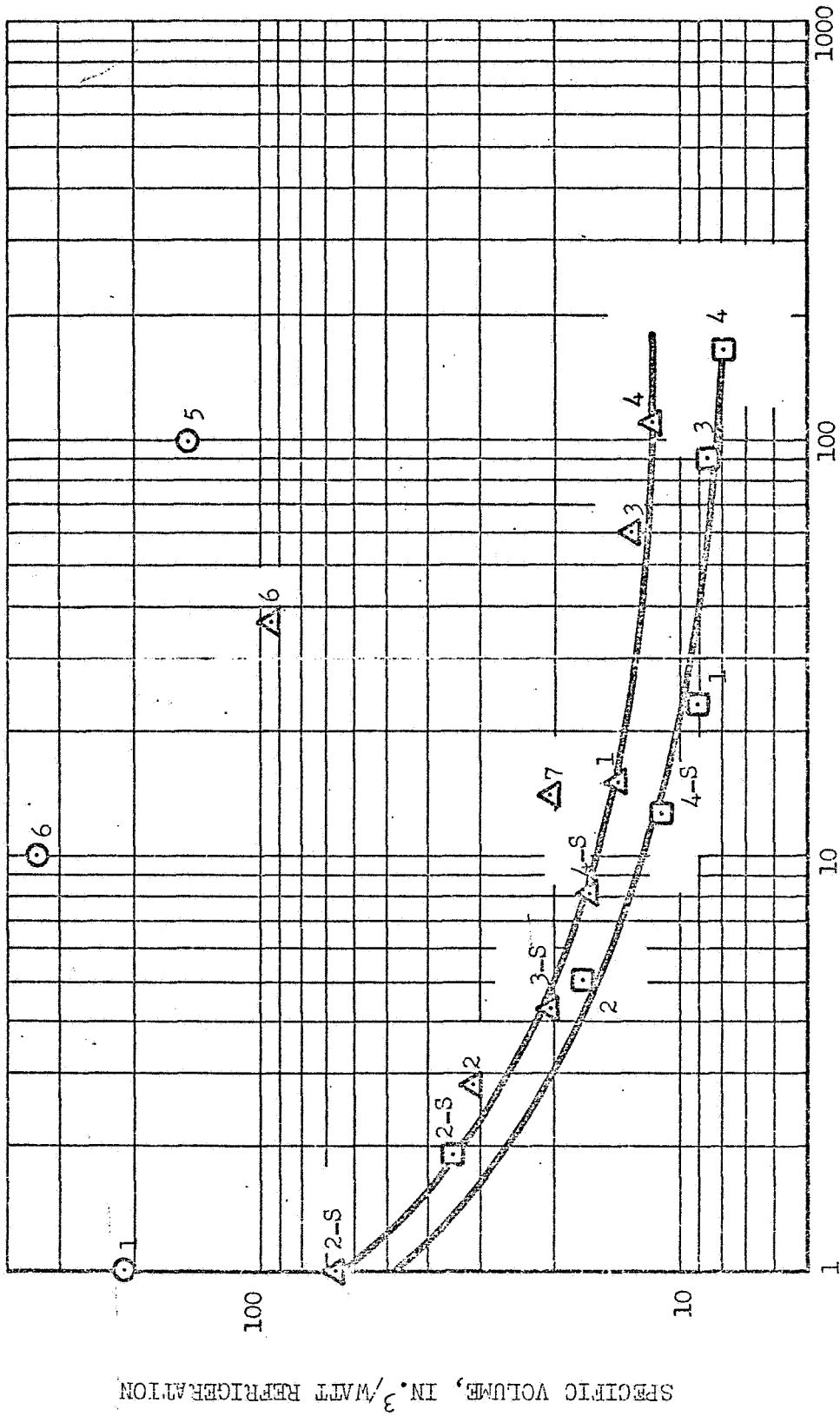


Fig. 3-31 SPECIFIC WEIGHT VERSUS TEMPERATURE (STIRLING CYCLE)



WATTS REFRIGERATION

Fig. 3-32 Specific Volume Versus Refrigeration Load (Stirling Cycle)

SPECIFIC VOLUME, IN³/WATT REFRIGERATION

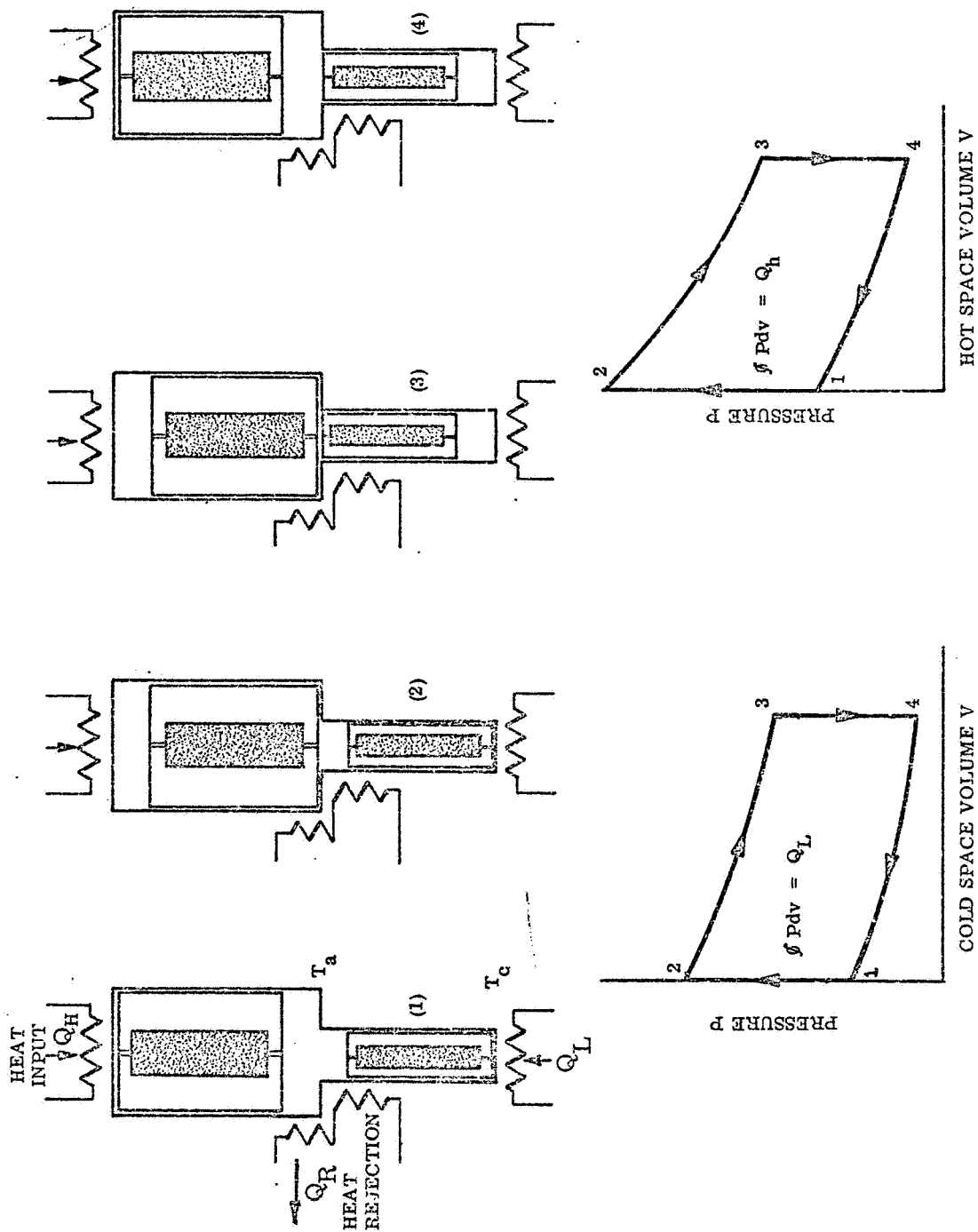


Fig. 3-33 Vuilleumier Cycle

must be greater than the compressive work by a factor equal to the reciprocal of the efficiency of the implied engine.

In practice the intermittent movement of the displacers is achieved by driving both of them from the same crankshaft but displaced in phase such that during compression most of the fluid is in the ambient space, and during expansion most of the fluid is in the cold space.

Thermal analysis of the VM refrigerator is very similar to that of the Stirling refrigerator and all comments made in Section 3.4.1 on this subject apply. Two analytical approaches are possible as in the Stirling case. The VM refrigerator is a constant volume device whereas the Stirling refrigerator changes overall volume at a prescribed rate. Otherwise the same general approach is employed.

In the case of the approximate analysis exactly the same approach is followed in analyzing the hot end as for the cold end, in that the heat input is equal to the gross work performed at the hot end plus the heat leakage to the ambient space. In the VM refrigerator power is supplied as thermal rather than mechanical energy. This required thermal energy, q_h , is given by

$$q_h = \oint_h Pdv + \sum \text{losses}$$

Here, $\oint_h Pdv$ is the gross work performed at the hot end and the losses represent the additional heat which has to be supplied to make good the heat lost by various mechanisms to the environment. The loss mechanisms are qualitatively identical to those occurring in the cold end and listed in Section 3.4.1.

3.4.2.2 Companies Engaged in the Development of Vuilleumier Refrigerators.

VM refrigerators exist only as prototypes with somewhat smaller cooling capacities than in the context of this study. Large size units are currently being designed. Several companies are engaged in the development of miniature units in the range of 0.1 to 2 watts, however, and several prototype units have been built and tested. Many of these units are being developed with the express goal of long term orbital operation. The VM cycle has certain potential advantages over other cycles considered which make it sufficiently interesting to explore for this application, even though its suitability for larger outputs has not been established. The following list summarizes the development efforts known to be currently underway:

Hughes Aircraft Company Inc.: Hughes has been actively engaged in the development of the VM cycle for at least 3 years. Their activities include the fabrication and testing of five prototype units. HAC is preparing to put one of their VM prototype units in space for extended orbital use in the near future. Some of the prototype models developed were under contract to Air Force Flight Dynamics Laboratory, WPAFB, during the period March 1967 to April 1968 (Contract F33615-67-C-1532) (3-19).

Philips Laboratories: Philips Laboratories has built two small prototype units recently and has successfully tested these. The units have been built with the application of military infrared systems in mind, utilizing the quiet operation to advantage (3-18).

AiResearch Manufacturing Co.: AiResearch presently is engaged in a contract (NAS 5-21096) with NASA/Goddard SFC to develop and test a VM cryogenic refrigerator for approximately 5W cooling at 75°K for space-flight usage. The lifetime goal of the system is 2 years to 5 years.

RCA: RCA has been developing a breadboard unit under a company-sponsored program in conjunction with their studies in ICICLE (Integrated Cryogenic Isotope Cooling Engine) for NASA/Goddard SFC.

Submarine Systems (Division of Sterling Electronics): Submarine Systems has recently entered the VM development area. The principal man responsible for this work is Kenneth Cowans, formerly with Hughes Aircraft Company. Work on VM units includes programs under contract to WPAFB for development of a space flight unit and Ft. Belvoir in the area of night vision, Contracts F33615-70-C-1130 and DAAK 02-70-C-0436, respectively. These contracts call for development, fabrication and testing of VM units. In addition, a three stage unit is being built and tested under contract to WPAFB. The unit was designed to operate down to 5°K.

Recently Wright Patterson AFB has funded Hughes and Phillips Laboratories to build larger VM refrigerators of cooling capacities of 2 watts at 15°K plus 40 watts at 35°K.

3.4.2.3 Analysis of Data on Units

Data on prototype units from Hughes and Phillips were the only information available on this recently developed unit. The data for six Hughes prototype

units and two Philips prototype units are presented in Table 3-2.

In drawing the curve fits for the various parameters, the characteristic shape of the curves was based on the more extensive data of the Stirling units, to which the VM cycle is closely related, in areas where specific data on the VM units were lacking.

The coefficient of performance of these units is plotted as a function of refrigeration capacity in Figure 3-34. As shown, the cooling capacity only goes to 2 watts, substantially below the requirements of this study. Figure 3-35 presents the C.O.P. as a function of the refrigeration temperature, and Figure 3-36 presents the percent Carnot efficiency, as a function of refrigeration capacity, showing efficiencies in the range of 1 to 4% for the small prototype units.

Figures 3-37 through 3-39 present the data on specific weight and specific volume for the VM system.

It should be anticipated that since the units are prototype and the development history is quite limited, significant improvements may be forthcoming in the performance of units based on this cycle. The comparison between the performance of this cycle and others is discussed in Section 3.6.

3.4.3 The Joule-Thomson Refrigerator

3.4.3.1 Operation

The practical Joule-Thomson refrigerator is shown in Figure 3-40. The cycle is identical to the Brayton cycle of Figure 3-50 except for one important modification. The expansion process, 4 to 5, is accomplished by isenthalpic expansion through a throttling valve rather than by expansion in a work producing device. Since no expansion work is produced, no heat addition is required in the load exchanger to replenish the lost internal energy of the working fluid. The cycle produces refrigeration by virtue of a useful side effect of non-ideal behavior at the sink temperature. The cooling effect is given by

$$\begin{aligned} q_c &= \dot{m} (h_6 - h_5) \\ &= \dot{m} (h_6 - h_4) \end{aligned}$$

where \dot{m} is the working fluid mass flow rate, and h is enthalpy.

FOLDOUT FRAME

Manufacturer	Hughes Aircraft	Hughes Aircraft	Hughes Aircraft
Trade Name			
Model	Prototype	Prototype	Prototype
I.D. Number	11	12	13
Refrigeration Range	$\approx 77^{\circ}\text{K}$	$\approx 77^{\circ}\text{K}$	15K - 75°K
Cycle	Vuilleumier	Vuilleumier	Vuilleumier
Working Fluid	Helium	Helium	Helium
High Pressure		600 psi	
Low Pressure			
Minimum Temp			
Cool-Down Time	30 min	10 min	30 min
Expander RPM		600	
Volts-Phase-Frequency	28 VDC	28 VDC	28 VDC
Cooling Means	Air	Air	Liquid
Ambient Temp Reqmts		-55°C to 71°C	
Required Attitude	Any	Any	Any
Cryostat Dimensions	7.15 x 7.15 x 8	6.5 x 5.7 x 5.1	10.5 x 13.6
Compressor Dimensions			
System Volume	410 in. ³	190 in. ³	1,110 in. ³
System Weight		5.75 lb	
MTEF		5,000 hr goal	
Maintenance Interval	3,000 hr goal	1,000 hr	10,000 hr goal
Near 20°K	Refrigeration		0.15W at 15°K
	Power Input		370W
	COP		.000405
	% Carnot		0.77%
	Lb/Watt		
	In. ³ /Watt		16,700
77°K	Refrigeration	0.6W	1.5W
	Power Input	60W	200W
	COP	.01	.0075
	% Carnot	2.9%	2.2%
	Lb/Watt		3.83
	In. ³ /Watt	683	127

(1) Same units at two different operating conditions
(2) Based on 350°K ambient

FOLDOUT FRAME 2

Table 3-2

Hughes Aircraft	Hughes Aircraft	Hughes Aircraft	Phillips Lab.	Phillips Lab.	PHL
Prototype	Prototype	Prototype	Prototype	Prototype ⁽¹⁾	Pro
3	14	15	16	17	18
5K - 75°K	25 - 75°K	30 - 75°K	77 - 200°K	7:°K	7
Vuilleumier	Vuilleumier	Vuilleumier	Vuilleumier	Vuilleumier	Vu
Helium	Helium	Helium	Helium	Helium	Hel
		400 psi	23 atm	30 atm	40
30 min	16°K 30 min	30 min	70°K		
23 VDC	115 - 3 - 400	240 28 VDC	450	600	60
Liquid	Liquid	Liquid	Air	Air	Air
Any	Any	Any	Any	Any	Ar
10.5 x 13.6 x 7.8	7.5 x 9.5 x 10"	10.5 x 13.6 x 7.8"	12 x 8 x 6	16.5 x 7.1 x 7.1"	16
1,110 in. ³	712 in. ³	600 in. ³	580 in. ³	820 in. ³	82
		18.1 lb	10.3 lb	15 lb	15
10,000 hr goal	1,000 hr	10,000 hr goal	800 hrs + demonstrated		
0.15W at 15°K	2W at 25°K	0.4W at 20°K			
370W	1,200W	550W			
.000	.00167	.00073			
0.77%	1.84	0.66%			
		45			
16,700	365	2780 (2nd Stage)			
		6W	0.5W	1W	
		500W	70W	120W	
		(1st Stage)	.00715	.00833	
			2.07%	2.9% ⁽²⁾	
			20.6	15	
			1,160	820	

FOLDOUT FRAME 3

LMSC-A981632

Table 3-2 Existing Vuilleumier Prototype Refrigerators (Small Units)

Phillips Lab.	Phillips Lab.	Hughes Aircraft	
Prototype (1)	Prototype (1)	P/N X447525-100 Prototype	
77°K	18 77°K	19 77°K	
Vuilleumier	Vuilleumier	Vuilleumier	
Helium	Helium	Helium	
40 atm	40 atm	600 psi charge press.	
		64°K	
		7 min	
	600	600	
		28 VDC	
	Air	Air	
	Any	Any	
5 x 7.1 x 7.1"	16.5 x 7.1 x 7.1		
108 in. ³	820 in. ³	108 in. ³	
15 lb	15 lb	3.4 lb incl. inverter	
		744 hr +	
2W	2W	1.6W	
191W	191W	163W	
.105	.105	.00983	
3.7% (2)	3.7% (2)	2.85%	
7.5	7.5	2.12	
410	410	67.5	

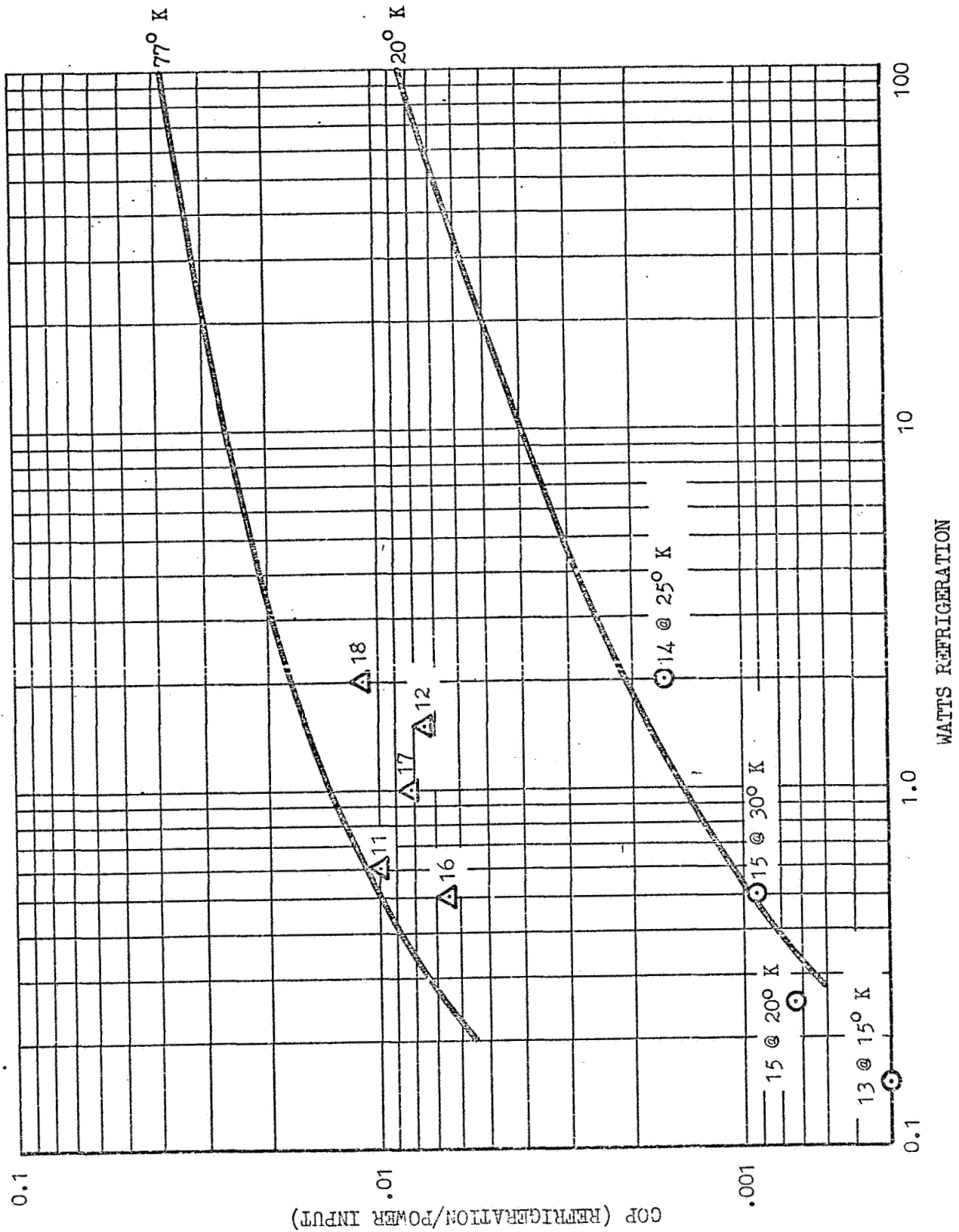


FIG. 3-34, COEFFICIENT OF PERFORMANCE VERSUS COOLING CAPACITY (VUILLEUMIER CYCLE)

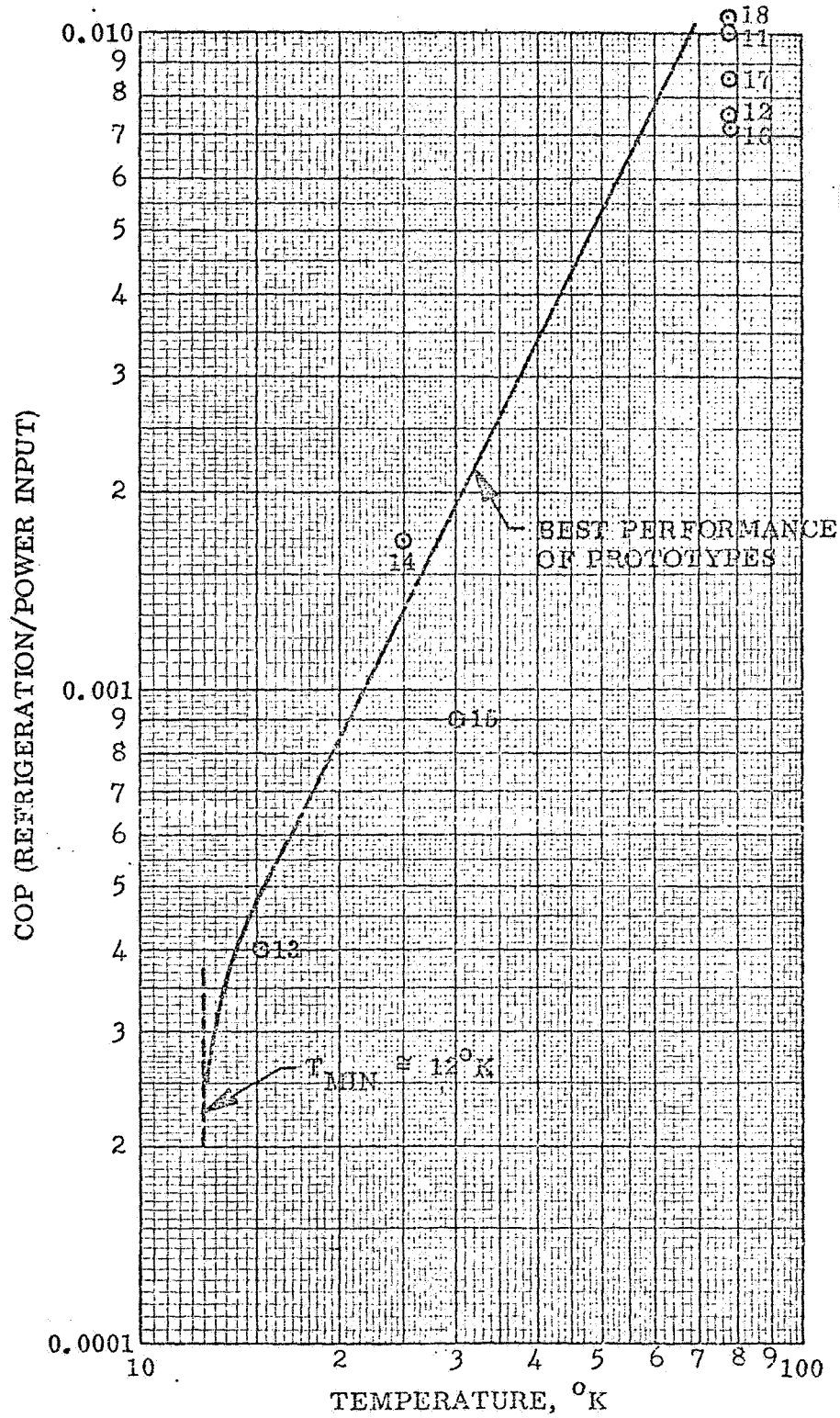


Fig. 3-35 Coefficient of Performance of Prototype Vuilleumier Refrigerators (Small Units)

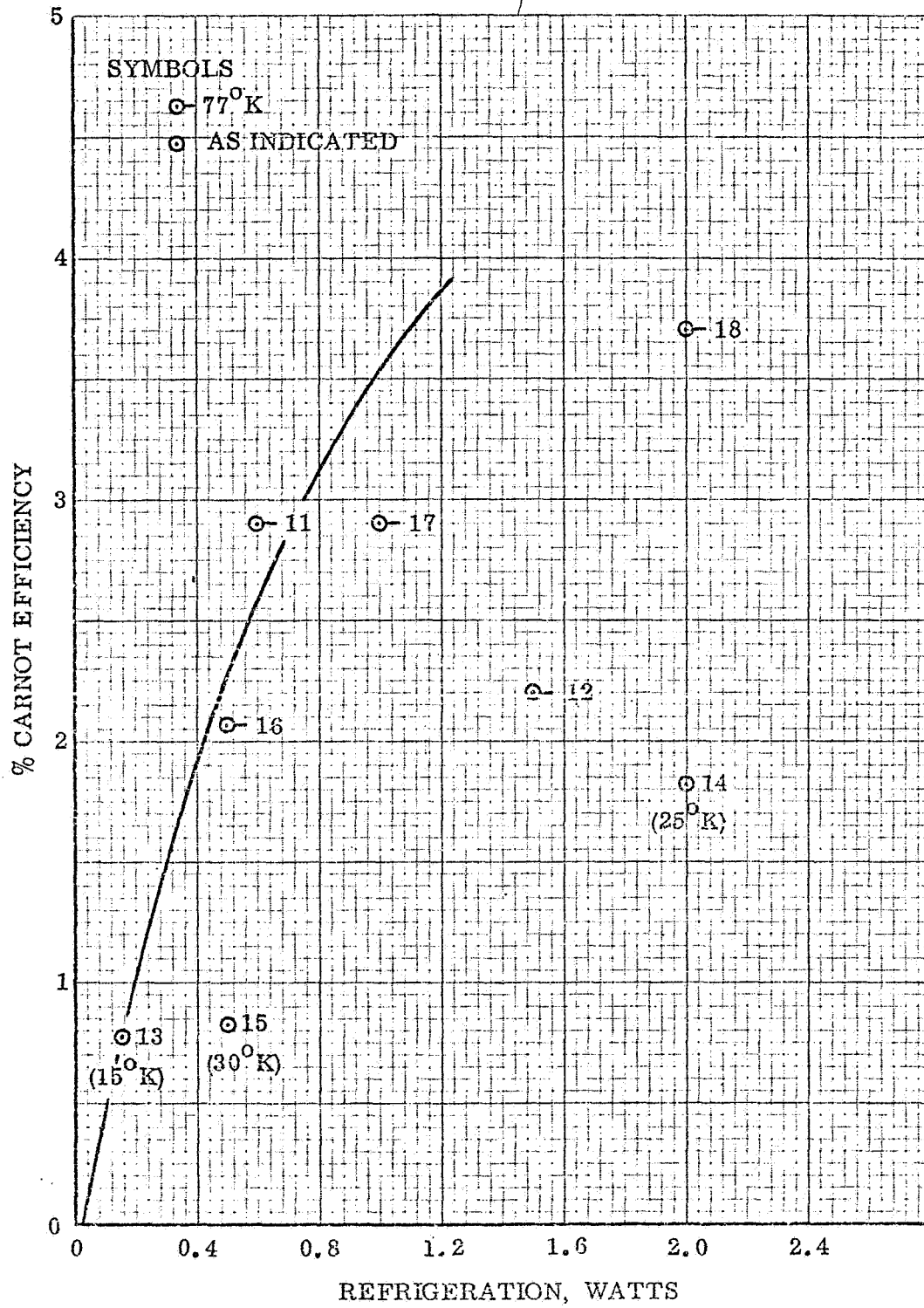


Fig. 3-36 Percent Carnot Efficiency of Vuilleumier Prototype Refrigerators

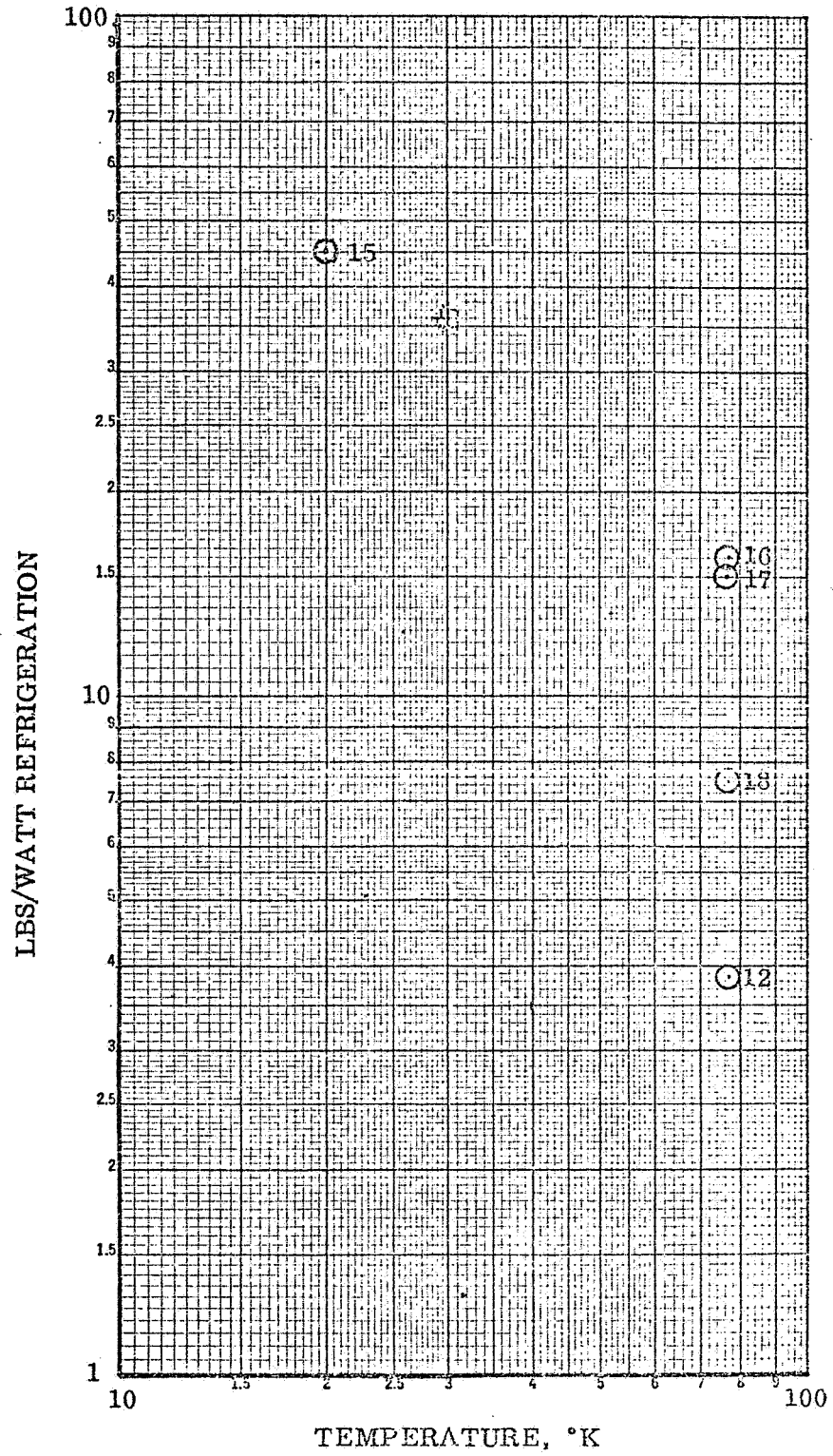


Fig. 3-37 Specific Weight Versus Temperature (Vuilleumier Cycle)

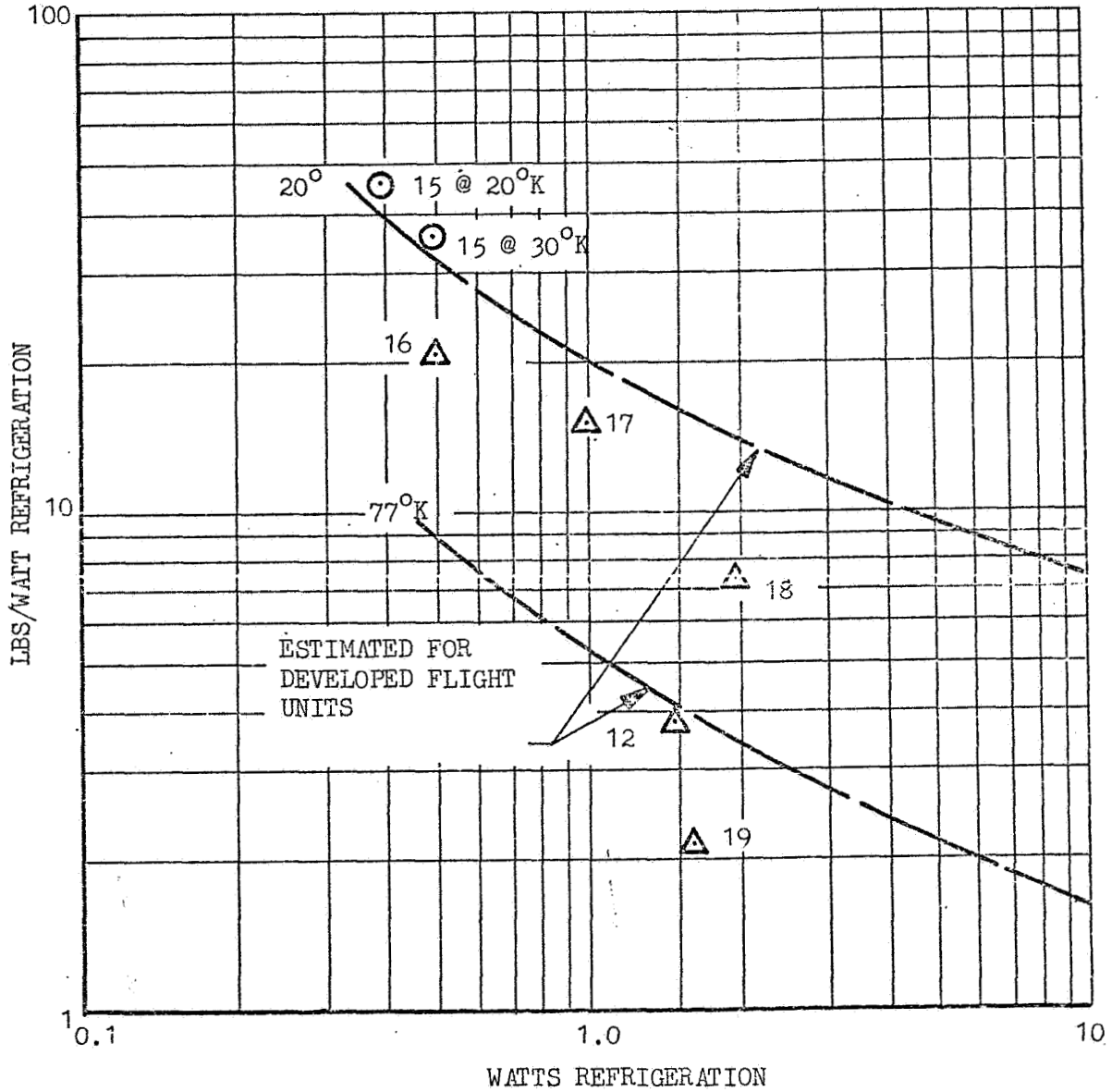


Fig. 3-38 Specific Weight Versus Refrigeration Capacity (Vuilleumier Cycle)

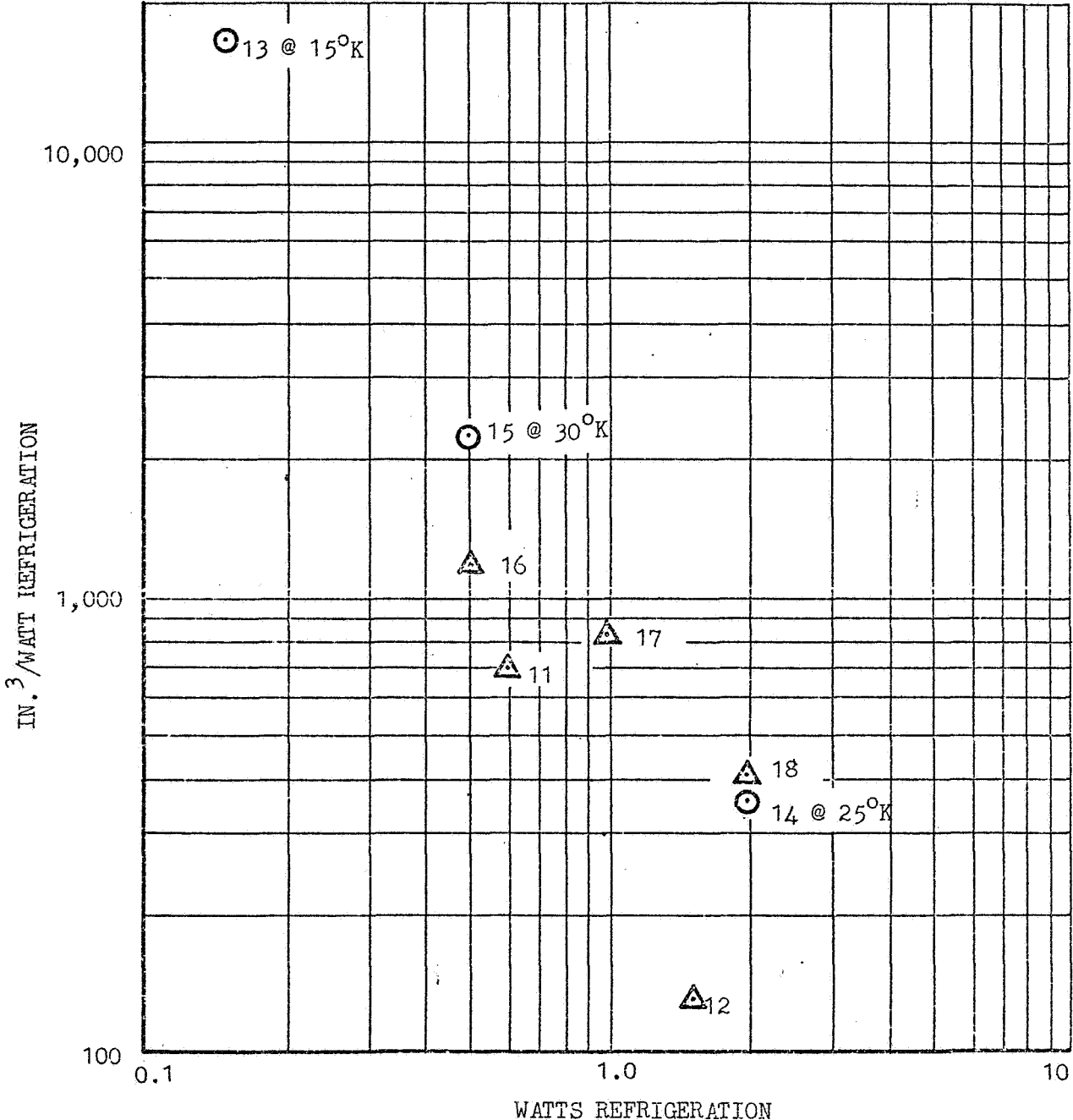


Fig. 3-39 Specific Volume Versus Refrigeration Capacity (Vuilleumier Cycle)

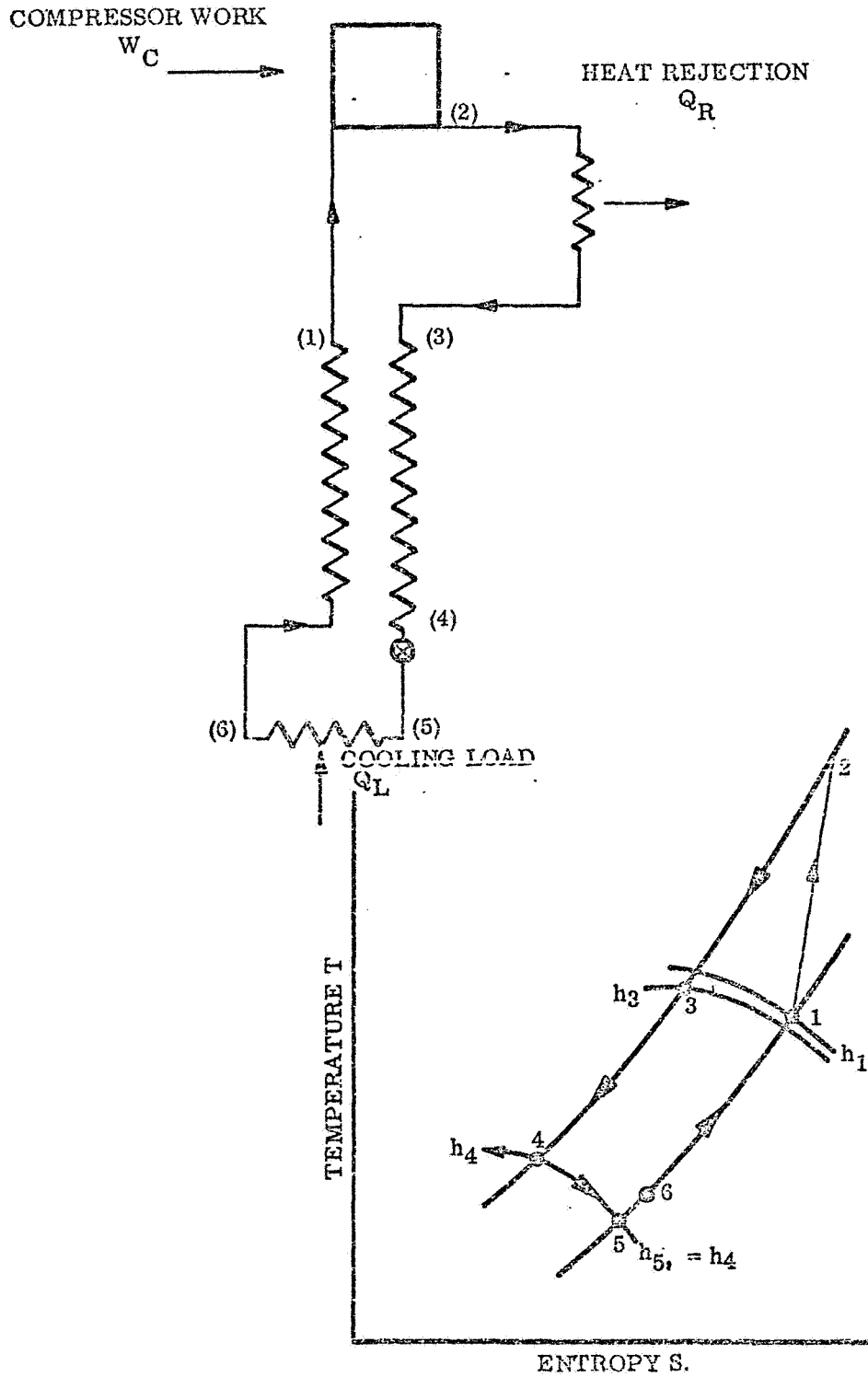


Fig. 3-40 Joule-Thomson Cycle

A heat balance on the main heat exchanger yields

$$h_1 - h_6 = h_3 - h_4$$

Hence:

$$q_c = \dot{m} (h_1 - h_3) \quad (3-12)$$

For q_c to be positive, $(\partial h / \partial p)_{T_3}$ must be negative.

With a 100 percent efficient main heat exchanger

$T_1 = T_3$ and the maximum value of q_c is given by

$$q_c (\text{max}) = \dot{m} [h(P_1 T_3) - h(P_2 T_3)] \quad (3-13)$$

With less than 100 percent efficiency, q_c is given by

$$q_c = \dot{m} [h(P_1 T_1) - h(P_2 T_3)] \quad (3-14)$$

As T_1 is reduced due to less efficient heat exchange, $h(P_1 T_2)$ will decrease and q_c will eventually become zero. The performance of a Joule-Thomson system is therefore limited by the sign and magnitude of $(\partial h / \partial p)_{T_3}$, and by the ability of the main heat exchanger to permit utilization of this effect.

For the present application only nitrogen has both a negative value of $(\partial h / \partial p)_{T_3}$ at normal ambient temperatures and is still a vapor in the temperature range of interest. Those fluids which condense at temperatures lower than nitrogen -- neon, hydrogen, and helium -- can be used for very low temperature Joule-Thomson refrigerators if T_3 is reduced to a point where $(\partial h / \partial p)_{T_3}$ is negative. This can be done by precooling the fluid using another type of refrigeration system. Thus, Joule-Thomson systems can be used in double or triple cascade to obtain cooling in the range of liquid hydrogen or liquid helium temperatures, as shown in Figure 3-41.

The cooling capacity, q_c , of a single-stage Joule-Thomson system is given by

$$q_c = \dot{m} (h_1 - h_3) \quad (3-15)$$

The power required, W , is given by

$$W = \dot{m} (h_2 - h_3) \quad (3-16)$$

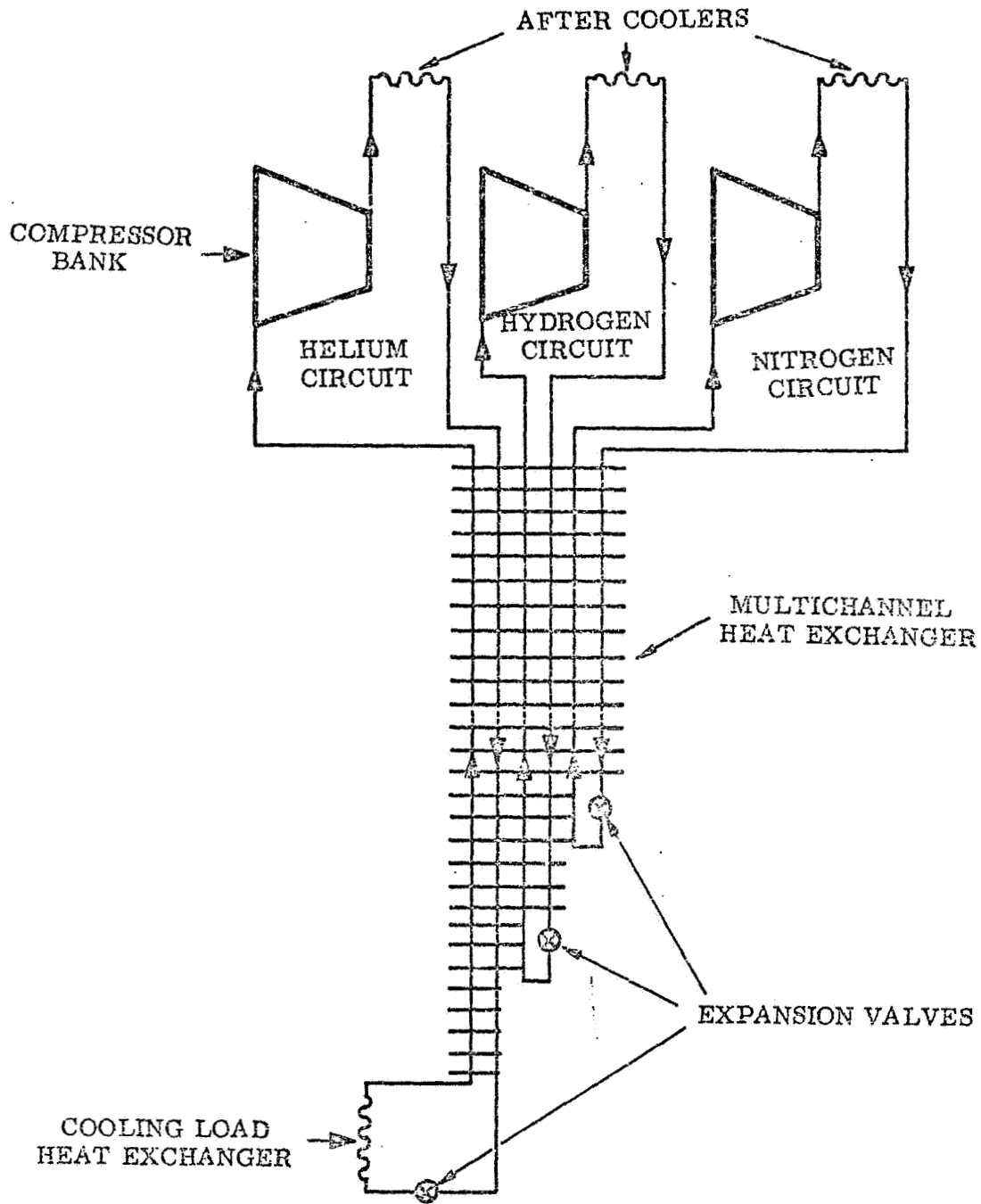


Fig. 3-41 A Three-Fluid Cascaded Joule-Thomson Refrigerator

The significant parameters for assessing the performance of a Joule-Thomson refrigerator are the compression ratio, the gas properties at the warm end, and the heat exchanger effectiveness. Dean and Mann (3-20) present values of W/q_c as a function of these quantities for J-T refrigerators using nitrogen, hydrogen, and helium as working fluid. Available data on closed-cycle systems is sparse and generally limited to a few watts of cooling. The parameters of larger J-T units, in the range of this study, may be obtained by combining the data from this study with the physical dimensions, capacity, and efficiency of practical compressors, and heat exchangers, from Section 3.3.

3.4.3.2 Manufacturers of Joule-Thomson Refrigerators

The following companies are, or have been, engaged in production and development of J-T refrigerator systems:

Air Products and Chemicals, Inc.

AiResearch Manufacturing Co.

Santa Barbara Research Center

Hymatic Engineering Company Ltd.

The majority of J-T units produced by these companies are open-cycle systems, in which the working fluid is supplied by a high-pressure stored gas source. In this usage, only relatively short cooling periods are available. J-T units have been used in space in various applications, but their principal advantage is in providing short-term cooling (i.e., minutes or hours) after extended durations in space. For example, a two-stage J-T unit was supplied by Air Products for cooling of an infrared system on the Mariner missions.

Data on existing closed-cycle J-T units are quite sparse, and there appear to be no production models available which meet the refrigeration requirements of this study. The performance of the closed-cycle J-T system is keyed to the compressor, and data in Section 3.3 can be utilized to make fairly close estimates of the performance which would be expected from closed-cycle J-T systems in the range of 5 - 100 watts.

AiResearch Manufacturing Co.: AiResearch makes several closed-cycle units primarily for use in aircraft. These units use N_2 as the working fluid, and are therefore limited to a lower temperature of $75^\circ K$. These units provide cooling up to 5 watts.

Air Products and Chemicals Inc: APCI produces a wide variety of open-cycle J-T units. In addition, they produce two closed-cycle J-T units, one a single-stage unit to provide 2W at $77^\circ K$, and a two-stage unit which supplies 0.35 W at $23^\circ K$.

Santa Barbara Research Center: SBRC has produced a variety of open-cycle J-T refrigerators and also has produced a single, closed-cycle J-T unit for aircraft use. It is believed that they are not active in the development of closed-cycle J-T systems at this time.

Hymatic Engineering Co., Ltd.: Hymatic Engineering Company specializes in open-cycle-type J-T coolers for infrared detectors. Hymatic has been engaged to a small degree in closed-cycle J-T systems.

Hughes Aircraft Company: Hughes has produced several units in the past for cooling systems on aircraft, but is not now engaged in development of J-T units, and does not produce a unit which is generally available to industry.

3.4.3.3 Discussion of Data on J-T Units

Characteristics of Existing Joule-Thomson Refrigerators Data have been assembled on the characteristics of closed-cycle J-T systems made by five companies. None of these units produces the degree of refrigeration required in this study; however, the data are useful in assessing the relative performance of units.

Complete data on some units were not available, and primarily cover the near $77^\circ K$ temperature range where a single-stage unit with N_2 as the working fluid can be used. Exceptions to this are the two-stage units produced by Air Products which provide cooling to approximately $23^\circ K$, and a unit produced by Fairchild Stratos Corp. The largest cooling capacity of the units is 12 watts.

The data on the closed-cycle systems are tabulated in Table 3-3. The COP of existing closed-cycle units is presented in Fig. 3-42 and 3-43. The ideal performance of a J-T unit operating at near optimum pressure (2400 psi) is also shown for comparison at 75° to 95°K. The system which provides the highest thermodynamic performance (No. 26) delivers about 25% of the ideal performance of the J-T cycle.

A curve fit of the data points was made only at 77°K, and is shown in Fig. 3-43.

Although the maximum theoretical performance of the J-T system is not given by the Carnot efficiency, the % Carnot efficiency vs refrigeration capacity is shown in Fig. 3-44 so that it may be compared with other cycles on the same basis. The plot shows that the J-T systems considered produce approximately 2% of the Carnot efficiency. A considerable improvement should be experienced for units of greater capacity; however, data were not available for large closed-cycle units.

Figure 3-45 shows the specific weight of the units as a function of refrigeration capacity at 77°K only. Figure 3-46 presents the specific volume of three units for which system volume was available.

The Joule-Thompson system is not considered to be a serious candidate for long term space operation because of its low efficiency and highly loaded compressor will not be considered further. It has been included because of its wide usage and hence the need to satisfy the curiosity of those not familiar with its disadvantages.

3.4.4 Split Component Regenerator Refrigerators (Gifford-McMahon, Solvay, and Taconis)

The practical Stirling and VM refrigerators achieve compression, expansion, and heat transfer processes in a single mechanical unit; however, refrigerators can be built which use regenerative exchangers in which the compression, expansion, and heat exchange components are completely separate, if switching valves and surge volumes are used to isolate the time-dependent operation of the exchanger from the operation of the compressor and expander. Valving introduces irreversibility which causes more harm to system efficiency if it occurs at the cold end than at the ambient end. It is therefore possible to conceive a partially split refrigeration system in which the main regenerative heat exchanger, load exchanger and expander operate as one unit, and the compressor as another.

FOLDOUT FRAME

Manufacturer	Garrett AiResearch	Garrett AiResearch	Air P	
Trade Name	None	None	None	
Model	133488	144406	J-80-	
I.D. Number	21	22	23	
Refrigeration Range	≈ 77°K	≈ 77°K	≈ 77°K	
Cycle	J-T	J-T	J-T	
Working Fluid	N ₂	N ₂	N ₂	
High Pressure	155 atm	176 atm		
Low Pressure	1 atm	1 atm		
Minimum Temperature	75°K	75°K	75°K	
Cool-Down Time	12 min	6.5 min	5 min	
Compressor RPM			3,850	
Volts-Phase-Frequency	115/208 - 3 - 400	115/208 - 3 - 400		
Cooling Means	Air	Air	Air	
Ambient Temp. Reqmts.	-40°C to 56°C	-40°C to 71°C		
Required Attitude	Any	Any		
Cryostat Dimensions				
Compressor Dimensions	6.5"D x 12"L (3-stage)		5" x (2-st)	
Cryostat Wt.				
Compressor Wt.				
System Wt.	22.5 lb	19.5 lb	13 lb	
Compressor Volume				
Cryostat Volume				
System Volume	500 in. ³ (est.)	0.45 ft. ³ (777 in. ³)		
MTBF	1,000 hr est	2,000 hr est		
Maintenance Interval	300 and 500 hr	400 hr	500 hr	
System Cost	\$9,000	\$8,000	\$9,000	
23°K 250K	Refrigeration			
	Power Input			
	COP			
	% Carnot			
	Lb/Watt			
77°K	In. ³ /Watt			
	Refrigeration	5W	3W	2W
	Power Input	650W	450W	600W
	COP	.0077	.0067	.0033
	% Carnot	2.23%	1.9%	0.9%
Lb/Watt	4.5	6.5	9	
In. ³ /Watt	100	259		

Table 3-3 Closed Cycle Joule-Thomson Refrigerators (Small Units)

	Air Products	Santa Barbara Research Center	Hughes Aircraft	Fairchild Stratos Corp.	
	None J-30-3500 24 23°K J-T N ₂ and He	None 25 ≈ 79°K J-T N ₂	Prototype 26 77°K J-T N ₂	Prototype 27 ≈ 30°K J-T N ₂ and He	
	3,850 Air	75°K 5 min Air	75°K 5 min	23°K 50 min Air	
12"		7"D x 12.5"L 16 lb	40 lb	52 lb	
	500 hr	0.35 ft. ³ (603 in. ³) 500 hr \$10,000		1765 in. ³ \$15,244	
	0.35W (23°K) 1,050W 0.000333 0.4%			0.5W (25°K) 1,000W .00050 .6% 104 3,520	
		5W 326W .015 4.5% 3.2 121	12W 750W 0.016 4.8% 3.33		

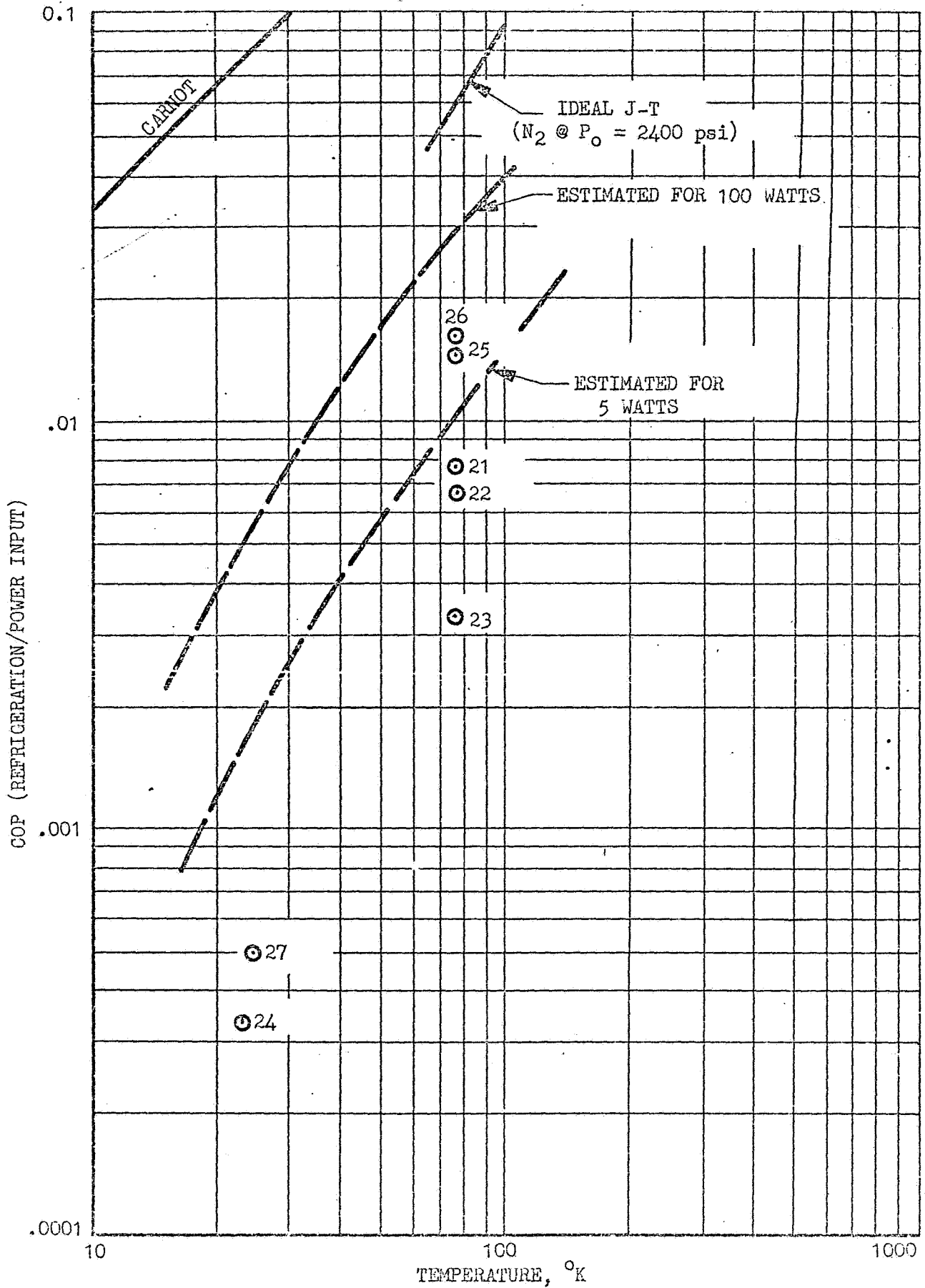
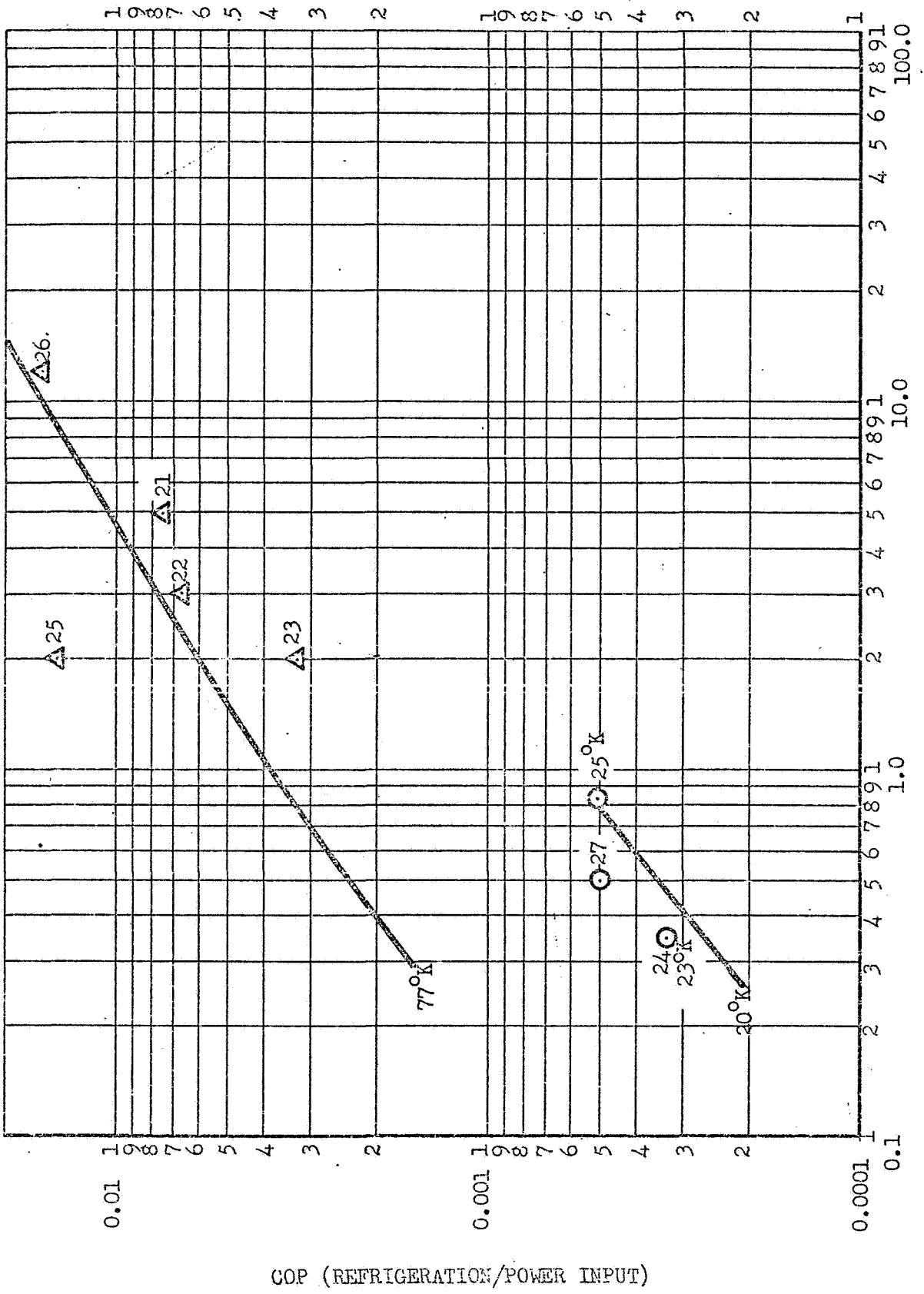


FIG. 3-42, COP VERSUS TEMPERATURE FOR JOULE-THOMSON CLOSED CYCLE SYSTEMS



WATTS REFRIGERATION

Fig. 3-43 C.O.P. VERSUS CAPACITY FOR JOULE-THOMSON CLOSED CYCLE SYSTEMS

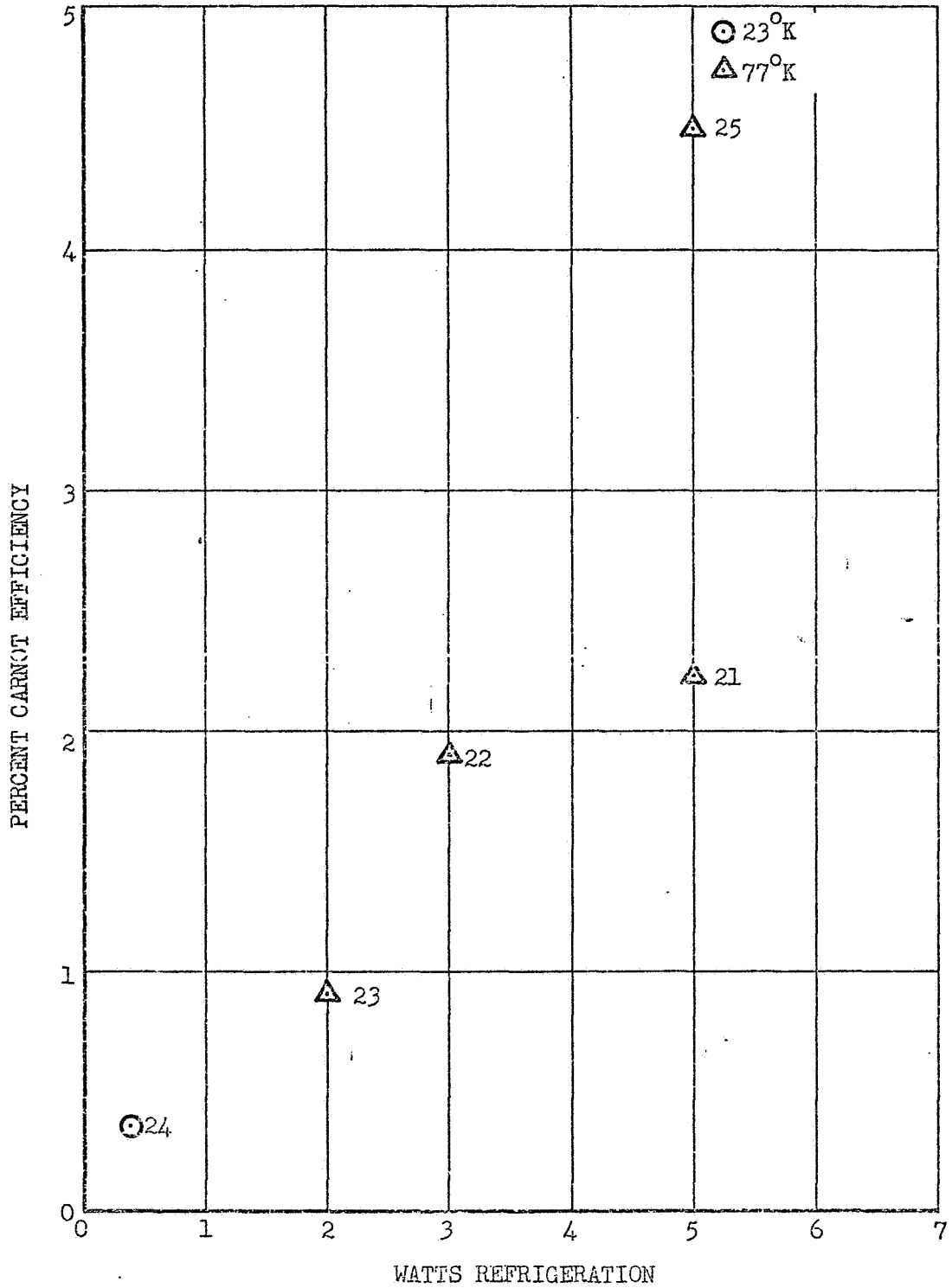


Fig. 3-44 PERCENT CARNOT EFFICIENCY FOR JOULE-THOMSON SYSTEMS

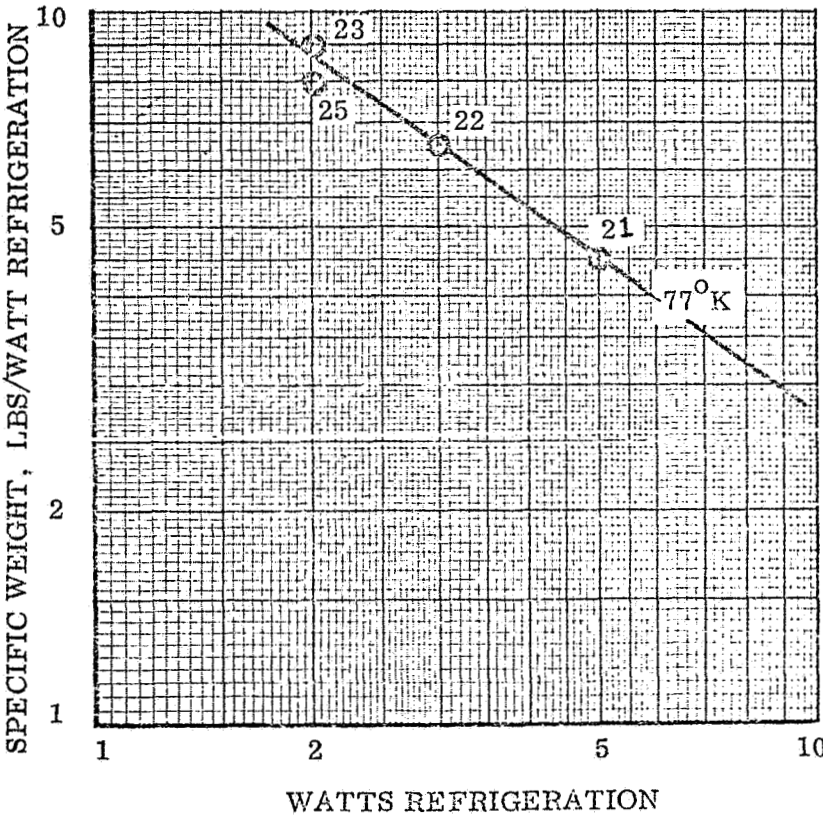


Fig. 3-45 Specific Weight vs. Capacity for Closed Cycle Joule-Thomson Units

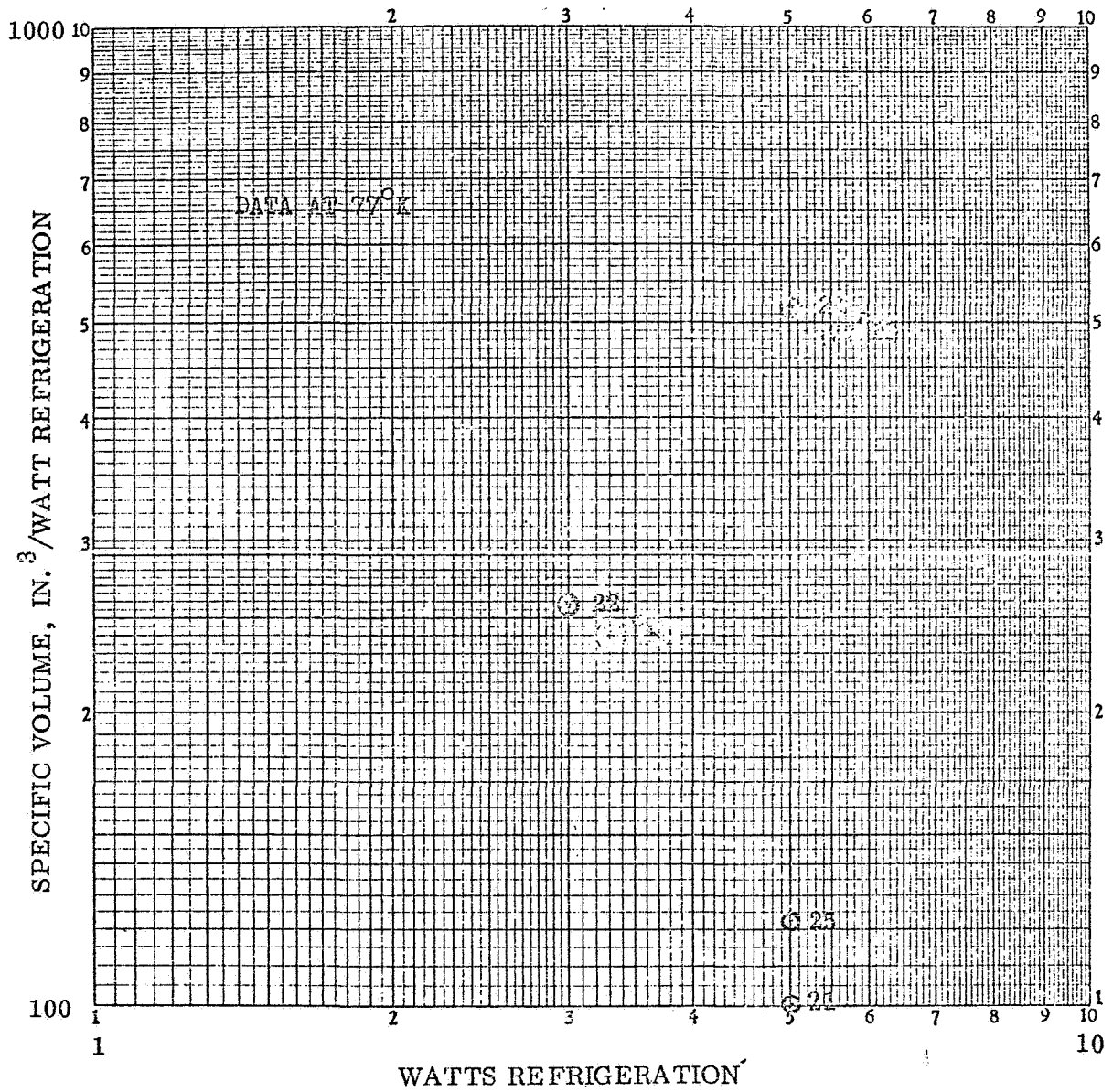


Fig. 3-46 Specific Volume of Closed Cycle Joule-Thomson Units Vs Capacity

Such a system has many practical advantages in that separation of components is achieved, but no low temperature valving is required. Valves and surge tanks are used only at the ambient end. This arrangement permits many areas design freedom by comparison with the Stirling or VM refrigerator. The compressor and heat exchanger-expander interface requirements are confined to working fluid flow rates and pressures. The type of compressor used to supply the working fluid at these rates and pressure can be selected optimally from all possible types - dynamic, positive displacement, or thermal.

The exchanger-expander unit will be very similar to the cold end of a Stirling or a VM refrigerator. With separation, however, there is greater freedom of choice of displacer drive and means of extracting expansion work. By changing the valve timing, the shape of the P-V diagram can be influenced to some degree.

In recent years, this split component system has gained a great deal of popularity. By separating the expander from the compressor, it is possible to construct a system consisting of a simple lightweight compact cooling unit which can be more easily integrated with the load, and a compressor which can be located remotely and connected to the expander with long flexible lines carrying the high- and low-pressure working fluid. Because of this remote location, the compressor design can be optimized for convenience and reliability rather than compactness. Because of the use of valves, the fluid flow is unidirectional and oil separators and filters can be inserted in the gas supply lines, permitting the use of reliable and proven oil-lubricated compressors instead of solid lubricated compressors.

It was noted above that this type of refrigerator permits many design variations to be considered within the same basic concept. Because of this characteristic and the commercial attractiveness of the system, there are many varieties of split-component refrigerators on the market. These systems are basically the same in that they nearly all use modified hermetically-sealed freon compressors, so that the system variations are confined to the method of operating the exchanger-expander unit. However, for reasons of commercial

advertising and patent justification, plus a certain amount of pedantry, a profusion of names has been applied to the individual expander types. They include Taconis, Solvay, and Gifford-McMahon, with and without the adjective "modified." There seems to be some justification for crediting Taconis with first appreciating the full possibilities of this type expander, although many persons have proposed devices using regenerators all the way back to Robert Stirling and earlier. It is outside the scope of this report to establish the correct name for this family of devices. However, there is a tendency to confuse expansion processes with thermodynamic cycles, and this point should be noted.

3.4.4.1 Operation

There are two major techniques for operating exchanger-expanders. One technique is exemplified by the basic Solvay process. In Figure 3-47 the expander consists of an expansion piston connected to the working fluid and the inlet and exhaust valves through a regenerator. In position 1 the inlet valve is open and the exhaust closed. The regenerator and other void volumes are filled to the higher pressure. From 1 to 2, the piston moves outward and working fluid enters the cylinder after first being cooled in the regenerator. At point 2, the inlet valve is closed and the fluid pressure falls until the piston reaches its outermost position. At position 3, the exhaust valve is opened and the fluid in the system expands irreversibly to point 4. From 4 to 5, the piston moves inward, expelling the working fluid from the system after its first being warmed in the regenerator. At 5, the exhaust valve is closed and the piston continues to move until it reaches the innermost position at 6. At position 6, the inlet valve is opened and the fluid in the system is compressed irreversibly from 6 to 1. The valve timing points 2 and 5 can be selected such that compression and expansion are reversible, i.e., position 3 and 4, and 6 and 1 are identical. Alternatively, the valve timing can be chosen so that 2 and 3, and 5 and 6 are identical, maximizing the area of the P-V diagram.

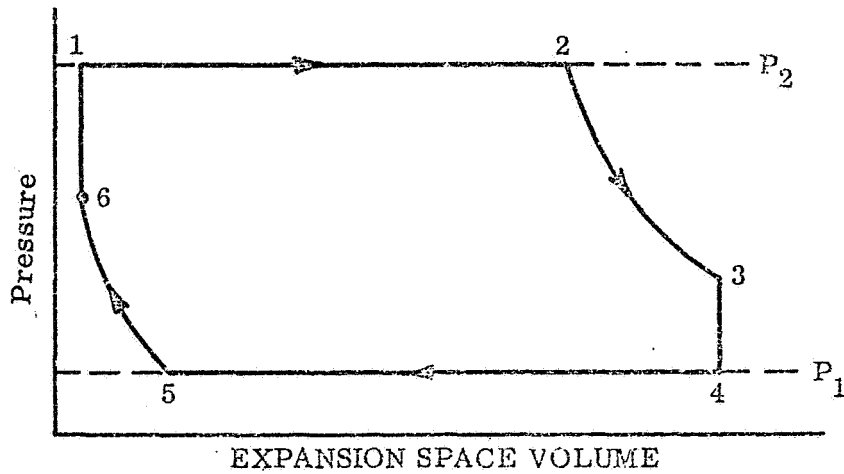
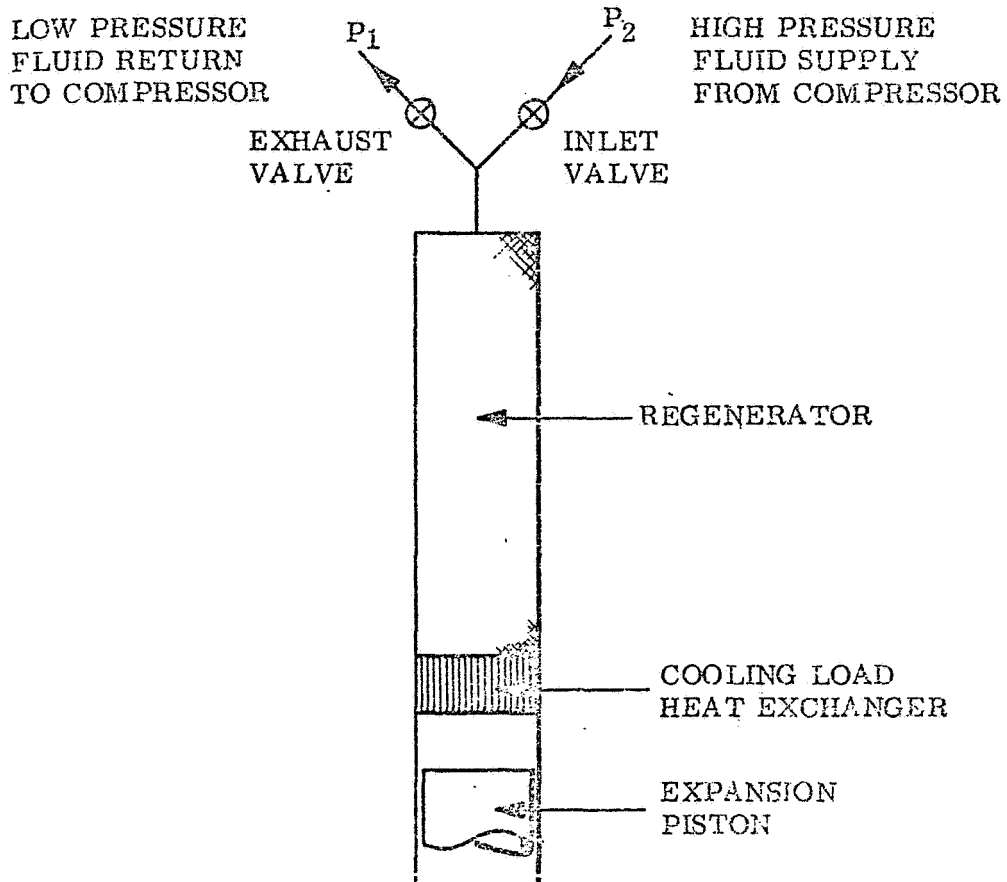


Fig. 3-47 The Solvay Expansion Process

In the Solvay process the work of expansion can be extracted mechanically by connecting the piston to a crank mechanism. Alternatively, the opposite end of the expansion piston can be operated as a compression piston which consumes the expansion work either as work of compression, or in the form of heat, by causing fluid to pass through a throttle valve and heat exchanger.

The other significant expansion technique is the Taconis process (Fig 3-48). The system consists of a cylinder containing a movable displacer. Working fluid can be introduced or rejected from the system via inlet and exhaust valves which communicate directly with the ambient temperature end of the cylinder, and with the cold end through a regenerative heat exchanger. In position 1, the inlet valve is open, the exhaust valve is closed, and the displacer is at the cold end. The ambient space and the regenerator contain high-pressure working fluid. From 1 to 2, the displacer is moved from the cold end to the ambient end, and the cold space fills with high-pressure fluid. At point 2, the inlet valve closes and the displacer continues moving until it reaches the ambient end at 3. The pressure at 3 is lower than at 2 by virtue of the cooling which occurs when fluid is transferred from ambient to cold spaces. At 3, the exhaust valve is opened and the fluid expands irreversibly to 4. At point 4, the displacer is moved back towards the cold end, expelling low-pressure fluid, until the exhaust valve is closed at 5. From 5 to 6, the fluid is compressed by displacement—from cold to ambient spaces. At 6, the displacer is at the cold end and the inlet valve is opened, compressing the gas in the ambient space irreversibly to point 1. As in the case of the Solvay cycle, the valve timing points 2 and 5 can be varied to maximize either cycle efficiency or unit performance.

In the Taconis process the work of expansion is extracted from the system by a somewhat devious route. When the inlet valve is opened the working fluid performs work as it flows into the expander to compress the fluid in the ambient space. When this fluid is displaced to the cold end the heat of compression is deposited in the regenerator. During the exhaust phase, this heat is picked up by the exhausting fluid and removed from the system.

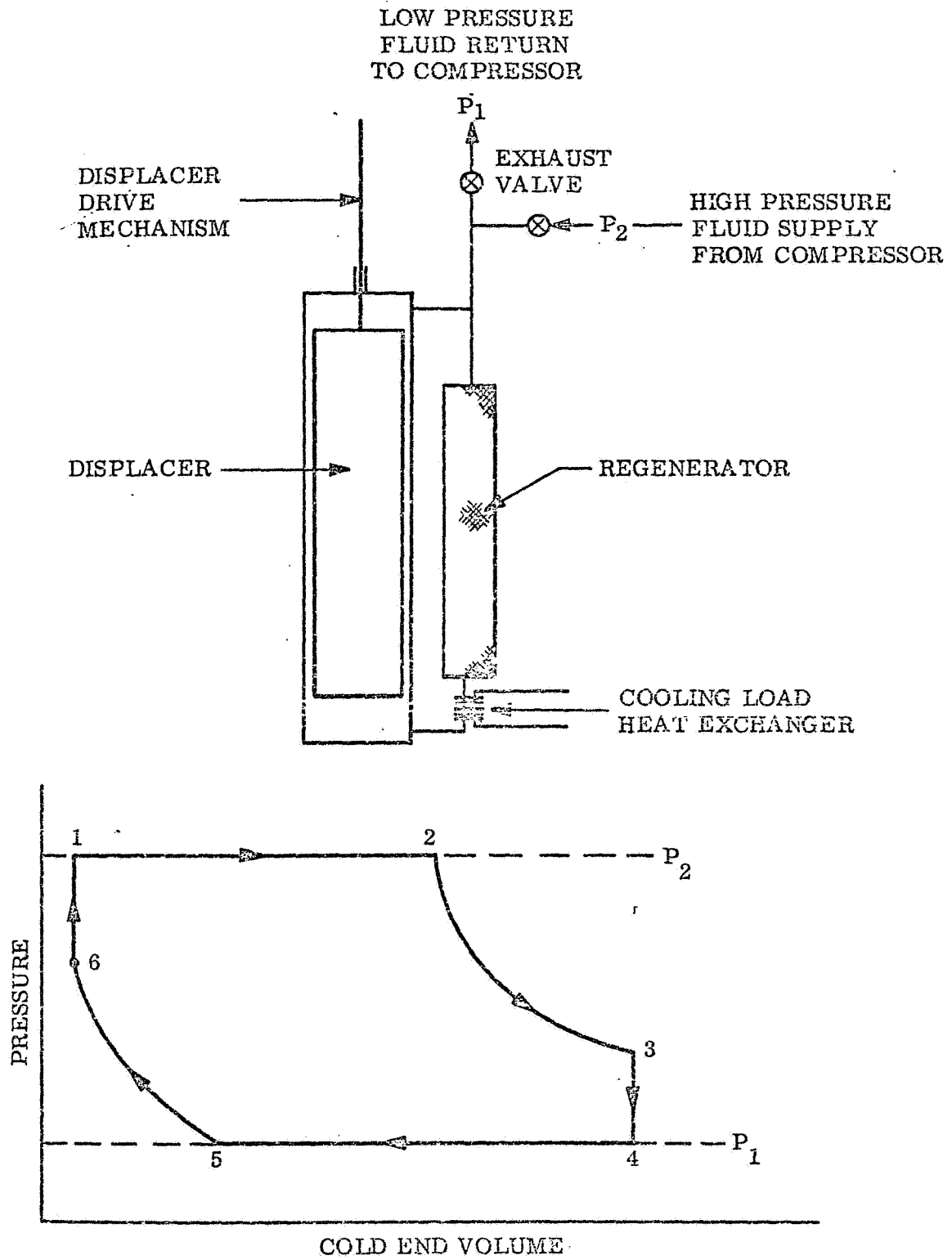


Fig. 3-48 The Taconis Expansion Process

The variations upon the Solvay and Taconis process usually involve valve timing, method of operation of displacer or piston, and geometric configuration.

The thermal analysis of the Taconis process is very similar to that of the Stirling and VM refrigerator in that remarks relating to the complex (differential) and simplified (integral) analysis approaches apply.

In the case of the Taconis expander the boundary conditions differ in that the system is open and the condition of constant mass is replaced by the valve timing and flow rate equations and the specified inlet and exhaust fluid pressures. The work required by the overall cycle comprising compressor and exchanger-expander is equal to the work needed to compress the fluid consumed by the expander.

The boundary conditions for the differential method for the Solvay process analysis will be the motion of the working piston, as governed by the crank mechanism or the dynamics of the free piston-compressor arrangement, and the inlet and exhaust valve timings and fluid inlet and exhaust.

3.4.4.2 Manufacturers of Systems

The following companies are engaged in the manufacture and development of systems which incorporate separate expanders and compressors in conjunction with regenerators.

Cryogenic Technology, Inc.

Cryomech Inc.

Air Products and Chemicals

British Oxygen Co., Ltd.

The Welch Scientific Company

U.S. Philips Corporation

Cryogenic Technology, Inc.: Cryogenic Technology, Inc., evolved from Arthur D. Little, Inc., originally. In 1967, an outgrowth of the activity of ADL was established as 500 Incorporated, a subsidiary of ADL, whose purpose was to produce and market low-temperature equipment. The company name was later changed to Cryogenic Technology, Inc., and established and operated as a

separate company. CTI did the pioneering work in the development of units of this type. Their units have been used since 1959 to provide cooling for amplifiers. Several hundred units of this type have been placed in use and CTI has the largest backlog of experience in this area. CTI produces a standard line of approximately 15 units based on the Gifford-McMahan system, which provide cooling from approximately 10°K to 150°K at capacities of from 1 to 100 watts. Like other manufacturers they utilize freon compressors which have been developed for aircraft service. Some of their units are utilized in aircraft, and these are lightweight, compact units. Extensive data on the system performance is available from CTI, primarily due to their long operating history and this data is readily available.

Cryomech, Inc: Cryomech, Inc. is a small company which was started in 1964 by Dr. W. E. Gifford. Dr. Gifford is a well-known, recognized authority in the field of cryogenic refrigeration and did much of the early development of the system which bears his name. Cryomech has a standard line of seven Gifford-McMahan refrigerators which provide cooling from 7.5°K (minimum temperature) to 200°K at rates from approximately 0.5 to 100 watts. The system uses a standard oil lubricated modified freon compressor.

Air Products and Chemicals, Inc: APCI has recently introduced a new cryogenic refrigerator system based on the modified Solvay system. APCI manufactures four units at present, which include a militarized version utilizing a dry lubricated compressor. These units provide cooling of 1 to 30 watts over a temperature range from 12°K to 200°K .

British Oxygen Co., Ltd.: British Oxygen manufactures a Taconis system unit which has a capacity of 1.5 watts at 16°K .

The Welch Scientific Company: Welch Scientific Company makes a Gifford-McMahan system unit which uses compressed air as the working fluid. The unit is not applicable to requirements here since it is open cycle and does not provide low enough temperature using air as the working fluid. It is closely related to the CTI line of refrigerators.

U.S. Philips Corp: Philips has recently fabricated a Solvay system which was designed for use in aircraft and delivers 0.4 watts at 20°K. It utilizes a dry lubrication compressor and is weight optimized.

3.4.4.3 Discussion of Data on Units

The parameters and operating data for cryogenic refrigerators based on the Gifford-McMahon, modified Solvay and modified Taconis systems are tabulated in Table 3-4. Most of the available units are tabulated, regardless of cooling level.

Figs. 3-49 through 3-53 present net refrigeration capacity vs. temperature for the individual units. Most of the units provide additional cooling on the first stage at approximately 77°K and this feature could be convenient for application to vehicle systems which utilize fuel and oxidizer that require cooling at two temperatures. Data on first stage refrigeration are presented where available. In most cases the first stage cooling exceeds the second stage (lower temperature) cooling. Most manufacturers do not include data on the coupling between first and second stage cooling rates. Second stage cooling rates are reduced as heat loads are introduced on the first stage. This effect is shown in Fig. 3-51 which presents data for Cryomech GB02.

The coefficient of performance of the various machines are presented in Figs. 3-54 to 3-56 vs. refrigeration and temperature. The data are curve fit using the technique as described for the Stirling cycle. The highest values for C.O.P. are shown by the Cryomech units. The minimum temperature achieved by the various units is approximately 7°K. The machines which provide the data on C.O.P. represent a substantial amount of experience, and it is not expected that large improvements in thermal performance will be forthcoming in the near future, although some improvements will almost certainly evolve.

Figs. 3-57 and 3-58 present the system weight per watt of refrigeration (specific weight) vs. temperature and cooling capacity. The data clearly show the effect of both cooling capacity and temperature level. As in the

FOLDOUT FRAME

Cryomech, Inc.	Cryomech, Inc.	Cryomech, Inc.	Cryomech, Inc.	CTI	CTI
None	None	None	None	Cryodyne	Cryodyne
AL01	AL02	GB02	GB12	350	355
31	31	32	33	34	35
23 - 150°K	23 - 150°K	7.5 - 150°K	9 - 150°K	15 - 150°K	15 - 150°K
G-M	G-M	G-M	G-M	G-M	G-M
He	He	He	He	He	He
24 atm	24 atm	24 atm	24 atm	185 psi	275 psi
10 atm	10 atm	10 atm	10 atm	65 psi	75 psi
23°K	23°K	7.5°K	9°K	15°K	15°K
25 min	25 min	25 min	35 min	45 min	35 min
144	144	144	144	72	82
220 - 1 - 50/60	220 - 1 - 50/60	220 - 1 - 50/60	220 - 1 - 50/60	200/300 - 1 - 50/60	200/400
Air	Air	Air	Air	Air	Air
NI	NI	NI	NI	-25°F - +125°F	-25°F - +125°F
Cryostat any	Cryostat any	Cryostat any	Cryostat any	Cryostat any	Cryostat any
5 x 5 x 13	5 x 5 x 13	5 x 5 x 21	5 x 5 x 24	19 x 5 x 9	18 x 5 x 9
29W x 19 x 27H	29W x 19 x 27H	29 x 19 x 27	29 x 19 x 27	28 x 17 x 16	41 x 27
15,350	15,350	15,420	15,500	8,460	29,200
175 lb	175 lb	175 lb	175 lb	175 lb	425 lb
25 lb	25 lb	25 lb	25 lb	22 lb	22 lb
300 lb	300 lb	200 lb	200 lb	229 lb ⁽²⁾	468 lb
5000	5000	5000	5000	10,050	10,000
3000/1500	3000/1500	3000/1500	3000/1500	3000/3000/6000	3000/3000
\$10,290	\$10,290	\$13,200	\$13,200	\$13,000	\$16,000
		2.4W	3.4W		
		3000W	3000W		
		.0008	.00113		
		1.92%	2.5%		
		83	59		
		6430	4560		
		4.0W	6.0W		1.5W
		3000W	3000W		560W
		.0013	.0020		.0001
		2.47%	3.8%		0.2%
		50	33.3		468
		3860	2580		29,200
2.5W @ 25°K		5.5W	8W	3W (2nd Stage)	5W (1st Stage)
3000W		3000W	3000W	2100W	5000W
.0011		.00184	.00267	.00143	.0001
1.1%		2.57%	3.7%	2%	1.2%
36.4		36.4	25	76	93
2200		2200	1940	2220	5720
	754			5W (1st Stage)	5W (1st Stage)
	3000W			2100W	5000W
	.025				
	7.2%				
	2.67				
	8.7W				
	3000W				
	.0247				
	4.7%				
	102				

FOLDOUT FRAME 2

CTI	CTI	CTI	CTI	Air Products	Air Products	Air Products
Cryodyne 350 34 15 - 150°K G-M He 185 65 psi 15°K 45 min 72 200/300 - 1 - 50/60	Cryodyne 355 35 15 - 150°K G-M He 275 psi 75 psi 15°K 35 min 82 208/440 - 3 - 50/60	Cryodyne 1020 36 13 - 150°K G-M He 275 psi 75 psi 13°K 50 min 82 208/400 - 3 - 40/60	Cryodyne 10077 38 30 - 150°K G-M He 300 psi 100 psi 25°K 30 min 82 208/440 - 3 - 50/60	Displex CS-102 38 30 - 300°K Mod. Solvay He 320 psig 115 psig 30°K 20 min 144 208/440 - 3 - 60	Displex CS-202 30-S 12°K - 300°K Mod. Solvay He 12°K 45 min 115V - 50/60	Displex (Airtone) 31-S 77°K - 1 Mod. Solvay He 290 psi 90 psi NI 5 min 385 NI
Air -25°F - +125°F Cryostat any 19 x 5 x 9 28 x 17 x 16 8,460	Air -25°F - +125°F Cryostat any 18 x 10 x 6 41 x 27 x 26 29,900	Air -25°F - +125°F Cryostat any 20 x 13 x 8 41 x 27 x 26 30,880	Air -25°F - +125°F Cryostat any 16.5 x 13 x 8 41 x 27 x 26 30,500	Air 40 - 110°F Cryostat any 4D x 19L 22 x 17 x 15 5,600	Air 40 - 110°F Cryostat any 4D x 17L 22 x 17 x 15 5,700	Air 65°C Any 0.5" x 1.7D x 5.0 x 5. 202
175 lb 22 lb 229 lb(2) 10,000 3000/3000/6000 \$13,000	425 lb 22 lb 468 lb(2) 10,000 3000/3000/6000 \$16,000	425 lb 33 lb 488 lb(2) 13,000 3000/3000/6000 \$17,000	425 lb 30 lb 420 lb(2) 14,000 3000/3000/6000 \$18,000	150 lb 10.6 lb 161 lb 3000 - 5000 est 3000/6000 \$7,000	150 lb 10.6 lb 161 lb 3000 - 5000 est 3000/6000	7.5 lb 3.5 lb 11 lb 26.12/2 1200
	1.0W 5600W .00018 0.32% 468 29,900	4.6 5600 .00082 1.45% 106 6720			0.7W 1735W .00040 0.77% 230 8150	
3W (2nd Stage) 2100W .00143 2% 76 28.0	5W (2nd Stage) 5600W .00089 1.2% 93 5920	11W (2nd Stage) 5600W .00197 2.7% 44 2810			1.5W (load station) 1735W .00026 1.2% 197 3800	
5W (1st Stage) 2100W	5W (1st Stage) 5600W	10W (1st Stage) 5600W	100W 5600W .0179 5.4% 4.8 205	17W 1700W .01 2.9% 9.5 370		
				22W 1700W .015 2.9% 7.2 255		

FOLDOUT FRAME

FOLDOUT FRAME 3

Air Products	Air Products	Cryomech, Inc.	Cryomech, Inc.	CTI	CTI
Displex (Airborne) 31-S 77°K - 150°K Mod. Solvay He 100 psi 100 psi NI 5 min 385 NI	Displex CS-1003 32-S 77°K - 150°K Mod. Solvay He NI NI NI 5 min 400 NI	None DT01 33-S 15°K - 150°K G-M He 24 atm 10 atm 23°K NI 144 220 - 1 - 50/60	None GB05 34-S 15°K G-M He 24 atm 10 atm NI NI 144 220 - 1 - 50/60	Cryodyne 0120 35-S 17.5°K - 150°K G-M He 17.5°K 10 - 15 min Ref. 200 - 3 - 400 Comp 208 - 3 - 400	Cryodyne 0110 36-S 6.5°K - 150°K G-M He 6.5°K 240 min Ref. 130 - 1 - 50/60 Comp 208 - 3 - 400
Air 65°C Any 0.5"D x 3.0"L 1.7"D x 5.7"L (4) 5.0 x 5.5 x 7.2 202	Air 80°F Any 0.5"D x 4.8"L 2.5"D x 5.4"L (4) 15.2" x 21.8 x 11.1 3,720	Air NI Cryostat any	Air NI Cryostat any	Air -63°F - +131°F Cryostat any 10 x 20 x 10 10 x 4 x 8 270 in ³	Air -25 - +125°F Cryostat any 10 x 20 x 21 26 x 17 x 17 7500 in ³
7.5 lb 3.5 lb 11 lb 26312/2156/8493 1200	65 lb 2 lb 67 lb NI 4500/4500	35 lb 4 lb 39 lb 5000 3000/1500	75 lb 6 lb 81 lb 5000 3000/1500	20 lb 5 lb 25 lb 10,000 3000/500/2000 \$10,000	175 lb 30 lb 205 lb 10,000 3000/3000/2000 \$23,000
					1.6W 2100W .000763 1.07% 128 4750
			1.0W 900W .0011 2.1% 81		2.4W 2100W .00114 2.2% 117
		0.5W @ 25°K 600W .00083 .32% 78		0.5W 680W .00073 1.0% 50 510	
1.5W 30W .0024 1.08% 7.3 135	1.0W 50W .002 .58% 67 3720				

FOLDOUT FRAME 4

PRECEDING PAGE BLANK NOT FILMED

LMSC-A981632

Table 3-4. Existing Gifford-McMahon Refrigerators

CTI	CTI	Phillips	British Oxygen
Cryodyne 0110 36-S 6.5°K - 150°K G-M He 6.5°K 240 min Ref. 130 - 1 - 50/60 Comp. 208/130 - 1 - 50/60	Cryodyne 20 37-S 19.0° - 150°K G-M He 19.0°K less than 15 min 115/100 - 1 - 60/50	Airborne P/N 460217 36-S 16 - 100°K Solvay He 16°K 20 min (75 gms cu) 115 - 3 - 400	None IR16 - Mk II 39-S 12 - 22°K Mod. Taconis He 20 atm 10 atm 12°K 40 min 166 RPM 240 - 1 - 50
Air -25 - +125°F Cryostat any 10 x 20 x 21 26 x 17 x 17 7600 in ³	Air +40 to +110°F Cryostat any 3.5D x 7 x 11.2 13 x 13 x 19 3280	Air NI Any 3" x 5" x 12" 5 x 7.5 x 9" 517 in ³	Air and Water 30°C Cryostat any 8"D x 13"L 36" x 21" x 27" 21,000 in ³
175 lb 30 lb 205 lb 10,000 3000/3000/6000 \$23,000	70 lb 11 lb 81 lb 10,000 3000/3000/6000	9.5 lb 5.5 lb 15.0 lb 2,000 2,000	240 lb 20 lb 260 lb NI \$9,100
1.6W 2100W .000763 1.07% 128 4750			
2.4W 2100W .00114 2.2% 117			0.7W 2640W .000265 0.51% 372 30,000
	0.2W 1000W .0002 0.27% 405 16,400	0.4W 639W .000627 .85% 37.5 1300	2.5W 2640W .000950 1.3% 104 3400
		3.3W 639W .00095 1.73% 3.9% 136	

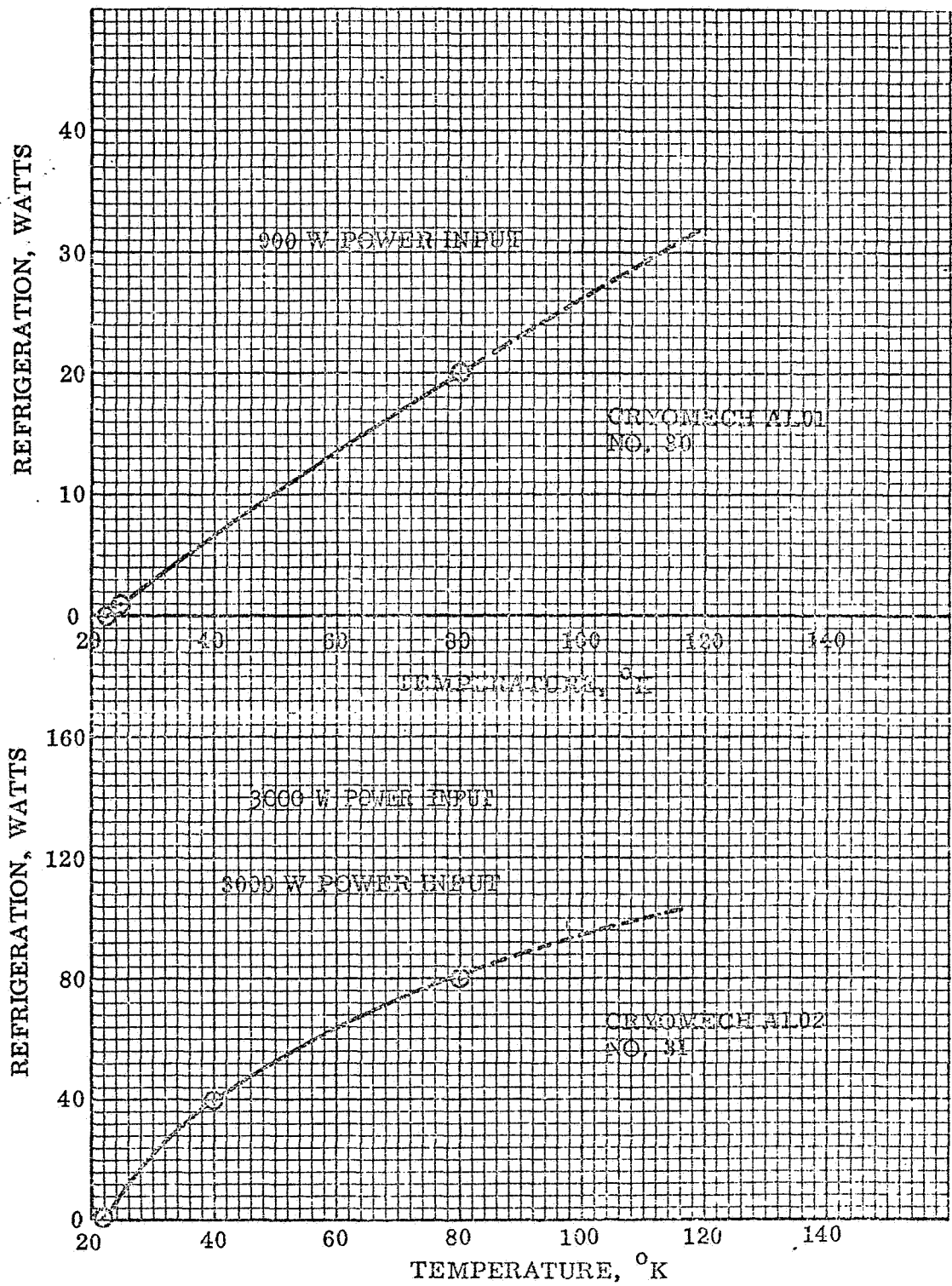


Fig. 3-49 Refrigeration vs. Temperature (Gifford-McMahon Cycle)

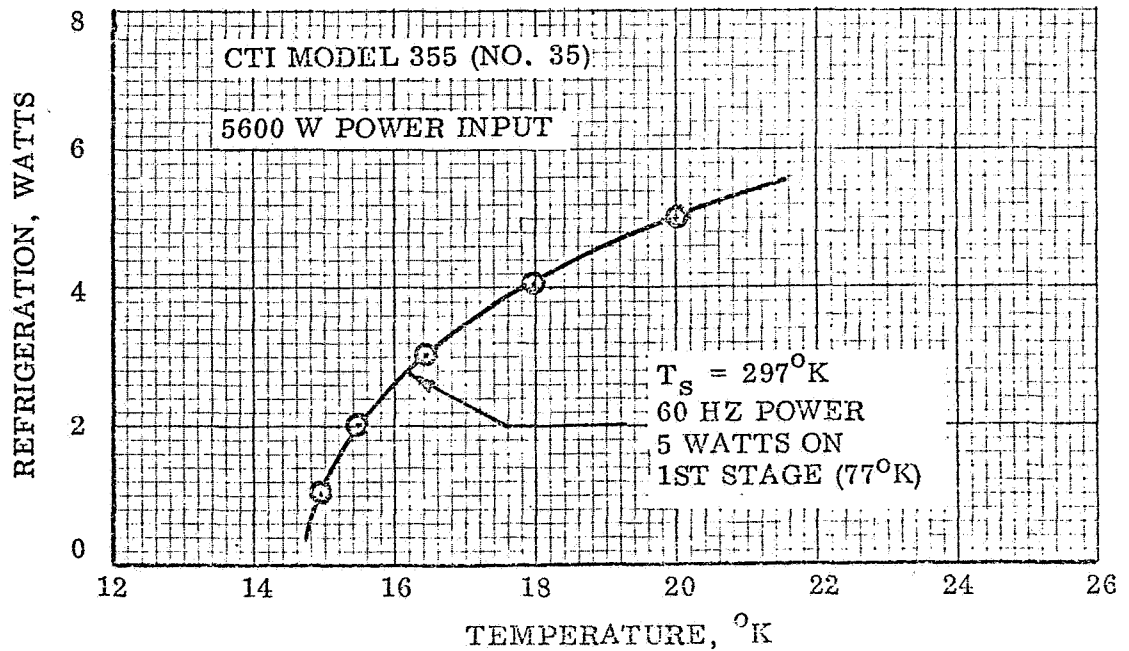
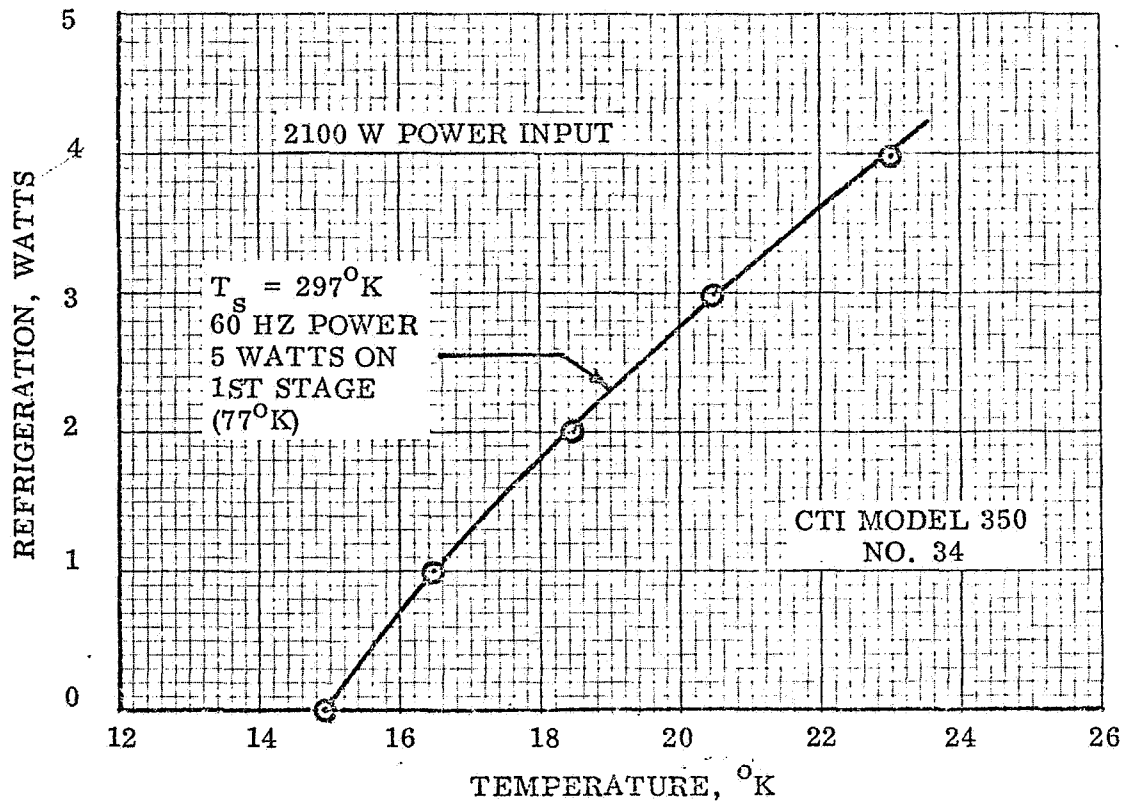


Fig. 3-50 Refrigeration vs. Temperature (Gifford-McMahon Units)

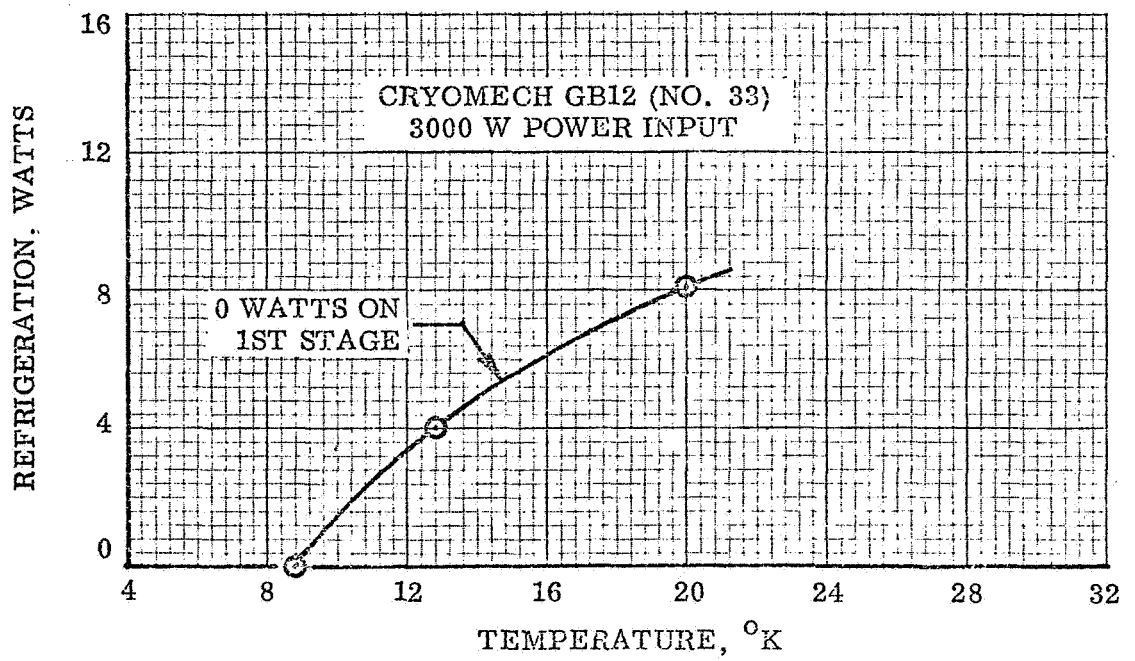
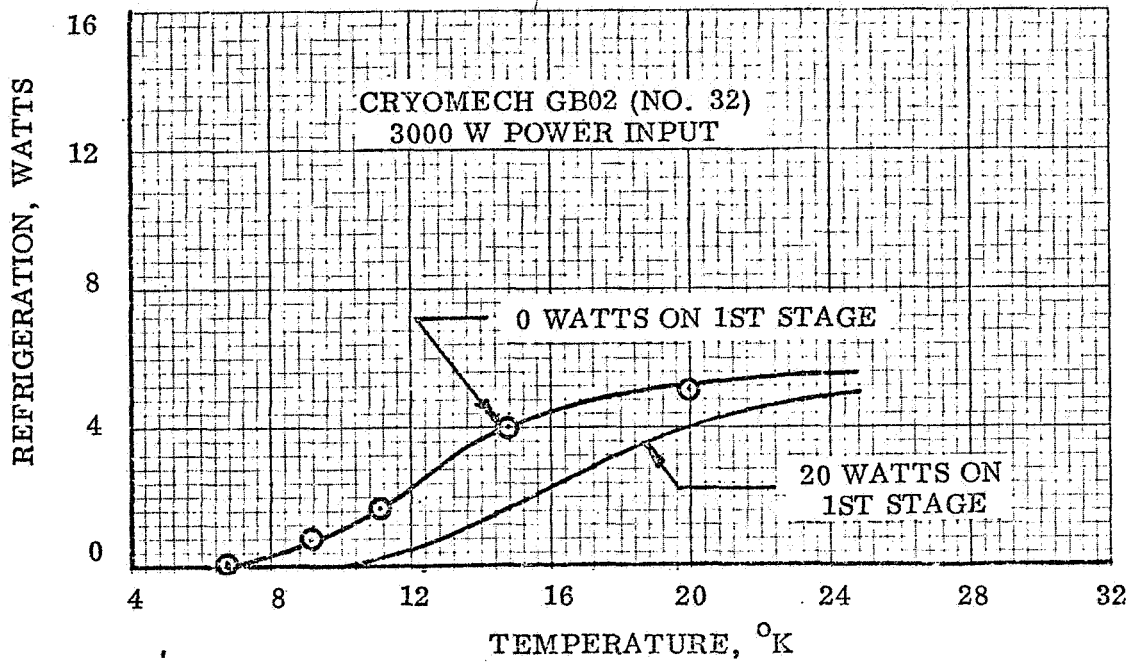


Fig. 3-51 Refrigeration vs. Temperature (Gifford McMahon Units)

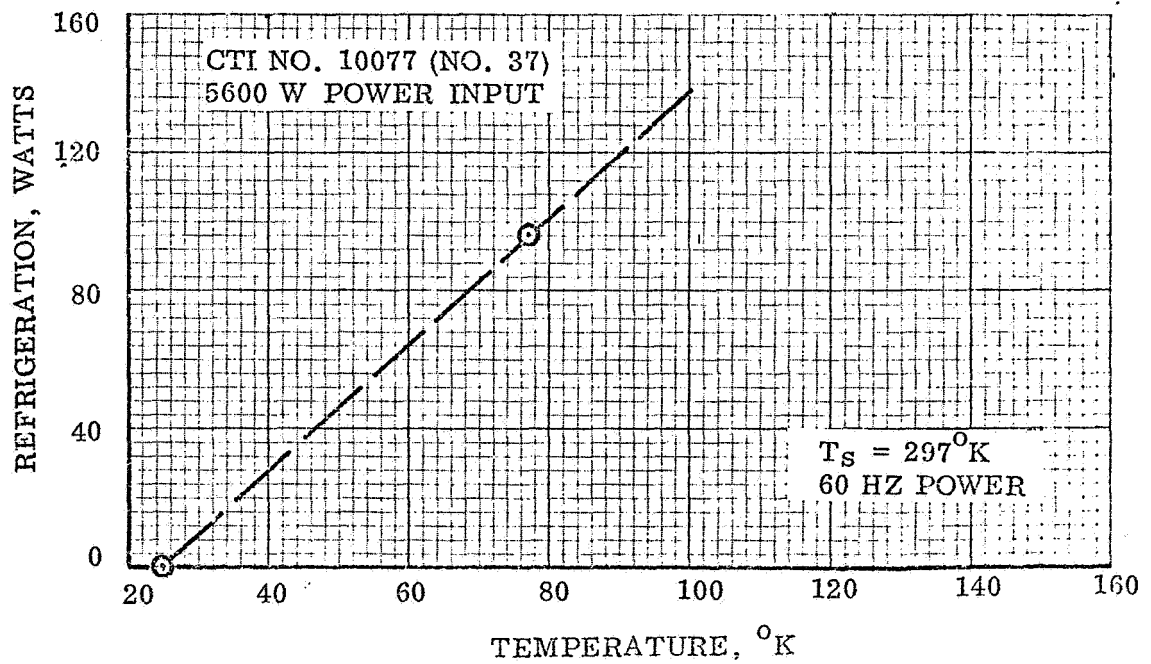
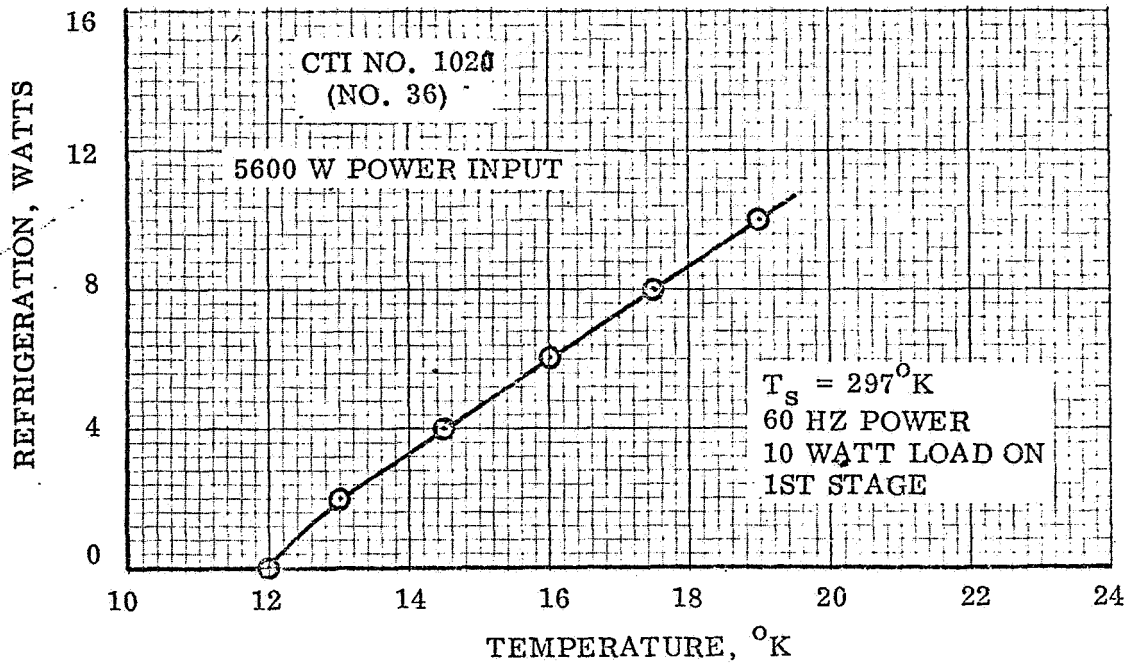


Fig. 3-52 Refrigeration vs. Temperature (Gifford-McMahon Units)

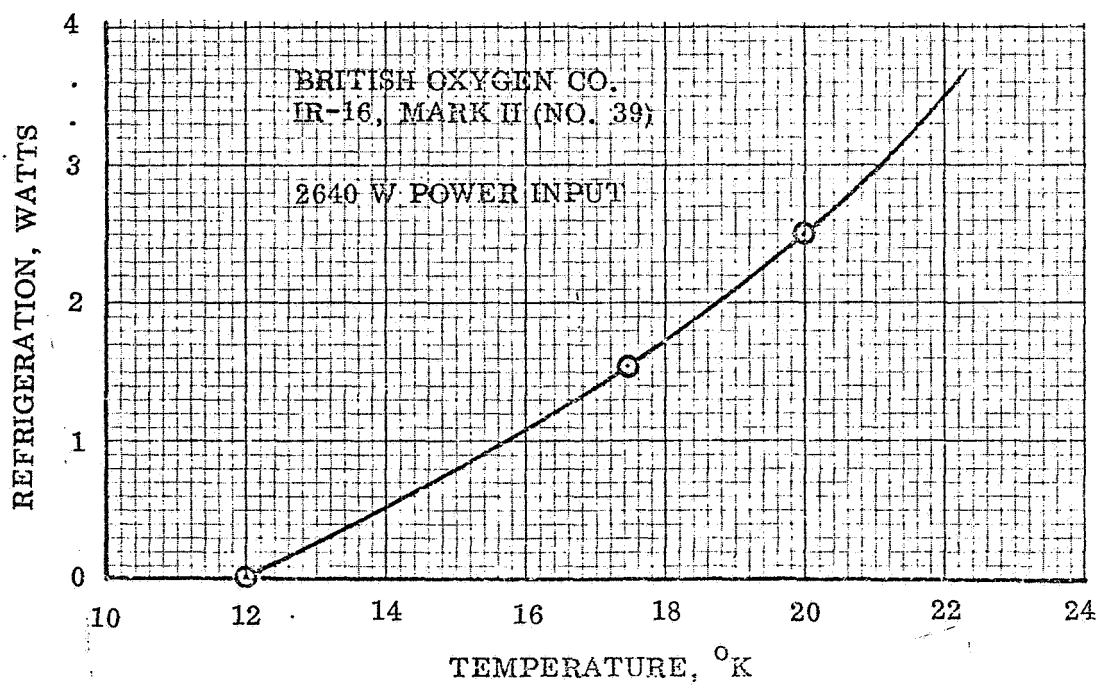
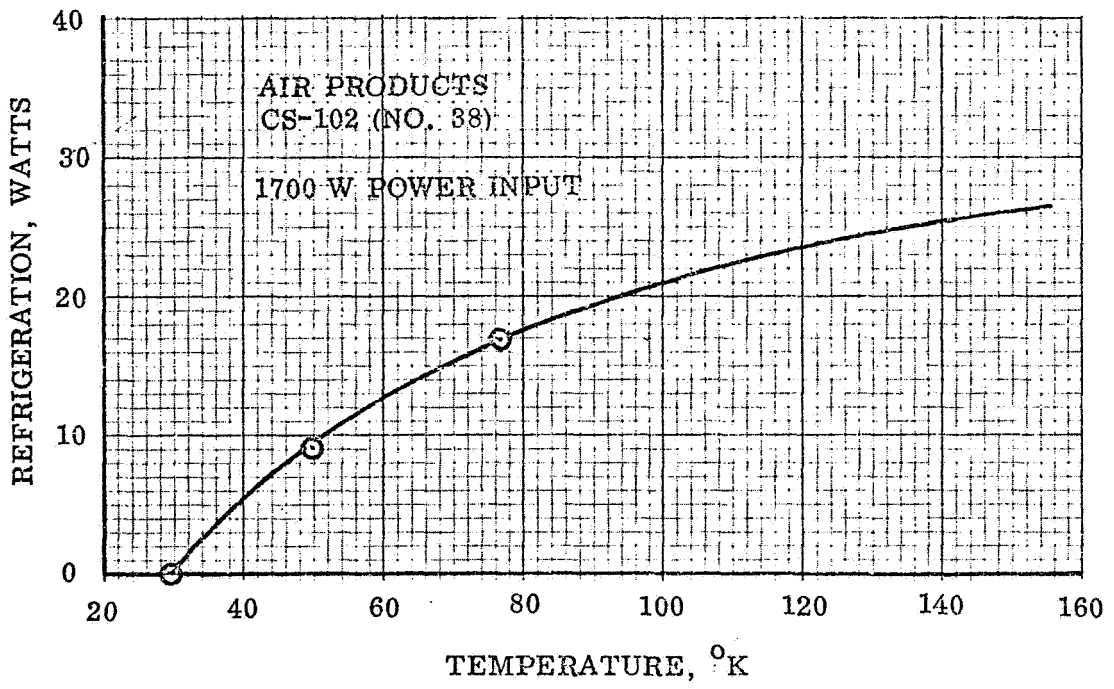


Fig. 3-53 Refrigeration vs. Temperature (Gifford-McMahon Units)

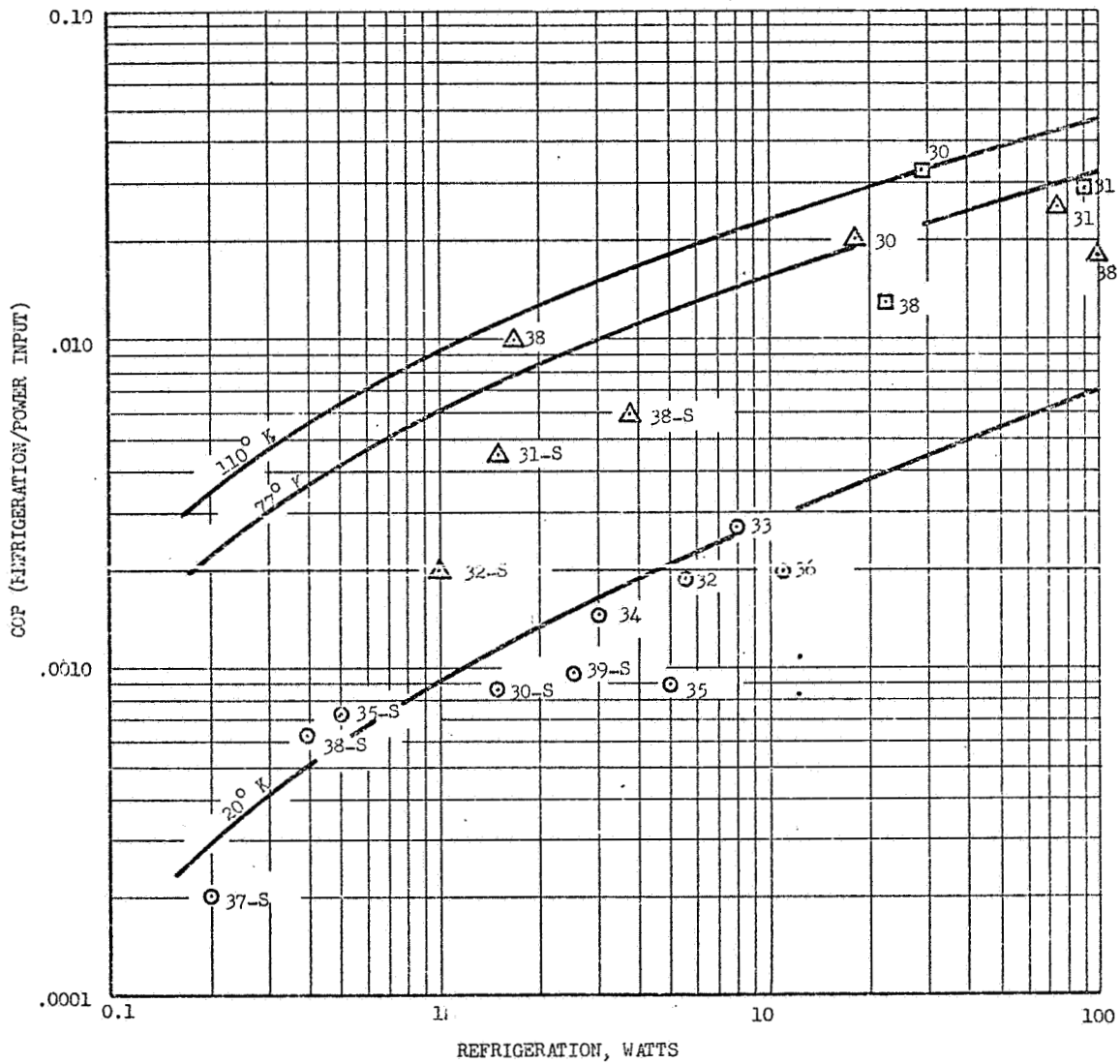


Fig. 3-54 COP Versus Refrigeration Capacity for Gifford-McMahon, Solvay and Taconis Systems at 20° K, 77° K, and 110° K

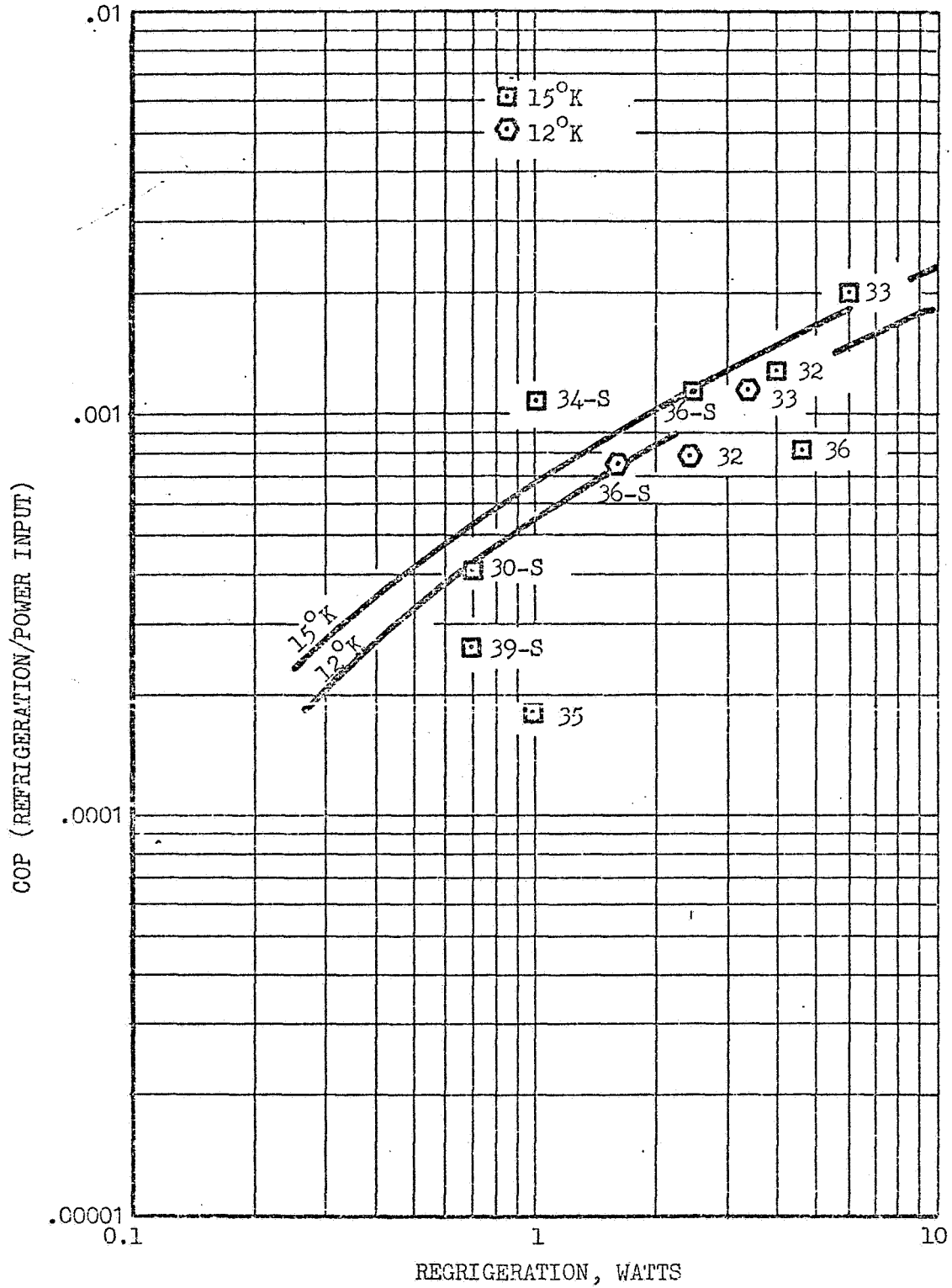


Figure 3-55 COP vs. Refrigeration Capacity for Gifford-McMahon, Solvay, and Taconis Systems at 12°K and 15°K

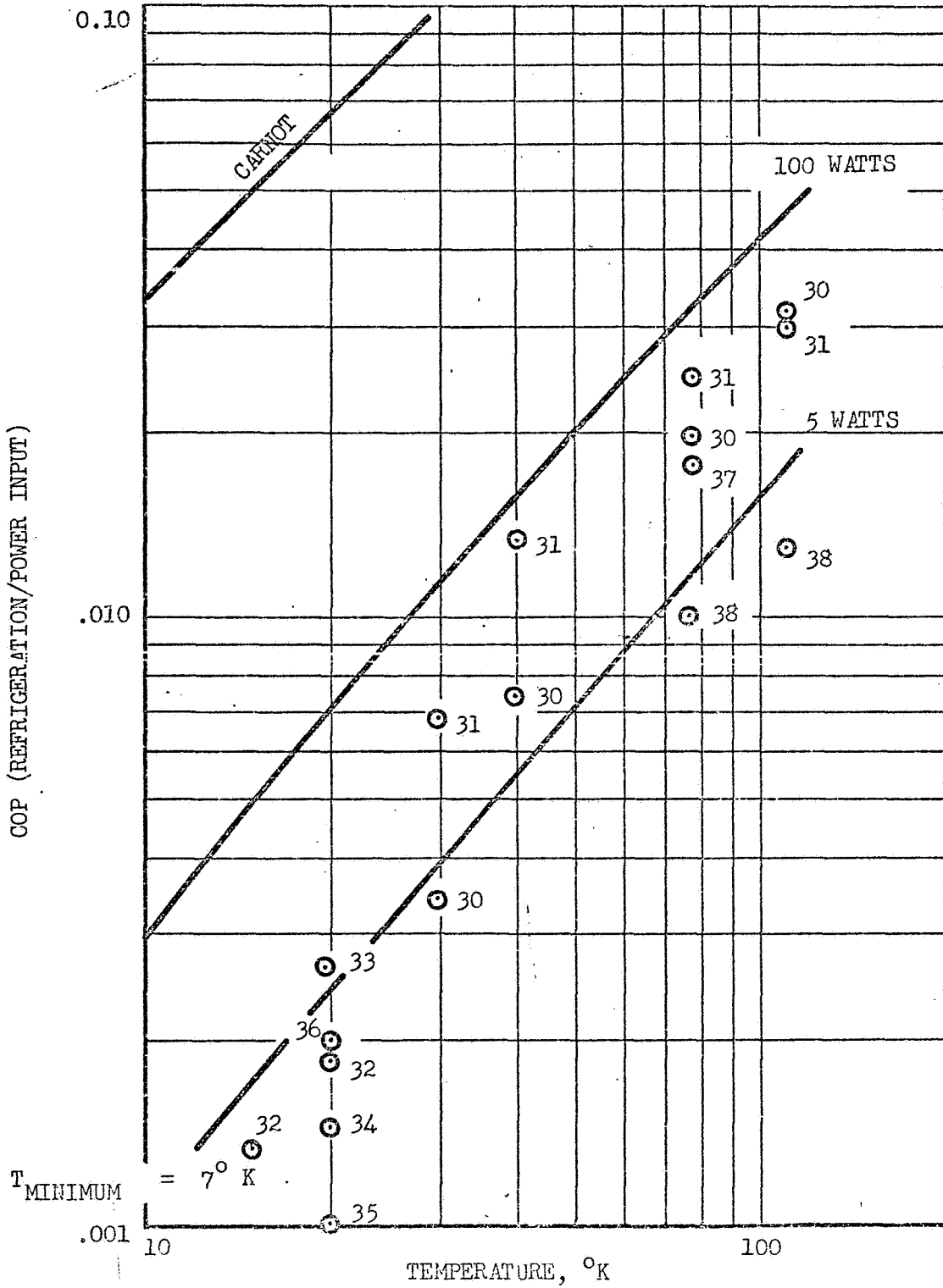


Fig. 3-56 COP of Gifford-McMahon, Taconis, and Solvay Refrigerators

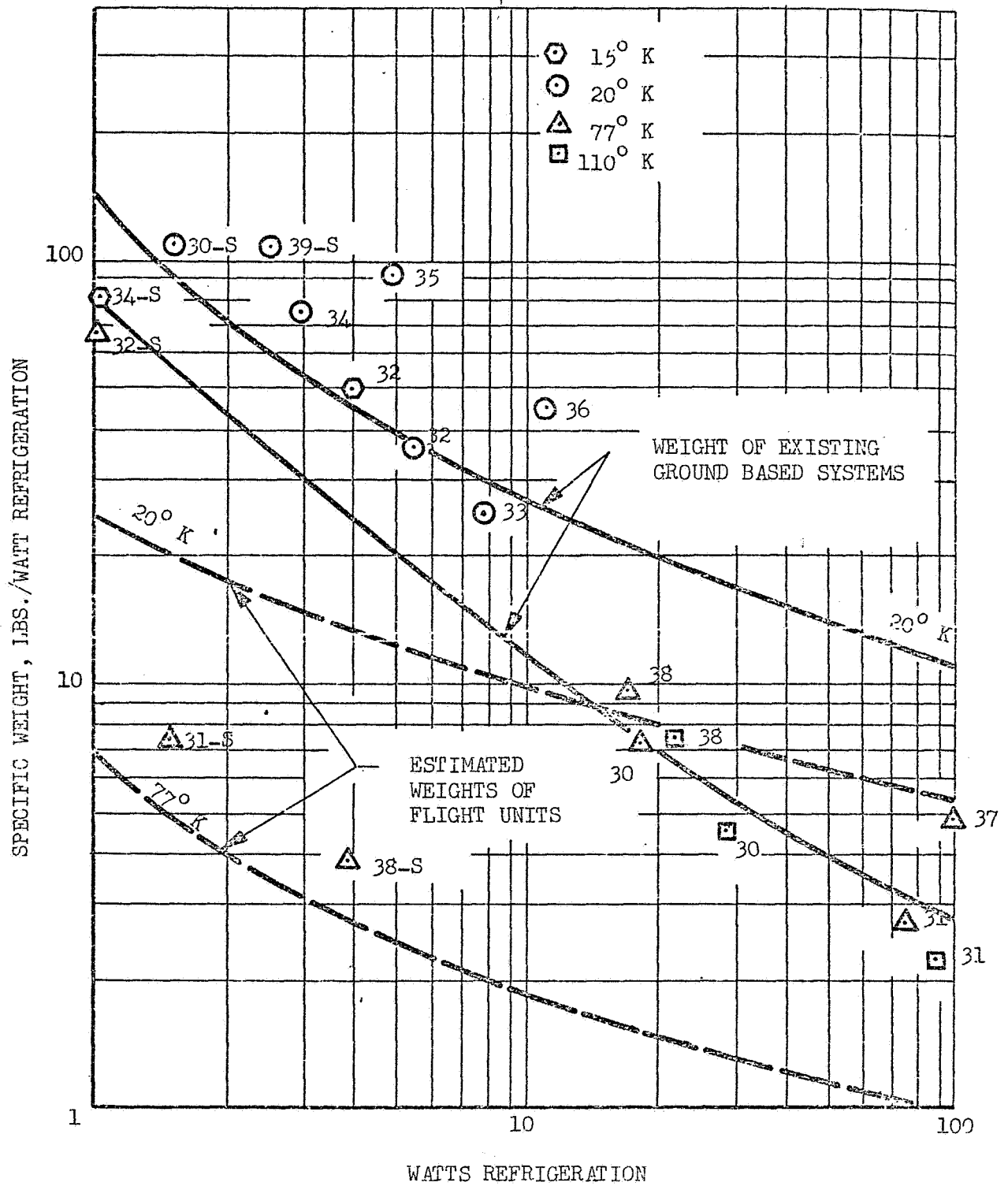


Figure 3-57 Specific Weight vs Refrigeration for Gifford-McMahon Solvay and Taconis Refrigerators

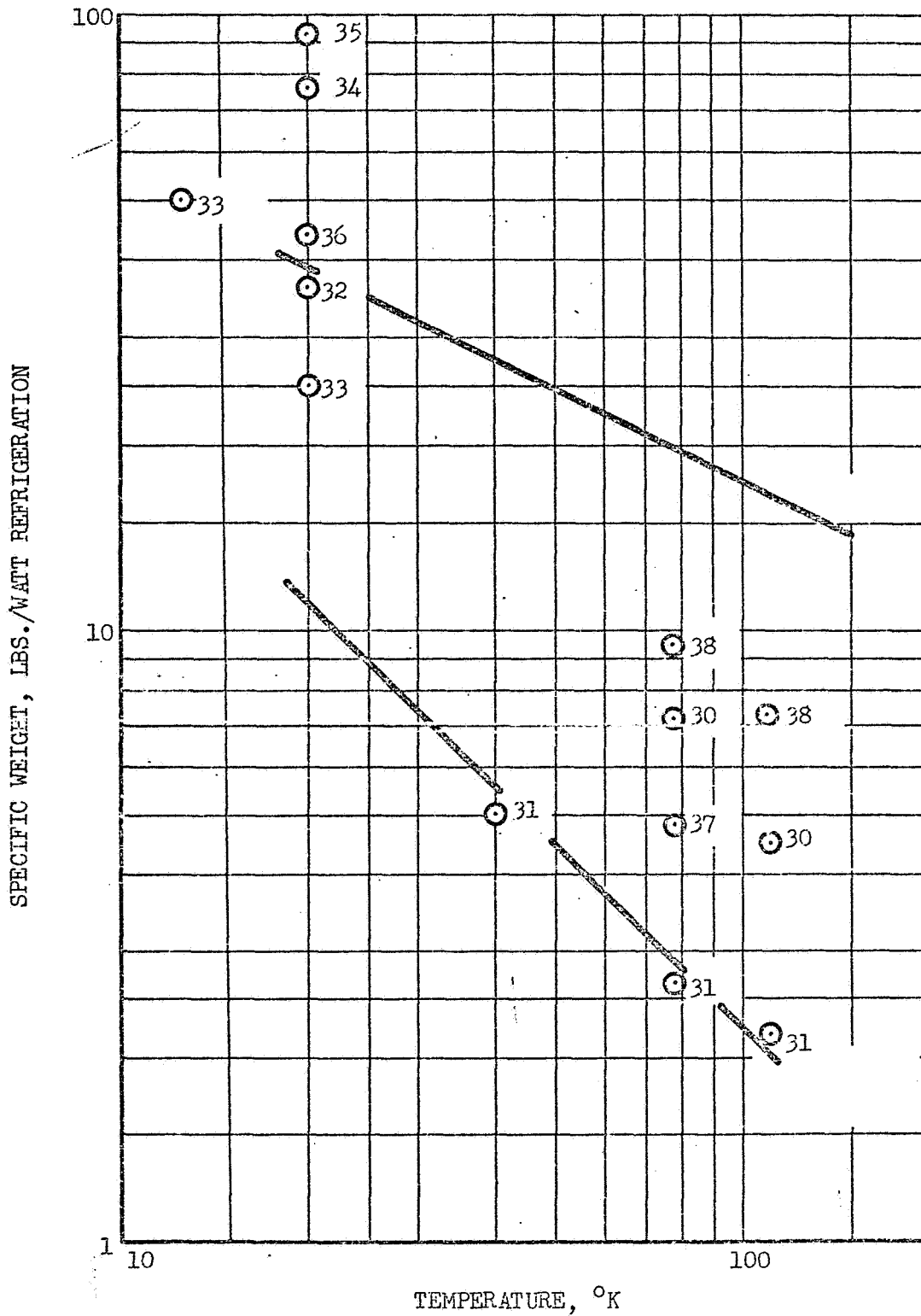


Fig. 3-58 SPECIFIC WEIGHT VERSUS TEMPERATURE OF GIFFORD-McMAHON, SOLVAY, AND TACONIS REFRIGERATORS

other cycles the curve fits were made through the "best" points (i.e., highest C.O.P. and minimum specific weight).

Unlike the C.O.P. data it is expected that substantial weight reduction could be made in the systems by selecting compressor units which are optimized for minimum weight. Data from units Nos. 31-S and 35-S are for flight weight-dry lube compressors and clearly show the weight improvement which can be obtained. Section 3.3.1 discusses the various compressors available and indicates the relative weight gains which appear obtainable in the compressor unit. Included in Fig. 5-37 is the estimated weight of flight optimized systems at 20°K and 77°K. These systems would use non-lubricated compressors as do units Nos. 31-S and 35-S. The technique of estimating these weights is fully described in Section 3-6, the primary purpose of this section being to present data on existing units.

Fig. 3-59 presents the specific volume of the systems (In^3/Watt) and the curve fits at the three temperatures. It is expected that large reductions in the specific volume of the units would likewise be achieved by optimization of the compressor for space use.

The percent Carnot efficiency is presented in Fig. 3-60 and shows that the units provide from 1 to 7% Carnot efficiency, which is substantially below that achieved with the most efficient cycle considered here, the Stirling cycle, which provides from 10 to 20% in the same operating range.

In spite of this shortcoming the G-M and similar cycles provide a high degree of flexibility due to the separable components and more importantly currently provide the longest unattended lifetime for the refrigerators which fall within this study.

3.4.5 Brayton/Claude Cycles

3.4.5.1 Operation

Brayton Refrigerator: A practical Brayton cycle refrigerator is shown in Fig. 3-61. Gas is compressed with some increase in entropy from 1 to 2. The heat of compression is rejected to the ambient temperature heat sink in an after-cooler from 2 to 3. The high pressure fluid is cooled from 3

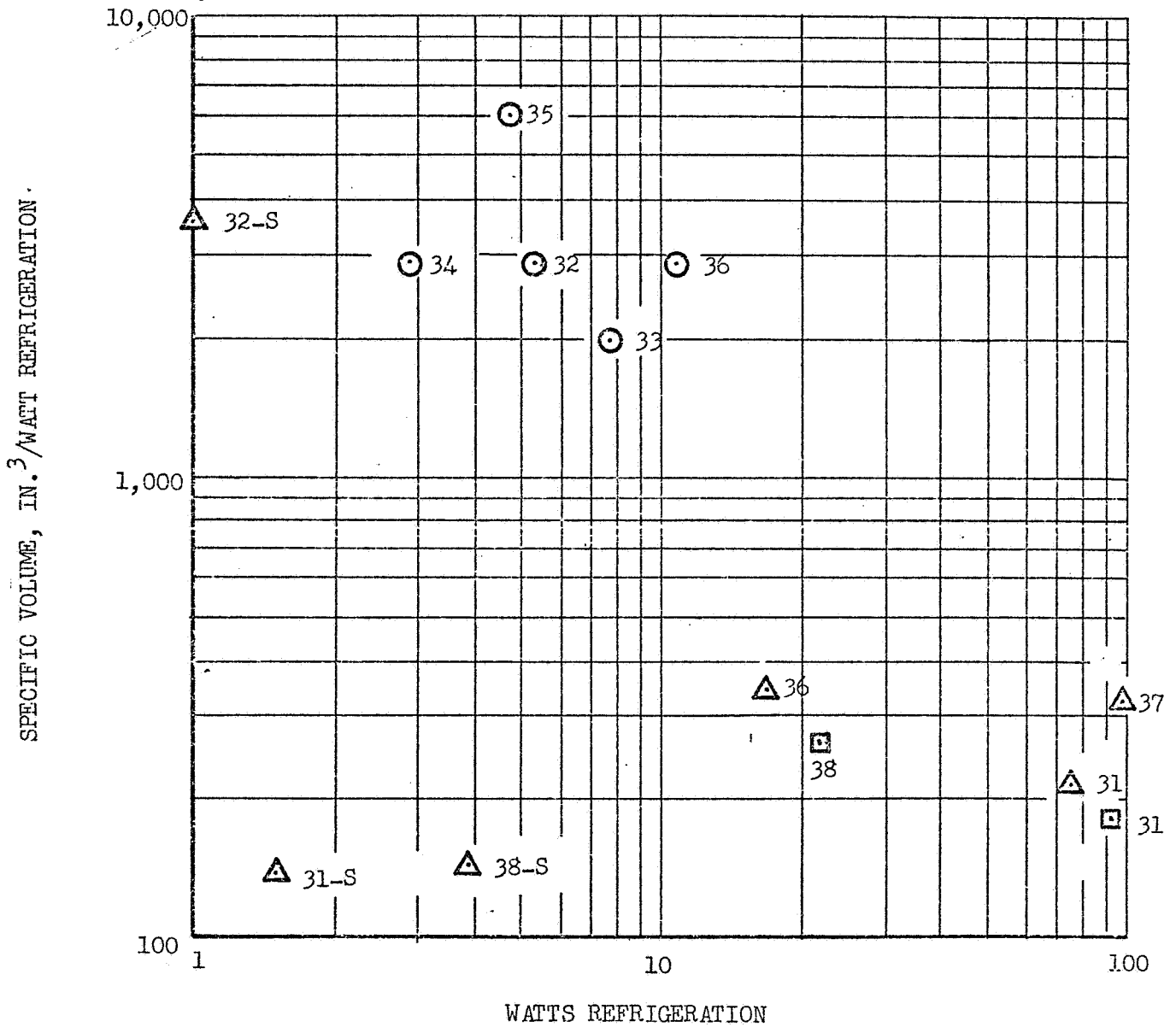


Fig. 3-59 SPECIFIC VOLUME VERSUS CAPACITY OF GIFFORD-McMAHON SYSTEMS

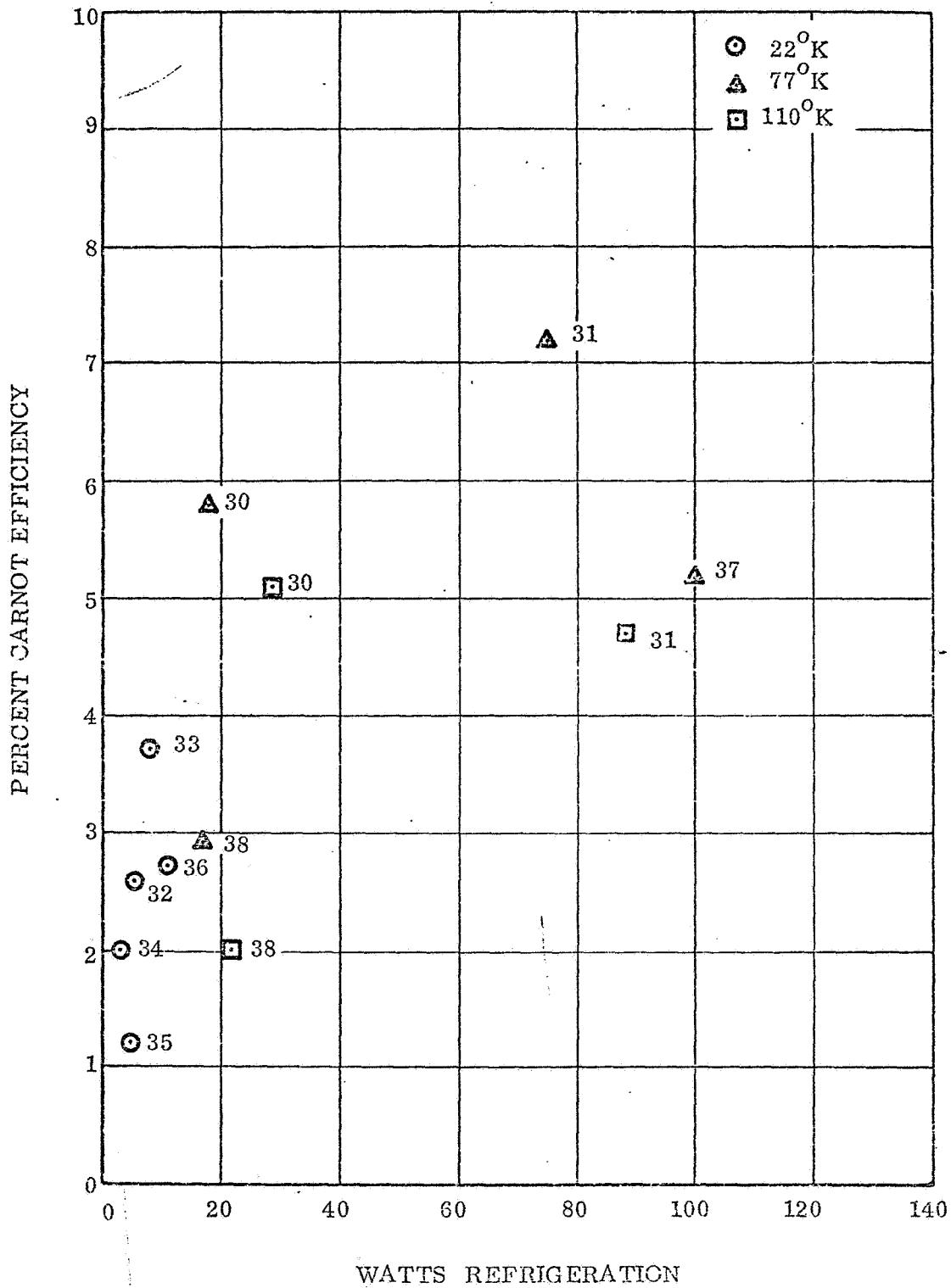


Fig. 3-60 Percent Carnot Efficiency of Gifford McMahon Systems

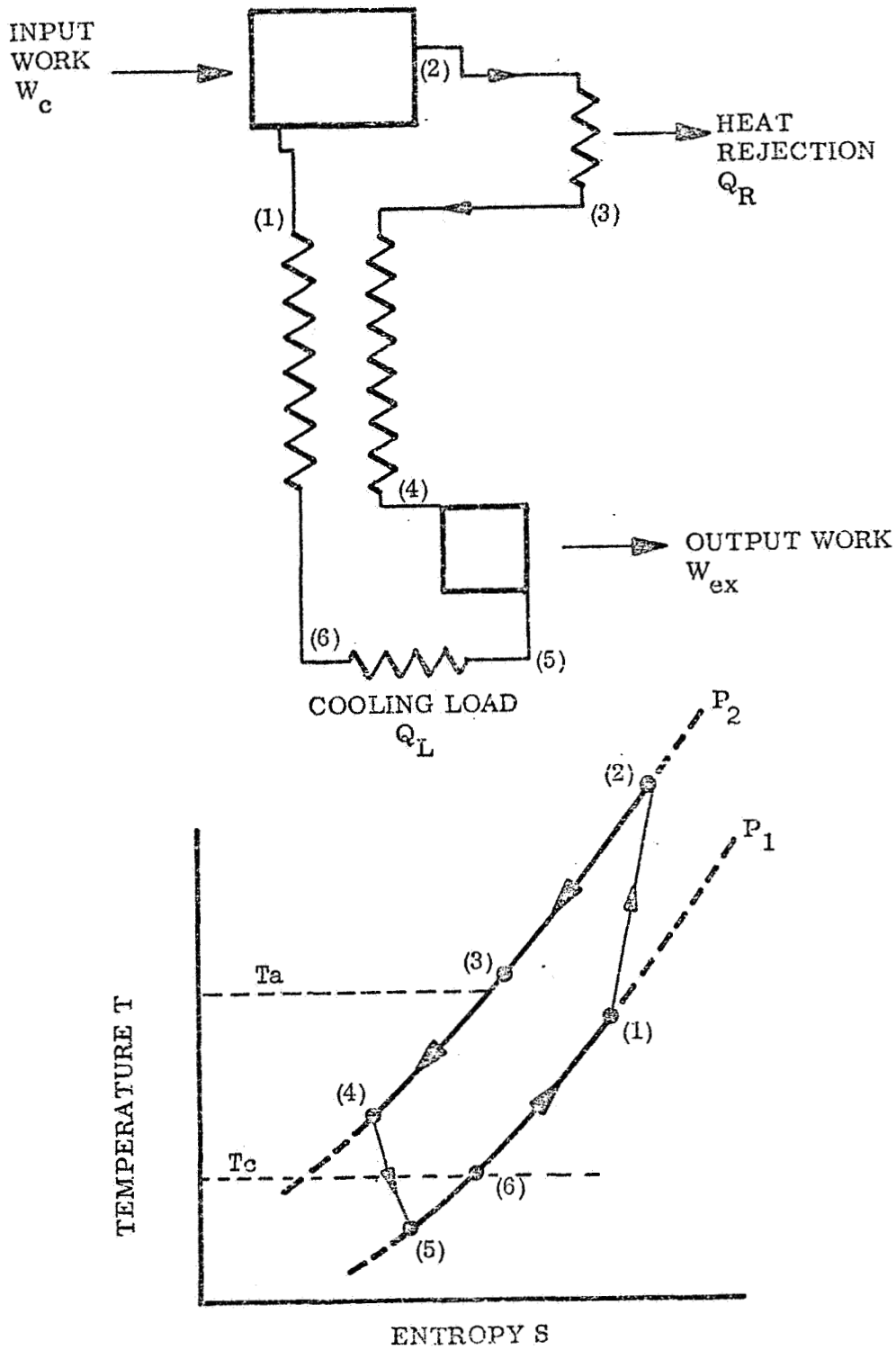


Fig. 3-61 The Brayton Cycle

to 4 in the main heat exchanger. The pressure at 4 is slightly less than at 2 due to the flow losses in the two heat exchangers. The fluid is expanded from 4 to 5 with some entropy increase, and is then warmed to 6 by passage through the load heat exchanger. The fluid is warmed from 6 to 1 in the main heat exchanger as it returns to the inlet side of the compressor. The pressure at 4 is slightly higher than at 1 because of pressure losses in the heat exchangers.

Analysis of the cycle is performed by selecting high and low fluid pressures, load and sink temperatures, and either choosing mass flow rates and component dimensions from which efficiencies can be determined (as described in Section 3.3), or assuming efficiencies from which required component dimensions may be found in a separate calculation (as described in Section 3.2). The analysis begins by assuming a value for T_1 , and hence, h_2 is found from the assumed or calculated compressor isentropic efficiency, η_{isc}

$$\eta_{isc} = \frac{h(P_2, S_1) - h_1}{h_2 - h_1} \quad (3-17)$$

T_2 is found from h_2 and P_2 .

$$T_2 = T(P_2, h_2)$$

P_3 is found from the assumed or calculated after-cooler loss coefficient K_a

$$P_3 = P_2 - \left(\frac{P_2 + P_3}{2} \right) K_a \quad (3-18)$$

h_3 is found from the assumed or calculated after cooler effectiveness ϵ_a , T_2 , and the sink temperature T_a

$$\epsilon_a = \frac{h_2 - h_3}{h_2 - h(P_3, T_a)} \quad (3-19)$$

T_3 is found from the fluid equation of state

$$T_3 = T(P_3, h_3)$$

h_4 is found from the assumed or calculated main heat exchanger effectiveness, ϵ_m

$$\epsilon_m = \frac{h_3 - h_4}{h_3 - h_6} \quad (3-20)$$

P_4 is found from the assumed or calculated main heat exchanger high pressure side pressure loss coefficient, K_{mh}

$$P_4 = P_3 - \frac{(P_3 + P_4)}{2} K_{mh} \quad (3-21)$$

T_4 is found from the fluid equation of state

$$T_4 = T(h_4, P_4)$$

P_5 is found from an assumed expander pressure ratio

P_6 is found from the assumed or calculated load heat exchanger pressure loss coefficient, K_L

$$P_6 = P_5 - \left(\frac{P_6 + P_5}{2} \right) K_L \quad (3-22)$$

h_5 is found from the assumed or calculated expander isentropic efficiency, η_{isc} .

$$\eta_{isc} = \frac{h_4 - h_5}{h_4 - h(P_5, S_4)} \quad (3-23)$$

T_5 is found from the fluid equation of state

$$T_5 = T(P_5, h_5)$$

h_6 is found from the assumed or calculated load heat exchanger efficiency, ϵ_e

$$\epsilon_e = \frac{h_6 - h_5}{h(P_6, T_c) - h_5} \quad (3-24)$$

T_6 is found from the fluid equation of state

$$T_6 = T(P_6, h_6)$$

P_1 is found from the assumed or calculated main heat exchanger low pressure side loss coefficient, K_{me}

$$P_1 = P_6 - \left(\frac{P_1 + P_6}{2} \right) K_{me} \quad (3-25)$$

h_1 is found from the assumed or calculated main heat exchanger effectiveness ϵ_m .

$$\epsilon_m = \frac{h_1 - h_6}{h_3 - h_6} \quad (3-26)$$

T_1 is found from the fluid equation of state

$$T_1 = T(P_1, h_1)$$

The calculated values of P_1 and T_1 will not, in general, agree with the assumed values. Adjustments are made in the assumed expander pressure ratio and the cycle is recalculated using the new T_1 . The process is repeated until a consistent set of figures is obtained. If component efficiencies rather than dimensions were assumed then the component sizes and flow rates required to provide this performance must then be determined.

The cooling capacity of the refrigerator, q_c , is the heat absorbed by the load heat exchanger.

$$q_c = \dot{m} [h_6 - h_5] \quad (3-27)$$

The power required by the refrigerator, W , is the work of compression .

$$W = \dot{m} [h_2 - h_1] \quad (3-28)$$

It is apparent that the analysis of continuous flow Brayton Cycle refrigerators is relatively straightforward. Performance data can be prepared quite readily as a function of component efficiencies and the results of two extensive parametric studies are reported in the literature (3-21) (3-22). Muhlenhaupt and Strobridge present calculated values of W/q_c for a wide range of expander and exchanger efficiencies and helium, hydrogen and nitrogen working fluids. A total of 66 charts are presented for W/q_c as a function of P_2 , each presented for a range of three other cycle parameters. Wilson and D'Arbeloff (3-23) present a similar range of calculated performance data with component efficiencies as parameters. These data are calculated for helium, hydrogen, and neon as working fluids. The effects of multiple stage compression, multiple stage expansions and the use of intermediate temperature expansion stages to improve apparent effectiveness are shown.

The dimensions and performance characteristics of a practical Brayton cycle refrigerators may thus be determined by combining the parametric system performance data of these two studies with the physical dimensions, capacity, and efficiency of practical compressors, heat exchangers and expanders.

The Claude Refrigeration Cycle: As the operating temperature of the Brayton refrigerator is lowered, point 5, (Fig. 3-61) will enter the two-phase region of the working fluid, and the fluid will leave the expander as a two-phase mixture. Up to the present time, it has not been considered good engineering practice to permit expanders to operate in the two phase region because of possible mechanical damage to the expander. For refrigeration at temperatures within the two-phase region of the working fluid it has therefore become accepted practice to perform the expansion process isenthalpically through a throttle valve as in the Joule-Thomson cycle, rather than in an expansion engine.

As explained in Section 3.4.3, this process will not produce net refrigeration unless the value of $(\partial h / \partial P)_T$ is negative at the effective sink temperature. For helium, hydrogen and neon this means that the effective sink temperature must be reduced by use of an auxiliary heat exchanger. The Claude cycle is effectively a Joule-Thomson cycle in which the effective sink temperature is lowered by a Brayton cycle refrigerator. It is designed so that the two systems share the same working fluids.

Fig. 3-62 shows a practical Claude cycle. The cycle closely resembles the Brayton and Joule-Thomson cycles, Figs. 3-61 and 3-40, and the cycle description is similar. The difference is that upon reaching point 4 the flow divide and a portion of the flow is expanded as in a Brayton refrigerator and is returned to the compressor via a combined load and precooling exchanger, and the main exchangers. The remaining portion of the stream at 4 is passed through the other side of the load/precooling refrigerator and is cooled to T_{4a} . The system $4-4_a-4_b-5_a-5_b-5-6$ is a standard Joule-Thomson refrigerator and functions like the system 3-4-5-6-1 in Fig. 3-40. The fluid is cooled in the main Joule-Thomson heat exchanger, 4_a to 4_b , after which it is expanded isenthalpically to 5_a . From 5_a to 5_b , the fluid is warmed in the Joule-Thomson load heat exchanger and then is reheated in the main exchanger to point 5 where the two flows are united and pass back to the compressor via the load/precooling exchanger and main exchanger.

It can be seen that the Claude cycle is essentially more complex and less efficient than the Brayton cycle inasmuch as a Joule-Thomson refrigerator has been added and that because of this the cooling effect at the load is produced by isenthalpic expansion, which produces a greater increase in entropy than even the most inefficient expander. Recently a reciprocating expander has been operated successfully in the two-phase region (3-24).

If it proves possible to develop expander technology to the point where such expanders become generally available, the technical advantage of the Claude cycle would be eliminated.

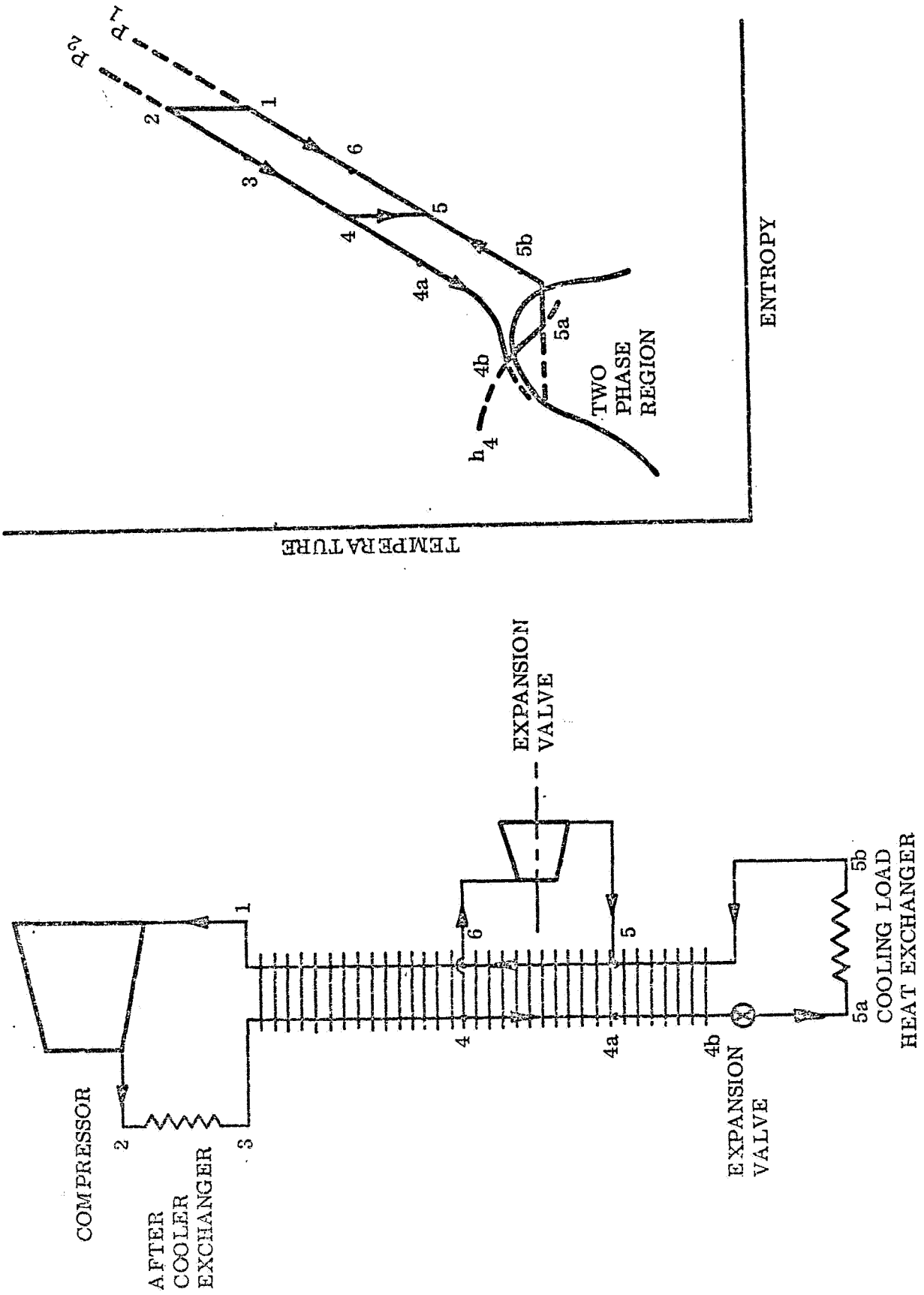


Fig. 3-62 The Claude Refrigeration Cycle

The Claude cycle can be analyzed in a manner analogous to the Brayton-cycle and Joule-Thomson-cycle analyses. For the temperature range of interest to this program, 20°K - 100°K, the possible working fluids are helium, neon, hydrogen, and nitrogen. Because of the low condensation temperature of helium, there is no necessity for adding a Joule-Thomson stage to a helium Brayton refrigerator. Neon or hydrogen Claude systems would be appropriate for the 20°K - 30°K range. A Claude system using nitrogen could be used in the 75°K to 85°K range, where its efficiency would be higher than that of a single-stage Joule-Thomson system.

An extensive parametric study of a helium Claude-cycle refrigerator for use in the temperature range of 4.2°K is presented by Muhlenhaupt and Strobridge (3-22). The temperature range of this refrigerator is below the range of current interest, and although the technique of analysis would be applicable to hydrogen, neon, or nitrogen system, the data are of no direct interest. However, the data do show that the efficiency passes through a maximum with increasing magnitude at high pressure, and that the optimum pressure is higher than that found for Brayton-cycle systems (3-22).

3.4.5.2 Companies Engaged in Brayton/Claude Cycle Refrigerator Development

The following companies have been engaged in research and development activities associated with a miniature Brayton-cycle refrigerator. Unlike activities on many of the other cycles, nearly all work in this area has been government-funded.

General Electric Company
 AirResearch Manufacturing Company
 Arthur D. Little, Inc.
 Hymatic Engineering Co., Ltd.

In addition to these companies, whose activities have been directed toward miniature units for aircraft and space usage, the following companies have built large-capacity industrial units, using the Claude and Brayton cycle:

Linde	British Oxygen Cryoproducts
L'Air Liquide	CVI Corporation
National Bureau of Standards	Sulzer Brothers Limited

AiResearch Manufacturing Co.: AiResearch began activities on the design and development of a miniature non-reciprocating closed-cycle cryogenic cooler in 1962 under contract to WPAFB (AFO4(695)-313), and AF 04(695)-146. The objective of this contract was to develop a refrigerator with a cooling capacity of approximately 2 watts at 77°K which would be suitable for use with space-based infrared sensor devices. The work conducted on this system resulted in the fabrication of a non-reciprocating system based on the Brayton cycle and using nitrogen as the working fluid. The system parameters for this unit are shown in Table 3-5 (No. 40).

Long-term unattended operation, one of the goals of this effort, was not demonstrated, the actual run time of the unit being limited to approximately 700 hours. The work on this unit terminated in March 1967. A second development contract carried on at Garrett was begun in February 1964, and ended in December 1965. This effort was funded by U.S. Army Satellite Communications Agency under Contract DA-36-039-AMC-30725. The program objective was the development of a helium refrigerator system suitable for cooling low-noise amplifiers at 4.2°K. The work accomplished under this contract consisted of component feasibility studies. A working model was not built under this contract. (Reference 3-25)

A third effort by Garrett was funded by WPAFB during the period April 1964 to October 1968. The objective was to develop a turbomachinery-type closed-cycle refrigeration system to provide 1 W of cooling at 3.6°K for a continuous operating period of 10,000 hours minimum in a space component environment. Fabrication and testing was conducted during this contract; however, a complete prototype unit was not fabricated. (Reference 3-26) This work was done under Contract AF33(615)-1015.

Arthur D. Little, Inc. Arthur D. Little, Inc., began their activities on Brayton-cycle systems in mid-1962. Their activities, like Garrett's, have been funded by WPAFB, and the objective of their initial work was the development of a refrigerator to provide 2 watts of cooling at 77°K in a space environment. Work in this area was completed in May 1967 and resulted in the fabrication and testing of a development model. In addition to this, a lightweight model

was constructed but not tested. Further information on this development effort is contained in Reference 3-27.

Additional work was performed by A. D. Little under contract to WPAFB from July 1966 to October 1968, on Brayton-cycle refrigeration (3-28). The design objectives of this study were to provide 1 watt of refrigeration at 3.6°K. The system was to operate in space, and had an operating lifetime goal of 10,000 hours. The major components of the refrigerator system were built and tested; however, a complete working model of the system was not built.

General Electric General Electric has investigated small cryogenic refrigeration units based on the Brayton cycle for a period of approximately 5 years. These activities have been conducted using in-house funds, and, more recently, under contract to WPAFB. Like Garrett and A. D. Little, two cryogenic refrigeration systems have been investigated. The first unit designed and built was an 80°K refrigerator. This was a prototype unit which was tested. Test data on this unit were not reported. As a result of this testing, a compact 77°K unit was designed.

In addition, a second unit for cooling at 4.4°K was designed, and various components were tested. General Electric has published various papers on their development effort (Ref. 3-30, 3-31, 3-33, 3-34) and presented operating data on components. Extensive testing of a complete refrigeration system was not accomplished in these programs.

Hymatic Engineering Hymatic Engineering has developed a prototype Brayton-cycle unit which produces 0.3w at 28°K. Additional information on their activities is not available at this time. The available parameters of their prototype model are listed in Table 3-5 along with the other Brayton-cycle units.

Other companies produce large Brayton- and Claude-cycle units for much higher refrigeration rates, and at generally lower temperatures ($\approx 4^{\circ}\text{K}$). These companies were included in the list, and limited data on the parameters of these units can be found in Reference 3-29. Additional information on available miniature gas bearing cryogenic turbines with low to moderate flowrate is presented in Reference 3-30, which includes the results of a survey of these units.

3.4.5.3 Discussion of Data for Brayton/Claude Systems

Data have been assembled on the various prototype units which operate on the Brayton cycle, and are presented in Table 3-5.

All of these units are prototype units, and a complete list of operating characteristics was not available, but available data are indicated in Table 3-5.

Figures 3-63 and 3-64 present the C.O.P. and specific weight data as a function of refrigeration temperature. Since experimental data on these units are severely limited, predicted performance data are also shown from two sources (3-25, 3-31).

Table 3-5 Prototype Brayton Cycle Refrigerators

Manufacturer	Garrett A/R Research	Hymatic	A.D. Little	A.D. Little	A.D. Little
Trade Name	None	None	None	None	None
Model	Prototype	Prototype	Prototype	Prediction (2)	Prototype
I.D. Number	40	42	44	45	46
Refrigeration Range	≈80°K	19 - 28°K	3.6°K	77°K	90°K
Cycle	Brayton	Brayton	Brayton	Brayton	Brayton
Working Fluid	N ₂	He	He	He	He
High Pressure	0.72 atm	20 - 30 atm			
Low Pressure	0.30 atm	1 atm			
Minimum Temperature	≈75°K	19°K			
Cool-Down Time	≈6 hr	30 min			
Expander RPM		1500			
Volts-Phase-Frequency	115 - 1 - 60				
Cooling Means	Water		Radiative	Radiative	
Ambient Temp. Reqnts.	NI	-40°K to 70°K	NI	NI	Any
Required Attitude	NI	NI	NI	Any	Any
Cryostat Dim. (in.)	8.5 x 10.6 x 28.3	6 x 4 x 15	8 D x 60 L	6.5" D x 32" L	7.8" D x 32" L
Compressor Dim. (in.)	2,500 in. ³	NI	5.5 D x 52 L	1,060 in. ³	1,530 in. ³
System Volume			7,700 in. ³		
Compressor Wt.	15 lb	NI	72 lb		
Cryostat Wt.	15 lb	20 lb	52 lb		
System Wt.		NI	124 lb	20 lb	90 lb
Refrigeration		0.3W at 28°K	1W at 3.6°K		
Power Input			1310W		
COP			.000763		
% Carnot			6.25%		
Lb/Watt			124		
In. ³ /Watt			7700		
Refrigeration	2W at 80°K			2.5W @ 77°K	2.1W @ 84°K
Power Input	375W			100W	125W
COP	.00533			.025	.0168
% Carnot	1.5%			7.25%	4.9%
Lb/Watt	7.5			8	42.8
In. ³ /Watt	1,280			425	727

(1) Excluding vacuum case.
 (2) Based on extrapolation from prototype tests to refined spacecraft unit.

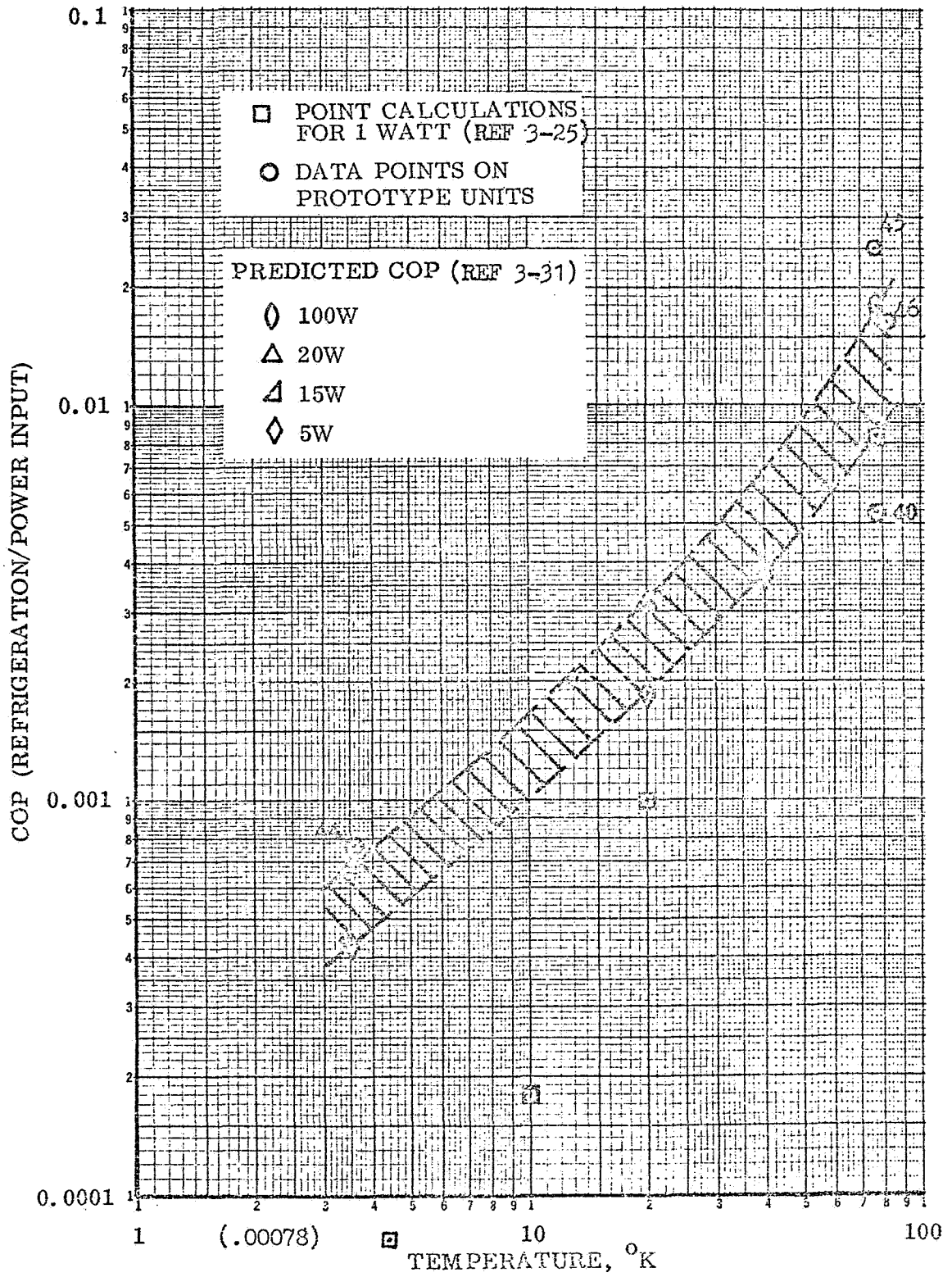


Fig. 3-63 Thermodynamic Performance of Brayton/Claude Cycle for Prototype Units and Prediction

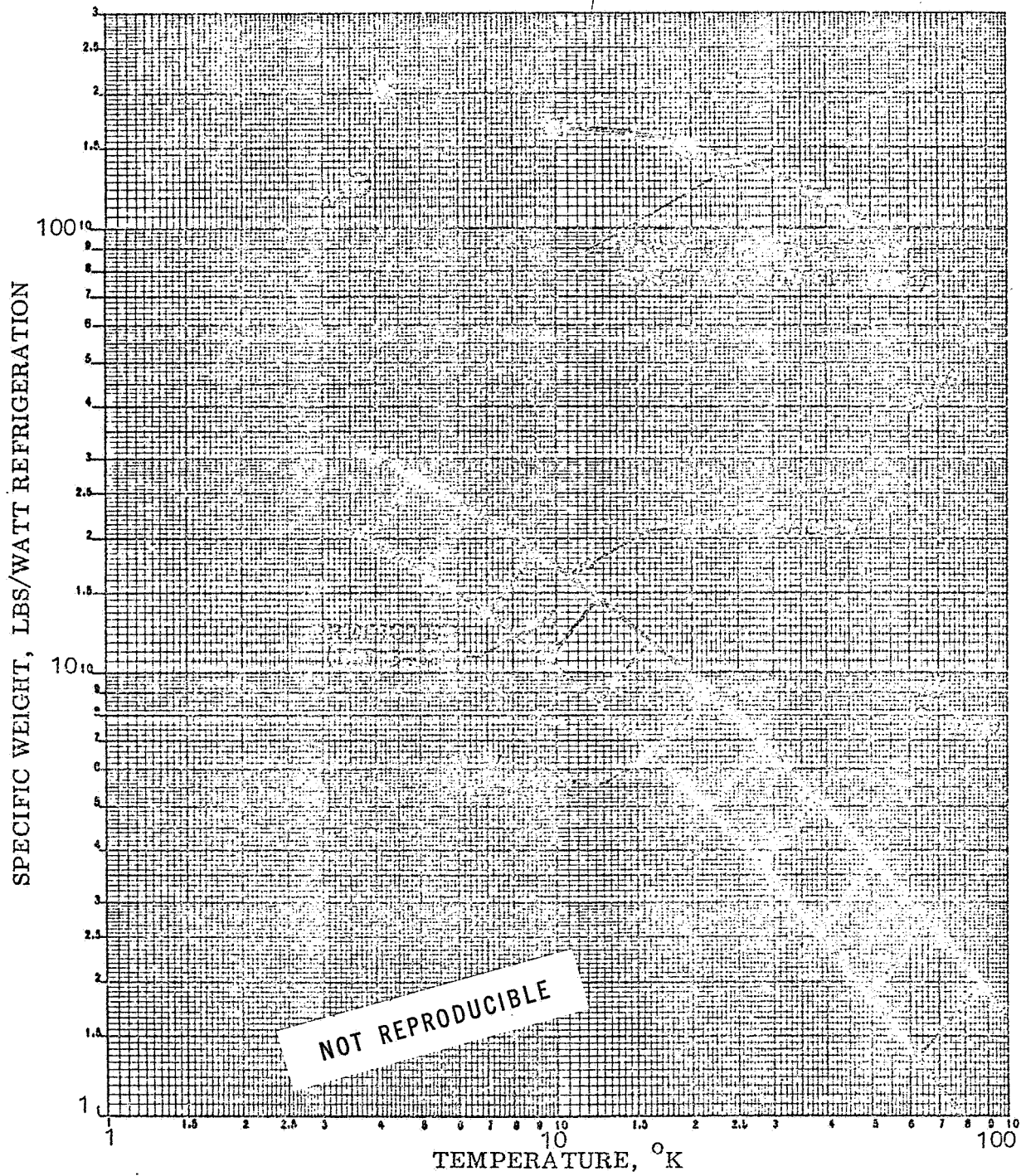


Fig. 3-64 Specific Weight of Brayton/Claude Cycle Refrigerators for Prototype Units and Prediction

3.5 ADDITIONAL OPERATING DATA

Several areas are of interest to the designer of spacecraft refrigeration systems in which little or no experimental data is available and analytical predictions are outside the scope of this contract. In these areas what little information that is available was collected and presented. In addition, analytical procedures are suggested which will yield first rough estimates of the effects of these parameters on system performance.

3.5.1 Cooldown Time of Refrigerators

Data have been included, where available, on the cooldown times of the various refrigerators in the data tabulations. The cooldown times of the units specified by the manufacturers are generally for conditions of minimum heat load and little or no mass attached to the cold head of the unit. The primary usage of the small units has been in cooling infrared detectors in which the mass of the focal plane assembly unit is small, generally in the range of 50-100 gms. In addition, the heat load to the cold finger is minimized to levels often in the area of 100-200 mw. As a result, most of the data available on cooldown of the closed cycle units is for those conditions where the heat to be removed is minimal.

For other applications where the mass to be cooled is substantially higher and where intermittent operation is desirable, the time for the refrigerator to cool down to its required operating condition can be an important design consideration. One example is an IR telescope where the barrel and optical elements, which represent a significant mass, must be cooled. Another is the case of intermittent refrigeration of propellant tanks in which it is desired to eliminate venting of the tank. In this case, heat exchanger elements and/or secondary fluid coolant systems must be cooled down to operating conditions prior to efficient propellant refrigeration.

The required information to determine the cooldown rate for various systems is the net refrigeration as a function of temperature for the unit being considered. If this information is available, then a transient analysis can be made which accounts for both external heat inputs and heat removal from items being cooled. Unfortunately, most of the manufacturers specify refrigeration rate versus

temperature only in the general region of the operating temperatures, and cooling rates up at higher temperatures near 200°K to 300°K are not generally available. It is felt that analysis techniques of predicting cooldown rates are extremely complex and not suitable. A discussion of analytical techniques for cool-down prediction is described in Ref. 3-67.

In order to form a rough guide in estimating the general cooldown characteristics of various refrigerators Figs. 3-65 and 3-66 were prepared. They show the cooling rate at temperature (T) normalized to the cooling rate at a specific temperature of interest as a function of temperature. As expected, the various units show a wide variation. It is suggested that in order to make an order of magnitude estimate the conservative or lower curves be used for design tradeoff purposes. It should be noted that a lengthy extrapolation of data to 300°K is required for all units except a Stirling unit for which data to 250°K was obtained.

A useful technique in obtaining general cooldown data is to obtain the time required to cool two different masses on the end of the cold finger to a desired temperature. The cooldown time is proportional to the mass attached to the cold finger, and this proportionally can be determined from the two measurements. Data obtained in this manner is normally for initial temperatures of 300°K and limits the utility of the data when lower initial temperatures exist, for example, on a space application. An example of this type of data is shown in Fig. 3-67. The cooldown time versus mass of copper is shown for various units, primarily for the Cryogenic Technology Inc. units for which this data is available, and for a single Stirling unit. The cooldown time is naturally a strong function of the steady state cooling rate and the minimum temperature. Figure 3-67 is shown only as an illustration, unfortunately sufficient data is not available to generate general curves of this nature for design purposes. This data is for a mass of copper at the cold finger; copper is normally utilized to minimize temperature gradients in the cooled block. The heat removed in cooling copper from 300°K to 40°K is 12,700 J/lb as noted on Fig. 3-67.

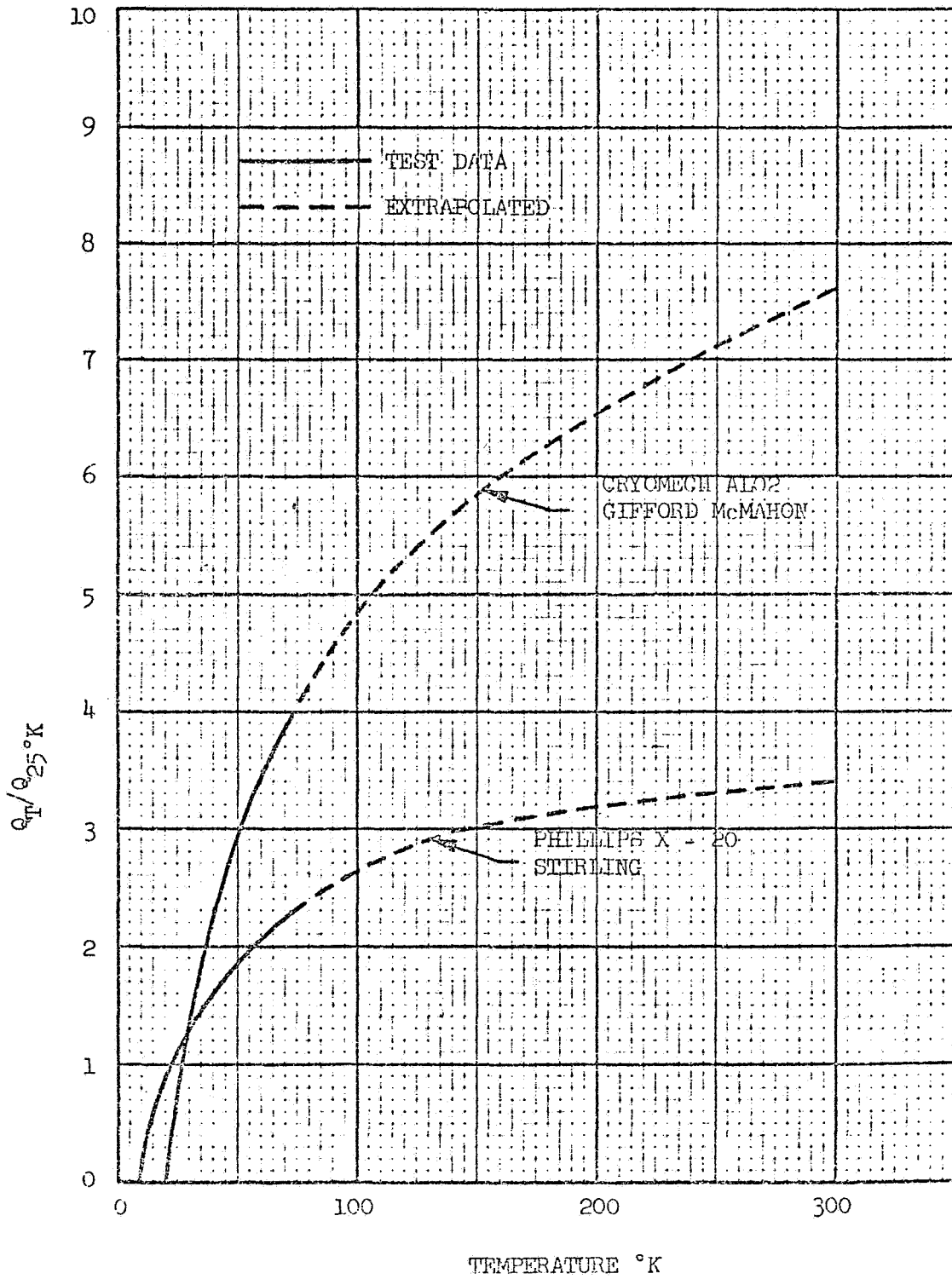


Figure 3-65. Estimated Cool-Down Characteristics of Various Refrigerators for 25°K Cooling

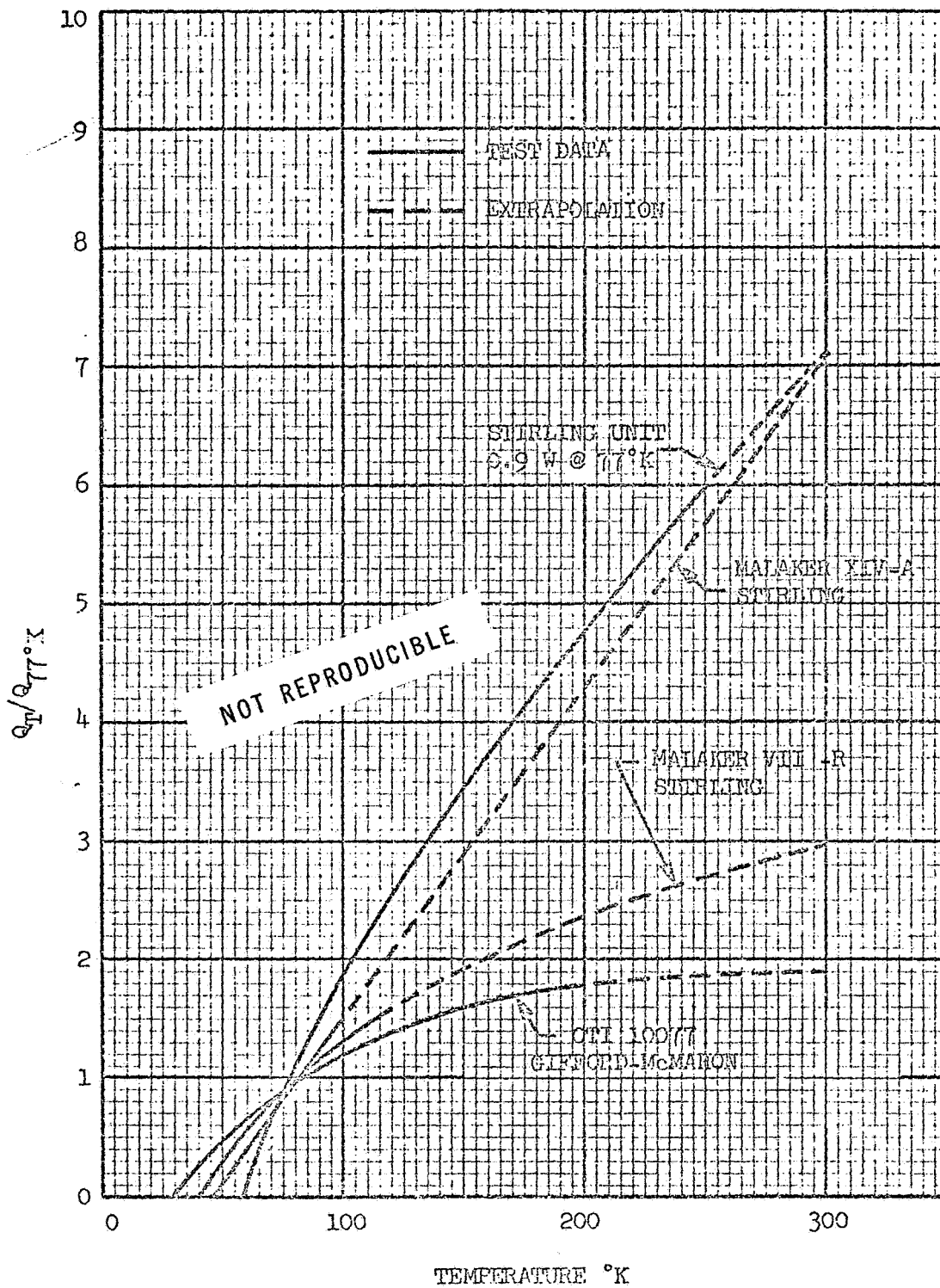


Figure 3-66. Estimated Cool-Down Characteristics of Various Refrigerators for 77°K Cooling

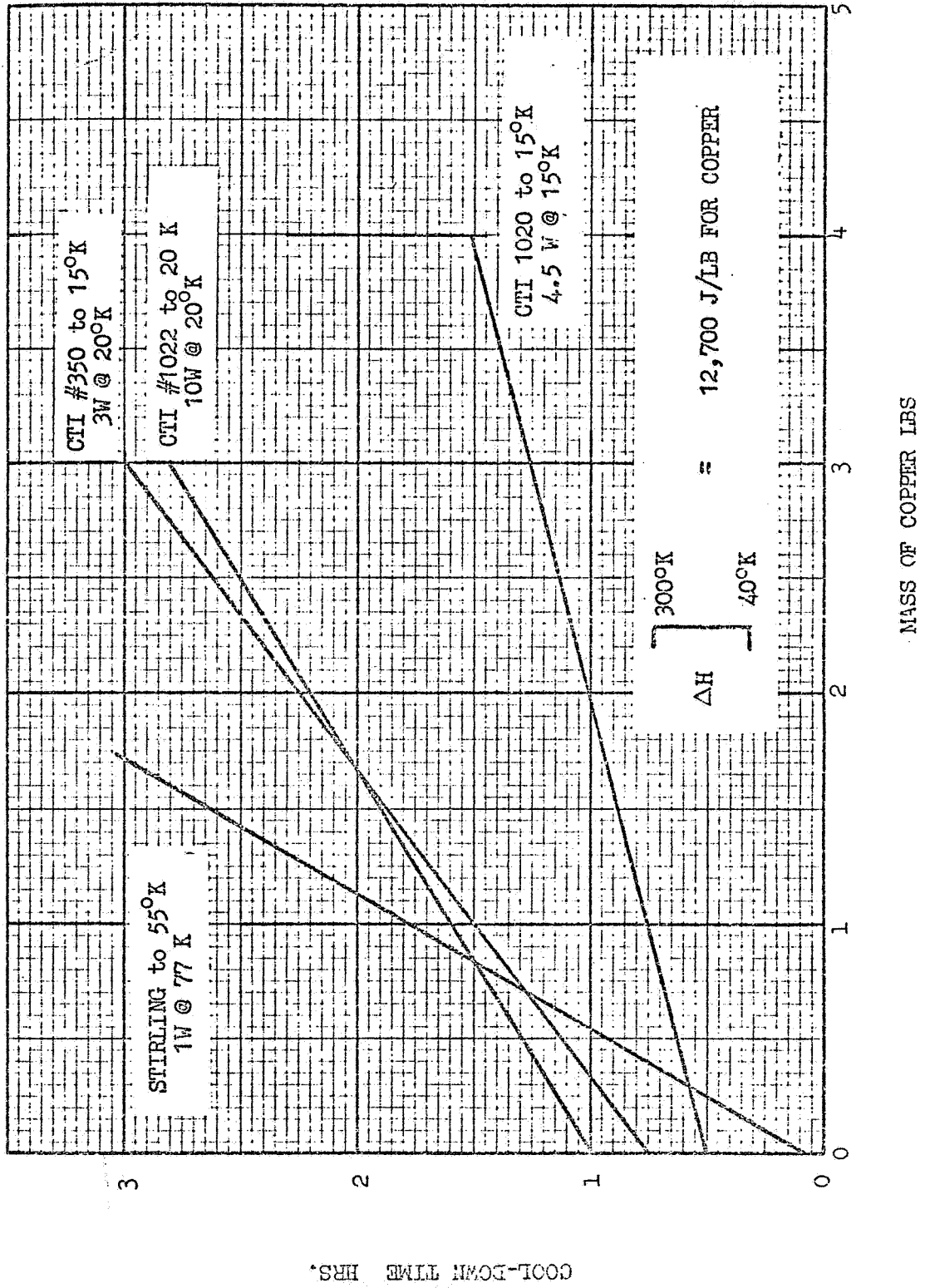


Figure 3-67. Cool-Down Times for Various Refrigerators (from 300°K)

3.5.2 Effect of Heat Rejection Temperature on Refrigerator Performance

Refrigeration systems in use at this time reject heat at temperatures near ambient ($\sim 300^{\circ}\text{K}$). This is due primarily to the convenience of rejecting the waste heat by air or water circulation to the atmosphere. No systems are known which reject heat at temperatures significantly different than this. It is felt that significant efforts would be required to develop systems which operate at temperatures substantially different from ambient. Lower temperatures leading to improved thermal efficiency may require modified sealing techniques for the working gas (rubber O-rings are used in most present systems) and wear characteristics of rubbing surfaces would undoubtedly change with temperatures. Let it suffice to say that this area has not been explored to a significant degree.

The advantage of reducing the heat rejection temperature of the refrigerator is to improve the thermal performance. The thermal performance of the ideal Carnot cycle is given by:

$$\frac{\text{refrigeration output}}{\text{power input}} = \text{C.O.P.} = \frac{T_c}{T_h - T_c}$$

As indicated in the previous sections the actual performance of operating systems is a fraction of the Carnot performance. In order to make system trade-off studies where it is desired to study the effect of variations in the heat rejection temperature it is recommended that the actual performance (COP) of a unit being considered at ambient temperature be modified, according to the Carnot efficiency for various temperatures.

$$(\text{COP})_{T_h} = (\text{COP})_{300^{\circ}\text{K}} \times \frac{300^{\circ}\text{K} - T_c}{T_h - T_c} \quad (3-29)$$

For a given cooling rate, the required power input can be reduced by rejecting heat at a lower temperature as given by the Carnot relationship. Contrarily, an increased heat rejection temperature requires greater power input than the 300°K base point, but leads to a more efficient, lighter radiator for waste heat rejection.

Data correlations for refrigeration systems and compressors investigated in this contract indicate that the weight and size of these units can be correlated as a function of their power input. Other investigators have shown this correlation (Ref. 3-68). An example of this correlation for the units considered is presented in Fig. 3-72.

Figures 3-72 and 3-77 may be used to find the change in refrigeration system weight and volume as a result of a change in the heat rejection temperature.

In summary, the following procedure is recommended to perform tradeoff studies for a perturbation of heat rejection (radiator) temperature:

- (1) Establish the characteristics (i.e., cooling load, weight, size, and power input) of the refrigerator rejecting heat at 300°K .
- (2) Modify the COP of the unit corresponding to the new rejection temperature (assuming the required refrigeration level remains constant) using equation (3-29).
- (3) Determine the power input for the new rejection temperature.
- (4) Find the new weight and size of the unit for the new power input utilizing Figs. 3-72 and 3-77.

Some studies have been performed to determine the effect of the heat rejection temperature on the total system weight (refrigerator, power supply, and radiator) and the results have indicated the optimum to be near 300°K and fairly flat (Ref. 3-69, 3-70) for the particular conditions assumed. For other conditions the effect of heat rejection temperature may be more significant.

3.6 SUMMARY OF PERFORMANCE DATA FOR VARIOUS CYCLES

In this section the weight, size and power requirements of the various cycles considered is presented. In general, the characteristics are included for cooling in the range of 5-100 watts at 20°K to 110°K which is the range of parameters specified by NASA/MSC. Additional data is included outside these parameters, both for the purpose of providing better curve fits in the primary range of interest, and to broaden the scope of use. A partial list of the areas of application of cryogenic cooling, and the general range of parameters is shown in Table 3-6.

Table 3-6
 AREAS OF APPLICATION OF
 CRYOGENIC COOLING

Application	Temperature Requirements °K	Cooling Requirements
1. Extra terrestrial propellant reliquefaction (contract application)	20 to 110	5 to 100
2. Masers	2 to 5	1
3. Parametric amplifiers	20 to 78	1 to 2
4. Super conducting circuits	4.2 to 12	0.5 to 2
5. Superconducting applications	2 to 15	1
6. ray detector devices	77 to 120	0.2 to 1
7. Infrared devices	77 to 4.2	0.1 to 2

The performance curves which follow are primarily a result of an extensive literature survey which was conducted during the contractual period, in which the performance data of various units was obtained. The operating characteristics of specific units which are operating or have been proposed are tabulated in Section 3.4. In curve fitting the data from existing units the intended use of the unit was taken into consideration, since it is the purpose of this study to present data for units applicable to spaceflight in which weight, volume, and required input power are at a premium. Data for units which are intended for application where weight and volume are not important were modified where possible for space use or discarded in obtaining the curves which follow. The source of data utilized to make the curve fits follows in order of preference.

1. Operating data on existing units intended for space-flight or aircraft use. (Section 3.4)
2. Predicted performance characteristics for space-flight systems from detailed studies by potential manufacturers.
3. Characteristics predicted by LMSC based upon more general data, on individual components; for example compressor, and cryostat weights were added for some cycles to obtain system weights.

In general, all three techniques were utilized to obtain the performance curves, but where possible the methods were selected in order of preference. Consideration of the maturity of the development of the cycles was also made. For example, the Vuilleumier and small Brayton cycles machines have not reached the same state of maturity in their development as the Stirling and Gifford-McMahon units. This consideration led to some instances where a curve fit through the best points for the newer cycles was made while for the more mature units a least squares fit was made. The individual data points are not shown on the cycle performance curves for ease of reading, however they are shown in Section 3.4.

It should be apparent from these comments that some significant extrapolations were required in making these curve fits and the authors judgment was used in many cases. For these reasons it is suggested that the following performance

data be used as a guide in performing trade-off studies and not as an absolute indication of the characteristics of units intended for space-flight cryogenic cooling.

3.6.1 Coefficient of Performance vs. Cooling Load

An indication of the thermal efficiency of the refrigerator is given by the coefficient of performance (COP) defined as the net refrigeration produced divided by the input power

$$\text{COP} = \frac{Q_{\text{ref.}}}{Q_{\text{input}}}$$

Figure 3-68 shows the COP data for five different cycles at 20°K as a function of the net refrigeration produced. In general, a large amount of applicable data was available for the various units. An exception was that of the Brayton cycle where predicted performance data was utilized. Data for large industrial units at higher cooling capacities are also shown, and the results of a previous study for the Stirling unit shows good comparison.

The value of COP for a reversible (Carnot) refrigerator is given by

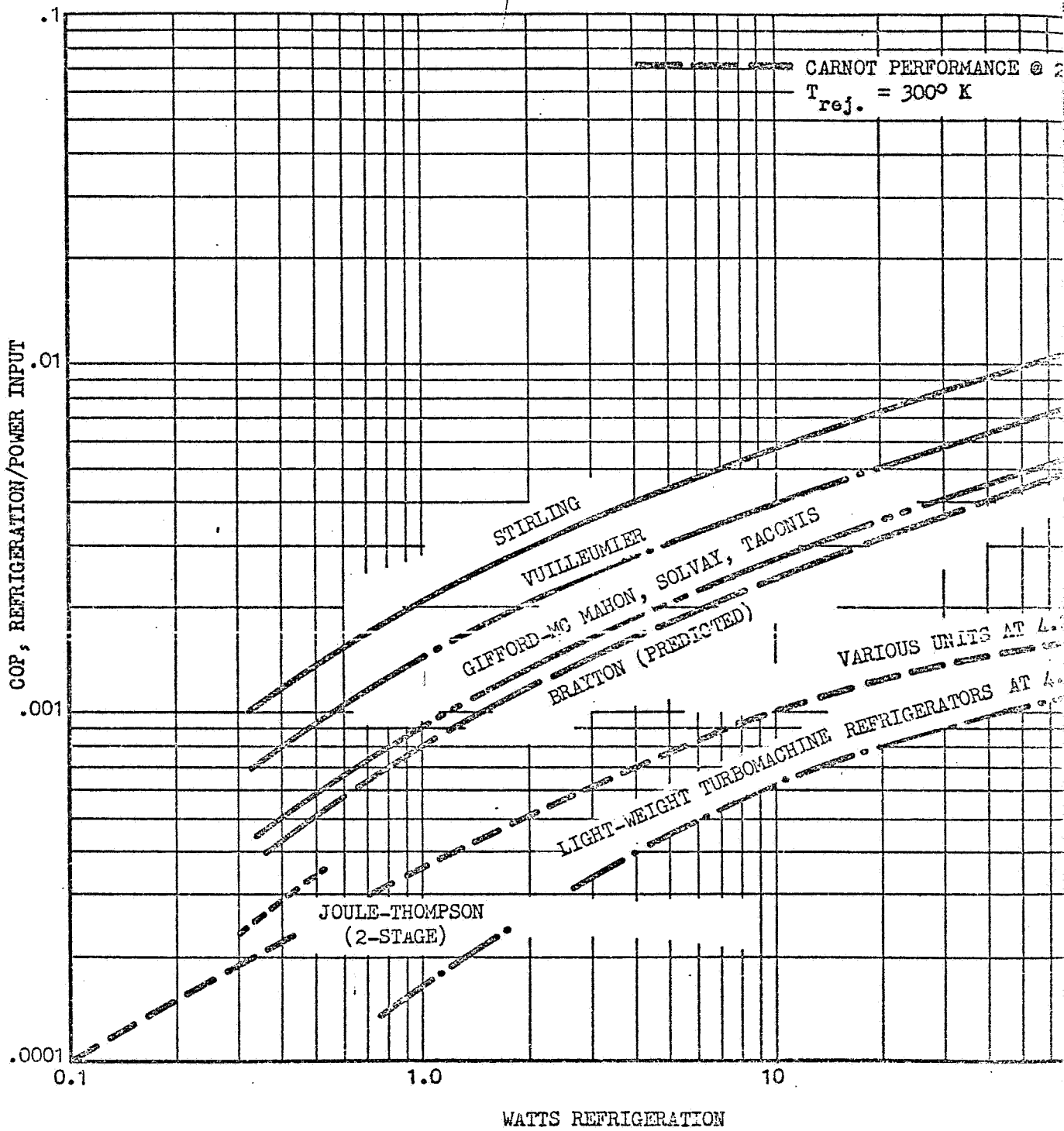
$$\text{COP} = \frac{T_c}{T_h - T_c}$$

where T_c is the temperature at which cooling takes place and T_h is the temperature of the surroundings (300°K for these units). The approach of the real refrigerators to the ideal (Carnot) performance can be seen by comparison with the COP for the Carnot engine of 0.0715.

The adverse effects of miniaturization are easily seen from Figure 3-68. The COP decreases substantially as the unit becomes smaller. This is due to the fact that relatively higher heat leaks are present for the smaller units because of the unfavorable area to volume ratios, and some components of the system become more difficult to fabricate efficiently in small size. Frictional losses are also proportionally higher.

The relative efficiency of the various cycles has been fairly well established with the exception of the Brayton cycle for which only predictions were available

FOLDOUT FRAME



FOLDOUT FRAME 2

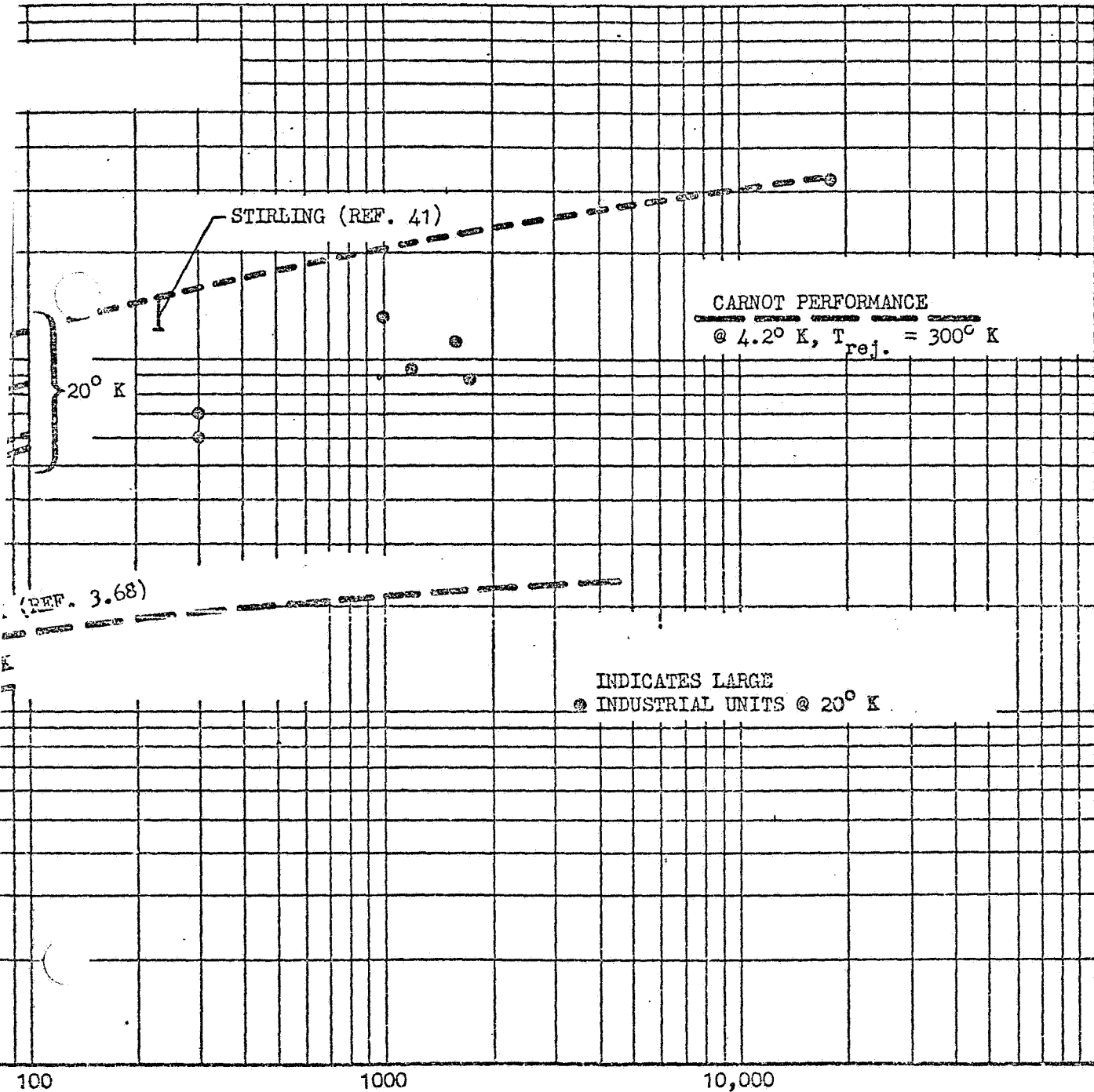


Fig. 3-68 Summary of Refrigerator Coefficient of Performance for Various Cycles at 20°K and 4.2°K

in the range of interest here. It is expected that if the performance of actual Brayton units is obtained, the values may be somewhat lower than shown since inefficiencies are generally higher than predicted. Performance for the Joule Thompson unit is shown only in the area of 0.4 W where data is available, predictions or extrapolations were not made, since the interest in a J-T unit for application in this area is limited.

Data for various units operating at 4.2°K is also shown in Figure 3-68 and is taken from reference 3-68. No attempt was made to show the relative performance of various cycles at this temperature, the curve being included only as a rough guide.

The units shown on the dotted curve represent for the most part ground based units where weight optimization was not performed. An additional curve is shown for lightweight turbomachinery refrigerators at 4.2°K, some of which were developed specifically for space flight. These reductions in weight are achieved with some loss in efficiency. As shown, the lightweight units are less efficient than the others.

Figure 3-69 shows COP data for the various cycles at 77°K, a temperature at which the majority of data is available. The same observations hold; the curve for the Brayton cycle is based on prediction plus one experimental point and the agreement with a previous study at higher cooling loads is satisfactory. The value for COP are substantially higher than at 20°K, and this is shown by the expression for the Carnot performance.

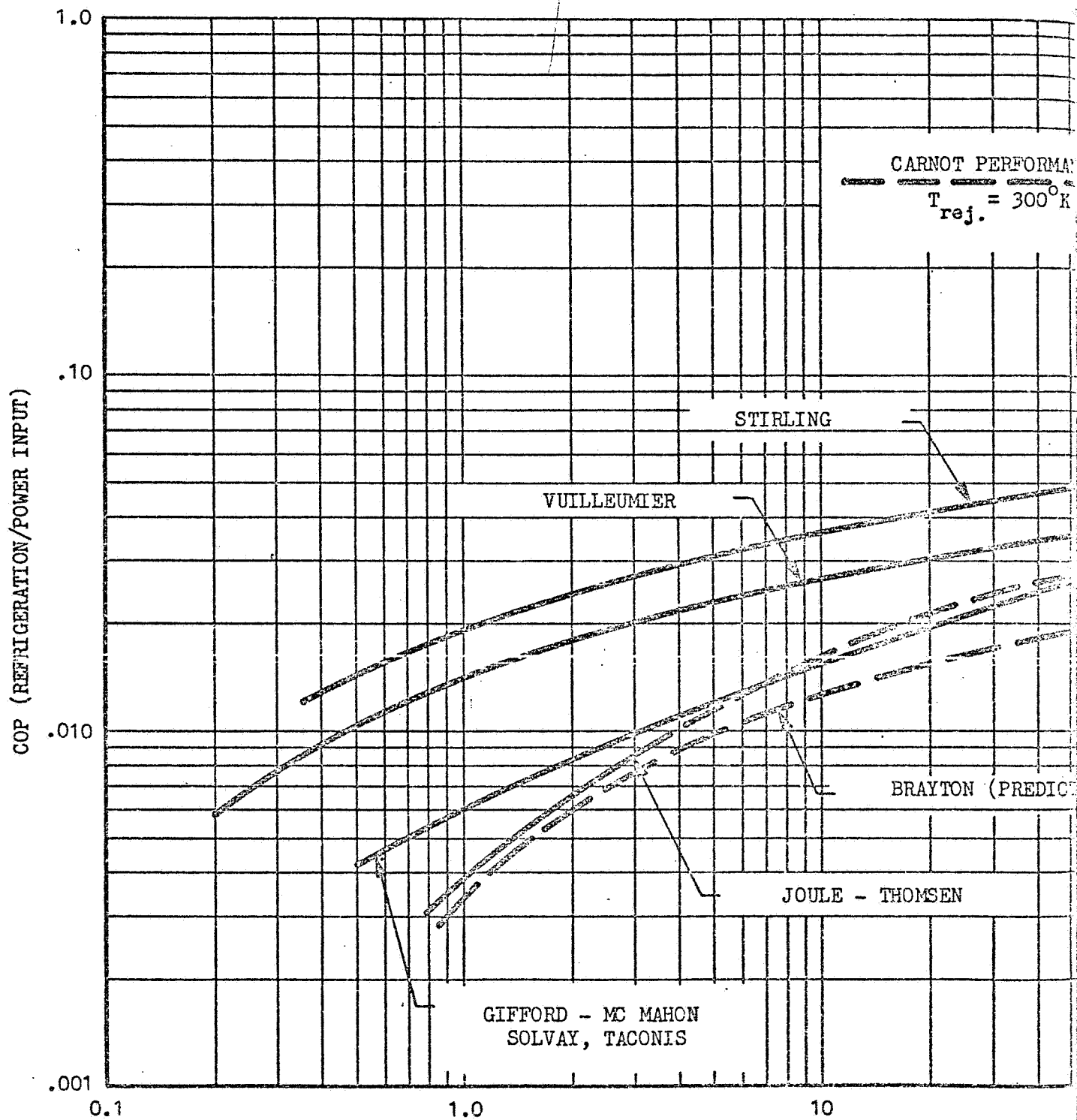
3.6.2 Coefficient of Performance vs. Temperature

Figure 3-70 and 3-71 show the effect of temperature on the COP at two cooling loads, 5W and 100W which correspond to the range of parameters for the study. The variation of COP with temperature is governed by two primary effects: (1) The COP begins to decrease rapidly as the minimum temperature for the particular cycle is approached. For example, as approximately 12°K is approached for the Stirling unit, the COP begins rapidly decreasing due to the rapidly decreasing specific heat of the regenerator material and corresponding loss of efficiency. The approximate minimum temperature achieved by the various cycles are indicated on the curves. (2) The curves generally parallel

FOLDOUT FRAME

CARNOT PERFORMANCE

$T_{rej.} = 300^{\circ}K$



FOLDOUT FRAME 2

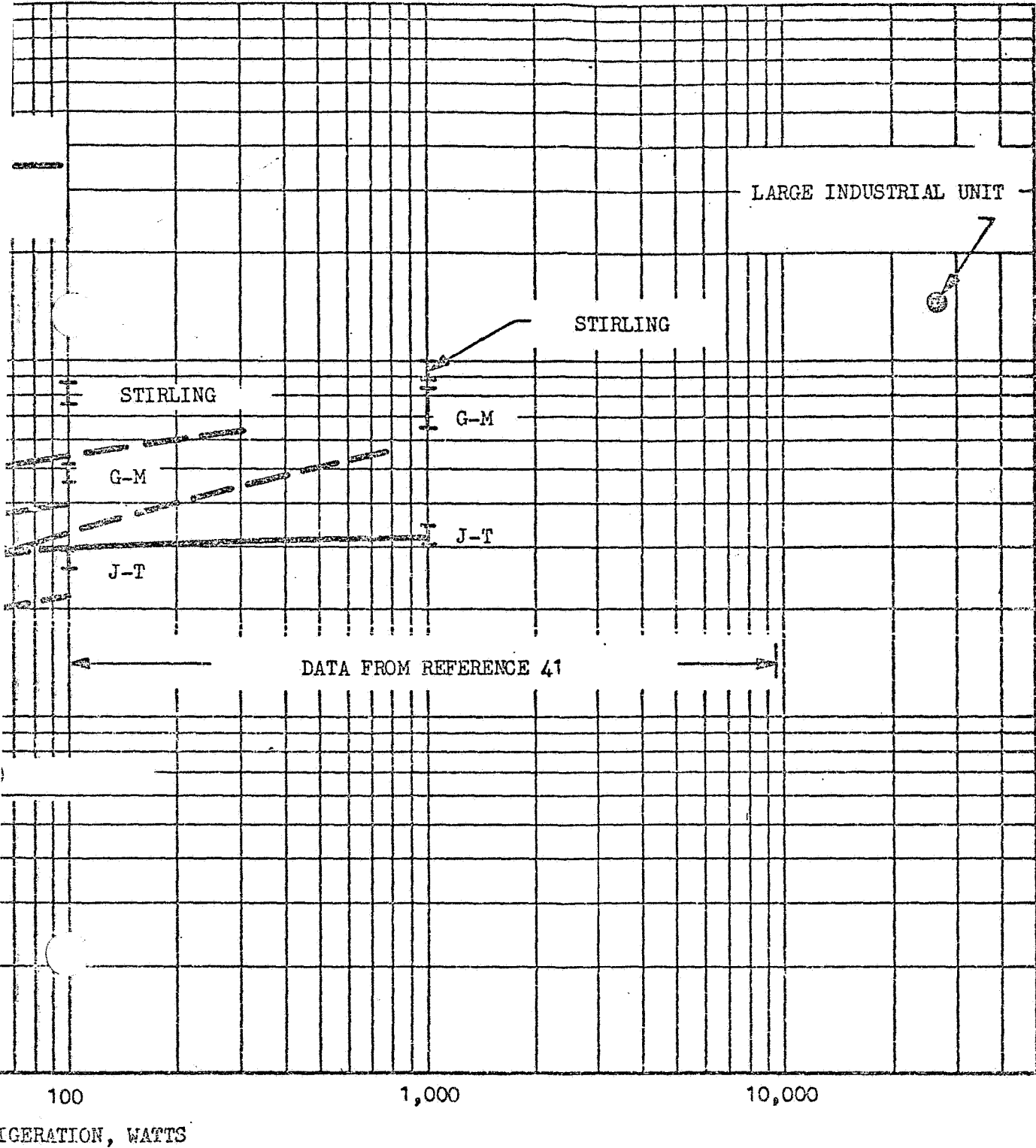


Fig. 3-69 Summary of Refrigerator Coefficient of Performance versus Refrigeration for Various Cycles at 77°K

PRECEDING PAGE BLANK NOT FILMED

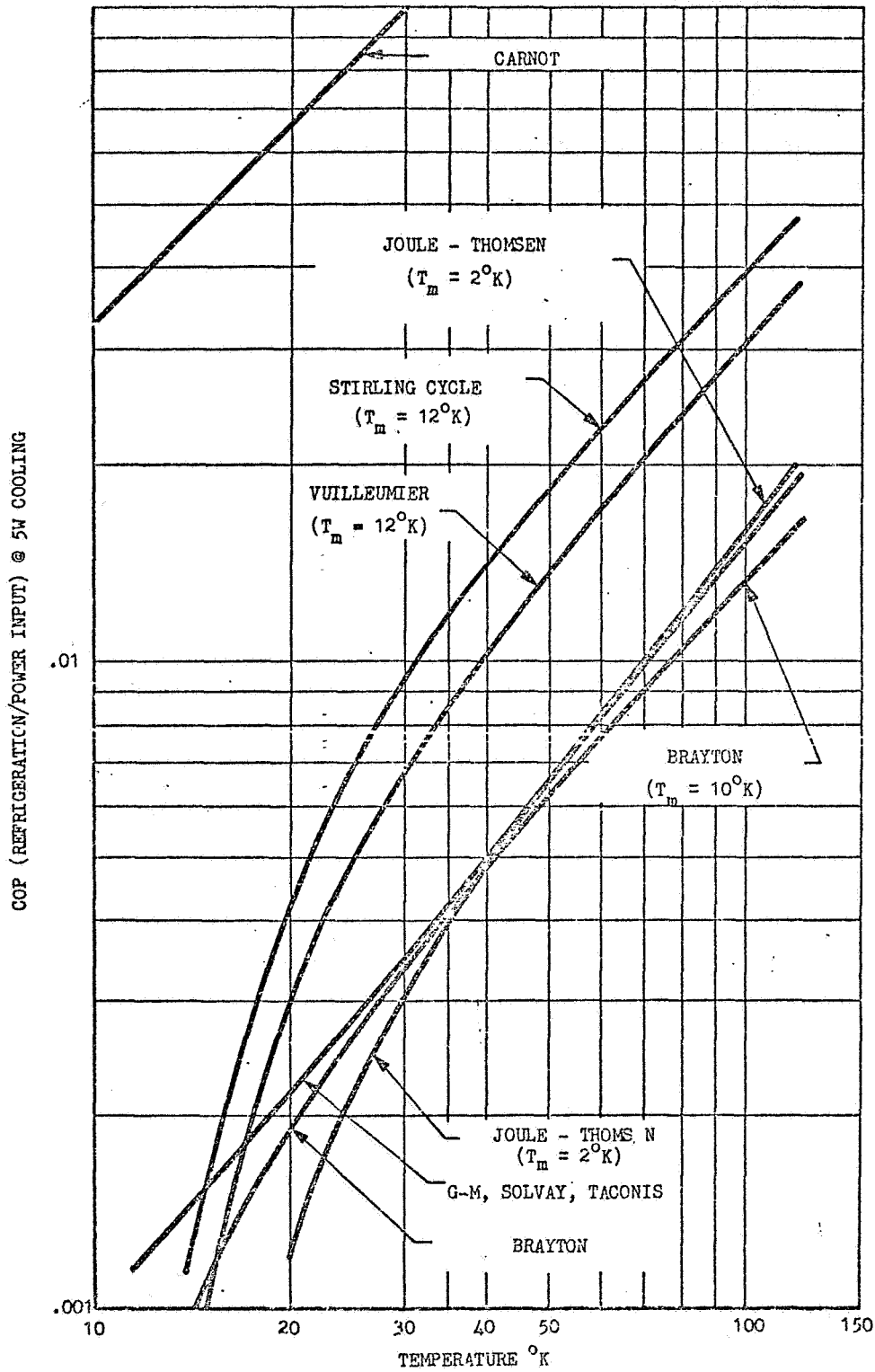


Fig. 3-70 Coefficient of Performance at 5 Watts versus Temperature

PRECEDING PAGE BLANK NOT FILMED

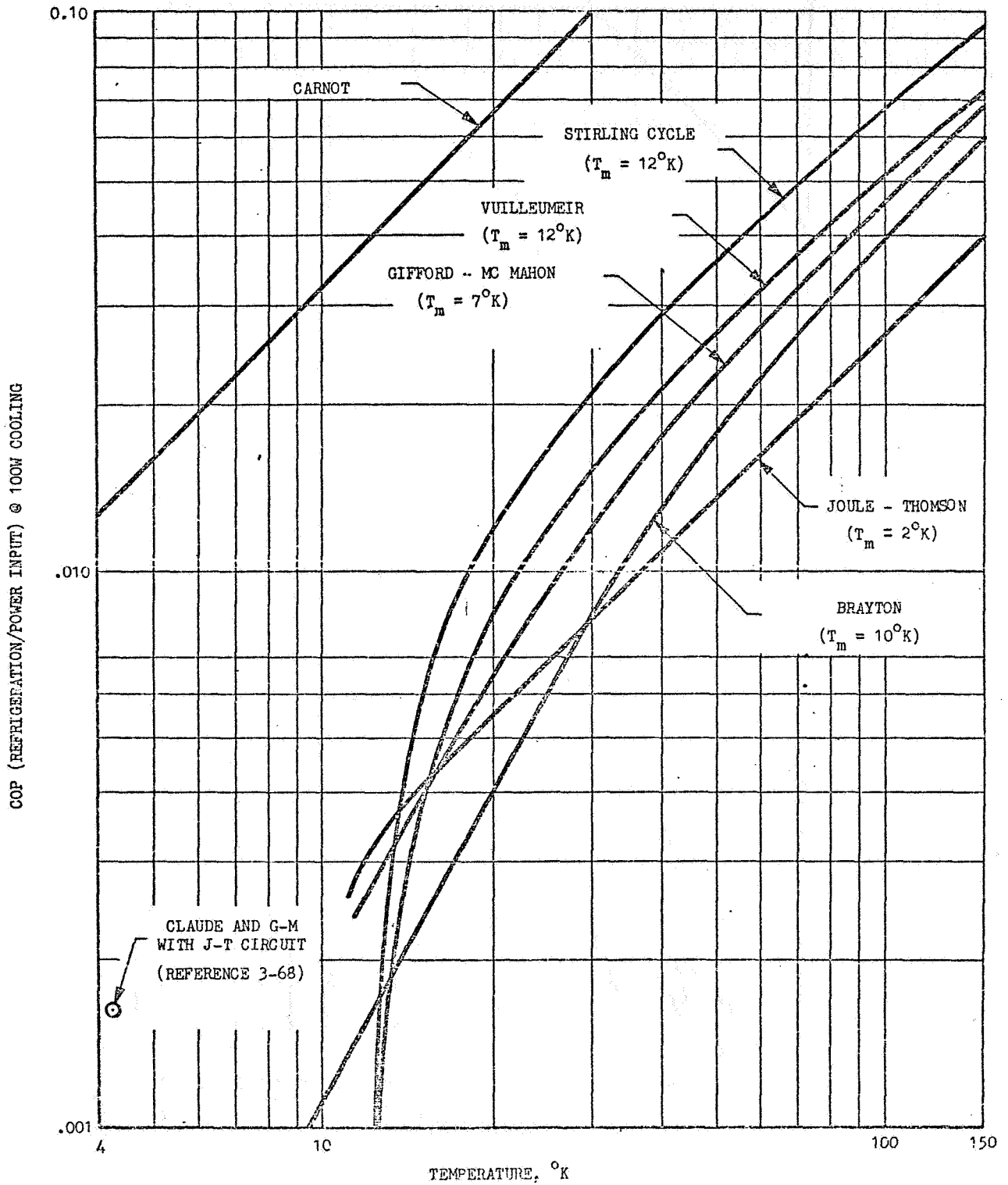


Fig. 3-71 Coefficient of Performance at 100 Watts versus Temperature

PRECEDING PAGE BLANK NOT FILMED

the Carnot efficiency curve at temperatures substantially higher than their minimum values, as shown on the figures.

Also shown is the performance of 4.2°K Claude and G-M units which both employ a Joule-Thomson expansion circuit to reach 4.2°K; the normal boiling point of helium.

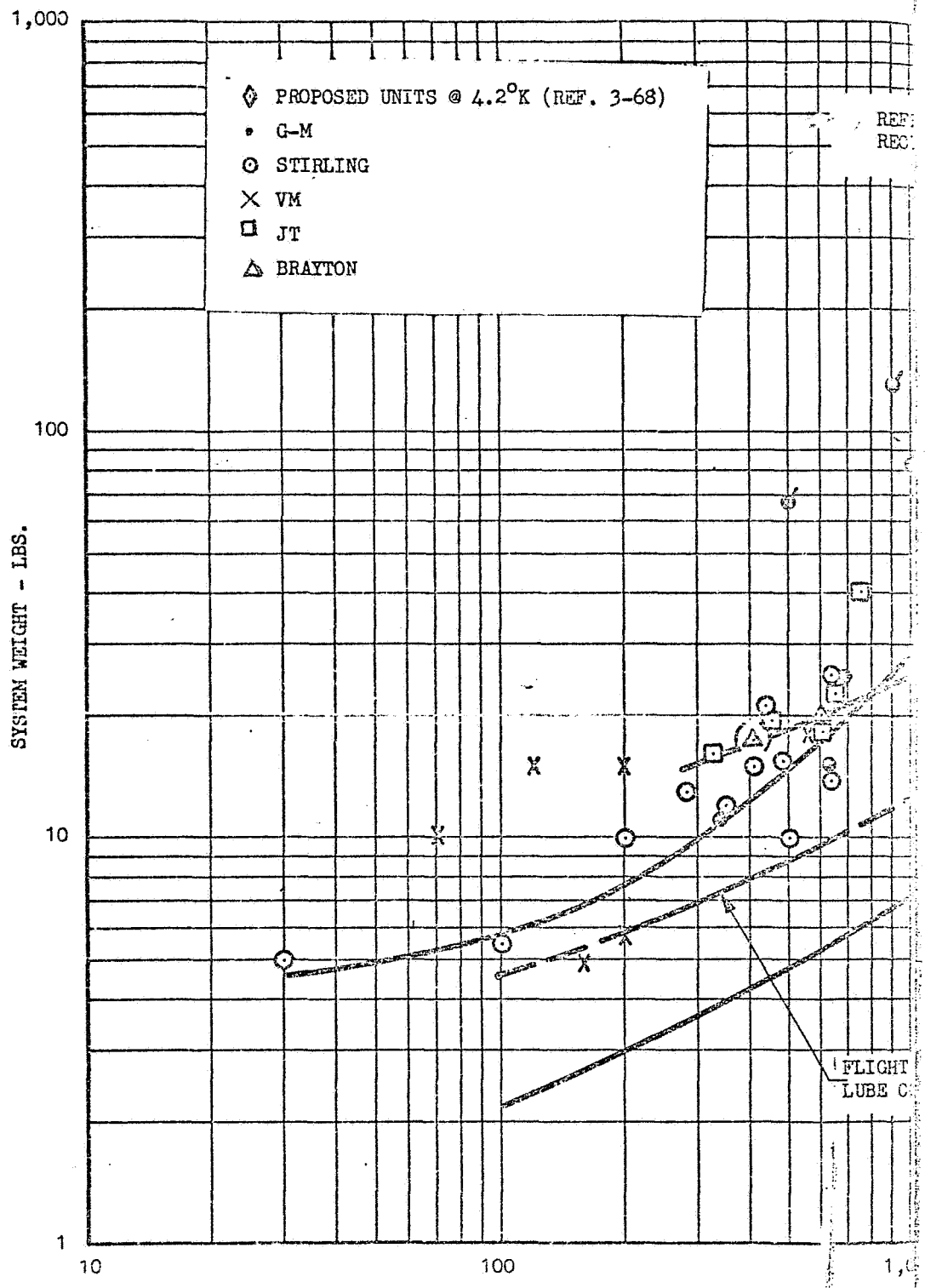
3.6.3 Refrigerator Weight vs Power Input

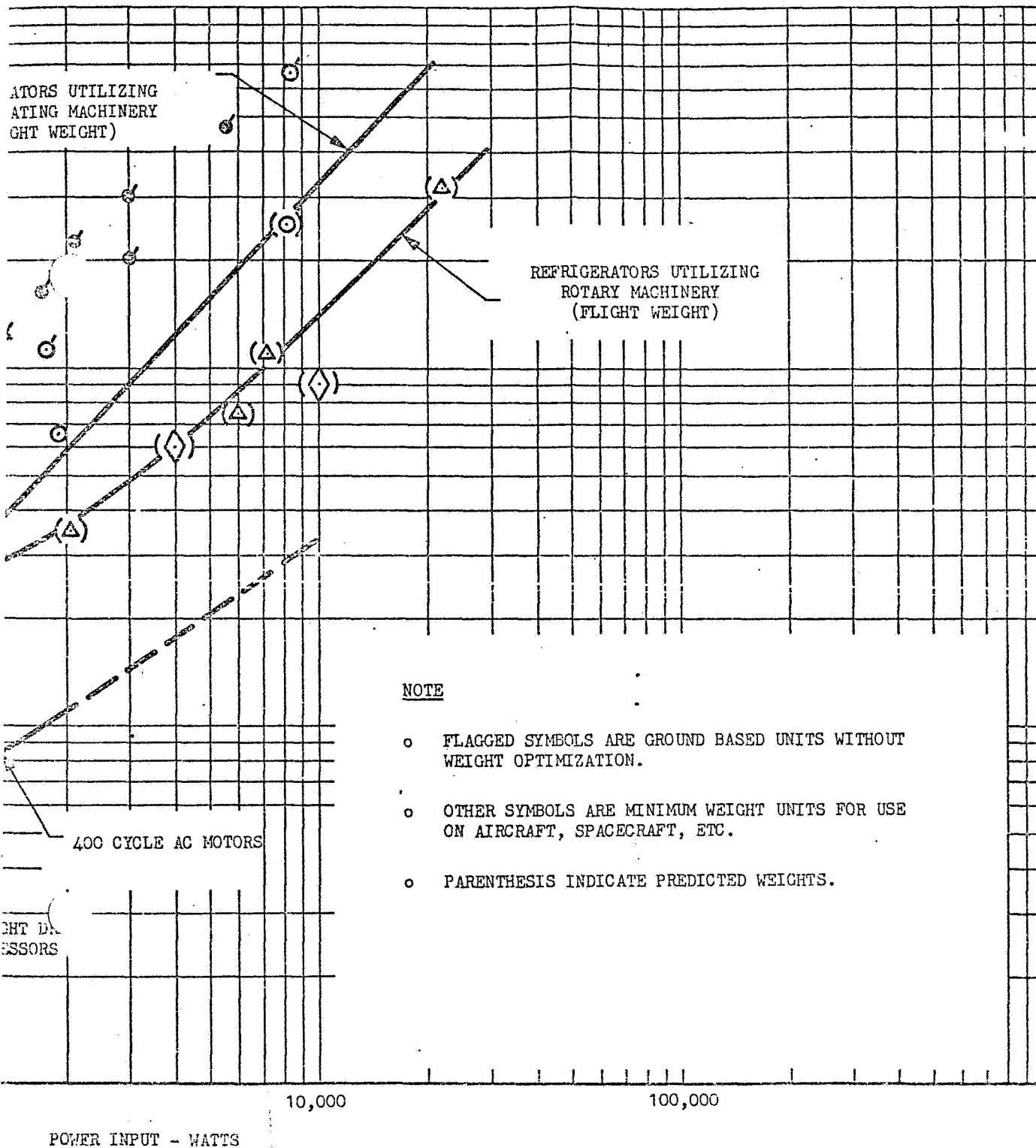
The weight of most machinery can be correlated quite successfully with the power input to the unit providing units with common design ground rules are utilized. For example, if the machinery is designed for space-flight where weight is a premium then this common basis will provide a consistent correlation. Data for compressors, motors, and complete refrigeration units was correlated on this basis. The complete results for compressors and motors are presented in Section 3.3. Figure 3-72 presents the correlation for refrigeration system weight as a function of input power. Some of the data for 400 Hz motors and dry lubricated compressors is also indicated in the figure to help discern the relative contribution of the different components to make up the total system weight. In fitting curves through the data, various cycles are indicated, and no differentiation was made as to cycle except for those cycles employing rotating machinery. These machines were considered separately from those employing reciprocating machinery. The curve fits were made through minimum weight systems rather than through the mean of the data to indicate the expected best weight that is currently attainable for weight optimized systems.

Data points are shown for units which are obviously designed for ground use with no weight minimization as flagged points, and are shown for general interest, although they were not used in the curve fits.

The curves presented in Figure 3-72 can be utilized in predicting weights of various units for which specific weight data is not available, and this technique was used in some instances where important data was lacking. The data also show the importance of obtaining a high coefficient of performance in order to minimize weight. For the higher power inputs, little data on weight optimized systems was available, and some extrapolations were necessary

FOLDOUT FRAME





NOTE

- FLAGGED SYMBOLS ARE GROUND BASED UNITS WITHOUT WEIGHT OPTIMIZATION.
- OTHER SYMBOLS ARE MINIMUM WEIGHT UNITS FOR USE ON AIRCRAFT, SPACECRAFT, ETC.
- PARENTHESIS INDICATE PREDICTED WEIGHTS.

Fig. 3-72 Refrigerator System Weight Versus Power Input for Various Machines

PRECEDING PAGE BLANK NOT FILMED

to cover the desired range. For the Brayton cycle systems employing turbomachinery a combination of predicted values and a few experimental points were used.

The results show a weight advantage for the turbomachinery units for power inputs in excess of about 800-900 watts.

3.6.4 Weight vs Cooling Capacity

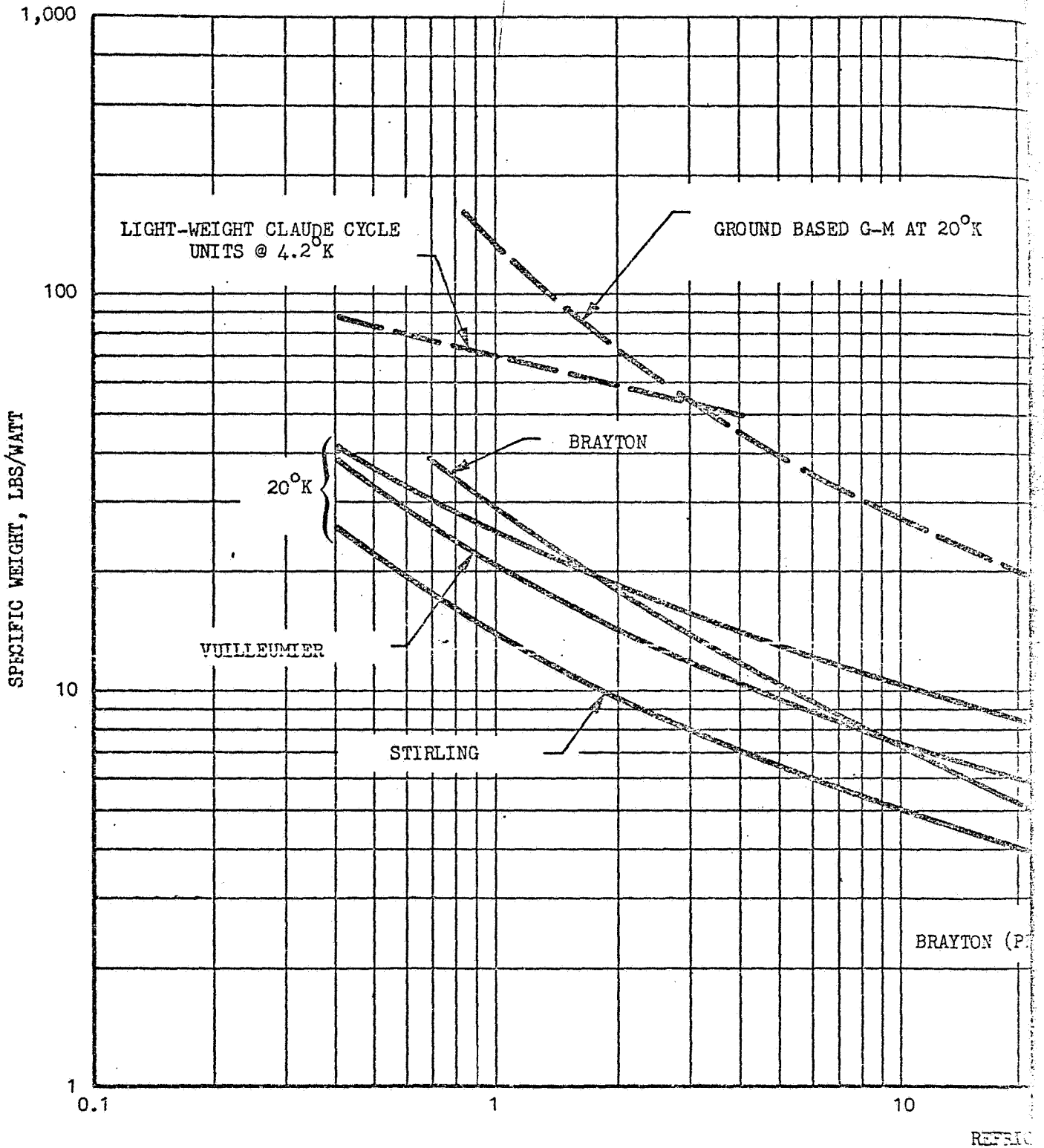
Figure 3-73 shows the comparison of weights for the various cycles at 20°K. Wherever possible data for operating flight weight systems was utilized. For those cases where sufficient data was lacking, weights were estimated based on a combination of the curve fits for COP previously described and the system weights vs power input. As might be expected the lower weight cycles are those with the highest thermal performance (COP) values, the Stirling units being the lightest weight systems, while the Brayton cycle shows a relatively improved position at the higher cooling rate. Comparison with a previous study (Ref. 3-41) at higher cooling rates is again shown. The weight of heavy units for ground use (oil lubricated compressor, etc.) is shown for the G.M., Taconis and Solvay units for comparison with what is expected for a weight optimized unit for those cycles. Weight optimized versions of the Solvay and G.M. cycle units have been built and are operating in the cooling range near one watt.

In addition, a curve is shown for lightweight Claude cycle refrigerators at 4.2°K. This curve is based primarily on predicted values and requires experimental verification before it can be used with any degree of confidence.

All of the curves show a reduction in specific weight as the refrigeration level is increased. This tendency is primarily a consequence of the variation of the coefficient of performance vs cooling rate, and the character of the curves is similar to the COP vs refrigeration curves.

Figure 3-74 shows the specific weight data for the 77°K cooling level. More operating data on actual units was available for this case than at 20°K. The same general comments are applicable to this curve as for the 20°K case. The weight of the units is substantially less than at 20°K.

FOLDOUT FRAME



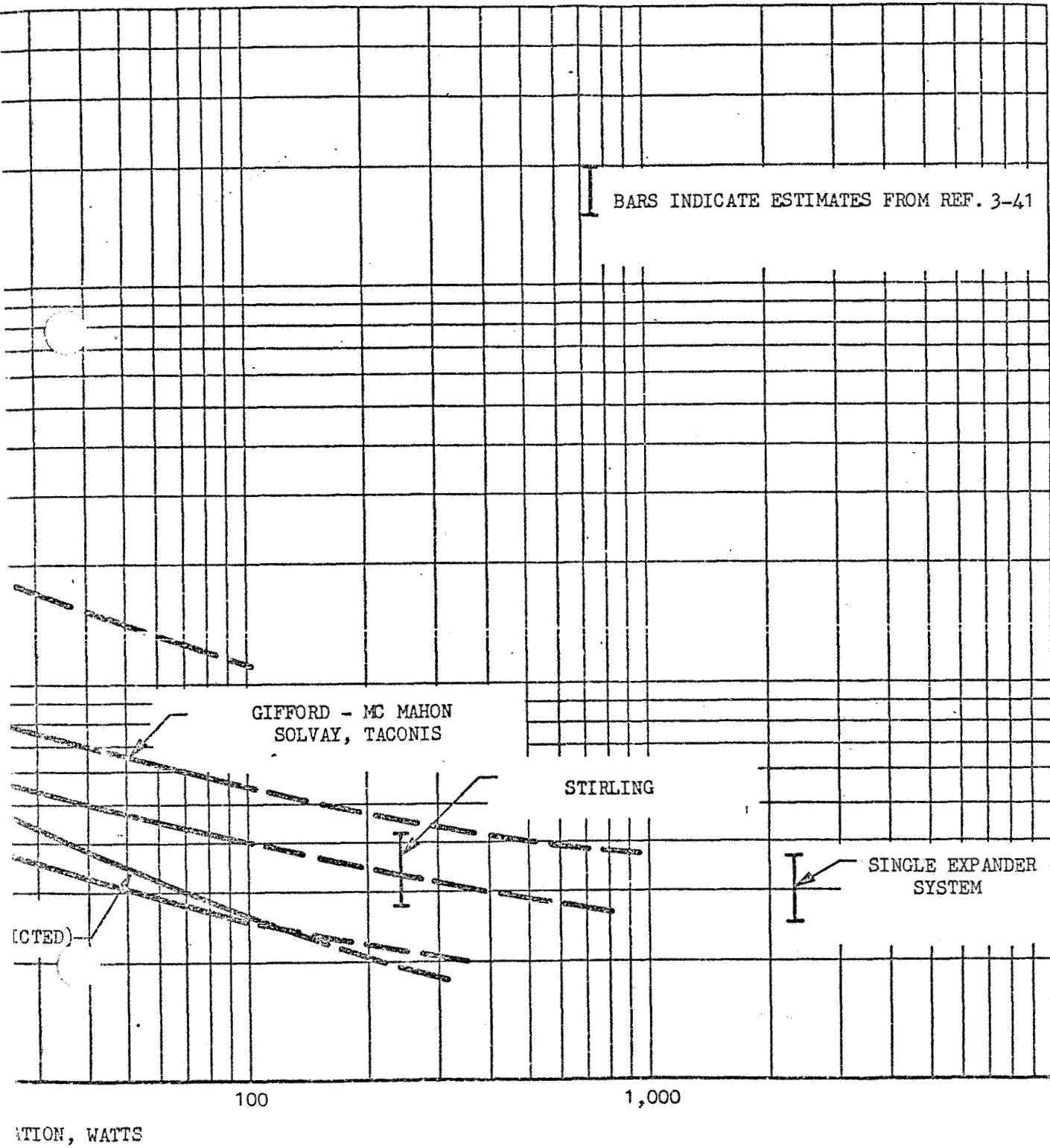
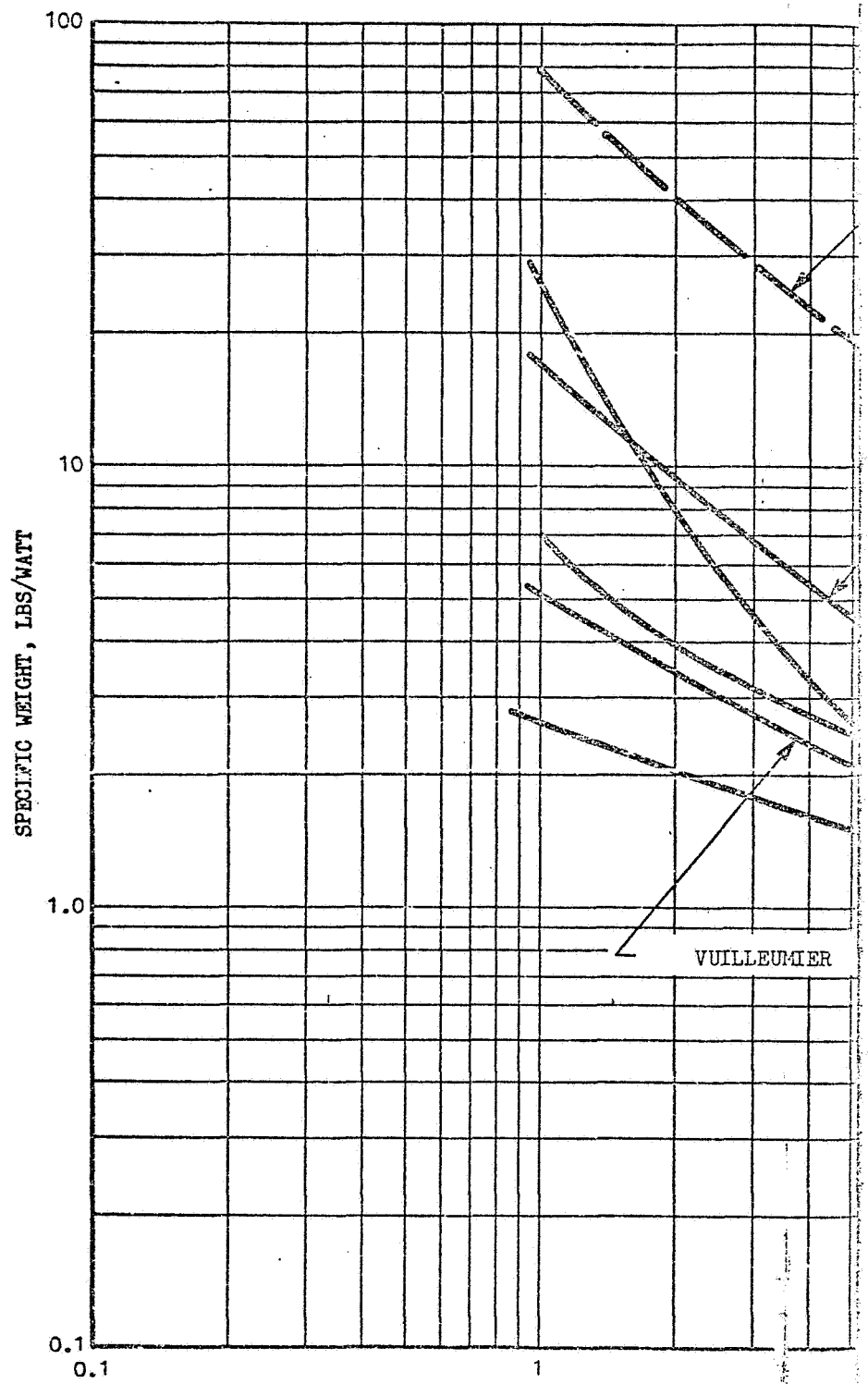


Fig. 3-73 Summary of Refrigerator Weights Versus Refrigeration for Various Cycles at 20°K and 4.2°K

FOLDOUT FRAME |



FOLDOUT FRAME 2

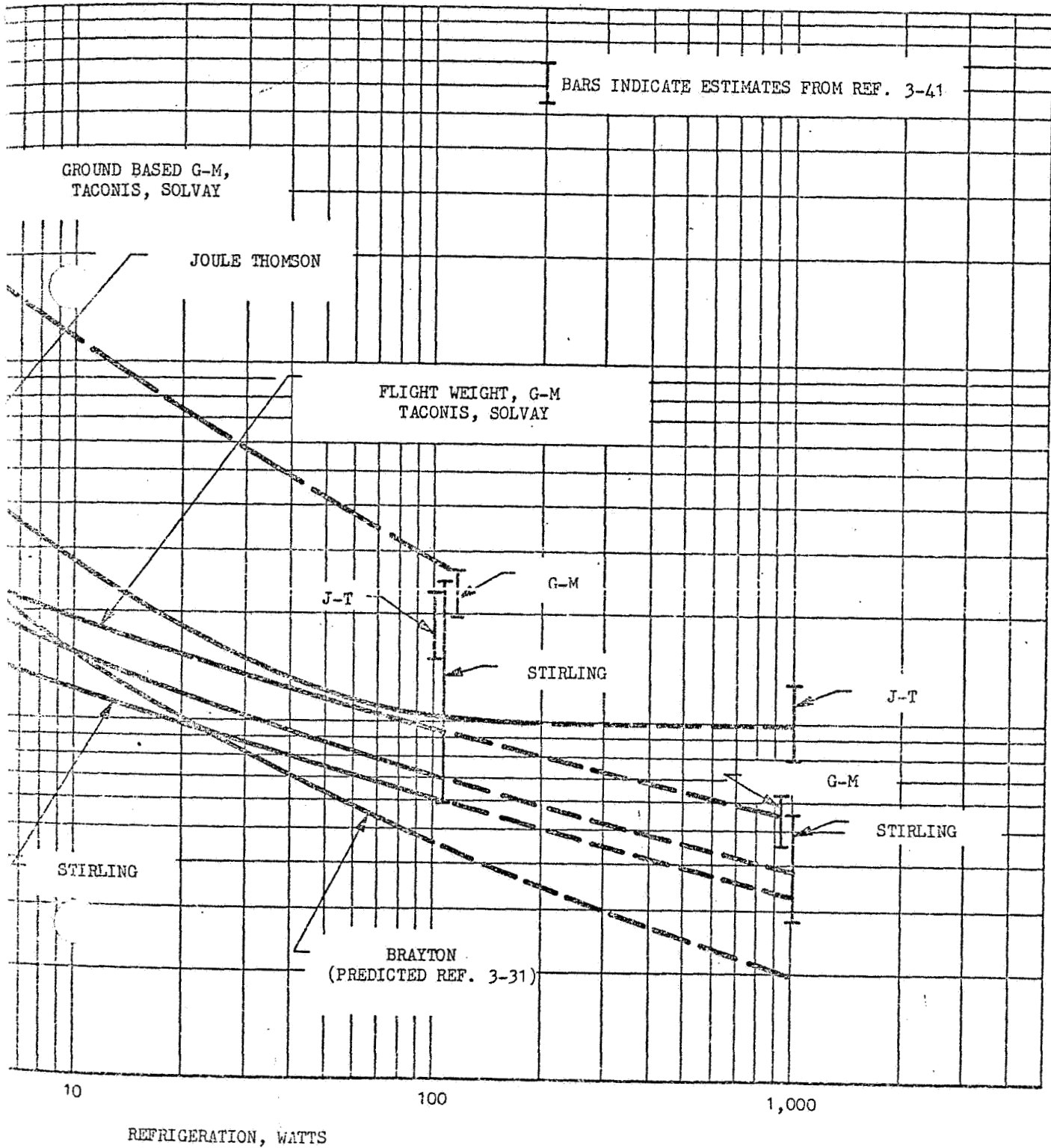


Fig. 3-74. Summary of Refrigerator Weight Versus Refrigeration for Various Cycles at 77°K

PRECEDING PAGE BLANK NOT FILMED

3.6.5 Weight vs Temperature

The specific weight vs temperature is shown in Figures 3-75 and 3-76 for cooling levels of 5 watts and 100 watts. The characteristics of the curves are similar to the COP vs temperature curves.

As the minimum temperatures are approached the weights rapidly increase as the thermal efficiency rapidly decreases, while at the higher temperature the slope becomes nearly constant. These curves can be utilized to make estimates of weight requirements at intermediate temperatures. Additional cross-plotting will be necessary to assess weight penalties at other cooling rates than the 5 watts and 100 watts selected here.

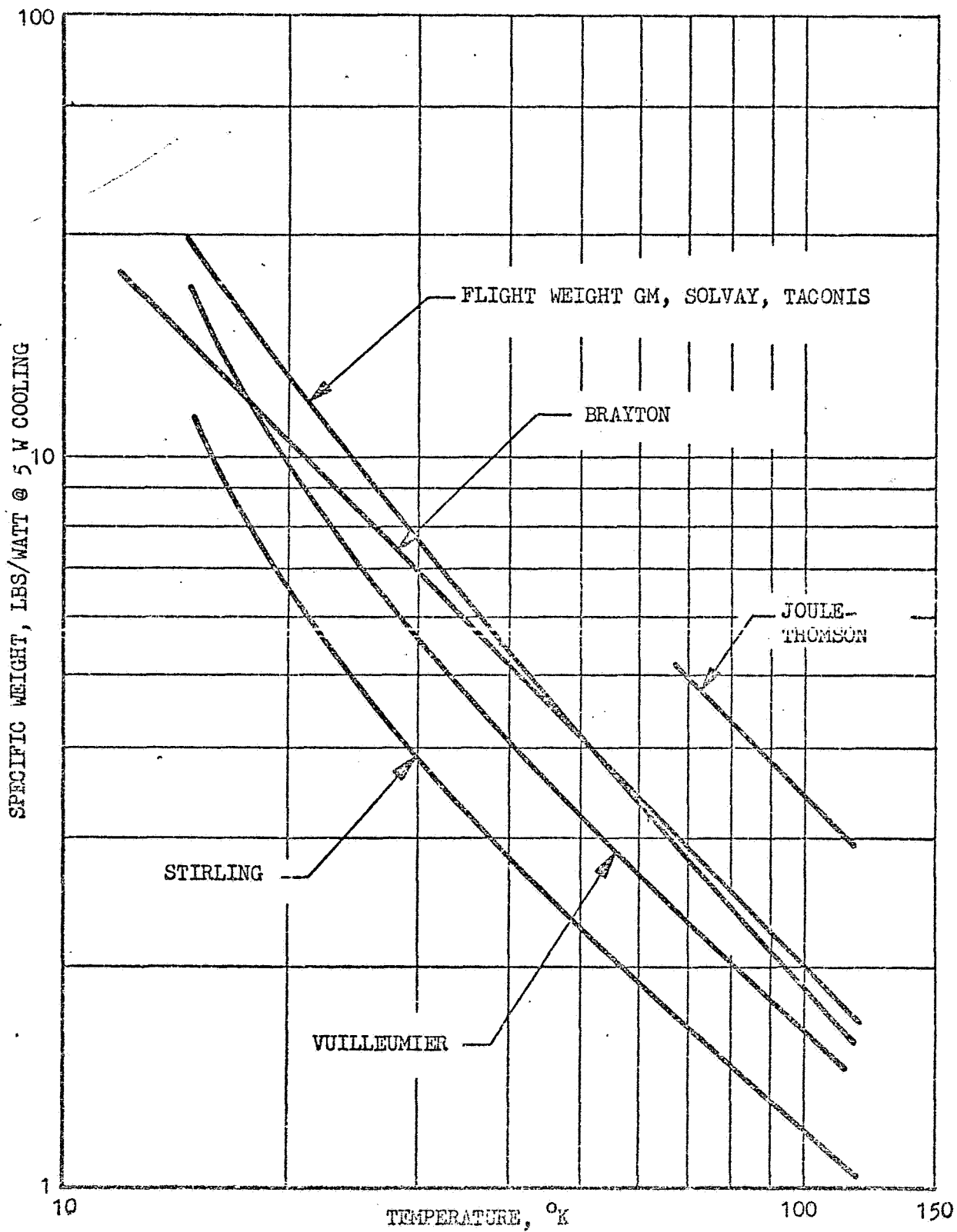


FIG. 3-75 SUMMARY OF REFRIGERATOR WEIGHTS VS. TEMPERATURE AT 5 WATT COOLING CAPACITY

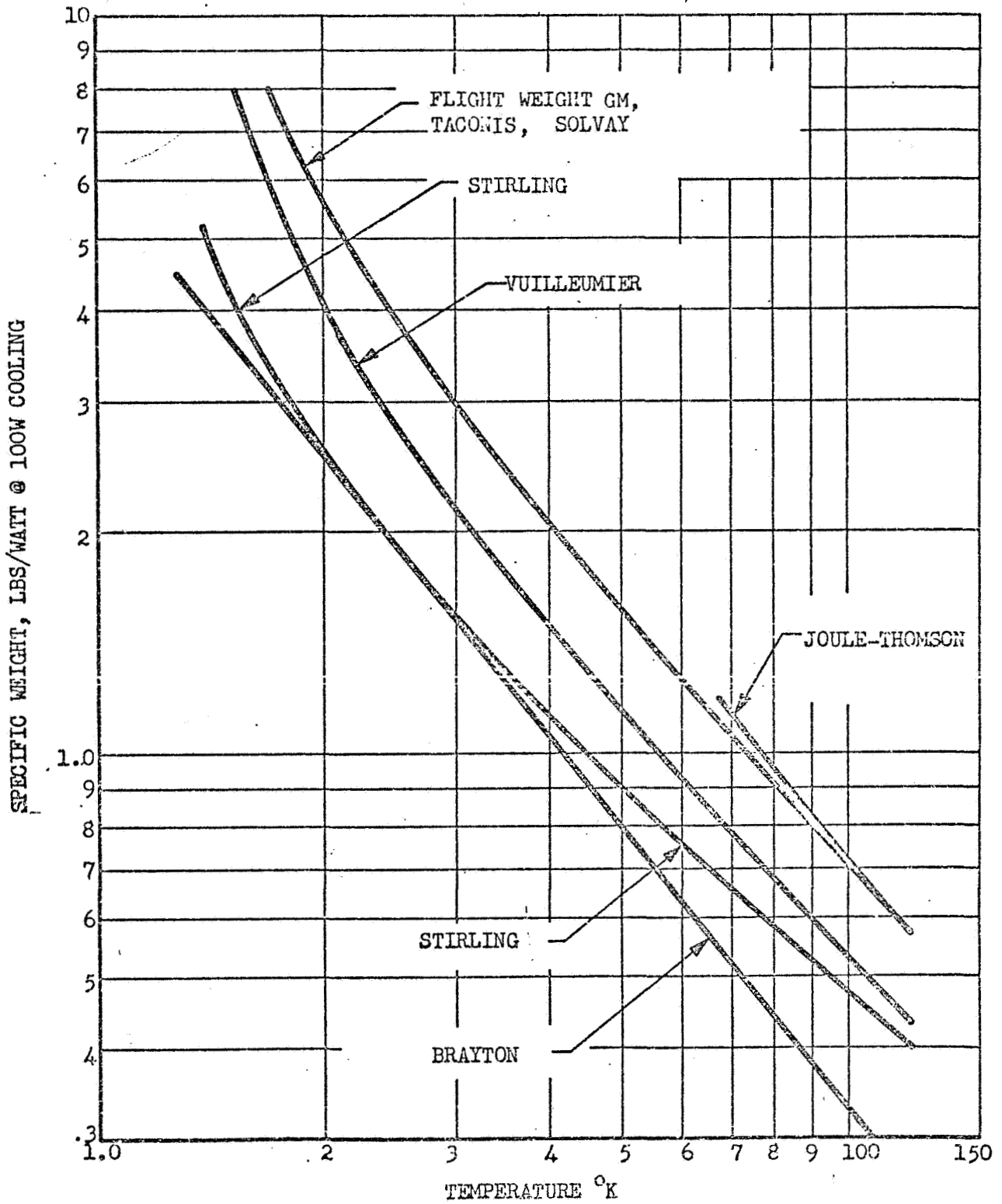


Figure 3-76 Summary of Refrigerator Weights vs. Temperature at 100 Watt Cooling Capacity

3.6.6 System Volume

The volume of the refrigeration systems showed the greatest spread and least correlation of the various parameters. One reason for this is that volume data were not readily available for most units. Reported data did not specify if actual (displaced) volume was reported or if the volume envelope was specified. In the majority of cases the drawings of the units were utilized to calculate the volumes. The system volumes for specific units are presented in the tables. Some cycles are inherently more compact than others. For example, the Stirling cycle can be conveniently fabricated in a single unit and lends itself to compact packaging. The Solvay cycle or Gifford-McMahon may consist of two or three separable units (compressor, cryostat, valve assembly) in which the overall volume is somewhat higher. The Solvay or Gifford-McMahon unit, on the other hand, offers greater flexibility since the cryostat is quite small and can be more easily integrated into a cryogenic system, while the compressor can be mounted in a remote location, connected to the cryostat only by the gas supply and return lines.

Several correlations of the volume data were attempted, the first being system volume vs power input. The result showed excessive scatter. A more successful correlation is shown in Figure 3-77 which shows the system density as a function of system weight. The data show considerable scatter. Also shown on the curve is data on large industrial units which provide cooling at 4.2°K (Reference 3-68). The following trends are in evidence from the data.

1. The density of lightweight units intended for flight is quite low. This is felt to be due to the greater use of lightweight materials such as aluminum in place of the more commonly utilized steel.
2. The lightweight Stirling units seem to form a separate trend at a higher density. This may be due to the basic character of the cycle which lends itself to very efficient packaging compared with the other units.

3. The data appear to show a reduction in density with increased weight. A possible explanation for this is that the larger units were specifically intended for terrestrial use in which the design goals were ease of installation and servicing of components. A greater potential for volume reduction therefore exists for the large units.

It is suggested that in the absence of better volume data for a unit the two density lines shown be utilized; one for the Stirling units and one for the other units as shown on the figure.

The system volume data which follows is based on Figure 3-77 in the absence of more specific data on units.

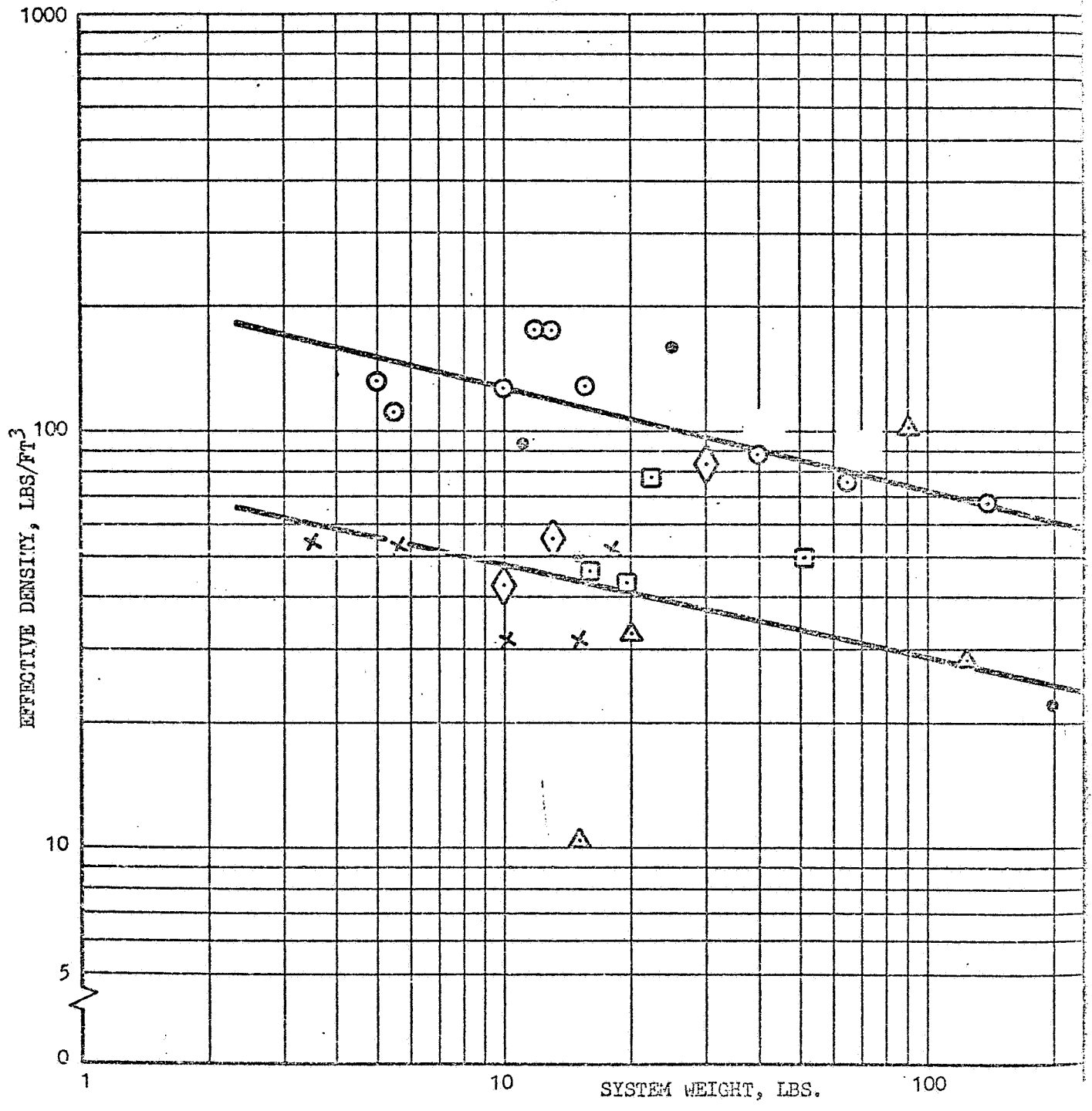
3.6.7 System Volume vs Cooling Rate

Figures 3-78 and 3-79 present the curve fits for specific volume as a function of cooling rate at 20°K and 77°K for the cycles considered. The general character of the curves is again similar to the COP and weight curves. The volume curves represent the largest uncertainty of the various parameters and a substantial reduction in volume should be obtainable with proper design techniques. Most of the units have provisions for either air or water cooling included in the volumes, which may be eliminated, or at least reduced for space application.

3.6.8 System Volume vs Temperature

Figures 3-80 and 3-81 present a cross plot of the data for specific volume as a function of temperature at cooling rates of 5 and 100 watts. The same general considerations govern the character of these curves as for the COP and weight data.

FOLDOUT FRAME



FOLDOUT FRAME 2

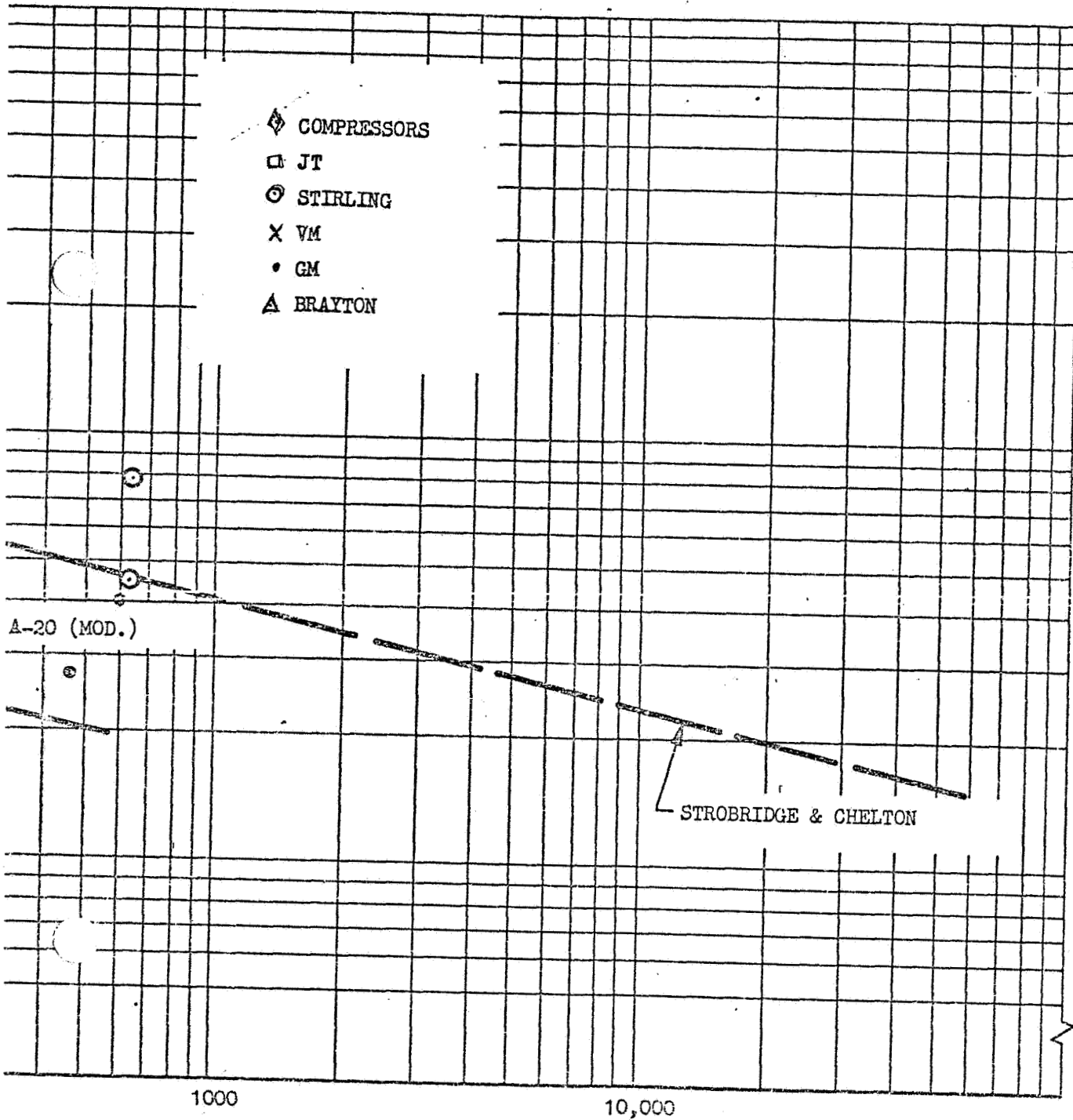
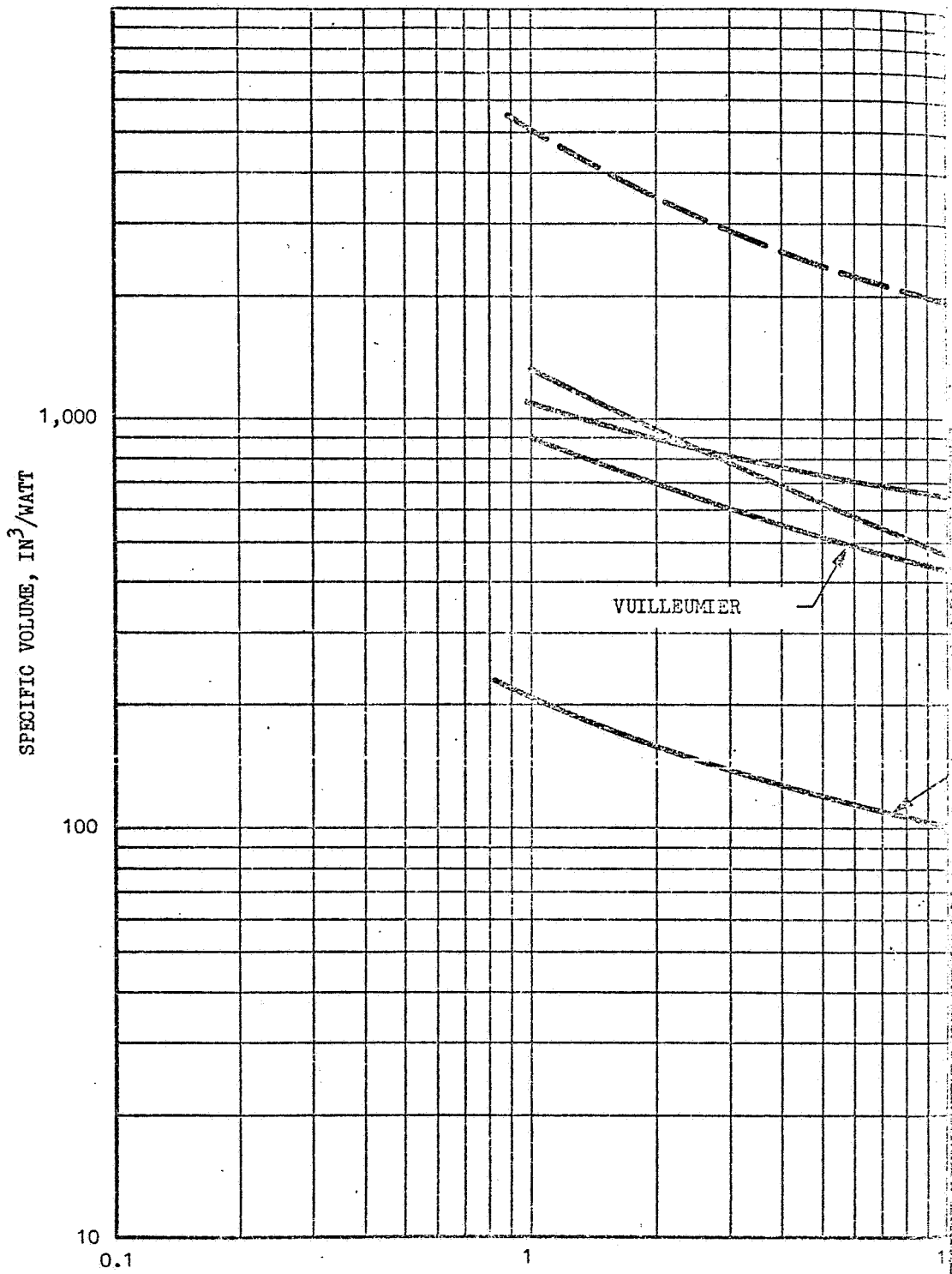


Fig. 3-77 Refrigerator System Density Versus System Weight

FOLDOUT FRAME)



FOLDOUT FRAME 2

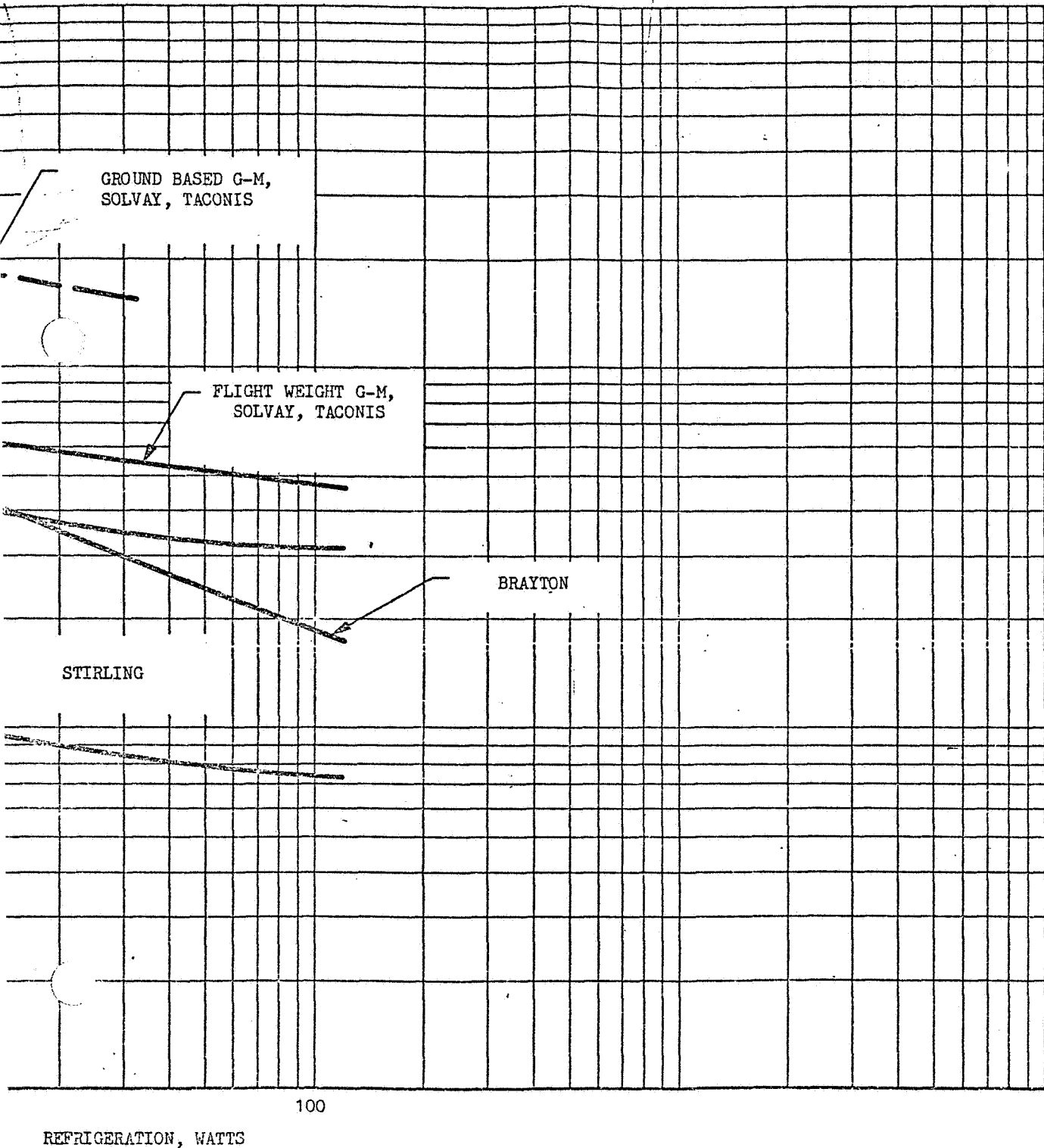
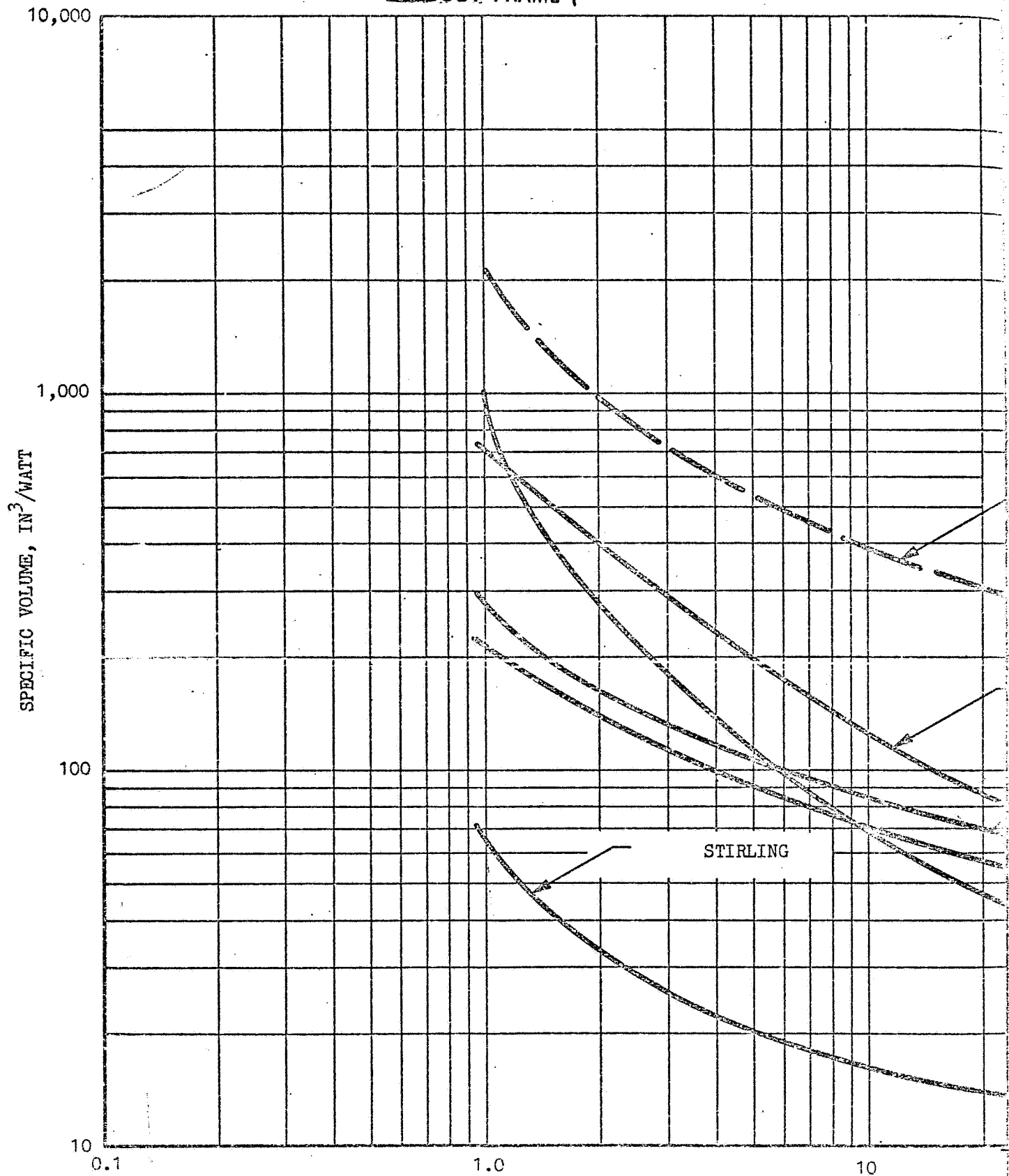


Fig. 3-78 Summary of Refrigerator Specific Volume Versus Refrigeration at 20°K

FOLDOUT FRAME (



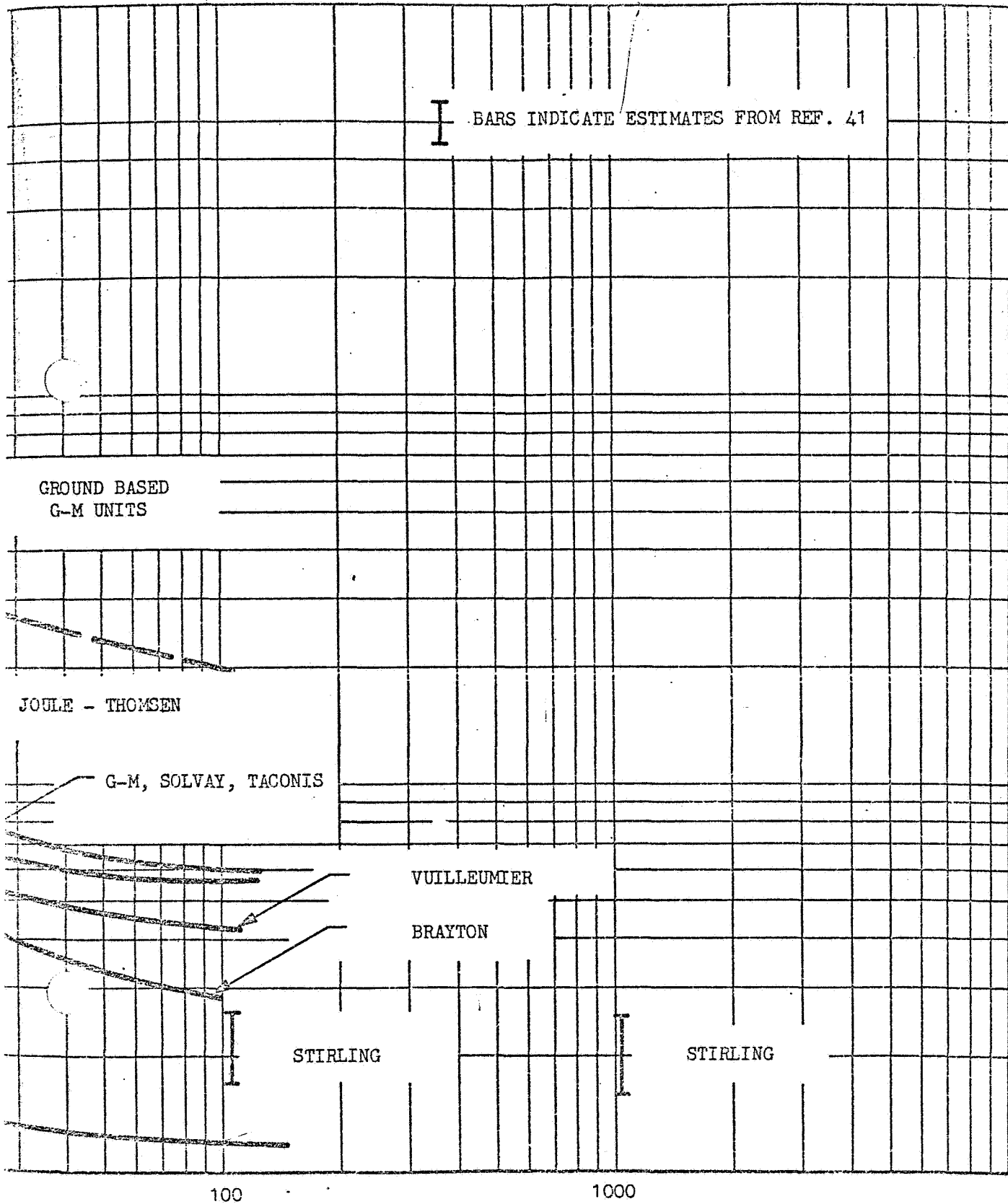


Fig. 3-79 Summary of Refrigerator Specific Volume Versus Refrigeration at 77°K

PRECEDING PAGE BLANK NOT FILMED

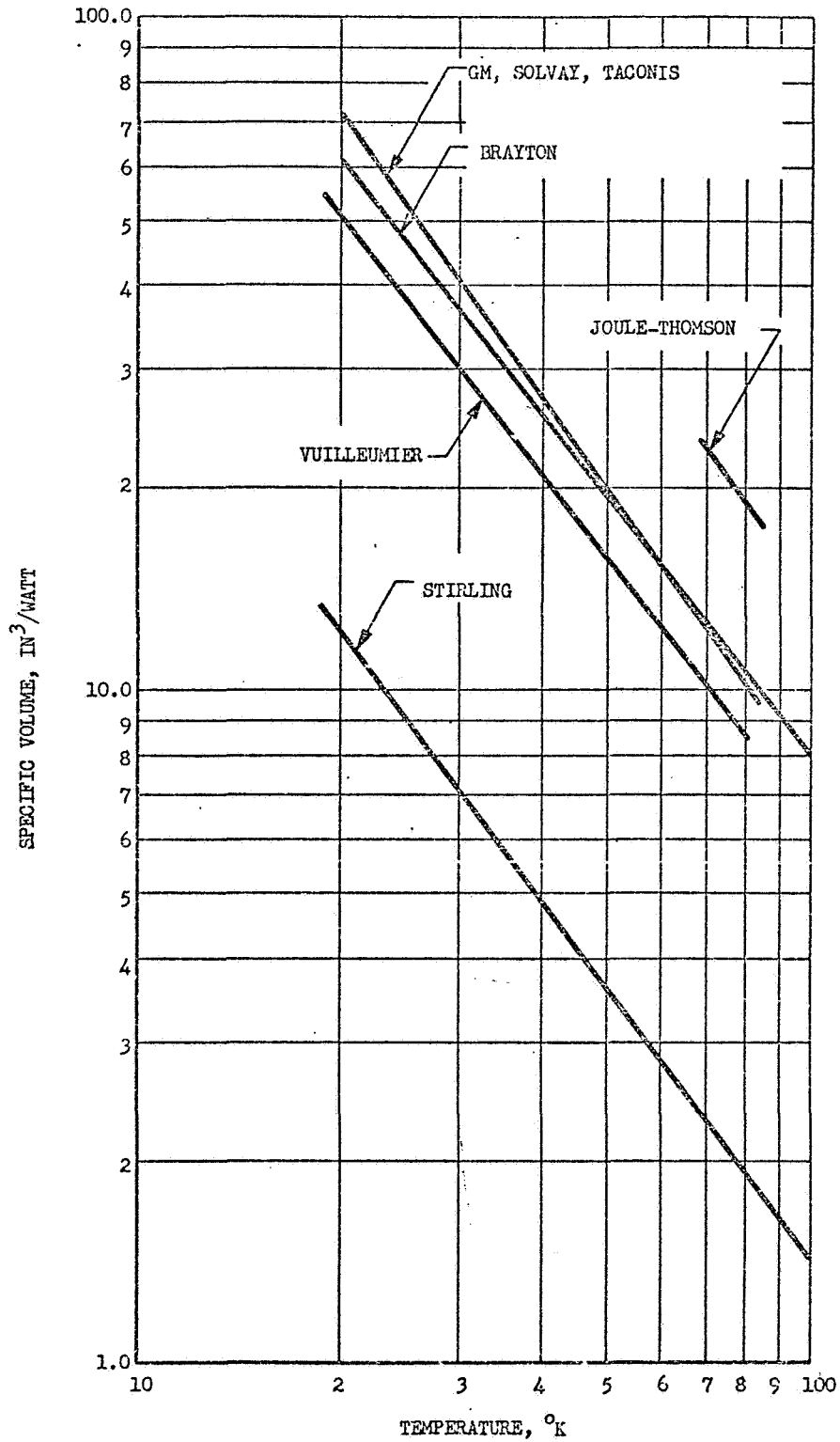


Figure 3-80 Summary of Refrigerator Specific Volume Versus Temperature for Various Cycles at 5 Watts

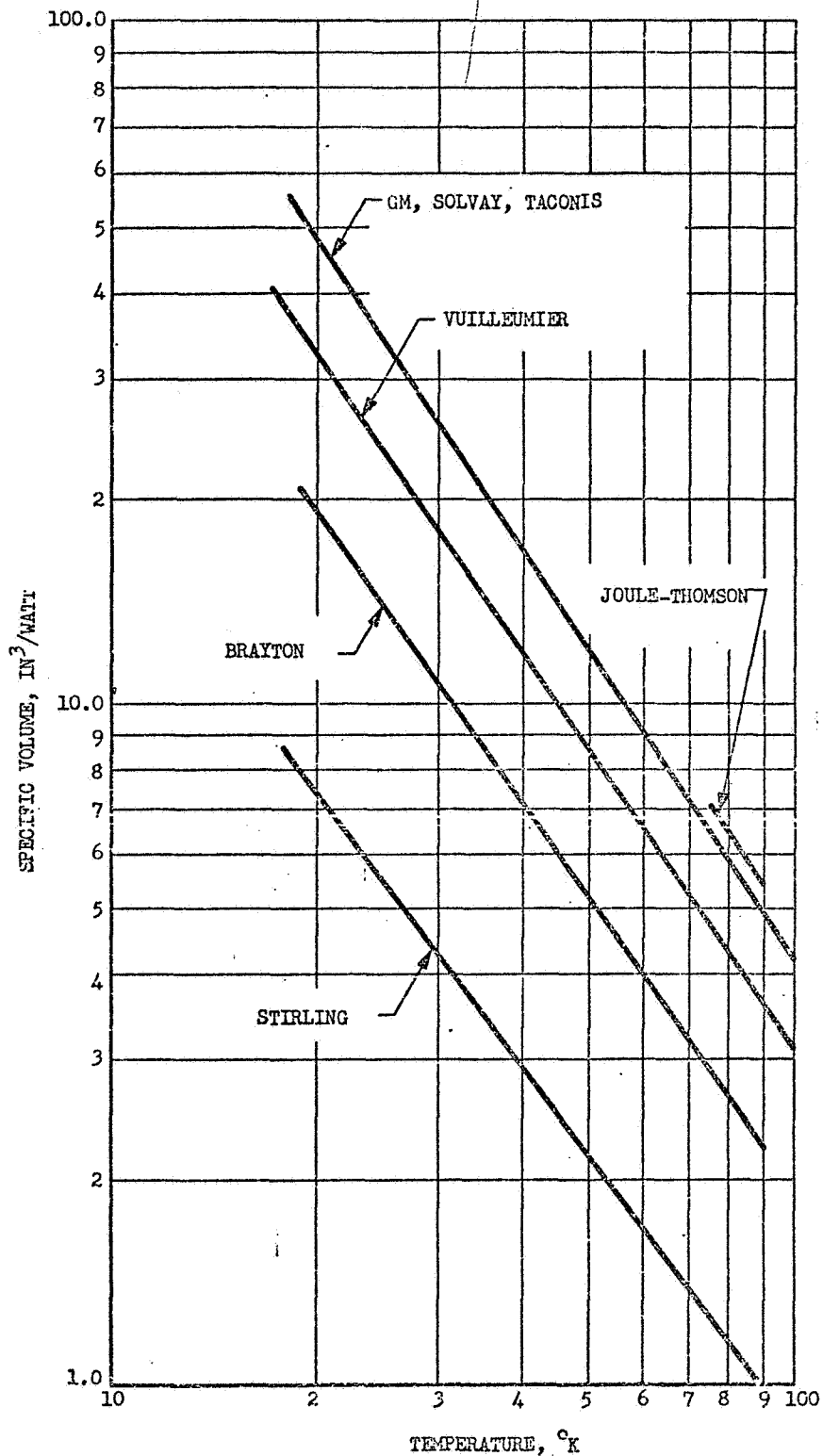


Figure 3-81 Summary of Refrigerator Specific Volume versus Temperature for Various Cycles at 100 Watts

LIST OF REFERENCES REVIEWED

- 3-1. Zefex, Inc., Bulletins 114-2, 114-118-1, 118-1, 118-3
- 3-2. Gast Manufacturing Corp., Bulletin ROC-169
- 3-3. Tecumseh Products Company, Bulletin 108-8.
- 3-4. Bendix-Westinghouse Automotive Air Brake Company, Form No. BWE-581-9.
- 3-5. Copeland Refrigeration Corporation, Form No. 5907-R-10
- 3-6. Maddocks, F. E., "3.6°K Closed-Cycle Turborefrigerator" AFFDL-TR-67-134, Air Force Flight Dynamics Laboratory, Wright-Patterson Air Force Base, Ohio, October 1968
- 3-7. Breckenridge, R. W., "Exploratory Development of a 1 watt, 3.6°K Reciprocating Refrigerator for Space Applications", AFFDL-TR-68-59, Air Force Flight Dynamics Laboratory, Wright-Patterson Air Force Base, Ohio
- 3-8. Colyer, D. B., "Miniature Cryogenic Refrigerator Turbo alternators", Advances in Cryogenic Engineering, Vol. 14, Plenum Press, New York, (1969.)
- 3-9. Kohler, J. W. L., "The Stirling Refrigeration Cycle", Scientific American, April 1965, Vol. 212, No. 4, pp. 119-127.
- 3-10. Kohler, J. W. L., "Principles of Gas Refrigerating Machines", Advances in Cryogenic Engineering, Vol. 2, Plenum Press, New York (1960), pp. 243-249
- 3-11. Kohler, J. W. L., "Refrigeration Below -100°C", Advances in Cryogenic Engineering, Vol. 5, Plenum Press, New York (1960), pp. 518
- 3-12. Prast, G., "A Modified Philips Stirling Cycle for Very Low Temperatures", Advances in Cryogenic Engineering, Vol. 10, Plenum Press, New York (1964), p. 40-45
- 3-13. Cowans, K. W., Walsh, P. J., "Continuous Cryogenic Refrigeration for Three to Five Micron Infrared Systems", Advances in Cryogenic Engineering, Vol. 10, Plenum Press, New York (1964), pp. 468-476
- 3-14. Rios, P. A., Smith, J. L., Jr., "An Analysis of the Stirling-Cycle Refrigerator", Advances in Cryogenic Engineering", Vol. 14, Plenum Press, New York (1968), p. 332
- 3-15. Qvale, E. B., "An Analytical Model of Stirling-Type Engines", PhD Thesis, Massachusetts Institute of Technology, Jan. 1967.
- 3-16. Rios, P. A., "An Analytical and Experimental Investigation of The Stirling Cycle," PhD Thesis, Massachusetts Institute of Technology, Sept. 1969.
- 3-17. Malaker Laboratories, "Miniature Stirling Cycle Cooler", AFAL-TR-65-15, July 1964
- 3-18. Pitcher, G. E., DuPre, F. K. "Miniature Vuilleumier Cycle Refrigerator", Advances in Cryogenic Engineering, Vol. 15, Plenum Press, New York (1969)

- 3-19. Magee, F. N., Doering, R. D., "Vuilleumier Cycle Cryogenic Refrigerator Development", AFFDL-TR-68-67, August 1968.
- 3-20. Dean, J. W., Mann, D. B., "The Joule-Thomson Process in Cryogenic Refrigeration Systems", NBS TN 227, National Bureau of Standards, Feb. 1965
- 3-21. Muhlenhaupt, R. C., Strobridge, T. R. "An Analysis of the Brayton Cycle as a Cryogenic Refrigerator", NBS TN 366, National Bureau of Standards, August 1968
- 3-22. Muhlenhaupt, R. C., Strobride, T. R., "The Single-Engine Claude Cycle as a 4.2°K Refrigerator." NBS TN 354, National Bureau of Standards, June 1967
- 3-23. Wilson, D. J., d'Arbeloff, B. J., "The Performance of Refrigeration Cycles Below 100°R." Advances in Cryogenic Engineering, Vol. 11, Plenum Press, New York (1965), pp. 160-170.
- 3-24. Johnson, R. W., Collins, S. C., "A Hydraulically Operated Two-Phase Helium Expansion Engine", Advances in Cryogenic Engineering, Vol 16, Plenum Press, New York, 1970 (E-4)
- 3-25. Wapato, P. G., "Design and Development of a Miniature Non-Reciprocating Closed-cycle Cooler, TR AFFDL-TR-67-9, March 1967.
- 3-26. Maddocks, F. E., "3.6°K Closed-Cycle Turborefrigerator", AFFDL-TR-67-134, Oct. 1968
- 3-27. Breckenridge, R. W., "Development of a Miniature Reciprocating Cryogenic Refrigerator for Space Applications", AFFDL-TR-67-78, May 1967.
- 3-28. Breckenridge, R. W., "Exploratory Development of a 1 Watt, 3.6°K Reciprocating Refrigerator for Space Applications," AFFDL-TR-68-59, Oct. 1968.
- 3-29. Crawford, A. H., "Specifications of Cryogenic Refrigerators", Cryogenics, Vol. 10, No. 1, Feb. 1970, pp. 28-37.
- 3-30. Colyer, D. B., Gessner, R. L., "Miniature Cryogenic Refrigerator Turbomachinery", Advances in Cryogenic Engineering, Vol. 13, Plenum Press, New York (1967), pp. 485-493
- 3-31. Gessner, R. L., Colyer, D. B. "Miniature Claude and Reverse Brayton Cycle Turbomachinery Refrigerators, Advances in Cryogenic Engineering, Vol. 13, Plenum Press, New York, (1967), pp. 474-484.
- 3-32. Wapato, P. G., "Development of a 4.2°K Cryogenic Refrigerator System", AiResearch Manufacturing Corp. Rept. 66-0347, June 1966
- 3-33. Fleming, R. B., "A Compact Perforated-Plate Heat Exchanger", Advances in Cryogenic Engineering, Vol. 14, Plenum Press, New York (1968), pp. 197-204
- 3-34. Colyer, D. B., "Miniature Cryogenic Refrigerator Turboalternators", Advances in Cryogenic Engineering, Vol. 14, Plenum Press, New York (1968), pp. 405-415

- 3-35. "The Development of Closed-Cycle Cryogenic Coolers for Long Duration Continuous Operation", AiResearch Manufacturing Co., 1966
- 3-36. Schonewald, Roger, "Cryogenic Refrigeration Systems", Industrial Research, Vol. 7, No. 10, Sept. 1965, pp. 86-91
- 3-37. Rochkind, Mark M., "Long Duration Cooling Using Open-Cycle Joule-Thomson Refrigeration", Review of Scientific Instruments, Vol. 38, No. 8, Aug. 1967, pp. 1171-3
- 3-38. Daunt, J. G., Goree, W. S., "Miniature Cryogenic Refrigerators", Report to Office of Naval Research Contract Nonr-263(70) (Stevens Institute of Technology) and Contract N0014-67-C-0393 (Stanford Research Institute.) 1969
- 3-39. Gifford, W. E., "Refrigeration Below 20°K". Cryogenics, Vol. 10, No. 1, Feb. 1970, pp. 23-27
- 3-40. "Conceptual Design Study of Space-borne Liquid Hydrogen Recondensers for 10 and 100 Watts Capacity". Arthur D. Little, May 1962. Report No. 63270-11-02 NAS 5-664.
- 3-41. Malaker Laboratories, "Investigation of Gas Liquefiers for Space Operation." ADS-TDR-63-775, August 1963
- 3-42. Hagedorn, N. H., "Parametric Mass Analysis and Comparison of Two Types of Reactant Cooling- and-Storage Units for a Lunar-Based Hydrogen-Oxygen Regenerative Fuel Cell System." NASA TND-4386, February 1968
- 3-43. Stephens, S. W., "Advanced Design of Joule-Thomson Coolers for Infra-Red Detectors." The Hymatic Engineering Col. Ltd. Infrared Physics, Vol. 8, No. 1, 1968, pp. 25-35
- 3-44. Breckenridge, R. W., "Spaceborne Refrigeration Systems." Cryogenics and Infrared Detection Systems Technical Colloquium, Frankfurt, W. Germany, April 1969
- 3-45. McCormick, J. E., "Cryogenic Refrigeration Efficiency Nomograph." ASHRAE Journal, Vol. 8, No. 11, 1966, pp. 60-65
- 3-46. Strobridge, T. R., "Refrigeration for Superconducting and Cryogenic Systems." MBS., Particle Accelerator Conference, Washington, D. C., March 1969
- 3-47. Higa, W. H., "A Practical Phillips Cycle for Low-Temperature Refrigeration.", NASA TR-32-712, Nov. 1965
- 3-48. Kirkley, D. W., "A Thermodynamic Analysis of the Stirling Cycle and a Comparison with Experiment," SAE Paper 949B, Jan. 1965
- 3-49. Heffner, F. E., "Highlights from 6500 Hr of Stirling Engine Operation," SAE Paper 949D, Jan. 1965
- 3-50. Rios, P. A., "An Analytical and Experimental Investigation of the Stirling Cycle." PhD Thesis, Massachusetts Institute of Technology, Sept. 1969

- 3-51. Ackermann, R. A., and Gifford, W. E., "A Heat Balance Analysis of a Gifford-McMahon Cryorefrigerator", *Advances in Cryogenic Engineering*, Volume 16, 1970
- 3-52. Lucek, R., Damsz, G., Daniels, A., "Adaptation of Rolling Type Seal Diaphragms to Miniature Stirling Cycle Refrigerators." AFFDL-TR-67-96, July 1967
- 3-53. Curwen, P. W., "Recent Developments of Oil-Free Linear-Motor Resonant-Piston Compressors." ASME Publication 69-FE-36, June 1969
- 3-54. Meier, R. N., Currie, R. B., "A 4.^oK Single-Engine Cycle Helium Refrigerator." Air Products and Chemicals, Inc., *Advances in Cryogenic Engineering*, Vol. 13, Plenum Press, New York, 1967, pp. 442-449
- 3-55. Higa, W. H., Wiebe, E., "A Simplified Approach to Heat Exchanger Construction for Cryogenic Refrigerators." *Cryogenic Technology*, Vol. 3, No. 2, March/April 1967, pp. 47-51
- 3-56. "Experimental Testing of Size 204 Ball and Roller Bearings for Use in Miniature Cryogenic Compressors." AFFDL-TR-66-223, January 1967
- 3-57. Walker, G., "Operations Cycle of the Stirling Engine with Particular Reference to the Function of the Regenerator." *Journal Mechanical Engineering Science*, Vol. 3, No. 4, 1969, pp. 394-408
- 3-58. Gifford, W. E., "Basic Investigation of Cryogenic Refrigeration Methods," AFFDL-TR-67-41, July 1967
- 3-59. Rios, P. A., Smith, J. L., Qvale, E. B., "An Analysis of the Stirling Cycle Refrigerator." *Advances in Cryogenic Engineering*, Vol. 14, Plenum Press, New York, 1968, pp. 332-342
- 3-60. Rule, T. T., Qvale, E. B., "Steady-State Operation of the Idealized Vuilleumier Refrigerator." *Advances in Cryogenic Engineering*. Plenum Press, New York, 1968, pp. 343-352
- 3-61. Walker, G., "Dynamical Effects of the Rhombic Drive for Miniature Cooling Engines." *Advances in Cryogenic Engineering*, Vol. 14, Plenum Press, New York, August 1968, pp
- 3-62. Stuart, R. W., Hogan, W. H., Rogers, A. D., "Performance of a 4.^oK Refrigerator." *Advances in Cryogenic Engineering*, Vol. 12, Plenum Press, New York, June 1966, pp. 564-575
- 3-63. McMahon, H. O., Gifford, W. E., "A New Low-Temperature Gas Expansion Cycle." *Advances in Cryogenic Engineering*, Vol. 5, Plenum Press, New York, September 1959, pp. 354-367
- 3-64. Trepp, G., "Refrigeration Systems for Temperatures below 25^oK with Turboexpanders." *Advances in Cryogenic Engineering*, Vol. 7, Plenum Press, New York, August 1961, pp. 251-261
- 3-65. Schulte, C. A., Fowle, A. A., Heuchling, T. P., Kronauer, R. E., "A Cryogenic Refrigerator for Long-Life Applications in Satellites." *Advances in Cryogenic Engineering*, Vol. 10, Plenum Press, New York, August 1964, pp. 477-485

- 3-66. Gifford, W. E., "The Gifford-McMahon Cycle." Advances in Cryogenic Engineering, Vol. 11, Plenum Press, New York, August 1965, pp. 152-159
- 3-67. Suslov, A. D., "Starting Period of Microgenic Apparatus," Izv. Vuz, Mashinostroenie, No. 5, 1969, pp. 97-101. (In Russian)
- 3-68. Strobbridge, T. R., Chelton, D. B., "Size and Power Requirements of 4.2°K Refrigerators," Advances in Cryogenic Engineering, Vol. 12, Plenum Press, New York, Aug. 1966, pp. 576-584
- 3-69. Leo, B., "Designer's Handbook for Spaceborne Two-Stage Vuilleumier Cryogenic Refrigerators", Technical Report AFFDL-TR-70-54, June 1970
- 3-70. Johnson, J. C., "Design and Selection of Miniature Cryogenic Refrigerators", Thesis, Ohio State University, 1969
- 3-71. Finkelstein, T., Joshi, T. J., and Walker, G., "Design Optimization of Stirling Cycle Cryogenic Cooling Engines by Digital Simulation", Advances in Cryogenic Engineering, Volume 16, 1970

LIST OF COMPANIES CONTACTED

From the beginning of the program to the present a comprehensive survey of refrigerator development has been made. This has included establishing communication with the following specialist refrigerator manufacturers.

Arthur D. Little, Inc.
520 Acorn Park
Cambridge 40, Mass.
R. W. Breckenridge, Jr.

Cryogenic Technology, Inc.
Kelvin Park
266 Second Ave.
Waltham, Mass. 02154
John Sheppard

The Malaker Corporation
West Main St.
High Bridge, N. J. 08829
Jim Burr

British Oxygen Company
Cryoproducts Div.
Deer Park Road
London S.W. 19, England
J. B. Gardner

Garrett AiResearch Manufact. Co.
Cryogenic Systems
2525 West 190th St.
Torrance, Calif. 90509
R. Hunt

General Electric
Research and Development Center
P. O. Box 43
Schenectady, N. Y. 12301
R. B. Fleming

Hymatic Engineering (Bendix Representative)
Hickory Grove Rd.
Davenport, Iowa 52808
B. F. Gerth

U. S. Phillips Corporation
Norelco Cryogenic Div.
One Angell Road
Ashton, Rhode Island 02864
J. A. Halloran
Bob Smith
A. B. Austin, B. J. Ferro

Cryomech
314 Ainsley Dr.
Jamesville, W. V. 13078
W. E. Gifford

Sterling Electronics, Inc.
(Sub-Marine Systems Div.)
9174 DeSoto Ave.
Chatsworth, Calif.
Kenneth Cowans

Air Products and Chemicals
Allentown, Pa. 18105
R. F. Niehaus
J. V. Galdieri
R. L. Rerig
R. C. Longworth

Wright-Patterson AFB
(Flight Dynamics Lab)
AFFDL (FDFE)
Wright-Patterson AFB, Ohio 45433
W. J. Uhl, Jr.
Ronald White

The Welch Scientific Company
840 Cherry St.
San Carlos, Calif.
Ted Crane

Section 4

FAILURE CHARACTERISTICS OF REFRIGERATORS

4.1 INTRODUCTION

The inclusion of a refrigerator as an essential component of a space vehicle will reduce the operational reliability of the vehicle, since the refrigerator reliability will inevitably be less than 1.0. In order to make a quantitative assessment of the overall reliability of the space vehicle a figure must be assigned to this reliability. To determine the reliability one must first define what is meant by failure, and then obtain data for failure rate as a function of time. It is also desirable to know quantitatively how the refrigerator fails so as to know how the space vehicle will function after failure. For example, a failure by explosion has a considerably different influence on the system than a failure due to reduction of performance to an unsatisfactory level.

Failure rate data may be generated by two principal techniques. Failure rate can be predicted at the design stage from a knowledge of the stress levels in the various elements of a machine, and actual operational performance data for similar types of elements used in other types of machine. The failure rate data generated this way will apply to the developed machine and will not account for the higher infantile failure rate inevitable with a new device. The more satisfactory way, and ultimately the only reliable way to obtain failure rate data, is from actual experience with the particular refrigerator of interest operating under load and environmental conditions identical to those of the planned duty. At the present time it may be stated categorically that using this definition there are no operational failure rate data for spaceborne refrigerators. However, it is necessary for the spacecraft designer to have some idea of the lifetime that could be expected from a developed refrigerator of a particular type, and so an estimate must be made. Such an estimate must be based, on the one hand, upon operational data for currently available refrigerators in various non-space applications and speculation upon how such systems would perform in a redesigned, fully developed spaceflight form; and, on the other hand, upon the projected reliability that it is hoped will

ultimately be obtained from the various spaceflight configured prototype systems currently being developed. It was hoped that discussion of lifetime possibilities with persons either in the commercial refrigerator business or involved with the sponsoring and execution of refrigerator development programs would result in some reportable consensus as to the development potential of the various systems for the space application. This was not the case. While it is generally conceded that fully developed gas-bearing Brayton-cycle systems will ultimately show the longest lifetimes, there is much disagreement over the relative development potential of the closely related family of Stirling, Gifford-McMahon/Solvay and Vuilleumier refrigerators. The writers of this report are obviously less qualified to judge performance potential of particular refrigerators than those intimately involved with their development. However, as noted above, an opinion must be expressed. It is hoped, that the opinion presented will have some value because of its objectivity.

In the first of the following sections, the refrigerators are discussed from the viewpoint of reliability. In the second section, a brief discussion of reliability theory is presented to show how refrigerator failure rate data may be related to a system study.

4.2 RELIABILITY TERMINOLOGY

The reliability of a system is defined as the probability that the system will provide a specified performance level for a specified time in a specified operational environment. Failure of a system can be due to random effects such as gradual propagation of background defects, unusually high stress concentration due to sample-to-sample variation, or unanticipated excursions of the environment, etc., which will result in eventual and unpredictable sudden failure of a component. Failure can also occur by gradual systematic wear or other types of degradation of components which results in a gradual and anticipated fall of system performance. It follows that failure can be defined as a fall in performance below a specified level, either abruptly due to a loss of system or component integrity, or gradually due to systematic degradation. The fundamental information needed in order to calculate the reliability of a system is the characteristic failure rate, λ , of this type of system, as a function of time. The problem of failure can be viewed from at least two

standpoints. One might be concerned with operating a particular system over a long period and would consider replacing worn or broken parts periodically. In this case the important information is the average time between part replacement, i.e., the meantime-between failures, MIBF. On the other hand, one might be concerned with estimating the useful life of an arbitrary system chosen at random from many production samples for which no maintenance or repair is planned. In this case the important information is the average time to the first failure of a group of systems, i.e., the mean-time-to-failure, MTF. In the case of spacecraft usage it will be assumed that no maintenance or repair will be possible. Thus, the desired information will be of the second kind.

The failure rate of systems in a given sample can be defined in two ways. The instantaneous failure rate, $\lambda(t)$, is the fractional failure rate at time t . The average failure rate, $\bar{\lambda}(t)$, is defined as

$$\bar{\lambda}(t) = \frac{\text{fraction of original sample failed at time } t}{t} \quad 4-1$$

By definition the relationship between $\bar{\lambda}$ and λ is as follows

$$\bar{\lambda} = \frac{1}{t} \int_0^t \lambda(t) dt \quad 4-2$$

Techniques for predicting $\lambda(t)$ for untested systems based upon the performance of similar components or on a knowledge of the stresses in the individual components have been devised. However, in the final analysis failure rate data should be obtained by observing the behavior of actual systems in the operational environment.

Once $\lambda(t)$ is known, the number of systems from a given sample remaining operative at time t , denoted by N , is obtained by integrating the failure rate equation

$$-\frac{dN}{dt} = \lambda(t)N \quad 4-3$$

$$\frac{N}{N_0} = \exp\left(-\int_0^t \lambda(t) dt\right) \quad 4-4$$

N_0 is the number of systems at zero time. ($\lambda(t)$ is assumed, reasonably, to be finite at zero time).

The probability that a system will still be operative a time t is the reliability R and is equal to the fraction of components that remain at this time

$$R = \frac{N}{N_0} = e^{-\int_0^t \lambda(t) dt} \quad (4-5)$$

The average lifetime of a component or mean-time-to-failure, MTTF, is a function of time and is given by

$$\text{MTTF} = \frac{1}{\bar{\lambda}(t)} \quad (4-6)$$

The MTTF defined by equation 4-6 is useful in that it expresses reliability in terms of a time quantity which increases as reliability increases.

4.3 FAILURE RATE PATTERNS

Most engineering systems show failure rate patterns similar in general form to Figure 4-1, known as the "bathtub curve". At early times $\lambda(t)$ decreases with time, reflecting infant mortality or the weeding out of systems with material, manufacturing, and inspection faults, etc. These faults may be eliminated before service by inspection and by a running-in period. The failure rate then tends to flatten out to a value more or less constant with time. During this period failure occurs randomly. If some components are subject to wear or other processes of degradation, then at extended times, the failure rate will begin to rise once more. Most systems incorporate some degradable terms. It has become common engineering practice to admit this fact at the design phase and to concentrate wear, etc. on a few inexpensive easily removable components which can be replaced at a time just before $\lambda(t)$ begins to increase. The failure rate can thus be maintained at a constant level for an indefinite time if periodic replacement of degraded parts is permissible. For terrestrial systems subject to wear it is usual to quote the system reliability as MTBF with preventive maintenance. It is important to bear this fact in mind when considering space applications.

It has been found from experience that the reliability of many engineering systems can be expressed satisfactorily by the so-called Weibull distribution. It is inappropriate to become involved in the failure theory in the present context. However, the Weibull failure rate distribution function is a simple expression which can be made to represent infant, constant, and adult failure rates by the variation of a single parameter. The function is thus useful in making a point that the form of the variation of failure rate with time is very important in determining reliability figures from mean time to failure data. The Weibull failure distribution function is:

$$\lambda(t) = \frac{b}{t_c} t^{b-1} \quad (4-7)$$

where t_c and b are constants. t_c is the characteristic life and b is an exponent whose value can be modified to express the different types of time dependence of λ . If b is less than unity, $\lambda(t)$ falls with time, giving the infant mortality curve. If b is equal to unity, λ is constant, and if b is greater than unity, the rising or adult mortality curve is obtained. These types of behavior are shown qualitatively in Figure 4-2a. Integration of Equation 4-7 gives the reliability.

$$R(t) = \exp \left[- (t/t_c)^b \right] \quad (4-8)$$

The reliability of a given system cannot be predicted until failure rate data are obtained and plotted on special log-log versus log graph paper to find t_c and b . However, for the purposes of this report, an estimate of the form of failure rate data can be made in order to show trends and permit the making of rough order of magnitude approximations. Figure 4-2b shows qualitatively the incidence of failure, F , plotted against time for several values of b . F is given by

$$F = \lambda(t) R(t) \quad (4-9)$$

Figure 4-2a shows that values of b greater than unity correspond to an adult mortality rate such as would be expected from the wearing out of bearings and seals. It can be shown for $b > 1$ the time at which F is a maximum, t_{in} , is

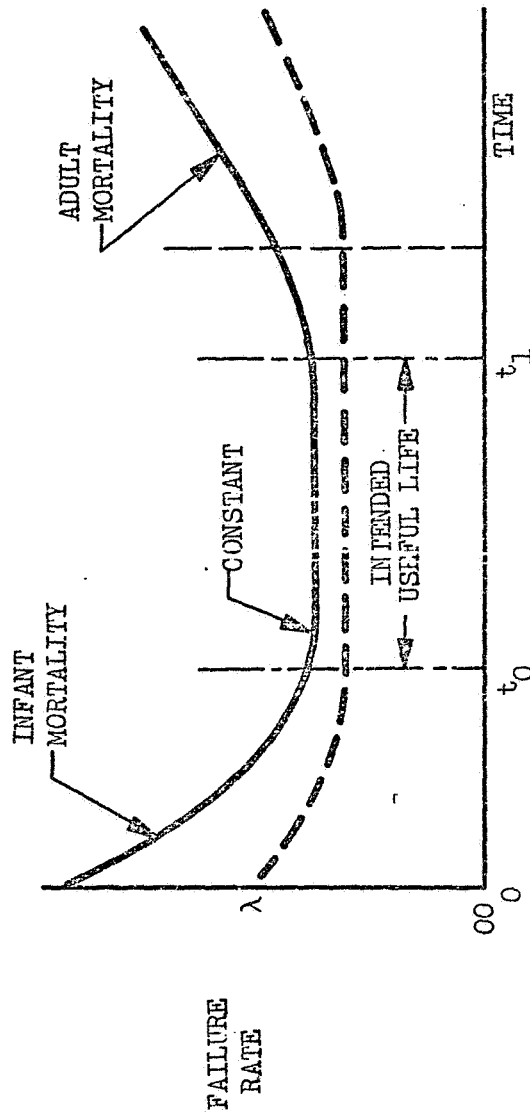


Figure 4-1 The "Bathtub" Curve

given by

$$t_m = t_c \sqrt[b]{\frac{b-1}{b}} \quad (4-10)$$

Systems which fail due to random effects such as mechanical failure would have $b = 1$. Figure 4-3 shows $R(t)$ equation 4-8 plotted for values of b of 1.0 and 3.44. The value of $b = 3.44$ is shown solely because it gives a symmetrical curve for F . It has no experimental significance.

The ordinate of Figure 4-3 is the ratio of MTF to operating life, which has been termed the "life ratio" for brevity.

For the case of $b = 1$, t_m and t_c are identical and the MTF of the system is equal to t_c . For $b = 3.44$, the MTF is equal to t_m . It is noted again that the figure 3.44 was selected solely to demonstrate the influence of b . In an actual case b must be found from experimental data. The curves illustrate the point that if failure is due to wear rather than random effects, then a higher reliability can be predicted for a given life ratio for times less than the MTF, but lower reliability at higher lifetimes. Practical systems are generally subject to infant, random, and adult types of failure, and it is to be expected that a practical failure rate equation should include at least three components, as follows:

$$\lambda(t) = \sum_{i=1}^3 \frac{b_i}{t_{c_i}^{b_i}} t^{b_i - 1} \quad (4-11)$$

$$b_1 < 1$$

$$b_2 \cong 1$$

$$b_3 > 1$$

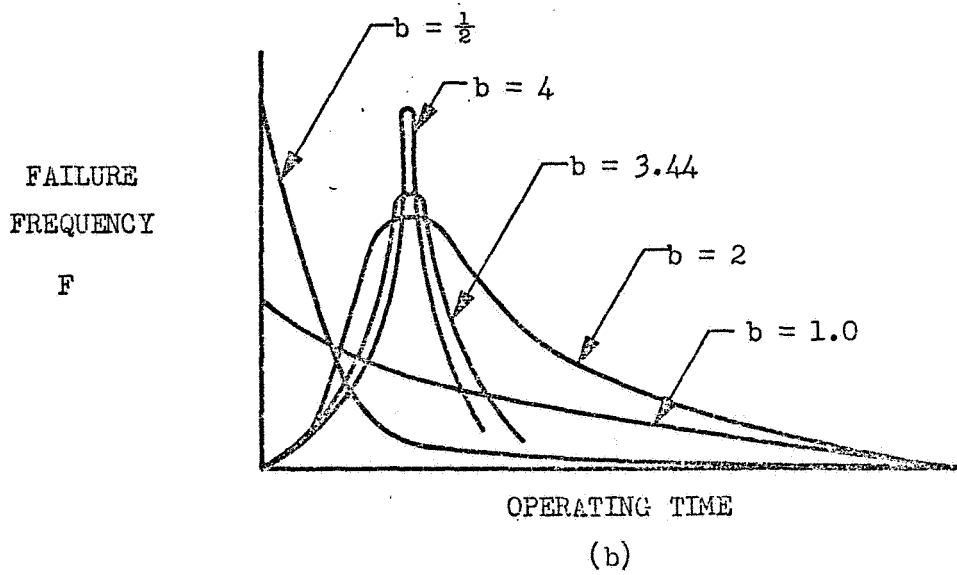
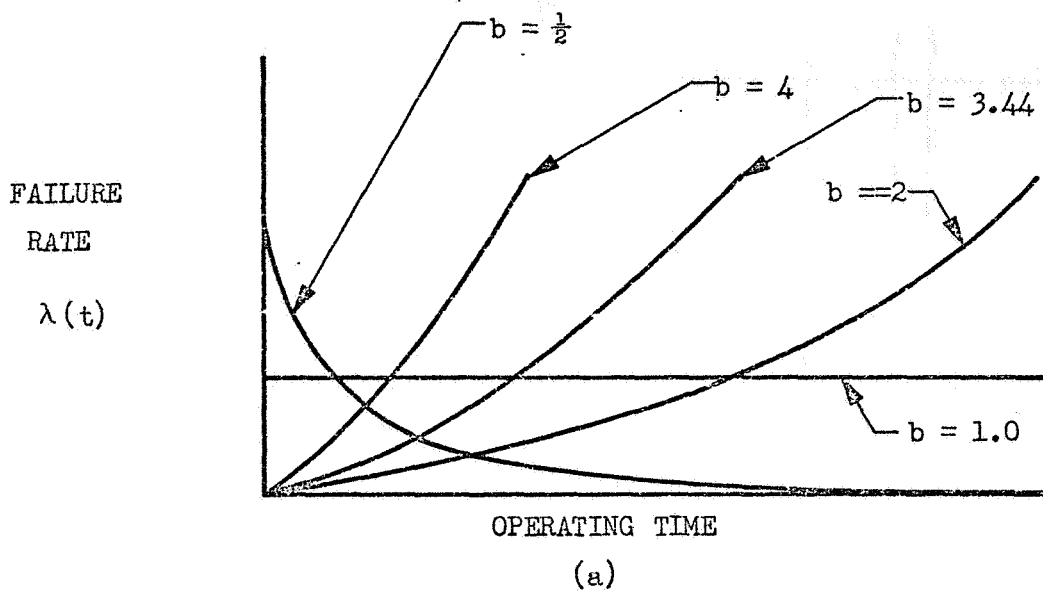


Figure 4-2 Weibull Failure Rate Distributions

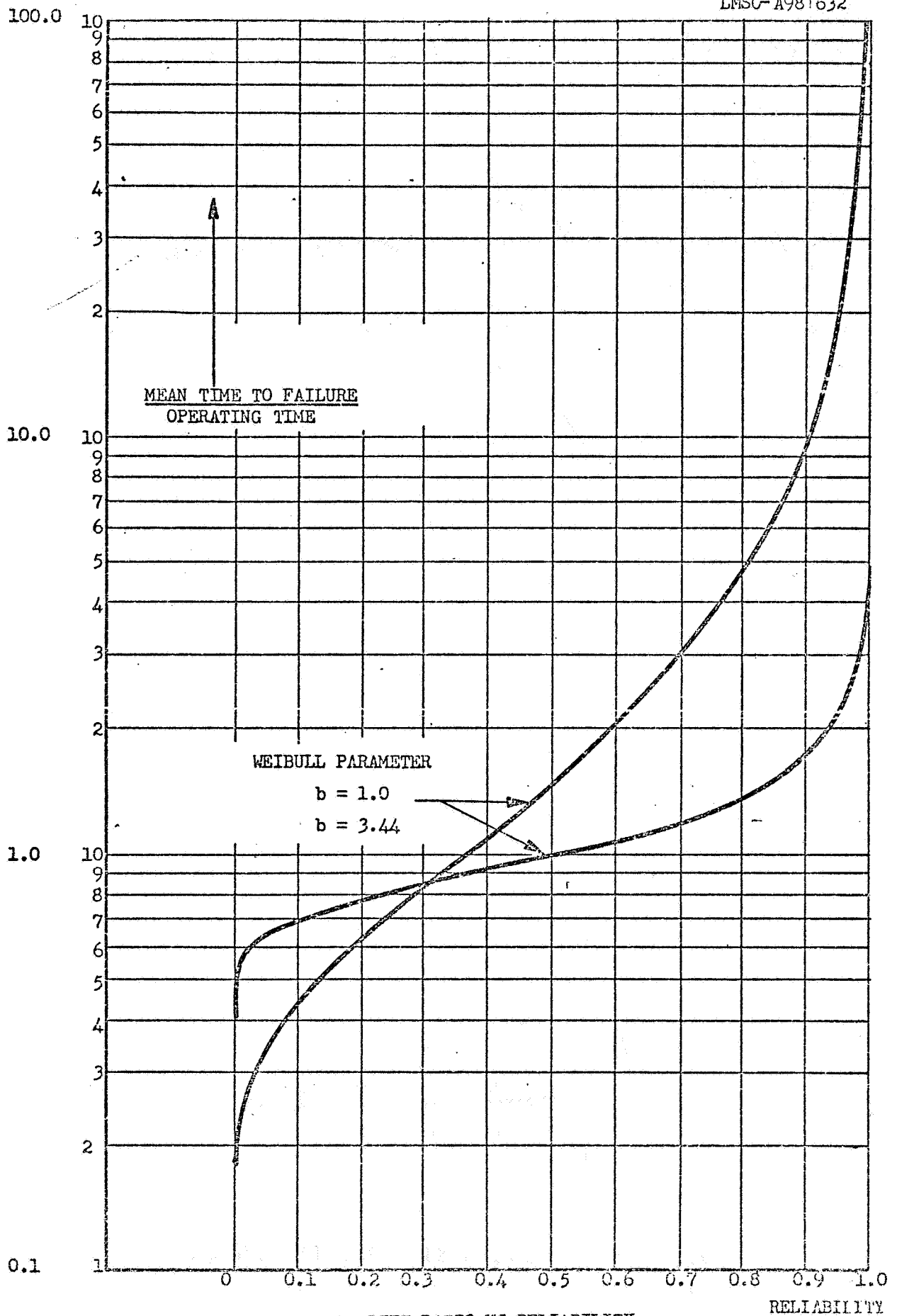


Fig. 4-3 LIFE RATIO VS RELIABILITY

4-9

4.3.1 Use of Redundancy

In order to increase the probability that the service demanded from a system for a given period is obtained, redundant systems can be used. In the cooling situation parallel redundancy in which more than one refrigerator is operating at a given time does not seem to be reasonable, since the storage vessel would be overcooled most of the time and power consumption would be excessive. Series redundancy, however, appears to offer a very significant increase in reliability. In this case additional refrigeration systems are provided to be switched on if the operational unit fails. The reliability of such a system can be estimated with the help of Figure 4-3. Suppose an operational lifetime of 4,000 hours is required from a unit whose MTF is 4,000 hours. Using the curve for $b = 3.44$ a reliability of 0.52 is obtained. Suppose two units were provided so that a lifetime of 2,000 hours was expected from each; the reliability of a 4,000-hour MTF unit on a 2,000-hour task is found to be 0.95. Since both must operate to perform the mission the overall reliability is 0.90. Such an analysis is somewhat oversimplified, but an approximate comparison of multi-unit systems can be made in this manner.

4.4 FAILURE RATE OF REFRIGERATORS

A refrigerator is basically a reversed heat engine, and its construction is essentially similar to that of gas compressors and heat engines. More care must be taken with the thermodynamic design of a refrigerator than a prime mover if a respectable efficiency is to be gained, but the mechanical features of motors, seals, and bearings and rotary or positive displacement expanders and/or compressors are generally common to both. This family of devices usually employs bearing and sealing features which are subject to wear. The wear is confined to components which can be replaced with little effort. Wear is generally minimized by the use of liquid lubricant between rubbing surfaces. Continuous reliable operation of these devices usually requires maintenance of optimum lubricant quality and periodic replacement of wearing parts. The life of such devices is usually specified as a certain number of hours, provided the necessary periodic maintenance is performed.

For the general family of thermodynamic machines with wet lubricated surfaces and seals, the following general order of maintenance-free lifetimes can be expected.

Prototypes; small, heavily loaded high-speed machines	30 → 300 hrs
Aircraft and automobile engines, compressors, many types of "average"-sized machines	300 → 3,000 hrs
Simple, large, slow, conservatively designed, generously lubricated machines	3,000 → 30,000 hrs

Conventional refrigerators of small to average size designed using conventional bearing and seal techniques would fall within the second category, and would thus be expected to have lifetimes of the order of 300 to 3,000 hours if refrigerator technology is, on the whole, as well developed as other forms of thermodynamic devices. This is, in fact, the case. It may be observed, therefore, that long-lived refrigerators can be obtained by either further development or better use of conventional technology, or by using a radically new technology. The refrigerators of interest to this study fall into one or other of these categories. The Stirling, Vuilleumier, and split-system Gifford-McMahon or Solvay refrigerators are currently designed using conventional technology. Refrigerators using gas bearings and operating on the Brayton cycle are being developed in an attempt to provide the necessary new technology.

In terrestrial use, most refrigerators are operated with periodic preventive maintenance. The reliability of the refrigerators is given as a certain number of hours mean-time-between-failures, with specified maintenance intervals. In this context, failure implies breakage of a component. In the spaceflight application it will be virtually impossible to perform maintenance and a conventional refrigerator would presumably suffer a gradual reduction of performance with time as the specified maintenance interval is exceeded. Failure should thus be defined as reduction of performance below an acceptable level either by gradual degradation or by abrupt breakage or seizure. Few data are available on the degradation rate of unmaintained conventional refrigerators. Even if they were available, they would be of little applicability. The use of preventive maintenance is a cost-effective manner of providing economical refrigerators for terrestrial use. It may be assumed that all conventional

refrigerators could be designed so as to reduce the rate of wear on those components which are normally replaced during terrestrial maintenance. The controversy surrounding the suitability of applying conventional technology refrigerators to space use lies in assessing what the ultimate performance and reliability of these redesigned refrigerators would be.

4.4.1 Conventional Technology Refrigerators

The Stirling, Vuilleumier and split-system Gifford-McMahon/Solvay refrigerators are closely related, not only by their use of conventional technology, but in the actual components required. The original, best developed, and most efficient of these systems is the Stirling refrigerator. The important features of the Stirling refrigerator from the reliability standpoint are:

- . electric motor bearings and brushes
- . drive train, including gearing and crank mechanism
- . lubrication system for motor and drive train
- . moving seals between high-pressure working spaces and crankcase on the working piston(s) and/or displacer drive
- . regenerator matrix
- . housing

The useful lifetime of these machines is strongly influenced by the moving seals. If these seals are not 100 percent effective, contaminants such as lubricant and desorbed gas can migrate into the working spaces and can plug the regenerator or bind moving parts by condensing in the colder regions. The migration rate could be lowered by lowering the crankcase operating pressure, but this will increase the stress in the seals. Assuming that conventional seals (i.e., less than perfect) are used, the problem can be minimized by using dry lubrication in the crankcase, and by taking special pains to bake out the components within the crankcase before assembly to reduce outgassing. The use of dry lubrication will result in a shorter lifetime for the bearings. The crankcase can also become contaminated by wear particles from the motor brushes. A typical Stirling refrigerator can thus be subject to performance degradation due to regenerator contamination, wear of seals, wear of brushes, or bearing failure. Other modes of failure are possible, of course, such as

structural failure, electrical insulation breakdown, etc., but these are far less likely to occur. Stirling refrigerators are generally operated with routine preventive maintenance, which includes replacement of the brushes, replacement of the contaminated working fluid, and bearing and seal replacement. There are no comprehensive data available upon the maximum allowable time between maintenance to prevent a "substantial" degradation in performance. Discussions with manufacturers of Stirling refrigerators suggest that this period may be as low as 300 hours for small refrigerators of the capacity of 1 watt at 77°K to more than 4,000 hours for larger size units of 100 watts at 20°K. The time between maintenance of a Stirling refrigerator can clearly be extended by the development of suitable brushless motors for those units which operate on D.C., and the use of positive seals, such as the rolling diaphragm, which would permit the use of a wet crankcase lubricant. Both these areas are currently being investigated.

A Stirling refrigerator can fail gradually due to regenerator or seal degradation. In this case service will not cease when the performance falls below the required level. Some refrigeration will continue to be provided. The refrigerator could fail due to internal mechanical breakage on seizure, in which case no harm would be done to surrounding systems, but service would stop and the refrigerator would act as a passive heat leak. If the outer housing fails, some damage may be caused to adjacent systems, but this is unlikely since the working fluid is inert and housing failure is not likely to be explosive.

For the purposes of this report it is necessary to estimate the reliability that might reasonably be expected from a specially built, extensively tested Stirling refrigerator utilizing the best in current and near-future technological developments. It is suggested that the following figures for refrigeration in the range of 5 watts at 100°K to 100 watts at 20°K be used as indicated in the table below.

Lifetime of Stirling Refrigerators (Estimated)

	5 watts at 100°K	100 watts at 20°K
Optimistic	2,000	6,000
Conservative	1,000	3,000

For better information on a specific application, it is recommended that a refrigerator manufacturer be contacted.

The Gifford-McMahon and Solvay refrigerators are related to the Stirling refrigerator as follows: The compressor is detached from the expander and two sets of valves are used to isolate their operation from each other. The compressor can be located at some distance from the expander, gas being supplied via long connecting lines. The compressor is generally oil-lubricated and entrained oil is removed from the compressed gas stream by a simple filtering system in the delivery line. The operating speeds of the compressor and expander can be different, and one compressor can be used to drive several expanders. Those features of split-system refrigeration which influence the degradation of performance are as follows:

- . Compressor and expander drive motor bearings and brushes
- . Lubrication system for compressor and expander drives
- . Moving seals on compressor piston and expander drive
- . Drive train on compressor and expander
- . Regenerator matrix
- . Housing

These features are of the same type as those on the Stirling refrigerator. The qualitative comments regarding the influence of the failure mode on adjacent systems that were made for the Stirling refrigerator apply also to the split systems. However, the presence of an unidirectional gas flow in the supply lines permits the use of oil and particulate matter filters which both protect the expander and permit the use of an oil-lubricated compressor in terrestrial applications. The compressor can therefore be expected to have a longer lifetime. The use of different operating speeds permits use of a slower moving expander with correspondingly longer seal life. The presence of valves adds a source of wear, but the time between valve replacement can be made as long as that for the other wear components. The result is that for small size refrigerators manufacturers are able to specify times between maintenance of about 3,000 hours. This maintenance interval is based upon the requirements of the expander. On the spaceflight application, the oil-lubricated compressor cannot be used, and dry-lubricated compressors must be developed. A dry-lubricated

compressor is essentially similar to the working piston and drive mechanism of the Stirling refrigerator, and the same comments regarding motor, lubrication, and seals can be made. The compressor could be a somewhat simpler device but not markedly so. The best of currently available dry-lubricated helium compressors have times between maintenance of about 2,000 - 5,000 hours. These compressors are well past the prototype stage, but have not yet had anything approaching the usage of the oil-lubricated compressors. This suggests that in the range of cooling powers of interest here, the expected lifetimes of fully developed spaceflight-qualified refrigerators should be in the following ranges.

Lifetime of Split System Refrigerators (Estimated)

	5 watts at 100°K	100 watts at 20°K
Optimistic:	4,000	6,000
Conservative:	2,000	4,000

For further specific information, a manufacturer should be contacted.

The Vuilleumier (VM) refrigerator has been developed solely for specific applications. There is no production history and experience as there is with the Stirling and split-system refrigerators. The VM refrigerator appears attractive because it can use a primary source of power, and because it has certain mechanical features which would appear to give it a potentially longer life than the Stirling refrigerator. Most VM refrigerators have been powered electrically which significantly reduces the thermal attractiveness. Development of this refrigerator is thus currently based upon its promise of longer lifetime. However, as in the case of the Stirling and split systems, the VM includes many wearing surfaces and seems more likely to fail due to degrading processes than because of abrupt failure. Those aspects of VM design which affect reliability are as follows:

- Drive motor bearings and brushes
- Drive train lubrication

- . Moving seals
- . Cold end renenerator .
- . Housing

Again, the comments made regarding the impact of failure modes on adjacent systems apply.

The VM refrigerator can be designed with fully enclosed motor driven by magnetic coupling, in which case there are no heavily loaded moving seals. In this configuration, however, the motor and drive train bearings must be dry lubricated. An alternative VM configuration employs a separate wet-lubricated crankcase which drives the displacer through relatively heavily loaded moving seals. In the latter case, brushed or brushless motors can be used. On the first configuration the VM refrigerator has an advantage over the Stirling refrigerator in that there are no heavily loaded moving seals, but the drive mechanism must be dry lubricated. In the second configuration, loaded moving seals are necessary, but the use of a separate crankcase permits wet lubrication and also permits the refrigerator to drive itself by suitably sizing the connecting rods. This will minimize electric motor loading. However, the comments regarding seals applied to the Stirling refrigerator apply here. The choice between configurations would seem to be based upon whether wear of the dry-lubricated bearings would degrade the system performance more or less rapidly than working fluid contamination through the seals from the wet-lubricated crankcase. If a long-life 100 percent effective seal such as a rolling diaphragm can be developed, then the separate crankcase configuration would appear to be more attractive. In any event, it appears as if the basic mechanical design choices are similar in kind in both the VM and Stirling refrigerators, although the relative acuteness of the problem areas differs.

VM refrigerators currently exist only in prototype form. Accumulated experience on particular machines does not exceed 1,000 to 2,000 hours.

It does not seem that the advantages which the VM is claimed to have over the Stirling refrigerator are of first order significance. The differences between the systems are not basic, but are of degree of loading on similar components.

It is suggested, therefore, that until the VM has been developed to a point where the advantages of the lower degree of loading have been proven, its time between maintenance should be assumed about equal to that of a comparable Stirling refrigerator. The estimated useful life of a VM refrigerator designed and developed for a specific spaceflight mission is, then, as follows:

Lifetime of Vuilleumier Refrigerators (Estimated)

	5 watts at 100°K	100 watts at 20°K
Optimistic	2,000	6,000
Conservative	1,000	3,000

It is again noted that the figures given for the Stirling, Gifford-McMahon/Solvay and Vuilleumier refrigerators are highly speculative, and are intended to provide the spacecraft designer with rough order of magnitude information. They have been estimated by surveying present technology and making an intelligent guess as to the general order of magnitude of lifetimes that could be anticipated. The figures should be revised at the earliest opportunity by contact with individuals working in this field. No consensus opinion should be anticipated, however.

4.4.2 Advanced Technology Refrigerators

In conventional designs of refrigerators, the degradation of certain components due to wear is accepted and allowed for. The useful life of these refrigerators, defined as time between replacement of work or contaminated parts, is generally governed by the life of the wearing parts rather than by mechanical failure. The lifetime can therefore usually be substantially extended by eliminating wearing surfaces through the use of gas bearings and aerodynamic seals. Design studies have demonstrated that the Brayton cycle is more compatible with gas borne components than the Stirling, Vuilleumier, Gifford-McMahon, and Solvay cycles, which must use periodic displacement machinery with low void volume. Development work is being conducted on two different approaches to the exploitation of gas gearings. One system developed by General Electric Company and Airesearch Corporation employs rotary compressors and turbines. The design of

such machines is relatively well understood and the application of gas bearing technology to pure rotary machines is straightforward. However, with diminishing capacity the efficiency of rotary machinery decreases, and reciprocating devices become more attractive. Arthur D. Little, Inc., have developed a rotary free piston device in which gas borne shafts both rotate and oscillate to provide frictionless expansion and compression pistons. Rebound forces are absorbed by gas springs, and power is transmitted to and from the shafts electromagnetically.

These systems consist of the following principal components:

- . Gas bearings for expander and compressor
- . Several electrodynamic devices such as motors, generators, or linear actuators
- . Counter flow heat exchangers
- . Outer housing

Gas bearings will fail if metal-to-metal contact is made. This can be produced by heavy side loading, or by the intrusion of particulate matter. The bearings can be designed for adequate rigidity and dynamic stability, but the random generation of particulate matter in the system is less easy to control. The heat exchangers are relatively complex in construction, and present a possible source of breakage and contamination. The housing is a relatively simple component but nevertheless would present a possible source of leakage and stress concentration.

These gas bearing systems are all in the early prototype stage, and no meaningful failure rate data are available. As prototype systems they will require very extensive development before their useful life failure rate is established. However, the potential reliability of both systems can be assessed by breaking the system down into its components and using existing data for similar components. Using this technique, and assuming constant failure rate (random effects) it can be shown that the MTF of these gas-bearing systems in fully developed form, should be in the range of at least 20,000 to 30,000 hours. This figure is for developed systems and assumes a constant failure rate. A case could be argued for the occurrence of infantile failure modes for this type of refrigerator

because of its inherent mechanical complexity in terms of construction details and consequent difficulty of manufacture and inspection. Also, electrical components can degrade with time and there is the problem common to all very low temperature systems of leakage of the working fluid. Thus, the quoted MTF figures are at present no more than speculative. No prototype system has run more than a fraction of these times.

It is possible for the performance of these gas-bearing Brayton-cycle refrigerators to suffer a loss in performance below specified level by gradual degradation due to contamination or loss of working fluid. It seems more likely, however, that most failures will be abrupt, due either to purely random effects or to the contamination eventually becoming sufficient to fail the gas bearings. Even though much larger forces are involved in these systems than the Stirling, Gifford-McMahon/Solvay and Vuilleumier refrigerators, explosive failure does not seem likely. The impact of failure upon adjacent systems is thus likely to be abrupt loss of service while the refrigeration system becomes a passive heat leak into the propellant tank.

4.5 DISCUSSION

It is not possible to provide parametric reliability data for spaceflight application. It is difficult even to provide typical data for existing systems which are relevant to the space application. The intent of this section was to outline the general state of technology as it applies to spaceflight applications, and to indicate to the spacecraft designer the order of magnitude of lifetimes that might be expected from different types if they were subjected to an extensive development program. Some degree of oversimplification was introduced in order to avoid overall confusion. Specific refrigeration information relating to a particular mission may be gained by contacting manufacturers. It is hoped that enough information has been presented to permit the formulation of intelligent questions.

Practical refrigerators have been grouped into two categories for reliability discussion purposes. The Vuilleumier refrigerator has been developed relatively recently as part of a general U.S. Air Force-funded program to develop long-life refrigerators, which has included the gas-bearing systems. It bears a

closer family resemblance to the Stirling and Gifford-McMahon/Solvay systems, however, and in the first instance its performance should be measured against these systems.

It is not the intent of this section to pass judgment on the relative merits of different refrigeration systems. Obviously this cannot be done with present information. It is realized that the proponents of particular systems may take issue with the quoted figures, but such issue must be based on potential, rather than actual, performance; and the spacecraft designer must be provided with rough order of magnitude data with which to make the larger decision of whether or not an active system is desirable.

Sufficient reliability theory has been presented to indicate the type of reliability data that must be obtained before an estimate of mission reliability can be made. It was shown that the nature of the variation of failure rate with time is of critical importance in determining this reliability.

Section 5
THERMAL ENVIRONMENTS

5.1 DEFINITION OF THERMAL ENVIRONMENT PARAMETERS

The objective of defining parameters describing refrigerator system thermal environments is to enable the system designer to make rapid preliminary estimates of average spacecraft surface temperatures and radiator heat rejection limits for a range of possible missions. For the purpose of this study, the maximum incident solar heat fluxes were taken to be as high as that experienced near Venus, and provisions were made for estimating absorbed heat fluxes for three mission groups. These groups are planetary orbit operations, Martian and Lunar surface operations, and deep space operation, such as translunar or transmartialian flight.

The environmental parameters for these cases can be derived by considering the definition of the average net heat flux radiated by a surface in space or on an airless planetary surface. A general expression for this quantity may be written

$$\begin{aligned} \text{Net radiated} &= \text{Emitted} & - & \text{Absorbed Solar} & - & \text{Net Absorbed} & (5-1) \\ \text{Flux Density} &= \text{Flux Density} & - & \text{Flux Density} & - & \text{Planetary or} \\ & & & & & \text{Lunar Flux} \\ & & & & & \text{Density} \end{aligned}$$

where the flux densities are regarded as steady-state values or are averaged over an appropriate time interval (such as an orbital period for an orbiting vehicle). It has been assumed that no thermal interchange occurs between the surface in question and other portions of the spacecraft. Symbolically, equation (5-1) can be written

$$\frac{q_{\text{net}}}{A_{\text{eff}}} = G_E T^4 - G_A - G_P, \quad \text{Watts/Ft}^2 \quad (5-2)$$

where

$$G_E = \sigma \epsilon_I \quad (5-3)$$

$$G_A = \alpha_s \bar{F}_s G_s \quad (5-4)$$

and

$$G_P = \sigma \epsilon_I \bar{F}_P T_P^4 \quad \text{for lunar or planetary surface operation} \quad (5-5a)$$

$$G_P = \epsilon_I \bar{F}_P R_P + \alpha_s \bar{F}_{Ps} \rho_P G_s \quad \text{for orbital or near-planet operation} \quad (5-5b)$$

where

σ	=	Stefan-Boltzman Constant = $0.5267 \times 10^{-8} \text{ W/Ft}^2 \text{K}^4$
ϵ_I	=	Infrared Emittance
α_s	=	Solar Absorptance
\bar{F}_s	=	View Factor for solar radiation
G_s	=	Solar Irradiation flux density, W/Ft^2
\bar{F}_P	=	View Factor to planet surface
T_P	=	Planet temperature, $^{\circ}\text{K}$
R_P	=	Planet Infrared Radiosity, W/Ft^2
\bar{F}_{Ps}	=	Time Average view factor for planet-reflected solar radiation
ρ_P	=	Planet Albedo

An upper limit of 500 W/Ft^2 for the sum ($G_A + G_P$) is possible for near-Venus operation. These relations can be used to determine the average net heat rejection from a radiator having a known surface temperature, or the equilibrium surface temperature of a surface having a known net heat rejection.

5.2 DIRECT SOLAR HEAT FLUX

The value of G_A is the product of solar absorptance, view-factor to the sun, and local solar irradiance (i.e., the solar constant at a given distance from the sun). The view factor to the sun for a flat surface is the cosine of the angle between the outward normal to the surface and a line to the sun. The view factor for curved surfaces is the ratio of the area projected in the direction of the sun to the total surface area. The solar irradiance

is given by

$$G_s = \frac{130}{r_p^2}, \text{ W/Ft}^2 \quad (5-6)$$

where r_p is the distance from the sun in astronomical units.

Values of solar absorptance and infrared emittance are tabulated in Table 5-1 for a variety of materials. Also shown are values of these properties after vacuum and simulated solar radiation exposure for 1000 equivalent sun hours (ESH).

5.3 PLANETARY HEAT FLUX

Evaluation of the planetary or lunar heat input, G_p , is somewhat more complex. For an object resting on or near the planetary surface the evaluation of the view factor to the planet's surface is usually straight forward. View factors from vertical and horizontal surfaces to an adjacent lunar or planetary surface are shown in Fig. 5-1. View factors to a hill and to a crater are plotted as a function of elevation angle to the top of the hill or crater. The hill is assumed to be of infinite extent in the direction parallel to the vertical side A_V of the vehicle. The crater is assumed to be circular, surrounding the surface A_V .

In order to determine G_p for a radiating surface passing or orbiting near a planetary surface the terms in (5-5b) must be evaluated. The view factor from a flat surface to the visible portion of a planet, F_p , can be evaluated using the data of Ref. 5-1. Referring to the geometry illustrated in Fig. 5-2, two cases can be distinguished:

1. Entire Planet Visible from Surface

For this case $\lambda + \phi \leq \frac{\pi}{2}$, where

- λ = Angle between surface normal and a line to the planet center
- ϕ = $\sin^{-1}(R/H)$
- R = Planet radius

Table 5-1
Representative Values of Solar Absorptance and Infrared Emittance

Material	Solar Absorptance, α_s		Infrared Emittance, ϵ_I	
	Normal	After 1000 ESH Exposure	Normal	After 1000 ESH Exposure
Clad Aluminum	0.22 ± 0.04	0.24 ± 0.04	0.06 ± 0.03	No Change
Optical Solar Reflector	0.050 ± 0.005	No Change	0.80 ± 0.02	No Change
White Acrylic Paint	0.24 ± 0.04	0.40 ± 0.04	0.86 ± 0.03	No Change
White Silicone Paint	0.20 ± 0.03	0.34 ± 0.03	$0.90 \begin{matrix} + 0.03 \\ - 0.06 \end{matrix}$	No Change
Black Acrylic Paint	0.93 ± 0.03	No Change	0.88 ± 0.03	No Change
Solar Cell Assembly	0.78 ± 0.04	0.83 ± 0.04	0.80 ± 0.03	No Change

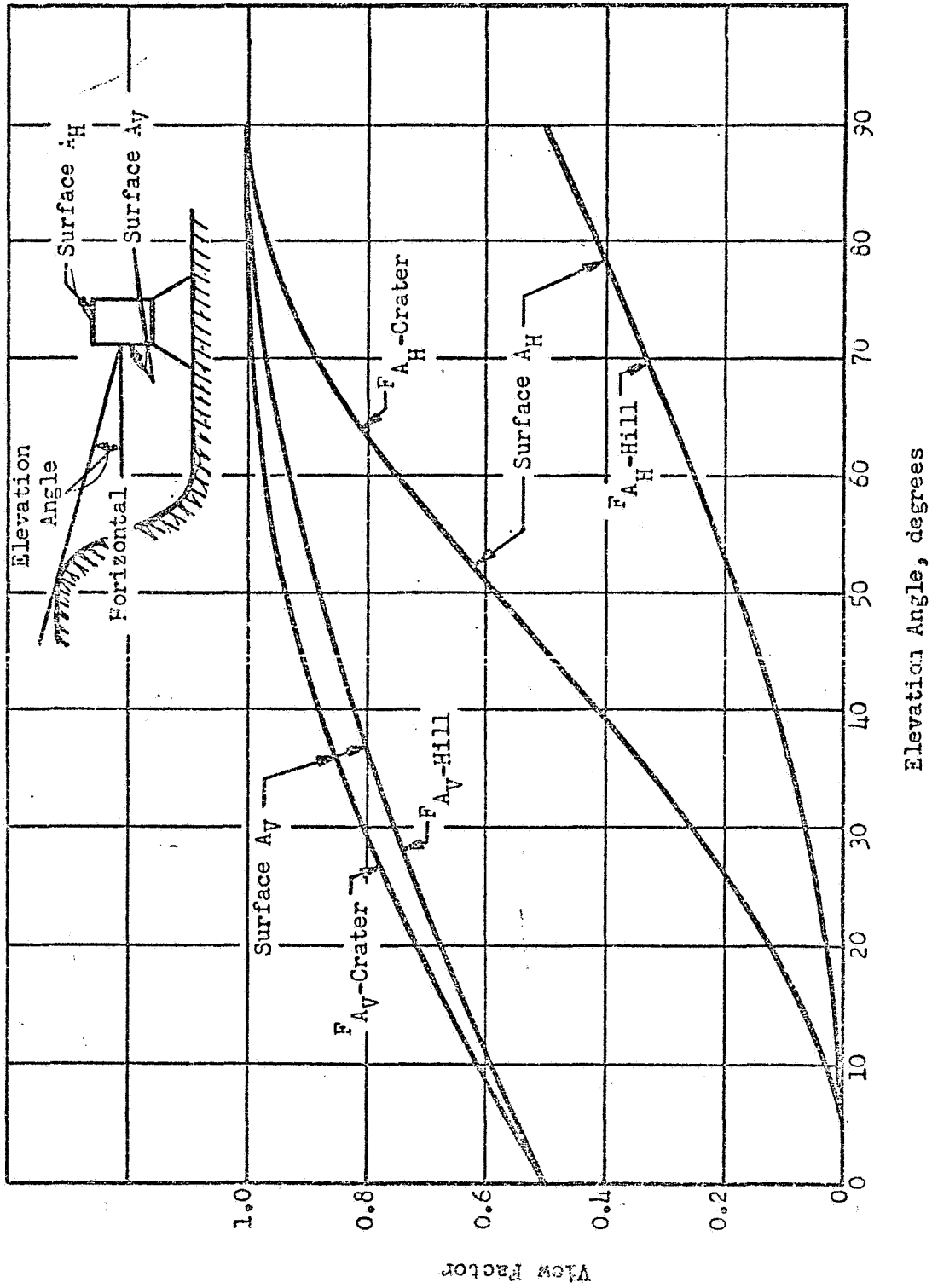
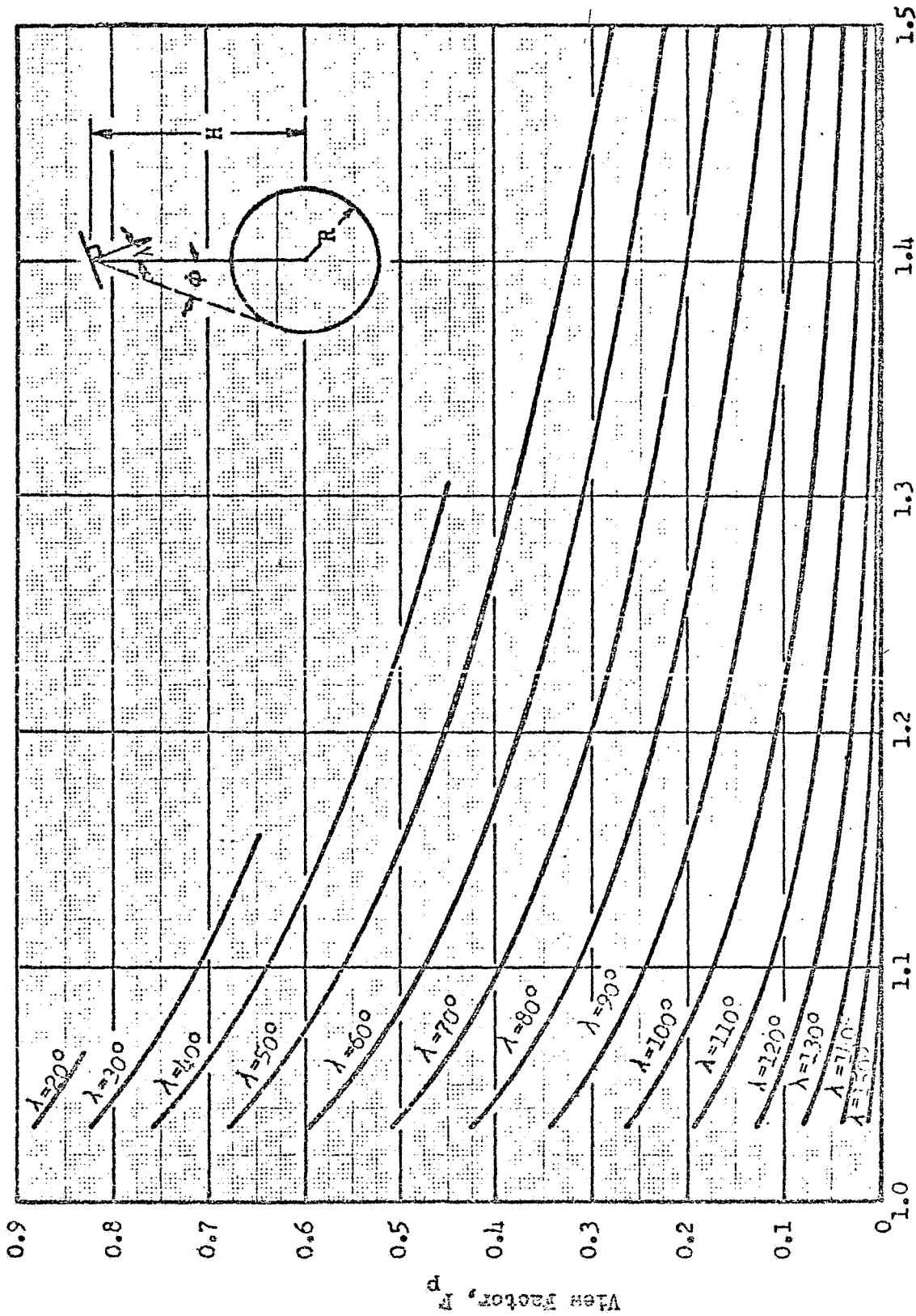


Fig. 5-1 View Factors from Vehicle Surfaces to Planetary Terrain



Dimensionless Altitude, H/R , Planet Radii
 Fig. 5-2 Planetary View Factor for Infrared Exchange

H = Distance from planet center to spacecraft surface

The view factor is given by

$$F_P = \left(\frac{R}{H}\right)^2 \cos \lambda$$

2. Part of Planet Visible

For this case

$$\left(\frac{\pi}{2} - \Phi\right) < \lambda \leq \left(\frac{\pi}{2} + \Phi\right)$$

and the view factor is given in Fig. 5-2.

Average values of planetary radius, surface radiosity, and reflectance (albedo) are given in Table 5-2 for Earth's moon and the planets. Also shown in Table 5-2 are surface temperature ranges for each of the planets. Values of lunar surface temperature are shown in Fig. 5-3 as a function of sun elevation angle. Values of the surface temperature of Mars are shown in Fig. 5-4. The value of the time-average view factor for reflected solar radiation is obtained by integration of an instantaneous view factor.

Thus,

$$\bar{F}_{Ps} = \frac{1}{2\pi} \int_0^{2\pi} F_{Ps}(\theta) d\theta \quad (5-7)$$

where θ is the orbit position angle measured as shown in Fig. 5-5.

The value of the view factor $F_{Ps}(\theta)$ may be approximated by the relation

$$F_{Ps} = C_R \cos \beta \cos \theta \quad (5-8)$$

where β is the angle between the orbit plane and a line to the sun, and C_R is a reflection coefficient given in Fig. 5-6.

5.4 TEMPERATURE OF NEAR-EARTH SATELLITES

Extremes in irradiation of a satellite are represented by the levels experienced on the six sides of a cube which always keeps the same side facing the

TABLE 5-2
PHYSICAL CHARACTERISTICS OF EARTH'S MOON AND THE PLANETS

Body	Mean Distance From Sun, (1) A.U.	Mean Radius		Orbital Period, Days	Period of Rotation, Days (3)	Gravitational Acceleration (Earth = 1)	Average Infrared Radiosity, W/Ft ²	Average Albedo	Surface Temperature Range, °K
		N.Mi.	Km.						
Mercury	0.3871	1263	2340	87.96	55.0	0.40	210	0.058	13 to 680
Venus	0.7233	3291	6100	224.70	(5)	0.89	60.5	0.76	240(6)
Earth	1.000	3438	6371	365.26	0.99769	1.00	21.8	0.39	220 to 320
Moon	(2)	938	1738	27.32	27.32	0.165	28.8	0.07	100 to 385
Mars	1.5237	1794	3324	686.98	1.02595	0.39	13.7	0.15	160 to 310
Jupiter	5.2037	37636	69750	4333.71	0.4115(4)	2.37	1.22	0.51	120 to 310
Saturn	9.5803	31387	58170	10829.5	0.4348(4)	0.90	0.355	0.50	100 to 225
Uranus	19.1410	12815	23750	30587.0	C.4458	0.97	0.0914	0.66	100 to 125
Neptune	30.1983	12087	22400	60612.3	C.5299	1.40	0.0404	0.62	100 to 125
Pluto	39.4387	1619	3000	90465.7	6.39	-	0.0204	0.16	~43

NOTES: (1) Orbit semi-major axis.

(2) Mean distance of Moon from Earth = 384 405 Km.

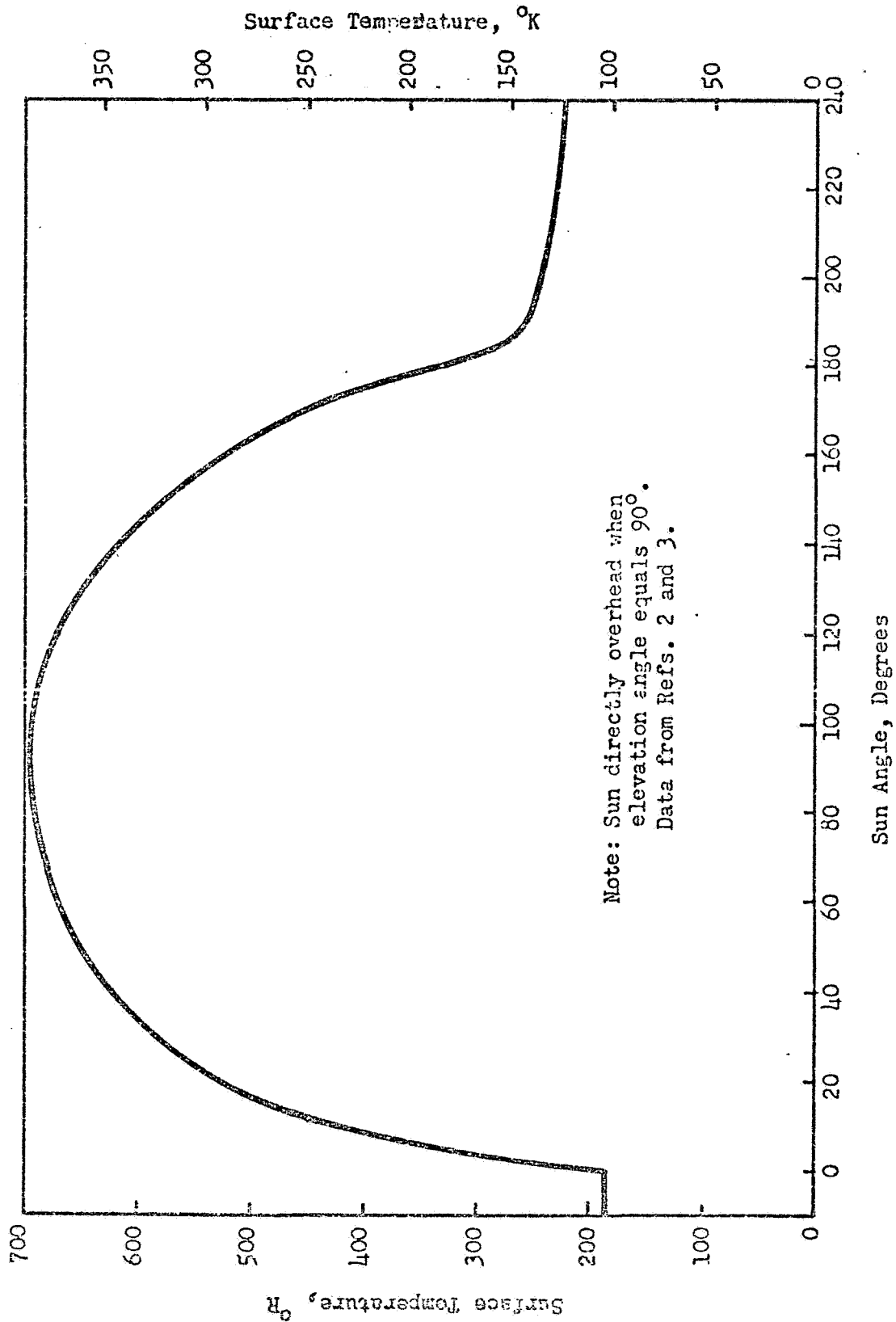
(3) Mean solar days

(4) Approximate, varies with latitude

(5) Not known. Venus rotates very slowly if at all.

(6) Temperature of top of clouds. Surface temperature is about 700°K.

LMSC-A981632



Note: Sun directly overhead when elevation angle equals 90°. Data from Refs. 2 and 3.

Fig. 5-3 Lunar Surface Temperatures

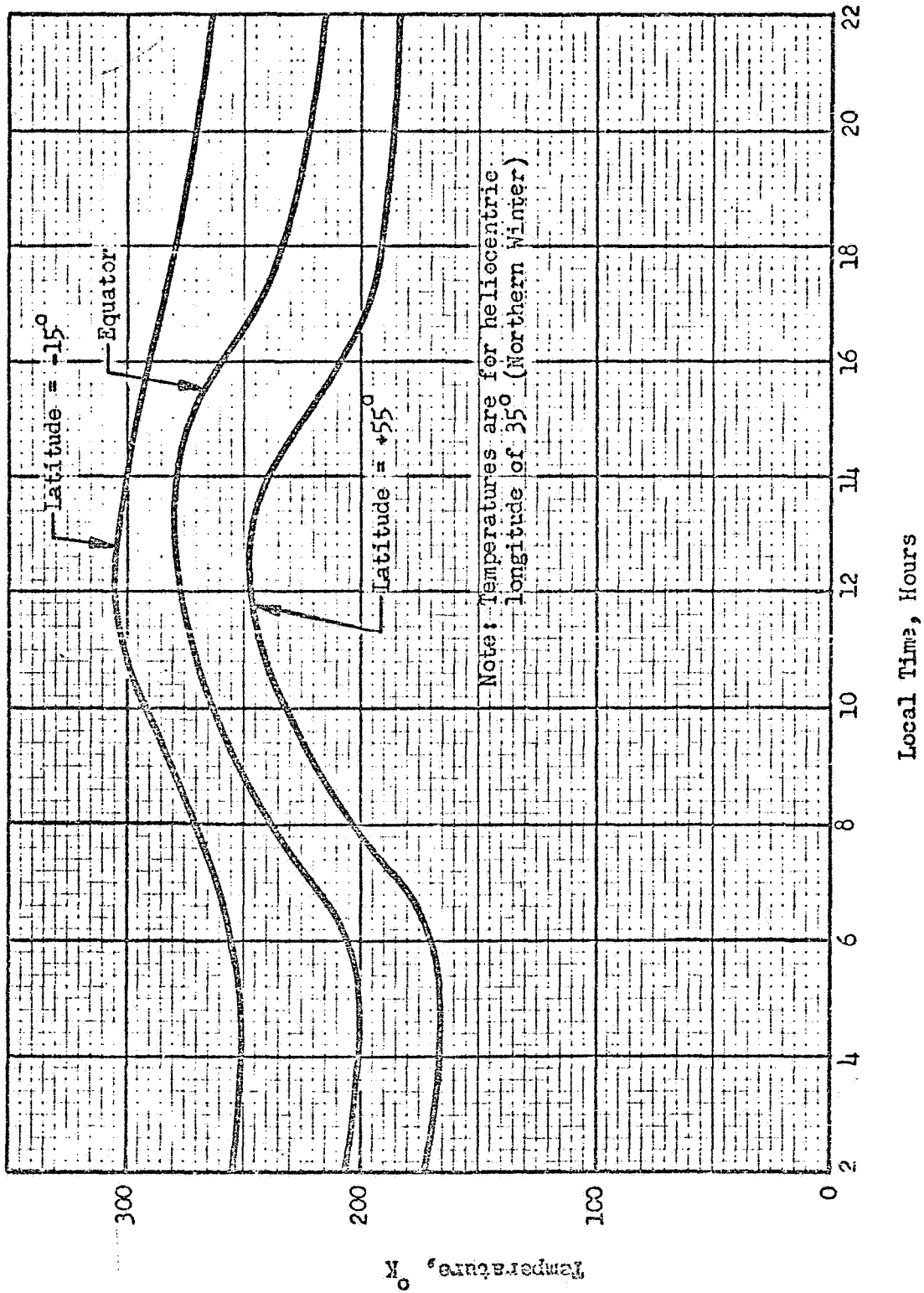


Fig. 5-4 Diurnal Temperature Variation of the Surface of Mars

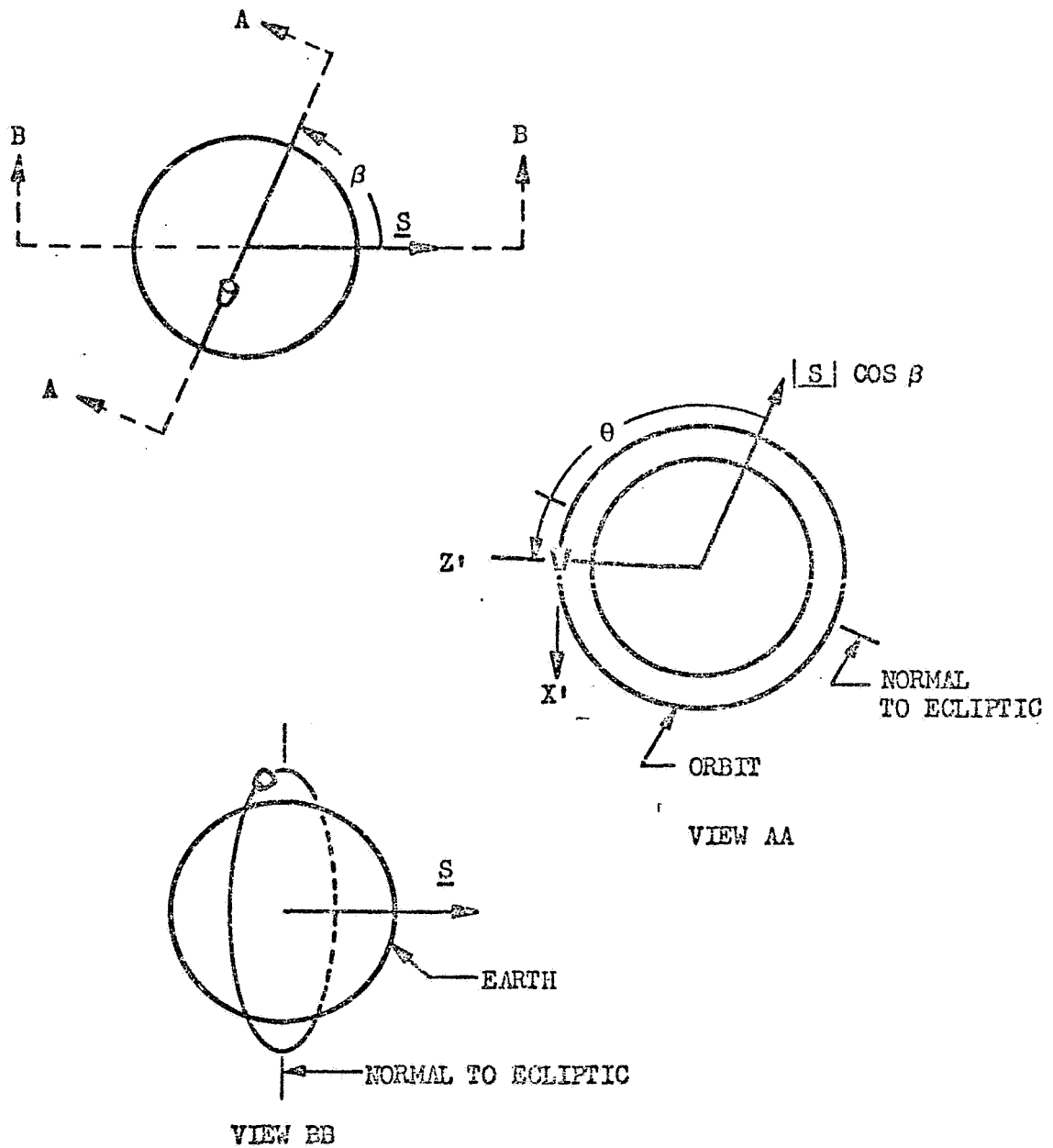


Fig. 5-5 Polar Orbit Geometry

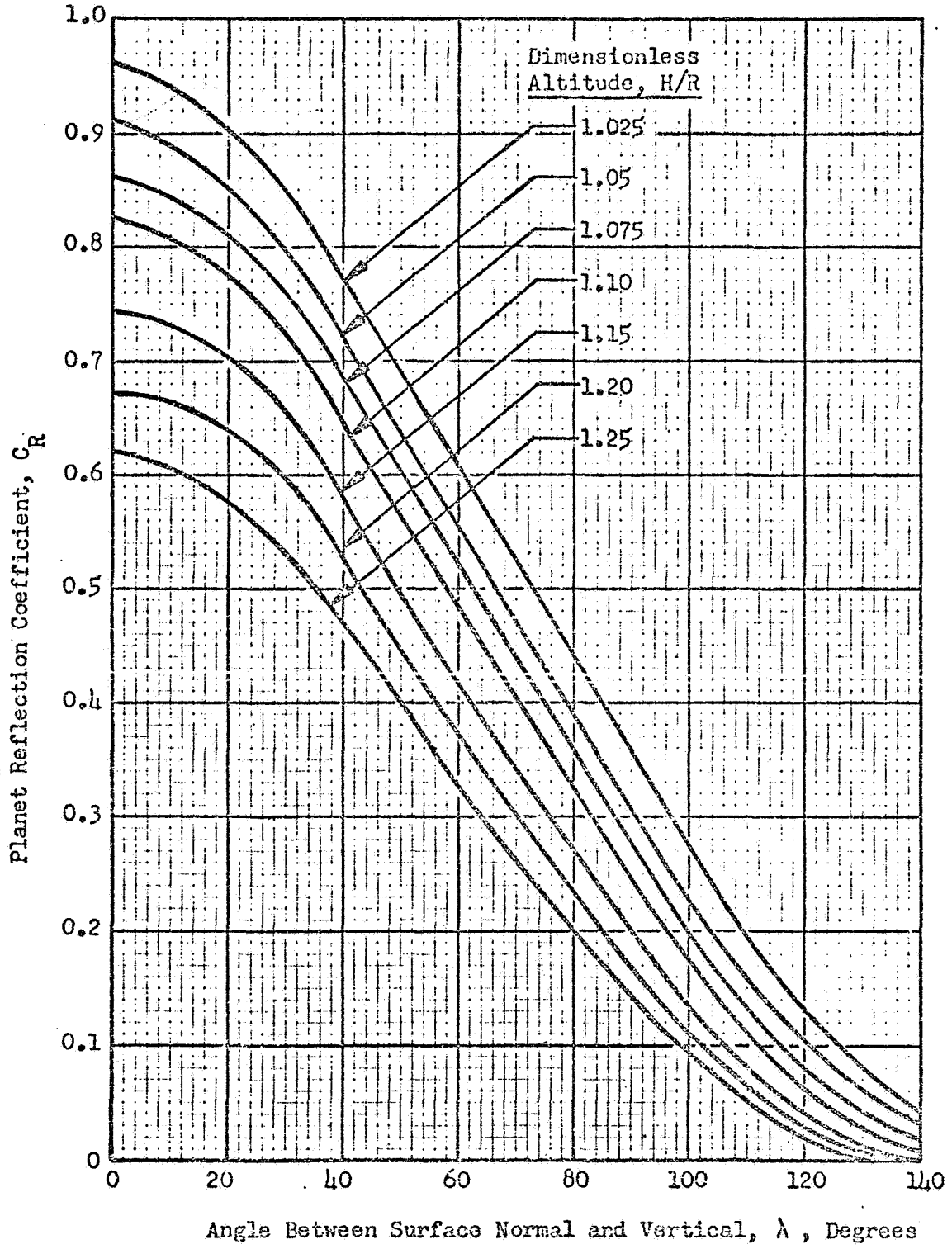
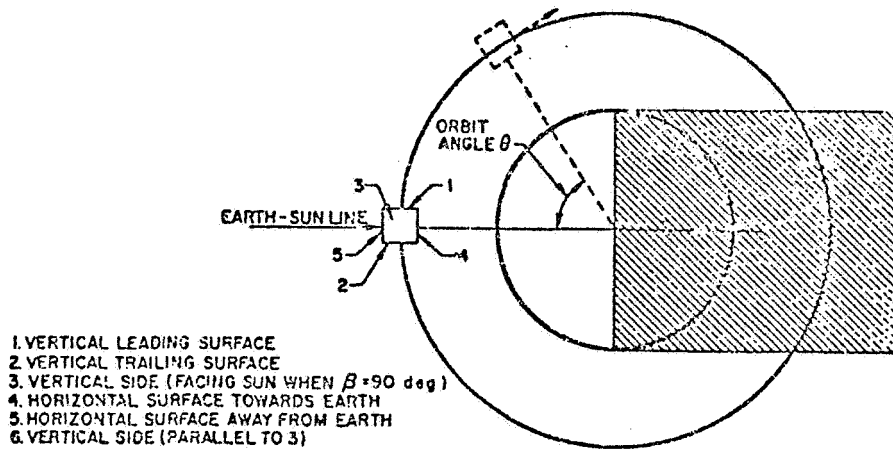


Fig. 5-6 Planet Reflection Coefficient for Flat Surface Element

Earth, as shown here below. In the noon orbit illustrated, for which the



Oriented Cube in Noon Orbit

orbit solar incidence angle, β , is zero, the satellite passes through the Earth's shadow. As a result the various faces of the satellite are subjected to widely varying incident heat fluxes. When $\beta = 90^\circ$ (the twilight orbit, which is always normal to the Earth-Sun line), there are no time variations in the incident fluxes. Average orbital temperatures have been computed for each face of the cube, assuming they are thermally isolated from each other. These time-average temperatures are shown in Figs. 5-7 through 5-10, for orbits with $\beta = 0^\circ$ and $\beta = 90^\circ$ and various orbital altitudes and surface optical properties.

For a spherical tank covered with high performance insulation, the average surface temperature can be approximated by computing the average of the six surface temperatures of the cube.

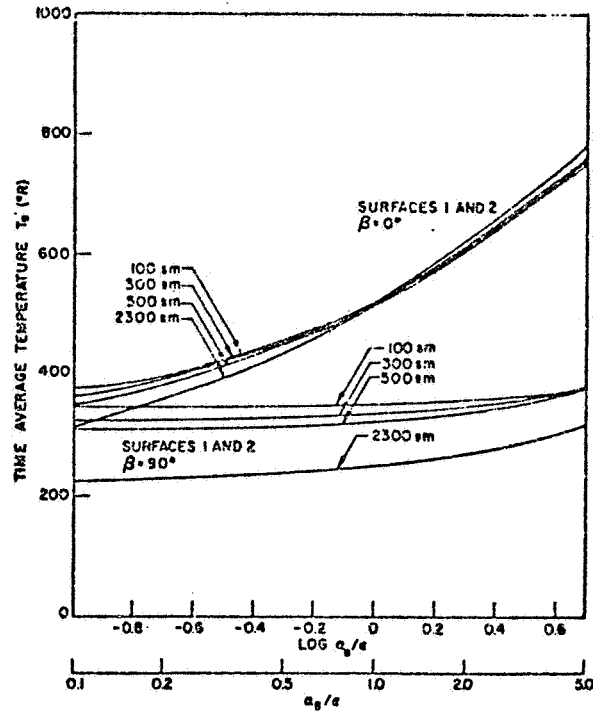


Fig. 5-7 Time Average Temperature as a Function of the α/ϵ Ratio (Surfaces 1 and 2)

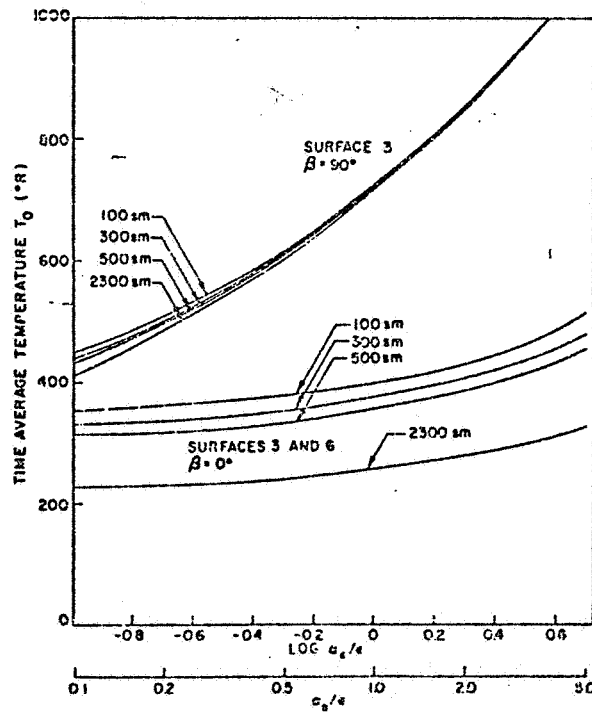


Fig. 5-8 Time Average Temperature as a Function of the α/ϵ Ratio (Surface 3)

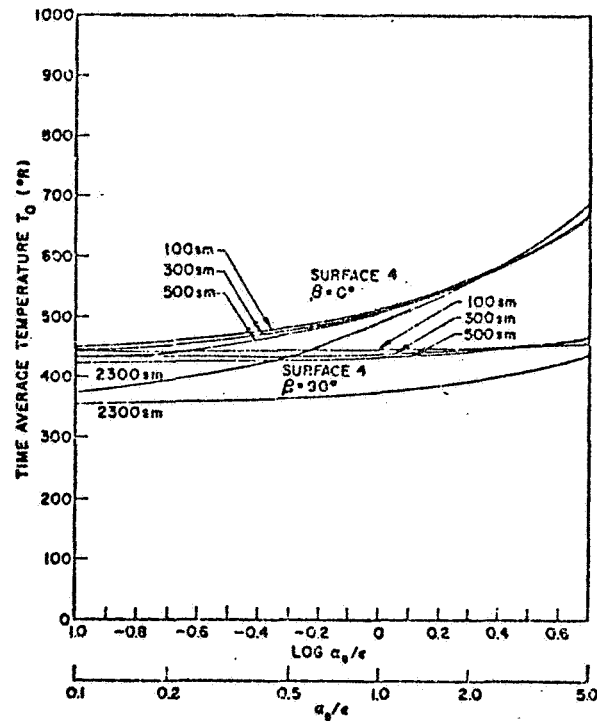


Fig. 5-9 Time Average Temperature as a Function of the α/ϵ Ratio (Surface 4)

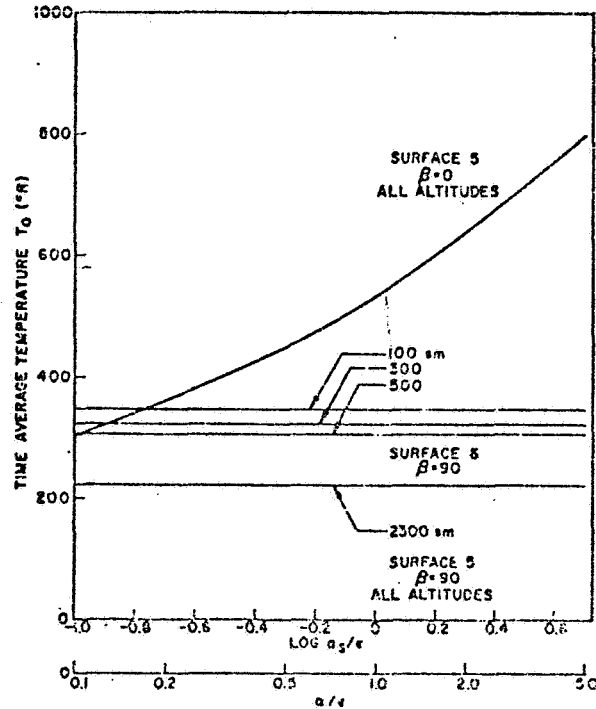


Fig. 5-10 Time Average Temperature as a Function of the α/ϵ Ratio (Surface 5)

Utilizing the data and methods outlined in this section the average surface temperature of an insulated tank was computed for several different space conditions. The conditions and temperatures are shown in Table 5-3.

Table 5-3
EQUILIBRIUM TANK SURFACE TEMPERATURES

Case I - Low Earth Orbit, h = 200 n. mi.

Circular, polar orbit

(Ia) 100% Sunlit Orbit - $\bar{T} = 214^{\circ}\text{K} (385^{\circ}\text{R})$

(Ib) 60% Sunlit Orbit - $\bar{T} = 204^{\circ}\text{K} (365^{\circ}\text{R})$

(Orbit plane parallel to sun's rays)

Case II - Lunar Surface Operation

(IIa) Lunar Noon (Sun Overhead) - $\bar{T} = 330^{\circ}\text{K} (595^{\circ}\text{R})$

(IIb) Lunar Night (Just before dawn) - $\bar{T} = 87^{\circ}\text{K} (157^{\circ}\text{R})$

Case III - Deep Space Operation (2 A.U.)

(IIIa) Unshielded Tank - $\bar{T} = 131^{\circ}\text{K} (236^{\circ}\text{R})$

(IIIb) Shielded Tank - $\bar{T} = 80^{\circ}\text{K} (144^{\circ}\text{R})$

External Solar Absorptance = 0.10

Infrared Emittance = 0.80

No Internal Heat Dissipation

Spherical Tank

REFERENCES

- 5-1 Cunningham, F. G., "Power Input to a Small Flat Plate from a Diffusely Radiating Sphere, with Applications to Earth Satellites," NASA TN D-710, 1961.
- 5-2 Lucas, J. W., et al, "Lunar Surface Temperatures and Thermal Characteristics," Surveyor V Mission Report, Technical Report 32-1246, Jet Propulsion Laboratory, Pasadena, California, 1 November 1967.
- 5-3 Lucas, J. W., et al, "Lunar Surface Temperature and Thermal Characteristics," Surveyor VI Mission Report, Technical Report 32-1262, Jet Propulsion Laboratory, Pasadena, California.
- 5-4 DeVaucouleurs, G., "The Physical Environment on Mars," Physics and Medicine of the Upper Atmosphere and Space, O.O. Benson and H. Strughold, Eds., John Wiley & Sons, Inc., New York, 1960.
- 5-5 Lockheed Missiles & Space Co., "Space Materials Handbook," C. G. Goetzl and J. B. Singletary, Eds., Contract AF 04(647)-673, January 1962.

Section 6 TANKAGE AND HEAT LEAKS

6.1 INTRODUCTION

The cryogenics will be stored in pressure vessels of various sizes and locations dependent upon the application. In this study, tank volumes of 20 to 200 ft³ were to be considered and the shape of the tanks were hemispherical domes with cylindrical midsections. The data presented in this section has been extended slightly to tanks having volumes up to 280 ft³. The emphasis has been placed on single-walled tanks having multilayer insulation. However weights have been included for a vacuum jacket shells capable of withstanding 15 psi crushing pressure.

To aid the designer or planner in computing the entire system weight for refrigeration trade-off studies, tank volumes, surface area, weights and heat transfer have been included. The tank weights are approximate and are mainly intended to provide weight increments for the trade studies. The heat rate to the tanks are based on a reasonable average for a large variety of multilayer insulations and supports. The heat rates through the multilayer insulation are based on calorimeter tests and modified by a factor of 2.8 to account for applications to real tanks. This modification was based on tests of a 109 inch diameter ellipsoid hydrogen tank tested at LMSC large cryogenic vacuum chamber.

6.2 TANK VOLUME AND SURFACE AREA

The tank volume and surface area have been plotted parametrically as a function of diameter, D, and length of the cylindrical section to diameter ratio, L/D. The tanks are spherical and cylindrical with hemispherical ends. The curves are shown in Figures 6-1 and 6-2. These same curves can be used to estimate the volume and surface area of a vacuum jacket by simply adding the vacuum annulus dimension to the pressure vessel diameter and reading the volume and area for the appropriate L/D.

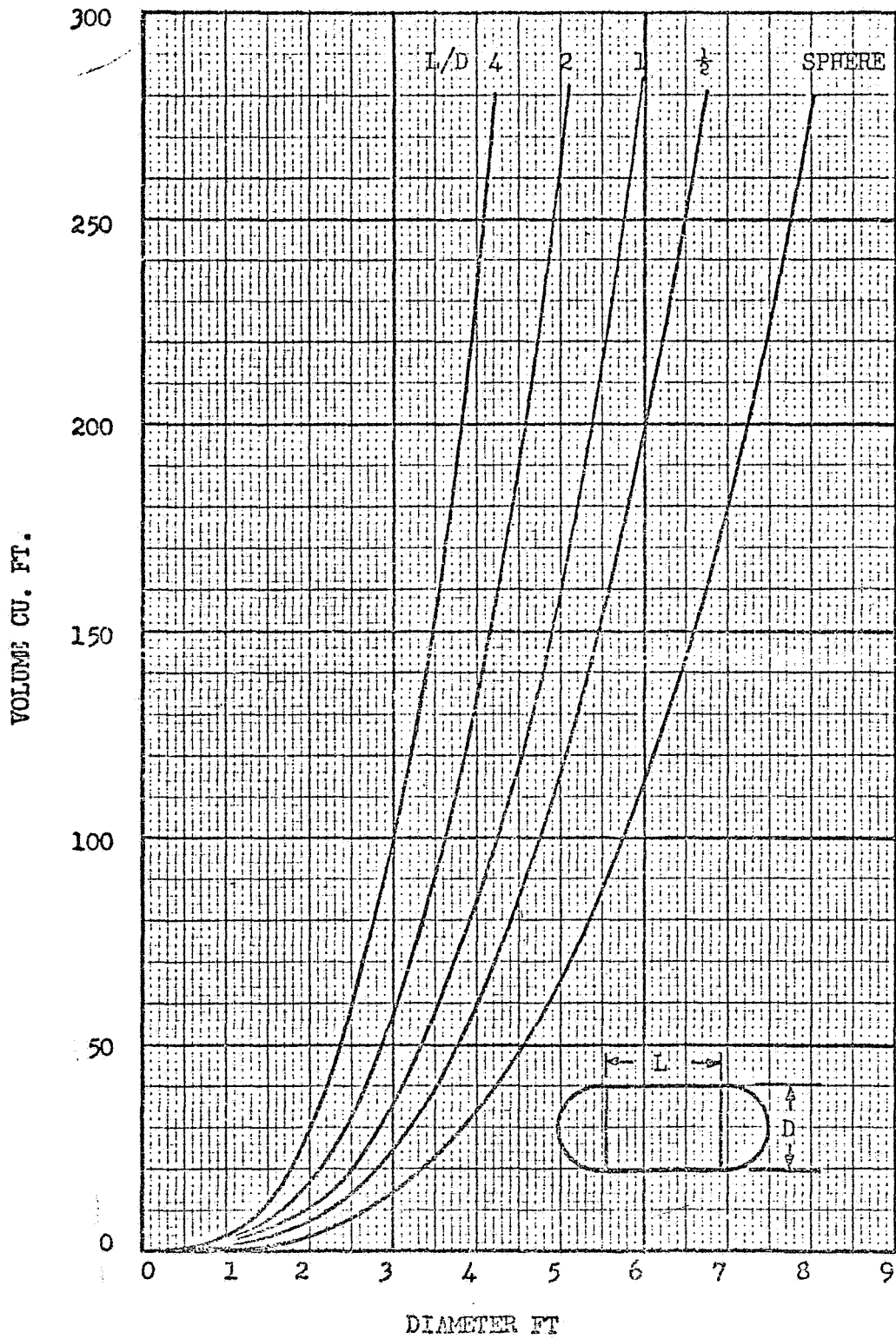


Figure 6-1 Tank Volume

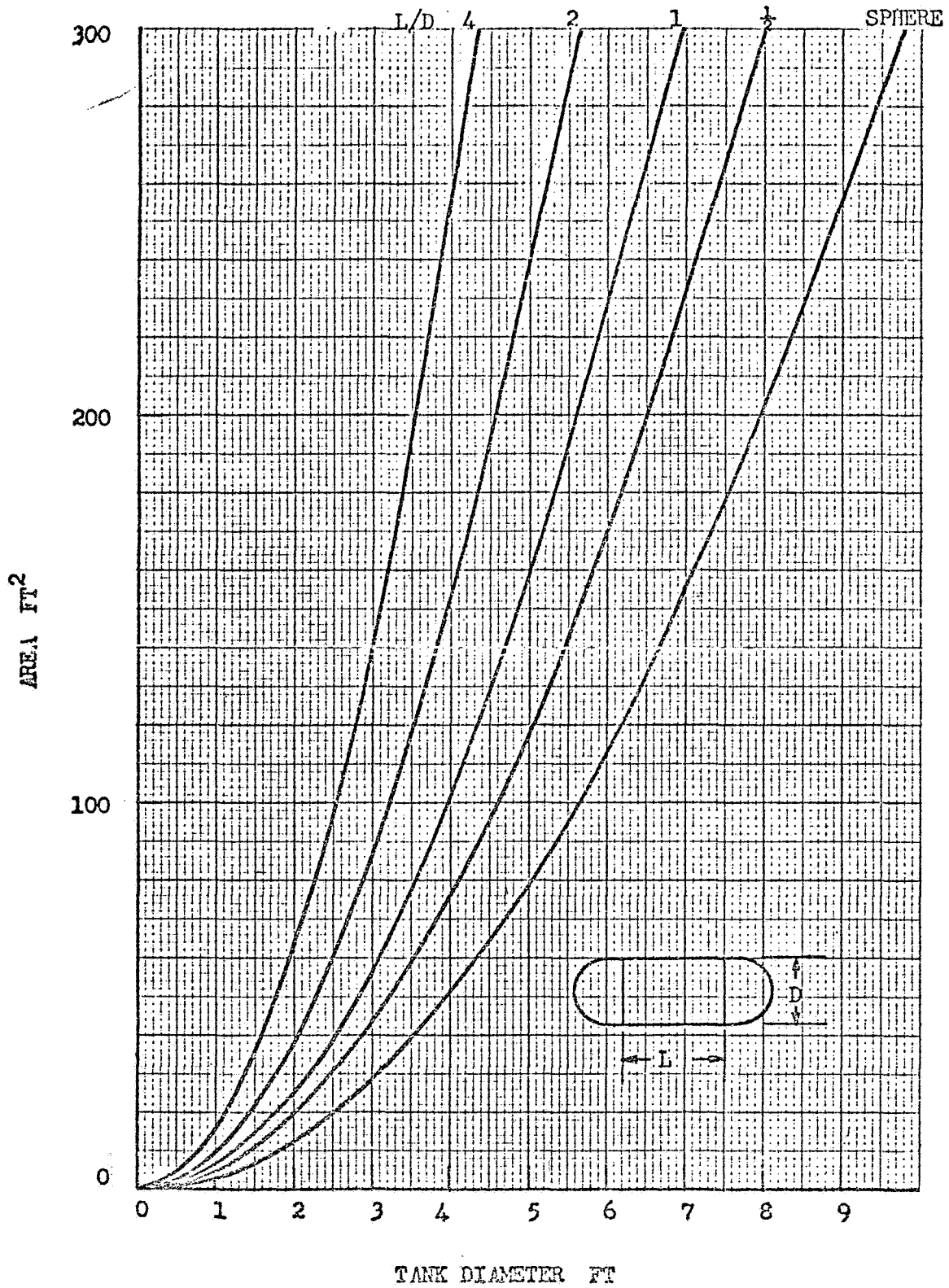


Figure 6-2 Tank Area

6.3 WEIGHT ESTIMATE OF CRYOGEN TANKS

Figure 6-3 can be used to estimate the weights of propellant tanks, spherical or cylindrical with hemispheroidal heads. The curves shown are for aluminum tanks with a maximum operating pressure of 100 psi and a design allowable tensile stress of 40,000 psi. The following assumptions were made:

- (1) The hemispheres used to fabricate the spherical tanks and the heads of the cylindrical tanks are one-piece with weld lands provided for assembly. If a gore construction is contemplated, additional weight should be introduced to provide adequate weld lands. For aluminum tanks, the weld lands were estimated to be twice the thickness of the membrane to take into account the reduced stress allowables in the weld and possible mismatch. Higher weld efficiency factors are obtained with stainless steel and nickel alloys and when that factor approaches 100% weld lands are not required.
- (2) Weights of the tank support attachments, baffles, access covers and sumps are not included in the weights shown in the figure.
- (3) The minimum weight curve is based on a minimum wall thickness of 0.040 in. and is shown for aluminum spherical tanks only. The variation of minimum weights between spherical and cylindrical tanks of the same volume is small if it is assumed the cylinder wall thickness to be twice that of the hemispherical heads.

The formulas used to evaluate the tank weights are as follows:

$$W_s = 0.785 \frac{\rho p}{\sigma} (D^3 + 3.82 D^2)$$

$$W_c = 0.785 \frac{\rho p}{\sigma} \left(2\left(\frac{L}{D}\right)D^3 + D^3 + 3.82 D^2 \right)$$

where:

W_s = Weight of spherical tanks, lbs

W_c = Weight of cylindrical tanks with hemispherical heads, lbs

p = maximum operating pressure, psi

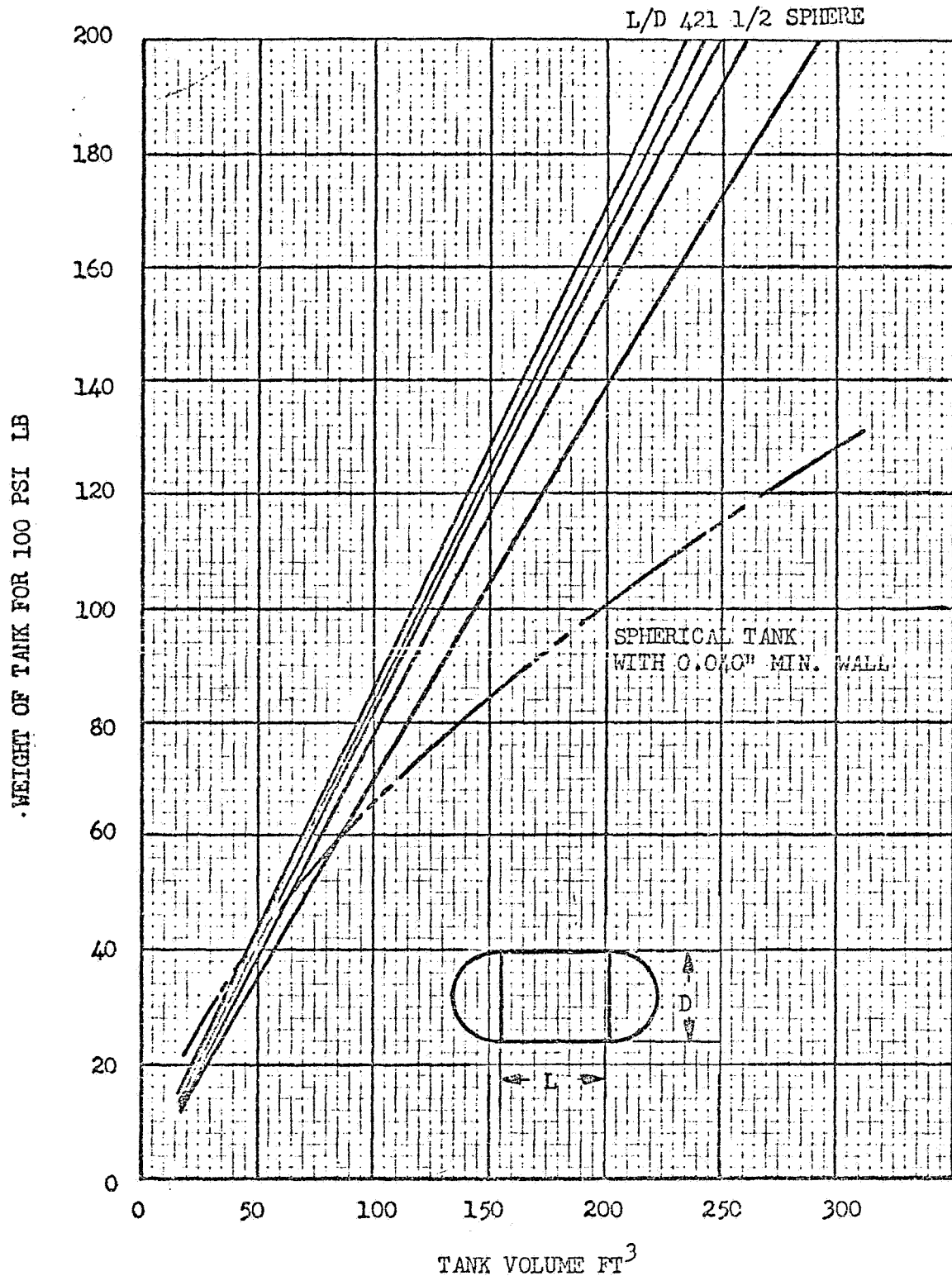


Figure 6-3 Aluminum Tank Shell Weight

- ρ = Density of tank wall material, lb/in³
 σ = Tank wall material design allowable tensile stress, psi
 D = Internal diameter of tank, in.
 L = Length of cylindrical section of tank, in.

In order to use the data in Figure 6-3 for other conditions the following steps should be followed.

When the volume and $\frac{L}{D}$ ratio of the tank are known, find the weight of 100 psi operating pressure aluminum tank from the figure. For operating pressures other than 100 psi, design allowable tensile stresses other than 40,000 psi and material densities other than .101 lb/in³ use the following formula:

$$W_a = W(\text{chart}) \times \frac{p_a}{100} \times \frac{40,000}{\sigma_a} \times \frac{\rho_a}{.101}$$

where:

- W_a = Actual weight of tank, lbs.
 p_a = Actual tank maximum operating pressure, psi
 σ_a = Actual material design allowable tensile stress, psi
 ρ_a = Actual tank material density, lb/in³

In all cases, but especially when the propellant density is high and the tank is submitted to high g-loads, the hydraulic head has to be added to the ullage pressure to determine the maximum operating pressure. If slosh is anticipated, another value depending on the shape of the tank and the number and shape of the baffles has also to be added. For preliminary estimates this term can be omitted.

The tank material design allowable tensile stress is the ultimate tensile stress of the material in the final formed condition corrected by the following factors:

- (1) Safety factor depending on manned or unmanned missions.
- (2) Temperature correction factor depending on maximum and minimum temperatures of the tank walls.

- (3) Discontinuity factor for thickness variations.
- (4) Manufacturing tolerance factor dictates by the fabrication processes.
- (5) Mismatch factor for welds only.

The design allowable used to compute the tank weights was 40,000 psi which is well below the ultimate stress.

6.3.1 Tank Support System Weights

Figure 6-4 shows a weight estimate of spherical tank support systems against the maximum propellant loading. These weights are based on axial loads of 4.5 g's forward and 1.0 g aft and a lateral load of ± 0.3 g's.

6.3.2 Baffles

The weight of baffles can be estimated between 2% of the tank weight for a 100 psi operating pressure for low density liquids and spherical tanks and 10% for high density liquids and long cylindrical tank with $\frac{L}{D}$ ratio of 4.

6.3.3 Vacuum Jackets

Figure 6-5 shows the estimated weights of aluminum self supporting vacuum jackets for spherical and cylindrical tanks. The weights are for vacuum jackets without reinforcing rings and the following formulas were used:

$$\text{For spheres: } \left(\frac{t}{D}\right)^2 = .685 \frac{P}{E_c}$$

$$\text{For cylinders: } \left(\frac{t}{D}\right)^3 = K \frac{P}{E_c}$$

where:

t = Thickness of shell, in.

D = Internal diameter of shell, in.

p = Critical external pressure, psi

E_c = Compression modulus of elasticity of shell material, psi

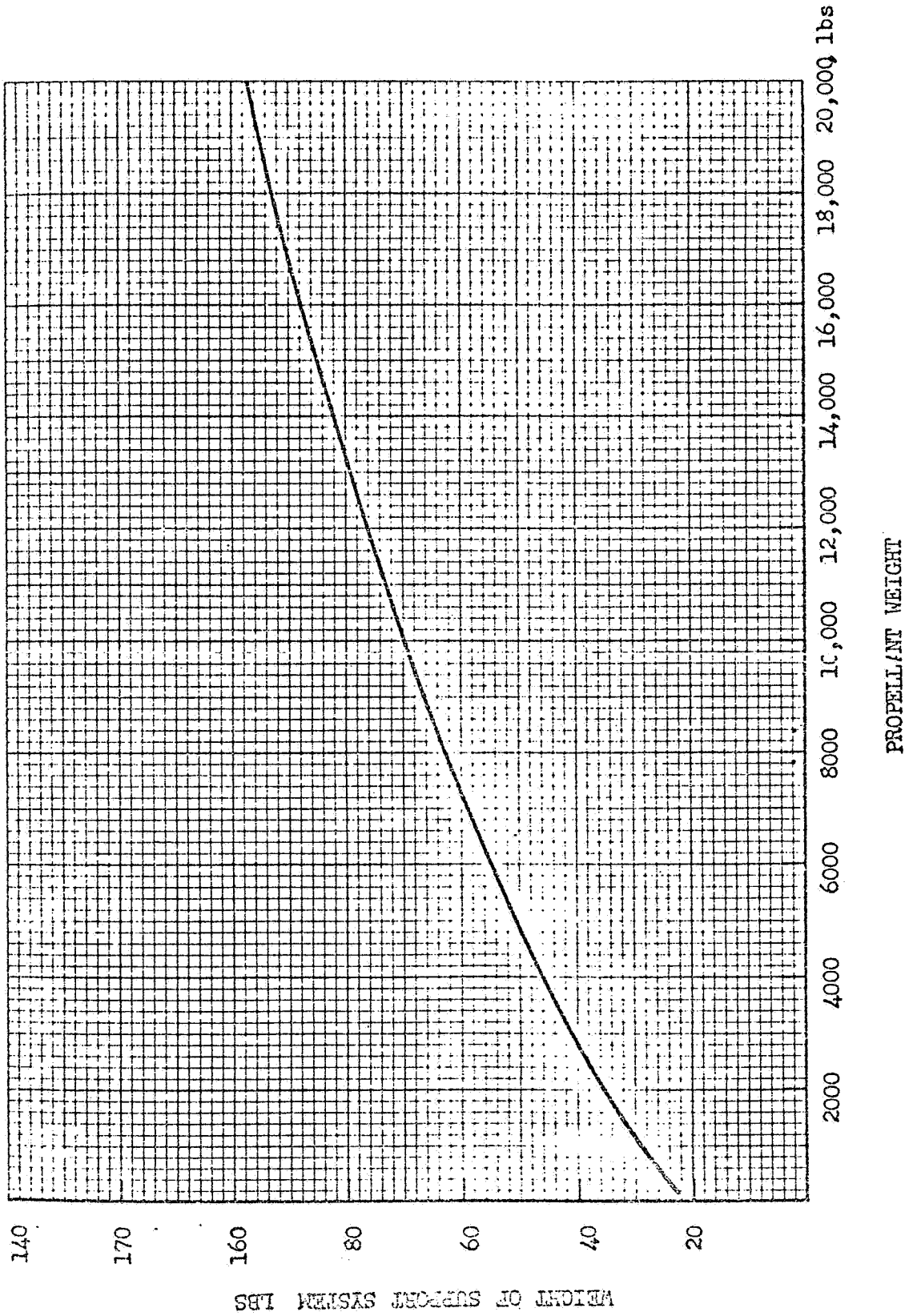


Fig. 6-4 Tank Support Weight

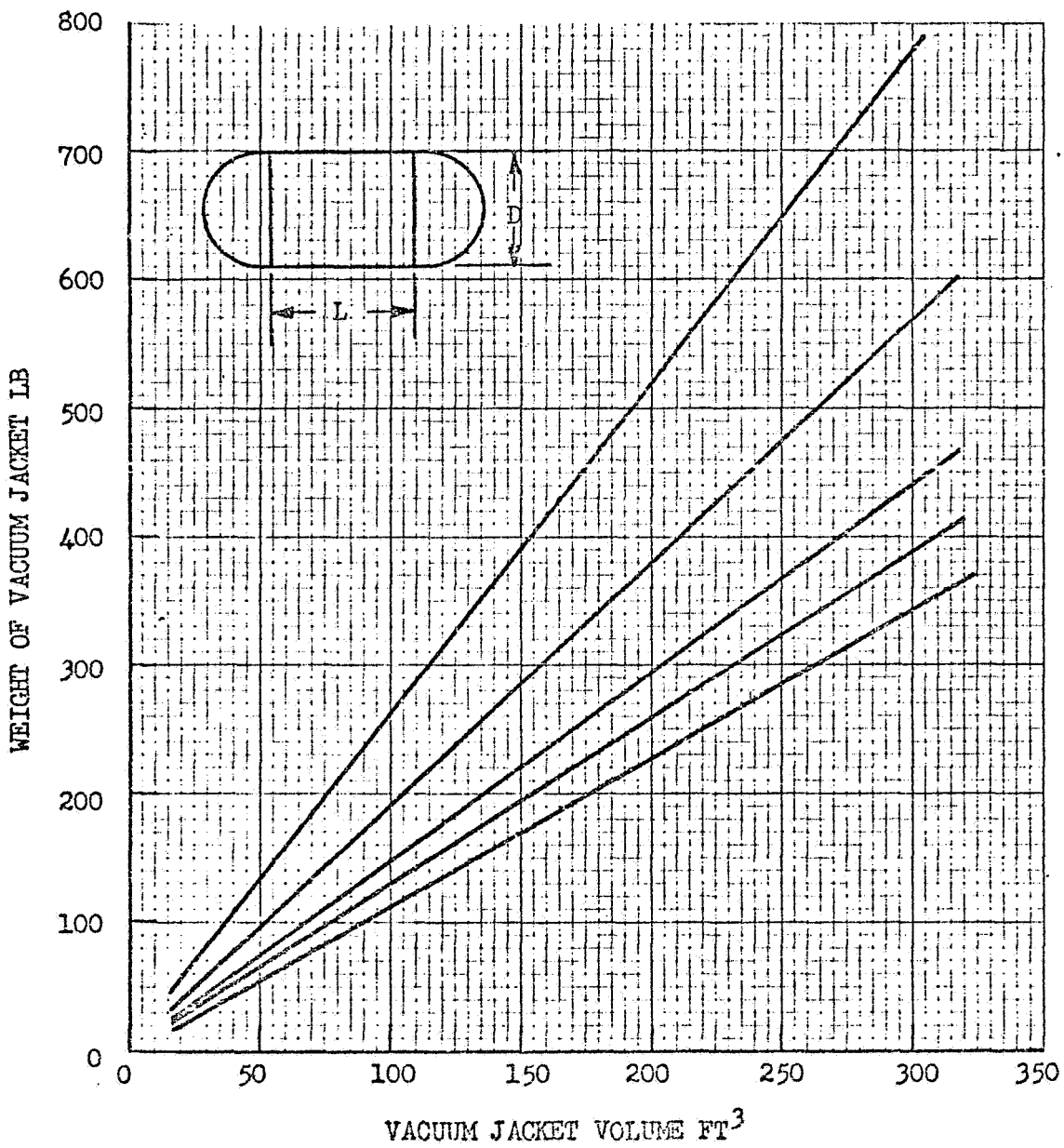


Figure 6-5 Vacuum Jacket Volume

Weight savings can be obtained by incorporating stiffening rings to cylindrical shells having high $\frac{L}{D}$ ratios, and by using honeycomb shells, but the weight evaluations of such designs are not in the scope of this study.

Some new concepts of flexible vacuum jackets in which the vacuum shell is allowed to deflect against supports attached to the tank wall or against non-crushable thermal insulation can achieve still greater weight savings. Data on such concepts are not available at the present time.

6.3.4 Access Covers

If a manhole is required, a minimum of 20.0 lb should be added to the weights given by the chart. This weight is for an aluminum manhole ring and cover having a minimum access diameter of 19.5 inches and a design maximum pressure of 150 psi. A handhold access ring and cover with an opening of 8.0-in-diameter adds about 5.0 lb to the tanks.

6.4 Heat Leak to Tanks

In order to estimate the heat load that a refrigerator system would have to be designed for, estimates of heat transfer rates to the propellant tanks have been made. The heat leaks are generally broken up into three groups: the leak through the insulation; the leak through the supports; and the leak through lines and instrumentation.

6.4.1 Heat Leak through Insulation

Several insulation systems have been under study over the last few years (References 6-1 and 6-2). For cryogenic tanks in a space environment it has been shown that multilayer insulation is among the better performers. One of the disadvantages of multilayer is the susceptibility to variations in performance due to compressive pressures and resultant insulation thickness variation for a given number of shields and spacers. In a recent study conducted for NASA/LeRC (Ref. 6-3) several types of multilayer insulation were evaluated. The results of those tests are summarized in Figure 6-6. The ordinate shows the insulation performance as measured by a term consisting of insulation weight and boiloff weight (assuming all heat transfer

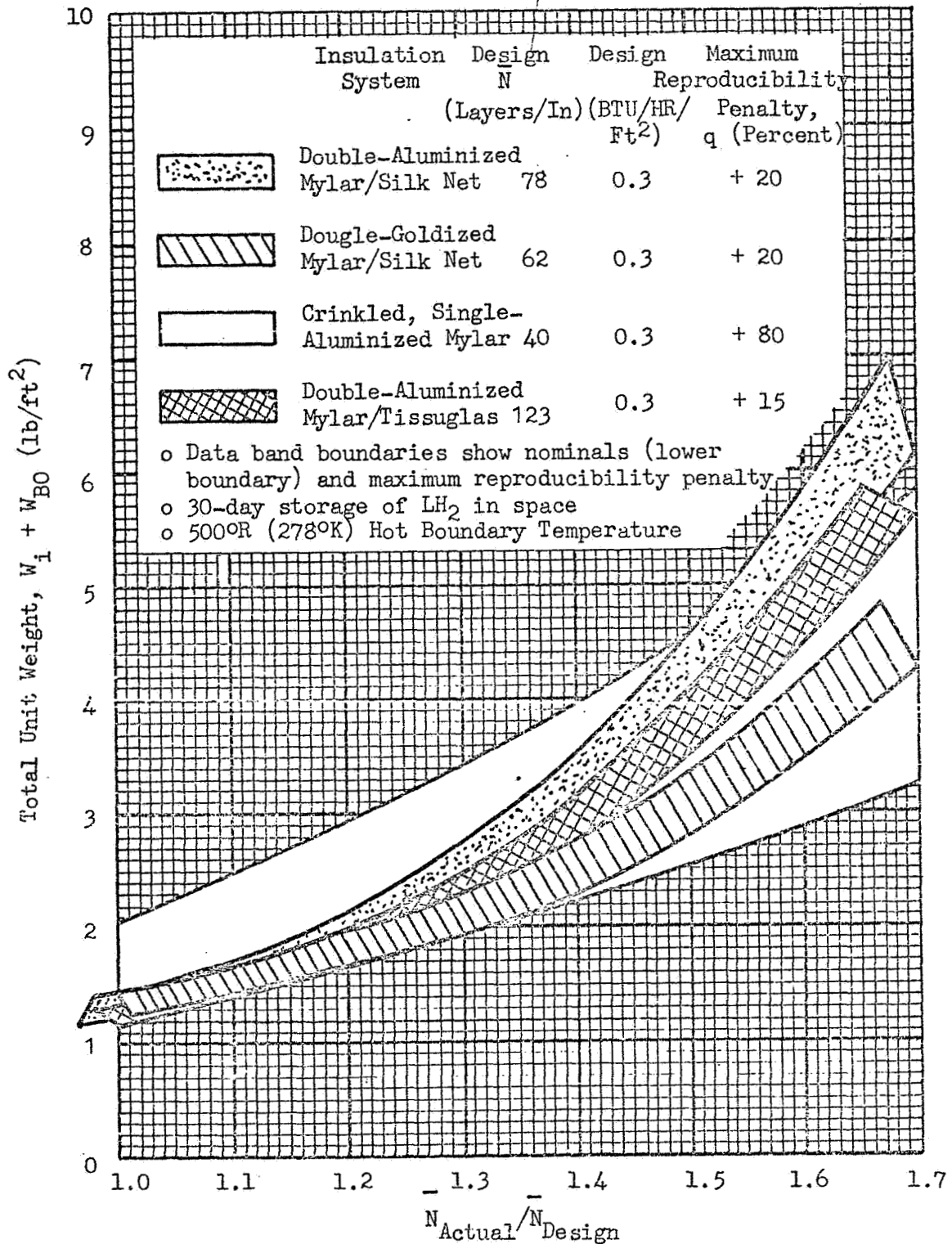


Figure 6-6 Total Unit Weight as a Function of Actual-to-Design Layer Density Ratio for Four Multilayer Insulations

results in boiloff). The abscissa shows the ratio of the actual to design layer density. As can be seen, a wide range of performance for any single design condition can exist. A good candidate for insulation performance is a double-goldized mylar with silk net spacers. It gives good performance, as well as relatively low performance variation. Therefore, for estimates of heat transfer, this type of insulation was selected.

Analytical investigations of double-goldized mylar/silk net, coupled with empirical data from calorimeter tests (Ref 6-3) have been employed to develop a relationship for the heat transfer as given by

$$q = .82 \left[\frac{4.37 \times 10^{11} (N)^{3.27} T_M (T_H - T_C)}{N_S + 1} + \frac{6.7 \times 10^{13} (T_H - T_C)^{4.51}}{N_S} \right]$$

where:

$$\begin{aligned} q &= \text{heat rate} \quad \text{Watts/Ft}^2 \\ N &= \text{Layer Density} \quad \text{No./in} \\ N_S &= \text{Number of Layers} \\ T_H &= \text{Hot Boundary Temp} \quad (^\circ\text{R}) \\ T_C &= \text{Cold Boundary Temp} \quad (^\circ\text{R}) \\ T_M &= \frac{T_H + T_C}{2} \quad (^\circ\text{R}) \end{aligned}$$

This relationship contains a multiplying factor of 2.8 to account for the degradation of the multilayer when it is applied to large tanks. This allows for fasteners, seams, and thermal degradation around supports. The value of 2.8 was determined as a result of thermal tests conducted on a 109-inch-diameter ellipsoidal hydrogen tank in the LMSC cryogenic flight simulator. Utilizing this equation, heat rates were computed for several hot and cold boundary temperatures and are shown in Figure 6-7. This curve can be quickly used to determine the heat rate through the insulation if the total surface area and surface temperatures are known. The surface temperatures can be estimated from the procedures and data given in Section 5.0 if the surface is exposed to the external environment. If the tank is enclosed within a vehicle, the environmental conditions of the vehicle are required. To attempt to estimate the thermal environment of the large variety of conditions that may exist

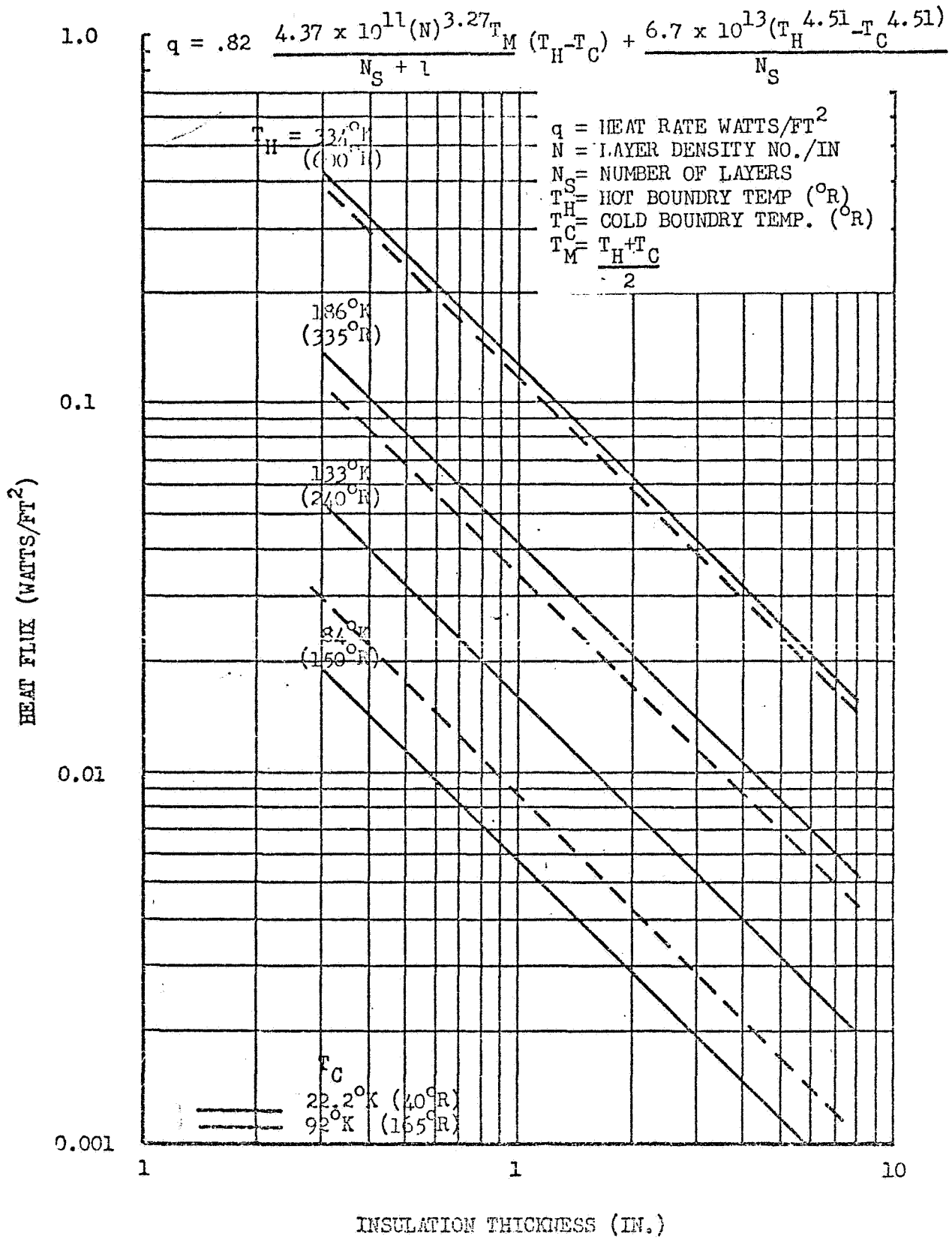


Fig. 6-7 Heat Flux Through Goldized Mylar/Silk Net Insulation

within a vehicle is beyond the scope of this study. However, in most instances rough estimates can be obtained by evaluating the type of equipment that is in the vicinity of the tank.

Because of the wide spread in thermal performance values associated with even the best multilayer insulation systems, various alternate insulation concepts have been investigated that will, hopefully, improve the thermal predictability and narrow the heat flux performance band.

One concept which is currently being tested by Lockheed substitutes low-emittance, 80-micron, hollow glass spheres for the multi layers. The major idea of the concept is to contain the spheres in a flexible vacuum jacket design so that compressive pressures imposed by atmospheric pressure and self-compression due to gravity during groundhold will markedly decrease and approach zero in orbit. The sphere acting like an incompressible fluid, will have minimal contact pressure in the weightless environment of space, reducing the solid conduction heat component to a low or negligible value. (The hard, perfect spheres contact each other only at a point under the low forces associated with orbital drag, on the order of 10^{-6} g, or electrostatic forces.) It is expected that the solid conductance component of the spheres will decrease on the order of 10^4 for a decrease in compressive load of 10^6 (i.e., from 1 g to 10^{-6} g). This reduction indicates the solid conduction value will be negligible in a weightless (10^{-6} g) environment. Heat transfer is then governed by radiation assuming sphere movement (convection) is minimal at low-g.

Other potential advantages of the system, such as high compressive strength (for flexible vacuum jacket use) are shown in Table 6-1. The thermal predictability value of $\pm 10\%$ shown is based on the estimated accuracy of IR transmittance measurements that are currently being made (solid conduction heat transfer is assumed to be negligible).

Since this concept has not been developed to the extent that multilayer insulation has, it is recommended that the heat rate given for the multilayer be used for refrigeration tradeoff studies.

TABLE 6-1

TYPICAL PROPERTIES OF ALUMINIZED, LOW-EMITTANCE MICRO-SPHERES

Thermal Conductivity, BTU/hr ft ² °R *	
530 to 140°R, 1-g, no mechanical load (Based on flat plate heat transfer test)	9 x 10 ⁻⁵
400 to 40°R, 0-g, no mechanical load (Based on IR transmittance tests, 0 solid conduction assumption; additional work will be done to optimize sphere size)	1.4 x 10 ⁻⁵ (Prelim. data)
Thermal Predictability	± 10% (estimated)
Isotropic (no thermal degradation at penetrations)	Yes
Min. Bulk Density. lb/ft ³ (commercially available; lower densities can be obtained on a development basis)	4
Maximum Temperature Capability, °F	900 (higher if gold is used)
Meteoroid Protection	Excellent (approximates theo- retical optimum of a powder)
Compressive Strength psi (Compressive Vacuum Jacket Application)	> 500
Cost Dollars/lb	10
Installation Complexity around Complex Shapes (supports, plumbing)	Low
Compatible with O ₂ or H ₂ leaking from propellant tanks	Yes
Nuclear Radiation Threshold Damage Level rads (c)	> 5 x 10 ⁸

* Aluminized sphere samples with a bulk density of 10.9 lb/ft³ were tested. Lower density spheres will be tested later.

6.4.2 Heat Leak Through Supports

Simple relationships can be developed to estimate the heat leak to a cryogen tank by computing the cross-sectional area required for the tank supports and estimating the solid conduction heat transfer. However, this approach generally results in much lower heat leak than is actually obtained in tests or as a result of detailed analysis which takes into account the radiation terms and the strut detail design and length. Therefore, several studies and tests performed over the years have been utilized to estimate the heat transfer to the cryogen tank. The data have been reviewed and normalized to put them in terms of the unit weight of the stored cryogens. In every case data were selected for fiberglass supports which were proven to be the best type of low heat leak support. For each case the design conditions include requirements for launch and ascent loads. The data are plotted in Figure 6-8, and a "best fit" curve has also been included. The identification of the data is given in Table 6-2. Most of the data fall into a fairly narrow band near the curve, with the exception of points 2, 5, and 8. Point 2 is for a slush hydrogen dewar that, due to the nature of the design, required the supports to be short compression members. This resulted in more than an order of magnitude increase in heat leak. Point 5 is a design for a cryogenic gas supply system where the supports were designed for oxygen loads due to commonality requirements. The point shown is for the case where hydrogen is used in the storage vessel, and therefore the heat leak per pound of hydrogen is high. Point 8 is for a propellant tank installation where the dense oxidizer could be supported in a near-ideal fashion. Also, the mission was such that the vehicle could be oriented away from the sun and the warm end of the supports were at a low temperature during steady-state operation. The combination of the good design conditions, mission profile, and the heavy propellant, gave a low value of heat leak per pound of cryogen.

It is suggested that for preliminary design estimates the curve shown in Figure 6-8 be used. For small hydrogen tanks, or for unusual design constraints the heat leak should be increased by as much as an order of magnitude, depending upon the installation.

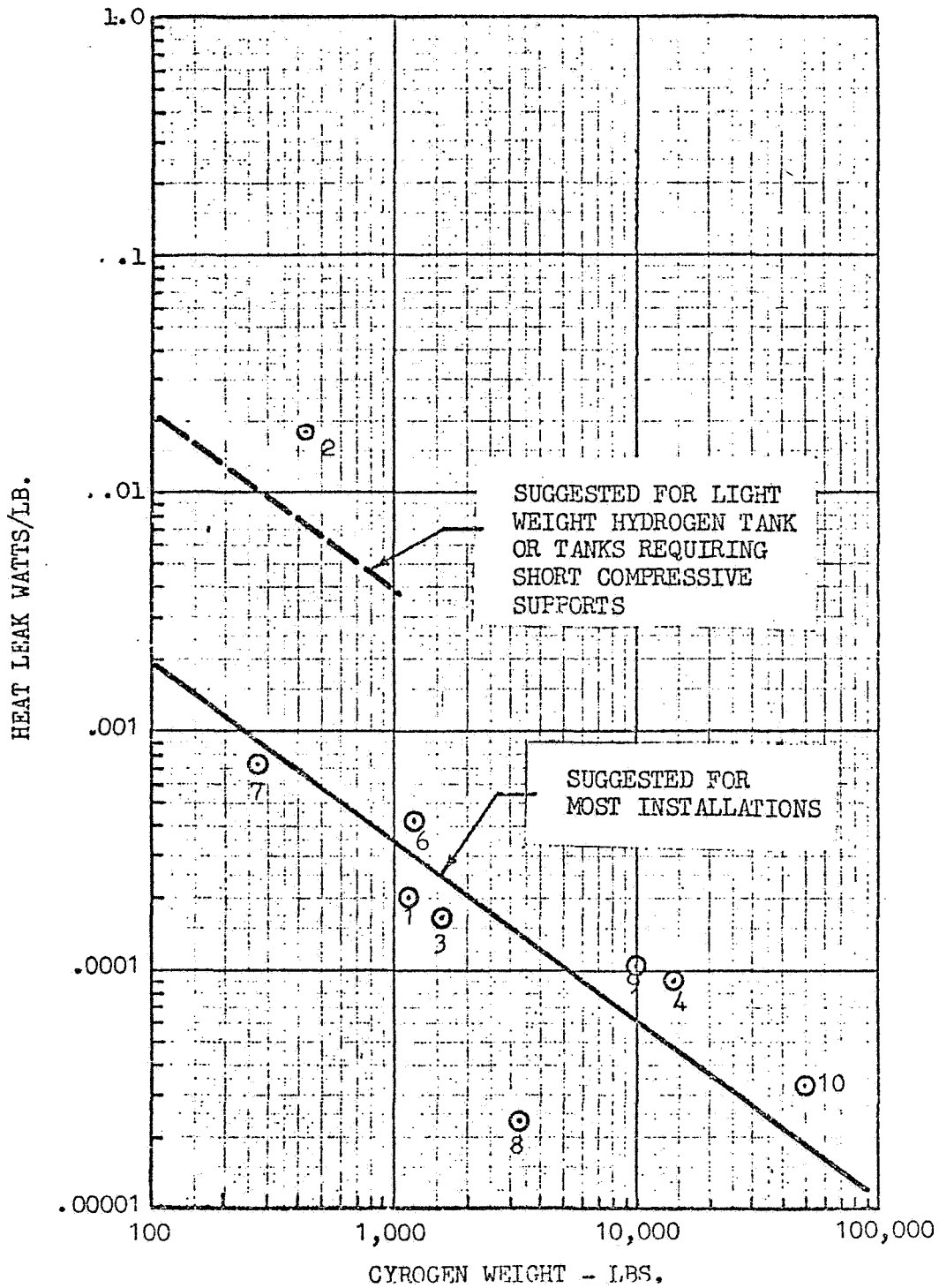


Figure 6-8 Heat Leaks through Fiberglas Supports

TABLE 6-2

HEAT LEAK THROUGH SUPPORTS AND LINES AND INSTRUMENTATION

Ident Point	Tank	Cryogen Wt Ib	--Heat Leak - Watts/lb --- Supports	Lines & Instrumentation	Ref
1	109.7" Ellipsoidal LH ₂	1,160	.0002	.00076	6-4
2	Slush H ₂ Dewar	436	.018	.0033	6-5
3	Ellipsoidal LH ₂	1,580	.00017	.00173	6-6
4	Ellipsoidal oxidizer	14,300	.000093	.000031	6-6
5	H ₂ Dewar	75	.0088	.00034	6-7
6	O ₂ Dewar	1,210	.00041	.00017	6-7
7	Ellipsoidal LH ₂	275	.00071	.00021	6-8
8	Cylindrical + Hemisphere IF ₂	3,300	.000024	.000012	6-8
9	Ellipsoidal LH ₂	10,000	.000103	.00012	6-9
10	Ellipsoidal IO ₂	50,000	.000033	.0000105	6-9

6.4.3 Heat Leak through Lines and Instrumentation

The same sources of data that were used to get the heat leak caused by the supports were used to get the heat leak caused by the lines and instrumentation. The term "lines and instrumentation" is used to include all sources of heat other than those caused by supports and insulation. However, it does not include the heat generated by the instruments themselves. A considerable amount of spread exists in the data as shown in Figure 6-9. This points up the fact that every design will have its own peculiarities that must be analyzed if a detail design is to be performed. However, to obtain rapid estimates of heat leak into the tank, the curve shown in Figure 6-9 can be used. The designer may want to adjust the heat upwards or downwards by an order of magnitude, depending upon his detail or peculiar design requirements.

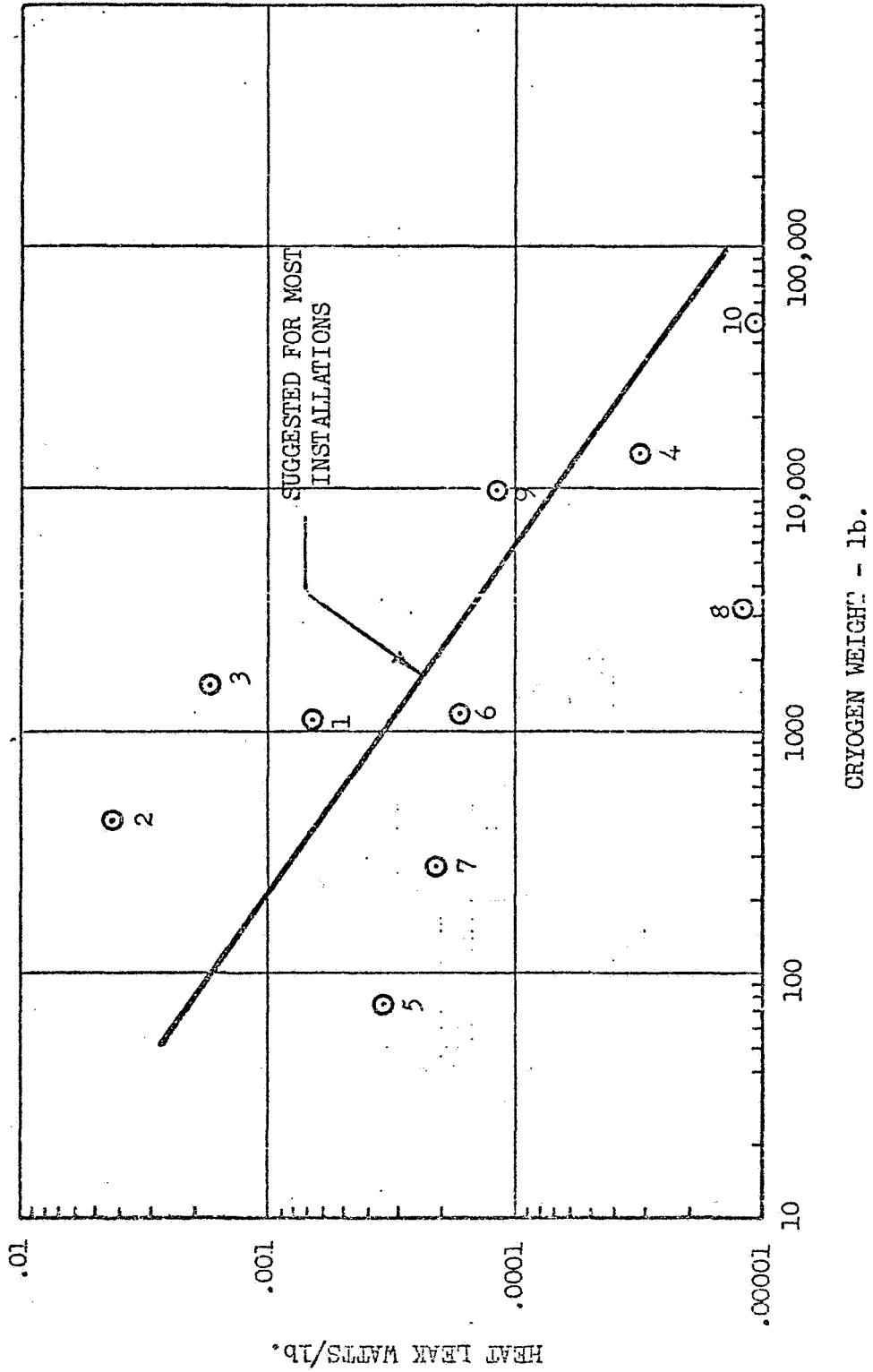


Figure 6-9 Heat Leak Through Lines and Instrumentation

REFERENCES

- 6-1 NASA-CR 54879, "Thermal Protection System for a Cryogenic Spacecraft Propulsion Module", Final Report for Contract NAS3-4199, Lockheed Missiles & Space Company, November 1966
- 6-2 LMSC K-17-68-5, "Investigations Regarding Development of a High-Performance Insulation System", Final Report for Contract NAS8-20758, July 1968
- 6-3 NASA-CR 72747, "Thermal Performance of Multilayer Insulations", Final Report for Contract NAS3-12025, Lockheed Missiles & Space Company, February 1971
- 6-4 LH₂ Storability in Space Propulsion Vehicles, Lockheed Missiles & Space Company, LMSC - 685104, 14 March 1968
- 6-5 LMSC K-11-68-1K, "A Study of Hydrogen Slush and/or Hydrogen Gel Utilization", Final Report for Contract NAS8-20342, Supplemental Program, Lockheed Missiles & Space Company, October 1968
- 6-6 Advanced Maneuvering Propulsion System. Lockheed Missiles & Space Company, LMSC-A960593, 31 January 1970
- 6-7 Cryogenic Gas Storage System. Lockheed Missiles & Space Company, LMSC 699613, 26 May 1967
- 6-8 Propellant Selection for Unmanned Spacecraft Propulsion Systems. Lockheed Missiles & Space Company, NASA CR 105202 NAS W 1644 15 September 1969
- 6-9 Improved Lunar Cargo and Personnel Delivery System. Lockheed Missiles & Space Company T-28-68-4 28 June 1968

Section 7 HEAT REJECTION SYSTEMS

7.1 INTRODUCTION

A significant portion of a cryogenic refrigeration system is the heat rejection system. The overall efficiency of the refrigerator at cryogenic temperatures tends to be low and therefore a considerable amount of heat must be rejected from the system.

Two basic methods of rejecting heat from the refrigeration system are generally available. One is to reject it to other components or cryogenics in the spacecraft, vehicle, or storage complex. The other method is to reject it to space. In order to evaluate the techniques of rejecting heat to other elements of a space vehicle or base requires considerable definition of the vehicles and elements themselves. Because of the large number of potential future applications and the large variety of arrangements that each vehicle may have, the task of defining the systems and requirements was beyond the scope of this study. Therefore, no attempt was made to integrate the refrigeration system heat rejection requirements with the heat absorption requirements of other elements or systems.

The effort in this study was concentrated on the techniques of rejecting heat to space. A radiator system design was analyzed in some detail and procedures presented for computing radiator area and weight. This was done for a standard fluid circulation radiator and for heat pipe systems. An evaluation of heat pipe design procedures was conducted and methods of estimating performance and weight are also presented in this section.

The designer can utilize the material in this section along with the material in the other sections to estimate overall system weight and performance.

As a first estimate in defining the applications and usefulness of a refrigeration system for space application where the heat is to be rejected to other system elements rather than to space, the designer can utilize the

elements in this section and substitute heat exchanger element in place of the radiator.

In order to estimate the heat rejection system characteristics the heat rejection rate must be known.

Values of required rates of heat rejection for a particular type of refrigeration system can be obtained using the definition of coefficient of performance presented in Section 3.

$$\text{COP} = \frac{\text{Cooling Load}}{\text{Power Input}} = \frac{q_c}{w}$$

The required rate of heat rejection is then

$$q_r = q_c + w = q_c \left(\frac{1 + \text{COP}}{\text{COP}} \right)$$

for mechanically powered refrigerators. For heat powered refrigerators,

$$q_r = q_h + q_c$$

where q_h is the rate at which heat is supplied to the refrigerator. Values of COP for a variety of refrigerators and conditions have been presented in Section 3.

7.2 RADIATOR DESIGN

7.2.1 Preliminary Design of Radiators for Space Operation

The preliminary design procedure presented below is directed toward the steady-state operation of a radiator rejecting (or absorbing) heat solely by means of radiative transfer. It is assumed that the cross section of the surface between coolant ducts is trapezoidal or rectangular and that no change of phase occurs within the coolant ducts.

7.2.1.1 Performance Analysis

A section of radiator using tapered fins is shown in Fig. 7-1. At the entrance to the radiator the fluid wall temperatures are T_{F1} and T_{W1} , respectively; at the exit the corresponding temperatures are T_{F2} and T_{W2} .

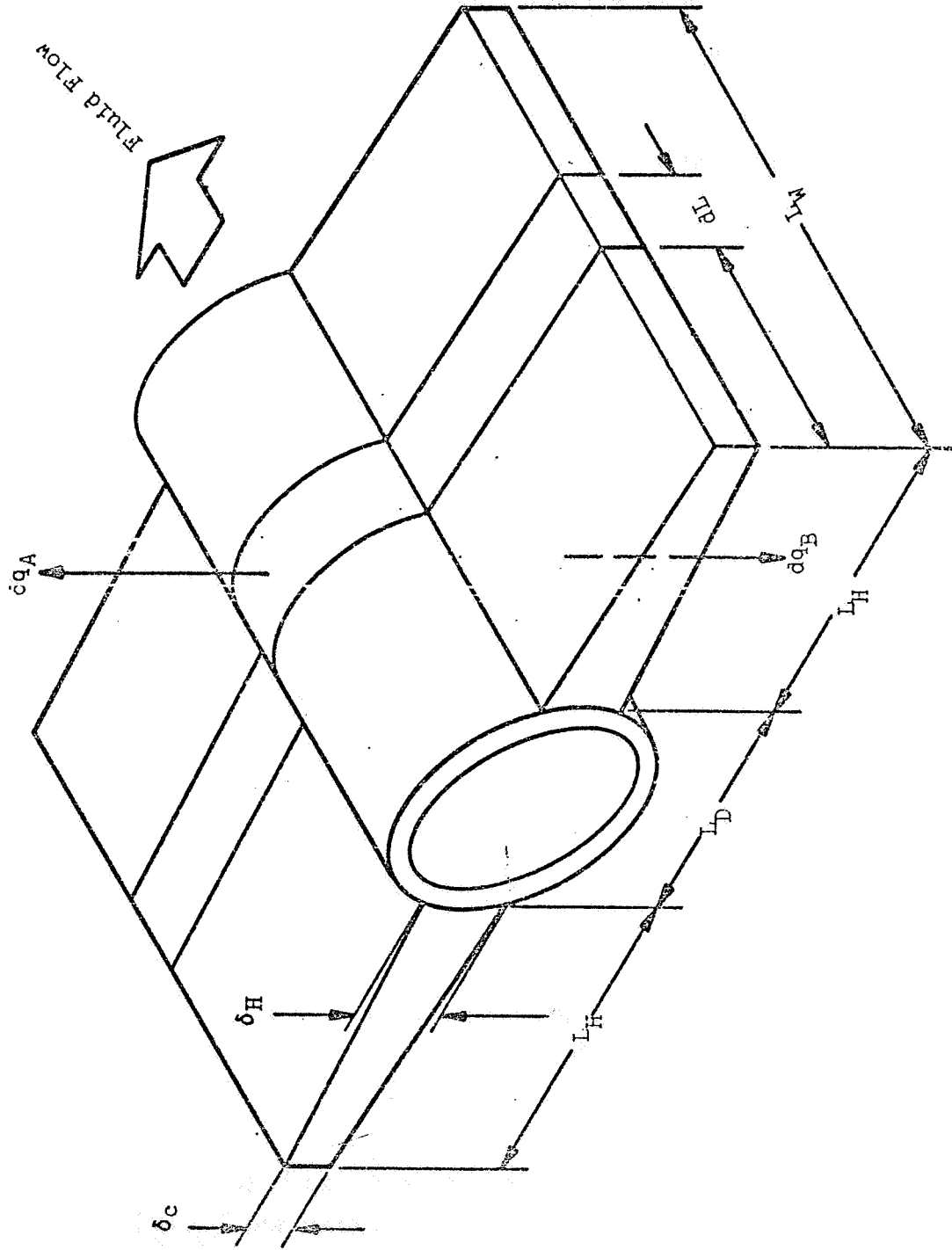


Figure 7-1 Radiator Duct with Trapezoidal Fins - Two Exposed Sides

Considering a differential element of length, dL , the heat rejected to space from both sides of the radiator is (Ref. 7-1):

$$dq = F_R \left[(G_E T_W^4 - G_A - G_P) L_D + 2 G_E T_W^4 \Omega L_H \right] dL \quad (7-1)$$

Where F_R is a factor accounting for radiant interchange between the coolant duct and the fin, Ω is a fin effectiveness factor, and G_E , G_A and G_P are environmental factors defined in Section 5. If an effective exchanger width is defined as

$$L_E = F_R \left[L_D + \frac{2 \Omega L_H}{1 - \frac{G_A + G_P}{G_E T_W^4}} \right] \quad (7-2)$$

Equation (7-1) can be written

$$dq = (G_E T_W^4 - G_A - G_P) L_E dL \quad (7-3)$$

The heat transferred from the fluid to the duct wall can be written

$$dq = p h (T_F - T_W) dL \quad (7-4)$$

where p is the perimeter of the duct cross-section and h is the heat transfer coefficient. Solving Equations (7-3) and (7-4) for T_F and differentiating the result yields

$$dT_F = \left(1 + \frac{4G_E L_E}{ph} T_W^3 \right) dT_W \quad (7-5)$$

The heat given up by the fluid to the walls is

$$dq = - \dot{W}_F C_{P_F} dT_F \quad (7-6)$$

Setting (7-3) equal to (7-4) and using Equation (7-5), we get

$$(G_E T_W^4 - G_A - G_P) L_E dL = - \dot{W}_F C_{P_F} \left(1 + \frac{4G_E L_E}{ph} T_W^3 \right) dT_W \quad (7-7)$$

Equation (7-7) can be solved for L_W if it is assumed that G_E , G_A , G_P and L_E are constant throughout the length of the radiator. Integrating Equation (7-7) over the radiator length gives

$$L_W = \frac{\dot{W}_F C_{PF}}{ph} \left[\phi_F + \phi_R \left(\frac{ph}{G_{E} T_{W1}^3 \bar{L}_E} \right) \right] \quad (7-8)$$

where \bar{L}_E is an average value of L_E over the length of the radiator,

$$\phi_F = \ln \left(\frac{1-G_H}{Z^4 - G_H} \right) \quad (7-9)$$

$$\phi_R = \frac{1}{4} G_H^{-3/4} \left[\ln \frac{\left(\frac{G_H^{1/4} + Z}{G_H^{1/4} - Z} \right)}{\left(\frac{G_H^{1/4} + 1}{G_H^{1/4} - 1} \right)} + 2 \left(\tan^{-1} \frac{Z}{G_H^{1/4}} - \tan^{-1} G_H^{-1/4} \right) \right] \quad (7-10)$$

$$G_H = \frac{G_A + G_P}{G_{E} T_{W1}^4} \quad (7-11)$$

and Z is the overall temperature ratio:

$$Z = \frac{T_{W2}}{T_{W1}} \quad (7-12)$$

The total quantity of heat removed from the fluid is

$$q = \dot{W}_F C_{PF} (T_{F1} - T_{F2}) \quad (7-13)$$

Radiators having a single active surface can be evaluated using the same equations provided the environmental factors are properly defined. For a two-sided radiator having different emittance values on each side,

$$G_E = \sigma (\epsilon_A + \epsilon_B)$$

and $G_A + G_p$ is the heat flux density from the environment reaching both surfaces. However, for a radiator having a single active surface (one side insulated) a value of zero is used for the underside surface emittance, ϵ_B , and $G_A + G_p$ is the environmental heat flux density incident only on the active surface. For a radiator whose underside is insulated the insulated portion of the coolant duct may be near the local fluid temperature. In this case the effective wetted perimeter of the duct must be modified to account for the reduced rate of heat transfer.

7.2.1.2 Design Charts

A solution to a preliminary design problem can be obtained from Equations (7-3), (7-4) and (7-8), providing required values of the environmental parameters and heat exchange factors are available. The values of the environmental parameters G_E , G_A and G_p are obtained as described above and Section 5. For coolant ducts or tubes of relatively small diameter the interradiation correction factor F_R can be set equal to one. For large diameter tubes the curves shown in Fig. 7-2 can be used. The profile number shown on the abscissa is defined by Equation (7-14):

$$P = \frac{G_E \pi^3 L_H^2}{K \delta_H} \quad (7-13)$$

where δ_H is the fin root thickness and K the fin thermal conductivity.

Values of the fluid-to-wall heat transfer coefficient, h , can be obtained from Ref. 7-2 for a variety of coolant duct cross-sections. For circular tubes a nomogram can be used to obtain the value of h . This nomogram is shown in Fig. 7-3. Values of fin effectiveness can be obtained from data

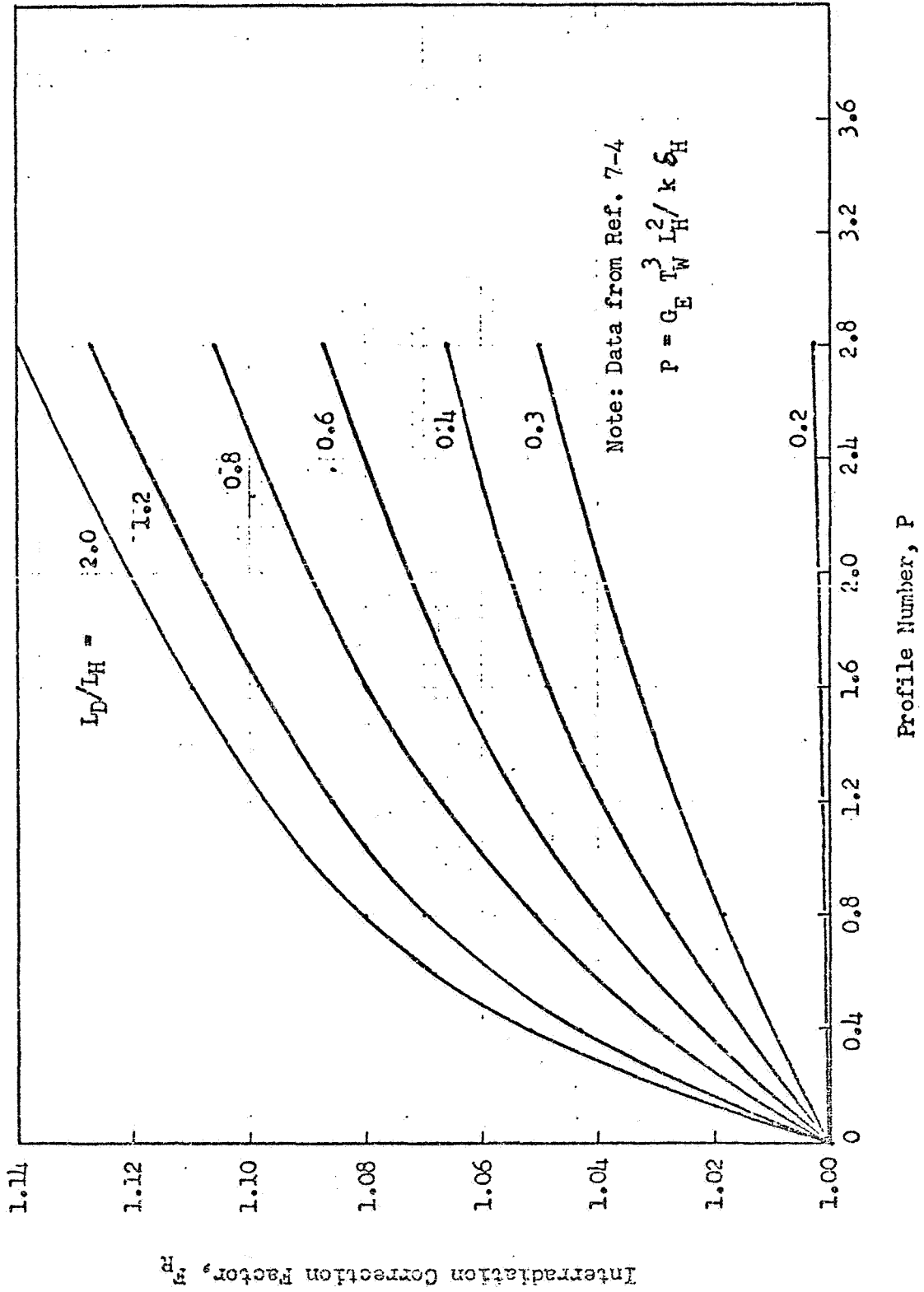
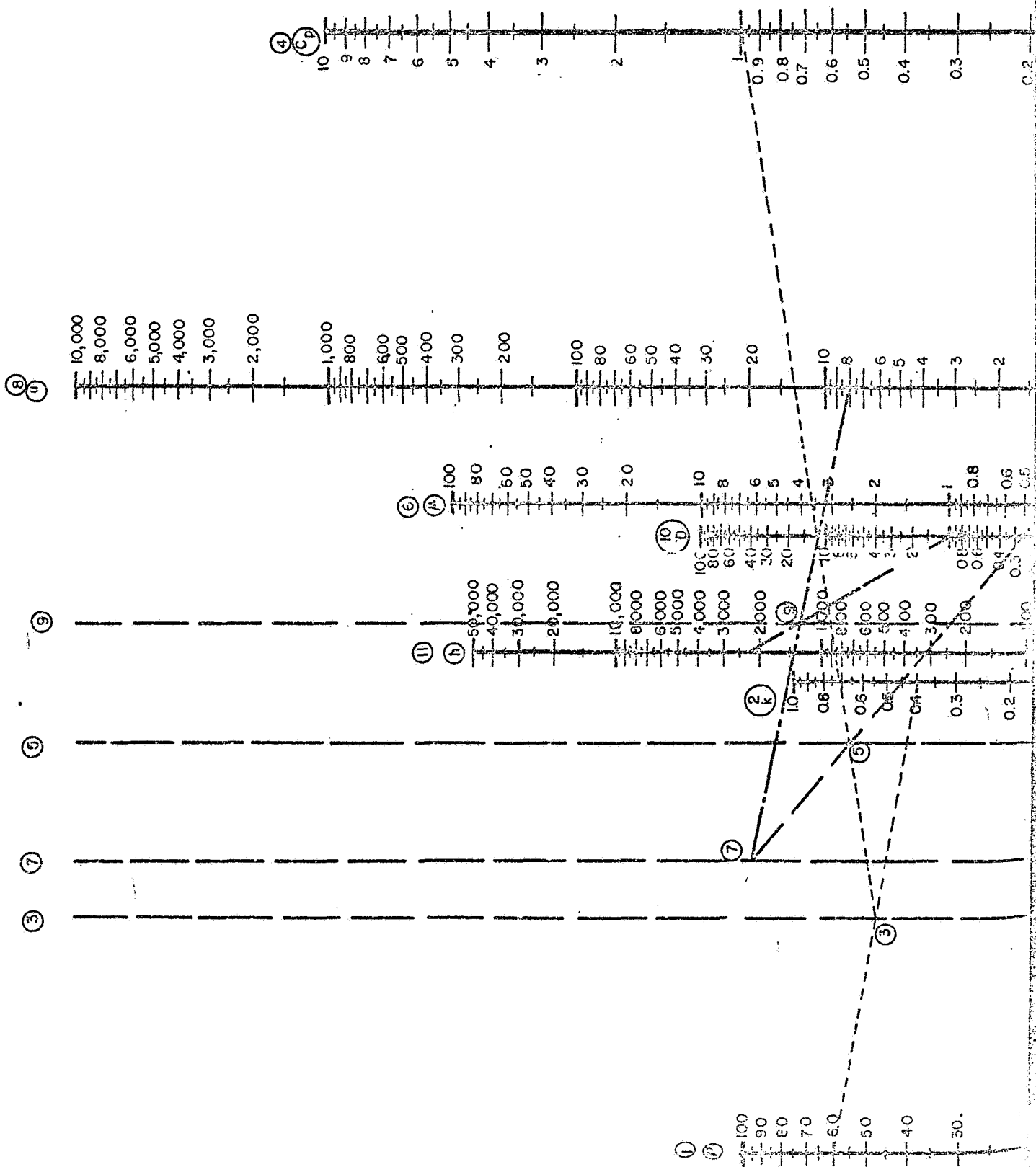
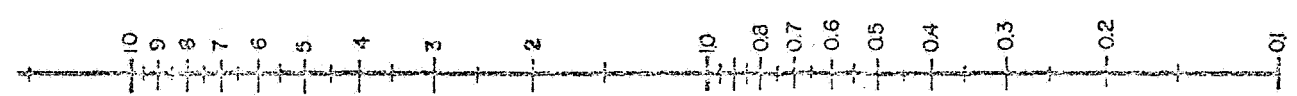
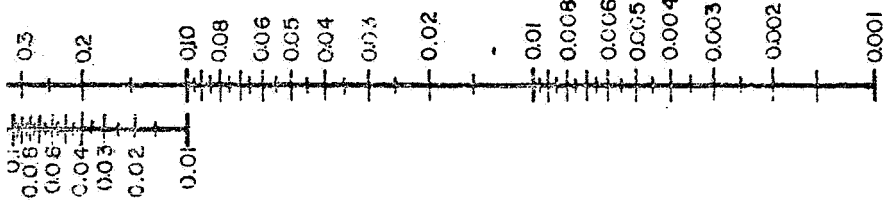
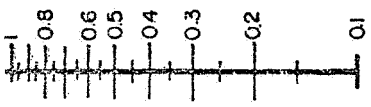


Figure 7-2 Correction Factor for Interradiation Between Coolant Tube and Fins

FOLDOUT FRAME





SYSTEM OF MIXED UNITS
DEFINITION

SYMBOL

UNIT

SYMBOL	DEFINITION	UNIT
ρ	DENSITY	Lb. cu.ft.
k	THERMAL CONDUCTIVITY	B.t.u. (hr)(ft ²)
c_p	THERMAL CAPACITY (numerically equal to sp. heat)	B.t.u. lb.ft.
μ	VISCOSITY	Centipoise
U	LINEAR VELOCITY	Ft./sec.
D	CHARACTERISTIC LENGTH (diameter for round tubes)	Inch
h	COEFFICIENT OF HEAT TRANSFER	B.t.u. (hr.)(sq. ft. ²)

Encircled numbers (e.g. 1 2 ---) indicate sequence of reference line usage

Fig. 7-3 Nomogram for Solution of Dittus-Boelter Equation

PRECEDING PAGE BLANK NOT FILMED.

presented in Ref. 7-1. These data give fin effectiveness as a function of thickness ratio, δ_C/δ_H , where

$$\delta_H = \text{fin root thickness}$$

and

$$\delta_C = \text{fin tip thickness}$$

Data from Ref. 7-1 for trapezoidal fins with thickness ratios of 1.0 (rectangular profiles), 0.75, 0.50, 0.25, and 0.01 (approximately triangular) are shown in Figs. 7-4 through 7-8 for a wide range of environmental parameters. Lines indicating minimum weight profiles are also shown. As pointed out in Ref. 7-1, the minimum weight profile may prescribe an unrealistically thin fin, or result in unacceptably large radiator areas. Thus, the minimum weight profile may not always be the optimum profile for a given application. However, fairly large deviations from the minimum weight profile can be tolerated without incurring large weight penalties.

In order to solve Equation (7-8), values of the film resistance number, ϕ_F , and the radiation number, ϕ_R , must be determined.

Values of ϕ_F , determined from Equation (7-9), are plotted in Fig. 7-9 as a function of the temperature ratio, Z , and the environmental parameter, G_H . Values of ϕ_R , computed from Equation (7-10), are plotted in Fig. 7-10.

7.2.1.3 Design Procedure

The usual design problem requires sizing a radiator to handle a given cooling load. Thus, given either q or the coolant flowrate, as well as coolant inlet and outlet temperatures, the length of a radiator having a given configuration is desired. The solution procedure for this case is outlined in stepwise fashion below.

1. Establish heat rejection rate for the given cooling load using the data in Section 3.

2. Select a fluid for the given inlet and outlet temperature range from Fig. 7-11, section 7.2.3.
3. Look up the fluid specific heat C_P from Table 7-1, section 7.2.3.
4. Compute the coolant flowrate from the known cooling load using Eq. (7-13).
5. Solve for G_A , G_P and G_E using the data of section 5.
6. Select values for the coolant duct dimensions and fin profile.
7. Solve for the heat transfer coefficient, h , using Fig. 7-3.
8. Assume the inlet and outlet tube wall temperatures, T_{W1} and T_{W2} , are equal to the adjacent coolant temperatures, T_{F1} and T_{F2} .
9. Obtain fin effectiveness values Ω_1 and Ω_2 from Figs. 7-4 through 7-8, with

$$P_1 = \frac{G_E T_{W1}^3 L_H^2}{K \delta_H}$$

and

$$P_2 = \frac{G_E T_{W2}^3 L_H^2}{K \delta_H}$$

10. Determine interradiation correction factors F_{R1} and F_{R2} from Fig. 7-2.
11. Compute equivalent lengths, L_{E1} and L_{E2} , at entrance and exit using Equation (7-2).
12. Use these values to compute "new" wall temperatures, T_{W1} and T_{W2} , by trial and error, using the heat balance resulting from Equations (7-3) and (7-4):

$$\left[G_E T_{W1}^4 - (G_A + G_P) \right] L_{E1} = p h (T_{F1} - T_{W1})$$

and

$$\left[G_E T_{W2}^4 - (G_A + G_P) \right] L_{E2} = p h (T_{F2} - T_{W2})$$

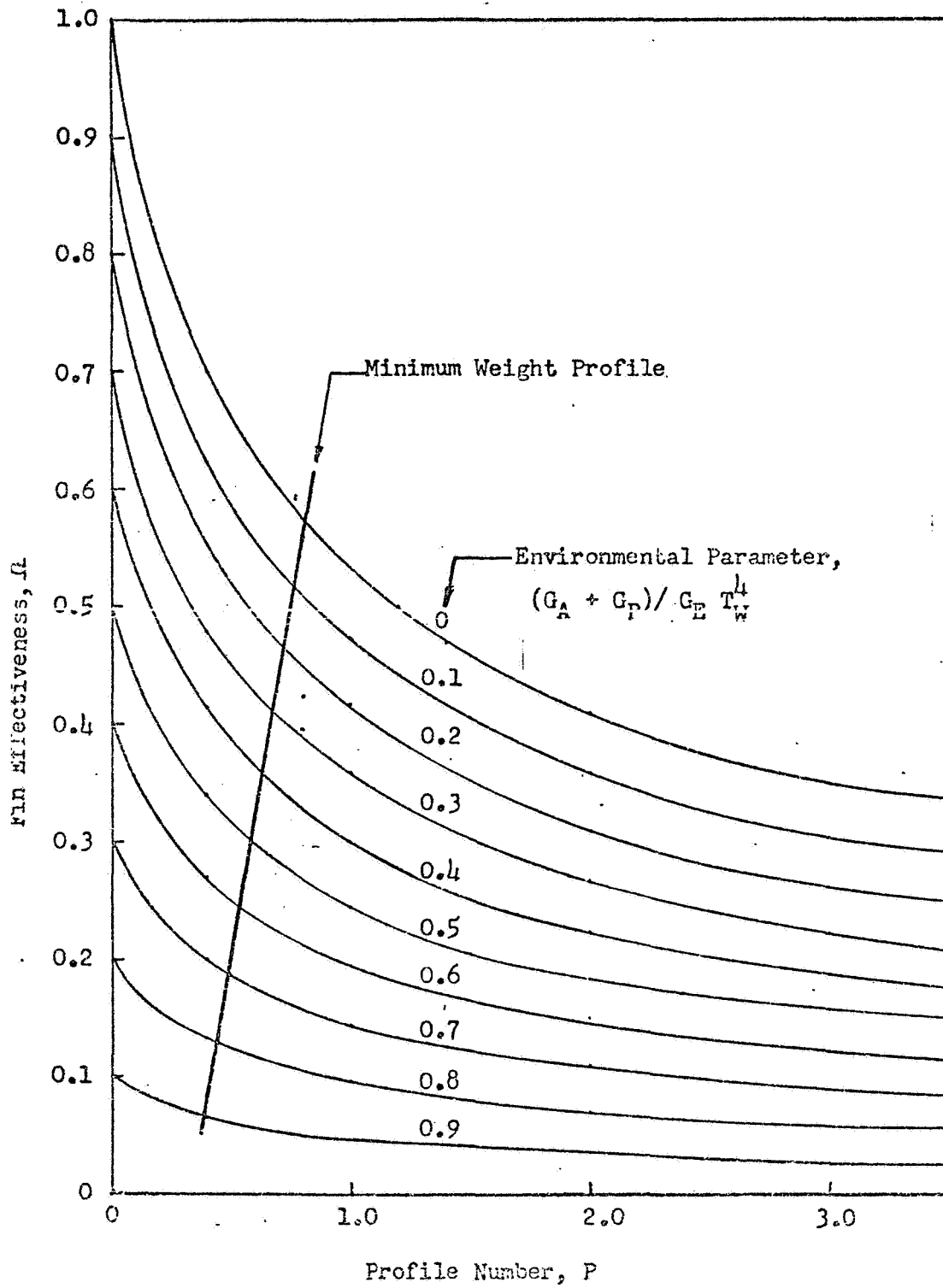


Fig. 7-4 Fin Effectiveness for Rectangular Fins

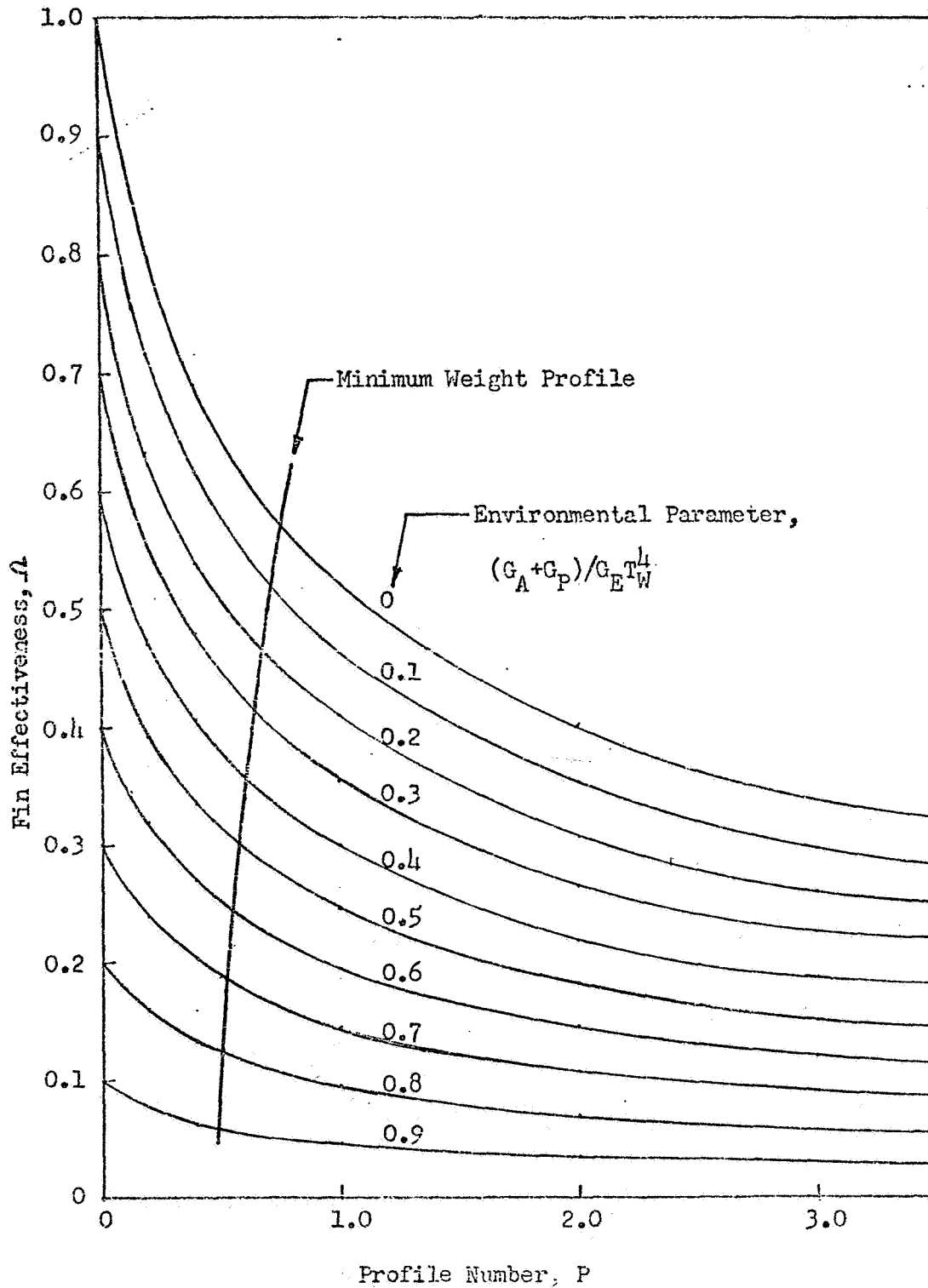


Figure 7-5 Fin Effectiveness for Trapezoidal Fin, $\delta_C / \delta_H = 0.75$

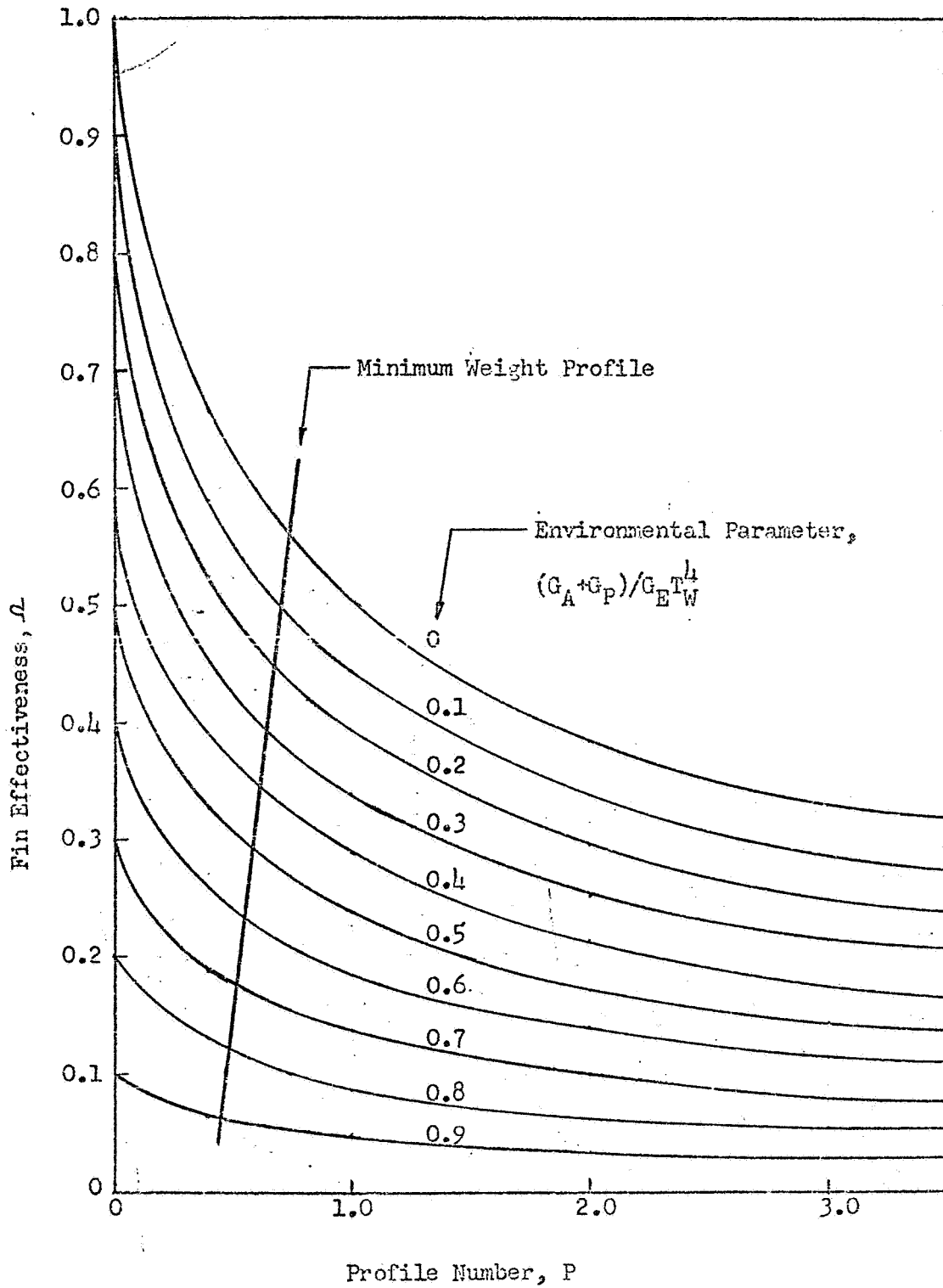


Figure 7-6 Fin Effectiveness for Trapezoidal Fin, $\delta_C / \delta_H = 0.50$

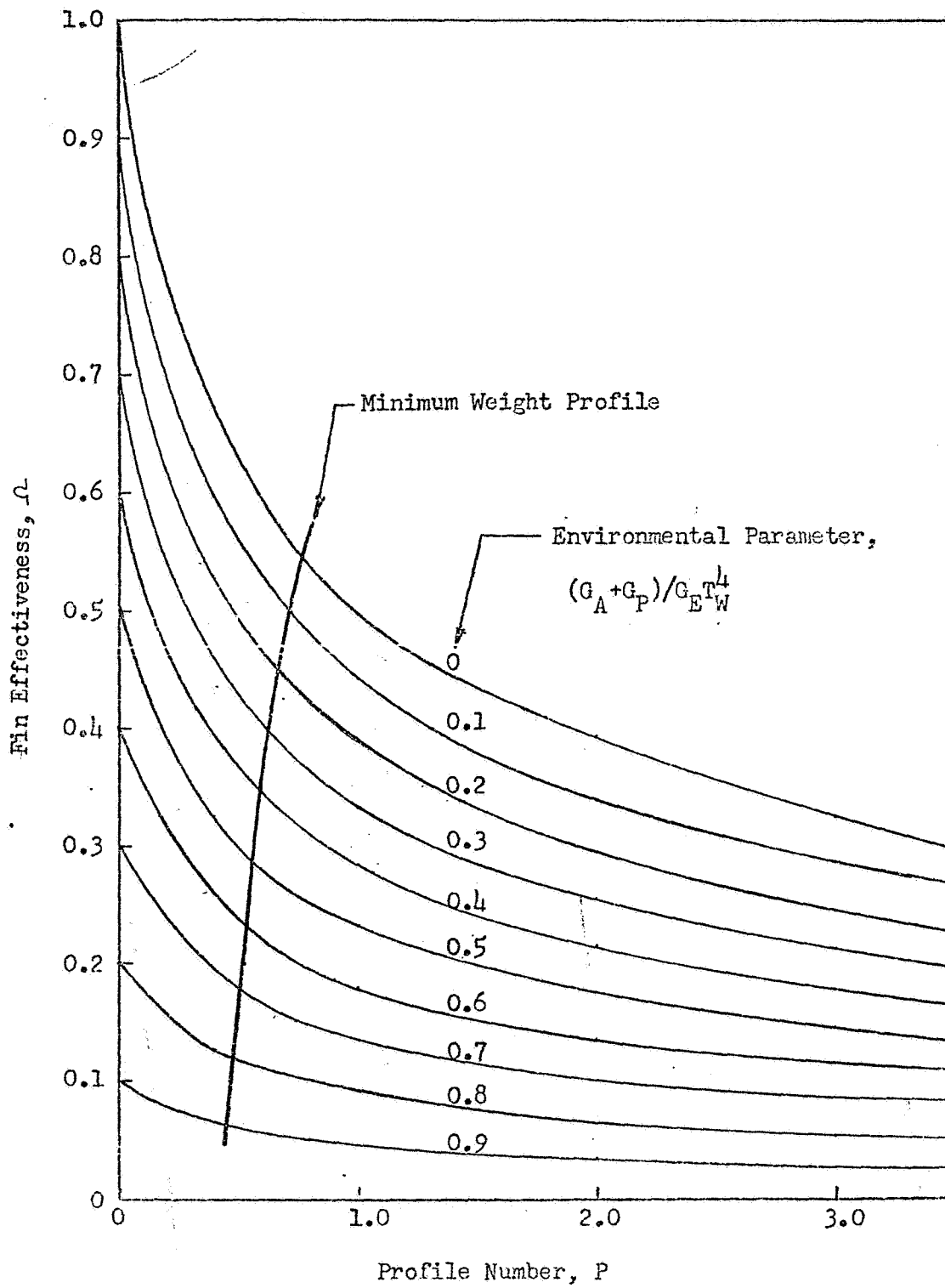


Figure 7-7 Fin Effectiveness for Trapezoidal Fin, $\delta_C / \delta_H = 0.25$

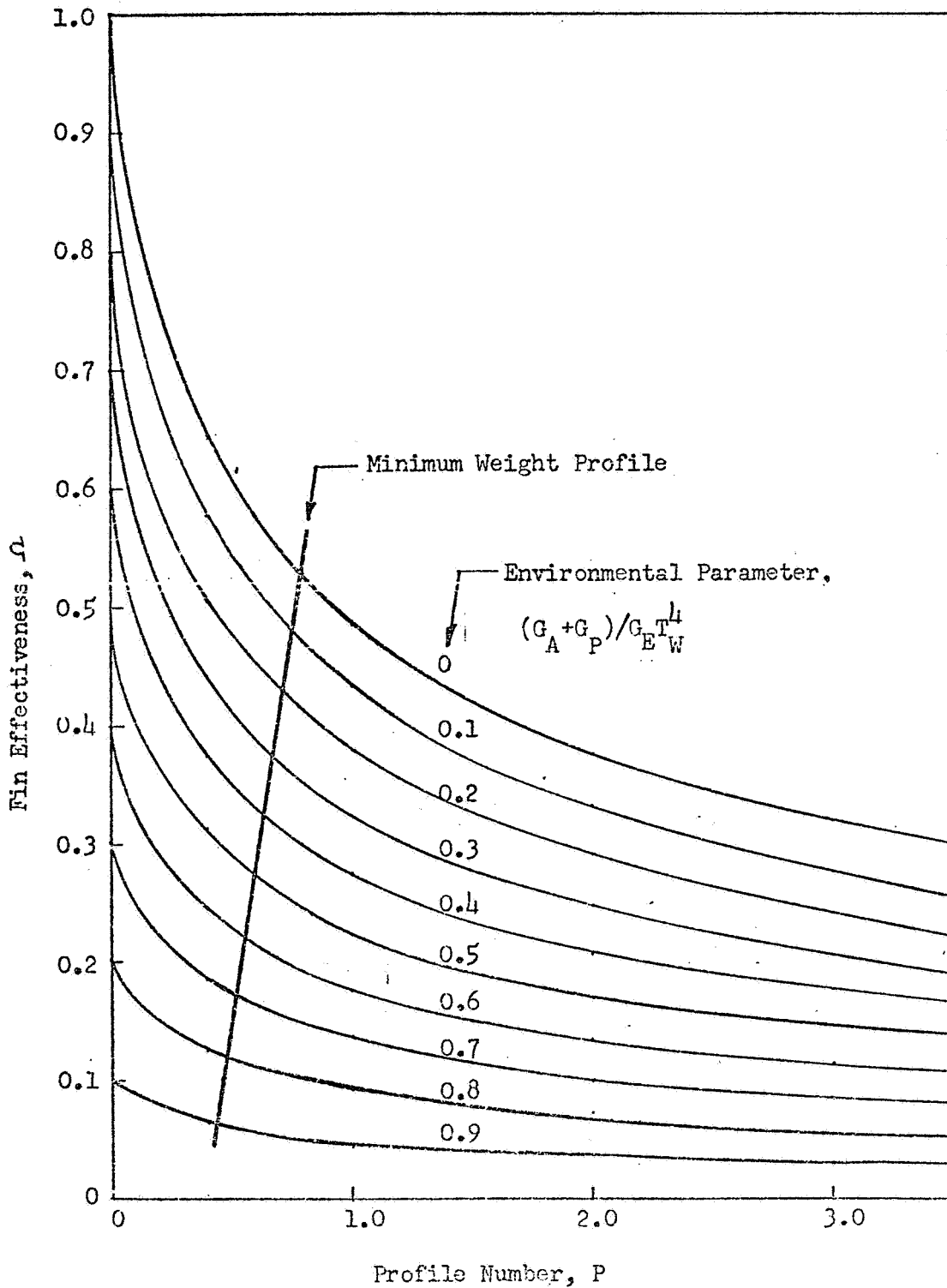


Figure 7-8 Fin Effectiveness for Trapezoidal Fin, $\delta_C / \delta_H = 0.01$

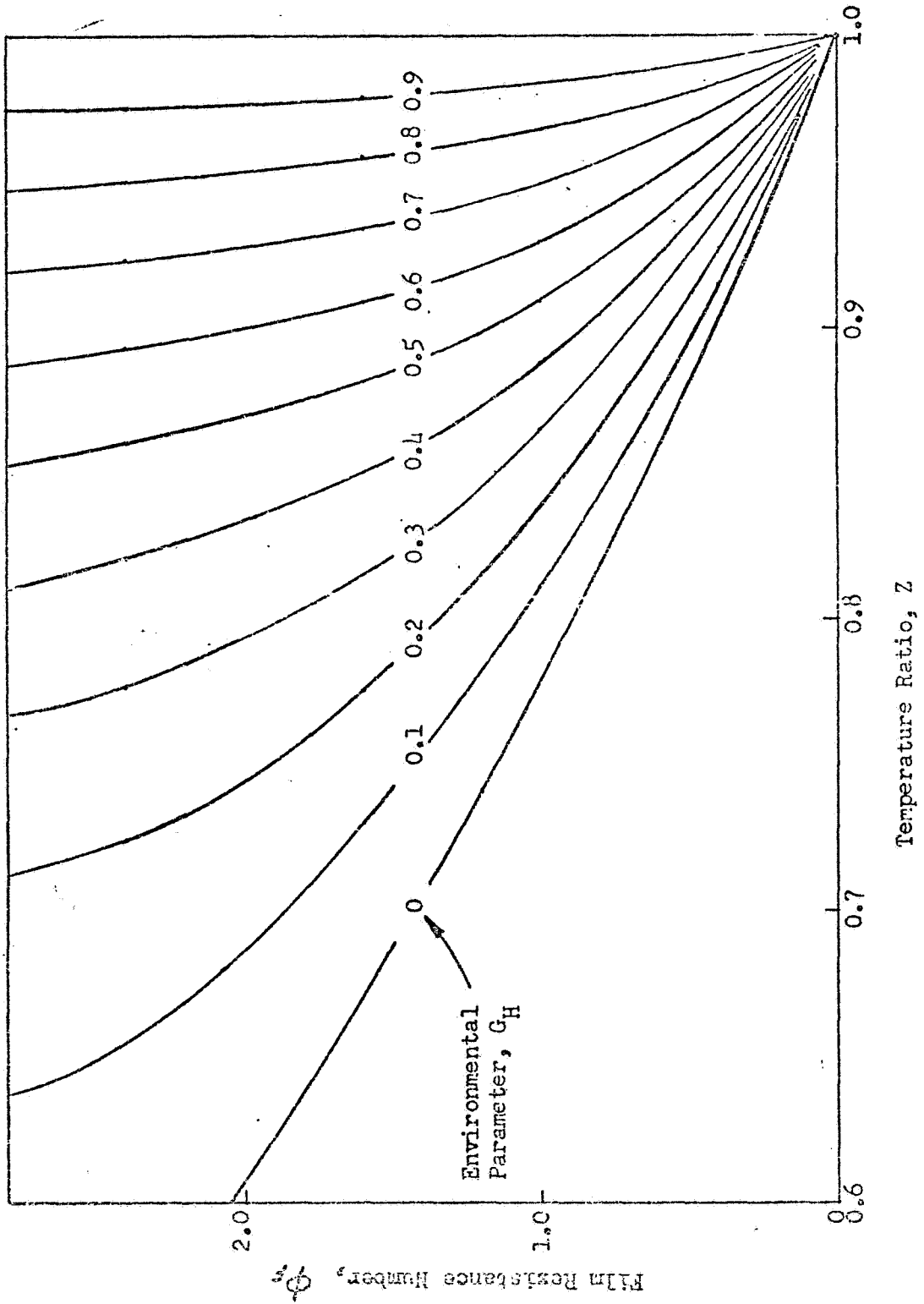


Figure 7-9 Film Resistance Number for Radiator Heat Rejection

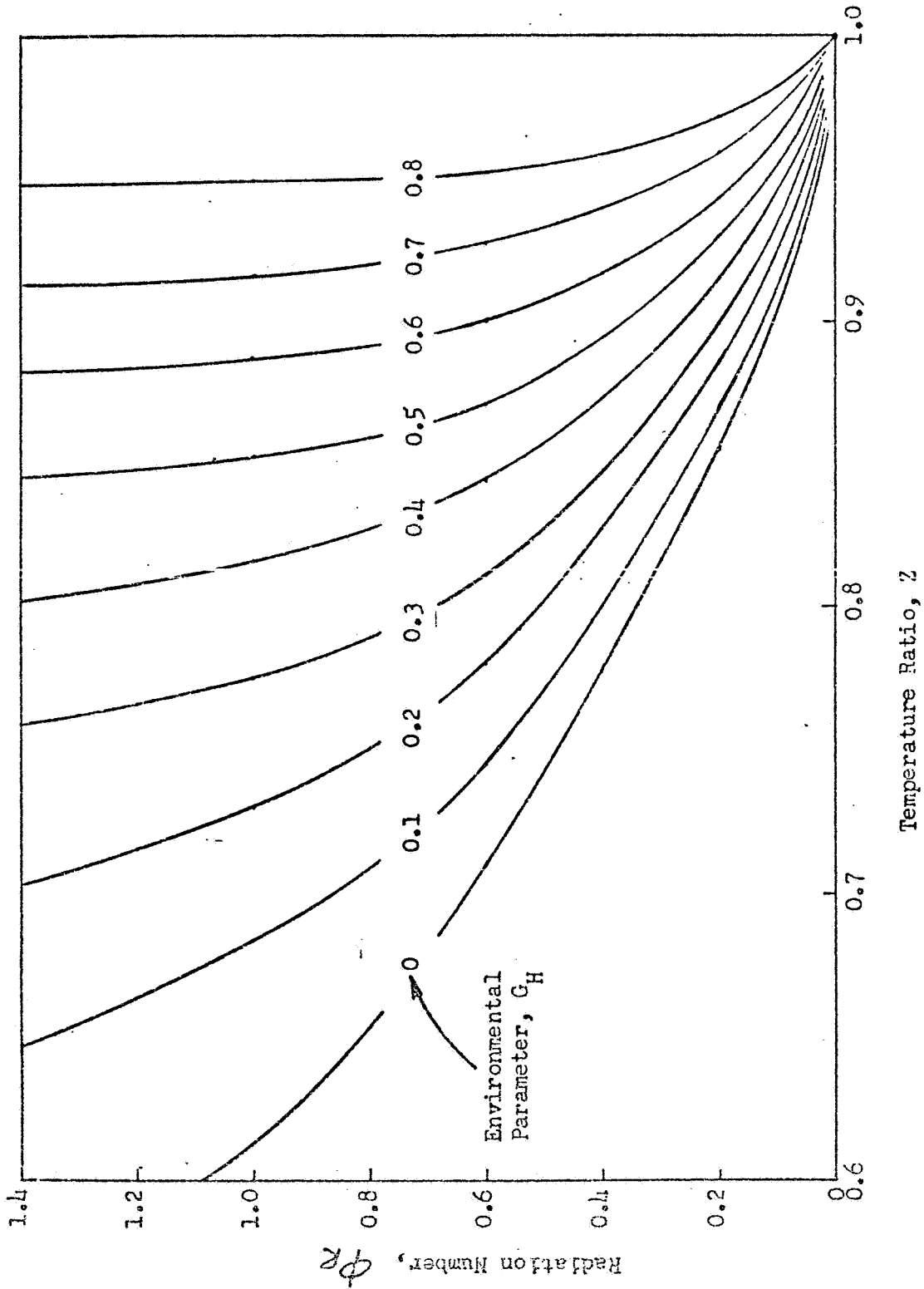


Figure 7-10 Radiation Number for Radiator Heat Rejection

13. With these wall temperatures steps 9 through 12 are repeated until consistent values of effectiveness and wall temperature are obtained.
14. Look up values of ϕ_F and ϕ_R from Figs. 7-9 and 7-10.
15. Compute required radiator length, L_W , from Equation (7-8).

7.2.2 Approximate Method for Radiator Design

The solution for radiator length, equation (7-8), can be written in the form

$$\frac{L_W}{W_F C_{PF}} = \left(\frac{1}{ph}\right) \phi_F + \left(\frac{1}{G_E T_{W1}^3 \bar{L}_E}\right) \phi_R \quad (7-15)$$

If the heat transfer coefficient, h , is high there will be a small temperature difference, $(T_F - T_W)$, between the coolant and the duct wall. In this case the radiator length is controlled primarily by the second term on the RHS in (7-15). It can be shown that, with some simplifying assumptions, the first term in (7-15) can be neglected if

$$\frac{L_D}{L_H} \frac{h}{\left(\frac{T_{W1}}{100}\right)^3} > 0.01 \quad (7-16)$$

where h is in Btu/hr ft²°R and T_{W1} is in °R. If this criterion is satisfied, an approximate value of L_W can be computed from equation (7-17):

$$L_W = \frac{W_F C_{PF} \phi_R}{G_E T_{F1}^3 \bar{L}_E} \quad (7-17)$$

Following the method outlined in Ref. 7-1, it can be assumed that the net heat dissipated by the radiator is given by a relation of the form

$$q = \bar{K} A T_{F1}^4 = 2\bar{K} L_W \bar{L}_E T_{F1}^4 \quad (7-18)$$

This heat rate is identical to that for the fluid,

$$q = \dot{W}_F C_{P_F} (T_{F1} - T_{F2}) = \dot{W}_F C_{P_F} T_{F1} (1-Z) \quad (7-19)$$

where now

$$Z = \frac{T_{F2}}{T_{F1}} = \frac{T_{W2}}{T_{W1}}$$

Equating (7-18) and (7-19) and solving for \bar{K} yields

$$\bar{K} = \frac{\dot{W}_F C_{P_F} (1-Z)}{2 L_W \bar{L}_E T_{F1}^3}$$

Using the radiator length, L_W , given by (7-17), we get

$$\bar{K} = \frac{G_E}{2} \frac{(1-Z)}{\phi_R} \quad (7-20)$$

So that equation (7-18) can be written

$$q = G_E \frac{(1-Z)}{\phi_R} L_W \bar{L}_E T_{F1}^4 \quad (7-21)$$

For most radiator configurations, further approximations can be made by neglecting the duct width, L_D , compared to L_H , and by assuming that F_R is equal to one. If, in addition, an average effective width is computed based on the mean temperature at the inlet and outlet, equation (7-21) can be rewritten as follows:

$$q = G_E \frac{(1-Z)}{\phi_R} L_W L_{E,AVG} T_{F1}^4 \quad (7-22)$$

where L_W is given by

$$L_W = \frac{\dot{W}_F C_{PF} \phi_R}{G_E T_{F1}^3 L_{E\text{AVG}}} \quad (7-23)$$

and

$$L_{E\text{AVG}} = \left(\frac{2 L_H \Omega}{G_A + G_P} \right) \left| \frac{1 - \frac{G_A + G_P}{G_E T^4}}{T = T_{\text{AVG}}} \right. \quad (7-24)$$

$$T_{\text{AVG}} = \frac{T_{F1} + T_{F2}}{2} \quad (7-25)$$

Equations (7-22) - (7-25) are sufficient for the rough, preliminary design of a radiator when the criterion given by equation (7-16) is satisfied. These equations may be combined to give additional insight into the factors affecting the ability of a radiator to reject heat. Substitution of equation (7-24) into equation (7-22) yields

$$q = 2 G_E \frac{(1-Z)}{\phi_R} L_W L_H \left(\frac{\Omega}{1 - \frac{G_A + G_P}{G_E T^4}} \right) T_{F1}^4 \quad (7-26)$$

AVG

The value of the factor $G_E(1-Z)/\phi_R$ indicates the effect of heat transfer from the environment and the heat loss due to temperature drop in the fluid. The factor

$$\left(\frac{\Omega}{1 - \frac{G_A + G_P}{G_E T^4}} \right)$$

AVG

is directly proportional to the effectiveness of the finned surfaces in rejecting heat.

7.2.2.1 Design Procedure Using Approximate Method

The solution for radiator length, using the approximate method outlined above, is given below in stepwise fashion.

1. Establish heat rejection rate for the given cooling load using the data in Section 3.
2. Select a fluid for the given inlet and outlet temperature range from Fig. 7-11, section 7.2.3.
3. Look up fluid specific heat C_{pF} from Table 7-1, section 7.2.3.
4. Compute the coolant flowrate from the known cooling load using Eq. (7-19).
5. Solve for G_A , G_P and G_E using the data of section 3.
6. Assume a value for the inside diameter of the coolant tubing and solve for the heat transfer coefficient, h , using Fig. 7-3.
7. Select values for the coolant duct dimensions and fin profile.
8. Check that the criterion given by Eq. (7-16) is satisfied:

$$\frac{L_D}{L_H} > 0.01 \frac{1}{h} \left(\frac{T_{W1}}{100} \right)^3$$

If not, select revised values of L_D/L_H until the inequality is satisfied.

9. Compute average radiator temperature from Eq. (7-25).
10. Compute fin profile number from Eq. (7-14) using $T_W = T_{AVG}$ and look up fin effectiveness values corresponding to T_{AVG} from Figs. 7-4 through 7-8.
11. Compute $L_{E_{AVG}}$ from Eq. (7-24).

12. Look up value of ϕ_R from Fig. 7-10 using an average environmental parameter:

$$G_H = \frac{G_A + G_P}{\frac{G_E(T_{W1}^4 + T_{W2}^4)}{2}}$$

13. Compute required radiator length, L_W , from Eq. (7-23).

7.2.3 Fluid Selection for Radiator Design

Using equations (7-18) and (7-19), the heat rejection density can be written

$$\frac{q}{A} = \bar{K} T_{F1}^4 = \frac{\dot{W}_F C_{PF} (1-Z) T_{F1}}{2 L_W \bar{L}_E} \quad (7-27)$$

for h (the heat-transfer coefficient) sufficiently large. In order to maximize the rate of heat rejection, Eq. 7-27 shows that we must maximize the quantity $C_{PF}/L_W \bar{L}_E$. But, from equation (7-23)

$$\frac{C_{PF}}{L_W \bar{L}_E} = \frac{G_E T_{F1}^3}{\dot{W}_F \phi_R}$$

Therefore, the maximum rate of heat rejection is independent of fluid properties except as they affect the value of h . The heat-transfer coefficient is proportional to the product of Reynold's number and the Prandtl number. For flow in a smooth tube,

$$h = \frac{CK}{D} (Re)^{.8} (Pr)^{.39}$$

Therefore, using the definitions of Reynold's and Prandtl's numbers, we wish to maximize the quantity

$$\psi_H = K \left(\frac{\rho}{\mu} \right)^{0.8} \left(\frac{Cp\mu}{K} \right)^{.33} = \frac{K^{0.67} \rho^{.8} Cp^{.33}}{\mu^{.47}} \quad (7-28)$$

Values of ψ_H are shown in Fig. 7-11 for several fluids of interest. Values of density, viscosity, specific heat and thermal conductivity are shown for these fluids in Table 7-1.

7.2.4 Pressure Drop in Coolant Ducts

The total frictional pressure drop of the fluid flowing in the coolant ducts can be estimated using the assumption that the tubing is smooth. The Fanning form of the pressure drop equation can be written

$$\Delta p = 2 \frac{fL}{D} \frac{1}{\rho} \left(\frac{\dot{W}_F}{A} \right)^2$$

or

$$\Delta p = 32 \frac{fL}{D} \frac{1}{\rho} \left(\frac{\dot{W}_F}{\pi D^2} \right)^2$$

where

- f - Fanning friction factor
- L = total tubing length
- A = Tube cross-sectional area
- D = Tube diameter
- ρ = density
- \dot{W}_F = Mass flowrate

The friction factor, f , for smooth pipes is given by

$$f = 16/Re, \quad 0 < Re \leq 3000$$

$$f = 0.0014 + 0.125 Re^{-0.32}, \quad 3000 < Re \leq 3 \times 10^6$$

where Re is the Reynold's number,

$$Re = \frac{\rho VD}{\mu}$$

The effect of bends or constrictions in the tubing (such as those due to valving) should also be added to the frictional pressure drop for an accurate estimate of the total Δp across the radiator.

Table 7-1
THERMOPHYSICAL PROPERTIES OF LIQUIDS AT ONE ATMOSPHERE

T (K)	ρ (lb_m/ft^3)	C_p ($\text{Btu}/\text{lb}_m\text{R}$)	$\mu \times 10^3$ ($\text{lb}_m/\text{ft}\cdot\text{sec}$)	K (Btu/HrFtR)	Pr
W A T E R					
273	62.4	1.01	1.20	0.319	13.7
278	62.4	1.00	1.04	0.325	11.6
289	62.3	0.999	0.76	0.340	8.03
294	62.2	0.998	0.578	0.353	5.89
311	62.0	0.998	0.458	0.364	4.52
339	61.2	1.00	0.202	0.384	2.74
367	60.1	1.00	0.205	0.394	1.88
A M M O N I A					
244	42.4	1.07	17.6	0.317	2.15
256	41.6	1.08	17.1	0.316	2.09
273	40.0	1.11	16.1	0.312	2.05
300	37.2	1.17	14.5	0.293	2.01
322	35.2	1.22	13.0	0.275	1.99
F R E O N 12					
233	94.8	0.211	28.4	0.040	5.4
256	91.2	0.217	23.1	0.041	4.4
273	87.2	0.223	20.0	0.042	3.8
289	83.0	0.231	18.0	0.042	3.5
322	75.9	0.244	15.5	0.039	3.5
N I T R O G E N					
114	55.0	0.479	0.202	0.0068	52
120	54.0	0.481	0.171	0.0072	41
130	52.35	0.486	0.135	0.0077	31
140	50.8	0.491	0.101	0.0082	22
M E T H A N E					
90	28.3	0.80	0.141	0.13	3.13
100	27.5	0.81	0.103	0.12	2.51
111	26.55	0.82	0.080	0.11	2.14
E T H Y L E T H E R					
173	54.7	0.50	1.137	0.084	24.4
193	51.4	0.51	0.644	0.082	15.03
213	50.0	0.515	0.428	0.080	9.90
233	48.6	0.52	0.310	0.078	7.43
253	47.3	0.527	0.243	0.076	6.07
273	45.9	0.53	0.191	0.074	4.93
293	44.4	0.54	0.157	0.073	4.18
F C - 7 5					
233	119	0.25	5.11	0.038	121
278	113	0.25	1.58	0.038	37.4
322	106.5	0.25	0.686	0.038	16.3
367	100	0.25	0.355	0.038	8.42

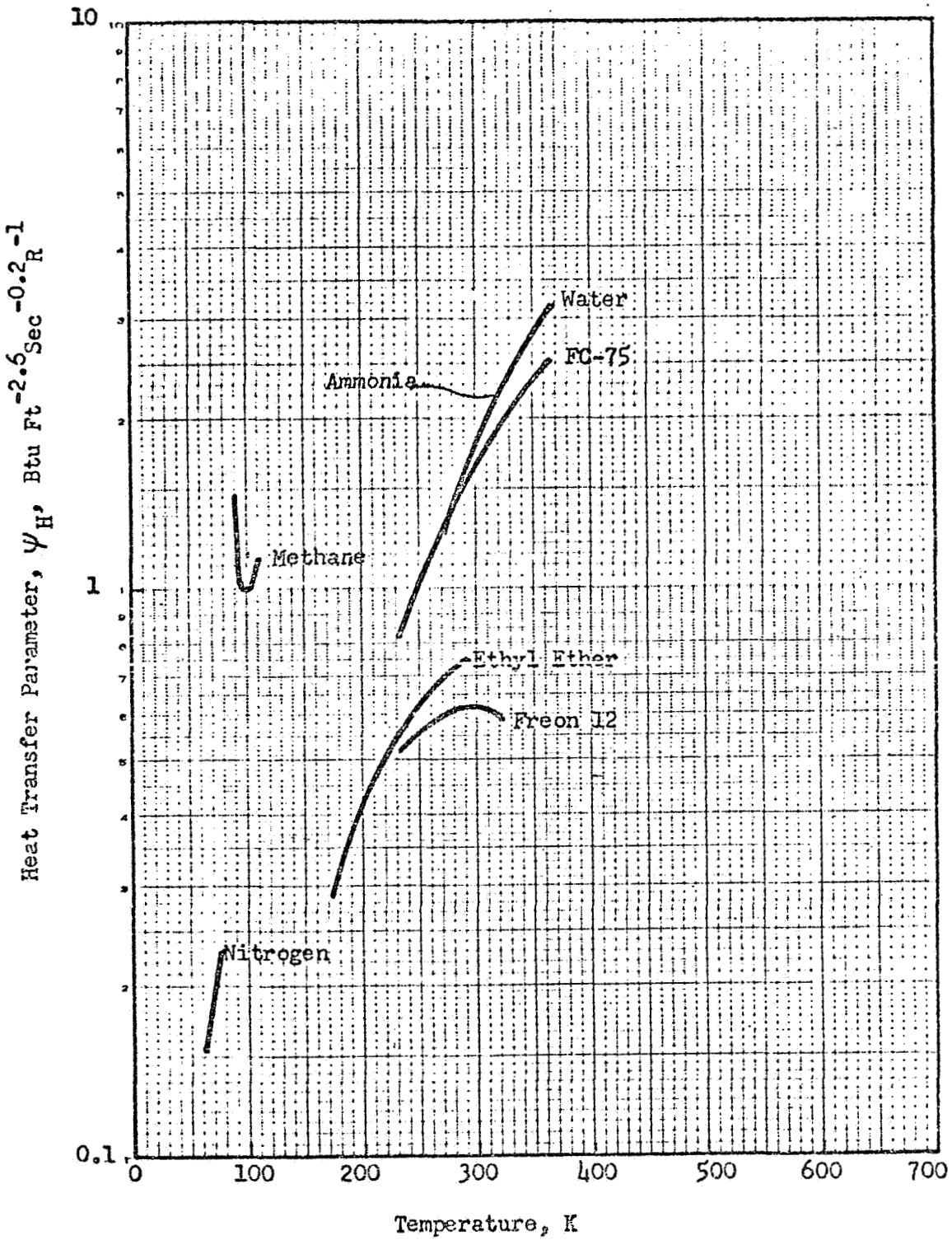


Figure 7-11 Heat Transfer Parameter for Various Liquids

7.2.5 Radiator Weight and Area Requirements

As an aid in estimating radiator weight and area requirements, values of these quantities have been computed for two extreme operating conditions:

- (1) Operation in free space with no solar or planetary heat inputs.
- (2) Operation on the lunar surface with the sun directly overhead.

Values of radiator weight and area were computed using the simplified procedure outlined in Section 7.2.2. No contingency was allowed to account for the weight of meteoroid protection or radiator headers. In all cases it was assumed that the rise in coolant temperature between inlet and outlet was 20°K. For operation in free space, fluid inlet temperatures of 110, 210 and 310°K were selected corresponding to feasible operating temperature ranges for methane, ethyl ether and water, respectively. Values of radiator area are shown in Fig. 7-12 as a function of net heat rejection rate. Only a single curve is shown for lunar surface operation since operation in the lunar environment with methane or ether was found to be unfeasible.

The computed radiator areas were converted to weight values using the appropriate relations for geometry of a triangular fin. For a trapezoidal radiator,

$$W = \rho L_W \left[\frac{\pi}{4} (D_o^2 - D_i^2) + L_H (\delta_c + \delta_H) \right]$$

where

- L_W = radiator length
- D_o = outside diameter of coolant tube
- D_i = inside diameter of coolant tube
- δ_c = fin tip thickness
- δ_H = fin root thickness
- L_H = fin width
- ρ = fin material density

For a triangular fin, of course, $\delta_c = 0$. Values of radiator weight as a function of heat rejection rate are shown in Fig. 7-13 for the same conditions as those used for the data of Fig. 7-12.

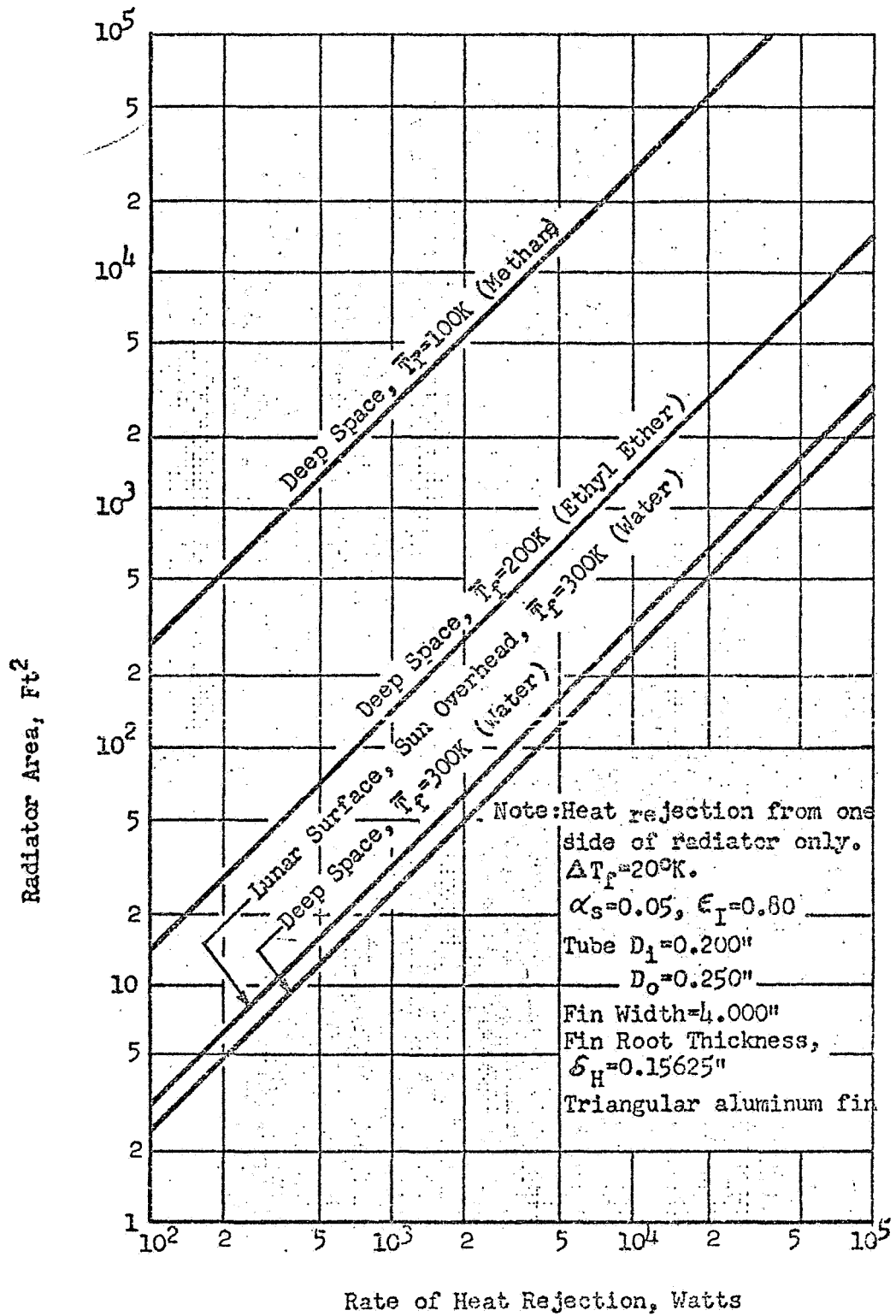


Figure 7-12 Radiator Area for Deep Space and Lunar Surface Operation

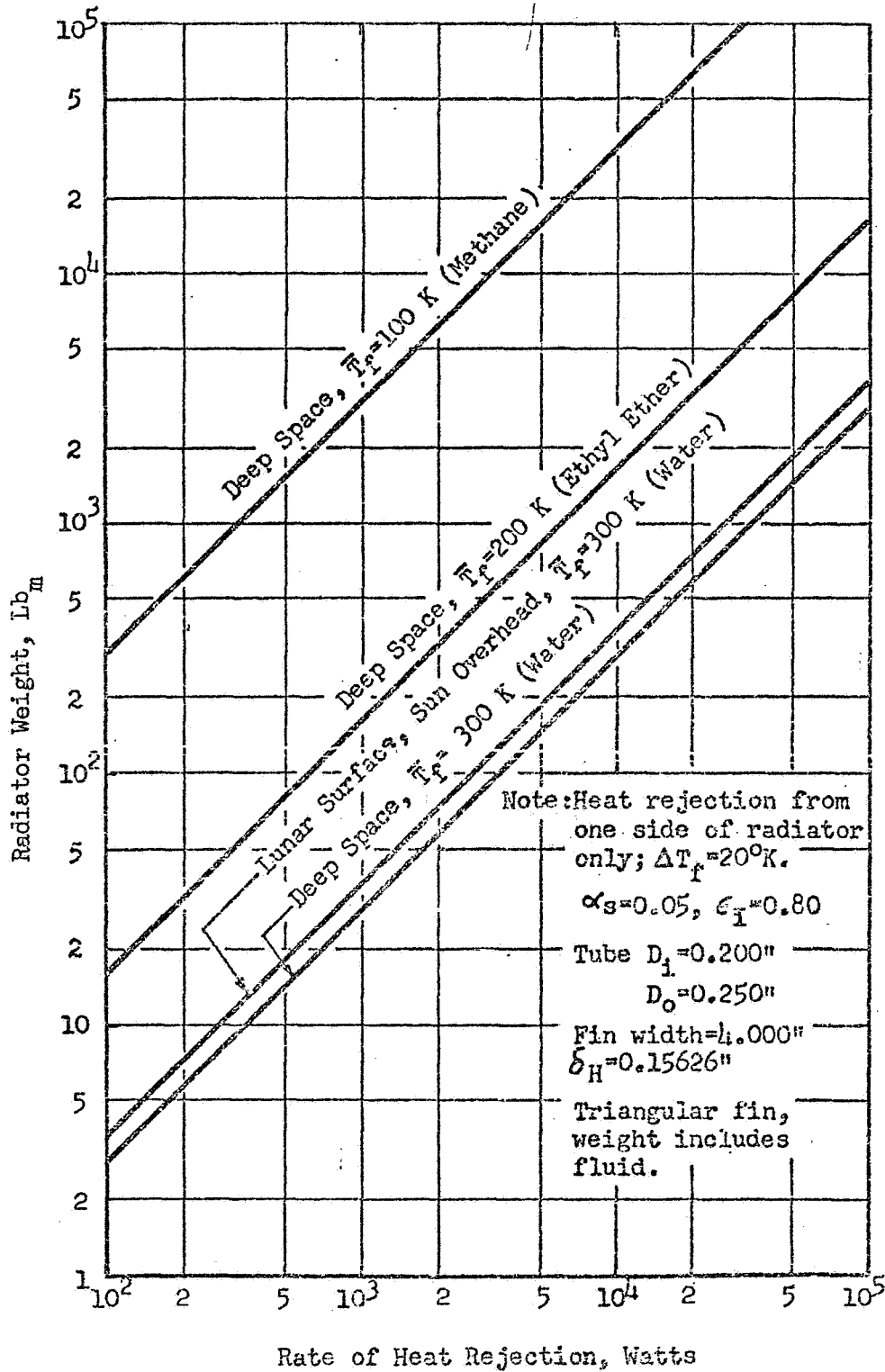


Figure 7-13 Radiator Weight for Deep Space and Lunar Surface Operation

7.3 DESIGN OF HEAT PIPE RADIATORS

The effectiveness of radiators for heat rejection systems can be increased considerably by replacing the coolant ducts with constant temperature heat pipes. Several possible configurations have been proposed for such a radiator (Refs. 7-5 to 7-8) and some experimental models have been built and tested (Refs. 7-5 and 7-9). A radiator design which has been successfully fabricated and tested is shown in Fig. 7-14. Since the condenser section of the heat pipe has a uniform temperature, the radiator design equations developed earlier may be used with T_W replaced by T_C . The required radiator area is then given by

$$A = \frac{q (L_D + 2 L_H)}{F_R \left[(G_E T_C^4 - G_A - G_P) L_D + 2 G_E T_C^4 \Omega L_H \right]} \quad (7-29)$$

where the symbols are as defined previously (Section 7.2). The condenser temperature T_C is determined by the thermal resistance of the heat pipe between the evaporator and condenser sections. Thus,

$$T_C = T_E - \frac{q R_{EC}}{N} \quad (7-30)$$

where

- T_E = temperature at evaporator end of heat pipe array, °K
- R_{EC} = thermal resistance between evaporator and condenser, °K/watt
- q = total rate of heat rejection, watts
- N = number of heat pipes connected in parallel

The values of R_{EC} and the maximum value of heat flux per pipe, q/N , are evaluated using heat flux limits based on either the heat pipe evaporator heat flux limit or the capillary pumping limit. Methods of evaluating these limits are given in section 7.5. The overall thermal resistance between the evaporator and condenser is equal to the sum of the evaporator and condenser resistances, $R_{EC} = R_E + R_C$. The evaporator resistance is given by equation (7-31):

$$R_E = \frac{t_e}{K_m A_e} \quad (7-31)$$

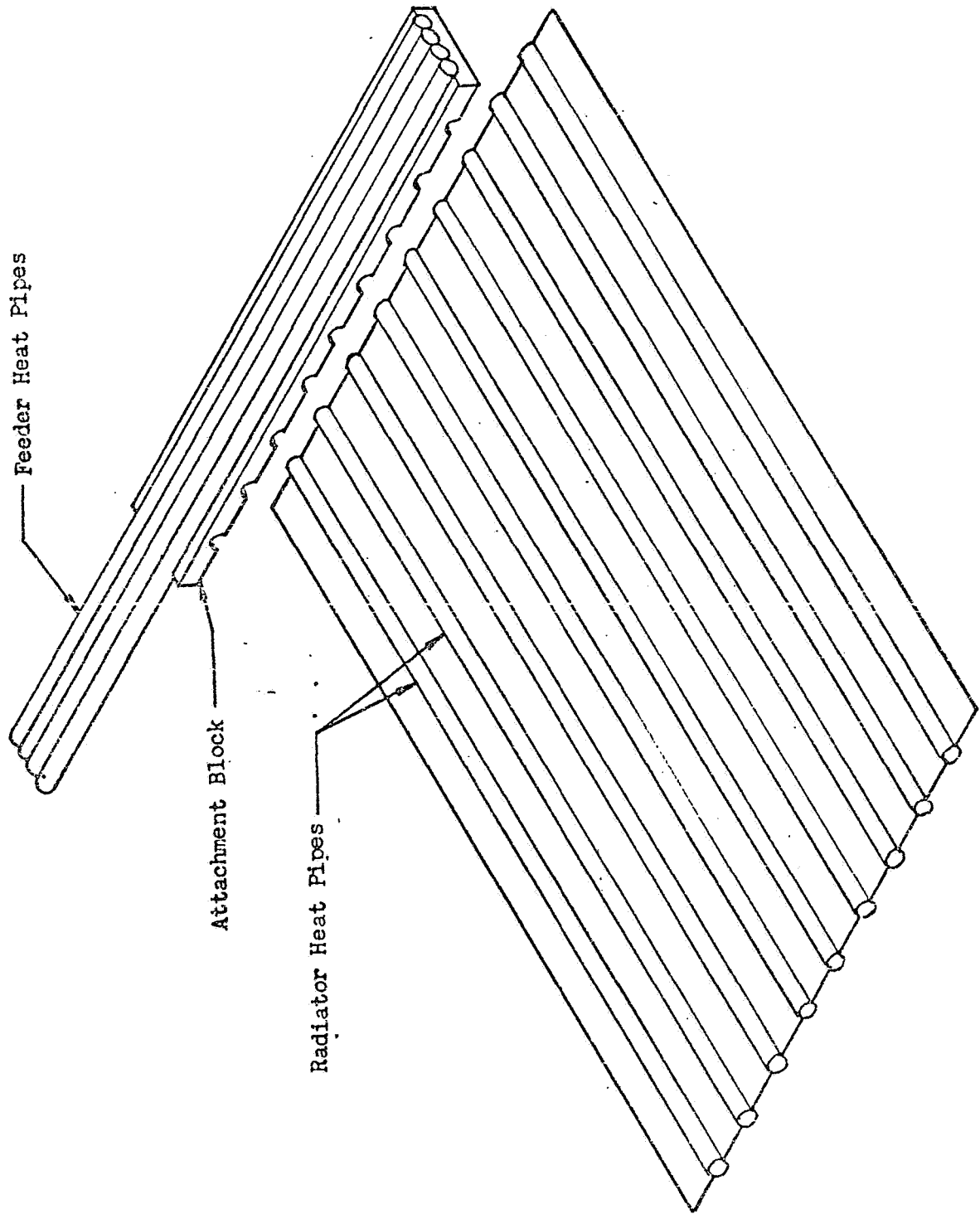


Figure 7-14 Rectangular Fin Radiator with Integral Heat Pipes

For homogeneous wicks, in heat pipes containing little or no excess fluid and having equal evaporator and condenser areas, $R_C = R_E$. However, in heat pipes having an excess fluid charge, the liquid layer thickness in the condenser may be up to twice that in the evaporator. Thus, in general

$$R_C = \frac{t_c}{\frac{K A}{m c}} \quad (7-32)$$

where t_c may be up to twice the value of t_e .

7.4 FLUID CIRCULATION

In order to provide the designer with a complete set of data to evaluate refrigeration systems the weight and power of coolant circulating pumps have been included. The weight and power as a function of flow rate is shown in Figs. 7-15 and 7-16, respectively. These data are estimates based on data provided in Reference 7-4 by AiResearch for a small thermal conditioning circulation unit. The electric motor weight was based on a brushless D.C. unit running at 6000 RPM. The fluid circulated is water. A check for different fluids did not significantly influence the weights of the motor and pumps. For example if ethyl ether at a density of 45 lb/ft³ were circulated instead of water at a density of 62.4 lb/ft³ the weight for a flow rate of 0.5 lb/sec and a pressure rise of 10 psi would increase to 6 lb from 5.75 lb for a water system. However, the power required should be proportionately increased by the ratio of the density of water to the density of the fluid to be circulated. The efficiencies of the pump and electric motor were assumed to be 0.80 and 0.85 respectively. The minimum weight of the case and supporting hardware was assumed to be 3.0 pounds.

7.5 HEAT PIPE DESIGN

The heat pipe is a self-contained passive device with an effective thermal conductance greater than that afforded by any solid material. The heat pipe is simply a closed, elongated tube containing a fluid, generally at low pressure, and a wicking material distributed along the inside of the tube. Heat is transferred from one end of the pipe to the other by continuous evaporation of the fluid at the hot end of the pipe and condensation at the cold end. Vapor flows

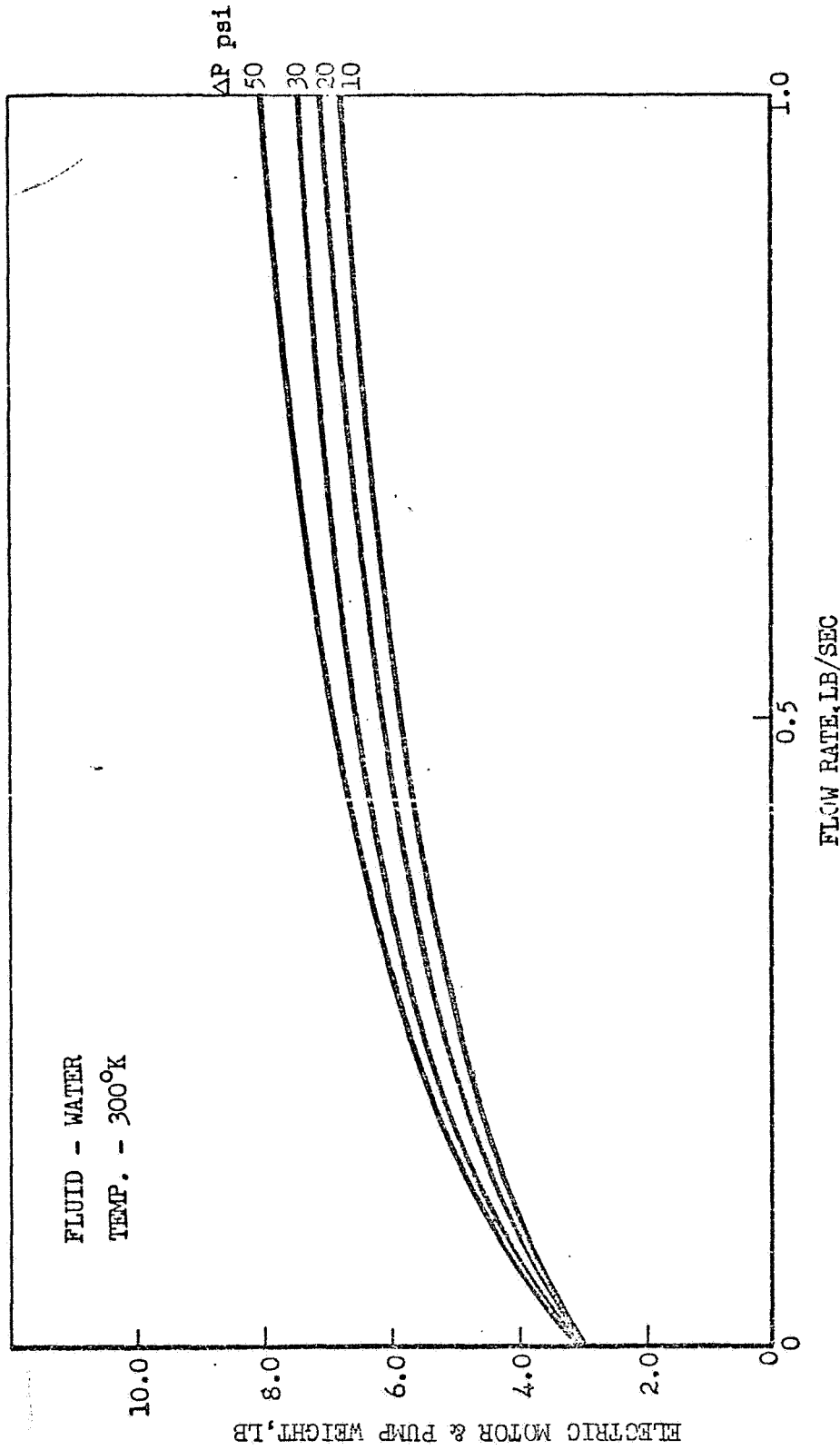


Figure 7-15 Weight of Circulation Pump and Motor

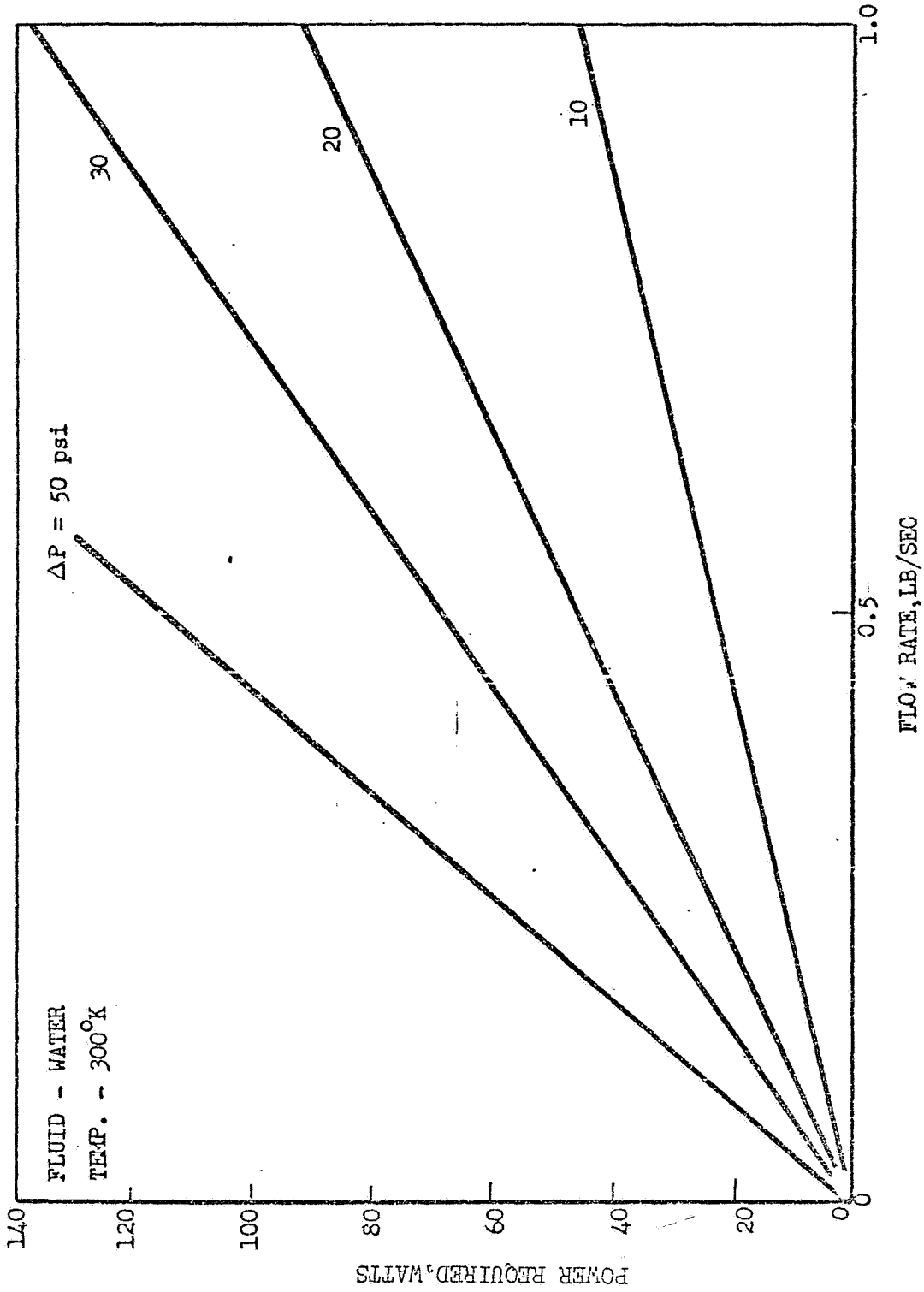


Figure 7-16 Power Required for Circulation Pump

from the hot end to the cold end as a result of the difference in vapor pressure between the two ends of the pipe; liquid condensed at the cold end is returned to the hot (evaporator) end as a result of capillary pressure developed within the wicking material. The heat pipe has been well established as a reliable device for long-life heat transport.

Figure 7-17 is a cross-sectional view of a heat pipe whose inner wall is lined with a porous wicking material having a thickness $R_W - R_V$. Under steady conditions the heat flux entering the evaporator, Q_e , causes evaporation of the liquid at a rate \dot{m} . The resulting vapor is carried along the pipe and condenses at the condenser end at the same rate, \dot{m} . Thus the product of the latent heat of vaporization, λ , and the mass circulation rate, \dot{m} , must be equal to the heat flux:

$$Q = \lambda \dot{m} \quad (7-33)$$

In the absence of gravitationally induced pressure gradients, the liquid condensate is pumped back to the evaporator by means of the capillary force developed at the liquid vapor-wick interface.

7.5.1 Fluid Selection

The normal operating range for a heat pipe fluid is between its triple point temperature and its critical temperature. The available temperature range between the triple point and critical point temperatures decreases markedly as the desired operating temperature is decreased. For instance, water has an operating temperature span of 374°K (273 to 647°K), nitrogen has 63°K (63 to 126°K) and helium 3°K (2.2 to 5.3°K). Concurrently, as the desired operating temperature is reduced the number of fluids which can exist in the saturated liquid state at the desired temperature is also reduced. Figure 7-18 shows the vapor pressure of several liquids over a wide range of temperatures.

Previous investigations have shown that there are three major limitations on heat pipe operation. These limitations are: the wicking limit, the boilout limit, and the vapor choking limit. Each of these limits can be related to the physical properties of the working fluid and/or the properties of the wicking material.

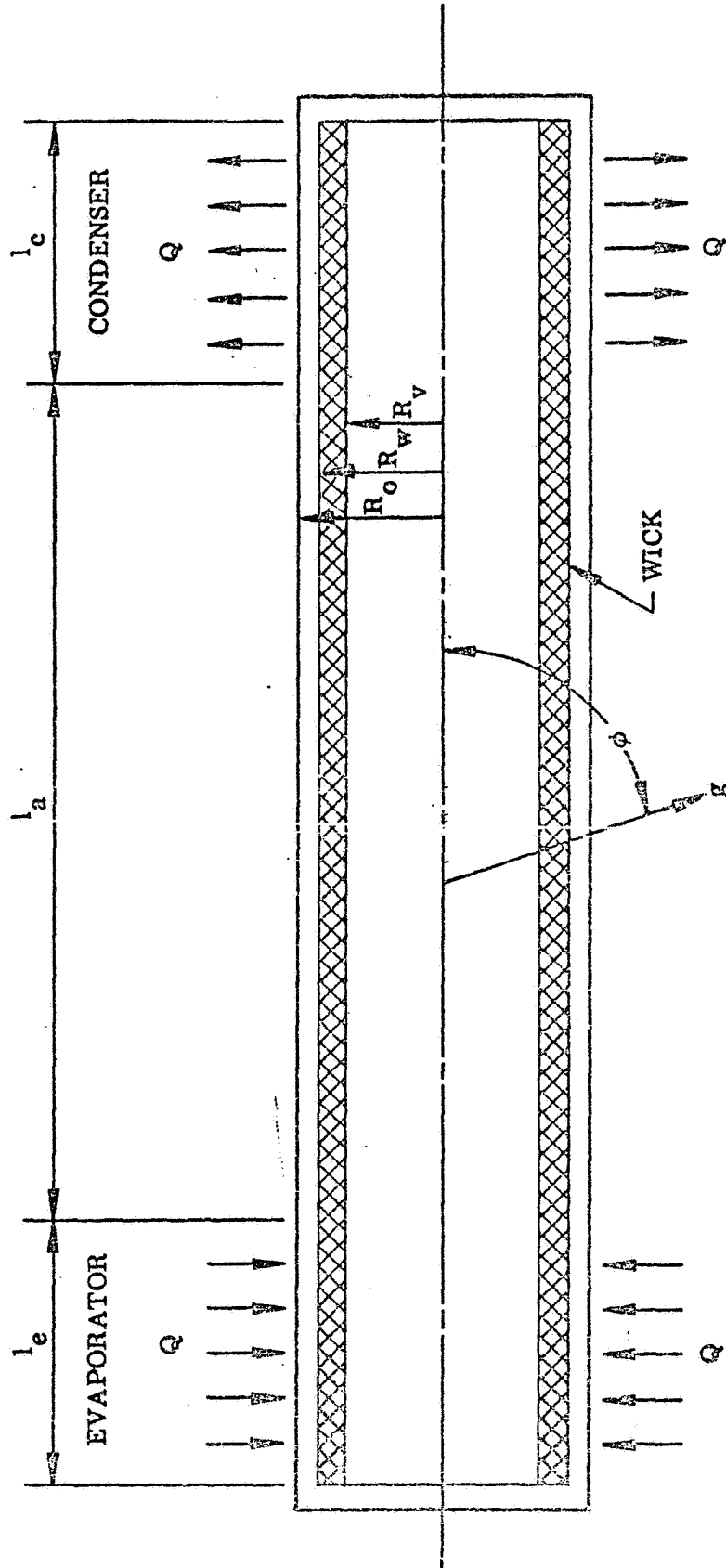
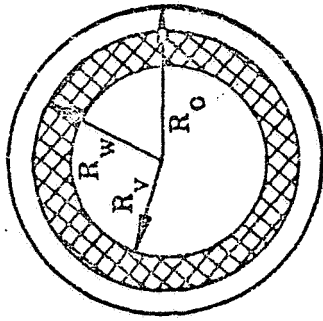


Figure 7-17 Heat Pipe Schematic

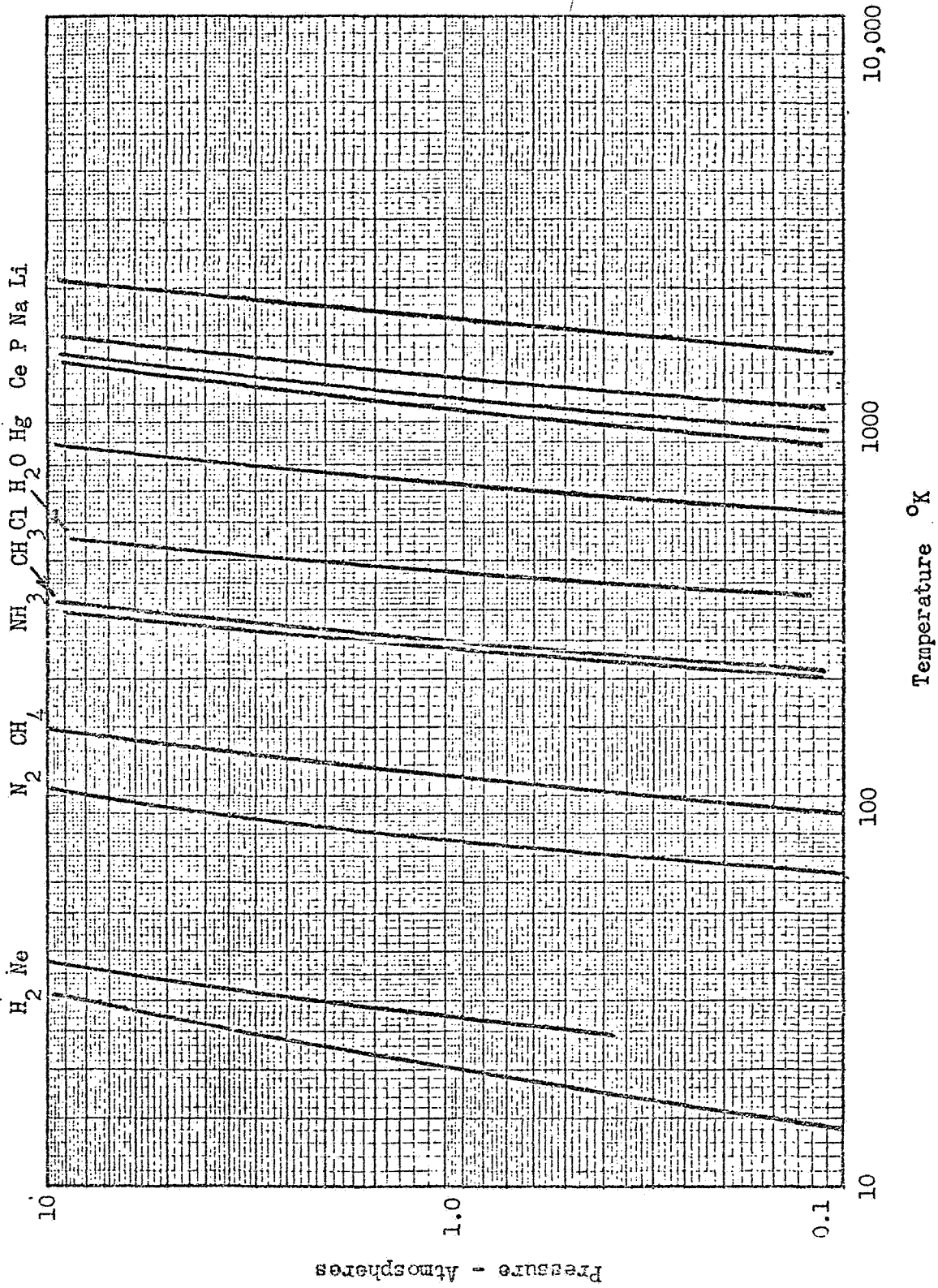


Figure 7-18 Vapor Pressure vs. Temperature for Various Liquids

7.5.1.1 Wicking Limit

The wicking limit is defined as that point at which the working liquid can no longer reach the evaporator through the wick in sufficient quantity to keep up with the required evaporation rate. In other words, it is reached when the pressure drops due to viscous effects and gravity are equal to the maximum capillary pumping head of the wick.

Cotter (Ref. 7-10) showed that in a zero-gravity field the maximum heat transfer rate for a cylindrical heat pipe with a homogeneous wick is given as:

$$Q_e = \frac{2\pi\sigma\lambda R_c \cos\theta}{(l+l_a)} \left[\frac{4\nu_v R_c^2}{\rho_v R_v^4} + \frac{b\nu_l}{2\rho_l \epsilon (R_w^2 - R_v^2)} \right]^{-1} \quad (7-34)$$

where the dimensions are shown in Fig. 7-17. Equation (7-34) may be optimized with respect to the capillary radius R_c and the wick and vapor core radii R_w and R_v . Following this procedure, it is found that maximum heat flux is obtained when $R_w/R_v = \sqrt{2/3}$.

By including a gravity term, an equation for the maximum axial heat transfer rate with an optimized wick can be found as

$$Q_{e\max} = \frac{2\sigma}{A(l+l_a)} \left(\frac{1}{\sqrt{B+C^2}} - \frac{C}{B} \right) \left(1 + \frac{B}{B+2C^2-2C\sqrt{B+C^2}} \right)^{-1} \quad (7-35)$$

where

$$A = \frac{3\nu_l}{2\lambda} \frac{1}{\pi R_w^2 (\epsilon/b)}, \quad B = 6 \frac{\nu_v}{\nu_l} \frac{\epsilon}{b} \frac{1}{R_w^2}, \quad C = \frac{\rho_l g z}{2\sigma}$$

For $g = 0$ equation (7-35) reduces to

$$Q_{e\max} = \frac{2}{3} \frac{\pi}{\sqrt{6}} \frac{R_w^3}{(l+l_a)} \frac{\sigma\lambda}{\sqrt{\nu_v \nu_l}} \sqrt{\frac{\epsilon}{b}} \quad (7-36)$$

The term z is the height to which the wick must raise the liquid against the gravity field g ; thus, for a horizontal heat pipe, $z = 2R_w$.

It is apparent from Equation (7-35) that a heat pipe designed for operation in a positive gravity field (i.e., condenser lower than the evaporator) will have a greater maximum performance in a zero gravity field. Therefore, a heat pipe configuration that meets the requirements of a particular flight design under a positive gravity test condition will exceed the operational requirements in the absence of gravity effects.

Examination of equation (7-36) shows that the heat transfer rate is dependent upon two separate parameters: one consisting of wick properties (R_w , ϵ and b) and the other consisting of fluid properties (σ , λ , ν_v and ν_l). (ϵ is the wick porosity.)

The performance of the fluid can be characterized in terms of a liquid parameter $\frac{\sigma\lambda}{\nu_l}$. This quantity is plotted as a function of temperature for several liquids in Fig. 7-19. For the higher temperature liquids (liquid metals), the vapor chocking condition will limit their performance at the low end of the indicated temperature ranges (as shown by the dashed lines). Heat pipes become considerably less efficient for the lower temperature liquids because of their lower surface tensions and smaller values of latent heat of vaporization. Therefore, the great advantage of heat pipes over solid conductors at moderate and high temperatures is considerably lessened at cryogenic temperatures.

To maximize Q_e with respect to the wicking limit, it is desirable to have a large value of $G_1 = \frac{\sigma\lambda}{\nu_v \nu_l}$. Figure 7-20 gives values of G_1 for water and ammonia. Such a comparison is helpful in the initial fluid selection, but it is not the only criterion to be considered during preliminary design considerations. It is also desirable to maximize the wick property group $\sqrt{\epsilon/b}$, which must be determined experimentally since it is a function not only of the wick material but of geometry as well.

Wicks other than the cylindrical homogeneous matrix can and have been used in heat pipe applications. These wicks, such as the channel and arterial, Fig. 7-21, also have wicking limits which can be predicted analytically.

Equation (7-35) can be used to obtain the maximum, wick-limited heat transfer rate for channel or arterial wicks if the parameter B is redefined as

$$B = 6 \frac{\nu_v}{\nu_l} \frac{1}{k \left(2 + \frac{t}{R_c} \right)}$$

In this relation k is a shape factor that is a constant dependent upon the geometry of the channel and arterial wicks and is defined under the assumption that the wick is completely wetted. Typical values of k are 1.5 for channel

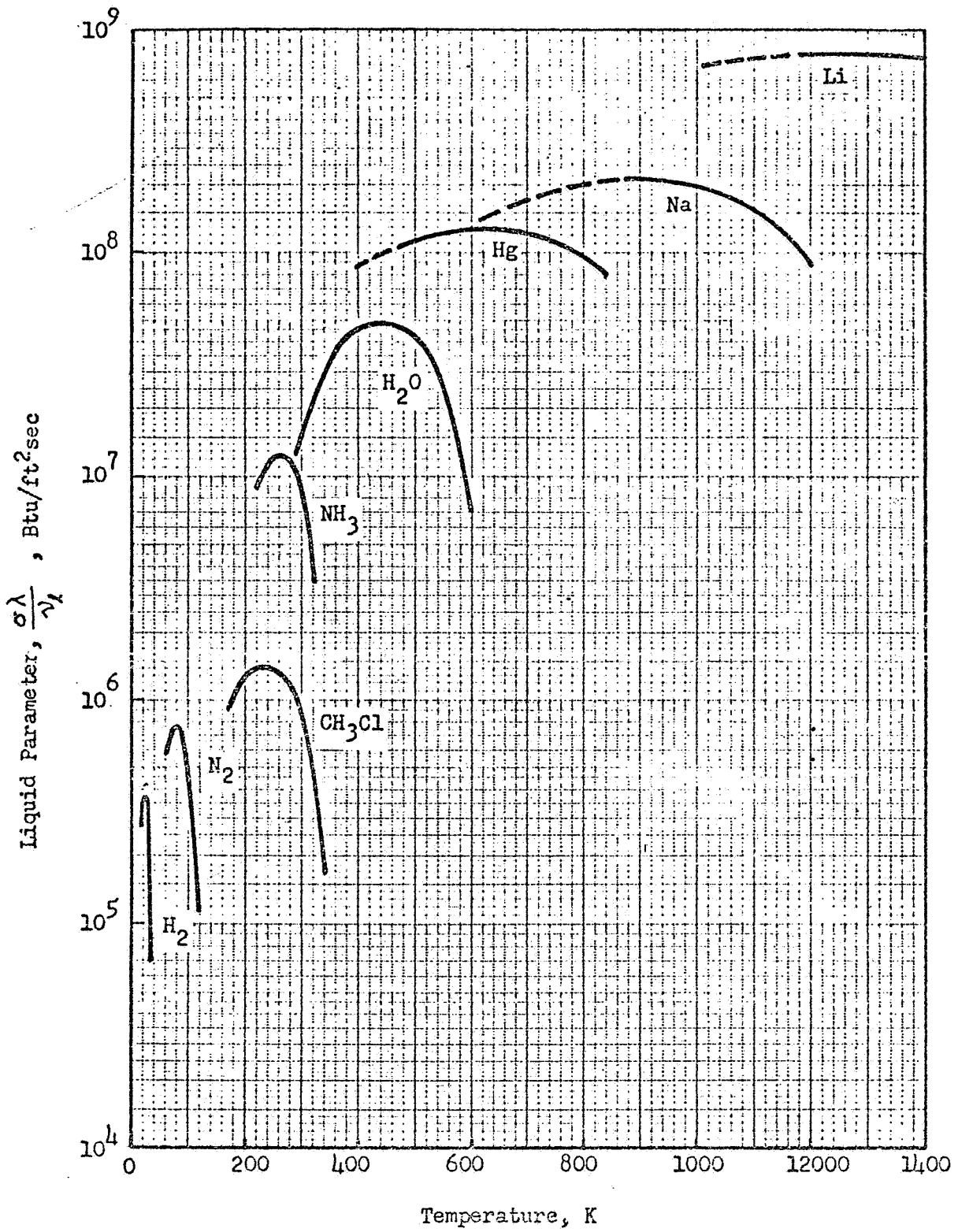


Figure 7-19 Liquid Parameter for Various Liquids

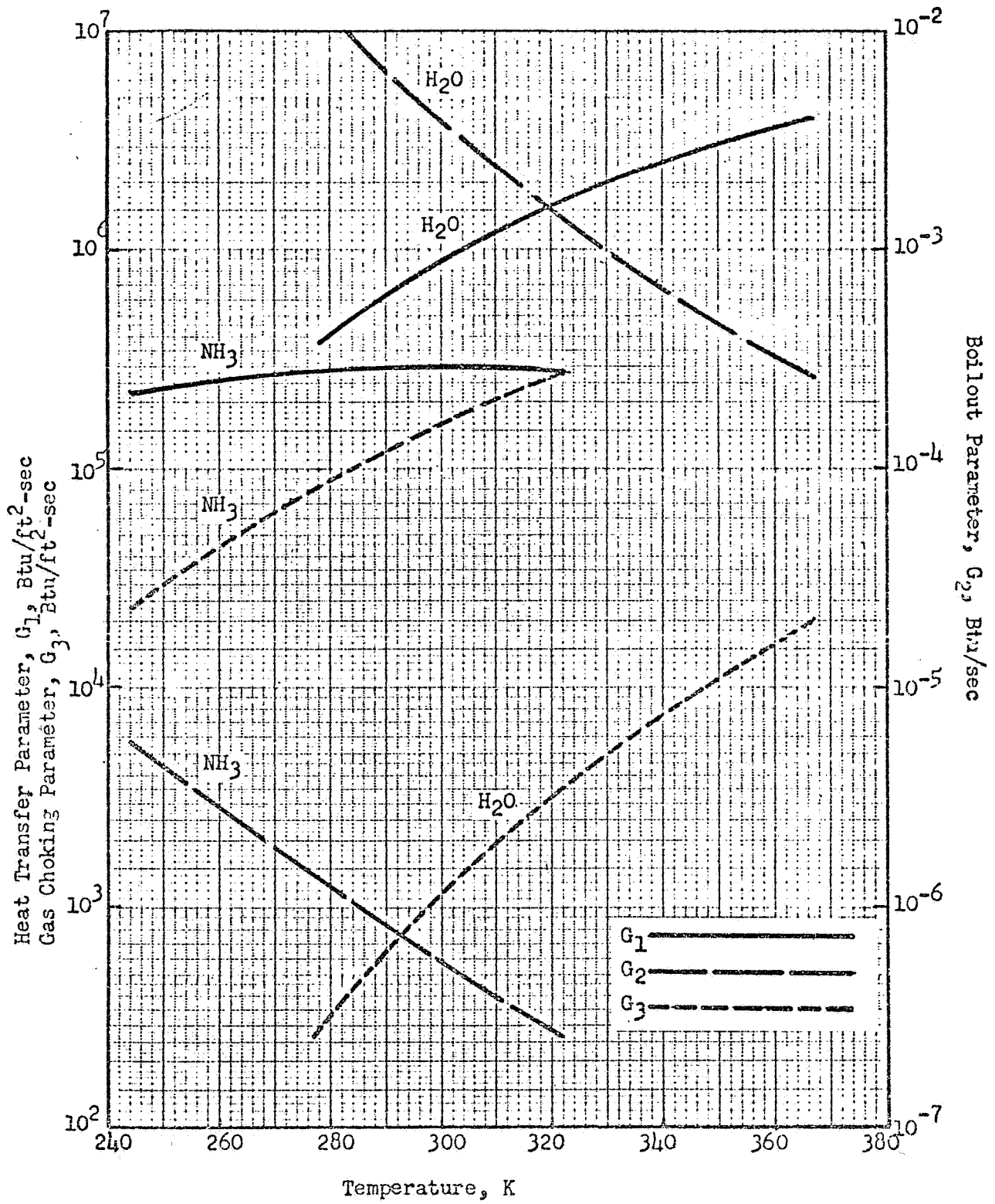
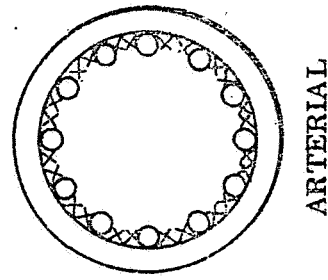
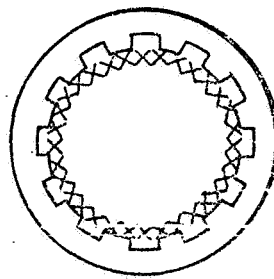


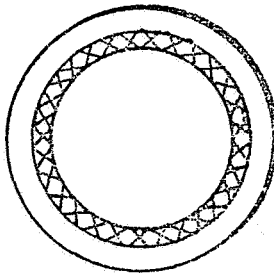
Figure 7-20 Fluid Property Groups at Moderate Temperatures



ARTERIAL



CHANNEL



HOMOGENEOUS

Figure 7-21 Cross-Sections of Three Wick Structures

⊕ 6

wicks having a channel depth-to-width ratio of 2.5 and $k = 1$ for arteries. When using a channel or arterial wick care must be taken not to exceed the maximum width or diameter at which the artery or channel will fill in an acceleration field. The maximum width or diameter is proportional to the square root of the surface tension divided by the specific weight ($D = \sqrt{\sigma/\gamma}$).

7.5.1.2 Boilout Limit

The boilout limit is reached when the liquid in the evaporator vaporizes in the wick structure and forms an insulating vapor film which disrupts liquid flow. The result is a rapidly increasing evaporator temperature with little or no increase in heat transfer rate. The cause of the boiling in the wick is the temperature gradient required for heat transfer across the wick matrix. Since the liquid at the inner surface of the wick in the heat pipe is at saturation temperature, the liquid at the pipe wall-wick-matrix interface is in a superheated state. When the vapor pressure corresponding to the super-heat temperature becomes greater than the local capillary pressure nucleation may occur.

Neal (Ref. 7-11) has determined that the onset of nucleation, which limits the maximum radial heat flux, is proportional to the fluid property group

$$G_2 = \frac{\sigma K_\lambda T_s}{\lambda \rho_v}$$

Values of G_2 are also plotted in Fig. 7-20 for water and ammonia. It is desirable to select a fluid with large values of this parameter. This selection must be made with due consideration given to providing satisfactory values of G_1 .

7.5.1.3 Vapor Choking Limit

The third heat pipe performance limit is that due to choking of the vapor flowing from the evaporator to the condenser. Levy (Ref. 7-12) has predicted that at low vapor pressures, such as operation near the triple point temperature, the vapor flow can reach sonic velocities and thus prevent an increase in the heat transfer rate. He showed that the choking limit is given by:

$$Q_{e_{\max}} = \frac{\rho_v \lambda V_a \pi R_v^2}{\sqrt{2(\gamma+1)}} \quad (7-37)$$

where

$$V_a = \sqrt{\gamma g_o RT} \quad (7-38)$$

Q is a function of a fluid property group ($\rho_v \lambda \sqrt{g_o RT}$) and the dimensions of the heat pipe. This fluid property group, designated G_3 , can be used in optimizing the fluid to be used in the heat pipe and is plotted on Fig. 7-20.

7.5.2 Wick Design

7.5.2.1 Evaporation and Condenser Sections

The primary function of the wick is to return liquid from the condenser end of the heat pipe to the evaporator. As long as a supply of liquid condensate is distributed throughout the evaporator wick, satisfactory heat pipe action will occur. Conversely, the heat pipe will fail to function properly should insufficient liquid be returned to the evaporator. This mode of failure is referred to as pumping failure. In this mode the strength of the capillary pumping mechanism is insufficient to provide the liquid required for evaporation rates corresponding to some maximum heat transfer rate; i.e.,

$$Q_{\text{failure}} > Q_{\max} = \lambda \dot{m}_{\max} \quad (7-39)$$

A second failure mode occurs as a result of liquid vaporization within the wick structure and subsequent vapor entrapment in the wick structure.

7.5.2.1.1 Wick Pumping Capability

Predictions of maximum liquid flow rate capability are based on analytical characterizations of the various pressure drops and losses in the heat pipe system. A schematic representation of the sources of these pressure drops is shown in Fig. 7-22. During evaporation the vapor pressure decreases in the axial flow direction as mass is added to the vapor stream. An additional slight drop in pressure is observed in the adiabatic section due to wall friction. In the condenser section the pressure increases in the direction of fluid motion due to

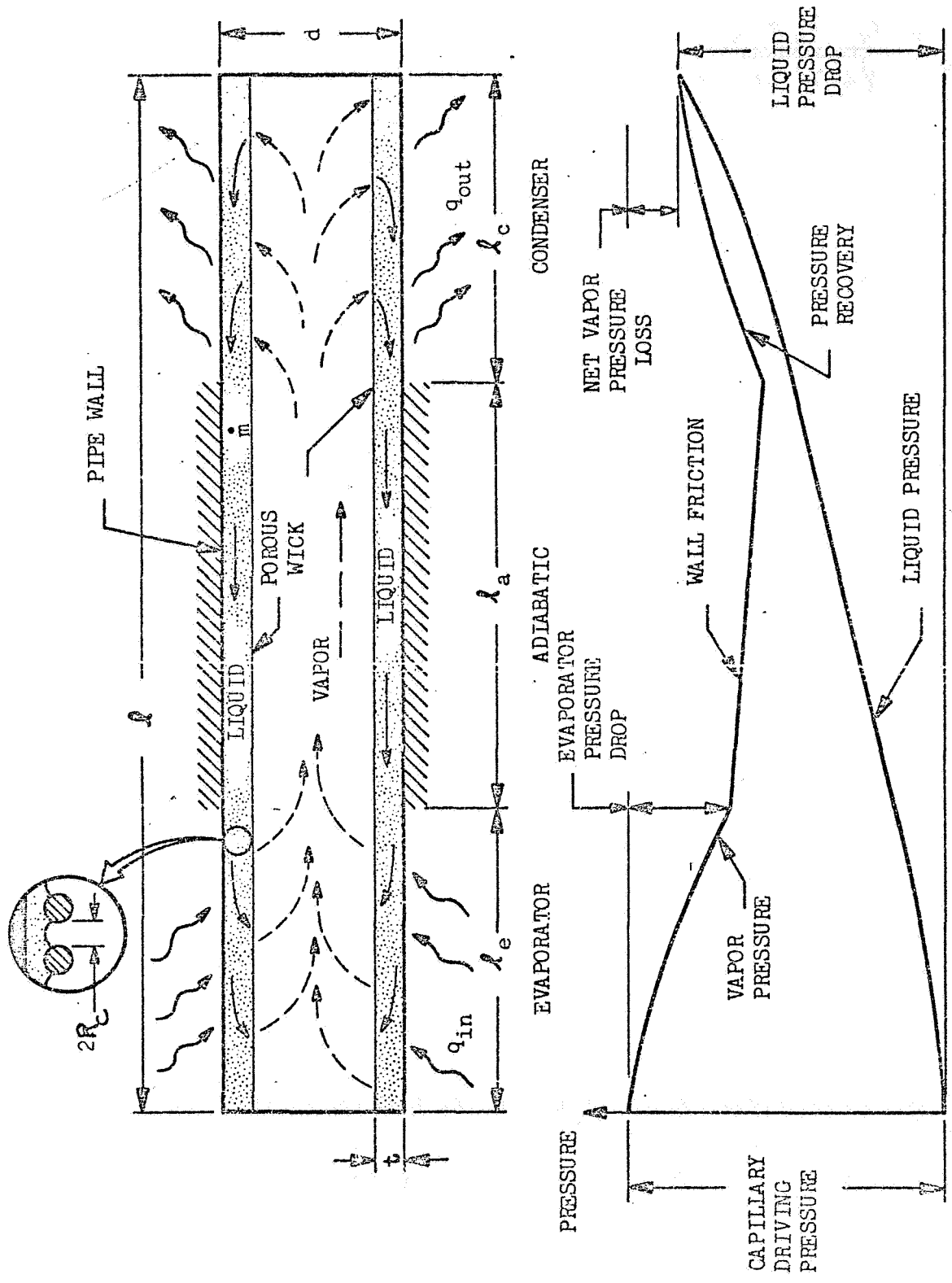


Figure 7-22 Heat Pipe Schematic and Pressure Diagram

partial dynamic recovery of the decelerating flow. The liquid condensate is then pumped back to the evaporator by means of the induced capillary driving pressure. The liquid pressure drop in the wick structure is due to internal friction between the fluid and the porous wick material.

For low temperature heat pipes the net vapor pressure loss is very small and may be neglected. Thus the fluid circulation rate is essentially fixed by a balance between the liquid pressure loss flowing in the wick structure and the available capillary pumping pressure. The maximum capillary pumping pressure is determined by the surface tension of the working fluid, the size of the holes or pores in the wick structure, and the wetting characteristics of the wick and working fluid combination. This pressure difference across the liquid-vapor interface, Δp_c , is expressed as follows:

$$\Delta p_c \Big|_{\max} = \frac{\sigma}{R_c} \phi \quad (7-40)$$

where R_c is the radius of holes in the wick (or $\frac{1}{2}$ hole size in a square weave mesh),

σ is the working fluid surface tension.

The quantity ϕ is an empirical constant related to the meniscus shape in the pores of the wick. Its value is dependent on the wetting characteristics of the liquid-solid system as well as the particular character of the wick pore geometry (i.e., round holes, square holes, irregular shapes, etc.). Many heat pipe theories assume a value of 2 for this constant for the common liquid-metal combinations such as alcohol, NH_3 , acetone, or water with aluminum or stainless steel. There is an interrelationship between ϕ and R_c , however, and it is necessary then to determine empirically values for R_c , the pore capillary radius (see equation 7-35). This approach is used by Kunz, et al, (Ref. 7-13) and Phillips, (7-14). Alternatively, one can measure the pore size or, for example, calculate it from the screen mesh weave geometry and then employ an empirically determined value for ϕ . Hollister, (Ref. 7-15) determined values for ϕ for a number of liquid and solid capillary systems. For conservatism a value of $\phi = 1.5$ is recommended in this regard.

7.5.2.1.2 Wick Pressure Drop

The liquid pressure loss due to flow through a wick structure is highly dependent on the wick geometry from the standpoint of both its gross dimensions and configuration and the flow geometry within the wick structure. Expressions for pressure loss due to liquid flow within a wick structure are usually based on Darcy's Law or the Blake-Kozeny equation for flow in porous media and packed beds. Analytical expressions (with empirically determined parameters) have been published in the literature to predict performance based on pressure drop for various types of wick configurations. Darcy's law is

$$\Delta p_L = \frac{\dot{m} \nu_L \ell}{A_w K_p} \quad (7-41)$$

This expression shows that wick pressure loss is minimized for maximum wick permeability values. Sample values of wick permeability, K_p , are listed in Table 7-2.

7.5.2.1.3 Boiling in Wick Structure

If fluid in the evaporator section of the wick is heated to its saturation temperature, gas bubbles will be formed within the wick structure. As these bubbles grow in size, they encounter pore openings smaller than their own diameter, and the bubble will not flow through the nonuniform section unless a critical force is exerted on it. This critical force is determined by the size of the bubble, the pore size, and the interfacial surface tension between the gas and liquid. The net effect is an equivalent reduction in permeability to flow of the gas-liquid mixture.

It is desirable to prevent the formation and possible trapping of bubbles in the wick. Therefore, the ΔT radially, across the wick must be kept as small as practicable. If boiling does not occur then the temperature drop across the wick is given by

$$\Delta T \doteq \frac{(Q/A)t}{K_m} \quad (7-42)$$

Table 7-2
WICK PERMEABILITY VALUES

<u>Wick</u>	<u>K_p (Ft²)</u>	<u>Source</u>
100 mesh screen (more than 3 layers)	0.16×10^{-8}	Kunz, et al (Ref. 7-13)
200 mesh screen (more than 3 layers)	0.08×10^{-8}	Kunz, et al
200 mesh screen		
o 1 layer, flat meniscus shapes	0.059×10^{-8}	Phillips (Ref. 7-14)
o 1 layer, moderately curved meniscus shapes	0.04×10^{-8}	Phillips
o 1 layer, highly curved meniscus shapes	0.014×10^{-8}	Phillips
o 2 layers, flat meniscus shapes	0.062×10^{-8}	Phillips
o 2 layers, curved meniscus shapes	0.045×10^{-8}	Phillips
Nickle Foam porosity 0.9	2.5×10^{-8}	Phillips
Felt Metal		
o porosity 0.9	0.5×10^{-8}	Phillips
o porosity 0.8	0.05×10^{-8}	Kunz, et al
o porosity 0.7	0.016×10^{-8}	Kunz, et al

The importance of having a wick-liquid matrix with a high thermal conductivity is obvious. Most previous heat pipe investigations have found that the thermal conductivity of a woven or mesh type of wick-liquid matrix approaches the value of a series conduction path given by

$$K_m = \frac{K_s}{1 + \epsilon \left(\frac{K_s}{K} - 1 \right)} \quad (7-43)$$

Since most wicks used for heat pipes have a high porosity (usually > 50%) and most working fluids have low conductivities relative to the wick material, the matrix conductivity given by equation (7-43) tends to approach the conductivity of the fluid alone.

It is suggested that for moderate and high temperature heat pipes the value of K_m be set equal to the value of liquid conductivity alone for a conservative design of the evaporator section. However, the thermal conductivity of cryogenic fluids, typically on the order of 10^{-1} to 10^{-2} Btu/ft hr $^{\circ}$ R negates this approach since the predicted temperature drop across the matrix is excessive even for extremely thin wicks and small heat fluxes. Therefore, for design of cryogenics heat pipes it is necessary to design using the wick material thermal properties.

Flow of liquid in the axial direction in the evaporator is impaired if the wick is made too thin. Therefore, a compromise must be reached between providing a minimum ΔT and minimizing axial pressure drop.

7.5.2.2 Adiabatic Section

As explained in the previous section the wick in the evaporator and preferably also in the condenser sections must be thin in order to prevent boiling and large temperature drops. However, the wick in the adiabatic section need not be optimized for radial conduction. Therefore, the adiabatic section is best designed according to optimum wicking conditions as given by equations (7-34) and (7-35).

For equations (7-34) and (7-35) the axial heat transfer rate is maximized when $R_v/R_w = \sqrt{2/3}$. Therefore, for a 1 cm ID heat pipe design the optimum wick

thickness would be $t = 0.092$ cm. This is approximately 3 times the maximum thickness allowable in the evaporator section according to the superheat criteria. If the heat pipe were 0.4 cm diameter, the optimum wick thickness would be $t = .037$ cm. This diameter would provide a wick of uniform thickness throughout the entire pipe assuming the parallel conduction condition stated in Section 7.5.2.1.3. However, the evaporator section would have to extend for 26 cm along the pipe to have an area of 32.3 cm^2 at a heat flux of $.216 \text{ W/cm}^2$.

The desire to have a short evaporator section suggests designing a three section wick with one section optimized for the evaporator section, one for the adiabatic section and one for the condenser section. Careful attention must be given to the interfaces between the sections to insure that proper wicking is obtained.

Work to date has shown the feasibility of manufacturing graduated wicks that provide near optimum conditions in each of the three heat pipe sections. These consist of separate sections of sintered felt metals sintered in turn to the pipe wall and have gradual changes in dimensions from one section to another.

7.5.3 Size and Weight

The size and weight of a heat pipe are dependent on a combination of design factors. The minimum surface areas of the evaporator and condenser sections are determined by the ΔT limitations described in section 7.5.2.1.3. The length of the adiabatic section is determined by the distance between the heat source and the heat sink. By assuming lengths for the evaporator and condenser sections, the total length of the pipe, l , is determined. Then, for a given fluid and wick material, equation (7-35) can be solved for the required wick radius for an optimum wick. The radius of the vapor flow channel is then given by

$$R_v = R_w \sqrt{\frac{2}{3}}$$

Values of $Q_{e \text{ max}}$ ($l + l_a$) have been calculated using equation (7-36) for a zero-g heat pipe. These values are plotted in Fig. 7-23 for two fluids, water and ammonia, operating at 300°K . The wick parameters ϵ , b and K must be determined experimentally. Typical values of $\epsilon = 0.8$ and $b = 20$ were used in obtaining the results plotted in Fig. 7-23 (a typical value for K is about 1.5).

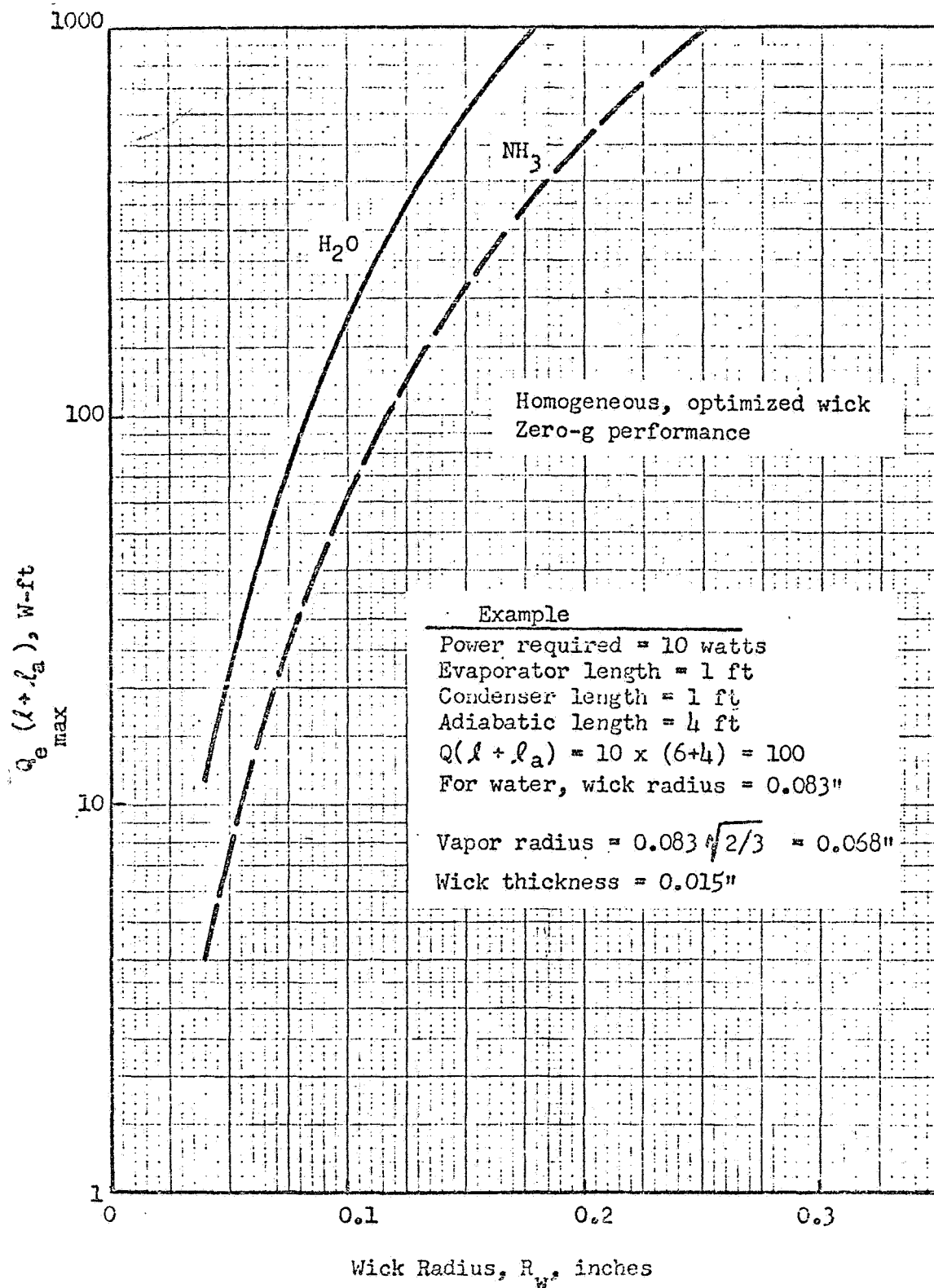


Figure 7-23 Heat Pipe Performance for Moderate Temperatures

Corresponding values of heat pipe weight are plotted in Figure 7-24.

Having determined the optimum values for R_v and R_w , the criteria for allowable evaporation area and wick pressure drops must be checked.

The minimum allowable evaporator area is given by equation (7-42):

$$A_{e \min} = \frac{Q_e t}{K_m \Delta T_{\max}} \quad (7-44)$$

where ΔT_{\max} is the maximum allowable ΔT to prevent boiling based on operation at the maximum heat flux. The maximum liquid pressure drop for laminar flow is given by Darcy's law:

$$\Delta p_{L \max} = \frac{\dot{m}_{\max} \nu_L \ell}{A \frac{K}{w p}} \quad (7-45)$$

where \dot{m}_{\max} is given by equation (7-39) and

$$A_w = \pi(R_w^2 - R_v^2) \quad (7-46)$$

For satisfactory operation we must have

$$\Delta p_{L \max} < \Delta p_{c \max} \quad (7-47)$$

where $\Delta p_{c \max}$ is given by equation (7-40).

The weight of the heat pipe is then simply equal to the sum of the fluid, wick and pipe wall weights. The pipe wall thickness is determined by the maximum hoop stress corresponding to the maximum internal vapor pressure. The total heat pipe weight is then given by

$$W = \pi \ell \left\{ \rho_w (R_o^2 - R_w^2) + [\epsilon \rho_s + (1 - \epsilon) \rho_l] (R_w^2 - R_v^2) \right\} \quad (7-48)$$

7.5.4 Design Procedure for Optimized Homogeneous Wick Heat Pipes

In the following, it is assumed that the required maximum heat flux, Q_e , the adiabatic length, ℓ_a and the nominal operating temperature are given. The heat pipe design procedure is then expressed in stepwise fashion below.

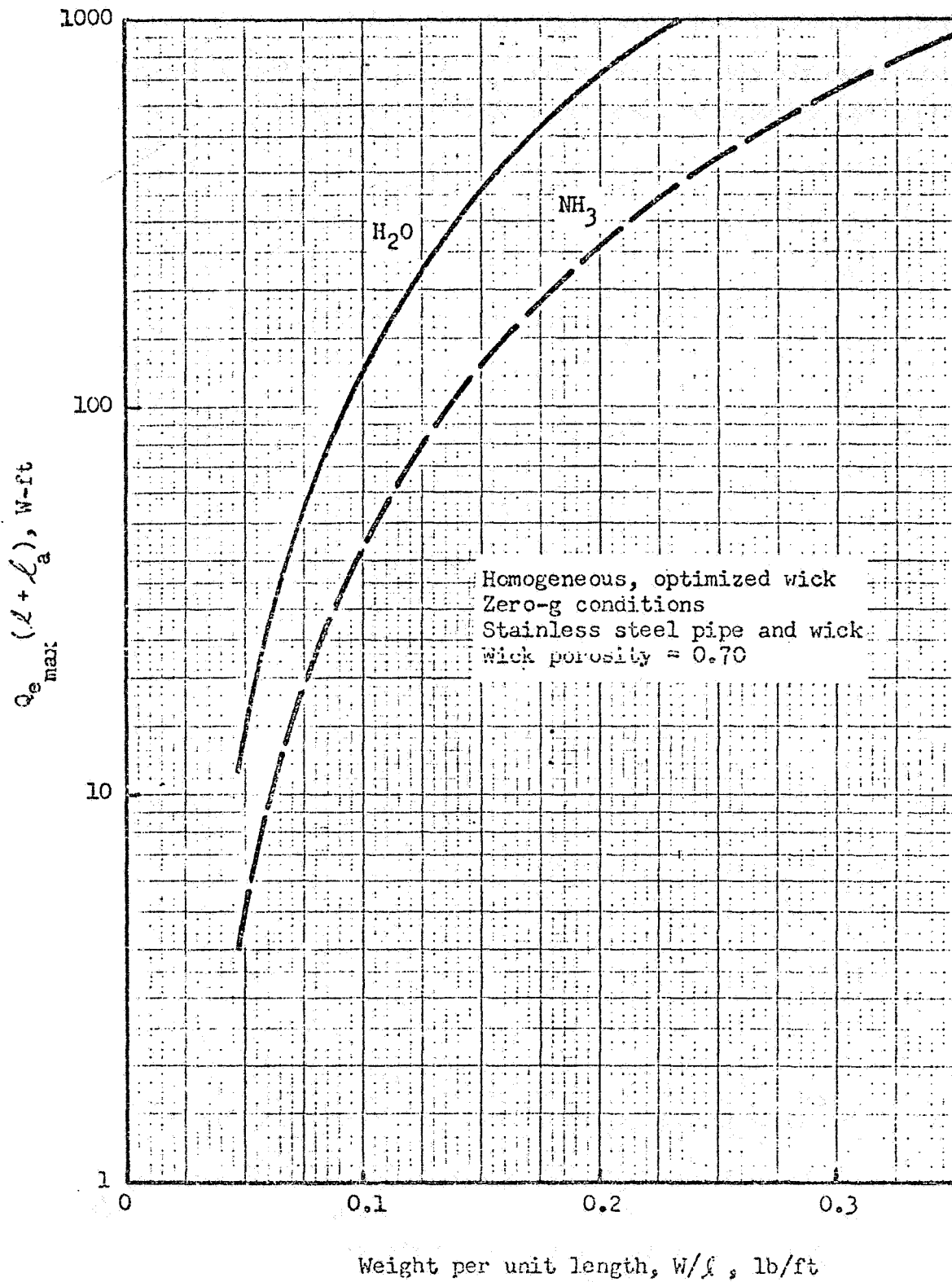


Figure 7-24 Weight of Moderate Temperature Heat Pipes

1. Select a fluid from Fig. 7-19 for the given operating temperature.
2. Select a wick material and assume a value of wick thickness, t .
Look up wick permeability, K_p and pore radius, R_c .
3. Compute the mean fluid-wick conductivity,

$$K_m = \frac{K_s}{1 + \epsilon \left(\frac{K_s}{K_l} - 1 \right)}$$

4. Look up the value of ΔT_{\max} for the selected fluid from Fig. 7-25.
5. Compute the minimum allowable evaporator area from equation 7-44:

$$A_{e \min} = \frac{Q_e t}{K_m \Delta T_{\max}}$$

6. Compute the required length of the evaporator section from

$$l_e = \frac{A_{e \min}}{2 \pi R_w}$$

7. Compute overall heat pipe length assuming equal evaporator and condenser lengths:

$$l = 2 l_e + l_a$$

8. Look up the optimum wick radius, R_w , from Fig. 7-23.
9. Compute wick thickness for the optimized wick:

$$t = R_w - R_v = 0.1835 R_w$$

10. Using this value of t repeat steps 5 through 10 until consistent values are obtained.
11. Compute wick cross-sectional area from

$$A_w = \frac{\pi}{3} R_w^2$$

12. Look up values for liquid heat of vaporization, λ , kinematic viscosity, ν_l , and surface tension, σ .

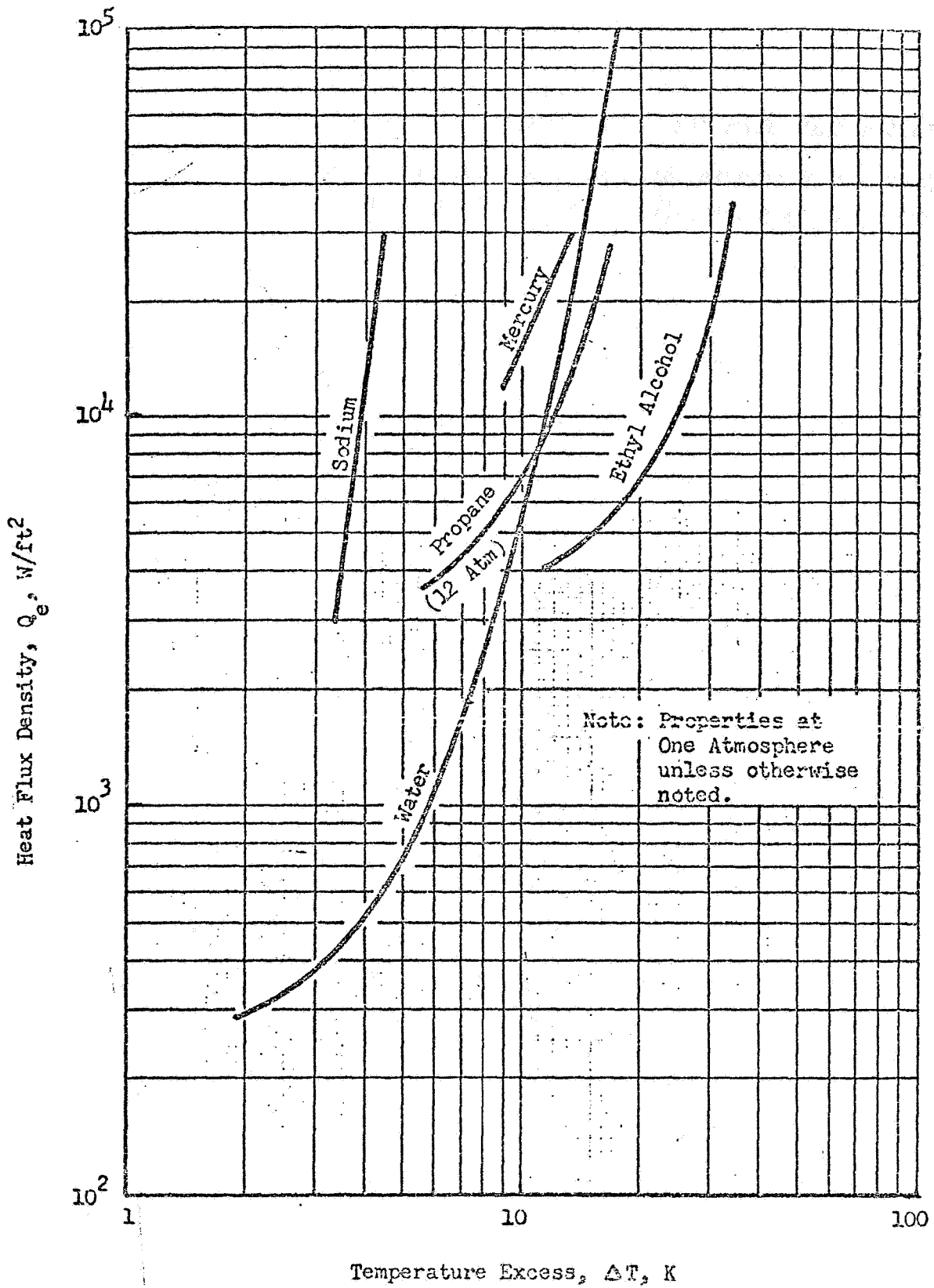


Figure 7-25 Nucleate Boiling Heat Fluxes for Moderate and High Temperature Fluids

13. Compute maximum liquid flowrate from

$$\dot{m}_{\max} = \frac{Q_e}{\lambda}$$

14. Compute wick pressure drop from equation (7-45):

$$\Delta p_{L_{\max}} = \frac{\dot{m}_{\max} \nu_l \ell}{A_w K_p}$$

15. Compute capillary pumping Δp_c from

$$\Delta p_c = 1.5 \frac{\sigma}{R_c}$$

16. If $\Delta p_{L_{\max}} > \Delta p_c$ select a new wick material having a higher permeability and/or a smaller capillary radius and repeat steps 13 and 14. Check that the mean conductivity for the new wick is not significantly different from that computed in step 3. If the new K_m is significantly smaller it will be necessary to repeat steps 4 through 16.

REFERENCES

- 7-1 Mackay, D. B., "Design of Space Power Plants," Prentice-Hall, Inc., Englewood Cliffs, N.J., 1963
- 7-2 McAdams, W. H., "Heat Transmission," 3rd ed., McGraw-Hill Co., Inc., New York, 1954
- 7-3 Sparrow, E. M., and Eckert, E. R. G., "Radiant Interaction Between Fin and Base Surface," A.S.M.E. J. Ht. Trans., V 84C, 1962, p. 12
- 7-4 Liquid Propellant Thermal Conditioning Unit - Interim Report, October 12, 1966, Airesearch Manufacturing Div., The Garrett Corp.
- 7-5 Lockheed Missiles & Space Company, "Heat Pipes for Active Thermal Control of Spacecraft, Report for 1969 Independent Development Program," LMSC/A965174, 13 February 1970
- 7-6 R. C. Turner, "The Constant Temperature Heat Pipe - A Unique Device for the Thermal Control of Spacecraft Components," AIAA Paper No. 69-632
- 7-7 H. C. Haller, S. Lieblein and B. G. Lindlow, "Analysis and Evaluation of a Vapor-Chamber Fin-Tube Radiator for High Power Rankine Cycles," NASA TN D-2836.
- 7-8 R. C. Turner and W. E. Harbaugh, "Design of a 50,000-Watt Heat-Pipe Space Radiator," ASME Aviation & Space Conference, Beverly Hills, California, June 1968
- 7-9 J. D. Hinderman, J. Madsen and E. D. Waters, "An ATS-E Solar Cell Space Radiator Utilizing Heat Pipes," AIAA Paper No. 69-630
- 7-10 Cotter, T. P., Theory of Heat Pipes, Los Alamos Scientific Laboratory Report No. LA-3246-MS, March 26, 1965
- 7-11 Neal, L. G., "An Analytical and Experimental Study of Heat Pipes," Report No. 99900-6114-R000, TRW Systems, Redondo Beach, California, June 1967
- 7-12 Levy, E. K., "Theoretical Investigation of Heat Pipes Operating at Low Vapor Pressures," Proceedings of ASME Aviation and Space Conference, PP 671-676, June 1968
- 7-13 Kunz, H. R., Langston, L. S., Hilton, B. H., Wyde, S. S., and Nashick, G. H., Vapor Chamber Fin Studies - Transport Properties and Boiling Characteristics of Wicks. NASA CR-812
- 7-14 Phillips, E. C., "Low Temperature Research Program" NASA CR 66792, June 1969

REFERENCES (Cont.)

- 7-15 Hollister, M. P., "Propellant Containment Utilizing Screen Mesh and Perforated Plate Surfaces," LMSC A665481, December 29, 1964

NOMENCLATURE

A	-	Area
A_w	-	Wick cross-sectional area
a	-	Land width divided by half the channel width
b	-	Geometric constant for homogeneous wicks, $b = 10 \text{ to } 20$
C_{p_f}	-	Fluid specific heat
D	-	Diameter
F_R	-	Radiant interchange factor
g	-	Acceleration
G_A, G_E, G_H, G_P	-	Environmental Parameters
g_o	-	Gravitational constant
h	-	Heat transfer coefficient
k	-	Channel wick shape factor
K	-	Constant, thermal conductivity
K_l	-	Thermal conductivity of liquid
K_m	-	Thermal conductivity of wick-liquid matrix
K_s	-	Thermal conductivity of solid wick material
K_p	-	Permeability
L_d	-	Width of fluid duct
L_e	-	Effective width of radiator
l	-	Total length of heat pipe, $l_e + l_a + l_c$
l_a	-	Length of adiabatic section
\dot{m}	-	Mass flow rate
P	-	Pressure, fin profile number
P_r	-	Reduced Pressure
P_c	-	Critical Pressure
Pr	-	Prandtl number

NOMENCLATURE (Cont.)

p	-	Perimeter of fluid passageway
Q_e	-	Axial heat transfer rate
q	-	Net rate of heat transfer
R	-	Gas Constant
R_c	-	Capillary radius
Re	-	Reynold's number
R_o	-	Pipe outside radius
R_w	-	Outer wick radius
R_v	-	Vapor core radius
t	-	Wick thickness
t_c	-	Wick thickness in condenser section
t_e	-	Wick thickness in evaporator section
T	-	Temperature
T_c	-	Critical Temperature
T_F	-	Fluid Temperature
T_r	-	Reduced Temperature
T_s	-	Saturation Temperature
T_w	-	Wall temperature
V_a	-	Sonic velocity
V_l	-	Volume of liquid in saturated wick
\dot{V}_{tot}	-	Total open volume of heat pipe
\dot{w}_F	-	Rate of fluid flow in radiator duct
z	-	Vertical height in an acceleration field
Z	-	Compressibility factor, Ratio of fin root temperature at radiator outlet to that at inlet
α	-	Solar absorptance

NOMENCLATURE (Cont.)

β	-	Angle between orbit plane and planet-sun line
δ	-	Fin thickness
ϵ	-	Infrared emittance, porosity of wick
σ	-	Surface tension, Stefan-Boltzmann constant
λ	-	Heat of vaporization
μ_v	-	Vapor viscosity
μ_l	-	Liquid viscosity
ρ_v	-	Vapor density
ρ_l	-	Liquid density
ρ_s	-	Wick material density
ρ_w	-	Pipe wall density
ν_v	-	Vapor kinematic viscosity
ν_l	-	Liquid kinematic viscosity
θ	-	Liquid-solid contact angle, orbit position angle
γ	-	Specific weight, ratio of specific heats in Equation 7-38
ψ_H	-	Heat Transfer Parameter
ϕ_F	-	Film Resistance number
ϕ_R	-	Radiation number
Ω_1	-	Fin effectiveness at fluid inlet
Ω_2	-	Fin effectiveness at fluid outlet

Section 8

HEAT ABSORPTION

8.1 INTRODUCTION

The material in this section has been prepared in order to provide the engineer with data and methods to quickly take into account the weight and performance of the devices required to transfer the heat from the cryogenic tank to the refrigerator. Many methods are possible to conduct the heat from the tank to the refrigerator and a few of them have been selected on which to provide data. Material is given in this section for on-tank heat exchangers, helium circulation devices, cryogenic heat pipes, and solid conduction devices. It is felt that a broad enough spectrum is covered by these devices that the engineer should be able to obtain a representative weight and performance estimate for nearly any space application that he may choose to analyze.

8.2 TANK WALL HEAT EXCHANGERS

A sketch of a typical heat exchanger installation is shown in Figure 8-1. It is assumed that the cold side fluid is helium at about 25 atmospheres pressure. The helium is pumped through a spiral wound tube which is fastened to the tank wall. It is assumed further that the cryogenic tank experiences an acceleration sufficient to mix the cryogenic liquid by natural convection, or that an internal mixer is provided as shown in Figure 8-1. The objective of preliminary design analyses is to find the heat exchanger wall area, the heat exchanger system weight, and the helium gas flowrate \dot{W}_{He} required to maintain a prescribed temperature difference ΔT_{He} between inlet and outlet for a given heat transfer rate q .

8.2.1 Design Analyses

The heat exchanger effectiveness, E , is defined as the ratio of the actual heat transfer rate to the maximum possible rate. For the range of ΔT_{He}

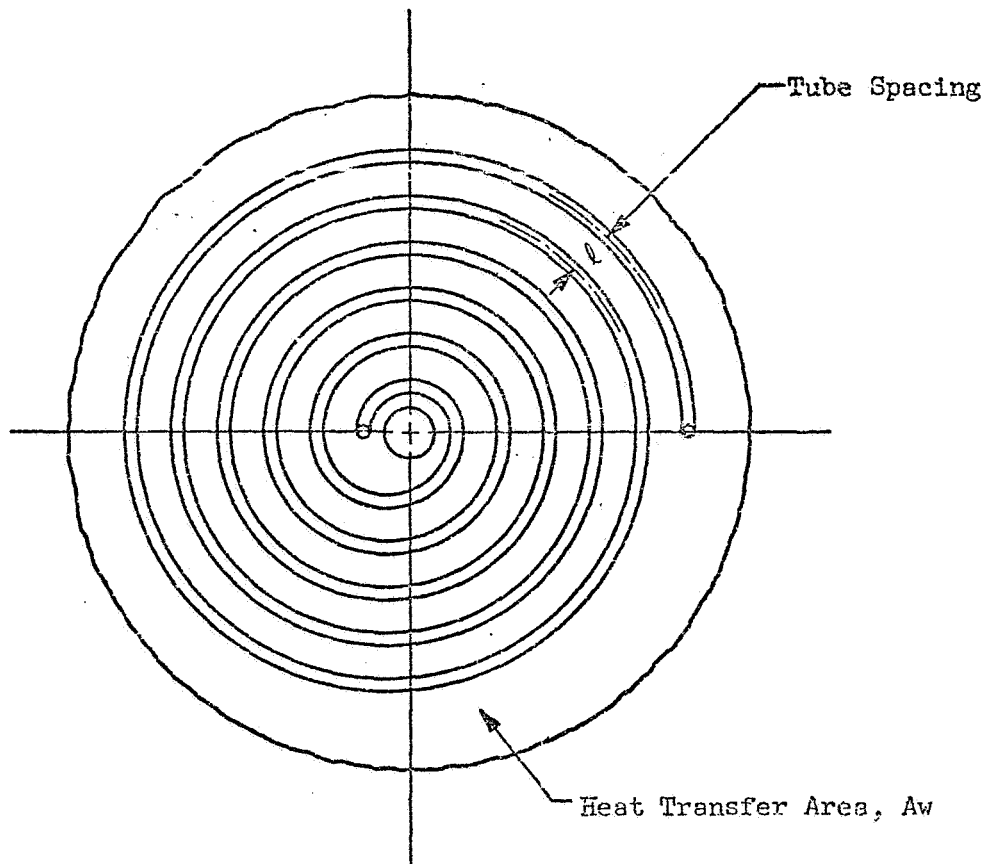
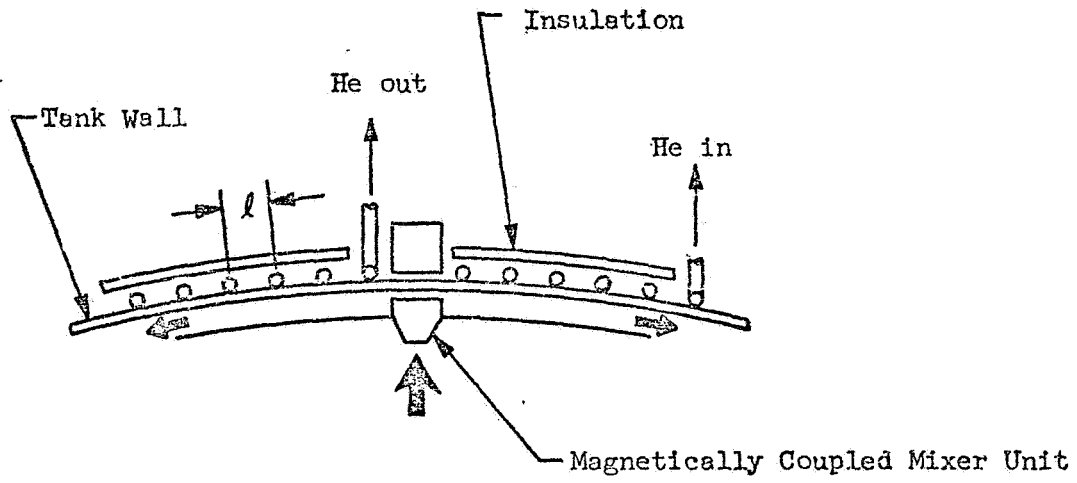


FIGURE 8-1 TANK WALL HEAT EXCHANGER

considered feasible for this application, the value of E can be estimated from reference 8-1. From Figure 2 of this reference, it can be seen that a value of E = 0.50 can be obtained for any fluid capacity ratio. If it is further assumed that the minimum fluid capacity rate, $\dot{W} C_p$, is on the helium side, and that the number of transfer units, NTU is one, we have

$$AU = C_{\min} = (\dot{W} C_p)_{\text{He}} \quad (8-1)$$

where A is the characteristic area of the heat exchanger and U is the overall heat transfer coefficient. If the characteristic area A is set equal to the heat exchange wall area, then Equation (8-1) can be written

$$A_W = \frac{(\dot{W} C_p)_{\text{He}}}{U} \quad (8-2)$$

The overall heat transfer coefficient can be related to its individual components through Equation (8-3):

$$\frac{1}{A_W U} = \frac{1}{A_W h_L} + \frac{1}{A_W h_W} + \frac{1}{A_T h'_g} \quad (8-3)$$

where h_L is the liquid-to-wall heat transfer coefficient, h_W is the tank wall conductance and h'_g is the equivalent heat transfer coefficient between the helium gas and the tube surface in contact with the tank wall. If the liquid-to-wall coefficient is sufficiently large, the first term on the right-hand-side of (8-3) can be neglected and

$$\frac{1}{U} = \frac{1}{h_W} + \frac{A_W}{A_T} \frac{1}{h'_g} \quad (8-4)$$

The wall conductance coefficient h_W is composed of the sum of two effects, the conduction of heat transversely through the tank wall plus the conduction along the tank wall between tubes. For conduction heat transfer normal to

the tank wall,

$$q = \frac{k_w}{t_w} A_w \Delta T_c \quad (8-5)$$

and for heat transfer through fins of width $\ell/2$,

$$q = \frac{8 t_w k_w A_w \Delta T_{\max}}{\ell^2} = \frac{12 t_w k_w A_w \Delta T_{\text{avg}}}{\ell^2} \quad (8-6)$$

where

$$\begin{aligned} t_w &= \text{tank wall thickness} \\ k_w &= \text{wall thermal conductivity} \\ \ell &= \text{tube spacing} \end{aligned}$$

and the ΔT values are defined in Figure 8-2. We now define h_w as

$$h_w = \frac{q}{A_w \Delta T_w} \quad (8-7)$$

$$\text{where } \Delta T_w = \Delta T_c + \Delta T_{\text{avg}} \quad (8-8)$$

Solving Equations (8-5) and (8-6) for ΔT_c and ΔT_{avg} , and substituting into Equation (8-7), we get

$$\Delta T_w = \frac{q}{A_w} \frac{t_w}{k_w} \left(1 + \frac{\ell^2}{12 t_w} \right)$$

Substituting the expression for T_w into (8-7), there results

$$h_w = \frac{h_w}{t_w \left(1 + \frac{\ell^2}{12 t_w} \right)} \quad (8-9)$$

The gas-side conductance is also composed of two effects, the internal gas film coefficient and the conduction coefficient around the tube walls. The equivalent conductance due to these effects is derived in Appendix III of reference 8-2. For this application, the thermal resistance between the

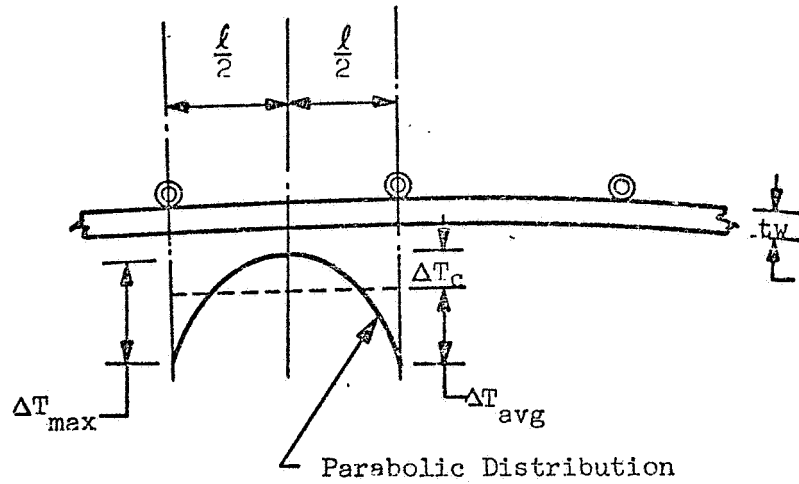


FIGURE 8-2 Wall Temperature Distribution

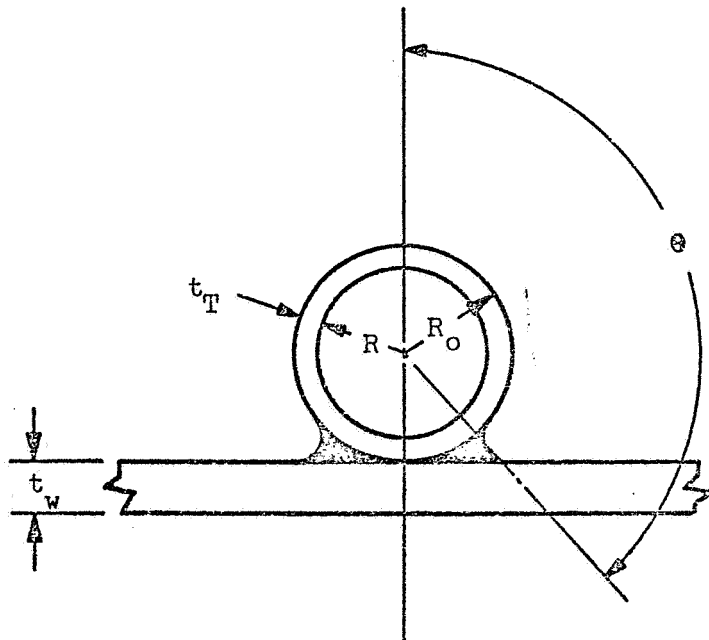


FIGURE 8-3 Tube-Wall Attachment Geometry

gas and the tube at the wall attachment point is given by

$$\frac{A_W}{A_T h'_g} = \frac{\ell}{2 \left[\sqrt{hg K_T t_T} \tanh \sqrt{\frac{hg}{K_T t_T}} R\theta + hg (\pi - \theta) R \right]} \quad (8-10)$$

where k_T is the tube thermal conductivity and the remaining symbols are defined in Figure 8-3.

The gas film coefficient, hg , can be obtained from Figure 7-3. The overall heat transfer coefficient is then given by Equation (8-4):

$$\frac{1}{U} = \frac{t_w \left(1 + \frac{\ell^2}{12 t_w^2} \right)}{K_w} + \frac{\ell}{2 \left[\sqrt{hg K_T t_T} \tanh \sqrt{\frac{hg}{K_T t_T}} R\theta + h_g (\pi - \theta) R \right]} \quad (8-11)$$

Using the value of U given by Equation (8-11) the required heat exchanger area can be computed from Equation (8-2).

If the conduction resistance around the tubing is small (i.e., if θ is small) then the second term in (8-11) can be simplified so that U can be found from the expression

$$\frac{1}{U} = \frac{t_w}{K_w} \left(1 + \frac{\ell^2}{12 t_w^2} \right) + \frac{\ell}{2 \pi R h_g} \quad (8-12)$$

8.2.2 Optimum Tube Spacing

Using the simplified expression for U , Equation (8-12), the value of A_W is given by

$$A_W = (\dot{w} C_p)_{He} \left[\frac{t_w}{K_w} + \left(\frac{1}{2 \pi R h_g} \right) \ell + \left(\frac{1}{12 t_w K_w} \right) \ell^2 \right] \quad (8-13)$$

This result shows that, for small tank wall thicknesses, the heat exchanger weight, is minimized by minimizing ℓ . Hence the tube wall spacing ℓ should be set equal to the minimum possible value, namely, the outside diameter of the tubing, $2 R_o$.

8.2.3 Design Procedure

In order to size the heat exchanger wall area, the design equations presented in Section 8.2.1 can be used. A summary of representative helium properties is given in Table 8-1. The design procedure is outlined in stepwise fashion below. It is assumed that the liquid storage temperature, the tank dimensions, the heat absorption rate q , and the helium gas temperature rise through the exchanger ΔT_{He} are all given.

Table 8-1

HELIUM GAS PROPERTIES AT
HIGH PRESSURE (25 ATMOSPHERES)

	<u>T = 20K (36R)</u>	<u>T = 90K (162R)</u>
Density, lbm/ft ³	3.81	0.847
Specific Heat, Btu/lbm R	1.40	1.25
Thermal Conductivity, Btu/Hr HR	0.016	0.040
Viscosity, lbm/hr ft	0.0087	0.0227
Prandtl Number	0.76	0.71

1. Look up values of helium gas properties from Table 8-1 or Reference 8-3.
2. Compute helium flow rate from the known capacity rate computed in Step 1:

$$\dot{w}_{He} = \frac{q}{C_{p_{He}} \Delta T_{He}}$$

3. Select a tubing material and values for tubing dimensions, R , R_o . Look up the thermal conductivity K_T of the tubing material.
4. Use Figure 7-3 to compute the helium gas heat transfer coefficient h_g .

5. Setting $\ell = 2 R_o$ use Equation (8-11) to compute the overall resistance $1/U$ or, if $\theta < 15^\circ$, use Equation (8-12).

6. Compute the required wall area A_w of the heat exchanger:

$$A_w = \frac{(\dot{w} C_p)_{He}}{U}$$

7. Compute the required number of tube turns N from

$$N = \frac{1}{\ell} \sqrt{\frac{A_w}{\pi}}$$

8. Compute the total tubing length L from

$$L = 2 \pi \ell \left[\frac{N}{2} + \sum_{n=1}^N (n-1) \right]$$

9. Compute the weight of tubing plus helium from

$$W_{TUBE} = \pi \rho (R_o^2 - R^2) L + \pi \rho_{He} R^2 L$$

10. The total weight of the tank wall heat exchanger system is then

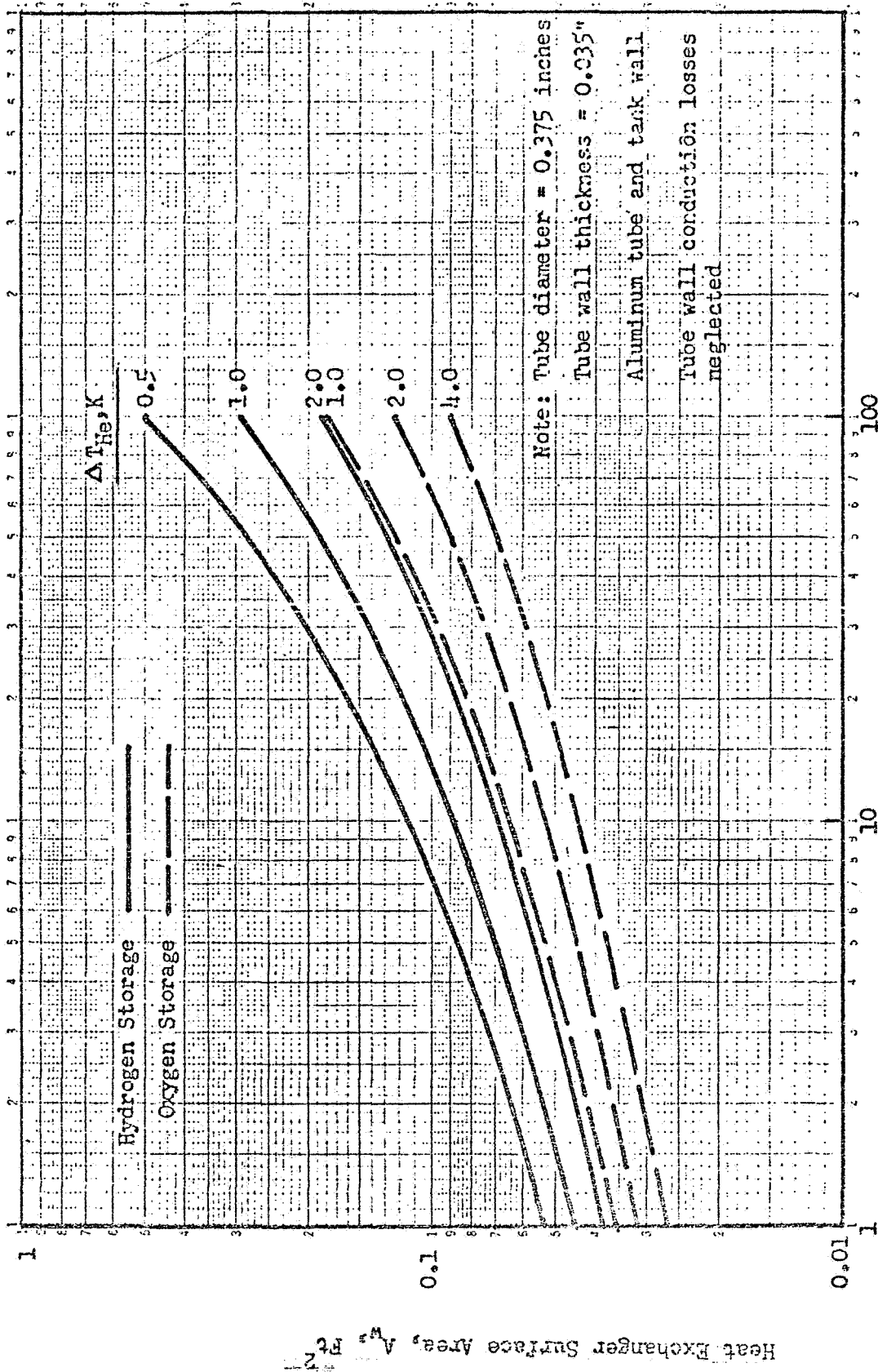
$$W_{HEX} = W_{TUBE} + W_{FILLET} + W_{MIXER} + W_{BAFFLE}$$

where W_{FILLET} refers to the weld fillet shown in Figure 8-3.

8.2.4 Sample Calculations

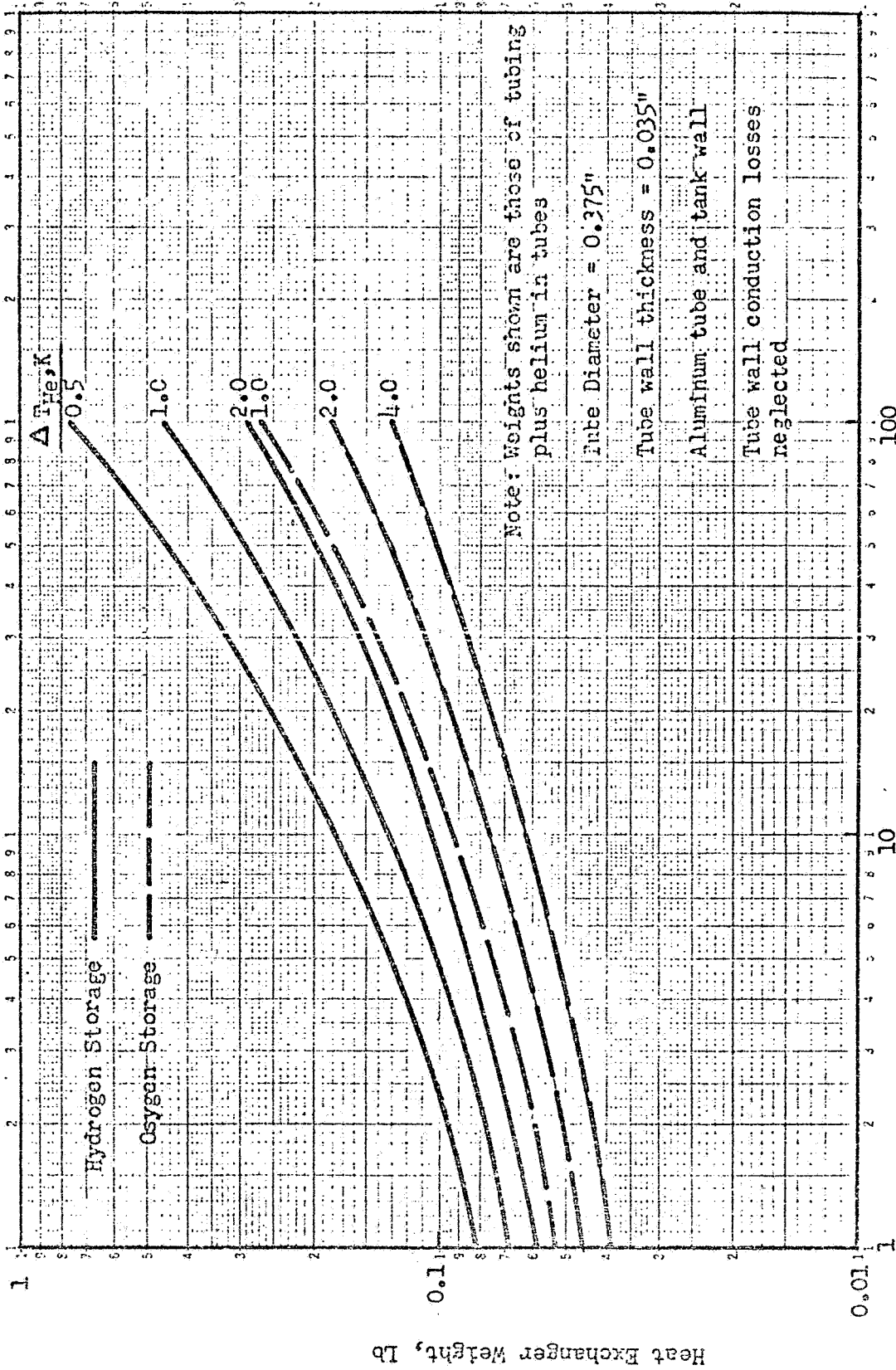
The procedure outlined in Section 8.2.3 has been carried out for a range of heat absorption rates and helium temperature rises. These calculations were performed for two cryogen storage temperatures, $20^\circ K$ (liquid hydrogen) and $90^\circ K$ (liquid oxygen) and for an assumed tubing diameter of 0.375 inches. It was also assumed that circumferential temperature gradients around the tubing walls were small, so that Equation (8-12) could be used.

The results of these computations are shown in Figures 8-4 and 8-5. The tank wall surface area required for the exchanger is plotted in Figure 8-4, and the tubing weight, plus the weight of helium contained in the tubing is plotted in Figure 8-5. It can be seen from these results that both the



Heat Absorption Rate, q , Watts

Figure 8-4 Heat Exchanger Surface Area Requirements



Heat Absorption Rate, q, Watts

Figure 8-5 Tank Wall Heat Exchanger Weight

area and weight penalties associated with such an exchanger are fairly small, even for the highest rates of heat transfer.

8.3 FLUID CIRCULATION PUMPS

If a separate cooling loop is used to transfer the heat from the cryogen tank to the refrigerator, a small pump or compressor is required. No attempt has been made to design such a unit; however, in order to be able to estimate a complete system weight approximate weight and power data (Figures 8-6 and 8-7) has been supplied for a circulation unit. These data are based on the same reference as in Section 7. The power was computed assuming an adiabatic compression and compressor and motor efficiencies of 0.80 and 0.85 respectively. Since the units are rather small, a positive displacement type of compressor was envisioned; however, no attempt was made to do a design analysis. The weights are based on a minimum case and hardware weight of 3.0 LB.

8.4 CRYOGENIC HEAT PIPES

The design of cryogenic heat pipes follows essentially the same procedures as that for moderate and high temperature heat pipes. Due to the high internal pressures in cryogenic heat pipes while inoperative at ambient temperatures, the pipe wall thickness, and thus the total weight, is somewhat higher than that of moderate temperature heat pipes. Internal pressures can range from 1 to 3000 psia.

The design equations presented in Section 7 may also be used for the design of cryogenic heat pipes. However, the unique properties of cryogenic fluids require special consideration.

8.4.1 Fluid Selection

The factors described in Section 7 related to the wicking limit, boilout limit and the gas choking limit also apply to cryogenic fluid selection.

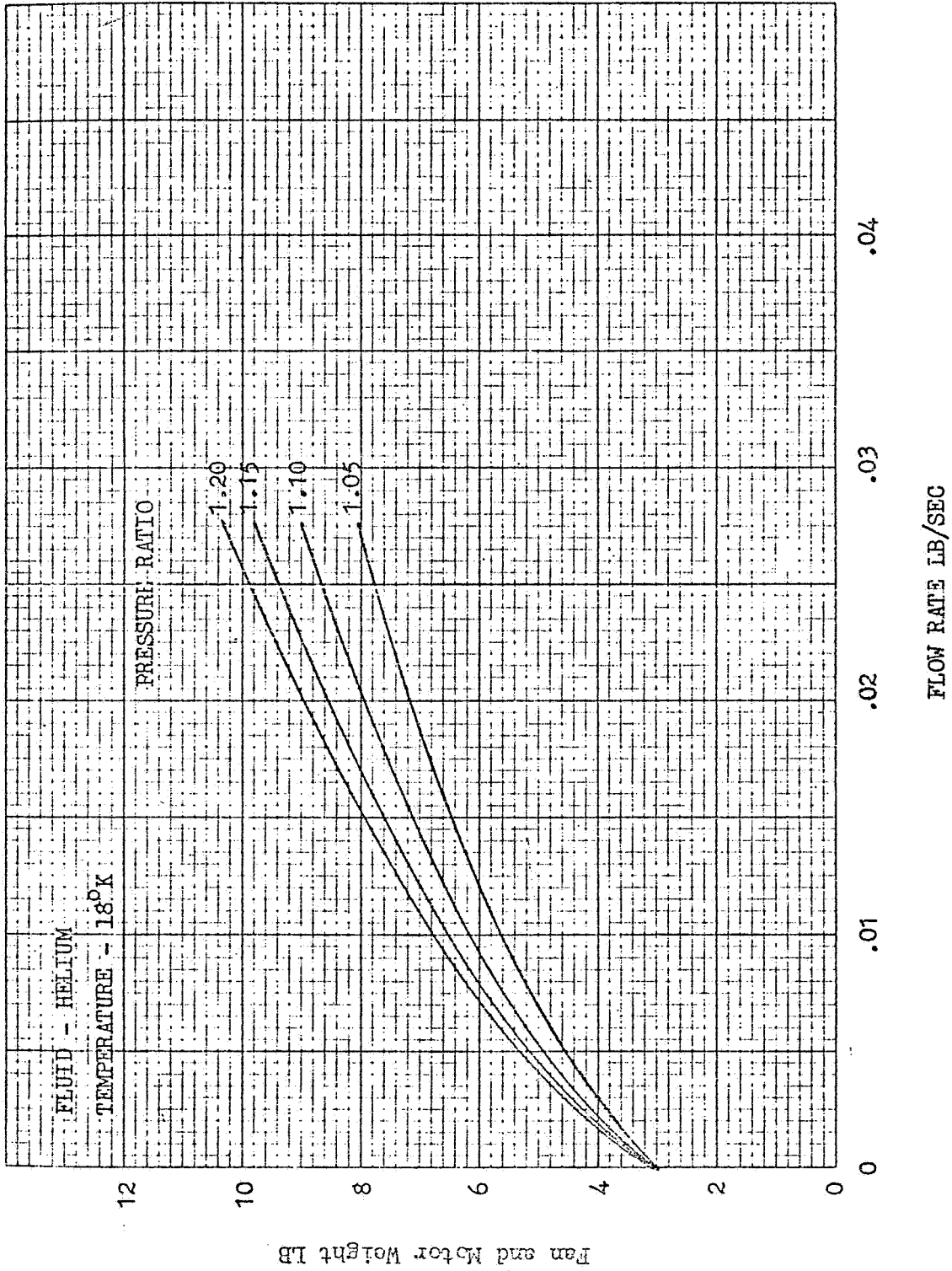


Figure 8-6 Helium Circulation Fan and Motor Weight

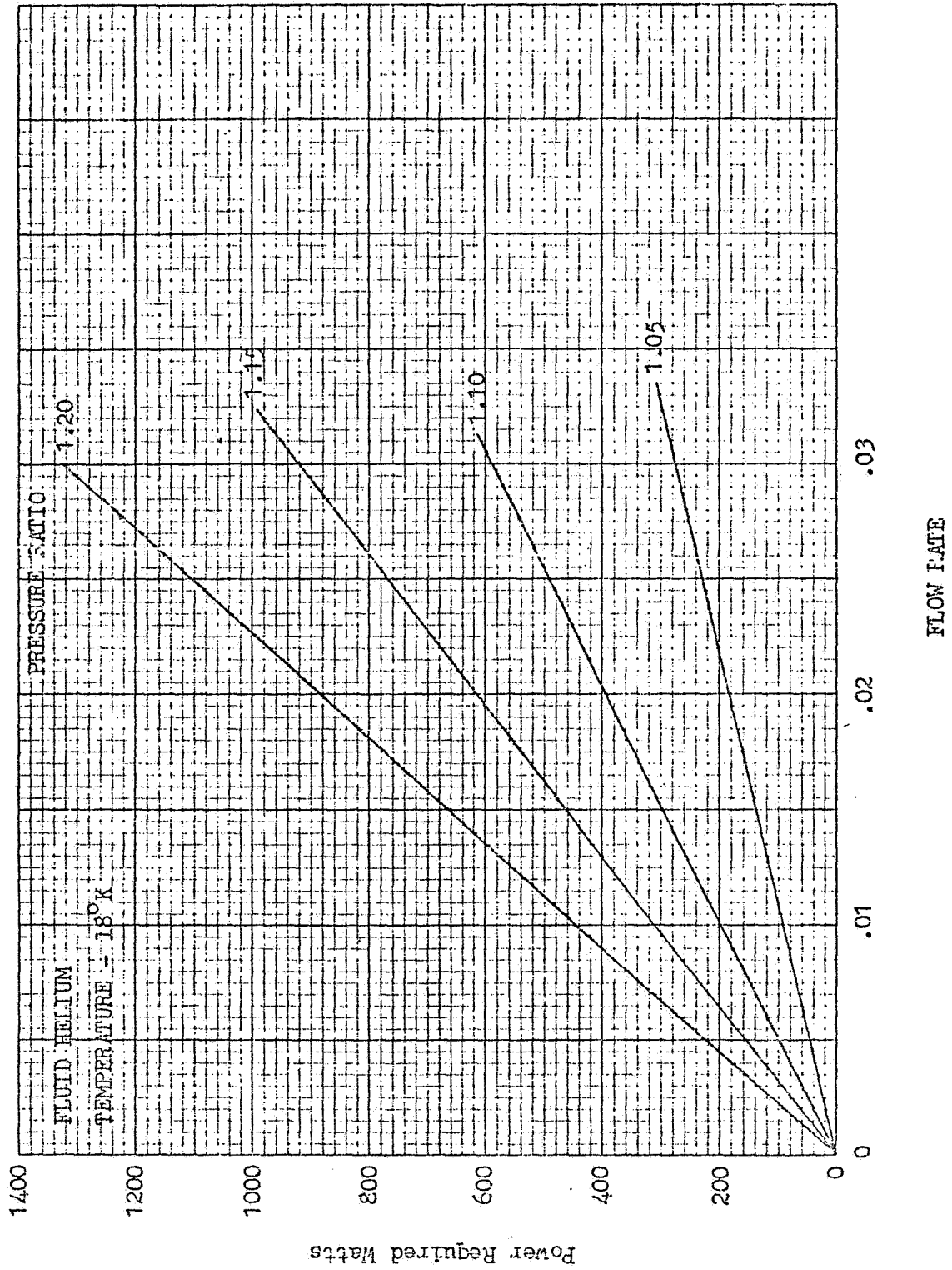


Figure 8-7 Helium Circulation Power

The optimization parameters G_1 , G_2 and G_3 are shown for three fluids, nitrogen, oxygen and fluorine, in Figure 8-8 in for hydrogen in Figure 8-9. The normal boiling point to critical point temperature range is shown in Figure 8-10 for several additional fluids.

8.4.2 Evaporator and Condenser Temperature Drops

A major cause of poor cryogenic heat pipe performance can be attributed to boiling in the evaporator. Brentari and Smith (Reference 8-4) have compiled data for nucleate boiling of LH_2 , LN_2 and LO_2 at one atmosphere. Values of nucleate boiling heat flux from this reference have been plotted in Figure 8-11 for these fluids. These data show that nucleation may begin at $2^\circ K$ of superheat and a heat flux of approximately 0.2 W/ft^2 for LN_2 or LO_2 . These small superheat values emphasize the need to minimize the temperature drop across the evaporator wick. This can be accomplished in three ways: (1) the evaporator area can be increased to reduce the radial heat flux density; (2) the wick-liquid matrix can be reduced in thickness; or (3) the thermal conductivity of the wick can be increased. The most appealing of these alternatives is generally that of reducing the wick thickness; however, this alternative may lead to practical difficulties. For example, with LN_2 or LO_2 the excess ΔT across the evaporator should be kept below $3^\circ K$ in order to prevent excess superheating in the wick structure. The corresponding value of (Q/A) maximum from Figure 8-11 is about 0.5 W/cm^2 . Rewriting Equation (7-42), we get

$$t = \frac{\Delta T}{Q/A_e} K_m = 6 K_m, \text{ cm} \quad (8-14)$$

If the thermal conductivity of the wick matrix is assumed equal to that of the liquid alone, then the wick thickness for LO_2 would be $8 \times 10^{-3} \text{ cm}$. This is an extremely thin wick which would be difficult to manufacture and would have very low capacity for axial flow.

On the other hand, the use of a sintered metal wick can provide conductivities close to those obtained assuming parallel conduction paths (see Section 7.5.2).

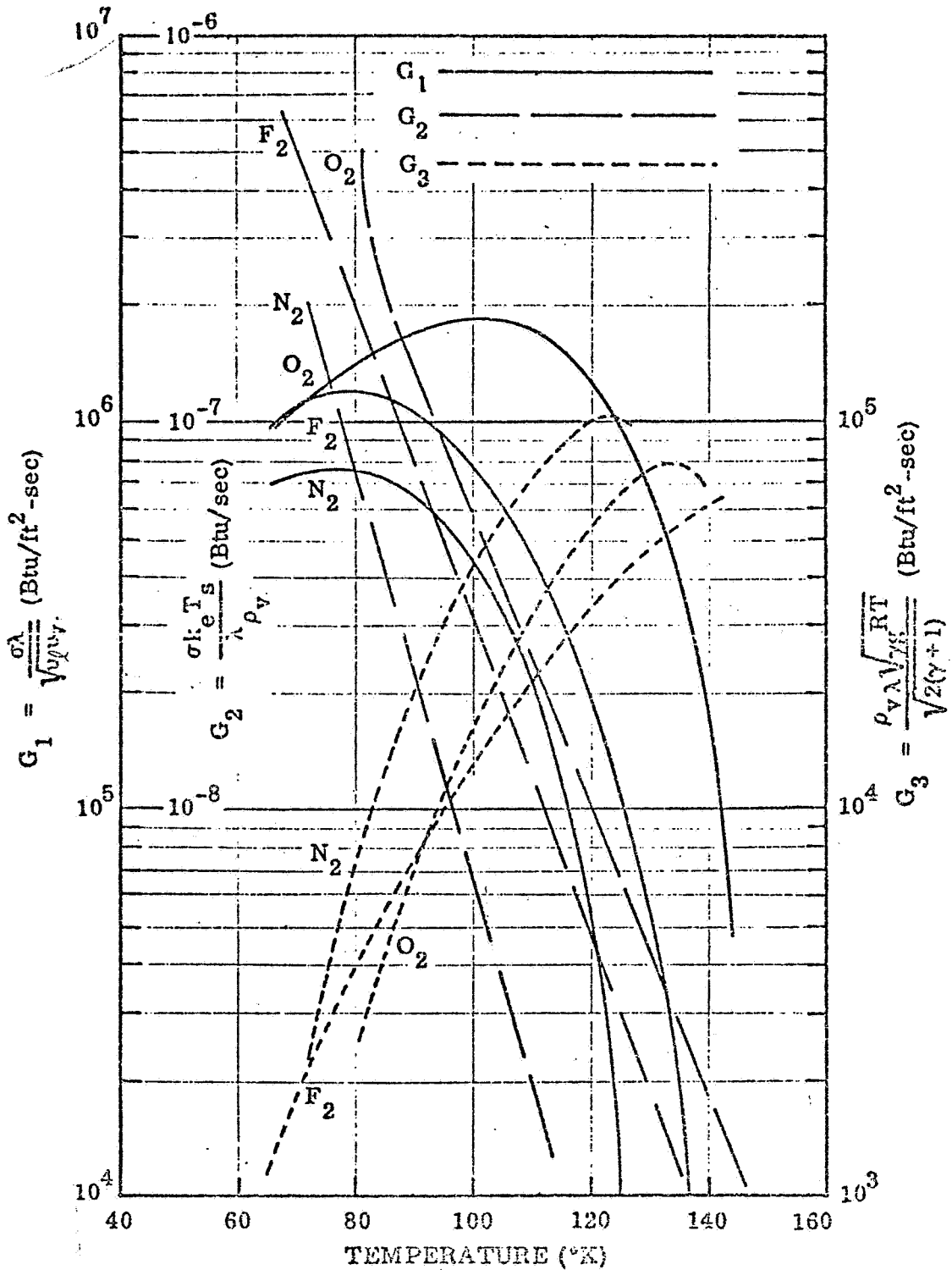


Figure 8-8 Fluid Property Groups at Low Temperatures

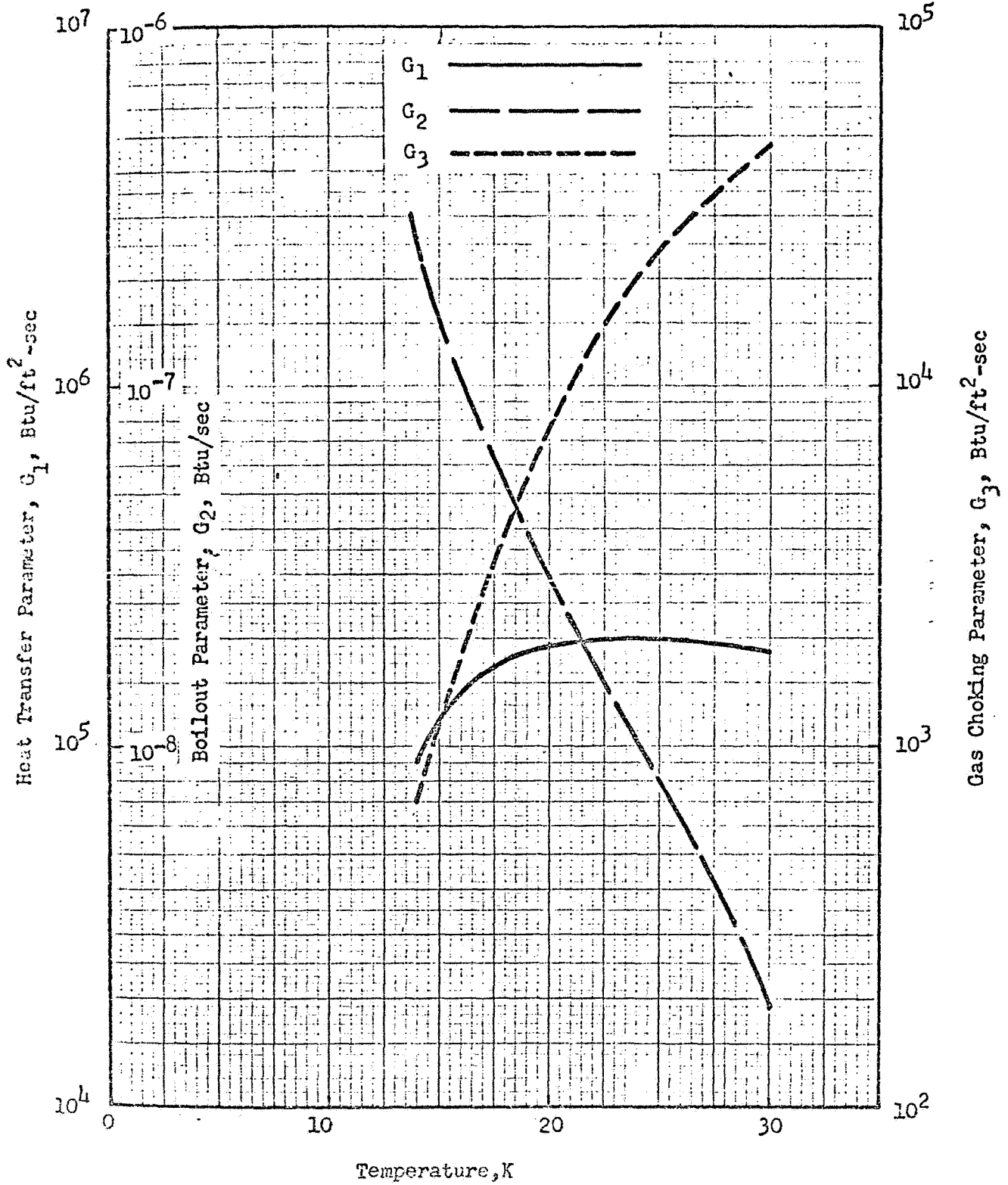


Figure 8-9 Fluid Property Groups at Low Temperatures (Hydrogen)

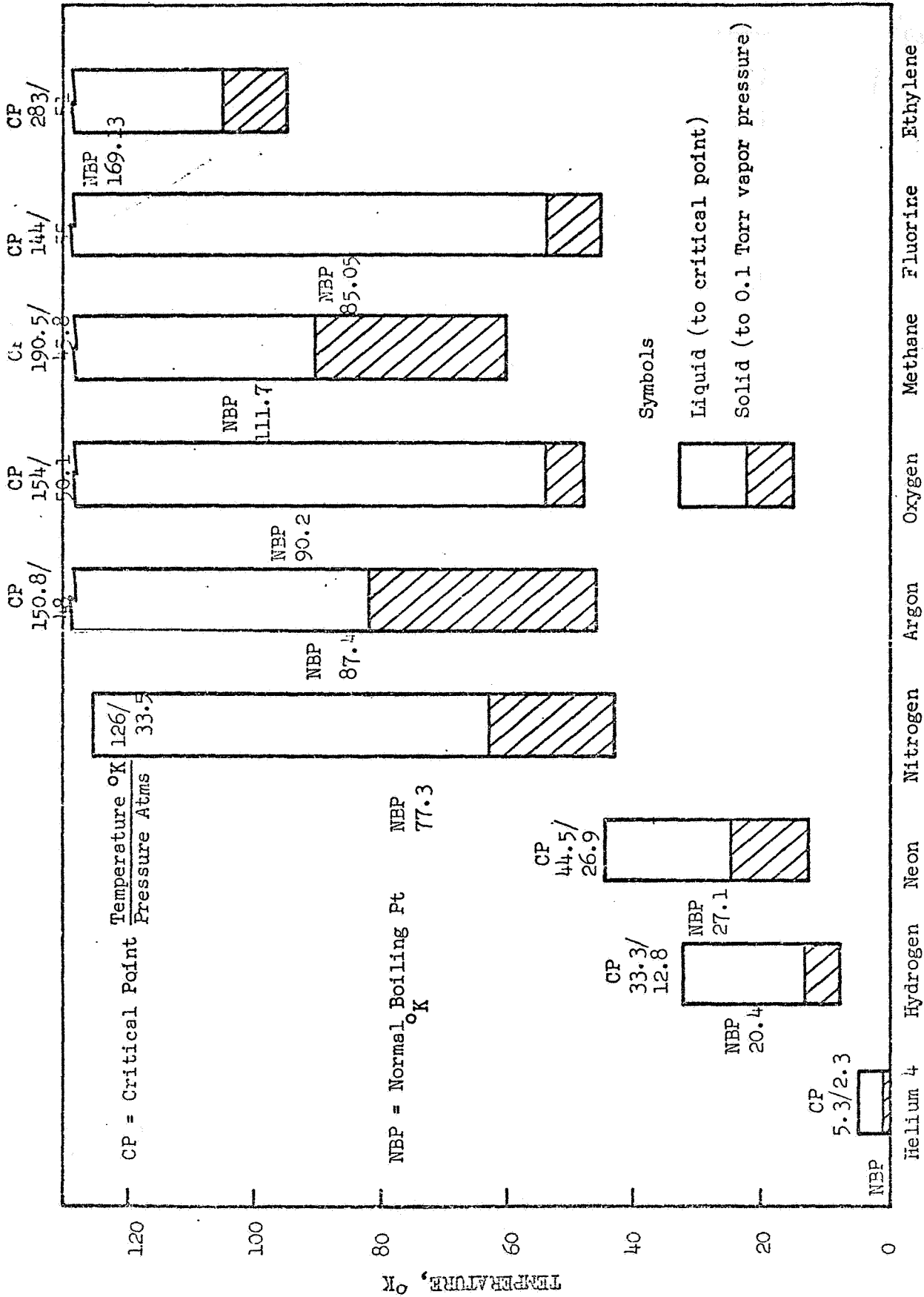


Figure 8-10 Cryogenic Heat Pipe Fluids

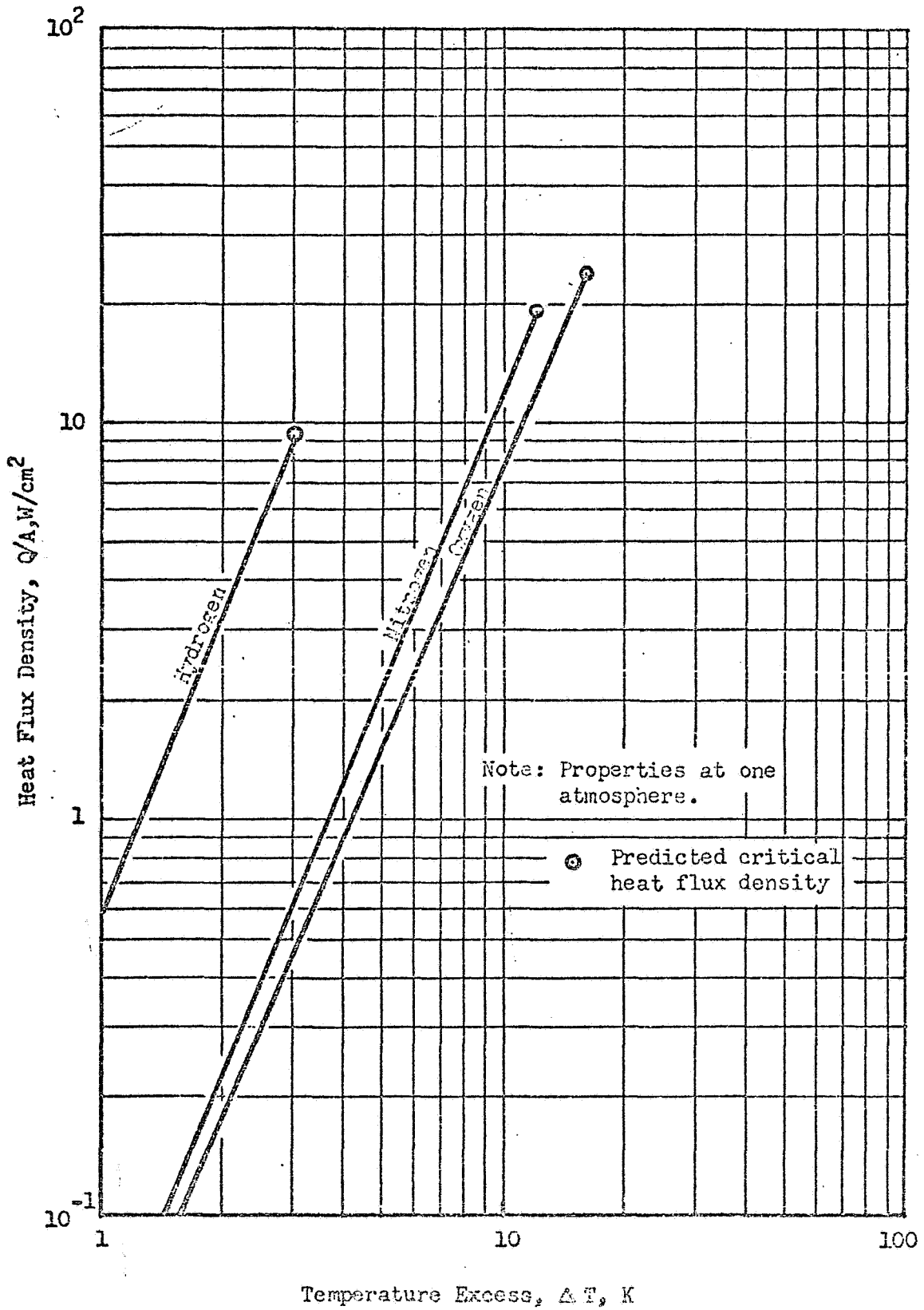


Figure 8-11 Nucleate Boiling Heat Fluxes for Cryogenic Fluids

Using such a wick, the matrix conductivity can be increased sufficiently to provide a maximum wick thickness on the order of 0.1 cm. It is for this reason that the use of thin sintered metal wicks in the evaporator section is desirable.

8.4.3 Wick Design

Figures 8-12 and 8-13 show a comparison of optimized homogeneous and channel wicks using equations (7-35) and (7-36). Values of the wick characteristic parameters used were $\epsilon = 0.8$, $b = 20$ and $K = 1.5$. These results show that channel wicks give better zero-g performance than homogeneous wicks, but degrade rapidly at higher acceleration.

8.4.4 Size and Weight

The size and weight of a cryogenic heat pipe are dependent upon a combination of design factors. These include the required heat transfer capacity, overall length and diameter, materials used and maximum internal pressure.

The internal pressure of a cryogenic heat pipe at ambient temperature ($0^{\circ}\text{F} - 120^{\circ}\text{F}$) is given by

$$P = Z\rho_{\text{HP}} RT \quad (8-15)$$

where

$$\rho_{\text{HP}} = \rho_{\ell} \frac{V_{\ell}}{V_{\text{TOT}}}$$

For a particular pipe and wick combination, the values of V_{ℓ} and V_{tot} are fixed for a saturated wick. Therefore, the pressure will be only a function of Z , ρ_{ℓ} , R and T . The compressibility factor Z for a real gas is pressure and temperature dependent. In evaluating the factor Z , it is useful to determine the reduced pressure and reduced temperature

$$P_r = \frac{P}{P_c} \quad (8-16)$$

$$T_r = \frac{T}{T_c} \quad (8-17)$$

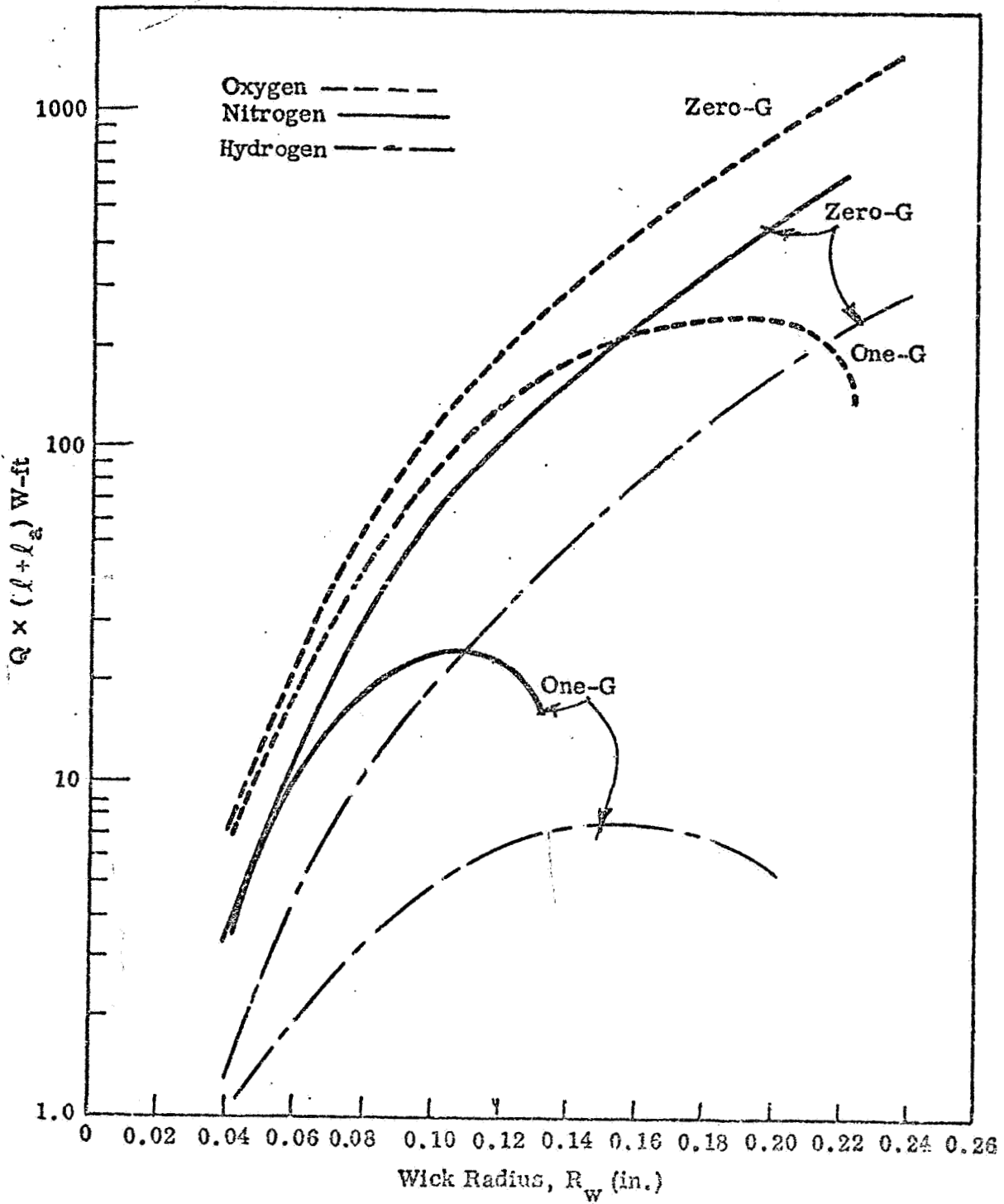


Figure 8-12 Homogeneous Wick Heat Pipe Performance

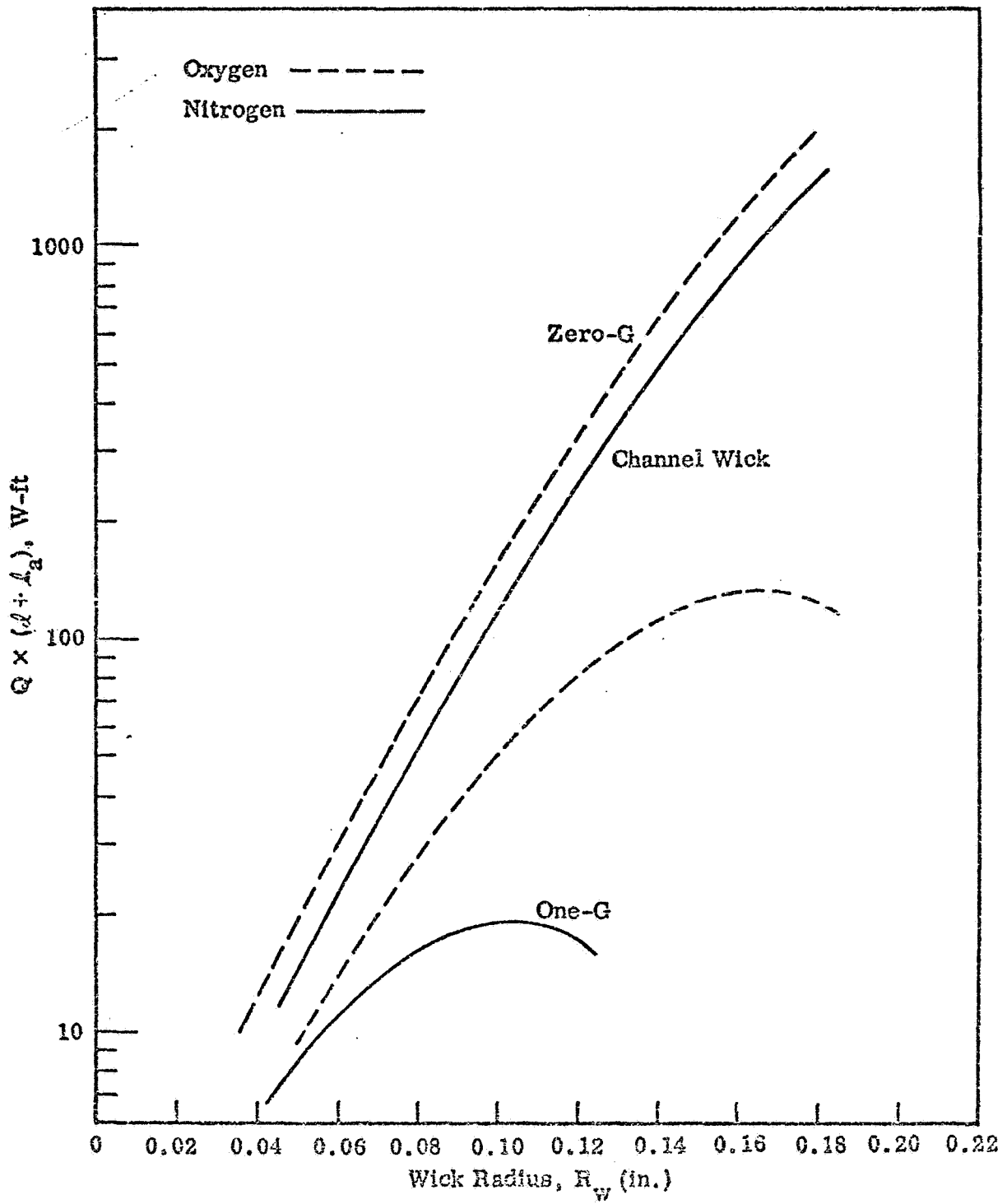


Figure 8-13 Channel Wick Heat Pipe Performance

The reduced temperature can be determined since the critical and ambient temperatures are known. However an iteration procedure using equation (8-10) and (8-17) and a Z versus P_r chart (Figure 8-14) is necessary for determination of the final pressure P.

Figure 8-15 is a plot of $\frac{PV_\ell}{V_{tot}}$ versus temperature for the three liquids. To apply Figure 8-15, the open volume of the wick and the total open volume of the heat pipe must be known. Since the ratio \bar{V}_g/V_{tot} is constant, Figure 8-15 shows that a nitrogen heat pipe would have the lowest pressure at ambient temperature.

The pressure at a given temperature can be significantly reduced by increasing the specific volume. This can be accomplished by decreasing the open volume of the wick; increasing the vapor volume or using a less dense working fluid.

Figures 8-12 and 8-13 can be used to calculate heat pipe size required for a given power and length. Once the pipe wall thickness has been determined, the system weight can be calculated from the known dimensions and material densities. Figure 8-16 is a plot of the power length product, $Q(l+l_a)$ as a function of heat pipe weight for two fluids, oxygen and nitrogen.

8.4.5 Heat Pipe Insulation

The possible long length of the heat pipe (up to 5 ft.) and the high surrounding temperatures dictate that some provision be made to reduce the radiation heat load into the adiabatic section. The simplest such provision would be to gold plate the outer surface of the heat pipe. Figure 8-17 shows the radiation heat load into a heat pipe at 80°K from surroundings at 320°K. Emittances of 0.01, 0.03 and 0.1 have been assumed in order to cover the range of possible metal surfaces.

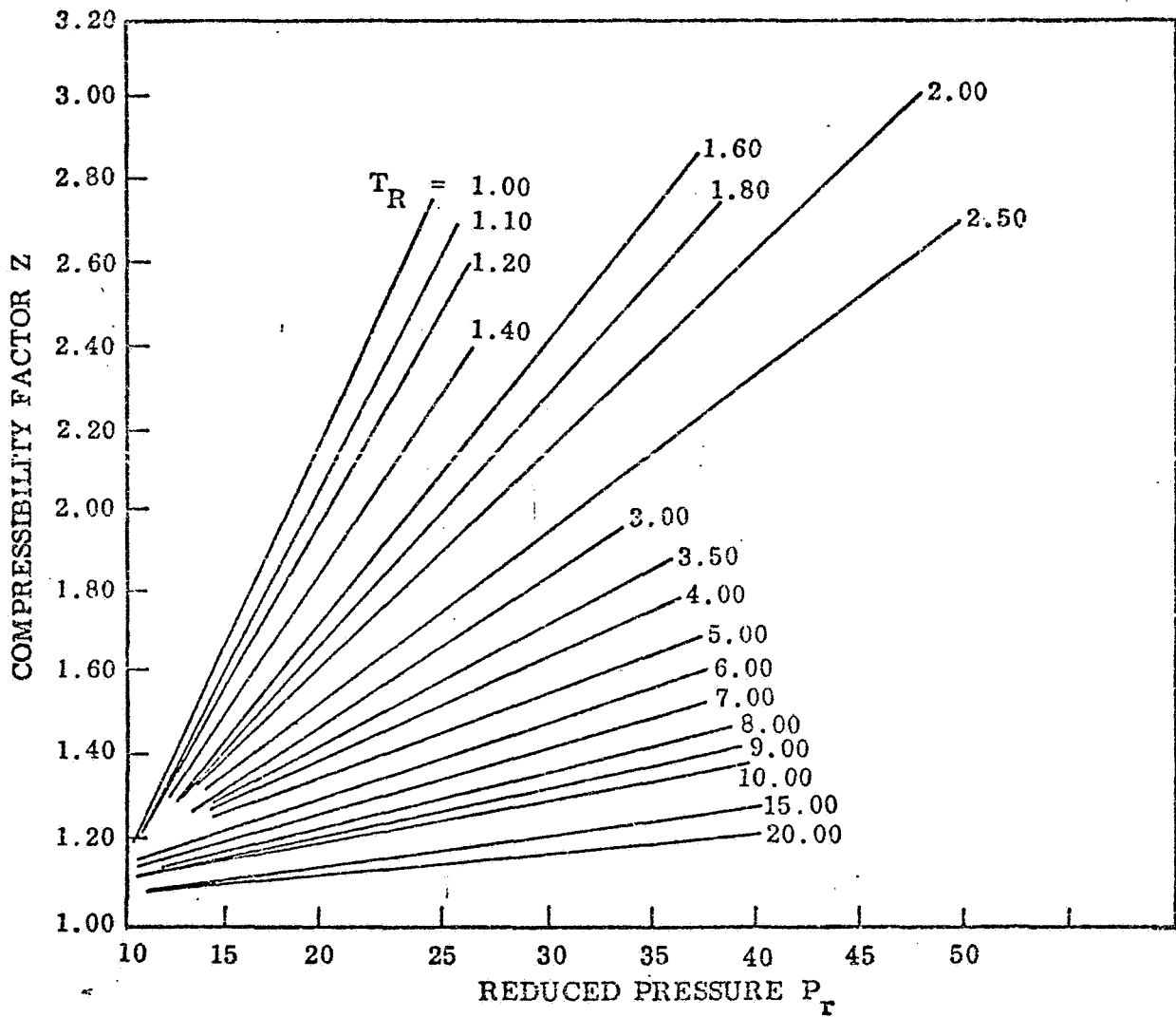


Figure 8-14 Compressibility Factor of Real Gases

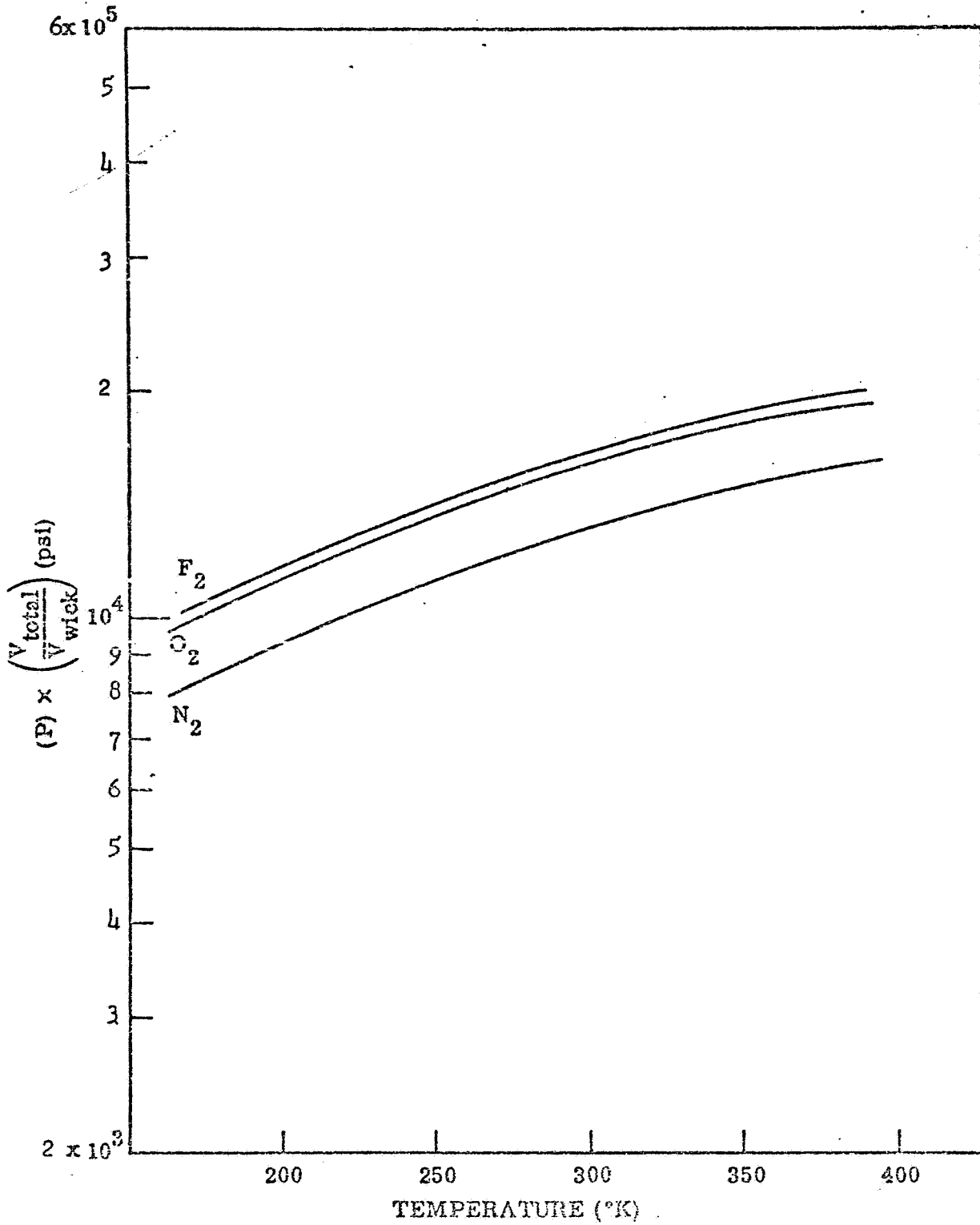


Figure 8-15 Relative Operating Pressures for Nitrogen, Oxygen, and Fluorine Heat Pipes

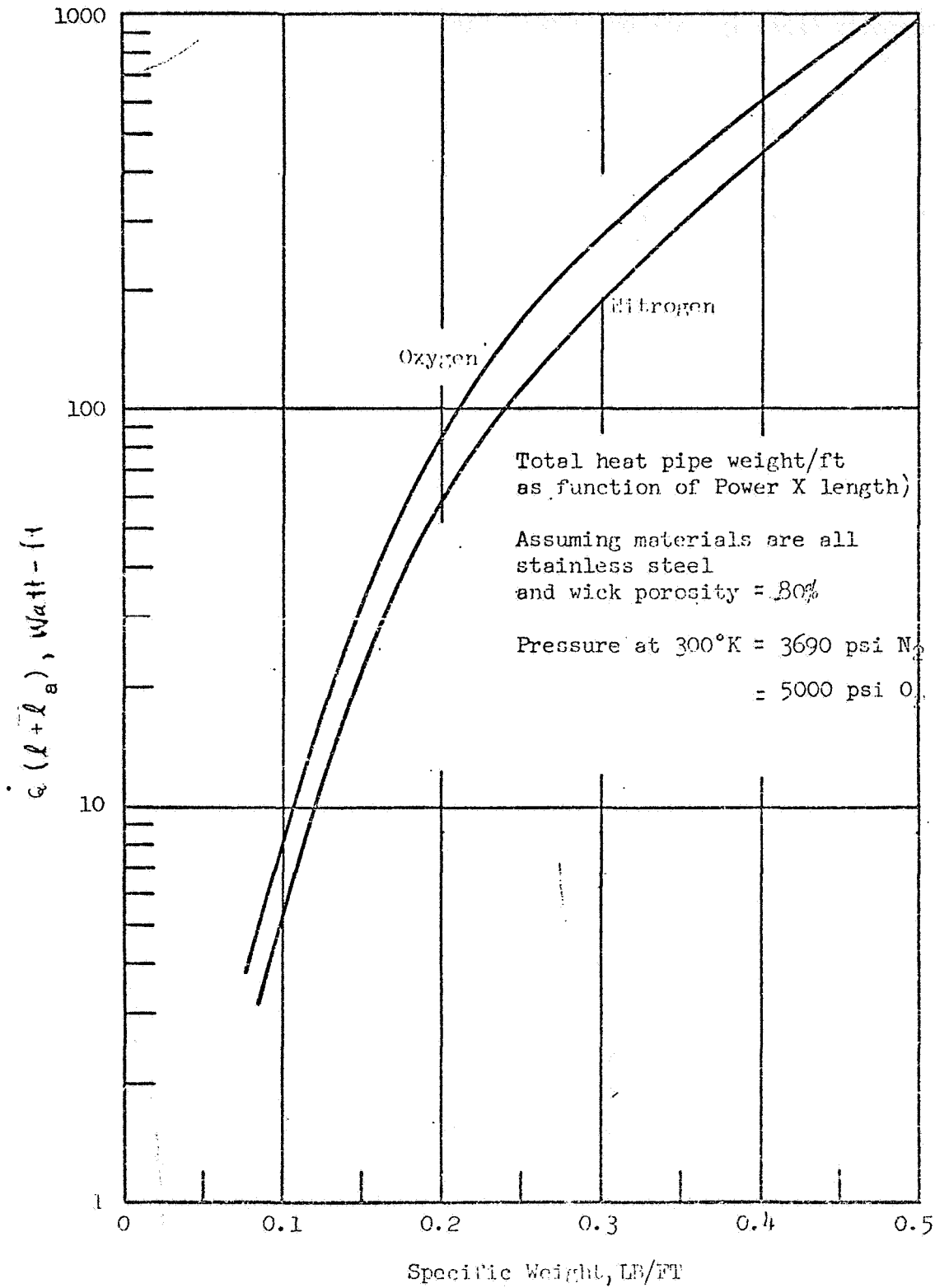


Figure 8-16 Cryogenic Heat Pipe Weight

A system using only a gold plated surface ($\epsilon = 0.03$) offers the advantage of simplicity of construction and a low heat capacity which is desirable since the heat capacity directly influences the start up time.

An improvement over a simple surface coating is achieved by using a few wraps of double goldized Mylar. The spacer between the wraps would be nylon net to reduce the level of offgassing and flaking experienced with glass cloth spacer materials, and to prevent absorption during storage in a humid environment.

Figure 8-18 shows a plot of the heat leak from 330°K into an insulated pipe at 77°K for a system with $\frac{1}{4}$ " of goldized mylar multilayer for various pipe diameters. The advantage gained with the multilayer system over that of a simple low emittance is obvious.

8.5 SOLID CONDUCTION DEVICES

If it is feasible to locate the refrigerator in close proximity to the cryogen storage tank, then the use of solid conduction devices may offer weight and space advantages in comparison to heat exchangers or cryogenic heat pipes. If the conductor is well insulated, the rate of heat conduction in a longitudinal direction is simply

$$q = KA \frac{\Delta T_{\text{COND}}}{L}$$

where

- K = thermal conductivity
- A = conductor cross-sectional area
- ΔT = temperature drop between refrigerator cold finger
and cryogen tank
- L = conductor length

From the above equation the weight per unit length of a solid conductor is given by

Heat Pipe Exterior Coated with Low Emittance Coating, No Additional Thermal Insulator

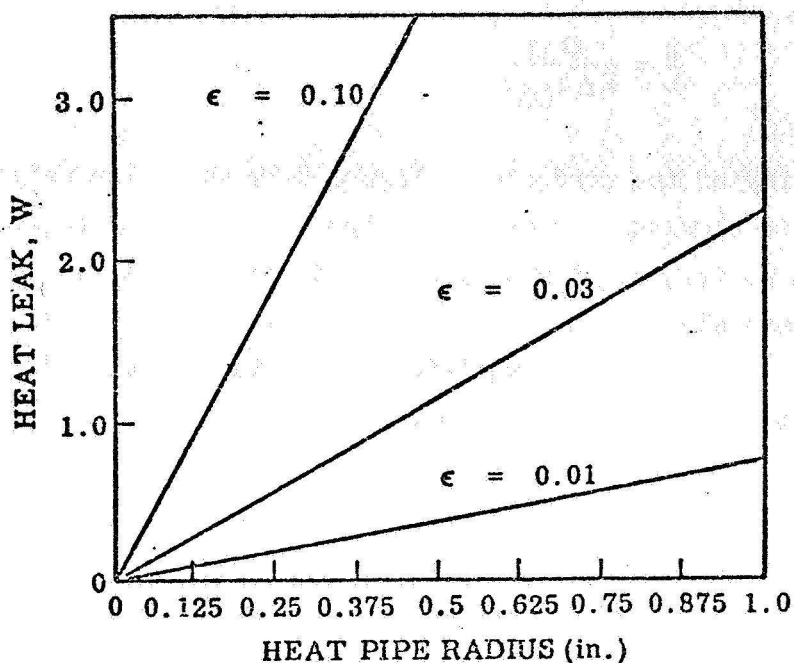


Figure 8-17 Heat Leak as a Function of Heat Pipe Radius for a 5-ft Long Pipe with No Exterior Insulation

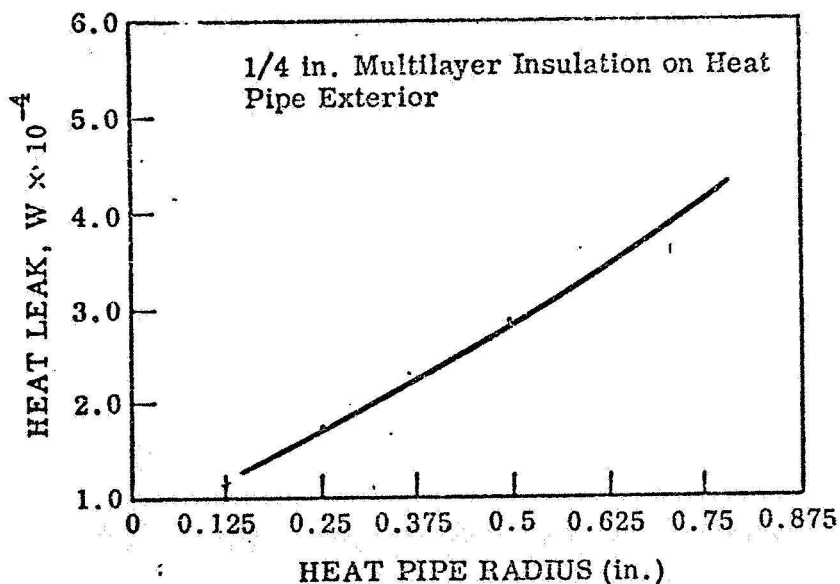


Figure 8-18 Heat Leak as a Function of Heat Pipe Radius for a 5-ft Long Pipe with a Multilayer Insulation

$$\frac{W}{L} = \frac{\rho qL}{K\Delta T_{\text{COND}}} \quad (8-18)$$

where ρ is the density of the conductor. Figure 8-19 shows the weight per unit length of a solid aluminum bar as a function of heat flux transmitted from a liquid oxygen container. For purposes of comparison similar data for an oxygen heat pipe are also shown. It can be seen that only for very low power-length products (less than 0.5 watt-feet) does the solid conductor compete in weight with the oxygen heat pipe.

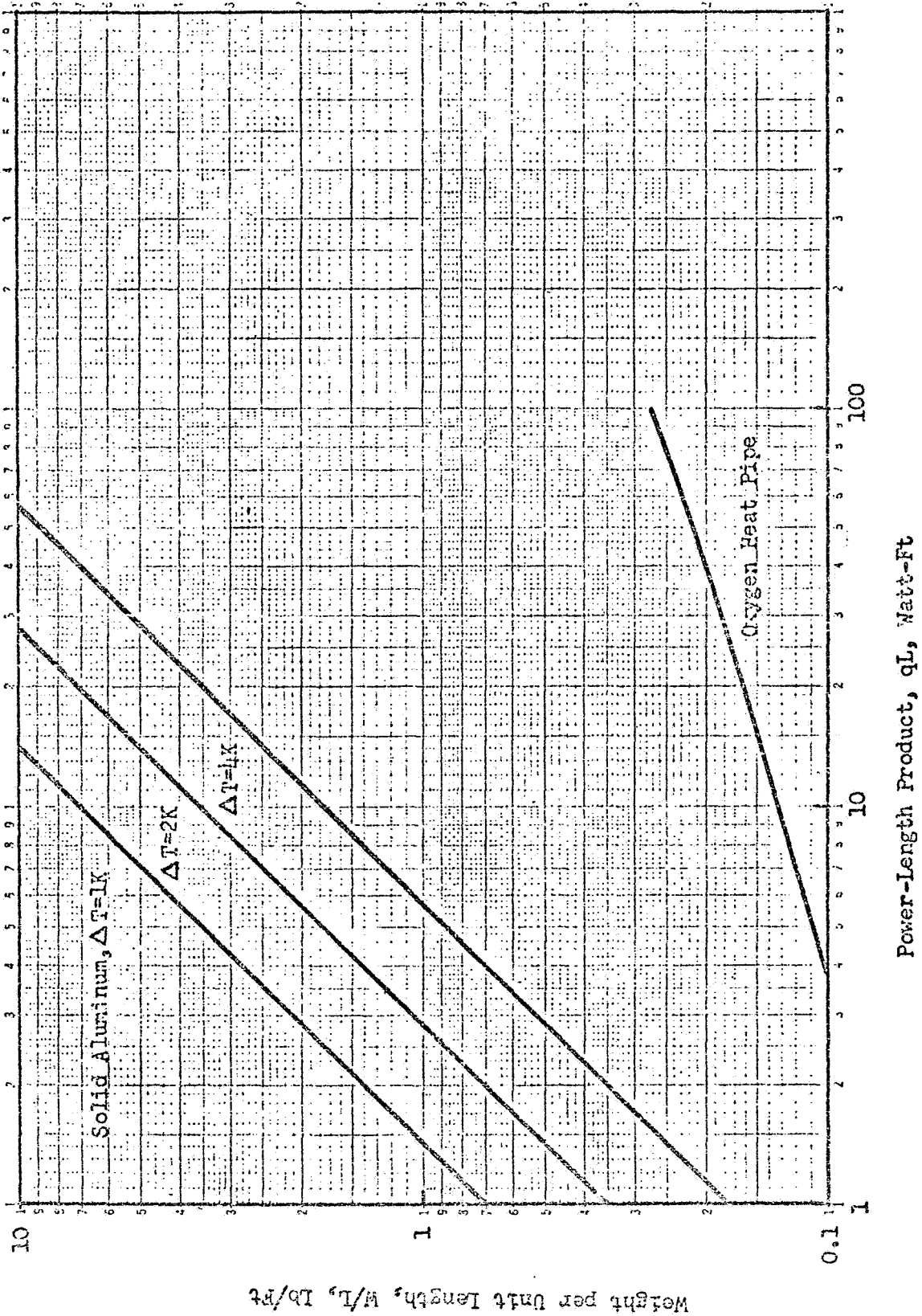


Figure 8-19 Weight of Solid Conductor for Liquid Oxygen Storage

REFERENCES

- 8-1 Kays, W. H. and A. L. London, "Compact Heat Exchangers," The National Press, Palo Alto, California, 1955.
- 8-2 Radiator Design for Space Vehicles, Airesearch Division, The Garrett Corporation.
- 8-3 Johnson, V. J., Ed., "Compendium of the Properties of Materials at Low Temperatures," Phase I, Cryogenic Engineering Laboratory, Boulder, Colorado, December 1959.
- 8-4 Brentari, E. G., Giarratano, P. J., and Smith, R. V., "Boiling Heat Transfer for Oxygen, Nitrogen, Hydrogen and Helium," NBS-TN-317, National Bureau of Standards, Boulder, Colorado.

Section 9

POWER SUPPLIES

9.1 SUMMARY

A survey of space electrical power systems which could serve as electrical power sources for external refrigeration systems for long-term cryogenic storage was conducted. Brief descriptions were prepared on the candidate power sources with schematics, figures, and tables to aid in screening and selecting an electrical power system.

The possible use of radioisotopes or solar collector/absorbers as a source of thermal energy for a heat-powered refrigeration device was also examined and descriptions of these two types of heat sources were prepared.

For long-life space electrical power systems in the 100 - 1,000-watt range, rigid solar photovoltaic systems and RTG's are the primary candidates. Typically, solar photovoltaics will provide 8 - 10 watt/lb and RTG's 1 - 2 watt/lb. RTG's are small (a 40-watt SNAP-19 requires about $2\frac{1}{2}$ ft³), are not constrained by sun-orientation requirements, but do create potential radiological hazards for the mission. Solar photovoltaic systems should be sun-oriented for maximum efficiency and large panel areas may be required (about 10 watt/ft²). Both solar photovoltaic systems and RTG's have been used in space missions and have been designed to satisfy launch environmental requirements.

Solar photovoltaic systems will require an auxiliary power system, e.g., batteries, if the particular mission involves periods of sun-shade and this added weight must be included under these conditions. Even with this constraint, unless there are overriding mission considerations that preclude the presence of external areas required for deployed solar photovoltaic panels, this will be the preferred source of electrical power in the 100 - 1,000-watt range. RTG's would be used when the solar photovoltaic systems were precluded.

In the 1 - 10-kilowatt electrical power range, solar photovoltaic systems will again be the primary candidate. Back-up candidates will be radioisotope-Brayton-cycle power systems and nuclear reactor power systems. Solar photovoltaic system's disadvantages of large external areas and sun-orientation requirements

apply and may preclude their use for certain missions. Development of deployable/retractable large area, lightweight solar photovoltaics (20 - 30 watts/lb) with specific stowage volumes of $1/2 - 1\frac{1}{2}$ kw/ft³ extends their application to this power range and strengthens their competitive position.

If mission considerations preclude the use of solar photovoltaic systems, then an isotope-Brayton-cycle power system becomes the preferred system. It has a specific weight of 1.0 watt/lb including an isotope re-entry vehicle and a 500-lb nuclear radiation shield. This system will require about 350 ft³ and, for a nominal 10-kw system, a radiator surface area of about 550 ft².

Nuclear reactor power systems would not normally be selected for space electric power below 10 kilowatts because of fixed weight penalties associated with the nuclear radiation shield required for space missions. However, if they were to be the primary spacecraft power system, then they would be competitive candidates to provide electrical power to external refrigeration systems for long-term cryogenic storage. Specific powers, without nuclear shielding, range from about 1.5 - 6 watts/lb. Depending on how the added power was to be obtained, e.g., off-design performance or optimized at the new power level, weight penalties would accrue primarily from increased radiator area and added nuclear shielding to accommodate the increased reactor power level since much of the other system weight would remain fixed.

9.2 ELECTRICAL POWER SYSTEMS

9.2.1 Solar Photovoltaic Power Source

Where spacecraft energy requirements have precluded the practical use of batteries, the primary power source generally used has been a solar photovoltaic conversion array. Such arrays have been used to provide power ranging from the 5-watt Vanguard to over 1 kw for the Orbiting Astronomical Observatory. Arrays are under development to provide multi-kilowatts of electrical power for future space missions.

Solar cell arrays are relatively lightweight and have proven to be very reliable power sources in a space environment. They have been used in sun-oriented and in unoriented configurations and as spacecraft body-mounted arrays, as well as deployed panels. Their operation requires exposure to sunlight and a supplementary power source must be on board if the mission profile results in the arrays being in shadow during some part of the mission. Projected use of solar cell arrays in the multi-kilowatt range emphasizes problems associated with their packaging, deployment, and orientation. Proposed solutions to these problems are under development by several contractors.

The basic element of a solar photovoltaic conversion system is a p-n junction semiconductor device which, when exposed to sunlight, converts the incident radiant energy in particular portions of the spectrum directly into electrical energy. Typically, 2x2 cm individual n/p silicon solar cells at 60°C and air mass zero will provide on the order of 0.4 volts and 115 milliamps at maximum power. Solar cell arrays contain thousands of these individual semiconductor devices (typically 2 cm x 2 cm x 0.010 in n/p silicon) mounted in supporting structure and electrically connected in a series / parallel arrangement to provide the desired output electrical characteristics and reliability. A transparent protective cover material is used on each of the individual cells. Solar cell output characteristics vary with temperature and solar intensity. The power capability of a solar cell will therefore fluctuate markedly over the range of space environments encountered in planetary exploration, e.g., the power output at Venus perihelion may be about three times the output at Mars aphelion. (See Table 9-1 for typical characteristics.)

While electrical power requirements of about 1 kw or less can be reasonably accommodated with current technology by rigid panels, multikilowatt solar arrays with their associated large areas will employ different techniques. Many companies are actively studying large area solar cell arrays which use flexible substrates and three basic approaches appear evident: the use of a drum roll-out technique; the use of a flat-plate fold-out technique; and the use of a flat roll-out technique. It is anticipated that the development work in progress will result in solar photovoltaic power systems that will be competitive for power requirements up to about 50 kw with storage volumes of 0.5 to 1.5 kw/ft³.

Rigid solar panels, sun-oriented at 55°C, 1 AU, and zero air mass, will typically yield 8 - 10 watt/lb and 10 watt/ft² with silicon solar cells. Use of 8 - 10 mil cells and 1 - 3 mil covers may allow this to increase to 15 - 25 watt/lb and 10 watt/ft². Roll-up designs exist which give 30 - 35 watt/lb and 10 watt/ft²; fold-up designs exist that give up to 40 watt/lb and 10 watt/ft²; and the LMSC fold-up flexible solar array design for NASA-Houston will give about 10 watt/lb and 10 watt/ft². These watt/lb numbers include the panels (with cells, substrates, etc.), structure and electrical wiring, and deployment and orientation devices, but do not include any battery weight.

Power allowance must be included in the design for power system degradation that will be experienced by the solar photovoltaic cells exposed to the space radiation environment. This degradation will be dependent upon the specific orbit parameters of the mission and may vary from 20 - 30% in 10 yr at synchronous orbit to as high as 40% in 2 yr at low earth orbit when the spacecraft transits in and out of the radiation belts during its orbits.

Although silicon solar cells have been the type used for space power, mention should be made of efforts directed towards development of thin-film cadmium sulfide solar cells. While these devices have a lower conversion efficiency, they are fabricated on a thin sheet of plastic that can conveniently be rolled up for storage and unrolled for deployment. Their use offers promise of a multi-kilowatt array with a specific power of 25 - 30 watt/lb and 5 - 6 watt/ft².

TABLE 9-1

SOLAR PHOTOVOLTAIC POWER SYSTEM CHARACTERISTICS*

<u>Type</u>	<u>Specific Power</u>	<u>Specific Area</u>	<u>Specific Volume</u>
Rigid Panel	8 - 10 w/lb	0.1 ft ² /w	-
Large Area Erectable Panel	10 - 40 w/lb **	0.1 ft ² /w	0.6 - 2 ft ³ /kw

* Typically:

Silicon n/p solar cells
 2 x 2 cm x 0.01 in thick
 with 0.03 - 0.04 in cover

Cell degradation with time is dependent on orbit parameters.

** Ranging from 10 - 12 w/lb for LMSC fold-up flexible array and Hughes large retractable array to designs of self-rigidized folded panels which offer up to 40 w/lb.

9.2.2 Battery Power Systems

Almost without exception, space power systems include chemical batteries. These batteries have served as primary batteries for providing launch vehicle power with attendant characteristics of high energy density, high current capacity, and good reliability. Batteries are also used as emergency power sources, requiring relatively long wet-stand capability, and as secondary batteries in conjunction with a primary power source, e.g., fuel cell or solar photovoltaic power systems. As secondary power systems they are used to provide peak power demands or during eclipse of the solar arrays, normal power demands. The discharge/charge periods for secondary batteries are determined by the specific type, their intended use, and the mission and power profiles. Reliability, longevity, and rechargeability are important characteristics of secondary batteries.

Batteries are electro-chemical devices. The basic element is a galvanic cell packaged in such a way that the oxidation-reduction reaction does not occur until an external circuit is closed. The reactants are mounted on current-collecting electrodes separated by a separator that acts as a carrier and immobilizer for the electrolyte. Individual cells are electrically connected to provide the desired output characteristics and physically enclosed in a case, typically prismatic for space batteries. The cell reaction proceeds at a rate controlled by the circuit resistance to electrical current. When a cell can be used only once, it is called a primary cell. When the chemical reaction can be reversed by applying electrical energy to the cell, it is called a secondary cell and can be used as an energy storage device. The need for careful control of quality and uniformity in cell and battery manufacture cannot be overemphasized for maximum utilization of battery weight and to avoid cell mismatching during discharging/charging cycles leading to different levels of state-of-charge and cell reversal or severe overcharge with pressure generation and cell rupture.

The types of space batteries used have been primarily nickel-cadmium, silver oxide-cadmium, or silver oxide-zinc. However, research is continuing on other battery systems, e.g., those which use organic solvents and high-activity

electrode materials to obtain energy densities above 200 watt-hr/lb. In common with many spacecraft systems, and despite their extensive use, the lack of performance characteristics data usable by power system design engineers and a lack of standardization of cells, testing conditions, and data reporting are frequently cited as shortcomings of battery technology.

The nickel-cadmium battery has the highest survivability and longest cycle life of the secondary batteries. It is frequently used in long-life applications even though heavier than the silver oxide-cadmium battery. Characteristics of an LMSC type XI, 20 amp-hr nickel cadmium battery are given in Table 9-2.

The silver oxide-zinc battery is a highly reliable primary battery (activated immediately prior to use) with energy densities up to 100 watt-hr/lb, and is often used in launch vehicles. As a secondary battery special separators are added to improve wet stand (up to 1 yr) and rechargeability. As a secondary battery high current performance is poorer than as a primary battery, but the energy density remains high. Characteristics of an LMSC Type 25 secondary battery are given in Table 9-2.

Silver oxide-cadmium batteries are seldom used as primary batteries, but as secondary batteries have an energy density about twice that of nickel-cadmium and a cycle life 1 - 2 orders of magnitude better than silver oxide-zinc batteries. Low cell voltage and power system voltage regulation are disadvantages but they are useful where rapid repetition of cycles is required. They have a wet-stand life of about 1 - 2 yrs. Typical characteristics of a silver oxide-cadmium battery are given in the table.

For battery power system design purposes, operating characteristics data are required for a wide range of system designs and environmental variables such as temperature, charge and discharge current, and system load characteristics and specifications. A NASA publication (NASA-SP-172)⁽¹⁾ identifies the maximum data required for a highly sophisticated battery power system as:

- discharge voltage as a function of time under the actual load conditions expected
- charge voltage and current as a function of time under the actual charging conditions expected

(1) Bauer, Paul: "Batteries for Space Power Systems", NASA SP-172, 1968

- . overcharge current requirements
- . quantity of electrical energy available from the battery at critical points in the mission and assurance that at all other periods energy availability exceeds requirements
- . rate of heat evolution as a function of time under the actual charge and discharge conditions expected and a complete temperature profile of the battery as a function of time
- . impedance and phase-shift characteristics of the battery as a function of frequency
- . efficiency of the battery's energy storage and its associated electronics
- . probability of battery failure as a function of time and conditions of use
- . battery voltage transients for critical load changes

Use of batteries as a primary source of electrical power for external refrigerator systems is constrained to relatively low-power, short-duration systems by the energy storage capacity of the battery. For example, an LMSC type I-E silver oxide-zinc battery has about 12,500 watt-hrs of energy, weighs about 125 lb, and occupies about 1.0 ft³. This battery could supply 100 watts of electric power to a small (45 watt thermal) refrigeration unit for only about 5 days.

TABLE 9-2
BATTERY POWER SYSTEM CHARACTERISTICS

<u>Type</u>	<u>Ni-Cd</u>	<u>Ag₂O-Zn</u>	<u>Ag₂O-Cd</u>
Oper Voltage	23.29 - 29.50	25	14.5
Oper Temp, °F	0 - 125	30 - 90	0 - 100
Dimensions	18.80"x7.750"x 6.50"	15.84"x 11.31"x 8.03"	~ 1 ft ³
Weight, Lb	62 (max)	116 (max)	~ 150
Rated Cap.	0 - 40°F, 17 ah 40 - 80 20 ah 80 -125 17 ah	300 ah	150 ah
Internal Impedance	0.05Ω (max) (70°F, 5 amp, 5 ah depth)	0.05 Ω	not avail.
Chg Rate	5 amp (max)	12 amp	6 amp
Wet Stand Life, 30°F	2.5 yr (disch)	0.5 yr	1 - 2 yr
Watt-Hr/Lb	8	65	~ 20
Number of cells	20	16	13
Typical Cycle Life *	4,000 cycles	100 cycles	1,500 cycles

* 50% depth of discharge; continuous 55-min charge and 35-min discharge cycling

9.2.3 Fuel Cell Power System

Fuel cells have been used as the primary electrical power source in Gemini, and the Apollo missions. In principle, a fuel cell can be considered as a battery in which fuel and oxidant are fed continuously from external storage tanks onto electrodes within the cell while reaction products are removed from the cell. Basic elements of a fuel cell power system include: the external case, negative and positive electrodes, electrolyte, inlets for the reactants, outlets for the chemical products and purging, fuel and oxidant storage and control equipment, heat removal and temperature control equipment, and chemical products removal equipment. Major variations in space-flight fuel cell systems from the different vendors occur in the electrodes and the techniques used in the control of reactants, product, and heat.

Within a fuel cell, chemical energy released by reactants via an electrolytic medium is converted into electrical energy. The electrodes serve as catalysts for the oxidation-reduction reactions and, in theory, remain chemically and structurally unchanged. Thermodynamically the cell voltage would correspond to the change in chemical free energy that occurs during the reaction if the system were reversible. In practice, as the current drawn increases, processes in the cell depart from equilibrium and the cell potential decreases. A key to success is the electrode, the catalyst it incorporates, and its design and construction. Suitable electrodes must admit correct amounts of reactants, provide catalyst surface for the reactions, and allow reaction products and electrons to flow quickly. The selection, design, and construction of the electrodes are determined by the type of fuel cell, i.e., nature of reactants, electrolyte composition, and overall design of the fuel cell.

Hydrogen and oxygen are the reactants used in the fuel cells that have been employed in space missions. Characteristics of the Gemini and Apollo fuel cells, as well as those under development at General Electric, Pratt-Whitney, and Allis Chalmers for space applications, are given in Table 9-3. A schematic of fuel cell power system elements is shown in Figure 9-1. In addition, General Electric has developed a 200-watt ion-exchange type fuel cell for the bio-satellite program. This fuel cell has a unit weight of about 30 lb and a

design life of 1,000 hours. Allis-Chalmers has developed a 200-watt radiatively cooled alkaline type fuel cell that weighs about 30 lb, occupies less than 0.5 ft³, and has a design life of 1,500 hours. The Allis-Chalmers fuel cell was flight-tested in 1966 and used a variable emittance technique (using louvers) to maintain the 190 - 220°F operating range. Both liquid- and gas-cooling techniques have also been used, e.g., Apollo fuel cells used a glycol cooling system.

Hydrogen-oxygen fuel cell performances are typically: 50 - 200 amperes per ft² of geometric surface area, 0.7 - 0.95 volts per cell, 0.75 - 1.5 kw per ft³, and 12 - 18 watts per lb. Specific fuel consumption ranges from 0.8 - 0.95 lb per kw-hr. Storage of hydrogen and oxygen for fuel cell operation to the fuel cell design life of 5,000 hr. becomes a major weight element that may constrain its competitive position. Reactants and tankage for 1 kw and 5,000 hr would typically weigh about 4,590 lb and 2,300 lb respectively when stored cryogenically and with no allowance for boiloff. Typical weight vs mission duration curves for 0.1, 1.0, and 10 kw hydrogen-oxygen fuel cell power systems are given in Figures 9-2, 9-3, and 9-4.

TABLE 9-3

HYDROGEN-OXYGEN FUEL CELLS

	<u>Gemini</u>	<u>Apollo</u>	<u>General Electric</u>	<u>Prett Whitney</u>	<u>Allis Chalmers</u>
Gross Pwr	1.05 kw	1.42 kw	5 kw	5 kw	2 kw
Type	Ion Exchange	Alkaline	Ion Exchange	Alkaline	Alkaline
Life	340 hr	400 hr	5,000 hr	5,000 hr	3,000 hr
Oper Temp	75°F	375 - 500°F	68 - 158°F	330 - 430°F	190 - 220°F
Weight	~ 175 lb	~ 220#	< 300#	< 300#	~ 170#
Efficiency	~ 50%	~ 70%	50 - 60%	65 - 70%	50 - 60%
Specific Power	~ 6 w/#	~ 6 w/#	> 16.7 w/#	> 16.7 w/#	~ 12.5 w/#
Specific Volume	~ 2 ft ³ /kw	~ 7 ft ³ /kw	~ 2 ft ³ /kw	~ 4.5 ft ³ /kw	~ 2.7 ft ³ /kw
Reactant Consum't'n	0.9 - 0.92#/kwh	1.166#/kwh at 1.42 kw	~ 0.9#/kwh	~ 0.8#/kwh	~ 0.85#/kwh
Parasitic Power	~ 5%	~ 5%	~ 4 - 5%	~ 4%	~ 5%
Tankage Wt	~ 100#	~ 1,600# *	--	--	--

9-12

* . Includes Life Support O₂

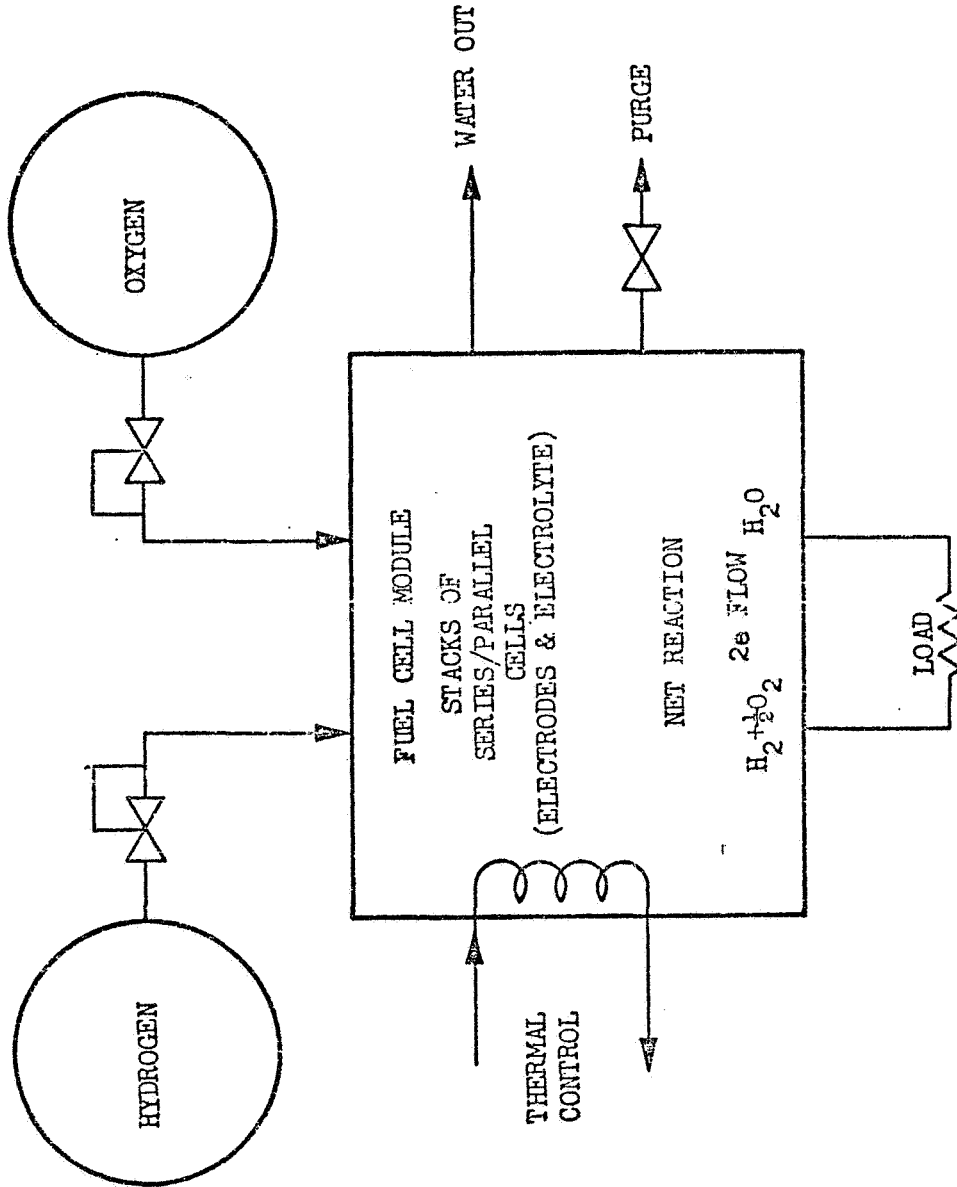


Fig. 9-1 SCHEMATIC OF HYDROGEN-OXYGEN FUEL CELL POWER SYSTEM

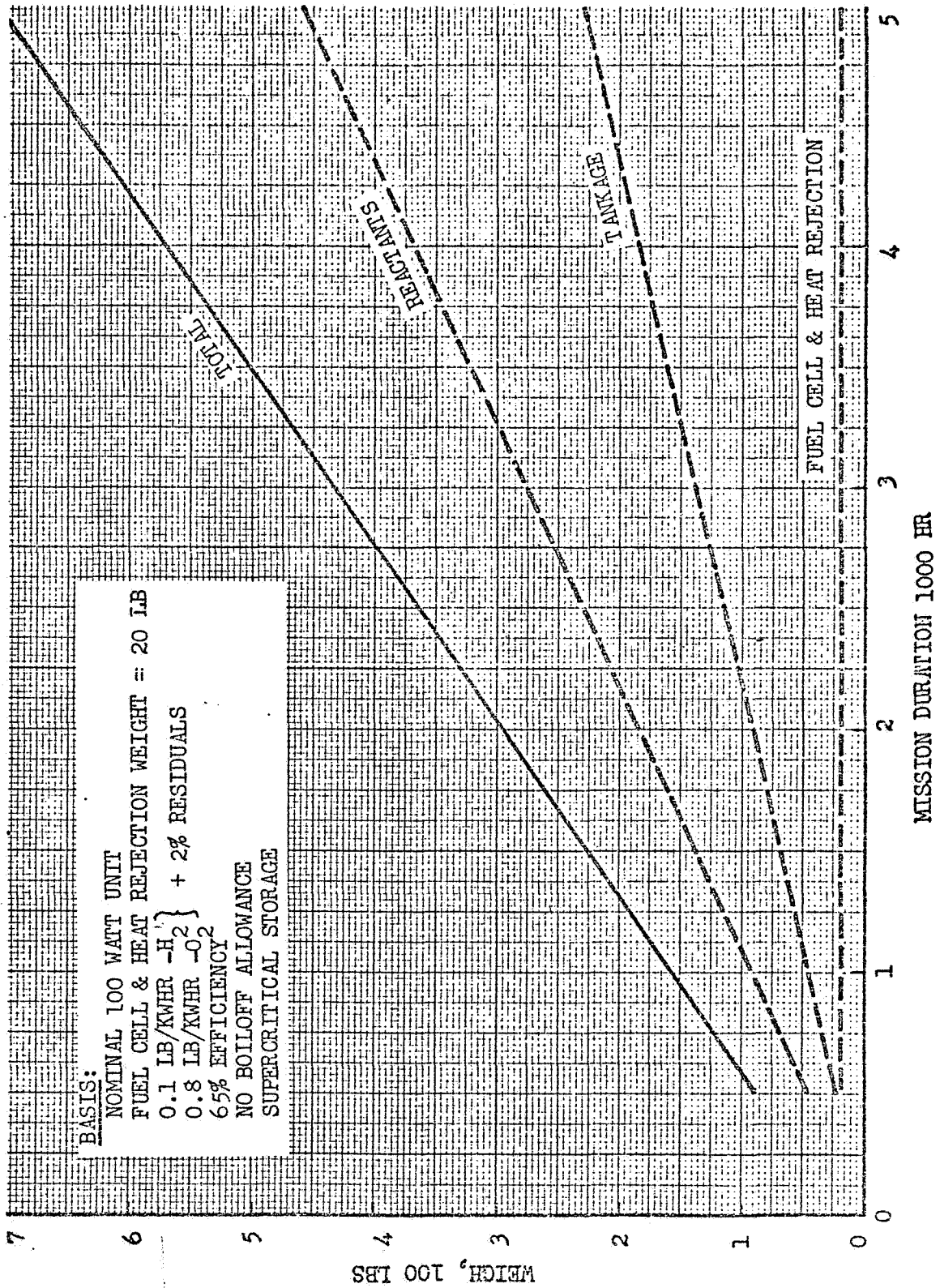


Fig 9-2 FUEL CELL POWER SYSTEM WEIGHT
 0.1 KW UNIT

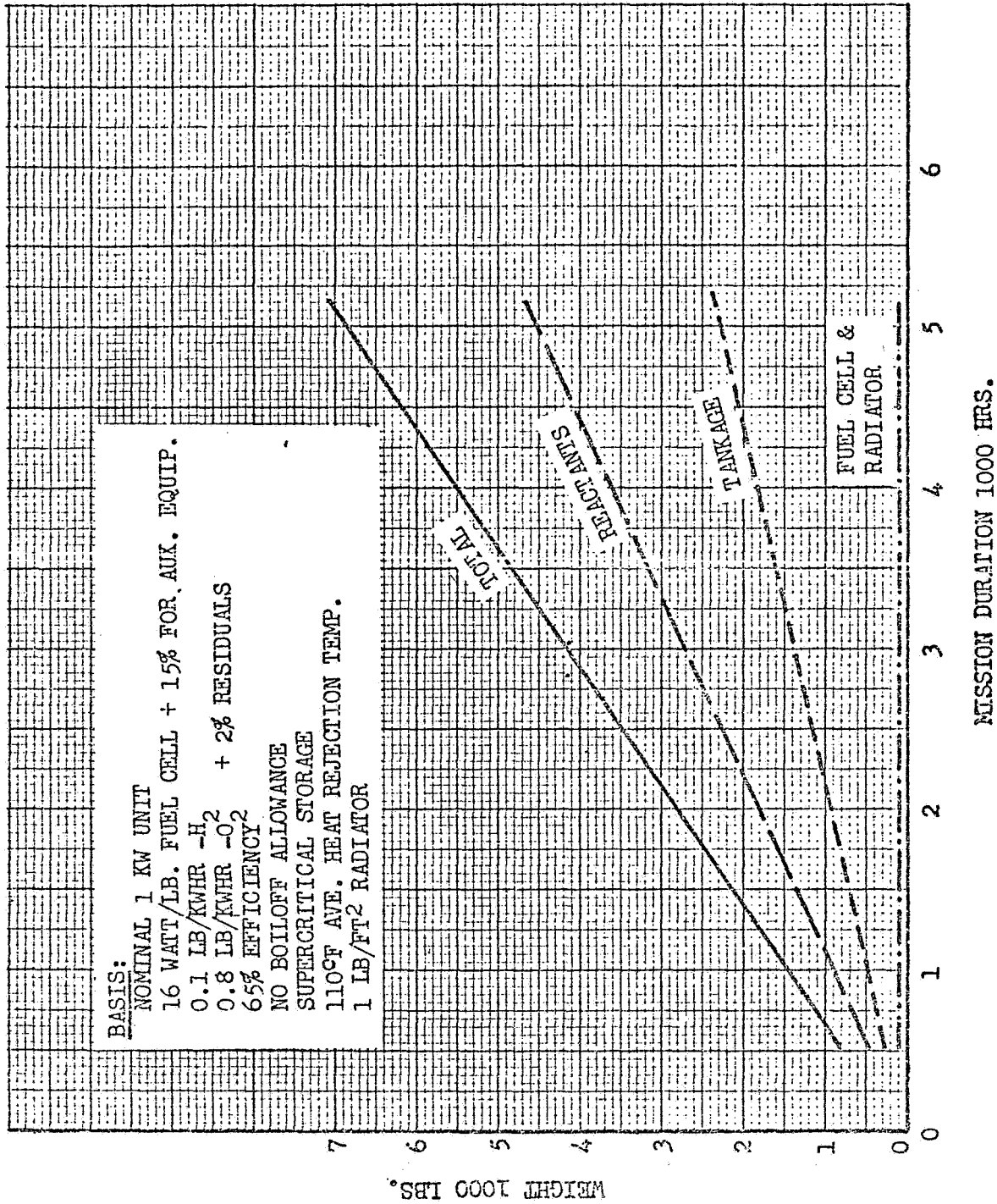


Fig 9-3 FUEL CELL POWER SYSTEM WEIGHT
 1.0 KW UNIT

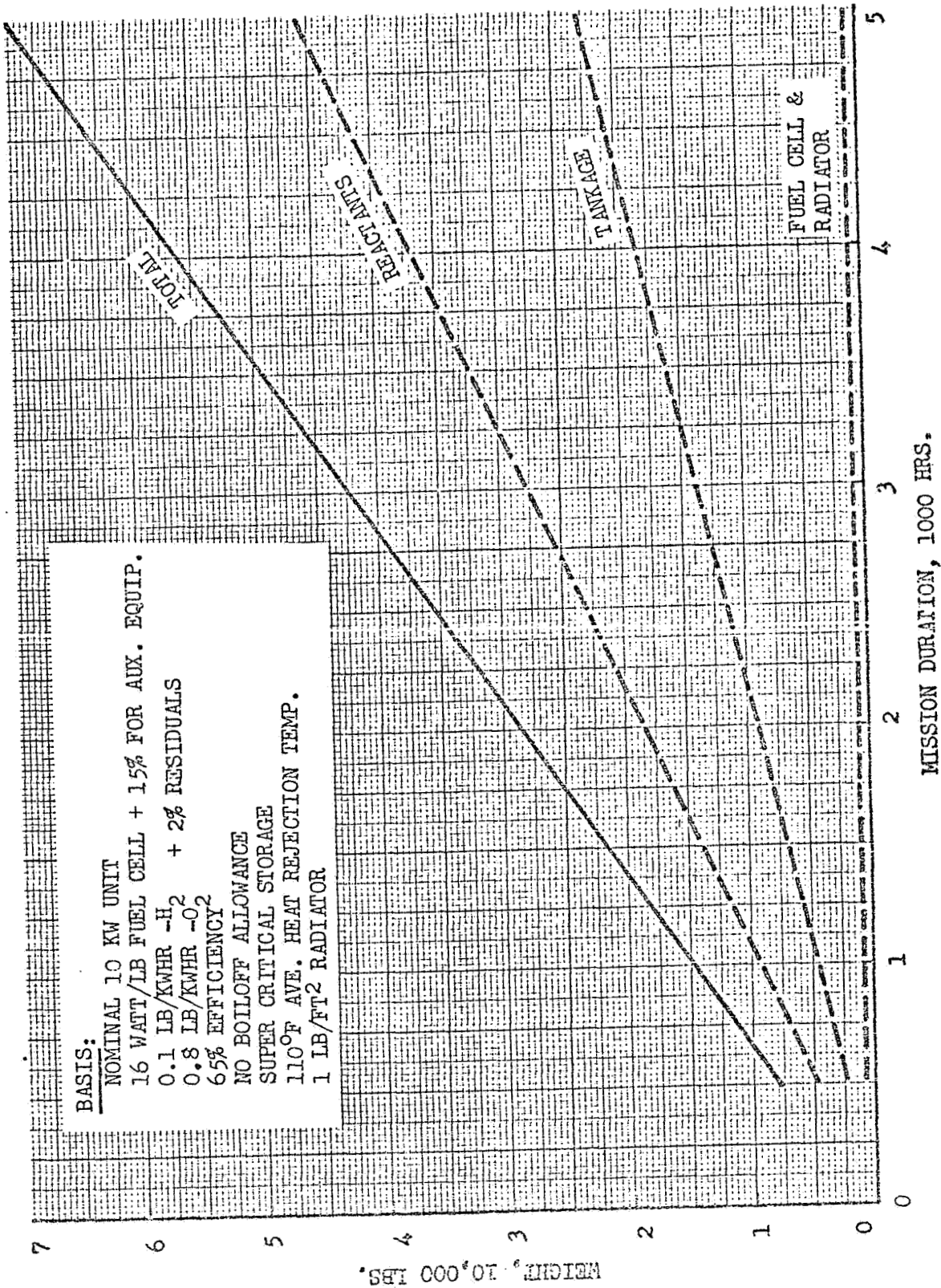


Fig 9-4 FUEL CELL POWER SYSTEM WEIGHT
 10 KW UNIT

9.2.4 Radioisotope Thermoelectric Generators (RTG)

RTG's are candidate electrical power sources for space power demands ranging from a few watts up to hundreds of watts. They are small, compact passive energy conversion devices that offer high reliability and long life. These devices have been used in Transit, Nimbus, and Apollo missions and are currently programmed for use in Pioneer F & G, Unified Nimbus Observatory, Viking Mars Lander, and NavSat. They are under active consideration as the electrical power source for a planetary Grand Tour mission.

The basic design of an RTG is relatively simple. It generally consists of a cylindrical external shell with fins to radiate unconverted heat to space. An encapsulated radioisotope is positioned in the center of the cylinder and transfers thermal energy to thermoelectric materials located between the heat source and the external shell. The schematic shown in Figure 9-5 illustrates this. Positive-type and negative-type thermoelectric elements are connected electrically in series to form thermocouples and thermally in parallel. The thermocouples are connected in series/parallel arrays to provide the desired output electrical characteristics and reliability. Thermal energy from the heat source flows conductively through the thermoelectric elements and then through the shell to space. The temperature difference established across the thermoelectric elements by the heat flow produces a voltage across the thermocouple due to the Seebeck effect, allowing electrical power to be extracted.

Thermoelectric conversion devices are based on the phenomenon that electric current will flow in a closed circuit formed by the junctions of two dissimilar metals if one junction is maintained at a higher temperature than the other. Important material properties in determining the relative merit of thermoelectric materials, the conversion efficiency and the converter design are: Seebeck coefficient, thermal conductivity, and electrical resistivity.

The low conversion efficiency of these devices (about 5%) generally limits the upper power range to less than 1,000 watts since the radioisotope used is both expensive and relatively scarce.

Plutonium-238 is the radioisotope used in all space RTG's launched and currently projected. Plutonium-238 has a long half-life (about 90 years) and produces

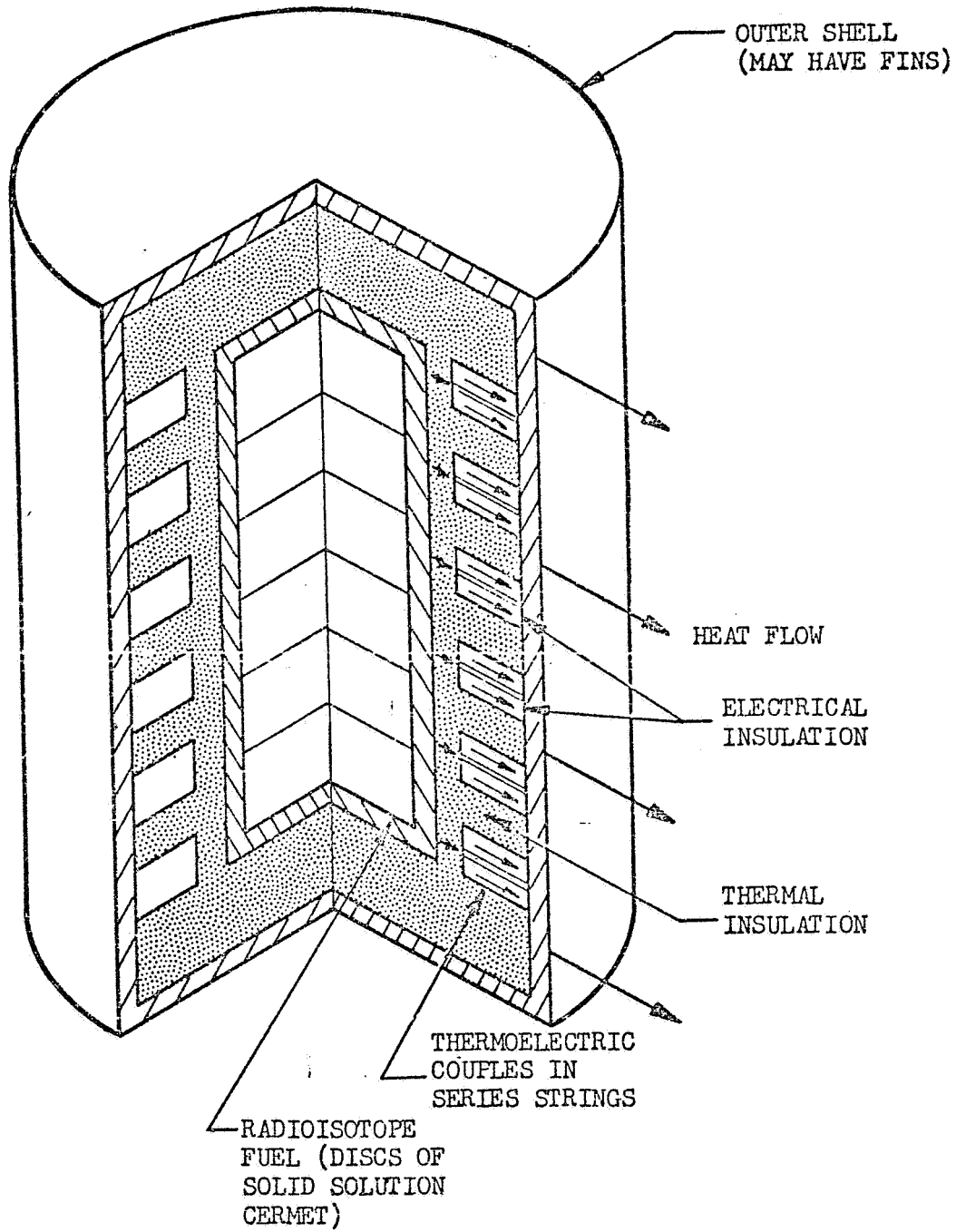


Fig 9-5 SCHEMATIC OF RADIOISOTOPE THERMOELECTRIC GENERATOR

a minimal radiation environment since it is primarily an alpha emitter with some spontaneous fission. The need for and amount of radiation shielding are dictated by the quantity of radioisotope, its geometric relationship to radiation-sensitive items, and the radiation levels that are acceptable before equipment performance does not meet design specifications.

The use of radioisotopes may present personnel radiological hazards and containment of the isotope under all normal and accident environments must be assured. The AEC is attempting to establish a standard heat source capsule design that satisfies safety criteria for use of plutonium-238 in space RTG's.

The thermoelectric materials used in space RTG designs have included lead telluride, silicon-germanium alloy, and an improved material of tellurium-antimony-germanium-silver (TAGS) for the modified SNAP-19 RTG. Since the efficient operating temperature of lead-telluride is lower than the silicon-germanium alloy, there is an effort to thermally cascade these two thermoelectric systems to increase the overall thermal efficiency from about 5% to as high as 10%.

There have been numerous design concepts of space RTG's proposed, but Table 9-4 presents characteristics of only those either currently available or under active development. Up to 100 - 200 watts can be obtained by using multiple SNAP-19 modified RTG's. For power demands above this range, the multihundred-watt RTG or a cascaded-Isotec RTG can be used. Both of these larger units are in an early design phase.

Waste heat from RTG's could be used by shrouding the generator exterior with a heat exchanger or by using heat pipes. However, the external surface temperatures are too low (See Table 9-4) to be of value with a heat-powered refrigeration device. A heat pipe could extract heat from the interior of the RTG but this would require increased thermal power of the radioisotope and it may not be conveniently located near the heat-using device. It would appear more practical to provide a separate isotope heat source for a heat-powered refrigeration device.

TABLE 9-4
RTG CHARACTERISTICS

	SNAP-19	SNAP-19 Modified	SNAP-27	ISOTEC	ISOTEC Cascaded	Multihundred
Power	28 w	~ 40 w	~ 73 w	~ 37 w	~ 100 w	To be defined
BOL *	~ 24 w	~ 35 w	~ 62 w	~ 30 w	~ 85 w	100-200 w (5 yr)
EOL **	~ 30 #	~ 30 #	~ 44 #	~ 28 #	~ 48 #	50 - 100 #
Weight	~ 3 vdc	~ 4 vdc	~ 14 vdc	~ 6 vdc	~ 6 vdc	6 v (min)
Voltage	3 yr	3 yr	1 yr	5 yr	5 yr	3 - 12 yr
Des Life	~ 630 w(th)	~ 635 w(th)	~ 1,450 w(th)	~ 790 w(th)	~ 980 w(th)	To be defined
Input Pwr	Cyl w/fins ~ 22" dia x 11"	Cyl w/fins ~ 22" dia x 11"	Cyl w/fins ~ 16" dia x 18"	12-sided prism ~ 23" dia x 15"	Similar to Isotec	To be defined
Size	350°F	350°F	520°F	290°F	290°F	
Heat Res Temp	Isotopes of Teledyne	Isotopes of Teledyne	General Electric	Gulf Gen Atomics & TRW	Gulf Gen Atomics	General Electric
Contractor	Used in NIMBUS	Scheduled for Pioneer, F&G & Viking Lander	Used in Apollo	Scheduled for NavSat	Under Developmt	Ref Des by end of FY '71 Grand Tour is ref mission
Status						

Based on
2.1 w/#
est.

* BOL Beginning of Life
**EOL End of Life

9.2.5 Radioisotope-Brayton-Cycle Power System

The radioisotope most applicable for long-life space power systems is plutonium-238. However, plutonium-238 is expensive and its availability is limited. Therefore, if it were to be used with 1 - 10 kwe power systems, the energy conversion system should have a better thermal efficiency than the 5% given by thermoelectric devices. Many candidate energy conversion systems have been studied for thermal coupling with a radioisotope heat source including thermionics and the more conventional dynamic systems. It appears from these studies that a Brayton cycle turbogenerator system offers the most promise with a radioisotope heat source. Efficiencies in the range of 20 - 30% seem achievable for 1 - 10 kwe power outputs.

An isotope Brayton cycle power system was selected as the base power system for the manned orbital research laboratory (MORL) and a flow schematic of the 5.5kwe system is shown in Figure 9-6. NASA/LeRC has initiated component ground testing of a 2 - 10 kwe Brayton cycle power conversion module. While initially in system ground tests the working fluid will be electrically heated, subsequent tests will use a large plutonium-238 heat source and a 30-ft-diameter solar collector. NASA has estimated that the Brayton cycle power system will be ready for operational use in the 1975 time period.

In the isotope-Brayton cycle system thermal energy from a radioisotope heat source, arrayed in an isotope re-entry vehicle for safe intact re-entry, is transferred by radiation to a heat source heat exchanger and an inert working fluid, e.g., a helium-xenon mixture, is heated to about 1,600°F. The heated working fluid is expanded through a turbine which drives an alternator and a compressor. The turbine exhaust flows through a recuperator to recover some of the heat and then flows either directly into a waste heat radiator or into an intermediate gas-liquid heat exchanger. In either case, the fluid is cooled to about 200°F and then flows into the compressor. After compression, the fluid flows through the recuperator and into the heat source heat exchanger to complete the cycle. If an intermediate gas-liquid heat exchanger is used, the waste heat is rejected through a liquid waste heat radiator by a secondary liquid cooling loop.

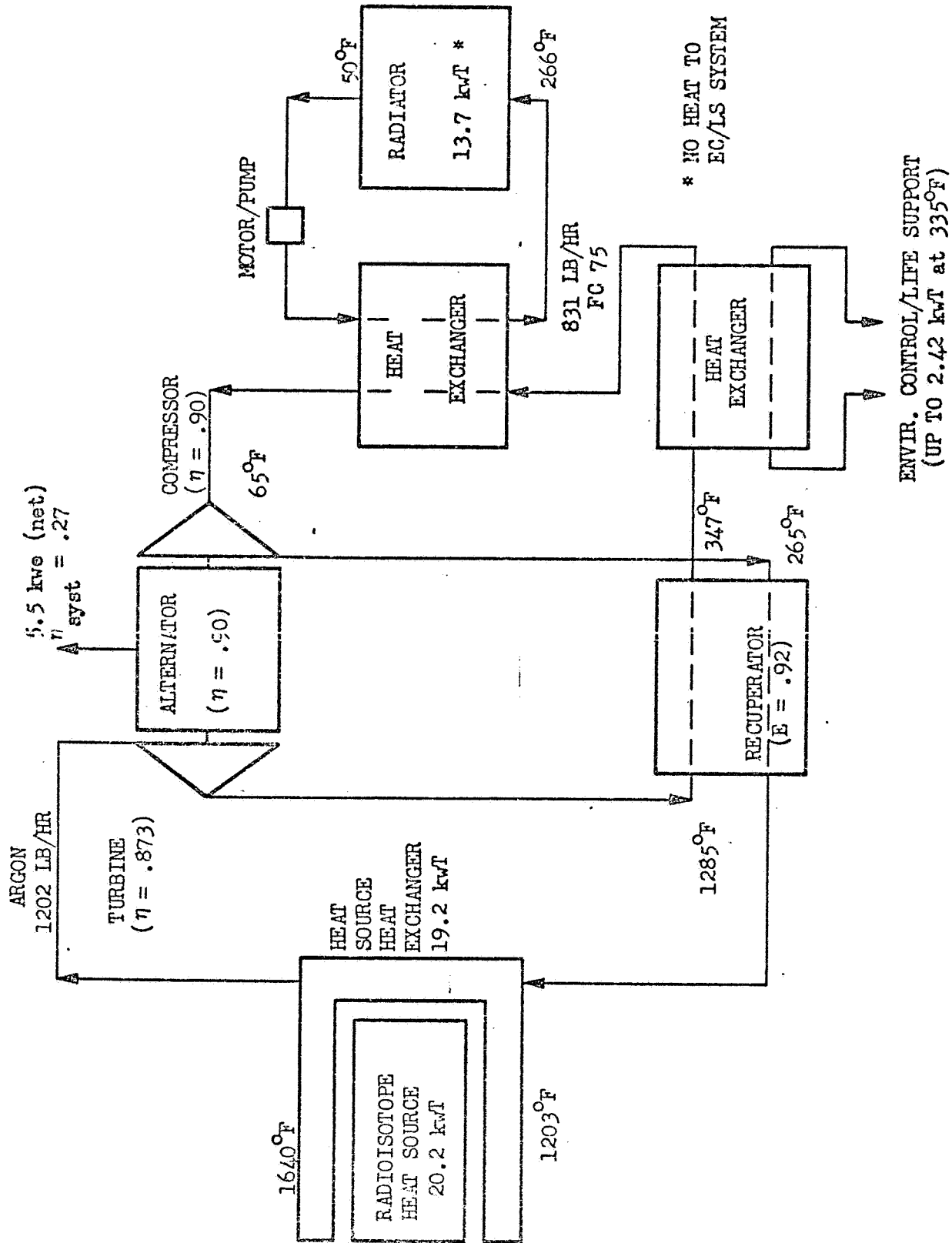


Fig 9-6 RADIOISOTOPE BRAYTON-CYCLE POWER SYSTEM

Preliminary designs of the isotope re-entry vehicle, the isotope heat source, and the heat source heat exchanger have been completed. The AEC is continuing development of plutonium-238 refractory metal fuel capsules. These capsules will be of flight quality for 5 years service at 2,000°F.

The NASA/LeRC isotope-Brayton cycle system is a nominal 7-kwe unit that weighs about 5,250 lb without a redundant power conversion module. This weight includes 1,980 lb for the isotope re-entry vehicle and the heat source array of plutonium-238 fueled capsules. This power system covers the 2 - 10 kwe range and at its nominal 7-kwe rating gives about 1.3 watt/lb. If used in a manned system with a redundant power conversion module and a 500-lb nuclear radiation shield (NASA estimate, with a 10-ft separation distance), it will give a nominal 1 watt/lb and occupy about 350 ft³. A heat rejection radiator area of about 550 ft² is required at an average heat rejection temperature of 154°F.

2.2.6 Nuclear Reactor Power Systems

When space missions are studied that require multikilowatts to megawatts of electric power for long periods of time, nuclear reactor power systems become a leading candidate to supply the power. They must compete with large solar photovoltaic arrays and isotope-Brayton cycle or solar collector-Brayton cycle in the lower kilowatt range (< 10 kwe) and with large solar photovoltaic arrays or larger solar collector-dynamic power systems in the 10 - 50 kwe range. Above about 50 kwe nuclear reactor power systems may be the only power source candidate.

A nuclear reactor power system offers a relatively compact space power system with 1 - 5 yrs design life that is not dependent on solar energy. The basic elements of a nuclear reactor power system are a thermal energy source, an energy conversion system, a waste heat rejection system, a nuclear radiation shield, and associated interfacing structure and accessories. Only one nuclear reactor power system (SNAPSHOT) has produced electric power in space. It produced a nominal 600 watts of electric power for 43 days before a voltage regulator failure terminated its mission. It used a compact zirconium-hydride-uranium reactor with a sodium-potassium (NaK) working fluid transferring the reactor thermal energy to a direct radiating thermoelectric power conversion system. The flight system weighed about 725 lb, had a 235-lb lithium hydride shield, and an efficiency of about 2%. A similar system was ground-tested for more than a year (about 10,000 hr) without malfunction in a simulated space environment.

In the power range where nuclear reactor power systems must compete with solar-dependent systems, they have an advantage in not requiring large deployable panels or collectors that may give unacceptable drag penalties at the lower orbital altitudes, or may need to be retracted for space maneuvers. They have the disadvantage that nuclear radiations emanate from the energy source. Therefore, radiation attenuation must be provided by shielding and separation distance between the source and radiation-sensitive items. In addition to the availability of fertile reactor core materials, contrasted to plutonium-238, a nuclear reactor power system has a distinct ground handling advantage over

large radioisotope heat sources since the reactor is not started up until the desired orbit has been achieved. For the same thermal power, shielding requirements are greater for a nuclear reactor than for a plutonium-238 heat source.

Because of fixed weights and shielding requirements, it is very difficult for nuclear reactor power systems to be competitive in the 1 - 10 kwe range unless there are mission considerations that override power system weight. It is therefore doubtful if a nuclear reactor power system would be considered as a separate source of electric power for external refrigerator systems. However, if there are missions which have a nuclear reactor power system as the primary spacecraft power source, they would be an excellent candidate to supply the additional power needed in an external refrigerator system at a minimal weight penalty. The penalty would be evident in extra radiator area and weight, any added shielding to reduce the increased radiation level, and possibly in reduced energy conversion cycle efficiency due to off-design operation, if the system were not optimized at the higher power load.

The thermal energy source is a compact nuclear reactor of the family flight-tested and now under development and testing for SNAP-8. The reactor uses zirconium-hydride as a neutron moderator, enriched uranium-235 fuel, liquid metal coolant (sodium-potassium mixture), beryllium reflectors with movable segments for reactor control, and stainless steel or hastelloy for most structural elements. If higher reflector temperatures may be encountered, e.g. with a 4π shielded reactor, beryllium oxide reflectors with poison -backed control drums can be substituted for the beryllium reflector and open-type drums. The SNAP-8-type reactor is designed to provide a nominal 600 kw of thermal power for 12,000 hours with a 1,300°F coolant outlet temperature. Design life can be increased by operating at reduced power or outlet coolant temperature. Design life can also be increased by using a slightly larger cone with additional fuel elements. Typically a SNAP-8-type reactor will weigh about 750 lb and occupy about 6 ft³. The 1,300°F outlet coolant temperature limit of zirconium hydride-uranium-type reactors constrains the performance of some of the energy conversion systems as will be noted later. Advanced reactor types that alleviate this constraint, e.g. SNAP-50-type, have been studied and considerable development work accomplished. However, they are not currently available or programmed for the near future.

The thermal energy released by the nuclear reactor must be coupled to an energy conversion system. Since the reactor coolant becomes radioactive during reactor operation, shielding and energy conversion system contamination considerations generally dictate the use of a primary loop heat exchanger to transfer the heat to the energy conversion system working fluid loop even though SNAPSHOT used the reactor coolant directly with the energy conversion system. In some applications it may even be advantageous to use an intermediate heat transfer loop between the reactor coolant loop and the energy conversion system fluid loop.

Many energy conversion systems have been studied for use with nuclear reactors. These have included thermoelectrics (both direct radiating and compact converters), thermionics, and dynamic systems, e.g. Rankine cycle, Brayton cycle, and more recently Feher cycle. A direct radiating thermoelectric system was used for SNAPSHOT with a system efficiency of about 2%. Subsequent development and the use of higher hot junction temperatures have improved the efficiency to 2.5 - 3%. In the direct radiating type, heated working fluid (sodium-potassium mixture) is pumped through a manifold and distributed to an array of tubes. From the tubes the fluid flows through a manifold and back to the heat exchanger to complete the loop. Silicon-germanium thermoelectric couples are bonded to the tubes and the other end of the couples are bonded to a heat rejection radiator. Heat flows from the hot fluid conductively through the n and p elements of the couples and the unconverted thermal energy is rejected to space. The temperature gradient set-up across the thermoelectric elements produces a voltage across the couple due to the Seebeck effect, allowing electrical power to be extracted. The couples are connected electrically in series/parallel arrays to provide the desired output characteristics and reliability. Such systems have been proposed for electrical power to the 20 - 30 kwe range. System characteristics are given in Table 9-5, and a schematic in Figure 9-7.

Compact thermoelectric converters provide a modular approach for energy conversion in which a number of thermoelectric modules are combined to give the desired total power. A typical module contains 4 tubular submodules

connected hydraulically in parallel and electrically in series. Each tubular submodule has an inner-tube on which rings of lead telluride thermoelectric material are mounted. Alternate rings of n-and p-type lead telluride are used with the rings isolated from each other by mica washers. An outer annular jacket is used on each submodule for coolant flow. Heated working fluid (sodium-potassium mixture) is pumped through the inner-tube of the submodule and circulated back to the primary heat exchanger to complete the loop. A heat rejection loop pumps coolant (sodium-potassium mixture) through the annular jacket surrounding the thermoelectric material and circulates the coolant to a heat rejection radiator and then back to the converter. Heat flows conductively from the hot working fluid radially through the thermoelectric rings to the heat rejection loop. A portion of the thermal energy is converted to electrical power because a closed circuit is formed by the junction of the two types of thermoelectric materials with different junction temperatures maintained by the heat flowing through the thermoelectric elements.

A typical module weighs about 56 lb and occupies about $1/3 \text{ ft}^3$. With an average hot junction temperature of $1,100^\circ\text{F}$ and cold junction temperature of 500°F , about 400 watts per module are generated. System characteristics are given in Table 9-5.

Unlike the direct radiating system, the compact converter system requires the provision of a heat rejection loop and radiator with associated plumbing and pump. These weights tend to offset the efficiency advantage that lead telluride couples offer over the silicon-germanium couples at the temperatures available from a SNAP-8-type nuclear reactor.

Both of these thermoelectric systems are static energy conversion systems with inherently high reliability and with the use of electromagnetic pumps in the various loops rotating machinery is not required.

The heat engine power cycles of primary interest for space dynamic power systems are the Rankine-cycle and the Brayton-cycle. In the Rankine-cycle both liquid and vapor-phases are used, while in the Brayton-cycle only the gas phase is used.

As a direct consequence of the development work performed on space power systems using solar collectors, e.g. Sunflower, and nuclear reactors, e.g. SNAP-2, -8, and -50, there exists a considerable reservoir of experience and data on Rankine-cycle energy conversion systems. A schematic of a version of the SNAP-8 power system is shown in Figure 9-8. This version contains four loops: a primary reactor coolant loop, a cycle working fluid loop, a heat rejection loop, and a lube/cooling loop. Thermal energy from the reactor is carried by the reactor coolant loop to a boiler where the Rankine-cycle fluid is heated and vaporized. The vapor is expanded in a turbine that drives an alternator. After expansion the fluid flows to a condenser where it is condensed and cooled before returning via a pump/motor assembly to the boiler for recycling. A heat rejection loop removes heat from the condenser and transfers it to a heat rejection radiator for disposal. A lower temperature lube/coolant loop with its own heat rejection radiator is provided for the pump/motor assemblies and the alternator.

Many working fluids have been considered for use in space power Rankine-cycle systems, including: water, organic fluids: mercury, rubidium, and potassium. Mercury is the fluid used in SNAP-2 and -8 and typically gives 8 - 12% system efficiencies with a nominal 1300°F turbine inlet temperature. Development work using an organic fluid, e.g. Dowtherm-A, is continuing. Although restricted, because of thermal decomposition, to temperatures less than 700 - 750°F, test results with a 12-kwe unit have given system efficiencies around 14% with promise of increasing to around 20%. If advanced nuclear reactors are developed with outlet temperatures greater than 1,300°F, mercury's vapor pressure becomes excessive, but potassium is then a prime fluid candidate. System efficiencies of 10 - 15% are estimated and a significant area and weight advantage would accrue in the heat rejection radiator because of the increased radiator temperature available. System performance characteristics of a SNAP-8 type power system are given in Table 9-5 for comparison with the other reactor power systems.

Even though only 5 - 6 years ago many believed a Brayton-cycle power system was not feasible for space applications, development work has progressed to the point that it may be the first dynamic energy conversion system qualified for flight

use. A schematic of a nuclear reactor Brayton-cycle power system is given in Figure 9-9 and its performance characteristics are given in Table 9-5. Efficiencies in the 20 - 25% range appear feasible even with the 1,300°F limit of the SNAP-8 family of nuclear reactors. The relatively low heat rejection temperature of a Brayton-cycle invokes a radiator area and weight penalty when compared with the other power systems. In a Bryaton-cycle system, thermal energy from the reactor is carried by the reactor coolant loop to a heat exchanger where the inert gas working fluid is heated to about 1,300°F. Operation of the rest of the Brayton-cycle system was described in the radioisotope-Brayton cycle section.

The waste heat rejection radiator is a major element of nuclear reactor power systems. The area required for a given quantity of heat rejected to space is a function of the average radiator temperature to the fourth power. The quantity of heat to be rejected is a function of the electrical power required and the power system efficiency. Radiator area requirements are given in Table 9-5 for the various reactor power systems for comparative purposes. Typically radiator specific weights will range from 0.9 to 1.2 lb per ft².

The shield weight for a nuclear reactor is a function of the reactor thermal power level; the radiation resistance of spacecraft equipment; mission considerations, e.g., manned, unmanned, exposure duration, equipment access, rendezvous and docking; and configuration considerations, e.g., reactor and equipment locations. Shielding must be provided for both neutron and gamma ray attenuation and typically lithium hydride and tungsten are used. Shield configurations can be shadow, split, or 4 π -type, depending on factors noted above. Without the factors noted above being specifically defined it is difficult to give typical shield weights. However, to give some indication of an order of magnitude, about 8,000 - 10,000 lb of reactor shielding would be required for a manned spacecraft with a 125-ft separation distance with a 422-kw reactor and a 2.3 mr/hr radiation tolerance at an 80-ft diameter dose plane.

TABLE 9-5

REACTOR POWER SYSTEM CHARACTERISTICS (TYPICAL)

	Nuc Reactor		Compact Conv't'r		Direct Rad	
	Brayton-Cycle	SNAP-8	Thermoelec	Thermoelec	Thermoelec	Thermoelec
Rated Power, Unconditioned, KW(e)	24 (net)	40 (net)	25.9 (net)	12 (EOL)		
Reactor Power, KW(t)	152	414	622	422		
System Efficiency	13.2	9.7	4.2	2.8		
Design Life	10,000 hr	10,000 hr	5 yr	5 yr		
Reactor Coolant Inlet Temp, °F	1,150	1,140	1,100	1,100		
Reactor Coolant Outlet Temp, °F	1,300	1,330	1,300	1,300		
Reactor Coolant Flow Rate, lb/hr	17,000	34,530	51,120	34,990		
Heat Rejection Avg Temp, °F	298	575	550	550		
Heat Rejection Area, ft ²	1,150	827	1,891	1,068		
Heat Rejection Loop Flow Rate, lb/hr	7,200	32,110	46,570	-		
Pwr Conversion Loop Flow Rate, lb/hr	11,070	9,410	49,285	28,800		
Lube/Coolant Loop Flow Rate, lb/hr	-	4,970	-	-		
Lube/Coolant Radiator Avg Temp, °F	-	227	-	-		
Lube/Coolant Radiator Area, ft ²	-	238	-	-		
Turbine Inlet Temp, °F	1,250	1,290	-	-		
Thermoelectric Hot Side Avg Temp, °F	-	-	1,150	1,150		

WEIGHTS, LB

Reactor & Primary Loop	912	1,329	1,258	1,025	
Power Conversion Unit	1,513	1,506	5,229 *	2,270 **	
Heat Rejection Loop & Pumps	578	313	1,763	-	
Lube/Coolant Loop & Pumps	-	197	-	-	
Heat Rejection Radiator	1,064	949	2,106	-	
Lube/Coolant Radiator	-	286	-	-	
Rad/Converter Support	553	790	870	2,256 **	
Miscellaneous Elect Equipment	308	324	510	390	
Thermal Shroud	844	698	1,484	1,095	
	5,772	6,392	13,220	7,036	
Specific Pwr, watt/lb (no shield or reactor disposal system)	4.2	6.3	2.0	1.4	

* Includes 6 active & 1 standby heat exchanger; 12 active & 2 standby compact converters

** Includes 5 active & 1 standby Power Conversion Loops and Units

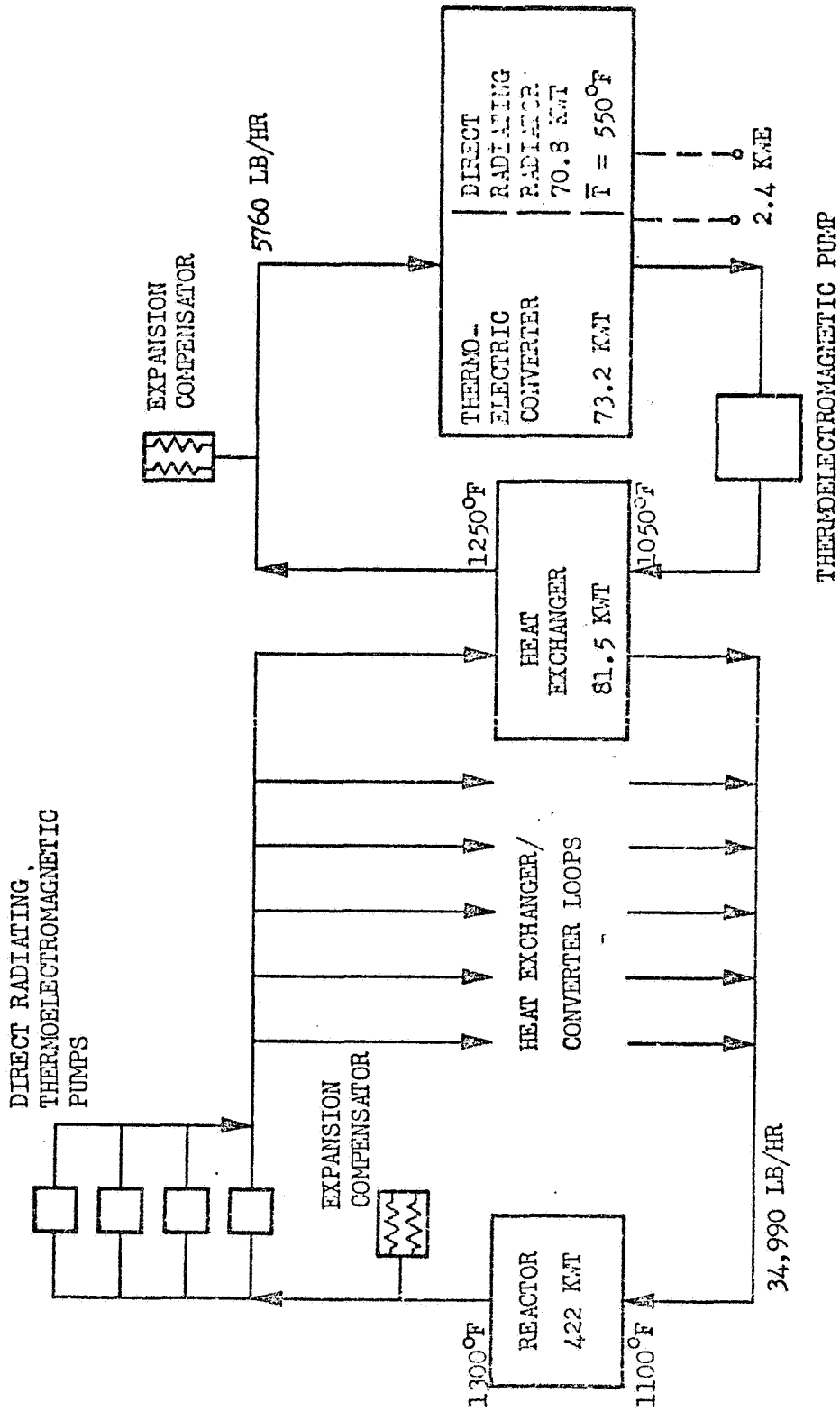


Fig 9-7 DIRECT RADIATING THERMOELECTRIC POWER SYSTEM

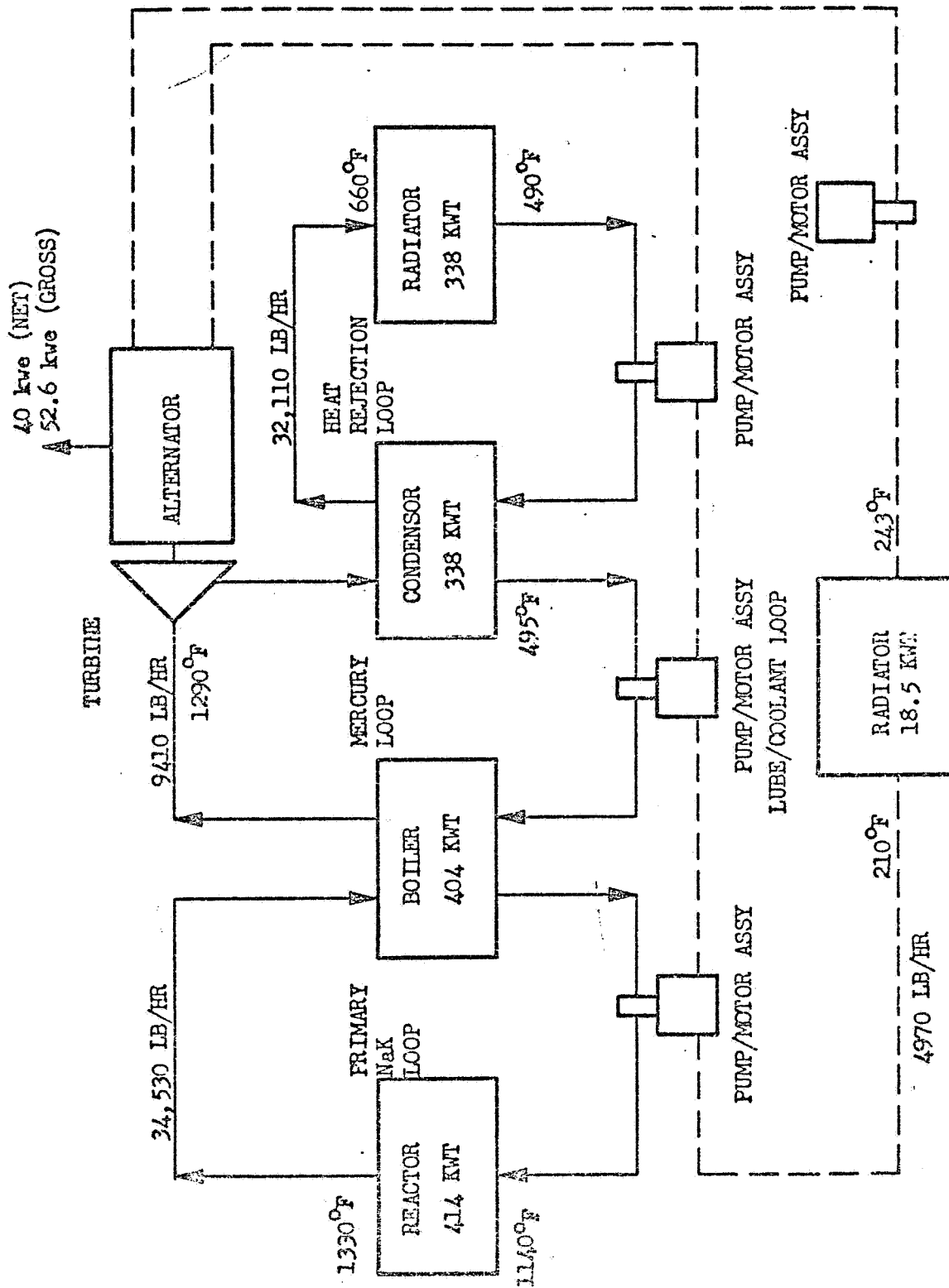


FIG 9-8 SNAP-8-TYPE RANKINE CYCLE POWER SYSTEM

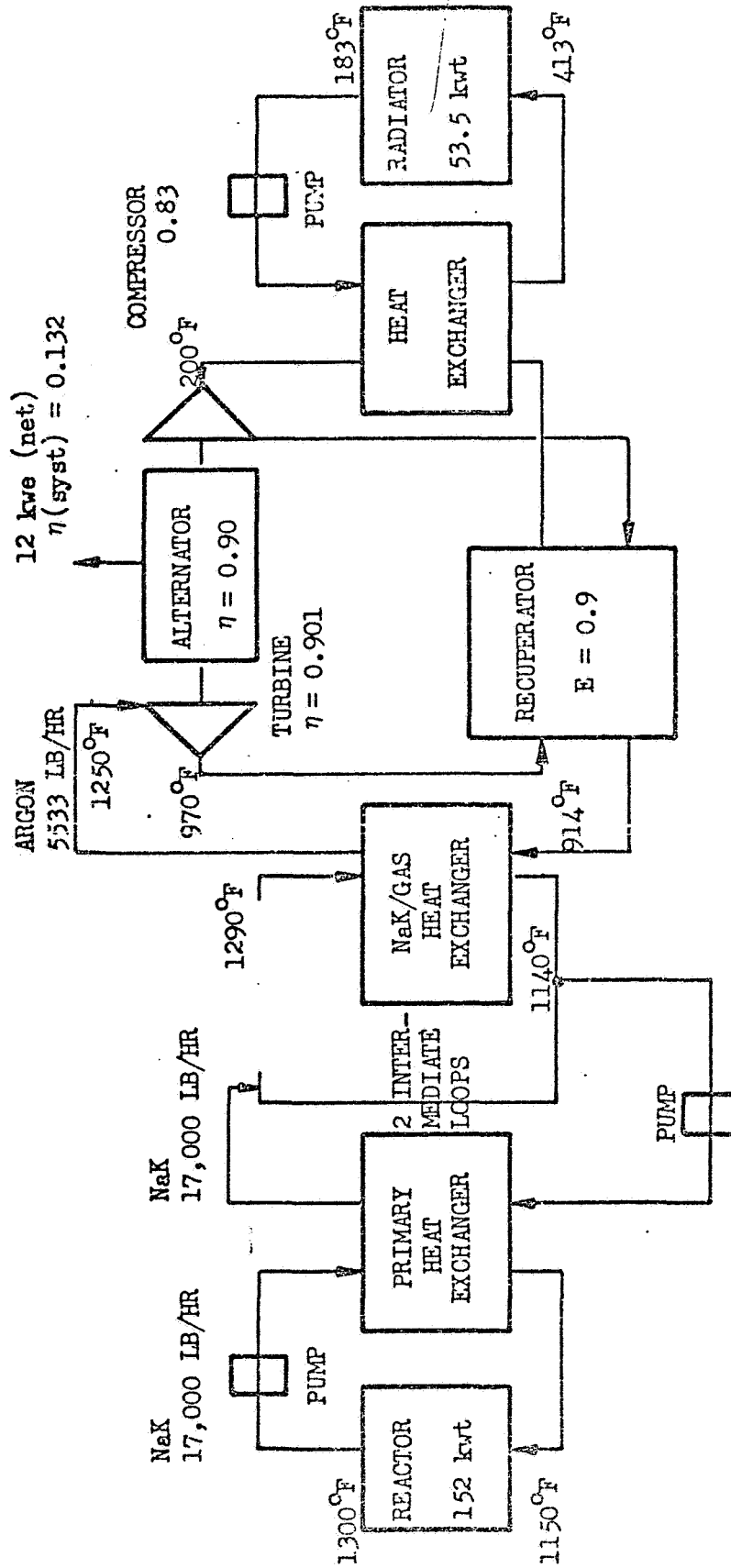


Fig 9-9 NUCLEAR REACTOR BRAYTON-CYCLE POWER SYSTEM

9.2.7 Power Conditioning

The power conditioning equipment may contribute a significant portion of the overall system weight for high power requirements. A limited amount of information is given here so that rough estimates can be made of weight and volume requirements. For detail analyses and designs more complete information must be obtained from other sources.

Power conditioning equipment may be required to transform, convert, invert, rectify, regulate, filter, or limit the power from a power source for use in spacecraft subsystems. The weight and volume requirements for power conditioning equipment will therefore be dependent upon the electrical characteristics specified for the power-using equipment and the output characteristics of the power source. In order to provide some insight into weight and volume allowances that must be provided, the following general guidelines are given for 28 vdc output DC/DC converters and for 3-phase, 115-volt, 400 cps inverters: DC/DC converters will generally range from about 18 - 20 lb/kw and 250 in³/kw to 5 - 8 lb/kw and 70 - 100 in³/kw as the input voltage varies from about 6 volts to 20 volts, respectively; 3-phase inverters will, in general, range from 30 - 40 lb/kw with 25 - 31 volt input to 15 - 25 lb/kw with 50 - 60 volt input. Inverter specific volume may range from several hundred in³/kw to 1000 in³/kw..

9.3 THERMAL ENERGY SOURCES

9.3.1 Radioisotope Heat Source

The use of radioisotope heat sources in space missions may present radiological hazards, particularly if the radioisotope were permitted to escape from the heat source capsule. Therefore, containment of the isotope under all normal and accident environments must be assured. This dictates that adequate thermal and structural protection be provided to allow the heat source capsule to withstand re-entry environments associated with mission aborts (which may include superorbital return) and remain intact after earth impact at the velocity and temperature conditions appropriate for the particular heat source configuration and re-entry characteristics. In addition, if the capsule design does not provide a means for venting the helium generated by the decay of plutonium-238, then sufficient structural strength must be provided within the capsule to withstand the maximum internal helium pressure developed.

The general approach has been to have the heat source capsule capable of remaining intact after earth impact and a graphite protective thermal shield around the capsule for re-entry protection. This approach was used, with a cylindrical capsule, for Nimbus SNAP-19, and is planned for Pioneer and NavSat RTG's. Studies by Douglas Nuclear Lab in isotope heater designs for NASA MSC have recommended a spherical capsule in a cubic ablator configuration. Others are also studying spherical capsule designs, but the AEC now considers a refractory metal multilayer cylindrical capsule with provisions for venting helium as their reference design.

NASA/LeRC requires a large radioisotope heat source (25 kw) for use with a Brayton-cycle power system. Their current reference design uses multiple unvented refractory metal cylindrical capsules in a planar array with an ablative blunted-cone isotope re-entry vehicle rather than individual capsule re-entry protection. This may become the preferred approach for thermal powers above several kw, but with vented rather than non-vented capsules.

The AEC reference fuel form is now a solid solution cermet of plutonium-238 dioxide and thorium dioxide in a molybdenum matrix rather than plutonium dioxide microspheres. Crushed particles are used in the fabrication process.

Single-capsule heat sources from 100 watts to over 1 kw can be fabricated based on the AEC reference design and technology developed for multilayer refractory metal capsules. Typical of the multihundred-watt type are the 635-watt heat source for the modified SNAP-19 and the 790-watt heat source for NavSat. The 790-watt heat source, with a composite graphite thermal shield in an inconel outer can is a 5" diameter x $7\frac{1}{8}$ " long cylinder and weighs about 14 lb. The capsule is vented and has T-111 as the strength member, Ta 10W for the inner liner, and Pt 20 Rh clad. It uses plutonium-238 solid solution cermet as the source of thermal energy.

For low thermal energy heat sources (100 watts) a refractory metal spherical capsule of about 1.8" diameter, weighing $1\frac{1}{4}$ - $1\frac{1}{2}$ lb fueled appears attractive if fuel form fabrication will permit its use. Enclosing this capsule in a 2.8" graphite cubic protective thermal shield with a thin outer inconel can will provide a 100-watt heat source weighing $1\frac{1}{2}$ - $1\frac{3}{4}$ lb. This source could be coupled by direct radiation to the heat-powered refrigeration device with a thermal shutter for decoupling during non-operational periods (see Figure 9-10).

If cylindrical isotope capsules with spherical ends are used as the reference capsule design, a 100-watt heat source could be configured in a 1"-diameter x 5" long refractory metal capsule, weighing $1\frac{3}{4}$ - 2 lb fueled, with the solid solution cermet discs only in the cylindrical section of the capsule. Addition of a $\frac{1}{2}$ " thick graphite protective thermal shield in an outer inconel can would increase the heat source to about 2" diameter x 6" long and add about 1 lb to the heat source weight. This cylindrical heat source could be directly coupled to the heat-powered refrigeration device in the same way as the spherical heat source.

For heat sources of around 1 kilowatt, isotope capsule designs similar to the Pioneer and NavSat RTG heat source design, but uprated in thermal power, appear appropriate. While this heat source could also be radiatively coupled directly to the heat powered refrigeration device with a thermal shutter for decoupling, consideration must be given to the nuclear radiation levels and the actual heat source geometry relative to nuclear radiation-sensitive items. This consideration may dictate the use of heat pipes for transferring the thermal energy

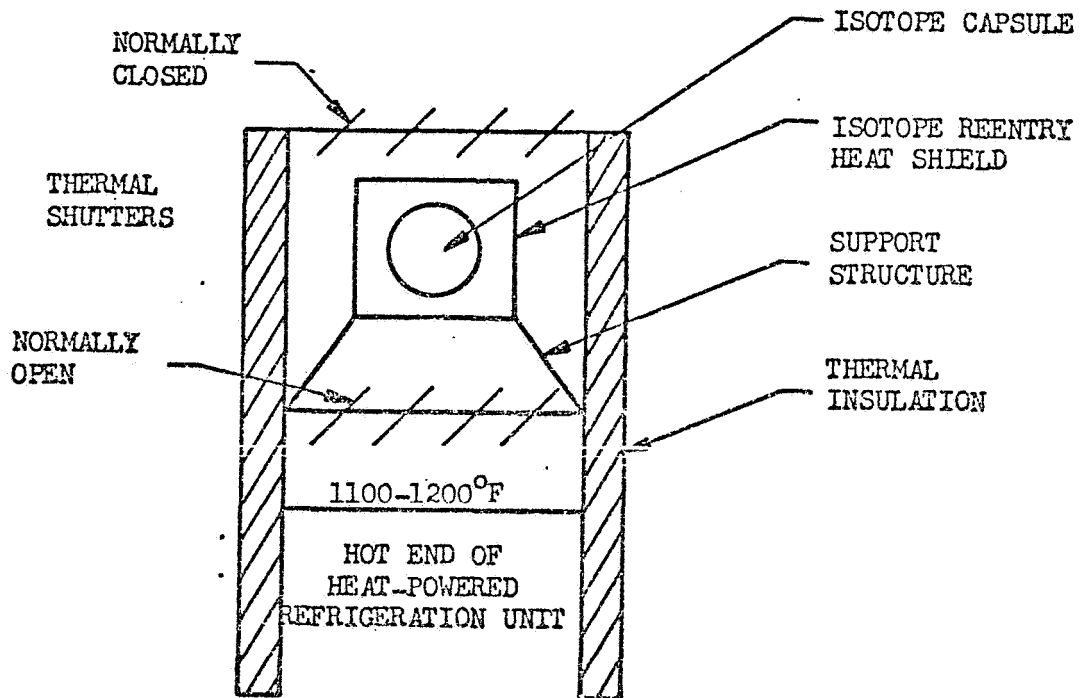


Fig 9-10 SCHEMATIC - DIRECT COUPLING OF RADIOISOTOPE HEAT SOURCE WITH HEAT-POWERED REFRIGERATION UNIT

with required nuclear shielding provided around the heat source. Figure 9-11 schematically shows this arrangement.

For heat sources of 10 kilowatts or higher, a planar array of vented refractory metal cylindrical capsules with an ablative blunted-cone isotope re-entry vehicle appears to be the best approach. The heat source is radiatively coupled to a heat source heat exchanger. For use with heat-powered refrigeration devices a forced-convection liquid metal (NaK) loop with the heat source heat exchanger (see Figure 9-12) would be preferred to the gas loop used by NASA/LeRC with their Brayton-cycle system. Multiple heat pipes could be used in place of the forced convection loop. Nuclear shielding will probably be required for the 10-kilowatt or higher heat sources, depending on the specific spacecraft configuration.

The 25-kilowatt heat source of NASA/LeRC has 164 unvented refractory metal cylindrical capsules, each a nominal 157 watts, supported by Cb-1Zr structure in a 49" diameter planar array. The isotope re-entry vehicle (IRV) with heat source weighs about 1,980 lb. Earlier studies indicated nearly a 400-lb reduction in IRV/heat source weight could be realized by the use of vented capsules with PuO₂ microspheres as the fuel form.

Use of 157-watt vented capsules with the solid solution cermet fuel form could be configured in a 25" diameter planar array for a 10-kilowatt heat source. Scaling from the 25-kilowatt heat source design gives a 10-kilowatt heat source weight of about 500 lb. Assuming a similar clearance between the heat source diameter and the aeroshell diameter, scaling of weights gives an IRV diameter of 44" and a weight of about 335 lb. This results in a total IRV/heat source weight of around 1,030 lb, including a spacer, hinge, and abort/de-orbit system.

The use of radioisotopes requires consideration be given to the radiations that emanate from the heat source. The radiation levels that will be experienced by equipment and personnel are a function of the quantity and purity of the isotope, its fuel form and constituents, the capsule materials and configuration, the separation distance between radiation source and equipments, and the shielding effectiveness of any intervening materials.

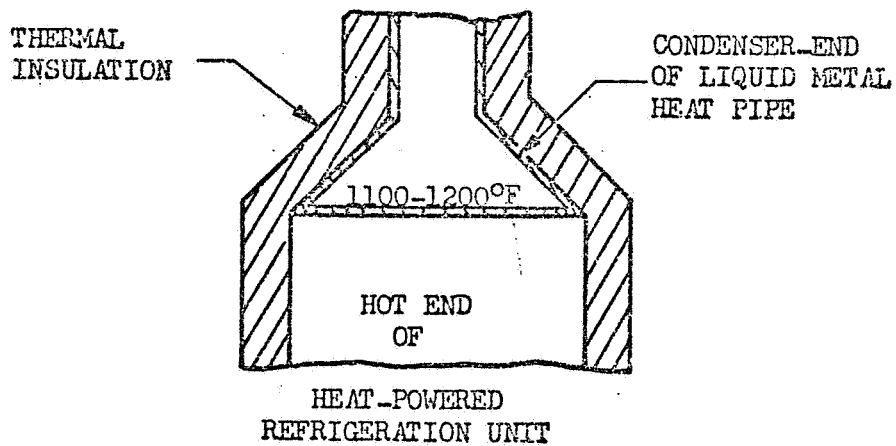
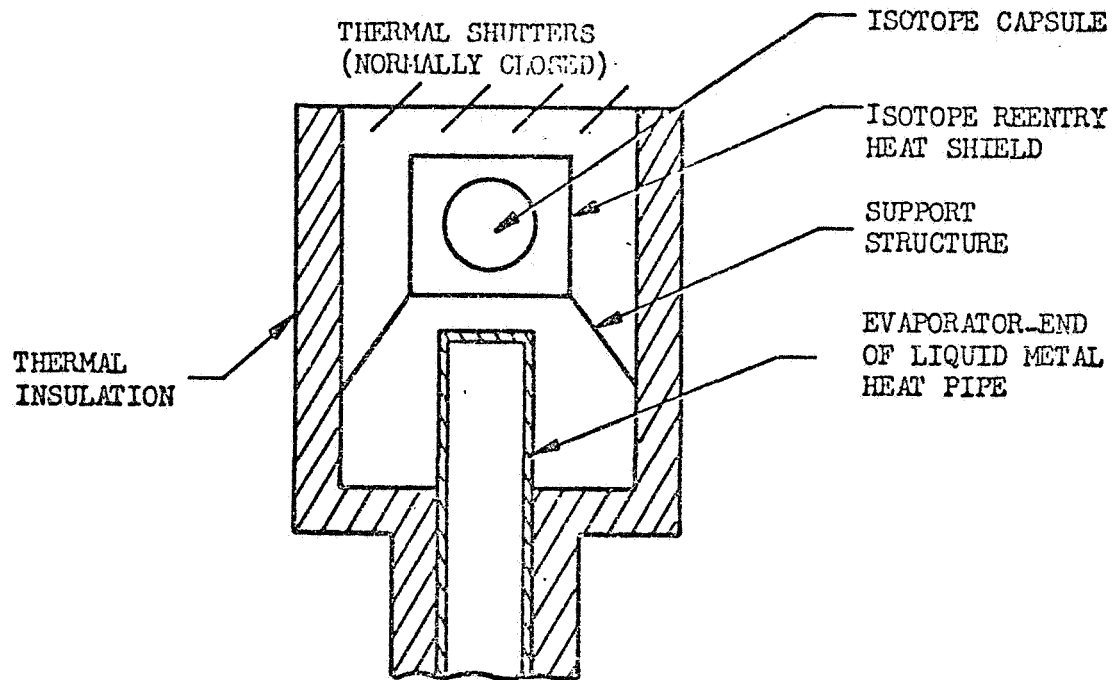


Fig 9-11. SCHEMATIC - HEAT PIPE COUPLING OF RADIOISOTOPE HEAT SOURCE WITH HEAT-POWERED REFRIGERATION UNIT.

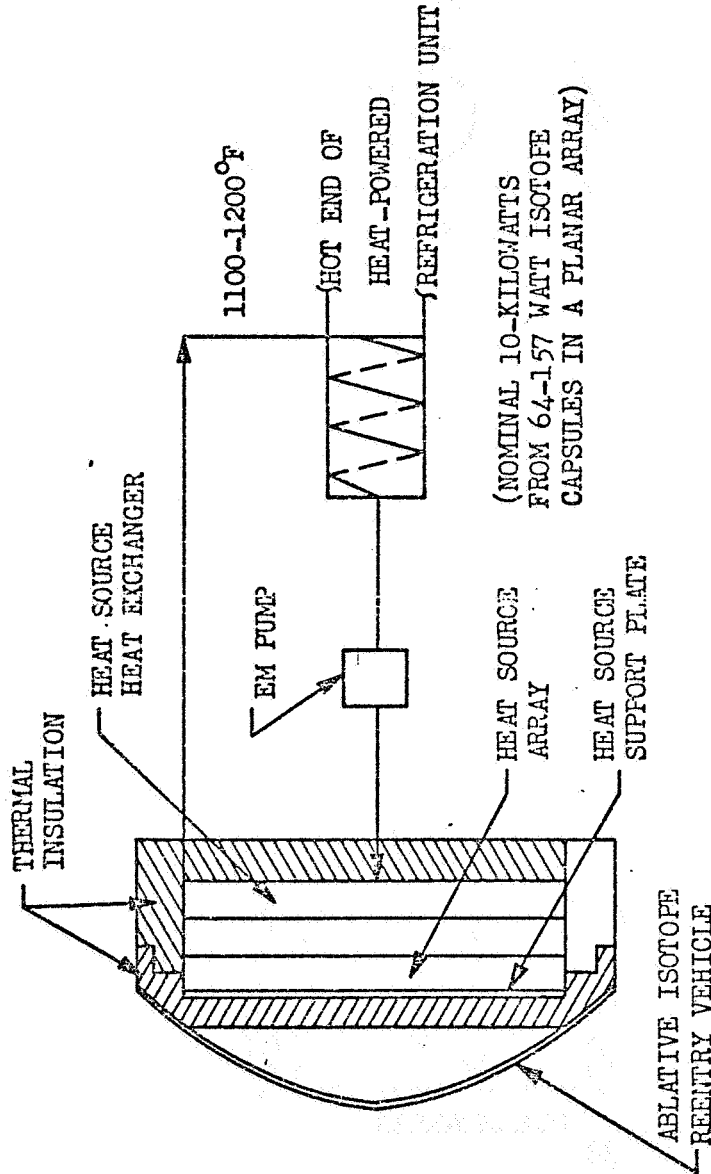


Fig 9-12 SCHEMATIC - LARGE ISOTOPE HEAT SOURCE FOR HEAT-POWERED REFRIGERATION UNIT

Plutonium-238 has a half-life of about 87.5 yr and decays to uranium-234 by alpha emission with primary energies of 5.495 Mev (72%) and 5.452 Mev (28%). Neutrons are produced by spontaneous fission, induced fission, and alpha-neutron reactions. Pure plutonium metal has a neutron production rate of about 3.5×10^3 n/sec-gm 238 which is essentially that produced by spontaneous fission. The oxide has a neutron production rate varying from about 1.5×10^4 to 2.5×10^4 n/sec-gm 238 depending on the light element impurities present. Gamma rays from plutonium dioxides come from a variety of processes including: intrinsic decay, prompt fission, decay of fission products, and isotopic impurities and their decay products. Typically the neutrons contribute about 90% of the radiation dose rate from the oxide.

The new reference plutonium-238 fuel form will have its radiation levels characterized in terms of neutrons/sec and a gamma spectrum of γ /sec per gram of solid solution cermet. Such characterizations are available in the open literature for PuO₂ microspheres.

Both SNAP-19 and -27 type isotope fueled capsules have had their radiation fields experimentally determined, e.g., a SNAP-19 capsule gave a maximum radiation level of about 38 mrem/hr at 100 cm from the capsule center. Estimates have been made of the radiation levels expected from the NASA/LeRC 25-kilowatt heat source and a 500-lb radiation shield has been determined as adequate for space station use of an isotope-Brayton cycle power system. A 100-watt spherical heat source would typically give about 7 mrem/hr at 100 cm without allowance for attenuation by the isotope or encapsulating materials.

Typical radioisotope heat source characteristics are present in Table 9-6 for thermal powers of 0.1, 1.0, and 10 kilowatts.

TABLE 9-6
TYPICAL RADIOISOTOPE HEAT SOURCE CHARACTERISTICS

Thermal Power	Re-entry Protection	Capsule		Heat Source		Unshielded Rad Level, 100 cm mrem/hr
		Dimensions	Wt (lb)	Dimensions	Wt (lb)	
0.1 kw	Graphite on indiv. capsule	~1.8" dia sphere	~1 ¹ / ₂	2.8" cube **	~2	~7
1.0 kw	Graphite on indiv. capsule	~2.8" dia x 6.3" cylinder, spherical cal ends	~10 ¹ / ₂	~3.8" dia x 7.3" cylinder spherical ends **	~15	~65
10.0 kw	Capsuled Arrayed in ablative re-entry vehicle *	~1.3" dia x 4.8" cylinder, spherical cal ends	~2 ³ / ₄	64 - 157 watt capsules in 25" dia array	~500 ***	~660

* Isotope re-entry vehicle is 44" dia blunted cone weighing ~335#

** 1/2" graphite protection

*** Includes capsule support structure, retention system heat sink & plate, truss support, and thermal insulation

9.3.2 Solar Collector/Receiver System

The primary elements of a solar collection/receiver system for supplying solar energy to a heat-powered refrigeration unit are:

- . a collector to gather solar radiation and concentrate it to a small focal image
 - . an absorber to receive the concentrated radiation and transfer the energy either directly to the heat-powered device or to a heat storage device
 - . an orientation device to keep the collector pointed at the sun
- a heat storage device to provide thermal energy storage during periods when sunlight is incident on collector and to provide thermal energy to the heat-powered device when the collector is shadowed from the sun
- a thermal switch to decouple the heat source and the refrigeration unit when refrigeration is not required
- a deployment/erection device to transform the collector from a stowed device to its deployed configuration
- structure to provide mechanical strength to the system

9.3.2.1 Solar Collector - Extensive development work has been accomplished over the past 10 years in solar collectors for use with spacecraft. Much of this work was motivated by the desire to use solar energy with space power conversion systems, e.g., dynamic systems, both Rankine-cycle and Brayton-cycle, and thermionic conversion devices. One-piece solar collectors up to about 30 ft diameter with specific weights from 0.25 - 0.6 lb/ft² of projected area were studied. Spacecraft stowage limitations and launch environmental effects placed considerable emphasis on large-diameter solar collectors that were capable of being erected in space. The lower temperature requirements of the dynamic power conversion systems compared to thermionic devices allowed concentration ratios that apparently could be met even with the erectable collectors. Perhaps typifying these types was the 32.2-ft diameter Sunflower paraboloidal solar collector with its ID of 9.2 ft to allow for the absorber and dynamic machinery. This collector provides about 75 kilowatts at the absorber with a collector efficiency of 0.736. The basis of

this design was a rim angle of $50^{\circ}41'$, 0.92 reflectivity, $3/4^{\circ}$ max solar misorientation, $\pm 1/2^{\circ}$ max surface slope deviation, $\pm 1''$ max surface translation deviation, and 130 watt/ft² solar constant.

Solar collector designs may be chosen from several possible shapes, but a highly reflective paraboloid is generally specified. Collector designs with specific weights as low as 0.25 lb/ft² of intercepted solar flux area have been proposed for erected diameters up to about 50 ft. Collector rim angles of $47 - 53^{\circ}$, i.e. angle subtended by the collector radius as seen from the focal point, appear optimum on the basis of concentration ability. The quantity of heat that a collector will focus on the absorber is a rather complex function of collector diameter, solar constant, angular diameter of sun disc, surface slope error at the collector surface, translation of the collector surface away from the true mathematical surface, the misorientation angle of the collector optical axis from the center of the solar disc, any blockage of the system by structure, the rim angle, and the reflectivity of the collector surface to solar radiation. Collector efficiencies are generally in the 70 - 85% range for single reflectance from the collector into the absorber. If the collector is to spend time shaded from the sun, then it must be sized to provide sufficient heat during periods of sun exposure for the heat storage system to accommodate the operating heat-load during shade time.

Use of a double-reflected collector system to focus the solar energy on an absorber located at the apex of the collector rather than at the focal length results in the accrual of additional losses and reduced collector efficiency. However, these losses may be acceptable for the configurational advantages of having the absorber nearer the refrigeration unit and the tankage being cooled. Even with a collector efficiency of only 0.50, a 4.5-ft-diameter one-piece paraboloidal collector, double-reflected, would give about 1 kilowatt incident on the absorber.

9.3.2.2 Absorber - In designing an absorber, one strives for a device with high solar absorptivity and low thermal emissivity to maximize the absorbed solar energy and minimize reradiation losses. Generally cavity absorbers are used and an optimum entrance diameter selected for the best combination of reradiation losses from the cavity entrance and losses due to solar

radiation not entering the cavity. While different shaped cavity absorbers have been studied, a common design is a spherical segment with its center offset from the focal point to reduce reradiation losses. A heat balance in the cavity absorber is required to establish the equilibrium surface temperature and the absorber efficiency. The absorber must be sized to accept the maximum heat flux that occurs when the ratio of shade-time to sun-time is a maximum. The end of a heat pipe could be incorporated in a cavity absorber and used to transfer heat to a heat storage unit or directly to a heat-using device. Efficiency of cavity absorbers discussed in the literature generally ranges from about 0.85 to 0.90. Weights will vary widely depending on what is included with the absorber, i.e., heat storage unit. Without heat storage material, specific weights of cavity absorbers appear to range from 4 - 6 lb/ft² of absorber surface area.

The Sunflower design offers an example of a cavity absorber. This design was to accept 76.5 kilowatts of energy from the solar collector through a 1.2-ft diameter aperture at extreme orbit/shade periods of 96/36-min at 300 nm and 1500/50 min at 20,000 nm. A spherical segment of 1.4-ft radius with a 1.2-ft aperture diameter was selected with its center offset from the focal point by about 1.25 ft. The absorber gave an efficiency of 0.903 and used lithium hydride located around the cavity for heat storage. The absorber also served as a mercury boiler for the Rankine-cycle power system. A shutter was devised to vary the aperture diameter during system startup. The unit weighed about 260 lb. and had sufficient lithium hydride to maintain the required heat flux and temperature during the 70-min. shade period at 20,000 nm.

Minneapolis-Honeywell, in a solar heat source design prepared under a USAF ML contract to provide 2.5 kilowatts at 1,250°F for a Vuellumier-cycle cryogenic cooler, used a different approach for a receiver design. They employed a low concentration ratio (about 50) to reduce sun-pointing requirements, a large rim angle (105°), and a hollow molybdenum spherical receiver (9.7-in diameter) as the evaporator section of a potassium heat pipe. The heat pipe (a nominal 1-in. diameter) then transported the heat from the receiver to a lithium-hydride heat storage device (a cylindrical bellows around the heat pipe) and the heat-using device. Pertinent characteristics of this design are given in Table 9-7.

Table 9-7

CHARACTERISTICS OF A SOLAR HEAT SOURCE
DESIGNED BY MINNEAPOLIS-HONEYWELL

Heat Intercepted by Collector	8.3 kw
Useful Heat for Refrig. (Ave. at 1250°F)	2.5 kw
Collector Diameter	9 ft
Rim Angle	105°
Collector Weight	75 lb
Receiver Diameter (Spherical)	9.7 in
Receiver Coating	$\alpha_s = 0.8, \quad \epsilon = 0.12$
Overall Efficiency	0.5
Potassium Heat Pipe Diameter	1 in
Percent Shadow Time	40%
Concentration Ratio	50
Heat Storage (Lithium Hydride in Cyl Bellows)	5.2 lb
Collector Pointing - 2 axes gimbal with 1° sun sensor and roll axis inertial wheel	

9.3.3 Heat Storage

Certain mission applications which might employ a solar collector experience periods when the collector will be shaded from the sun, e.g. earth orbital missions at 300 nm and 20,000 nm can typically have orbit-time/shade-time periods of 96/36-min and 1500/70-min respectively. The amount of heat that must be stored is a maximum at the mission condition that gives the maximum duration shade-time.

Over the years numerous studies of materials for use in storing heat have been conducted with the heat of fusion providing the heat to the using equipment during shade periods. For the temperature range of interest (1100-1200°F) for heat-powered refrigeration devices, lithium hydride appears to be a logical selection. Lithium fluoride has frequently been selected for temperatures appropriate for Ericsson-cycle applications (1500°F) but it has

a much lower heat of fusion than lithium hydride. Both of these materials undergo rather large volume changes in the liquid-solid transition, e.g., at its melting point lithium hydride as a solid has a density of 43.1 lb/ft^3 and as a liquid, 36.2 lb/ft^3 . Therefore the heat storage design must incorporate provisions to accommodate this volume change and still maintain acceptable heat transfer under zero-g conditions.

When a spherical-segment cavity absorber is used, the lithium hydride may be positioned around the surface in an annular area and heat absorbed in the cavity wall transferred by conduction to the lithium hydride. As noted earlier, heat pipes can be used to transfer the absorber heat to a heat storage unit located away from the absorber or directly to the heat using device. Transfer of heat from the heat storage material to the heat-using device can be by a forced convection (Nak) loop or by heat pipes.

Lithium hydride has a melt temperature of about 1260°F , a latent heat of fusion of about 1100 BTU/lb , and a heat capacity of about $2 \text{ BTU/lb-}^\circ\text{F}$. Operating a heat storage unit over a $1200\text{-}1500^\circ\text{F}$ range would provide storage of about 1695 BTU/lb of hydride. In order to provide 10 kilowatts for a 70-min shade period, the heat storage unit would have to supply about 40,000 BTU. This would require 36-lb of lithium hydride if only the latent heat of fusion were used and 23.6-lb of lithium hydride if the storage temperature were allowed to vary between $1200\text{-}1500^\circ\text{F}$ and both the latent heat of fusion and the sensible heat were used. The storage volume required for 36-lb of lithium hydride would be about 1.0 ft^3 at 1260°F and about 1.1 ft^3 at 1500°F .

Figure 9-13 can be used to estimate the solar collector diameter required to provide a given quantity of heat to a heat-using device in a typical earth-orbit. If some shade-time were to be encountered, the amount of heat required should be increased by the ratio of orbit time to sun time. As an example, if 5-kilowatts of heat were required with an orbit-time to sun-time ratio of 1.6 and with an overall collector efficiency of 0.78 and an absorber efficiency of 0.90, an ordinate value of 8-kilowatts (5×1.6) intersects the $0.7 \eta_{c/a}$ curve ($\sim 0.90 \times 0.78$) at a collector diameter of 10.4 ft. Table 9-8 indicates

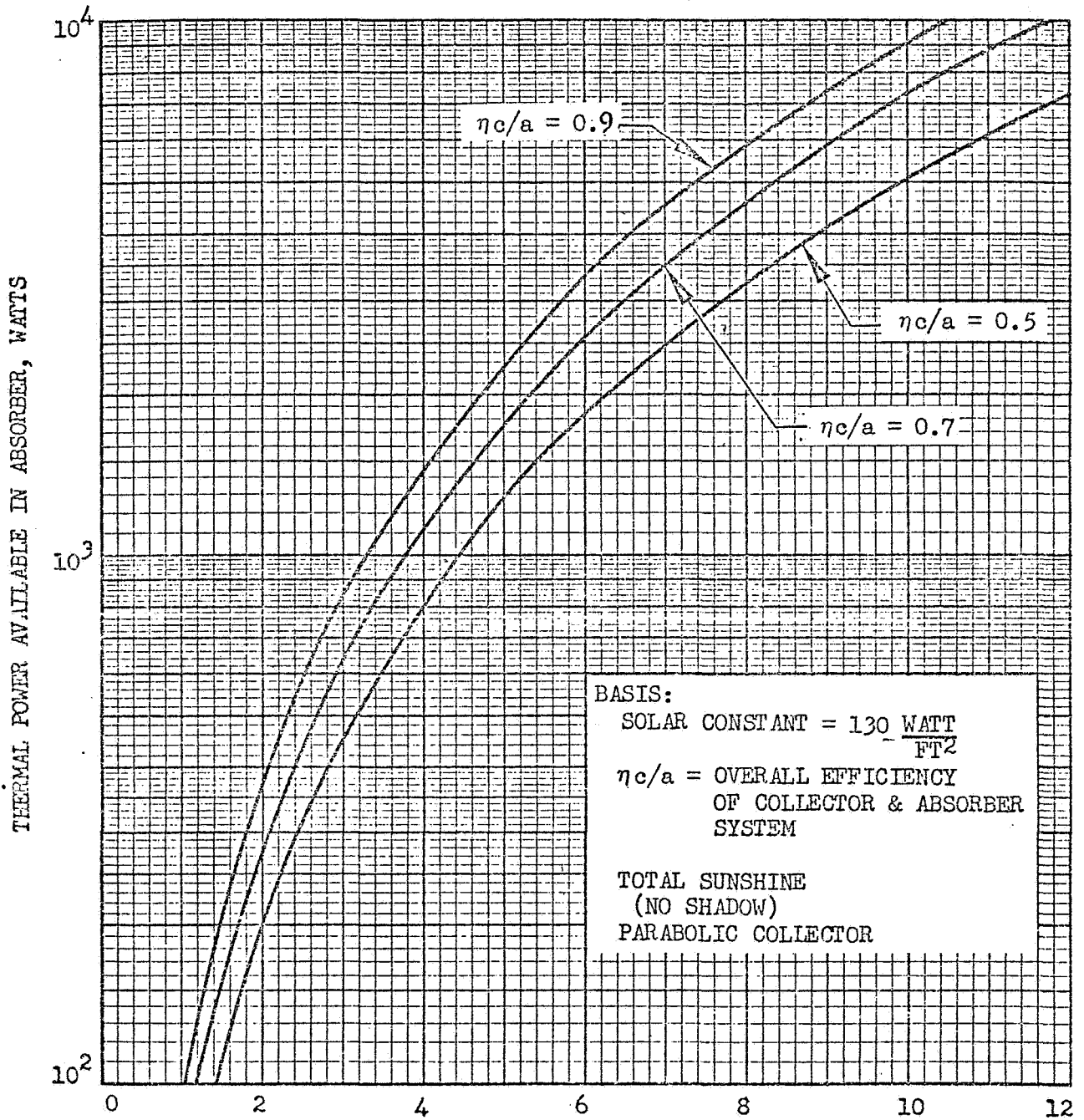


Fig 9-13 SOLAR COLLECTOR DIAMETER - FT

typical absorber aperture diameters as a function of heat in absorber and absorber/collector efficiency. Table 9-9 presents typical characteristics of solar collector/absorber heat sources.

Table 9-8
 TYPICAL ABSORBER APERTURE DIAMETERS* (FT)

$\eta_{c/a}$	100 Watts	1000 Watts	10,000 Watts
0.5	0.042	0.133	0.419
0.7	0.035	0.112	0.355
0.9	0.031	0.099	0.312

* Based on six times diameter of solar image at focal plane
 (Concentration ratio \sim 1100) (Rim angle = 50°)

Table 9-9

TYPICAL* CHARACTERISTICS OF SOLAR
COLLECTOR/ABSORBER HEAT SOURCES

Useful heat absorbed, kw	0.10	1.00	10.0
Collector diameter, ft	1.25	3.95	12.5
Collector weight, lb	0.61	6.10	61.0
Focal length, ft	0.67	2.12	6.7
Aperture diameter, ft	0.037	0.12	0.37
Cavity absorber inner diameter, ft	0.15	0.47	1.5
Cavity absorber weight, lb	0.17	1.70	17.0
System weight, lb	0.94	9.36	93.6

* Basis:

Collector overall efficiency = 0.7

Absorber overall efficiency = 0.9

Rim angle = 50°

Aperture diameter = six times solar image at focal plane

Heat flux limit into heat storage material = 2.93 kw/ft^2

Collector specific weight = 0.5 lb/ft^2

Absorber specific weight = 5.0 lb/ft^2

Near earth orbit

System weight includes 20% for structure support and contingency
but no allowance for heat storage material weight

Section 10
CRYOGENS PROPERTIES

A limited amount of cryogen property data have been included in this report so that the user will have a handy source of some of the more often used data that is pertinent to cryogenic refrigeration. No attempt has been made to provide a comprehensive set of data because most of this information is available in NBS technical notes. If detailed property data is required it is suggested that other sources be utilized.

The data included here is the liquid density, saturated pressure, and heat of vaporization versus temperature for each of the cryogens; hydrogen, oxygen, fluorine and nitrogen. A plot of pressure versus internal energy for each of these cryogens has also been prepared and is included. It has been found that these plots greatly facilitate heat-pressure balance calculations in liquid cryogenic tanks.

A summary of the figures are given below.

	Figure
Hydrogen -	
Density - Pressure - Heat of Vaporization - Temperature	10-1
Pressure - Internal Energy	10-2
Oxygen -	
Density - Pressure - Heat of Vaporization - Temperature	10-3
Pressure - Internal Energy	10-4
Fluorine -	
Density - Pressure - Heat of Vaporization - Temperature	10-5
Pressure - Internal Energy	10-6
Nitrogen -	
Density - Pressure - Heat of Vaporization Temperature	10-7
Pressure - Internal Energy	10-8

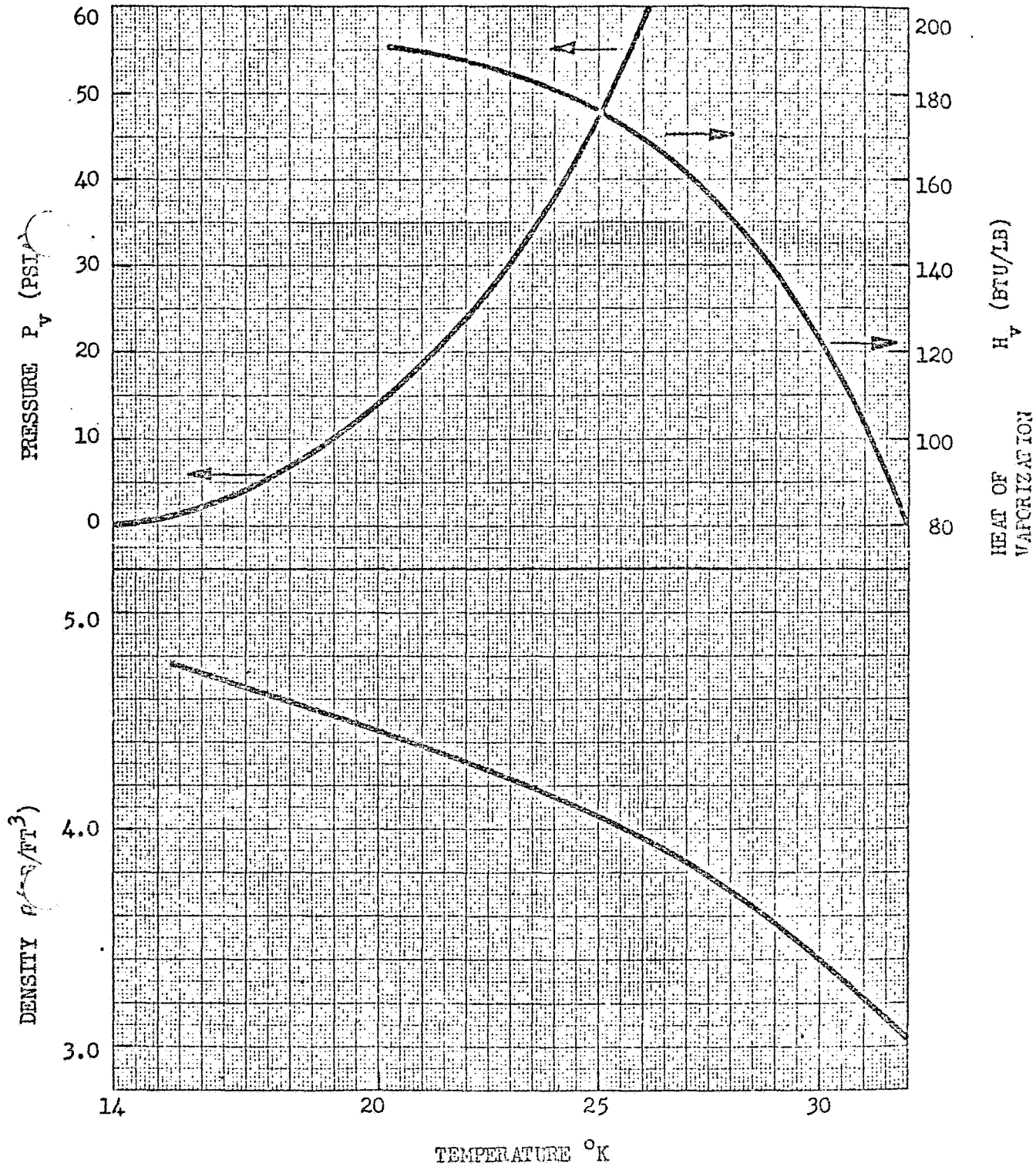


Fig. 10-1 PROPERTIES OF LIQUID HYDROGEN

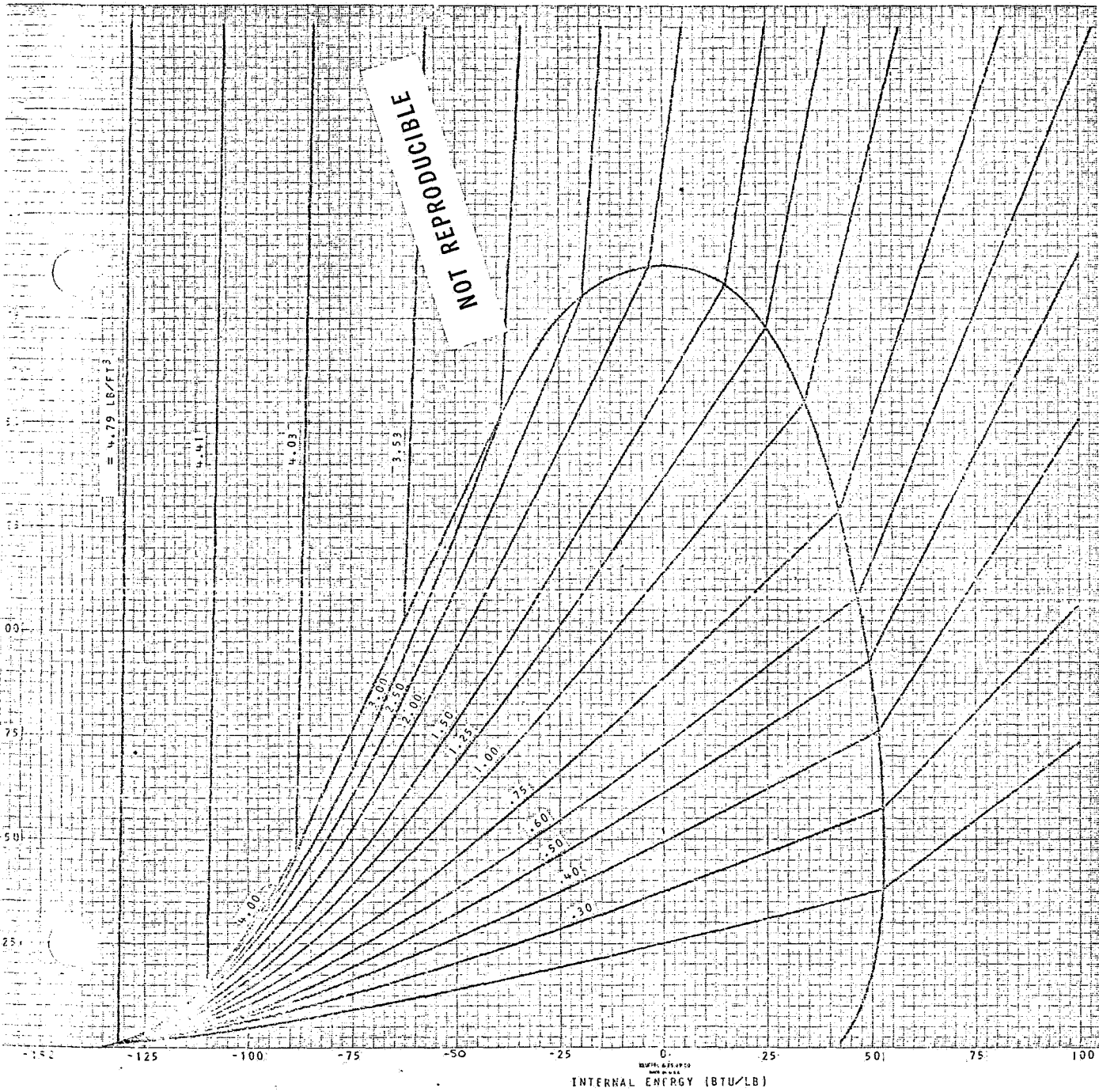


Fig. 10-2 Hydrogen Pressure Versus Internal Energy

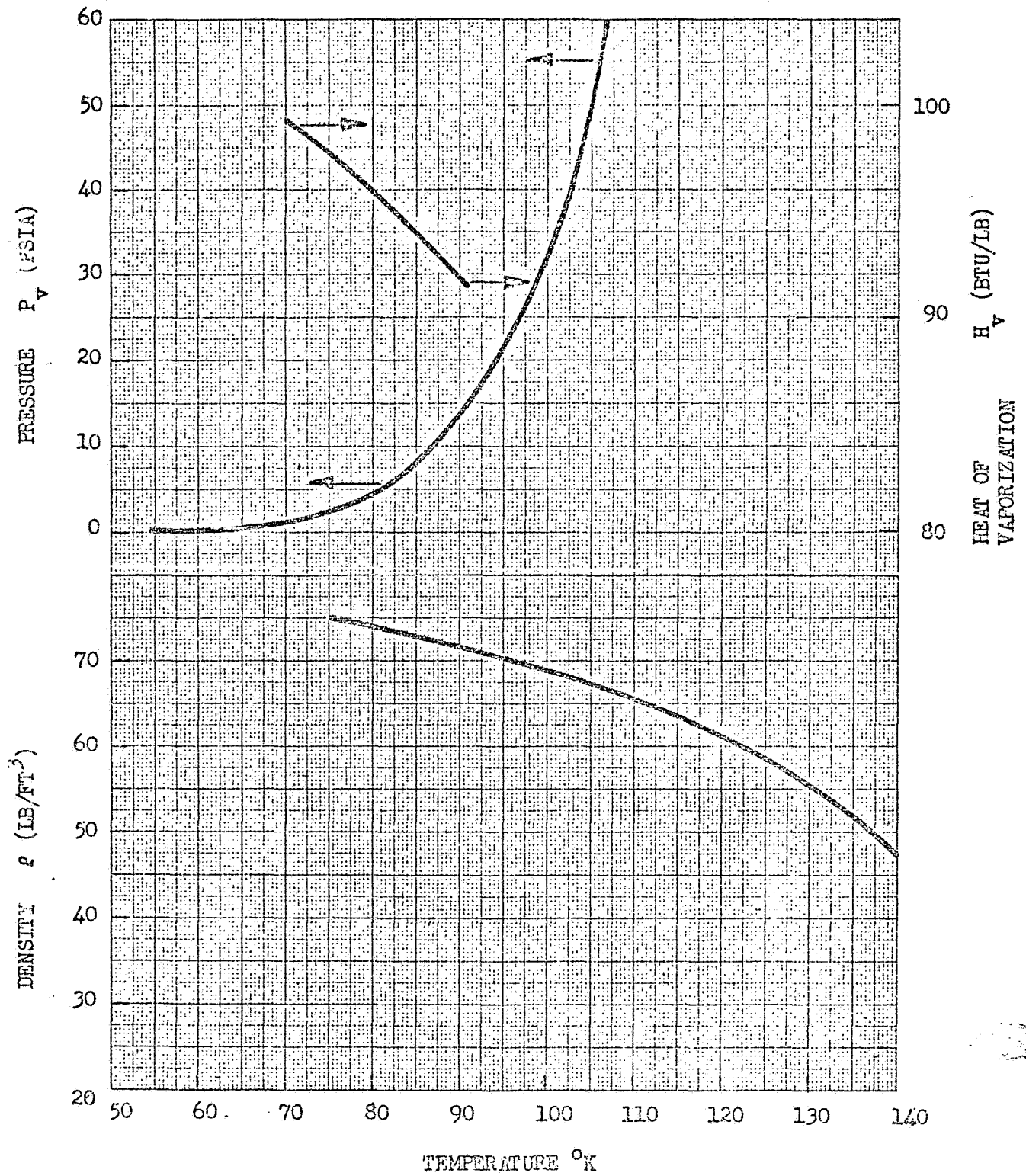


Fig. 10-3 PROPERTIES OF LIQUID OXYGEN

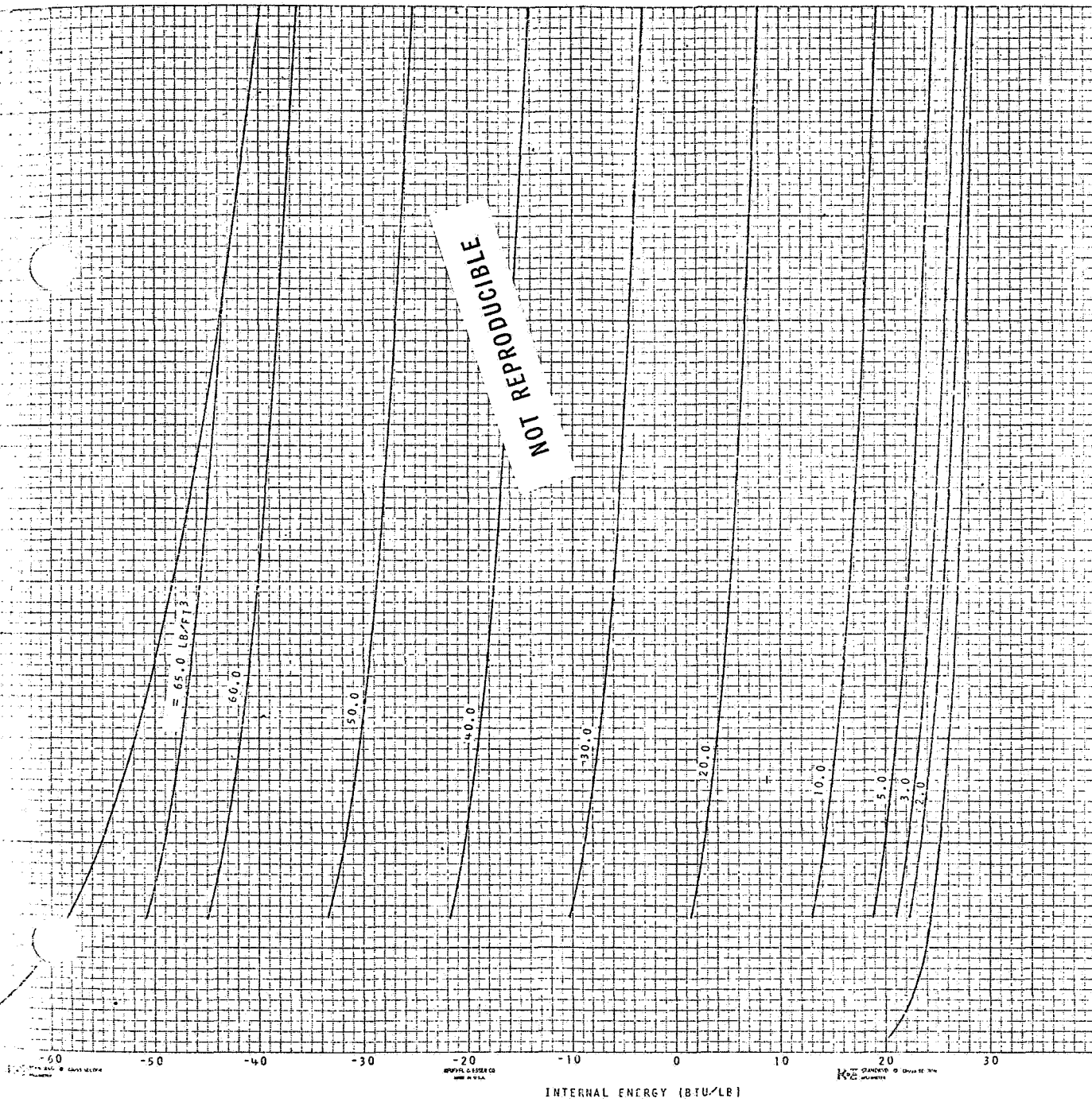


Fig. 10-4 Oxygen Pressure Versus Internal Energy

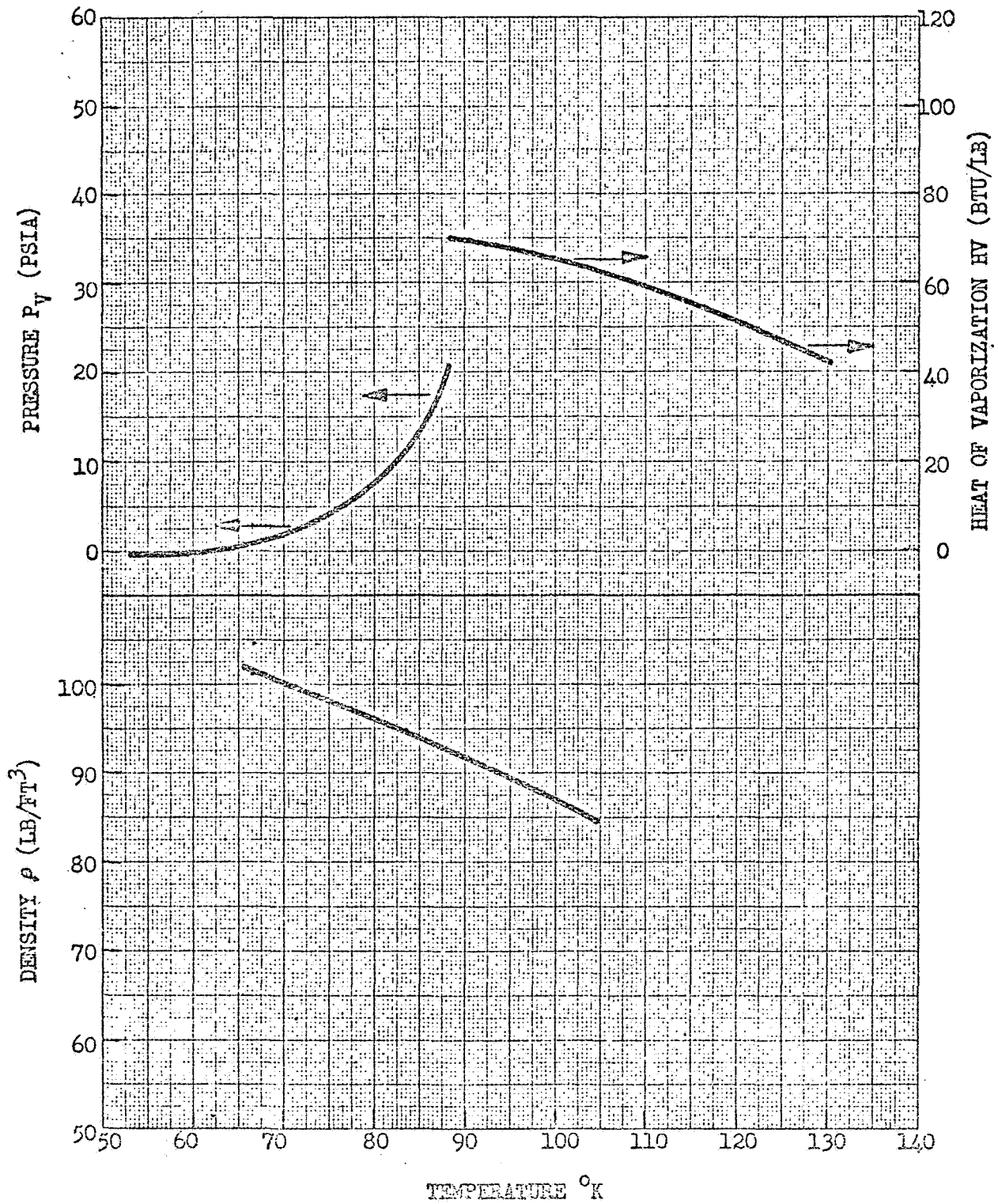


Fig. -10-5 PROPERTIES OF LIQUID FLUORINE

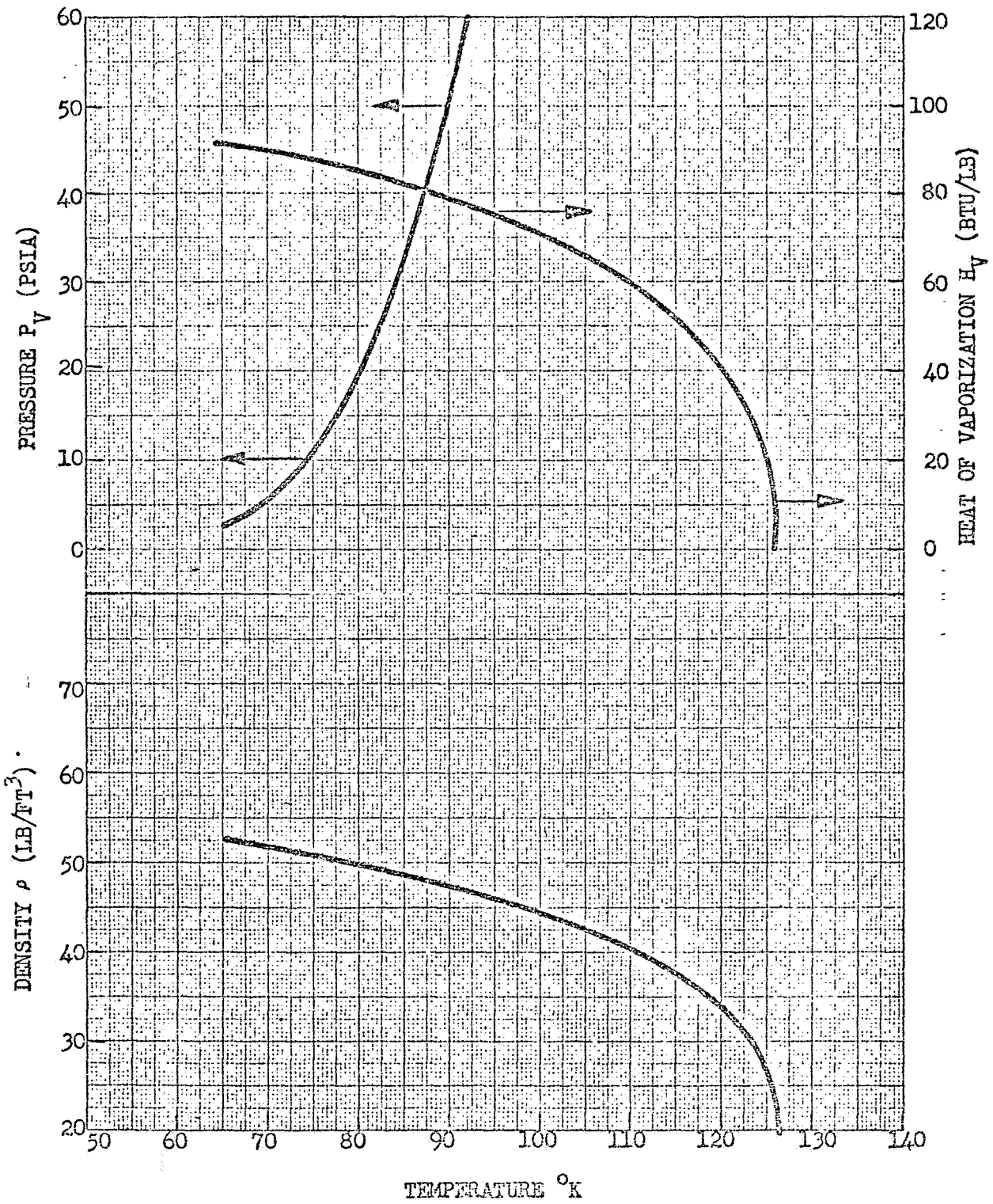


Fig. 10-7 PROPERTIES OF LIQUID NITROGEN

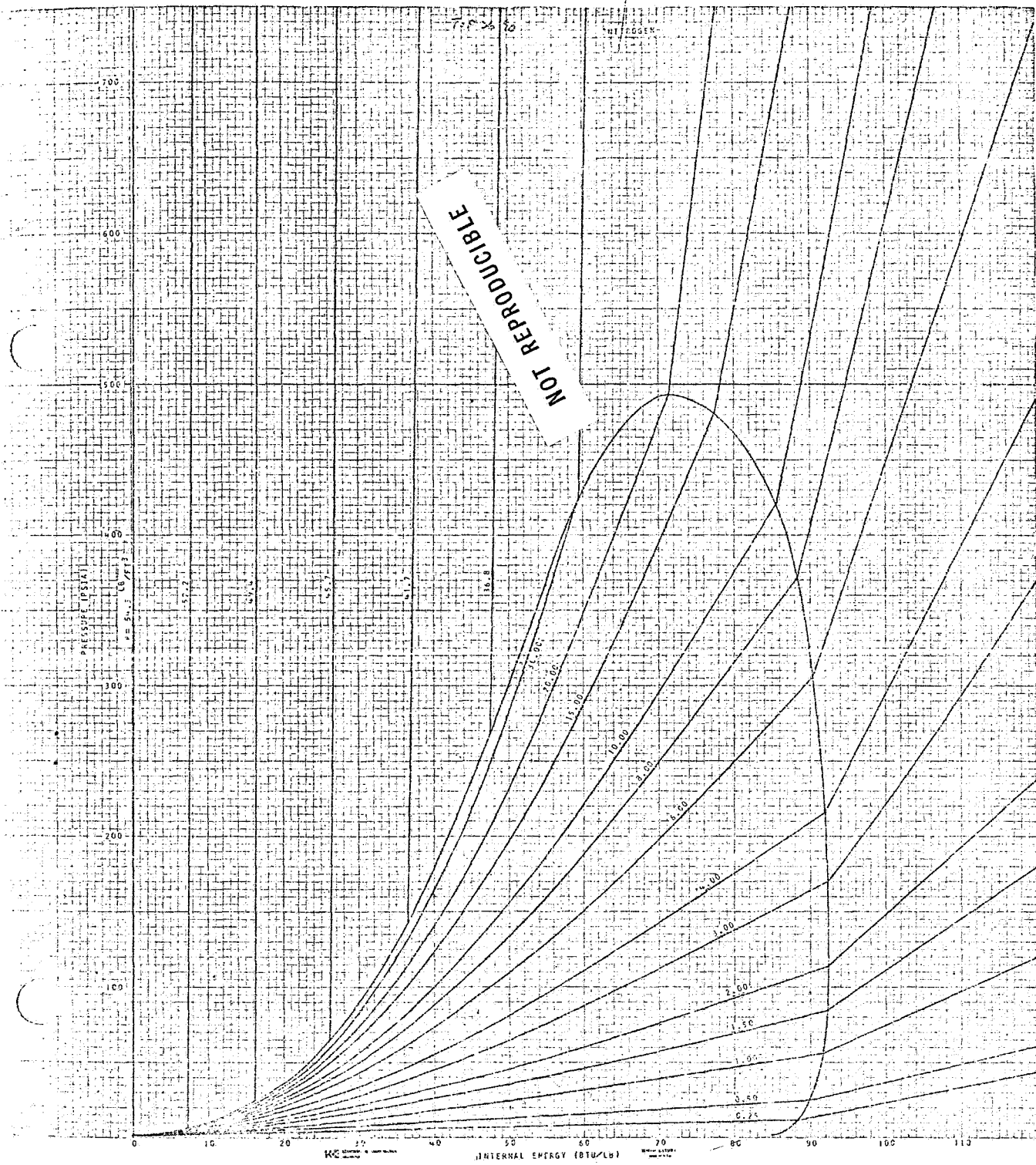


Fig. 10-8 Nitrogen Pressure Versus Internal Energy

Section 11 CONVERSION UNITS

11.1 INTRODUCTION

It has long been recognized that the use of varied and inconsistent systems of units in the various engineering and scientific disciplines has been a major source of inefficiency, errors and duplication of effort. Also, the lack of a common system of units has handicapped communication between engineers working in different fields of application of the same fundamental discipline.

To alleviate such communications problems on a world-wide basis, the International Committee on Weights and Measures has adopted a system referred to as the International System of Units (Reference 1). This system, abbreviated SI, is based on six fundamental units of measure as follows:

Length	meter	m
Mass	Kilogram	kg
Time	second	s
Electric Current	ampere	A
Thermodynamic Temperature	degrees Kelvin	°K
Light Intensity	candle	cd

The purpose of this section is to provide the user of this referation material a convenient set of conversion units. There is presented in this section the definitions of the SI units, a list of thermodynamic constants giving their values in SI units, and a set of conversion tables. Since it is likely that continued emphasis will be placed on using the SI units, most attention has been directed toward them.

11.2 THE INTERNATIONAL SYSTEM OF UNITS

The system based on the six basic units mentioned above is referred to as the International System of Units; the international abbreviation of the name of this system is SI. The defined values of the basic units of measure are given in Table I and a partial list of the set of values of the physical constants recommended by NAS-NRC is given in Table III.

The term "mass" denotes the quantity of matter contained in material objects, and "weight" denotes a force acting on an object. The preferred unit of force is the newton (N); the pound force (lbf) is equivalent to 4.4482216 newton and the pound mass (lbm) is equivalent to .45358 kilogram. Thus a man of 70.0 kg (154 lbm) mass, standing on the surface of the moon where the gravitational acceleration is 1.62 m/s^2 , weighs 113 newton (25.4 lbf). On the surface of the earth where the gravitational acceleration is 9.807 m/s^2 he would weigh 686 newton (154 lbf).

The preferred unit of energy (mechanical, electrical, thermal) is the joule (J). The mean British thermal unit (Btu) is equivalent to 1054.8 joules; thus a heat flow rate of 1 Btu per second (Btu/s) is equivalent to 1055 joules per second (J/s) or 1055 watts (W).

The preferred unit of pressure is the newton/meter² (N/m²) or newton/centimeter² (N/cm²). Thus 10.1 N/cm^2 is equivalent to 14.7 psi or 760 Torr.

11.3 SUMMARY OF CONVERSION DATA

The various basic and derived units are listed in the following tables. Also listed are the values of often used constants. An index to the various tables are given here.

	Table <u>No.</u>
Defined Values of Basic Units	1
Secondary SI Units	2
Values of Constants in the SI Units	3
Length	4
Area	5
Volume	6
Linear Velocity	7
Angular Velocity	8
Linear Acceleration	9
Angular Acceleration	10

	<u>Table No.</u>
Mass and Weight	11
Density	12
Force	13
Pressure	14
Torque	15
Moment of Inertia	16
Energy, Work and Heat	17
Power, Heat Flux	18
Power Density, Heat Flux Density	19
Temperature	20
Thermal Conductivity	21
Thermal Resistance	22
Thermal Capacitance	23
Thermal Diffusivity	24
Special Heat	25
Latent Heat	26
Viscosity	27
Kinematic Viscosity	28

These tables have been checked carefully; however, some errors may have escaped detection and the writer would appreciate having them brought to his attention so that corrections may be communicated to other users of these tables.

REF: (1) Translation of "Systeme International d'Unites. Resolution 12.",
NASA TTF-8365, February 1963

Table 1

DEFINED VALUES OF BASIC UNITS AND EQUIVALENTS

Meter (m)	1 650 763.73 wavelengths in vacuo of the unperturbed transition $2p_{10} - 5d_5$ in ^{86}Kr
Kilogram (kg)	Mass of the international kilogram at Sevres, France
Second (s)	1/31 556 925.974 7 of the tropical year at 12 ^h ET, 0 January 1900
Degrees Kelvin ($^{\circ}\text{K}$)	Defined in the thermodynamic scale by assigning 273.16°K to the triple point of water (freezing point, $273.15^{\circ}\text{K} = 0^{\circ}\text{C}$)
Ampere (A)	Current required to produce a force of 2×10^{-7} newton per meter of length in two straight parallel conductors of infinite length placed 1 meter apart in a vacuum
Candle (cd)	1/60 of the intensity of 1 square centimeter of a black-body radiator operated at the freezing temperature of platinum
Unified atomic mass unit (u)	1/12 of the mass of an atom of the ^{12}C nuclide
Mole (mol)	Amount of substance containing the same number of atoms as 12g of pure ^{12}C
Standard acceleration of free fall (gn)	9.806 65 ms^{-2} 980.665 cm s^{-2}
Normal atmospheric pressure (atm)	101 325 N m^{-2}

Table 2
SECONDARY UNITS IN THE INTERNATIONAL SYSTEM

<u>Physical Quantity</u>	<u>Unit</u>	
Area	square meter	m^2
Volume	cubic meter	m^3
Frequency	hertz	Hz, 1/s
Density	kilograms per cubic meter	kg/m^3
Velocity	meter per sec.	m/s
Angular velocity	radians per sec.	rad/s
Acceleration	meters per sec. squared	m/s^2
Angular acceleration	radians per sec. squared	rad/s^2
Force	newton per sq. meter	N, $kg.m/s^2$
Kinematic viscosity	sq. meter per second	m^2/s
Dynamic viscosity	newton-second per sq. meter	$N.s/m^2$
Work, energy, quantity of heat	joule	j, n.m
Power	watt	W, J/s
Electric charge	coulomb	C, A.s
Voltage, potential difference	volt	V, W/A
Electric field intensity	volt per meter	V/M
Electric resistance	ohm	Ω , V/A
Electric capacitance	farad	F, A.s/V
Magnetic flux	weber	Wb, V.s
Inductance	henry	H, V.s/A
Magnetic field	tesla	T, Wb/m^2
Magnetic field intensity	amperes per meter	A/M

Table 2 (Cont.)

<u>Physical Quantity</u>	<u>Unit</u>	
Magnetomotive force	ampere	A
Flux of light	lumen	lm, cd.sr
Luminance	candle per sq. meter	cd/m ²
Illumination	lux	lx, lm/m ²
Plane angle	radian	rad
Solid angle	steradian	sr
Pressure	newtons per sq. meter	N/m ²

Table 3
VALUES OF PHYSICAL CONSTANTS IN SI UNITS

<u>Constant</u>	<u>Symbol</u>	<u>Value</u>
Speed of light in vacuum	c	$2.997925 \times 10^8 \text{ ms}^{-1}$
Elementary charge	e	$1.60210 \times 10^{-19} \text{ C}$
Avogadro constant	N_A	$6.02252 \times 10^{23} \text{ mol}^{-1}$
Electron rest mass	m_e	$9.1091 \times 10^{-31} \text{ kg}$ $5.48597 \times 10^{-4} \text{ u}$
Planck constant	h	$6.6256 \times 10^{-34} \text{ Js}$
Gas constant	R	$8.3143 \text{ J } ^\circ\text{K}^{-1} \text{ mol}^{-1}$
Normal volume perfect gas	V_0	$2.24136 \times 10^{-2} \text{ m}^3 \text{ mol}^{-1}$
Boltzmann constant	k	$1.38054 \times 10^{-23} \text{ J } ^\circ\text{K}^{-1}$
First radiation constant	c_1	$3.7405 \times 10^{-16} \text{ Wm}^2$
Second radiation constant	c_2	$1.43879 \times 10^{-2} \text{ m } ^\circ\text{K}$
Wein displacement constant	b	$2.8978 \times 10^{-3} \text{ m } ^\circ\text{K}$
Stefan-Boltzmann constant	σ	$5.6697 \times 10^{-8} \text{ Wm}^{-2} \text{ } ^\circ\text{K}^{-4}$
Gravitational constant	G	$6.670 \times 10^{-11} \text{ Nm}^2 \text{ kg}^{-2}$
Mean solar constant	S	$1.40 \times 10^3 \text{ Wm}^{-2}$

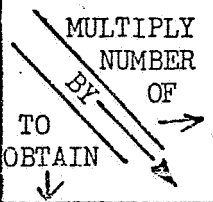
Table 4

LENGTH

MULTIPLY BY NUMBER OF TO OBTAIN	CENTIMETERS*	FEET	INCHES	KILOMETERS	NAUTICAL MILES	METERS*	MILES	MILLIMETERS*
CENTIMETERS*	1	30.48	2.540	10^5	1.853×10^5	100	1.609×10^5	0.1
FEET	3.281×10^{-2}	1	8.333×10^{-2}	3281	6030.27	3.281	5280	3.281×10^{-3}
INCHES	0.3937	12	1	3.937×10^4	7.296×10^4	39.37	6.336×10^4	3.937×10^{-2}
KILOMETERS*	10^{-5}	3.048×10^{-4}	2.540×10^{-5}	1	1.853	0.001	1.609	10^{-6}
NAUTICAL MILES	5.396×10^{-6}	1.645×10^{-4}	1.371×10^{-5}	0.5396	1	5.396×10^{-4}	0.8684	5.396×10^{-7}
METERS*	0.01	0.3048	2.540×10^{-2}	1000	1853	1	1609	10^{-3}
MILES	6.214×10^{-6}	1.894×10^{-4}	1.578×10^{-5}	0.6214	1.1516	6.214×10^{-4}	1	6.214×10^{-7}
MILLIMETERS*	10	304.8	25.40	10^6	1.853×10^6	1000	1.609×10^6	1

Table 5

AREA

	SQUARE* CENTIMETERS	SQUARE FEET	SQUARE INCHES	SQUARE KILOMETERS	SQUARE* METERS	SQUARE MILES	SQUARE MILLIMETERS
SQUARE* CENTIMETERS	1	929.0	6.452	10^{10}	10^4	2.590×10^{10}	0.01
SQUARE FEET	1.076×10^{-3}	1	6.944×10^{-3}	1.076×10^7	10.764	2.788×10^7	1.076×10^{-5}
SQUARE INCHES	0.1550	144	1	1.550×10^9	1550	4.015×10^9	1.550×10^{-3}
SQUARE KILOMETERS	10^{-10}	9.290×10^{-8}	6.452×10^{-10}	1	10^{-6}	2.590	10^{-12}
SQUARE* METERS	0.0001	9.290×10^{-2}	6.452×10^{-4}	10^6	1	2.590×10^6	10^{-6}
SQUARE MILES	3.861×10^{-11}	3.567×10^{-8}	2.4907×10^{-10}	0.3861	3.861×10^{-7}	1	3.861×10^{-13}
SQUARE MILLIMETERS	100	9.290×10^4	645.2	10^{12}	10^6	2.590×10^{12}	1

PRECEDING PAGE BLANK NOT FILMED

Table 6

VOLUME

TO OBTAIN by MULTIPLY NUMBER OF	CUBIC* CENTIMETERS	CUBIC FEET	CUBIC INCHES	CUBIC* METERS	GALLONS (LIQUID)	LITERS
CUBIC* CENTIMETER	1	2.832 $\times 10^4$	16.39	10^6	3785	1000
CUBIC FEET	3.531 $\times 10^{-5}$	1	5.787 $\times 10^{-4}$	35.314	0.1337	3.531 $\times 10^{-2}$
CUBIC INCHES	6.102 $\times 10^{-2}$	1728	1	6.102 $\times 10^4$	231	61.02
CUBIC* METERS	10^{-6}	2.832 $\times 10^{-2}$	1.639 $\times 10^{-5}$	1	3.785 $\times 10^{-3}$	0.001
GALLONS (LIQUID)	2.642 $\times 10^{-4}$	7.481	4.329 $\times 10^{-3}$	264.2	1	0.2642
LITERS	0.001	28.32	1.639 $\times 10^{-2}$	1000	3.785	1

80

Table 7
LINEAR VELOCITY

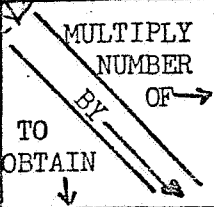
 TO OBTAIN BY OF	CENTIMETERS PER SECOND	FEET PER MINUTE	FEET PER SECOND	KILOMETERS PER HOUR	KILOMETERS PER MINUTE	METERS PER MINUTE	METERS* PER SECOND
CENTIMETERS PER SECOND	1	0.5080	30.48	27.78	1667	1.667	100
FEET PER MINUTE	1.969	1	60	54.68	3281	3.281	196.8
FEET PER SECOND	3.281×10^{-2}	1.667×10^{-2}	1	0.9113	54.68	5.468×10^{-2}	3.281
KILOMETERS PER HOUR	0.036	1.829×10^{-2}	1.097	1	60	0.06	3.6
KILOMETERS PER MINUTE	0.0006	3.048×10^{-4}	1.829×10^{-2}	1.667×10^{-2}	1	0.001	0.06
METERS PER MINUTE	0.6	0.3048	18.29	16.67	1000	1	60
METERS* PER SECOND	0.01	5.080×10^{-3}	0.3048	0.2778	16.67	1.667×10^{-2}	1

Table 8
ANGULAR VELOCITY

TO OBTAIN ↓ BY ↘ MULTIPLY NUMBER OF → ↙	DEGREES PER SECOND	RADIANS* PER SECOND	REVOLUTIONS PER MINUTE	REVOLUTIONS PER SECOND
DEGREES PER SECOND	1	57.30	6	360
RADIANS* PER SECOND	1.745 $\times 10^{-2}$	1	0.1047	6.283
REVOLUTIONS PER MINUTE	0.1667	9.549	1	60
REVOLUTIONS PER SECOND	2.778 $\times 10^{-3}$	0.1592	1.667 $\times 10^{-2}$	1

Table 9

LINEAR ACCELERATION

TO OBTAIN ↓ BY ↘ MULTIPLY NUMBER OF →	CENTIMETERS PER SECOND PER SECOND	FEET PER SECOND PER SECOND	KILOMETERS PER HOUR PER SECOND	METERS* PER SECOND PER SECOND	MILES PER HOUR PER SECOND
CENTIMETERS PER SECOND PER SECOND	1	30.48	27.78	100	44.70
FEET PER SECOND PER SECOND	3.281 $\times 10^{-2}$	1	0.9113	5.281	1.467
KILOMETERS PER HOUR PER SECOND	0.036	1.097	1	3.6	1.609
METERS* PER SECOND PER SECOND	0.01	0.3048	0.2778	1	0.4470
MILES PER HOUR PER SECOND	2.237 $\times 10^{-2}$	0.6818	0.6214	2.237	1

Table 10

ANGULAR ACCELERATION

<p>MULTIPLY NUMBER OF</p> <p>8γ</p> <p>TO OBTAIN</p>	<p>RADIANS* PER SECOND PER SECOND</p>	<p>REVOLUTIONS PER MINUTE PER MINUTE</p>	<p>REVOLUTIONS PER MINUTE PER SECOND</p>	<p>REVOLUTIONS PER SECOND PER SECOND</p>
<p>RADIANS* PER SECOND PER SECOND</p>	<p>1</p>	<p>1.745 $\times 10^{-3}$</p>	<p>0.1047</p>	<p>6.283</p>
<p>REVOLUTIONS PER MINUTE PER MINUTE</p>	<p>573.0</p>	<p>1</p>	<p>60</p>	<p>3600</p>
<p>REVOLUTIONS PER MINUTE PER SECOND</p>	<p>9.549</p>	<p>1.667 $\times 10^{-2}$</p>	<p>1</p>	<p>60</p>
<p>REVOLUTIONS PER SECOND PER SECOND</p>	<p>0.1592</p>	<p>2.778 $\times 10^{-4}$</p>	<p>1.667 $\times 10^{-2}$</p>	<p>1</p>

Table 11

TABLE 11 - MASS AND WEIGHT

TO OBTAIN ↓ BY ↘ MULTIPLY NUMBER OF →	GRAMS*	KILOGRAMS*	MILLIGRAMS	OUNCES	POUNDS
GRAMS*	1	1000	0.001	28.35	453.6
KILOGRAMS*	0.001	1	10^{-6}	2.835×10^{-2}	0.4536
MILLIGRAMS	1000	10^6	1	2.835×10^4	4.536×10^5
OUNCES	3.527×10^{-2}	35.27	3.527×10^{-5}	1	16
POUNDS	2.205×10^{-3}	2.205	2.205×10^{-6}	6.250×10^{-2}	1

Table 12

DENSITY

TO OBTAIN ↓ BY ↘ MULTIPLY NUMBER OF →	GRAMS PER CUBIC CENTIMETER	KILOGRAMS* PER CUBIC METER	POUNDS PER CUBIC FOOT	POUNDS PER CUBIC INCH
GRAMS PER CUBIC CENTIMETER	1	0.001	1.602 $\times 10^{-2}$	27.63
KILOGRAMS* PER CUBIC METER	1000	1	16.02	2.768 $\times 10^4$
POUNDS PER CUBIC FOOT	62.43	6.243 $\times 10^{-2}$	1	1728
POUNDS PER CUBIC INCH	3.613 $\times 10^{-2}$	3.613 $\times 10^{-5}$	5.787 $\times 10^{-4}$	1

Table 13

FORCE

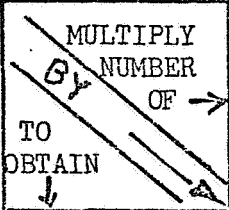
	DYNES	GRAMS	JOULES PER CM	NEWTONS* OR JOULES PER METER	KILOGRAMS	POUNDS	POUNDALS
DYNES	1	980.7	10^7	10^5	9.807×10^5	4.448×10^5	1.383×10^4
GRAMS	1.028×10^{-3}	1	1.020×10^4	102.0	1000	453.6	14.10
JOULES PER CM	10^{-7}	9.807×10^{-5}	1	0.01	9.807×10^{-2}	4.448×10^{-2}	1.383×10^{-3}
NEWTONS* OR JOULES PER METER	10^{-5}	9.807×10^{-3}	100	1	9.807	4.448	0.1383
KILOGRAMS	1.020×10^{-6}	0.001	10.20	0.1020	1	0.4536	1.410×10^{-2}
POUNDS	2.248×10^{-6}	2.205×10^{-3}	22.48	0.2248	2.205	1	3.108×10^{-2}
POUNDALS	7.233×10^{-5}	7.093×10^{-2}	725.3	7.233	70.93	32.17	1

Table 14

PRESSURE OR FORCE PER UNIT PER AREA

MULTIPLY BY TO OBTAIN	ATMOSPHERES	DYNES PER SQUARE CENTIMETER	MILLIMETERS OF MERCURY AT 0°C	INCHES OF MERCURY AT 0°C	KILOGRAMS PER SQUARE METER	POUNDS PER SQUARE FOOT	POUNDS PER SQUARE INCH	NEWTONS* PER SQUARE METER
ATMOSPHERES	1	9.869 $\times 10^{-7}$	1.316 $\times 10^{-3}$	3.342 $\times 10^{-2}$	9.678 $\times 10^{-5}$	4.725 $\times 10^{-4}$	6.804 $\times 10^{-2}$	9.869 $\times 10^{-6}$
DYNES PER SQUARE CENTIMETER	1.013 $\times 10^{-6}$	1	1.333 $\times 10^3$	3.386 $\times 10^4$	98.07	478.8	6.895 $\times 10^4$	10
MILLIMETERS OF MERCURY AT 0°C	760.0	7.501 $\times 10^{-4}$	1	25.40	7.356 $\times 10^{-2}$	0.3591	51.71	7.50 $\times 10^{-3}$
INCHES OF MERCURY AT 0°C	29.92	2.953 $\times 10^{-5}$	3.937 $\times 10^{-2}$	1	2.896 $\times 10^{-3}$	1.414 $\times 10^{-2}$	2.036	1.953 $\times 10^{-4}$
KILOGRAMS PER SQUARE METER	1.033 $\times 10^4$	1.020 $\times 10^{-2}$	13.60	345.3	1	4.882	703.1	0.1020
POUNDS PER SQUARE FOOT	2117	2.089 $\times 10^{-3}$	2.7845	70.73	0.2048	1	144	2.089 $\times 10^{-2}$
POUNDS PER SQUARE INCH	14.70	1.450 $\times 10^{-5}$	1.9337 $\times 10^{-2}$	0.4912	1.422 $\times 10^{-3}$	6.944 $\times 10^{-3}$	1	1.450 $\times 10^{-4}$
NEWTONS* PER SQUARE METER	1.013 $\times 10^5$	0.10	133.3	3.386 $\times 10^3$	9.807	47.88	6.395 $\times 10^3$	1

Table 15

TORQUE

TO OBTAIN ↓ BY ↘ MULTIPLY NUMBER OF →	DYNE-CENTIMETERS	GRAM-CENTIMETERS	KILOGRAM-METERS	POUND- FEET	NEWTON*- METER
DYNE-CENTIMETERS	1	980.7	9.807 $\times 10^7$	1.356 $\times 10^7$	10^7
GRAM-CENTIMETERS	1.020 $\times 10^{-3}$	1	10^5	1.383 $\times 10^4$	1.020 $\times 10^4$
KILOGRAM-METERS	1.020 $\times 10^{-3}$	10^{-5}	1	0.1383	0.1020
POUND- FEET	7.376 $\times 10^{-3}$	7.233 $\times 10^{-5}$	7.233	1	0.7376
NEWTON*- METER	10^{-7}	9.807 $\times 10^{-4}$	9.807	1.305	1

Table 16
MOMENT OF INERTIA

MULTIPLY NUMBER OF → BY ↓ TO OBTAIN ↓	GRAM- CENTIMETERS SQUARED	KILOGRAM- METERS SQUARED	POUND- INCHES SQUARED	POUND- FEET SQUARED
GRAM- CENTIMETERS SQUARED	1	10^7	2.9266 $\times 10^3$	4.21434 $\times 10^5$
KILOGRAM- METERS SQUARED	10^{-7}	1	2.9266 $\times 10^{-4}$	4.21434 $\times 10^{-2}$
POUND- INCHES SQUARED	3.4169 $\times 10^{-4}$	3.4169 $\times 10^3$	1	144
POUND- FEET SQUARED	2.37285 $\times 10^{-6}$	23.7285	6.944 $\times 10^{-3}$	1

Table 17)

ENERGY, WORK, AND HEAT

MULTIPLY BY TO OBTAIN	BRITISH THERMAL UNITS	CENTIMETER- GRAMS	ERGS OR CENTIMETER- DYNES	FOOT- POUNDS	HORSEPOWER HOURS	JOULES, WATT- SECONDS OR NEWTON - METERS	KILOGRAM- CALORIES	WATT- HOURS
BRITISH THERMAL UNITS	1	9.297 $\times 10^{-8}$	9.480 $\times 10^{-11}$	1.285 $\times 10^{-3}$	2545	9.4709 $\times 10^{-4}$	3.969	3.413
CENTIMETER- GRAMS	1.076 $\times 10^7$	1	1.020 $\times 10^{-3}$	1.383 $\times 10^4$	2.737 $\times 10^{10}$	1.020 $\times 10^4$	4.269 $\times 10^7$	3.671 $\times 10^7$
ERGS OR CENTIMETER- DYNES	1.055 $\times 10^{10}$	980.7	1	1.356 $\times 10^7$	2.684 $\times 10^{13}$	10^7	4.186 $\times 10^{10}$	3.60 $\times 10^{10}$
FOOT- POUNDS	778.3	7.233 $\times 10^{-5}$	7.367 $\times 10^{-8}$	1	1.98 $\times 10^6$	0.7376	3087	2655
HORSEPOWER- HOURS	3.929 $\times 10^{-4}$	3.654 $\times 10^{-11}$	3.722 $\times 10^{-14}$	5.050 $\times 10^{-7}$	1	3.722 $\times 10^{-7}$	1.559 $\times 10^{-3}$	1.341 $\times 10^{-3}$
JOULES, WATT- SECONDS OR NEWTON - METERS	1055.87	9.507 $\times 10^{-5}$	10^{-7}	1.356	2.684 $\times 10^6$	1	4186	3600
KILOGRAM- CALORIES	0.2520	2.343 $\times 10^{-8}$	2.389 $\times 10^{-11}$	3.239 $\times 10^{-4}$	641.3	2.389 $\times 10^{-4}$	1	0.8600
WATT- HOURS	0.2930	2.724 $\times 10^{-8}$	2.778 $\times 10^{-11}$	3.766 $\times 10^{-4}$	745.7	2.778 $\times 10^{-4}$	1.163	1

Table 18

POWER, HEAT FLUX, RADIANT FLUX

TO OBTAIN ↓ BY ↙ MULTIPLY NUMBER OF ↑	BRITISH THERMAL UNITS PER SECOND	BRITISH THERMAL UNITS PER HOUR	ERGS PER SECOND	FOOT-POUNDS PER SECOND	HORSEPOWER	KILOGRAM- CALORIES PER MINUTE	WATTS*	KILOWATTS
BRITISH THERMAL UNITS PER SECOND	1	2.777 $\times 10^{-4}$	9.480 $\times 10^{-11}$	1.285 $\times 10^{-3}$	0.707	6.614 $\times 10^{-2}$	9.480 $\times 10^{-4}$	0.9480
BRITISH THERMAL UNITS PER HOUR	3600	1	3.413 $\times 10^{-7}$	4.6275	2.545 $\times 10^3$	233.1	3.413	3.413 $\times 10^3$
ERGS PER SECOND	1.0548 $\times 10^{10}$	2.930 $\times 10^6$	1	1.356 $\times 10^7$	7.457 $\times 10^9$	6.977 $\times 10^8$	10^7	10^{10}
FOOT-POUNDS PER SECOND	778	0.2161	7.376 $\times 10^{-8}$	1	550	51.44	0.7376	737.6
HORSEPOWER	1.414	3.929 $\times 10^{-4}$	1.341 $\times 10^{-10}$	1.818 $\times 10^{-3}$	1	9.355 $\times 10^{-2}$	1.341 $\times 10^{-3}$	1.341
KILOGRAM- CALORIES PER MINUTE	15.12	4.20 $\times 10^{-3}$	1.433 $\times 10^{-9}$	1.943 $\times 10^{-2}$	10.69	1	1.433 $\times 10^{-2}$	14.33
WATTS*	1054.8	0.2930	10^{-7}	1.356	745.7	69.77	1	1000
KILOWATTS	1.0548	2.930 $\times 10^{-4}$	10^{-7}	1.356 $\times 10^{-3}$	0.7457	6.977 $\times 10^{-2}$	10^{-3}	1

Table 19

POWER DENSITY, HEAT FLUX DENSITY

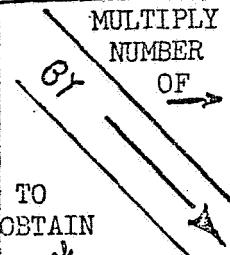
	BTU PER SECOND PER SQUARE FOOT	BTU PER HOUR PER SQUARE FOOT	ERGS PER SECOND PER SQUARE CENTIMETER	FOOT-POUNDS PER SECOND PER SQUARE FOOT	WATTS PER SQUARE CENTIMETER	WATTS PER SQUARE METER	WATTS PER SQUARE FOOT
BTU PER SECOND PER SQUARE FOOT	1	2.777 $\times 10^{-4}$	8.807 $\times 10^{-8}$	1.285 $\times 10^{-3}$	0.8807	8.807 $\times 10^{-5}$	9.480 $\times 10^{-4}$
BTU PER HOUR PER SQUARE FOOT	3600	1	3.171 $\times 10^{-4}$	4.626	3171	0.3171	3.413
ERGS PER SECOND PER SQUARE CENTIMETER	1.1354 $\times 10^7$	3153	1	1.459 $\times 10^4$	10^7	1000	1.076 $\times 10^4$
FOOT-POUNDS PER SECOND PER SQUARE FOOT	778	0.2161	6.852 $\times 10^{-5}$	1	685.2	6.852 $\times 10^{-2}$	0.7375
WATTS PER SQUARE CENTIMETER	1.1354	3.153 $\times 10^{-4}$	10^{-7}	1.459 $\times 10^{-3}$	1	10^4	1.076 $\times 10^{-3}$
WATTS PER SQUARE METER	1.1354 $\times 10^4$	3.153	10^{-3}	14.59	10^4	1	10.76
WATTS PER SQUARE FOOT	1054.8	0.2929	9.290 $\times 10^{-5}$	1.355	929	9.290 $\times 10^{-2}$	1

Table 20

TEMPERATURE

$X^{\circ}K =$	$(T^{\circ}C) + 273.16$	$0.556(T^{\circ}F - 32) + 273.16$	$0.556 (T^{\circ}R)$
$X^{\circ}C =$	$(T^{\circ}K) - 273.16$	$0.556 (T^{\circ}F - 32)$	$0.556 (T^{\circ}R - 491.6)$
$X^{\circ}F =$	$1.8(T^{\circ}K - 273.16) + 32$	$1.8 (T^{\circ}C) + 32$	$(T^{\circ}K) - 459.6$
$X^{\circ}R =$	$1.8 (T^{\circ}K)$	$1.8 (T^{\circ}C) + 491.6$.	.	$(T^{\circ}F + 459.6)$.	.

Note:

$^{\circ}K$ = Degrees Kelvin

$^{\circ}C$ = Degrees Centigrade or Celsius

$^{\circ}F$ = Degrees Fahrenheit

$^{\circ}R$ = Degrees Rankine

Table 21

THERMAL CONDUCTIVITY

MULTIPLY NUMBER OF ↓ TO OBTAIN ↓	WATTS PER* CM-°K	WATTS PER INCH-°R	CALORIES PER SEC-CM-°K	BTU-IN PER HR-FT ² -°R	BTU PER HR-FT-°R	BTU PER SEC-IN-°R	BTU PER HR-IN-°R	K CAL PER HR-M-°K
WATTS* PER CENTIMETER- °K	1	0.7087	4.184	1.4423 x 10 ⁻³	1.731 x 10 ⁻²	747.7	0.2077	1.1622 x 10 ⁻²
WATTS PER INCH-°R	1.4111	1	5.904	2.035 x 10 ⁻³	2.442 x 10 ⁻²	1.0550	0.2931	1.6400 x 10 ⁻²
CALORIES PER SECOND- CENTIMETER-°K	0.2390	0.1694	1	3.447 x 10 ⁻⁴	4.136 x 10 ⁻³	178.70	4.964 x 10 ⁻²	2.778 x 10 ⁻³
BTU-IN PER HR-FT ² -°R	693.4	491.4	2901	1	12	5.1840 x 10 ⁵	144	8.058
BTU PER HR-FT-°R	57.78	40.946	241.8	8.333 x 10 ⁻²	1	4.320 x 10 ⁺	12	0.6715
BTU PER SEC-IN-°R	1.337 x 10 ⁻³	9.478 x 10 ⁻⁴	5.596	1.9290 x 10 ⁻⁶	2.3148 ¹ x 10 ⁻⁵	1	2.778 x 10 ⁻⁴	1.5545 x 10 ⁻⁵
BTU PER HR-IN-°R	4.815	3.413	20.15	6.944 x 10 ⁻³	8.333 x 10 ⁻²	3600	1	5.596 x 10 ⁻²
K CAL PER HR-M-°K	86.04	60.97	360	0.12409	1.4891	6.433 x 10 ⁴	17.87	1

Table 22

THERMAL RESISTANCE

	°R PER WATT	°K PER WATT*	SECOND-°K PER CALORIE	HOUR-FEET-°R PER BTU-INCH	HOUR-°R PER BTU	SECOND-°R PER BTU	HOUR-°K PER KILOCALORIE
°R PER WATT	1	1.80	0.430	40.956	3.413	9.480 $\times 10^{-4}$	1.548
°K PER WATT*	0.5556	1	0.2389	22.76	1.896	5.267 $\times 10^{-4}$	0.860
SECOND-°K PER CALORIE	2.326	4.187	1	95.26	7.939	2.205 $\times 10^{-3}$	3.60
HOUR-FEET-°R PER BTU-INCH	2.442 $\times 10^{-2}$	4.396 $\times 10^{-2}$	1.050 $\times 10^{-2}$	1	8.335 $\times 10^{-2}$	2.315 $\times 10^{-5}$	3.780 $\times 10^{-2}$
HOUR-°R PER BTU	0.2930	0.527	0.126	12	1	2.778 $\times 10^{-4}$	0.4536
SECOND-°R PER BTU	1054.8	1898.6	453.6	4.32 $\times 10^4$	3600	1	1632.8
HOUR-°K PER KILOCALORIE	0.646	1.163	0.278	26.458	2.205	6.124 $\times 10^{-4}$	1

Table 23

THERMAL CAPACITANCE

<div style="display: flex; align-items: center; justify-content: center;"> <div style="writing-mode: vertical-rl; transform: rotate(180deg); font-weight: bold; margin-right: 10px;">BY</div> <div style="text-align: center;"> MULTIPLY NUMBER OF ↗ ↘ </div> </div> <div style="display: flex; align-items: center; justify-content: center;"> <div style="writing-mode: vertical-rl; transform: rotate(180deg); font-weight: bold; margin-right: 10px;">TO OBTAIN</div> <div style="text-align: center;"> ↘ ↗ </div> </div>	BTU PER °R	JOULES* PER °K	CALORIES PER °K	KILOCALORIES PER °K
BTU PER °R	1	5.26 $\times 10^{-4}$	2.2046 $\times 10^{-4}$	0.22046
JOULES PER °K OR WATT-SECONDS PER °K	1899.11	1	4.1868	4186.8
CALORIES PER °K	4536	0.2389	1	1000
KILOCALORIES PER °K	4.536	2.389 $\times 10^{-3}$	0.001	1

Table 24

THERMAL DIFFUSIVITY

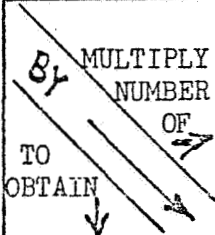
	SQUARE FEET PER HOUR	SQUARE FEET PER SECOND	SQUARE INCHES PER SECOND	SQUARE CENTIMETERS PER HOUR	SQUARE METERS PER HOUR	SQUARE CENTIMETERS PER SECOND	SQUARE METERS* PER SECOND
SQUARE FEET PER HOUR	1	3600	25	1.0764×10^{-3}	10.764	3.875	3.875×10^4
SQUARE FEET PER SECOND	2.778×10^{-4}	1	6.944×10^{-3}	2.990×10^{-7}	2.990×10^{-3}	1.0764×10^{-3}	10.764
SQUARE INCHES PER SECOND	0.040	144	1	4.306×10^{-5}	0.4306	0.1550	1.550×10^3
SQUARE CENTIMETERS PER HOUR	929.0	3.3445×10^6	2.323×10^4	1	10^4	3600	3.600×10^7
SQUARE METERS PER HOUR	9.290×10^{-2}	334.45	2.323	10^{-4}	1	.3600	3600
SQUARE CENTIMETERS PER SECOND	0.2581	929.0	6.452	2.778×10^{-4}	2.778	1	10^{-4}
SQUARE METERS* PER SECOND	2.5806×10^{-5}	9.290×10^{-2}	6.452×10^{-4}	2.778×10^{-8}	2.778×10^{-4}	10^{-4}	1

Table 25
SPECIFIC HEAT

BY MULTIPLY NUMBER OF TO OBTAIN	GRAM-CALORIES PER GRAM °K	* JOULES PER GRAM °K	BTU PER POUND °R	KILOGRAM-CALORIES PER GRAM °K
GRAM-CALORIES PER GRAM °K	1	0.239	1.000	1000
JOULES * PER GRAM °K	4.187	1	4.187	4187
BTU PER POUND °R	1.000	0.23825	1	1000.00
KILOGRAM-CALORIES PER GRAM °K	0.001	2.3901 x 10 ⁻⁴	1.00065 x 10 ⁻³	1

Table 26

LATENT HEAT

<p>MULTIPLY NUMBER OF</p> <p>BY</p> <p>TO OBTAIN</p>	<p>KILOCALORIES PER GRAM</p>	<p>CALORIES PER GRAM</p>	<p>JOULES *</p> <p>PER GRAM</p>	<p>BTU PER POUND</p>
<p>KILOCALORIES PER GRAM</p>	<p>1</p>	<p>0.001</p>	<p>2.39 $\times 10^{-4}$</p>	<p>5.56 $\times 10^{-4}$</p>
<p>CALORIES PER GRAM</p>	<p>1000</p>	<p>1</p>	<p>0.23901</p>	<p>0.556</p>
<p>JOULES *</p> <p>PER GRAM</p>	<p>4187</p>	<p>4.187</p>	<p>1</p>	<p>2.326</p>
<p>BTU PER POUND</p>	<p>1800.0</p>	<p>1.80</p>	<p>0.4279</p>	<p>1</p>

Table 27

VISCOSITY

TO OBTAIN ↓ BY ↘ MULTIPLY NUMBER OF →	GRAM PER CM SEC (POISES)	KILOGRAM PER METER SECOND	POUND MASS PER FOOT SECOND	POUND FORCE SECOND PER SQUARE FOOT	CENTIPOISES	POUND MASS PER FOOT HOUR
GRAM PER CENTIMETER SECOND (POISES)	1	10	1.488 $\times 10^1$	4.788 $\times 10^2$	10^{-2}	4.134 $\times 10^{-3}$
KILOGRAM PER METER SECOND	10^{-1}	1	1.488	4.788 $\times 10^1$	10^{-3}	4.134 $\times 10^{-4}$
POUND MASS PER FOOT SECOND	6.7197 $\times 10^{-2}$	6.7197 $\times 10^{-1}$	1	32.174	6.7197 $\times 10^{-4}$	2.778 $\times 10^{-4}$
POUND FORCE SECOND PER SQUARE FOOT	2.0886 $\times 10^{-3}$	2.0886 $\times 10^{-2}$	3.1081 $\times 10^{-2}$	1	2.0886 $\times 10^{-5}$	8.6336 $\times 10^{-6}$
CENTIPOISES	10^2	10^3	1.4882 $\times 10^3$	4.788 $\times 10^4$	1	4.1338 $\times 10^{-1}$
POUND MASS PER FOOT HOUR	2.4191 $\times 10^2$	2.4191 $\times 10^3$	3.6 $\times 10^3$	1.1583 $\times 10^5$	2.4191	1

Table 28

KINEMATIC VISCOSITY

TO OBTAIN ↓ BY ↘ MULTIPLY NUMBER OF →	SQUARE CENTIMETER PER SECOND	SQUARE METER PER SECOND	SQUARE FOOT PER HOUR	CENTISTOKES
SQUARE CENTIMETERS PER SECOND	1	10^4	2.5807×10^{-1}	10^{-2}
SQUARE METER PER SECOND	10^{-4}	1	2.5807×10^{-5}	10^{-6}
SQUARE FOOT PER HOUR	3.8750	3.8750×10^4	1	3.8750×10^{-2}
CENTISTOKES	10^2	10^6	2.5807×10^1	1